PROCEEDINGS OF THE FLUIDIC STATE-OF-THE-ART
SYMPOSIUM HELD AT NAVAL ORDNANCE LABORATORY,
WHITE OAK, MARYLAND ON 30 SEPTEMBER - 3 OCTOBER, 1974.
VOLUME III

Harry Diamond Laboratories

1974

FLUIDIC
STATE-OF-THE-ART
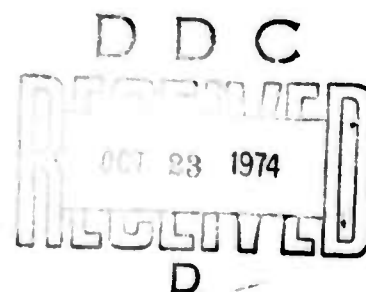# SYMPOSIUM

1974

30 SEPTEMBER – 3 OCTOBER

D D C

OCT 23 1974

D

VOLUME III

U.S. Army Materiel Command
Harry Diamond Laboratories
Washington, D.C.

DISCLAIMER NOTICE

THIS DOCUMENT IS BEST QUALITY AVAILABLE. THE COPY FURNISHED TO DTIC CONTAINED A SIGNIFICANT NUMBER OF PAGES WHICH DO NOT REPRODUCE LEGIBLY.

REPORT DOCUMENTATION PAGE		READ INSTRUCTIONS BEFORE COMPLETING FORM
1. REPORT NUMBER	2. GOVT ACCESSION NO.	3. RECIPIENT'S CATALOG NUMBER
4. TITLE (and Subtitle) Proceedings of the Fluidic State-of-the-Art Symposium, 30 Sep - 3 Oct 74, Vol. III		5. TYPE OF REPORT & PERIOD COVERED
		6. PERFORMING ORG. REPORT NUMBER
7. AUTHOR(s) Various		8. CONTRACT OR GRANT NUMBER(s) HDL Proj No. 302531
9. PERFORMING ORGANIZATION NAME AND ADDRESS		10. PROGRAM ELEMENT, PROJECT TASK AREA & WORK UNIT NUMBERS
11. CONTROLLING OFFICE NAME AND ADDRESS		12. REPORT DATE
		13. NUMBER OF PAGES 485
14. MONITORING AGENCY NAME & ADDRESS(if different from Controlling Office)		15. SECURITY CLASS (of this report) Unclassified
		15a. DECLASSIFICATION DOWNGRADING SCHEDULE

16. DISTRIBUTION STATEMENT (of this Report)

DISTRIBUTION STATEMENT A

Approved for public release;
Distribution Unlimited

17. DISTRIBUTION STATEMENT (of the abstract entered in Block 20, if different from Report)

Unlimited

18. SUPPLEMENTARY NOTES

19. KEY WORDS (Continue on reverse side if necessary and identify by block number) Digital fluidic components, digital fluidic systems, digital analog hybrid fluidic system, regenerative process fluidic switching circuits, fluid logic networks, fluidic threshold lgoic, state diagram synthesis of sequential feedback control circuits, signal analysis of fluidic networks, flueric controller, fluidic carrier techniques, fluidic notch filters, analog fluidic circuits, low power hydraulic control components

20. ABSTRACT (Continue on reverse side if necessary and identify by block number)

This volume contains twelve papers for a total of 485 pages.

DD ₁ FORM JAN 73 1473 EDITION OF 1 NOV 65 IS OBSOLETE

Volume III

DIGITAL FLUIDIC COMPONENT AND SYSTEM DESIGN

by

G.A. Parker, B.Sc., Ph.D.

Reader, Dept. of Mechanical Engineering

University of Surrey, Guildford, U.K.

1

Nomenclature

A	=	cross-sectional area
b	=	nozzle width
C	=	fluid capacitance
c_p	=	specific heat of gas at constant pressure
d	=	inlet diameter
D	=	tube diameter
F	=	frequency parameter $\left(= \sqrt{\dfrac{\omega P_R}{\upsilon}} \cdot \dfrac{D}{2} \right)$
h	=	channel depth
H	=	fluid inductance or inertance
k	=	thermal conductivity
L	=	tube length
$\dot{M}$	=	mass flow
n	=	polytropic constant
N	=	aspect ratio $(= h/b)$
Δp	=	pressure drop
$P_{m,s}$	=	mean and supply pressure (gauge)
P	=	pressure (absolute)
P_R	=	Prandtl number $(= \mu c_p/k)$
R	=	fluid resistance
R_e	=	Reynolds number $(= \overline{U}D/\upsilon)$
R_g	=	gas constant
s	=	LaPlace transform operator
T	=	absolute temperature

$\bar{U}_{s,j}$ = average supply and jet centre-line velocities respectively

V = volume

W_s = supply power

μ = absolute viscosity

ν = kinematic viscosity

ρ = density

t_c = connecting line and passive component rise time

t_D = pure time delay

t_s = switching time

ω = angular frequency

1. INTRODUCTION

The techniques of successful design often involve the fusing together of a wide range of apparently contradictory requirements involving mainly technological, social, economic and aesthetic considerations. While some of the facets of engineering design have the appearance of requiring only a mechanistic use of established information, nevertheless, technological progress has only been brought about by the designer's willingness to grapple with imperfectly understood ideas and transform them into marketable products in the present not the future. It is in this area that design is truly an art form.

It has been evident for a number of years that fluidics would present the designer with a variety of difficult problems, and to a large extent the growth of fluidics has reflected this. The component designer of pure fluidic devices has been faced with reconciling intractable fluid mechanics problems with a large volume of empirical data. The systems designer has found the dynamic processing of information in a fluid media equally severe. Finally, the non-specialist user in designing applications has experienced some difficulties in translating his experience of electronics, pneumatics and so on into the fluidics area.

Fortunately, technology is never static for long and some of the problems of the day disappear as new ideas and design philosophies emerge. While the component designer must still rely heavily on empirical data for new designs of pure fluid devices, the system designer and user now has a widening range of standard devices at his disposal which may be used with a high degree of confidence. Whether or not a designer chooses a fluidic solution to his control problem depends on many factors, but we are now at the stage where a comparison with other techniques may be made with some economic realism.

2. PASSIVE FLUIDIC SYSTEM COMPONENT CHARACTERISATION

The small signal analysis of lumped parameter characteristics associated with fluid components has to a large extent been developed over many years in the field of acoustics. Fluid characteristics analogous to the electrical parameters of resistance, inductance and capacitance have been identified and described for different flow regimes. The use of passive components in fluidic as opposed to acoustic systems does involve some practical differences, such as:-

   a) Higher power levels are usually transmitted through the system.

   b) Large steady flow levels may be superimposed on the signal.

5

c) Matching to pure fluid amplifiers and switches is required.

d) High velocities may occur in the system under compressible flow conditions.

The most easily measure independent variables in a fluid system are, of course, pressure and average volume flow which, unfortunately, loses generality by excluding compressible flow. The use of mass flow rather than volume flow is more complete but leads to inconsistent units when measuring power. Both Kirshner (Ref.1) and Taplin (Ref.2) have suggested modifications to the pressure parameter to retain consistency when using mass flow as the other parameter. Kirshner has proposed a mechanical potential from fluid mechanic considerations and Taplin from a fundamental thermodynamic approach used

$$R_g T \log_e P$$

Both suggestions have their merits but neither has found widespread acceptance for design work, probably due to their dissociation from the measured physical variable.

The lumped parameter characteristics of fluid components may be found from the properties of resistance, capacitance and inductance (or inertance) analogous to their electrical counterparts. Figure 1 indicates how pressure drop Δp and mass flow $\dot{M}$ completely specifies each of these characteristics in a linear system. Each will now be considered briefly from the design point of view.

The linear properties of laminar flow through tubular and rectangular capillary passages is attractive for providing resistance in analogue, and to a lesser extent digital, fluidic systems. Provided a fairly long capillary length is chosen (usually greater than 100 diameters) non-linear fluid entrance loss effects can be minimized to give a linear resistance characteristic at constant fluid temperature, with the resistance R given by (Ref.3).

$$R = \frac{128 \mu L}{\pi D^4 \rho} \tag{1}$$

where D = tube diameter
       L = tube length

provided the flow is laminar. This requires that the Reynolds Number, R_e, satisfies

$$R_e = \frac{\rho U D}{\mu} < 2000 \tag{2}$$

6

The effect of viscosity variations with temperature may not always be ignored in determining the resistance value, and indeed this property has been exploited for temperature sensing in some fluidic circuits. The main practical design problem in calculating laminar resistor values is the extreme sensitivity to errors in measuring the tube diameter in miniature sizes. Even the diameter variations in hypodermic tubing give considerable scatter in calculated values.

Many of the channels and orifices in fluidic systems are rectangular in shape with low aspect ratio (depth, h / width, b). In this case the resistance for laminar flow conditions is

$$R = \frac{3\mu L}{4hb^3} \cdot \left[1 - \left(\frac{b}{h} \right) \cdot f\left(\frac{h}{b} \right) \right]^{-1} \qquad (3)$$

where

$$f\left(\frac{h}{b} \right) = \frac{192}{\pi^5} \sum_{n=1}^{\infty} \frac{1}{n^5} \cdot \tanh\left(\frac{n\pi h}{b} \right)$$

Methods of calculating the capacitance associated with fluid passage-ways and volumes and the inductance or inertance associated with fluid inertia are well known for simple geometric conditions. For a simple chamber of volume V, it can be shown (Ref.3) that when it is filled with a perfect gas, such as air, the capacitance C caused by compression of the gas in the chamber is given by

$$C = \frac{V}{nR_g T} \qquad (4)$$

where n = polytropic constant

For air the value of n can vary between 1 and 1.4 depending on whether the pressure changes in the volume vary slowly or rapidly respectively. Katz and Hastie (Ref.4) have conducted experiments, using frequency response methods, to determine the actual value of n under different dynamic conditions. Their investigations on cylindrical chambers approximately confirms earlier theoretical work that the polytropic constant n is a function of a frequency parameter F, defined by

7

$$F = \left[\frac{-P_R}{\omega} \right]^{\frac{1}{2}} \cdot \frac{D}{2} \qquad (5)$$

where P_R = Prandtl number = $\dfrac{\mu c_p}{k}$

ω = angular frequency of oscillation

For air, approximately isothermal conditions occur when $F < 1$ and adiabatic conditions when $F > 0$ in long cylindrical tubes, although little error appears to arise when this is also applied to short cylinders. Further work is required on the heat transfer mechanism associated with fluid capacitance effects for more complex geometries and under varying load conditions.

In fluid circuitry, wherever high velocity transient flows occur a mass of fluid is accelerated or decelerated causing a significant pressure change due to the fluid inertia. In a relatively small diameter tube of cross-sectional area A and length L it can be shown that (Ref. 5) the fluid inductance or inertance H is given quite simply by

$$H = \frac{L}{A} \qquad (6)$$

The relationships of C and H to the mass flow and pressure drop are as defined in Figure 1.

The ideas of lumped fluid inertance could well be extended beyond the simple geometries of tubes, convergent and divergent ducts. Calculations involving inertance must almost invariably be coupled with a corresponding resistance term. When considering the frequency response of these parameters in fluidic systems, very commonly the inductive reactance is at least one order of magnitude smaller than the capacitive reactance or the resistance. The exception to this is in resonant circuits such as the Helmholtz resonator.

Some systems parameters, such as orifice flow resistance, are non-linear but their analysis is considerably simplified if algebraic manipulation of linear functions is used. Most systems designers use the linearizing approximations of small signal analysis to overcome this difficulty while digital computer simulation is increasingly being used for synthesizing systems with large signal changes.

When the physical size of a fluid component becomes significant compared with the wavelength of the acoustic signal being propagated through it, the concept of lumped parameter properties for the component breaks down and it must be considered to have spatial as well as time variations of pressure and flow. This is commonly known

as a distributed parameter system and is particularly relevant to the
characteristics of the connecting passages and lines in fluidic
systems. A considerable volume of literature has existed for many
years on electrical transmission lines and acoustic properties of long
lines but the growth of interest in fluidic systems has stimulated a
fresh surge of research into fluid transmission lines. Early papers
on fluid transmission lines were based on an elemental one-dimensional
model of the line consisting of constant resistance, inertance and
capacitance terms. However, it was observed that short pulses and fast
rise time steps, such as might occur in a fluidic digital circuit,
disperse much more rapidly than such models predict.

Although the actual transmission line is not strictly
one-dimensional, it is possible to include varying velocity profile
and heat transfer effects in the model which largely account for
signal dispersion. Classic papers by Nichols (Ref.5) and Iberall
(Ref.6) have given the frequency response of linear fluid lines
using this approach while Brown (Ref.7) has developed the
corresponding transient response based on the propagation operator
and characteristic impedance concepts familiar to electrical
engineers. More recently Schaedel (Ref.8) has extended the analysis
to fluid transmission lines with rectangular cross-section, which is
particularly relevant to the dynamic analysis of integrated fluidic
circuits. Using computer programmes based on these models, workers
such as Franke (Ref.9) have been able to show good correlation
between theoretical and experimental frequency response character-
istics for well defined linear load terminations to the line.

In practice a fluid transmission line is usually terminated
by a valve or orifice producing a non-linear pressure-flow
characteristic. As the control impedance of most fluidic elements
is not high, significant mean flows may be superimposed on the signal
level thereby increasing distortion. In a recent paper Strunk
(Ref.10) has analysed the distortion in the frequency response
caused by orifice type loads using a perturbation technique. He
shows that a second harmonic distortion is produced which is a direct
function of the ratio of the signal amplitude to the mean flow.
Using a load impedance greater than the characteristic value reduces
the distortion although at frequencies close to resonance conditions
distortion can be expected to increase.

From the designers point of view, fluidic transmission lines
remain a complex area and it is unlikely that accurate predictions
of their characteristics can be made without recourse to computer
programmes. The transient response required for digital systems
analysis is more laborious to handle than the frequency response
and at the present time no fast transform method appears to be
available to keep storage capacity requirements within reasonable
limits.

9

3.   FLUID DIGITAL DEVICES

Digital fluid devices may be broadly divided into non-moving part ('pure') and moving part and many of them perform similar functions. They may be classified as fluidic if they operate relatively rapidly compared with conventional pneumatic and electro-mechanical control valves and if they are also designed to have very high reliability. Operating pressures vary considerably from 0.1 to 20 bars and are generally dependant on whether they are 'open-centre', requiring flow through the device continuously, or 'closed-centre' requiring flow only during the switching action in most cases. Pure fluid devices fall into the former category and therefore operate at low pressures while moving part devices are usually closed-centre and may have a wide range of operating pressures. Fig. 2 taken from Bouteille (Ref.11) summarises the classification of fluid logic devices in terms of operating pressures.

The main types of pure fluidic digital devices are:-

(i) Wall re-attachment

(ii) Turbulence

(iii) Momentum interaction

although other effects such as jet impact modulation, vortex feedback, wall reflection, and so on have been used.

The wall re-attachment of a jet, first described by Coanda, was used by Bowles in the late 1950's in a series of practical fluid logic devices which have remained virtually the same in general operation to the present day. The two basic elements are the R-S memory device and the two input OR - NOR monostable device which may be used to generate all the standard logic functions, as shown in Fig.3 (Ref.11). In all cases the elements are active, that is to say that a separate fluid supply is required, in addition to the input and output signals, with pressure levels in the range 0.1 to 0.7 bar.

The turbulence digital element was developed by Auger (Ref.12) a few years later using the well known transition of a laminar jet of fluid to the turbulent state. It produces only an active multiple input NOR function and consequently the range of standard logic functions require rather more elements for their implementation as shown in Fig.4. (Ref.11). Supply pressures are usually very low in the range .015 to .15 bar.

Passive momentum interaction elements for digital applications seem to have been originally suggested by Greenwood (Ref.13) and has lead to the development of OR, AND, EXCLUSIVE-OR, and HALF ADDER

10

functions. Glaettli (Ref.14) and others have also suggested an active EQUIVALENCE element based predominantly on the same principle which is useful in some computational circuits. Because of signal degradation through a passive fluid logic device, care must be taken in cascading such elements and usually a prefered arrangement is to integrate passive elements into the inputs of active wall re-attach-ment elements thereby giving greater logic power and flexibility and minimising the danger of the user placing passive elements in unusable configurations.

While the early development of pure fluidics took place largely in America, the corresponding expansion of low pressure moving part devices took place mainly in Eastern Europe at approximately the same time. Of course, high pressure pneumatic poppet and spool valve systems had existed long before then and indeed had been designed in systems as logic devices by, for example, Martonair in England. However, the new generation of moving part devices were highly miniaturized and simple geometrically making them very reliable with good response so that they could be built into complex circuits.

The main types of moving part digital devices are:-

(i) Double diaphragm stack with static force balance.

(ii) Three diaphragm stack with static force balance or back-pressure operation.

(iii) Single diaphragm with flow over surface.

(iv) Single diaphragm with ejector nozzle.

(v) Free foil.

Although other moving part devices have been made based on different principles, undoubtably the high reliability possible with diaphragm actuation has lead to its inclusion in all the most successful configurations. Operating pressures are usually in the range 0.1 to 1 bar although higher pressures may be used.

Historically the triple-diaphragm Useppa unit developed in the USSR was the first of the low pressure moving part logic systems to be reported by Berends and Tal (Ref.15) and this was followed shortly by the Dreloba double diaphragm device in the GDR, operating on the force balance principle, attributed to Töpfer et al (Ref.16). Fig.5. shows the logic function of this device. The configuration was subsequently refined in a three diaphragm arrangement called Trimelog by Helm et al in Hungary. Yet a further system developed by Brychta (Ref.17) independently in Czechoslovakia consists of a diaphragm restricting the output from an ejector nozzle, which has

11

the advantage in some applications that the output pressure may be
switched between supply and suction pressures. More recently
diaphragm valves have been developed in West Germany and a novel
planar diaphragm element which performs the logical NOR function has
been reported by Jensen et al (Ref.18) in America. Very high
packaging densities appear to be possible with the latter
configuration together with rapid response. Fig.6. from Ref.11
summarises the standard logic functions for the element.

Possibly the simplest type of geometry for a moving part logic
device is provided by the foil element originally proposed by Bahr
(Ref.19) in 1965. The basis of the element is a free moving disc or
foil contained in a chamber of a shape to constrain the foil to move
in a direction normal to the plane of the foil. The parts of the
chamber to which the supply, input and output connections are made
determine the logic function of the element. The main configuration
give NOT, OR, bistable and diode functions.

A number of pure fluid and moving part devices fall into the
category of threshold logic devices; that is, elements with several
input connections arranged so that they switch when a given number
of input signals are present. Such devices have great logic power
but are usually very complex and rather slow in operation. Possibly
the most ingenious of these is a multiple bag diaphragm arrangement
developed by Stivin (Ref.37) in Czechoslovakia for machine tool
applications. It is possible that its complexity made it unreliable
in operation.

4. DIGITAL COMPONENT CHARACTERISTICS

The design of fluidic circuits using digital components require
the specification primarily of power consumption, fan-in and fan-out,
pressure and flow recovery, and switching characteristics.

Considerable attention has been paid to the power consumption
of pure fluid wall re-attachment devices, which by their nature are
open centre devices. For the flow of an incompressible fluid from a
rectangular cross-section nozzle, the supply pressure, p_s, and the
supply power W_s are given by

$$P_s = \frac{\rho}{2} \cdot \bar{U}_s^2 = \frac{\mu^2}{2\rho} \cdot \frac{R_e^2}{b^2} \tag{7}$$

$$W_s = \frac{\rho}{2} \cdot \bar{U}_s^3 \cdot Nb^2 = \frac{\mu^3}{2\rho^2} \cdot N \cdot \frac{R_e^3}{b} = \sqrt{\frac{2p_s^3}{\rho}} \cdot Nb^2 \tag{8}$$

12

Small (Ref.20) has shown that the minimum operating Reynolds Number for wall re-attachment is independant of elements size so that the minimum power consumption of an element, $(W_s)_{min}$, for a given fluid can now be expressed from equation (8) as

$$(W_s)_{min} = \frac{Const.}{b} \qquad (9)$$

In other words, the minimum power consumption is inversely proportional to element size. Müller (Ref.21) and others have confirmed the same relationship. It would also be expected that the turbulence amplifier would show the same characteristics although the power levels would be much lower.

Various workers, including Glaettli, Müller and Zingg (Ref.22), have shown that the minimum Reynolds Number of spontaneous turbulent wall re-attachment is in the region of 2,500 - 3,000 for a unity aspect ratio nozzle. This may be reduced somewhat for aspect ratios up to 3 or 4 but increases abruptly for aspect ratios of less than unity. Tests by Rechten and Zückler (Ref.23) show that it is possible to obtain re-attachment well into the laminar flow regime, at the expense of power consumption, by using aspect ratios of at least 10. In practice most wall re-attachment devices operating with gases are designed with an aspect ratio between 2 and 4 based on a nozzle width in the range 0.25 - 0.40 mm. Supply pressures are usually chosen well away from the minimum Reynolds Number condition, 0.2 to 0.7 bar being typical. This corresponds to a power consumption in the range 1 - 10 fluid watts. In comparison the turbulence amplifier normally consumes rather less than 0.1 watt.

Digital fluidic devices are not confined to air as the supply fluid but have been used with water, oil, steam, kerosine and so on. It is unlikely that complex logic circuits using pure fluidic devices operating with liquid supplies will be used to any significant extent due to high power consumption involved. For example, a small size wall re-attachment element using hydraulic oil typically consumes 100 fluid watts of power. However, there is an interesting trend to use large scale pure fluidic elements for process control applications in which the device is inserted directly in a liquid or gas stream to provide such functions as flow metering, diversion, regulation and mixing. Load matching vent channels are usually omitted to avoid re-circulating the process fluid and the element profile is designed for the particular load conditions required by the application.

Moving part devices, require little power when used in pneumatic logic circuits and may operate at pressures often in excess of 1 bar. Most of these elements do not require continuous power consumption in any switched state, apart from that due to small leakage flows, but rather a static pressure signal combination to

13

hold the device in the required state. However, during switching the supply and vent ports may be momentarily connected together thereby causing significant power losses for very short periods of time. Static switching elements may be designed in which the vent port is always closed before the supply port is opened during the switching cycle. They consume little power and are particularly useful for complex, low speed circuitry. However, the apparent advantage of moving part logic devices over their pure fluid counterpart is not straightforward as logic power, response time and so on must be taken into account in deciding the best type of device to use.

As the power consumption requirements of moving part devices is low, there is some attraction in using them for liquid systems. Of course, to a large extent this has been done for many years, particularly in hydraulic systems where relatively large spool valves are widely used for sequence control. Provided the oil is well filtered, there is little doubt that highly miniaturised valves could be used with the advantages of high packing density, improved response and reduced cost.

Fan-in, that is the number of input connections, to wall-attachment devices is usually limited by geometric considerations to 3 or 4 with the control channels converging into a passive OR junction, the output of which passes directly to the wall re-attachment control port. This allows improved signal isolation over earlier designs at the expense of some signal attenuation. Fan-out, or the number of parallel output connections, is governed by the signal amplification at switching in relation to the control input requirements. As the pressure-flow characteristics of both control and output ports are non-linear, the fan-out is conveniently determined by graphically superimposing control switching characteristics on the output pressure-flow characteristic as shown in Fig.7. A fan-out of 2 - 4 is usually obtained for conservatively designed elements with pressure recovery sacrificed to obtain improved reliability. Higher fan-in figures are possible using either planar or tubular turbulence amplifiers with good isolation between input signals. A moving part device, on the other hand, is often constructed with a fan-in of 1 or 2 but with an infinite fan-out.

One of the main advantages claimed for fluidic digital devices over conventional mechanical and electro-mechanical moving part control devices, large and small, is the fast response time. Typical values of switching rise time found in practical elements is 0.5-5 ms for pure fluid types as opposed to 1-100 ms for moving part elements, depending primarily on their size. In combinational, and most sequential circuits, for industrial applications the differences in switching speed are not crucial, except for modules such as counters, shift registers, pulse shapers and so on. Even when counters are used the cycling rate is often modest so that many solutions are possible.

Not unnaturally, considerable attention has been paid to the mechanism of switching in pure fluid elements and to the potential for increasing performance. In an early paper Johnston (Ref.24) demonstrated that over a wide range of Reynolds Numbers for a turbulent re-attached jet, the Strouhal Number based on the supply jet velocity and nozzle width was essentially constant. In other words, the switching time, τ_s, of a wall re-attachment element is

$$\tau_s = \text{const.} \ \frac{b}{\overline{U}_s} = \text{const.} \ \frac{b^2}{R_e} \tag{10}$$

where $\overline{U}_s$ = average supply jet velocity

For constant supply Reynolds Number, the switching time would be expected to decrease with the square of the nozzle width. However, element designs with nozzle widths much smaller than 0.25 mm run into difficulties with boundary layer growth affecting re-attachment, Mach Number effects, manufacturing problems and so on. It is therefore unlikely that significant decreases in present generation element switching times can be obtained in this way. Nor is it particularly attractive to decrease the switching time by increasing the Reynolds Number as power consumption incr..ses dramatically (Eqn.8). Another possibility is to reduce the supply nozzle aspect ratio while holding the supply nozzle velocity constant in the hope that power consumption can be lowered without affecting wall re-attachment too significantly. However, it would appear that at low aspect ratios (below perhaps 1.5) the switching time starts to noticeably increase which suggests that the simple expression for switching time given above (Eqn.10) should be modified. It is evident that although some reduction in power consumption may be made in this way these requirements are opposed to those of minimum switching time, so inevitably some design compromise must be made.

To complete the picture it must be remembered that the response time of a circuit must include the signal pure time delay through the connecting lines and the rise or decay time associated with its transmission characteristics. The pure time delay, τ_D, is given by the local speed of sound divided by the connecting line length, which varies directly with element dimensions, that is, with nozzle width. This we may write as

$$\tau_D = \text{const.} \ b \tag{11}$$

The transient response of a transmission line has already been discussed but if we assume a rather simple model with the line and load represented by lumped parameter resistance R and capacitance C, then the rise time τ_c of the passive components with a gas as the

15

working fluid can be shown to be

$$\tau_c = RC = \frac{\text{const.}}{p_m} = \frac{\text{const.} \cdot b^2}{R_e^2} \tag{12}$$

where p_m is the mean pressure in the capacitance. This is assuming that the component shapes are unaltered by scaling. The expression has a similar form to the switching time for the element although it is more sensitive to Reynolds Number. Most designers of fluidic circuits tend to reduce the Reynolds Number quite appreciably in the connecting lines so that the connection rise time may be significant in some fast operating circuits, such as one-shot pulse shapers.

The problems of predicting the dynamic performance of a turbulence amplifier are rather different as the transition between laminar and turbulent supply flow regimes produces unequal switch-on and switch-off characteristics. Hayes (Ref.25) has associated a pure time delay with both the rise time (switch-on) and the decay time (switch-off) of the amplifier.

The pure time delay and switching rise time expressions are similar in form to Eqn.10 for the wall re-attachment device. Decreasing size and increasing supply pressures would both be expected to improve response. However, as the size of the turbulence amplifier decreases, the static off state output pressure increases and the gain decreases, thereby limiting the fan-out. A minimum value of free jet length between the control port and receiver equal to 1 cm appears to be realistic from this consideration. Increasing the supply pressure significantly reduces the delay times and the switch-on rise time but the residual turbulence in the jet also appears to increase very markedly producing switch-on times approximately one order of magnitude greater than the switch-off time. Typical pure time delay times are 0.5 ms, switch-off time 1 ms, switch-on time 5-15 ms. It is therefore doubtful whether significant improvements in the dynamic performance of the turbulence amplifier can be made until switch-on rise times can be made appreciably more repeatable, probably by reducing residual turbulence in the supply jet.

The dynamic response of moving part devices is to a large extent dependent on the inertia of the fluid and moving parts, fluid compressibility, and viscous effects. Most moving part logic devices use free or clamped diaphragm configurations operating on force balance principles. The device capable of the greatest degree of miniaturisation with low inertia is the free foil element. Work by Fahr (Ref.19) has shown that the theoretical switching time of such elements has exactly the same form as Eqn.10 for wall re-attachment elements with dimension 'b' representing now a characteristic dimension of the foil chamber. He indicates a switching time of 0.1 ms for a typical air operated foil element of

diameter 2 mm although it is not clear whether this has been confirmed experimentally. The limitation on fan-in would appear to impede the successful developement of the foil element for fast acting high packaging density logic blocks but the development of the ridge diaphragm element from this concept has been commercially more successful. Jensen, Müller and Schaffer (Ref.18) in a comprehensive account give a switching time in the region of 1 - 1.5 ms for a push-pull inverter circuit consisting of three diaphragms. The standard arrangement is to use a separate diaphragm chamber for each input but even so high packaging densities are possible. Normally some flow is always present through the logic circuit so that the fan-out is no longer infinite. In practice a value of 4 is used although higher fan-outs are possible.

Inevitably with moving part logic devices, if they are designed to have greater logic power the mechanical complexity increases and so there is some loss of response. The well-known Russian and East German moving part logic elements use multiple stacks of diaphragms to achieve a variety of logic functions within one standard block. Power consumption is very low and switching times are rather longer than the ridge diaphragm element due to the higher inertia of the diaphragm stack. Töpfer (Ref.16) has given switching of approximately 1 ms for the two diaphragm stack, 2.9 ms for three diaphragms, 4.6 ms for five and 8.4 ms for ten diaphragms.

I have dealt at some length with the dynamic characteristics of fluidic devices in order to shed some light on future element design trends. It appears unlikely that miniaturisation can be taken much further without very high initial costs for tooling and it is probable that a larger scatter in element characteristics in a production batch would also have to be tolerated. None of the elements discussed showed any dramatic advantage due to scaling down or increasing the operating energy level so it is probable that element manufacturers will not be able to improve significantly on present day characteristics. However, there is still room for manoeuvre in deciding, not so much on element profile or diaphragm size, but what logic functions are best suited to a particular standard logic block.

Bouteille (Ref.11) has made a comparison between the power consumption and switching speeds of both fluid and electronic devices which is reproduced in Fig.8. This suggests that moving part pneumatic logic is the most economical in very low speed applications, such as supervisory systems and is very attractive even up to operating speeds of 1 HZ. At the other extreme, where very fast switching speeds are required electronic systems are unchallenged. Pure fluidic devices when compared in this way, are prefered to moving part devices in the range 1 - 100 HZ of operation. It must be emphasised that this comparison is not complete as many other aspects, such as overall system cost, sensor specification, reliability, environment, etc., must be considered before a final system choice is made.

17

5.   DIGITAL MODULES

Until comparatively recently, designers of pure fluidic devices were slow to exploit one of their advantages over most moving part devices. This was to assemble in one module several logic function profiles at very little extra cost and almost negligible increase in size. Early wall re-attachment elements suffered from poor input isolation until input vent ports were added at the expense of some input signal degradation. It was then a short step to make the input vent arrangement into a passive OR junction, commonly with two or three inputs. More recently passive AND and one-shot pulse shaper circuits have also been used as inputs in integrated designs with both OR/NOR and bistable profiles.

This has been beneficial in several respects. Logic function power has been increased without increasing air consumption. Packaging passive elements within the standard logic block has reduced the circuit design problems of the user, as signal matching becomes easier. Improved dynamic response is also possible in some cases.

Element designers are now more conscious of the need to make their fluidic components into standard logic blocks suitable for general industrial usage with the minimum of assembly difficulties and maximum immunity to air supply and environmental contamination. Most current commercial pure fluid devices have filters built into the profile to protect the supply and control nozzles from internal contamination and similar filters protecting the vent channels and bias ports from external contamination. Experience has shown that the high degree of reliability inherent in the concept of pure fluidic elements may only be realised by attention to this sort of detail.

Many processes have been tried for manufacturing pure fluidic elements but the main types which have involved for small elements are etched glass, etched metal and epoxy resin casting. With correct bonding the first two processes may be used over a very wide operating temperature range while the latter has the advantage of comparative cheapness. Although injection moulding has been successfully used, it has not lead to a mass produced very low cost element. This is largely due to the trend towards rather more complex profiles mentioned earlier which would significantly increase die costs. The etching processes are particularly useful for multi-layer configurations required in compact integrated designs which can be achieved without appreciably increasing manufacturing costs. Circuits of this complexity would be very difficult to achieve using injection moulding methods.

18

6.   SENSORS

In the majority of industrial fluidic applications the primary reason for choosing this type of control is the attractiveness of detecting or sensing pneumatically. The construction of many types of fluidic sensor is simple and may give rise to an appreciable improvement in reliability and lower cost compared with other methods of detection. If sensing is attractive pneumatically the extension to signal processing and amplification using fluidic circuits is a natural development. This can give rise to cheaper overall systems as, for example, expensive interface valves between different media are avoided.

The majority of fluidic sensors use the variations in the physical parameter being measured to modify the characteristics of one or more fluid jets. Position, liquid level, temperature, flowrate are examples of common parameters sensed directly with jets and this list may be extended if simple moving parts are used in conjunction with jets. For example, relatively inexpensive pressure gauges may be modified so that a high pressure may be detected with a low pressure fluidic circuit by attaching a back pressure sensor to a bourdon tube subjected to the high pressure. Alternatively, if multiple digital output signals are required for different pressures, interruptible jets may be placed round the periphery of a pressure dial gauge so that the pointer interrupts the jet at the desired pressure. This method can be extended to any dial indicator (for example, weight, temperature, voltage) with the advantage that the fluidic detecting circuit is completely isolated from the variable being measured.

The commonest types of jet configurations used for sensing are the back pressure, interruptible jet and conical or proximity jets. The back pressure sensor has been used for many years as an amplifying device in pneumatic and hydraulic circuits. A regulated supply passes flow through a restriction into the back pressure chamber which is then vented, usually to atmosphere. An object placed close to the venting flow causes the pressure in the chamber to increase, which in the extreme case has a value equal to the supply pressure when the vent nozzle is completely blocked. The device is very sensitive to changes in the position of the object when closer than approximately one-quarter of the nozzle diameter. However, as the vent nozzle diameter is usually kept as small as possible to limit power consumption, the useful working gaps are very small, 0.05 to 0.2 mm being typical. The signal generated by the sensor usually activates the fluidic digital switching element directly requiring the input nozzle to be sufficiently small so that no appreciable flow is taken from the sensing element. Apart from the good dynamic response of these sensors they also possess the advantage of negligible hysteresis, a factor which is important in sensing.

19

The interruptible pneumatic sensor is useful for sensing objects in the range 0.2 or 10 cms. The simple form of the sensor consists of a supply jet nozzle and receiver axially aligned but separated by a gap. A relatively high pressure signal can be recovered in the receiver when the supply jet passes across the gap. Any object passing through this gap interrupts the jet stream and reduces the receiver pressure nominally to ambient conditions. The two pressure levels may be readily detected by fluidic switching elements. The sensor has the important advantages that the texture of the objects is not important and the gap setting is not critical. The configuration does suffer from the disadvantage that the receiver may entrain ambient contaminated air with the jet thereby causing unreliable operation.

By slightly pressurising the receiver the problem of receiver contamination may be overcome. When no object is present, the supply jet impinges on the lower pressure jet leaving the receiver thereby restricting the vent flow which in turn raises the pressure at the sensor outlet. When an object interrupts the main jet the receiver vent flow increases causing a corresponding reduction in the outlet pressure. Another solution is to use a diaphragm operated back pressure sensor for the receiver. This has the advantage that the diaphragm isolates the contamination from the pneumatic circuit and also provides more sensitive detection. Jet gaps with this configuration may be increased to over 30 cm.

The sensitive laminar jet has been used to sense objects over much larger distances. A supplementary jet is used to trigger turbulence in a main jet-pressurized receiver configuration with the gap now being between the supplementary and main jets. When an object interrupts the supplementary jet a laminar main jet is re-established which causes the vent flow to fall, thereby increasing the sensor output pressure. Sensing distances may be as large as 100 cm with good shielding of the laminar jet from environmental noise.

If an annular nozzle is used for detection the structure of the conical jet issuing from it may be utilized to sense the presence of objects approximately one nozzle diameter away. The range of gaps is usually from 0.05 to 5 cms. By a suitable choice of cone angle, the jet may be deflected by the presence of an object into an asymmetric configuration so that an output sensing port located close to the deflected jet indicates a relative reduction in pressure. An advantage of the sensor is that it acts as a switch itself with a zero cross-over pressure for object distances of approximately one nozzle diameter. Against this must be weighed the relatively large air consumption of most of these sensors, together with their rather slow response. Hysteresis effects may also be present.

Air powered acoustic sensors are similar in principle to well-established electro-acoustic detection systems employing continuous wave and pulse echo transmission techniques. A continuous wave system involves a transmitter, which emits a continuous wave, and a target which reflects a portion of it back to the receiver. The received wave is time delayed compared with the transmitted wave thus giving an indication of the target distance. These sensors, while being in their infancy, show promise of distance resolution to one-half a wavelength with a range of from 2 cm to several metres. However, the circuitry involved with the sensor is appreciably more complex than with the types previously described.

7.   COMBINATIONAL AND SEQUENTIAL CIRCUIT DESIGN

        Digital fluidic elements are very largely assembled in combinational or sequential circuits configurations for industrial applications. Most simple circuits are combinational in nature; that is, the output signal combination is always a unique selection of the input signal combination. In more complex circuits a particular output signal may be required more than once during the complete machine duty cycle, so that it is no longer possible to specify a unique input signal combination. Sequential circuits are designed to overcome this problem by generating a memory function so that the time sequence of events in the cycle may be identified.

        The difference between these two fundamental types of circuit can be quite simply illustrated by an example of two mechanically interconnected pneumatic cylinders A and B, shown in Fig.9. A+ denotes the extension of the rod of cylinder A while A- signifies the retraction and so on. Small letters a-d denote the positions of limit switches at the end of cylinder strokes to detect completion of that part of the cycle. If a complete machine cycle is A+, B+, A-, B- then the rod of cylinder A traces a square pattern in space through a, b, c, d. Each limit switch signal then uniquely defines the next cylinder action required and the control logic required is said to be combinational as there is no signal ambiguity. However, if the cycle had been A+, B+, B-, A- then it is seen that the rod of cylinder A traces an L-shaped pattern in space which does not require the use of limit switch d but requires two signals from limit switch b which have to provide different cylinder actuation command signals. The circuit must therefore remember the order in which the actuation signals are performed which implies the use of memory elements. This would be an example of sequential circuit design.

        No particular problems should be encountered now in designing fluidic combinational circuits as element characteristics such as fan-in and fan-out, pressure recovery, and so on are conservatively specified by manufacturers. Standard synthesis and reduction procedures using Boolean Algebra, mapping and tabulation methods may

21

all be used to advantage by the designer familiar with these techniques. Fluidic combinational circuits rarely reach the level of complexity that excludes the intuitive approach of the practical engineer, and in some cases, alternative designs may all provide a correct solution to a problem while displaying different features. The criterion for selection under such circumstances is usually on the basis of overall system cost but air consumption may also be of considerable importance in a pure fluidic circuit.

High pressure pneumatic sequential circuits are still commonly designed by intuitive practical methods although systematic design procedures, such as the commercial Martonair, Lucas and Rn⋅ts methods in the U.K. are available. Taking the Martor air cascade method (Ref.3) as an example of this group, the cycle sequence is divided up into groups of operations in which no cylinder operation appears more than once. A three-port valve acts as a limit switch on each cylinder movement and each cylinder has a five-port pilot operated valve associated with it. In addition, one less five-port memory valves than the number of groups are needed. Fig.10 shows the resulting circuit to implement the A+, B+, B-, A-, sequence. The two groups are A+, B+, and B-, A- and the memory valve Y serves to energize the sensors x for the appropriate group of the sequence at the appropriate time whilst de-energizing those which are not required. In this particular circuit the limit switch x_{A-} is used instead as a start valve so that the circuit does not continually cycle. Limitations of the method are that it may lead to the use of rather more logic and memory components than absolutely necessary. With conventional high pressure pneumatic components this could be expensive and space consuming.

In a more general way sequential circuits using digital elements of any type may be designed systematically using the method of Huffman (Ref.26) and others, first developed for the synthesis of electronic circuits. This involves drawing a timing diagram for the sequence using the inputs x from the limit switches, called primaries, to give the logic functions required for the output signals Z which actuate the cylinders. This is then reduced to a minimum form using a merged flow table which enables the signals required for the memory functions, called secondary excitation, to be determined. Application of a modified form of Karnaugh map, with a separate map for each state of the memory elements, then allows the logic circuit for the output signals to be constructed (see, for example, Ref.3 for further details). For example, using such a procedure the sequence A+, B+, B-, A-, is obtained using the circuit shown in Fig. 11. The figure indicates that the memory element occurs in conjunction with AND gates on the outputs in circuits of this type which has lead Retallick (Ref.27) to suggest using these three elements in a fluidic standard block. The number of AND gates increases as more events are added to the cycle with a consequent limitation in practice due to fan-in problems with passive AND components. Cole and Fitch (Ref.28) have suggested

22

rather similar memory element blocks with a systematic synthesis
method for event controlled sequence circuits.

One of the big advantages of fluidic logic elements for
sequential control is the greater flexibility in the choice of logic
and memory functions possible compared with conventional high
pressure pneumatic elements. Also more complex fluidic elements
do not carry a significant packaging size and cost penalty. A
simple illustration of this is afforded by again returning to the
simple two cylinder sequence A+, B+, B-, A- but using instead
one-shot pulse shaping functions on the limit switches; that is,
when the pressure rises as the switch is activated a short duration
pressure pulse is generated. Such fluidic circuits are well known
and may be integrated into memory elements to perform set and reset
action with short pulses. Halford (Ref.29) has shown that using
pulsed memory elements a very simple solution to the above sequence
results, as shown in Fig. 12, which may be easily extended to other
cylinder sequences.

Of course, all cylinder sequences are not as simple as the
example which has been used up to now. Each event in a machine
cycle may be stored in a variety of memory units, such as a binary
counter, shift register, ring counter, tape or card reader, and
decoded to provide the appropriate command signal for the next
event in the sequence. Binary counters suitable for sequence
circuits have been discussed by Bantle (Ref.30), Foster and
Retallick (Ref.31) and others and are usually based on the T
Flip-Flop with pulsed inputs. The sequence may be time controlled
with synchronous operation of the counter using pulsed signals from
a reference oscillator or, alternatively, event controlled with
asynchronous counter operation. In this case the limit switch
associated with each event must produce a pulsed input to the
counter. Alternatively, an event based sequence may be controlled
using AND-OR memory modules (Ref.29) and is particularly useful as
a programmer.

In some cases part of the sequence is repeated which requires
each repetition to be counted as well as the provision for the
normal memory function in the sequence. This may be simply provided
by a binary counter circuit which counts each repetition of the
sequence and, with appropriate decoding, switches the control logic
out of the repetition after the specified number of cycles. Fig. 13
(Ref.29) shows a simple way of implementing A+, (B+, B-) repeated 7
times, A- using a binary counter and making use of composite fluidic
elements such as AND/OR memory and inhibited OR memory functions.

Some use has been made of ring counters, instead of binary
counters, as decoding the output to provide a command signal for the
next event is rather simpler. However pulsed inputs are still
required and a bistable element corresponding to each event in the
sequence is needed in the ring with a consequent difficulty in

23

fan-out for the input signal. More recently work by Foster and Cheng (Ref. 32 and 33) has suggested the use of special codes in conjunction with shift registers for the control of the sequence which has the advantage that pulsed operation is no longer required and decoding the register is fairly straightforward.

The designer of fluidic sequential circuits must also be aware of the possibilities of signal hazards within the system. In the event-based circuit the steady state behaviour is adequately described by the Boolean representation of the logic used. However, during the transient change of state when the system is responding to a change in input variables, signals entering some elements in the system may not change at precisely the same moment in time due to the unequal time delays of different connecting channels and also due to variations in element switching time. During this transition period the actual output may be quite different from the steady state value and is known as a hazardous condition. The effect of such hazards on overall system performance depends upon whether the circuit has memory. Combinational circuits are not permanently affected by hazards whereas sequential circuits many adopt improper stable states.

Hazards in fluidic circuits are likely to occur mainly in high speed sub-circuits such as counters and adders (Ref.34) and in sequential circuits with significant connecting channel differences (Ref.35). Recently Zissos and Grant (Ref.36) have given a design procedure for sequential circuits which provides hazard-free operation.

8.   CONCLUSIONS

Quite significant gaps remain in our knowlege of passive fluid component dynamic characteristics. For example, heat transfer effects in capacitive components and a more general representation of fluid inertias in complex geometries. While much attention has been devoted to transmission line characteristics, simple programming methods for identifying such systems with non-linear load conditions have not yet materialised.

The review has attempted to show that little commercial advantage can be expected from new basic designs of miniature pure fluid digital elements but we may expect more complex digital modules to appear as the design emphasis shifts towards circuit organisation. In low speed circuits an increasing use of moving part devices is to be expected. The decision to use pure or moving part fluidic devices, as opposed to conventional pneumatic valves, in sequential circuit applications is not clear cut. Undoubtedly pure fluidic modules will offer the greatest logic flexibility and packaging density thus allowing rather straightforward design procedures to be developed.

24

Some work remains to be done in optimising logic blocks for
particular design methods. Moving part devices will be particularly
useful in applications involving moderately complex circuits where
power consumption must be minimised or alternatively where the
higher signal pressures can be directly processed. For example, in
process control. Conventional pneumatic values must not be under-
estimated as, properly used, they have good reliability, can operate
as a high pressure amplifier and logic component and can be somewhat
miniaturised. However, it does appear that in most cases systematic
design procedures for sequential systems would carry a cost penalty
compared with fluidic solutions. The life expectancy generally of
fluidic devices, both non-moving and moving part, should exceed 50
million cycles which is better than can be achieved with most
electro-mechanical systems.

REFERENCES

1. Kirshner, J.M., 'Fluid Amplifiers' McGraw Hill, New York. 1966.

2. Taplin, L.B., 'Small Signal Analysis of Vortex Amplifiers'.

3. Foster, K. and Parker, G.A., 'Fluidics. Components and Circuits' Wiley. 1970.

4. Katz, S. and Hastie, E., 'The Transition from Isothermal to Adiabatic Capacitance in Cylindrical Enclosures' AD 735704. December, 1971.

5. Nichols, N.B., 'The Linear Properties of Pneumatic Transmission Lines' Trans.Instr.Soc.Am. Vol.1, No.1, p.5. 1962.

6. Iberall, A.S., 'Attenuation of Oscillatory Pressure in Instrument Lines' J.Res.Nath.Bur.Stds. Paper RP 2115, Vol.45. July, 1950.

7. Brown, F.T., 'The Transient Response of Fluid Lines' J. Basic Eng. p.547. December, 1962.

8. Schaedel, H., 'A Theoretical Investigation of Fluidic Transmission Lines with Rectangular Cross-Section' Third Cranfield Fluidics Conference. Paper K3. 1968.

9. Franke, M.E., Wilder, R.W., Miller, R.N., and Fada, C.V., 'The Frequency Response of Volume Terminated Pneumatic Lines with Circular and Rectangular Cross-Sections' JACC, University of Colorado, Boulder. p.410. 1969.

10. Strunk, R.D., 'Frequency Response of Fluid Lines with Non-Linear Boundary Conditions' J. Basic Eng. p.365. September, 1971.

11. Bouteille, D., 'Fluid Logic Controls and Industrial Automation' Wiley. 1973.

12. Auger, R.N., 'The Turbulence Amplifier in Control Systems' Second Fluid Amplification Symposium. Vol, 2. p.261. H.D.L., U.S.A. May, 1964.

13. Greenwood, J.R., 'The Design and Development of a Fluid Logic Element' B.Sc. Thesis M.I.T. 1960.

14. Glaettli, H.H., 'Circuits using Fluid Dynamic Components' First Cranfield Fluidics Conference, Paper D4. Cranfield U.K. September, 1965.

26

15. Berends, T.K. and Tal, A.A., 'Pneumatic Relay Circuits' First IFAC Congress, Moscow. 1960.

16. Töpfer, H., Schrepel, D., and Schwarz, A., 'Universelles Baukastensystem für pneumatische Steuerungen'. Sonderdruck aus der Zeitschrift für Messen, Steuern, Regeln. Vol.7. Pt.2. p.65. 1964.

17. Brychta, O., 'A Logic System using a Microdiaphragm Device and its use in Medical Process Control' IFAC Symposium on Fluidics Paper C5. London. November, 1968.

18. Jensen, D.F., Müller, H.R., and Schaffer, R.R., 'Pneumatic Diaphragm Logic' Advances in Fluidics. ASME. P.313. 1967.

19. Bahr, J., 'Das Folienelement, ein neues flüssigkeitslogisches Schaltelement' Electron. Rechenanl. Vol.7. No.2. p.69. 1965.

20. Small, D.A., 'Optimising Fluid Element Size for Speed and Power Consumption' ASME Paper No. 67-WA/FE-39.

21. Müller, H.R., 'Some Characteristics of Fluid Switching Devices' I.B.M. Report. RZ101. July, 1962.

22. Glaettli, H.H., Müller, H.R., and Zingg, R.H., 'Remarks on the Limitations of Pure Fluid Amplifiers' Fluid Amplification Symposium. Vol.1. p.317. 1964. H.D.L., U.S.A.

23. Rechten, S.W., and Zückler, Th., 'New Aspects of Miniaturisation of Fluid Logic Elements' Paper F5. Third Cranfield Fluidics Conference. May, 1968.

24. Johnston, R.P., 'Dynamic Studies of Turbulent Re-Attachment Fluid Amplifiers' M.Sc. Thesis. University of Pittsburgh. 1963.

25. Hayes, W., 'The Dynamic Response of Fluidic Turbulence Amplifiers' Fourth Cranfield Fluidics Conference. March, 1970.

26.1 Huffman, D.A., 'The Synthesis of Sequential Circuits' Journal of the Franklin Institute. Vol. 257. No.3. p.161. March 1954; No.4. p.275. April 1954.

27. Retallick, D.A., 'Switching Theory Applied to Fluidic Digital Systems' Ph.D. Thesis. University of Birmingham. 1968.

28. Cole, J.H., and Fitch, E.C., 'Synthesis of Fluid Logic Circuits with Combined Feedback Input Signals' ASME Paper No.70-Flcs-18.

29. Halford, J., 'Integrated Fluidic Circuit Modules Simplify the Design of Sequential Control Systems' Fluid Power International Conference, London, 1972.

30. Bantle, K., 'Counters with Bistable Fluid Elements' Paper H5. Second Cranfield Fluidics Conference. January, 1967.

31. Foster, K., and Retallick, D.A., 'Fluidic Counting Techniques' BHRA Fludics Feedback Aug. and Dec., 1969. February, 1970.

32. Cheng, R.M.H., and Foster, K., 'A Computer-Aided Design Method specially applicable to Fluidic-Pneumatic Sequential Control Circuits' ASME Paper No. 70-WA/Flcs-17.

33. Cheng, R.M.H., 'Logic Design of Pneumatic Sequential Circuits' Ph.D. Thesis, University of Birmingham. 1971.

34. Parker, G.A., and Jones, P., 'Protection against Hazards in Fluidic Adder and Subtractor Circuits' Paper B2. First IFAC Fluidics Symposium, London 1968.

35. Poix, A., Takahaski, Y., and Thal-Larsen, H., 'Hazards in Pneumatic Fluidic Circuits' ASME Paper No. 68-WA/AUT-18.

36. Zissos, D., and Grant, J., 'Design Algorithms for Fluidic Circuits' Paper B4. Second IFAC Fluidics Symposium. Prague 1971.

37. Stivin, J., 'Contribution to the development of pneumatic logic elements and their applications to machine tools' Proc. 9th Int. M.T.D.R. Conference. Manchester, U.K. 1968.
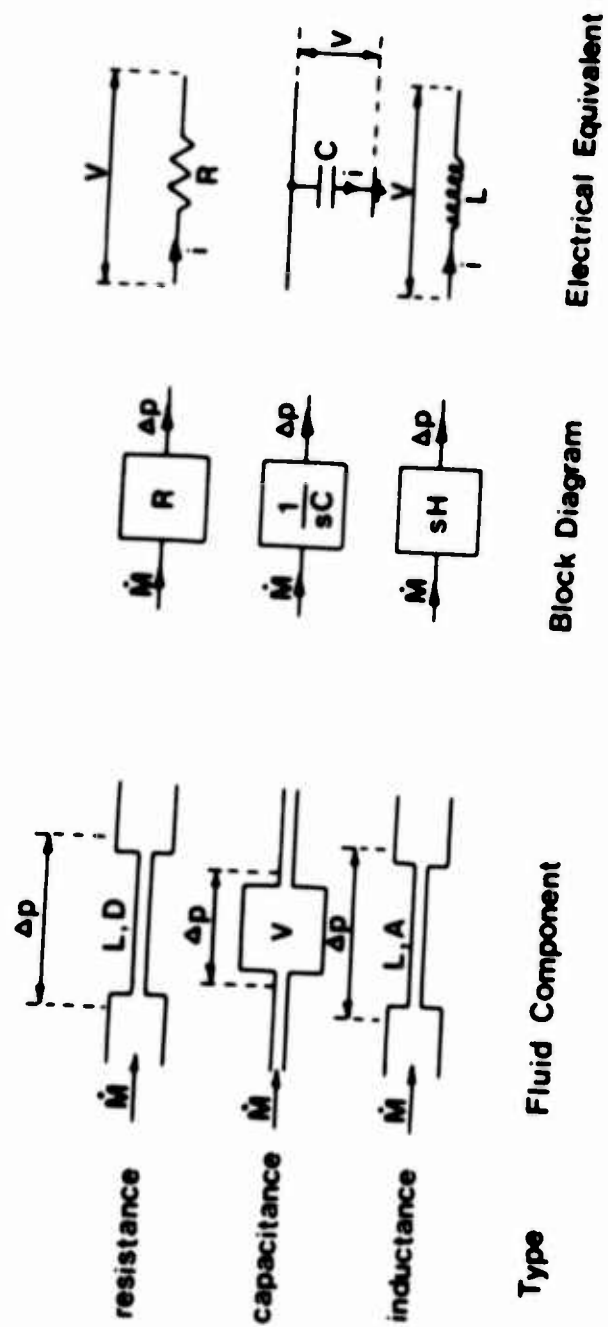
Fig. 1. System representation of lumped parameter fluid components.
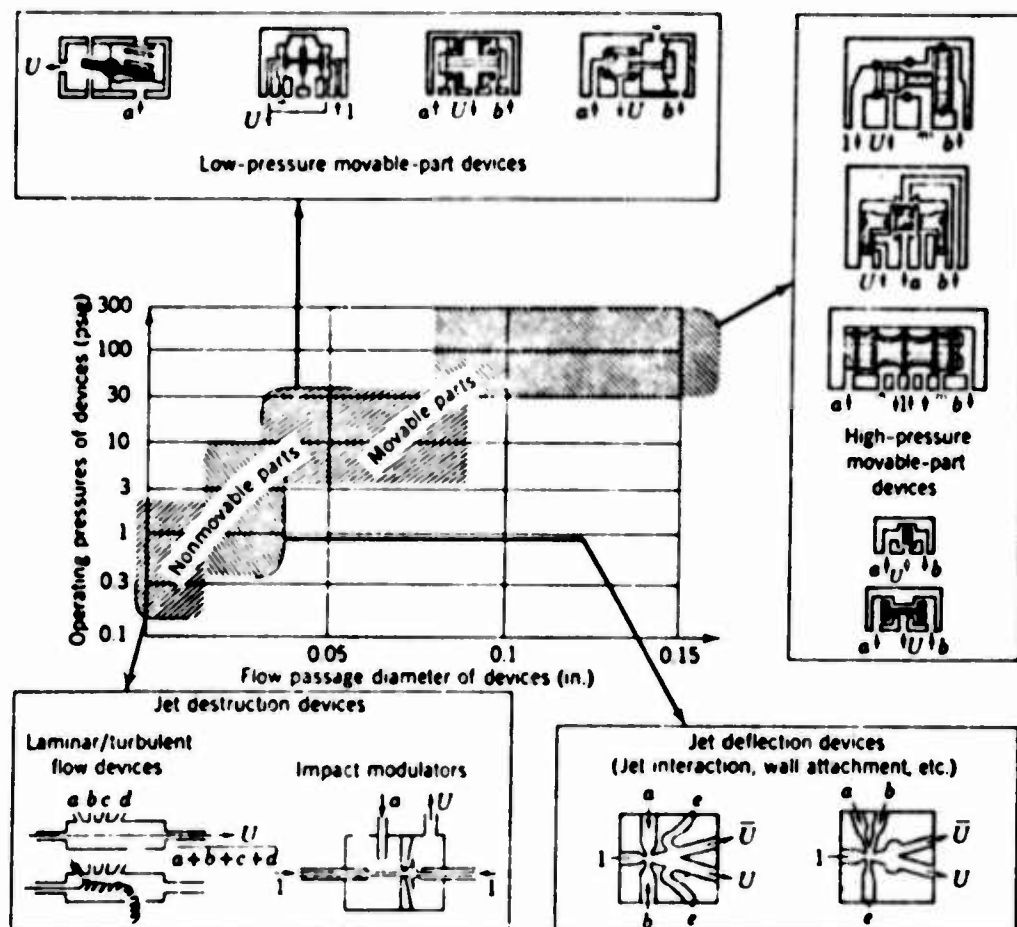
Fig. 2 Operating Regions for Fluidic Devices (Ref.11)
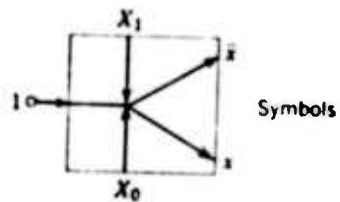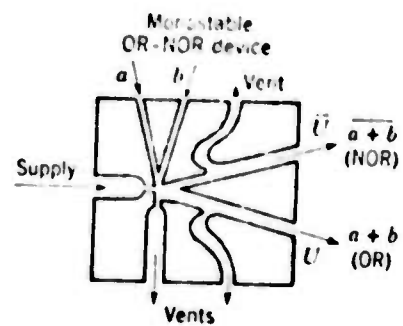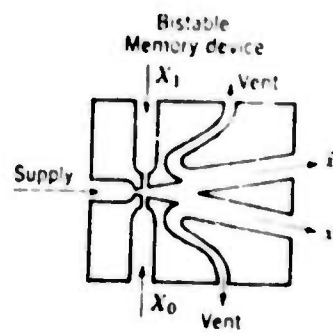
Fig. 3 Wall re-attachment Elements (Ref.11)
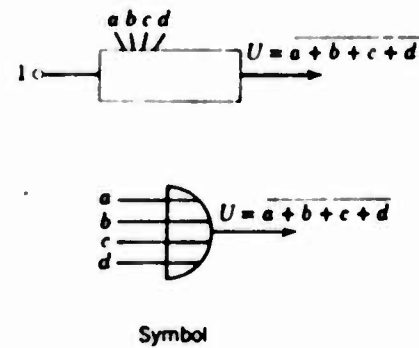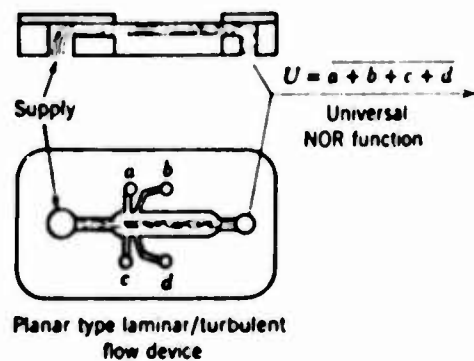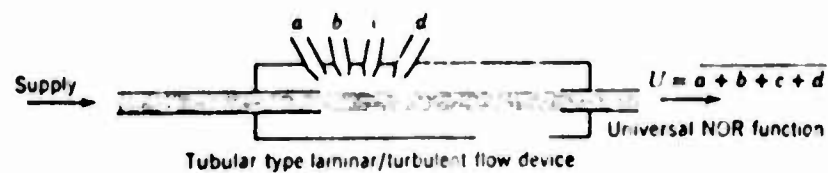
Fig. 4 Turbulence Element (Ref.11)
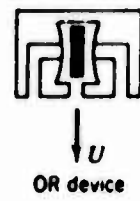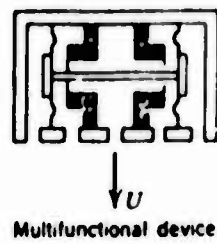
Fig. 5 Double Diaphragm and Foil Elements (Ref.11)

33
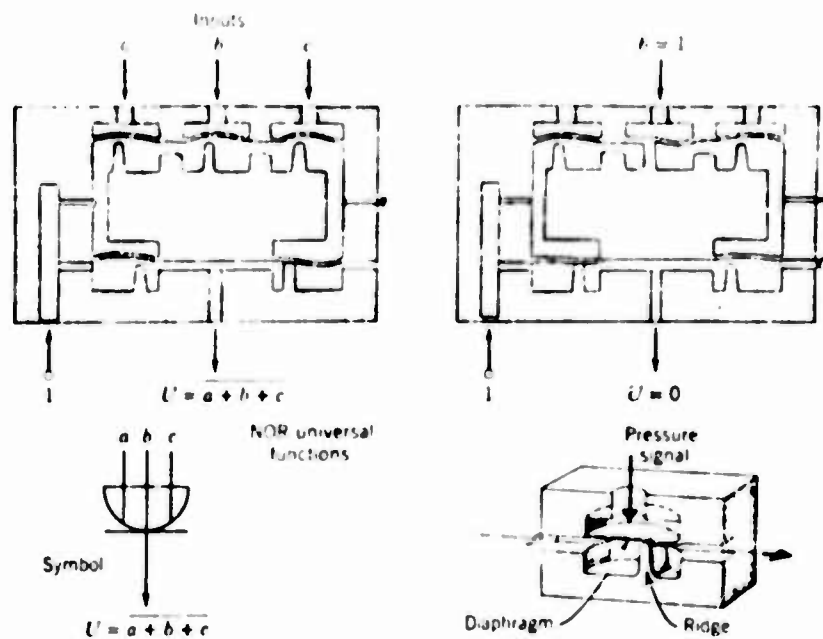
Fig. 6 Ridge Diaphragm Element (Ref.11)
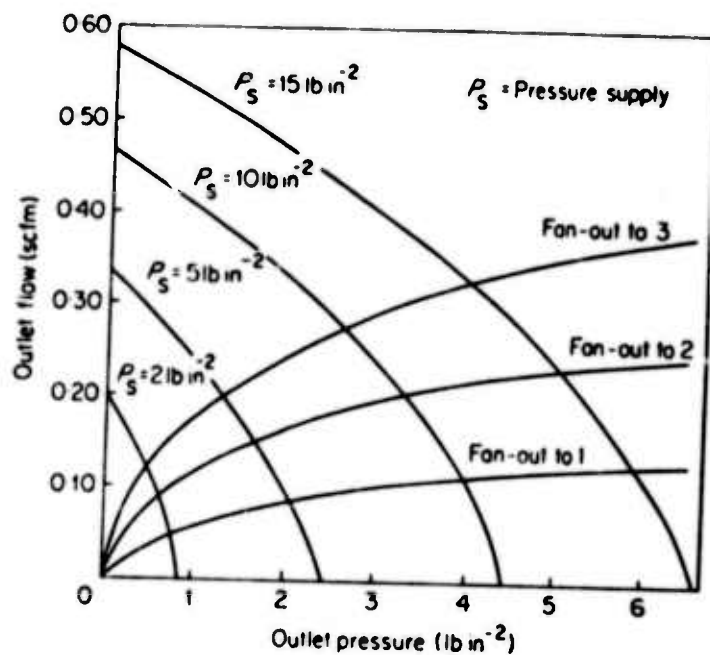
Fig. 7 Graphical Solution for fan-out from
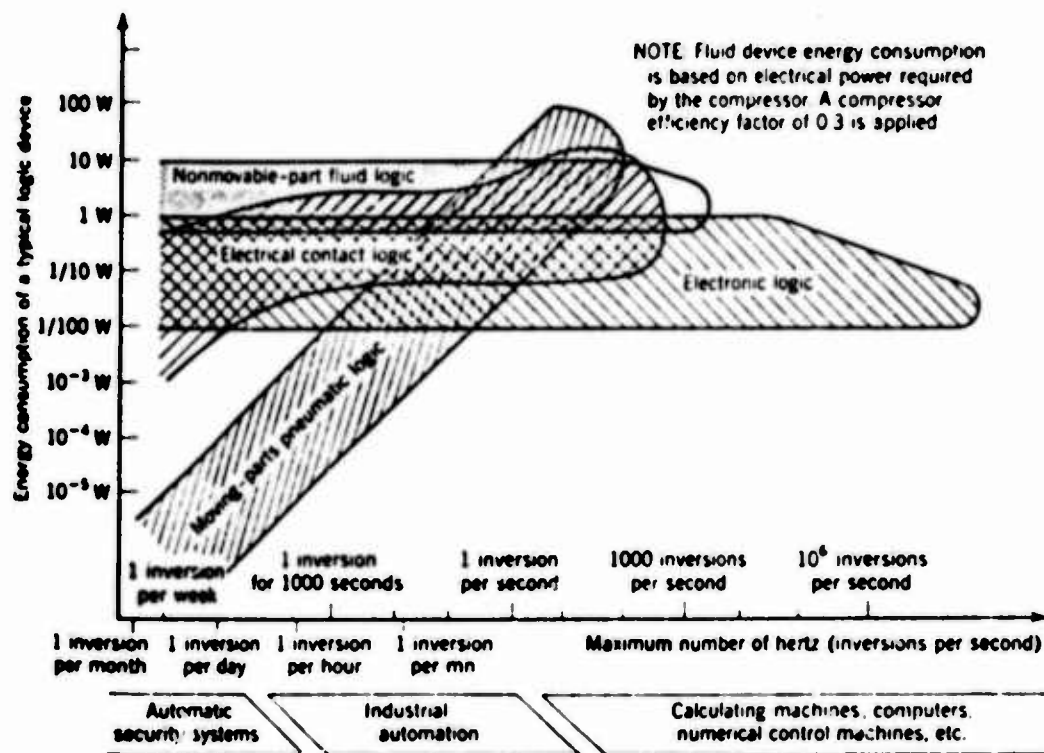non-linear output and input charac-
teristics.

35
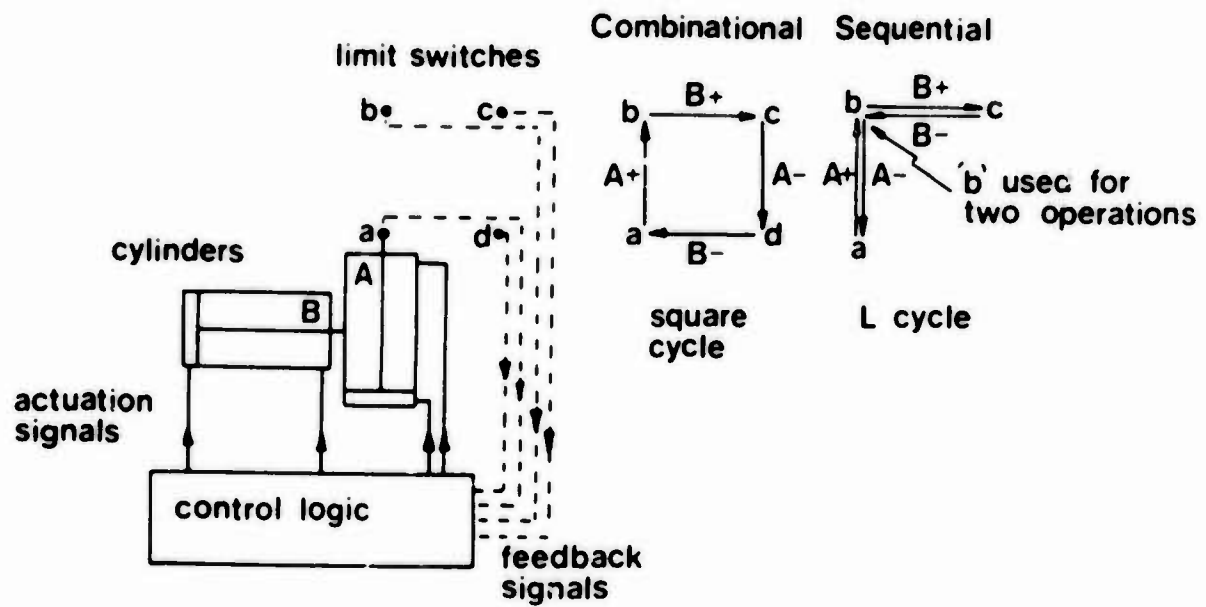
Fig.8   Comparison between Fluid and Electronic Logic (Ref.11)

Fig. 9. Combinational and Sequential Cycles in Pneumatic two-cylinder circuits.
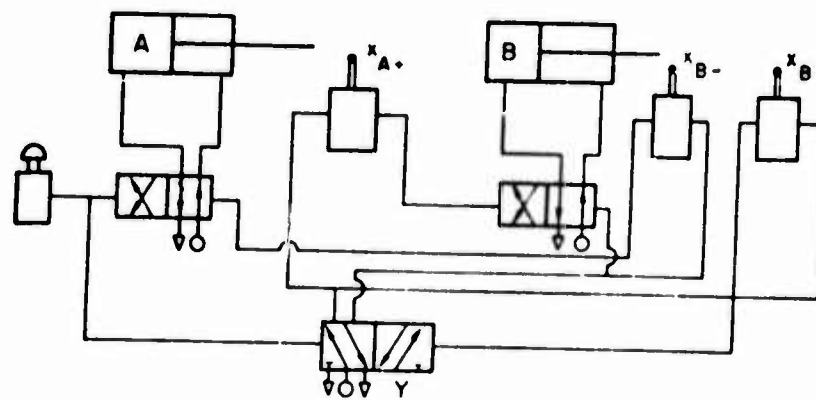
Fig. 10   Circuit for the Sequence A+, B+, B-, A- according to
the Cascade Method using spool valves.
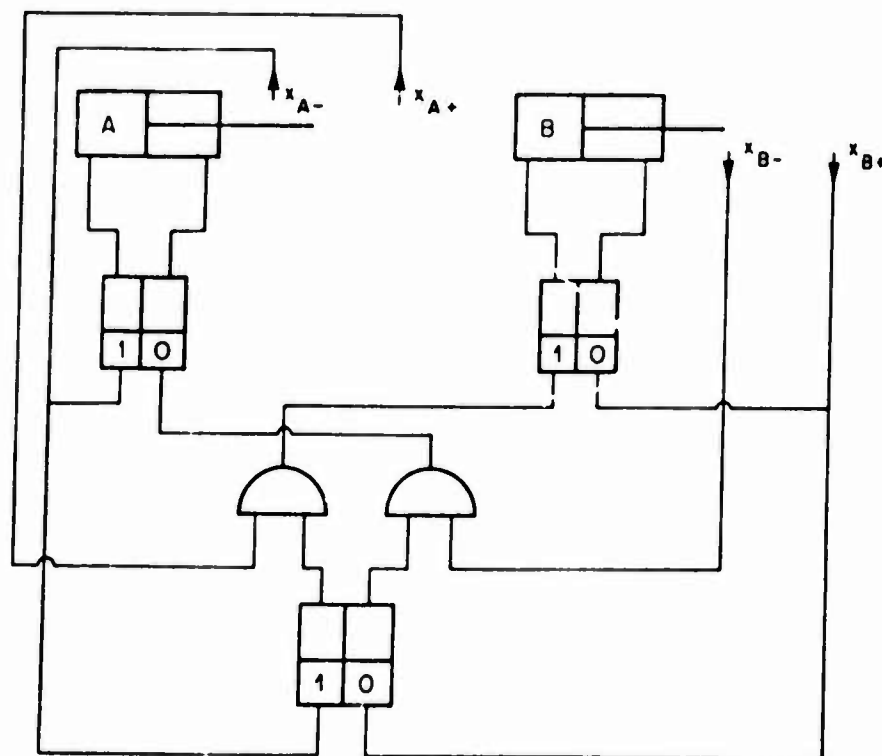
Fig. 11   Circuit for the Sequence A+, B+, B-, A- using the
Logical reduction method of Huffman.

38
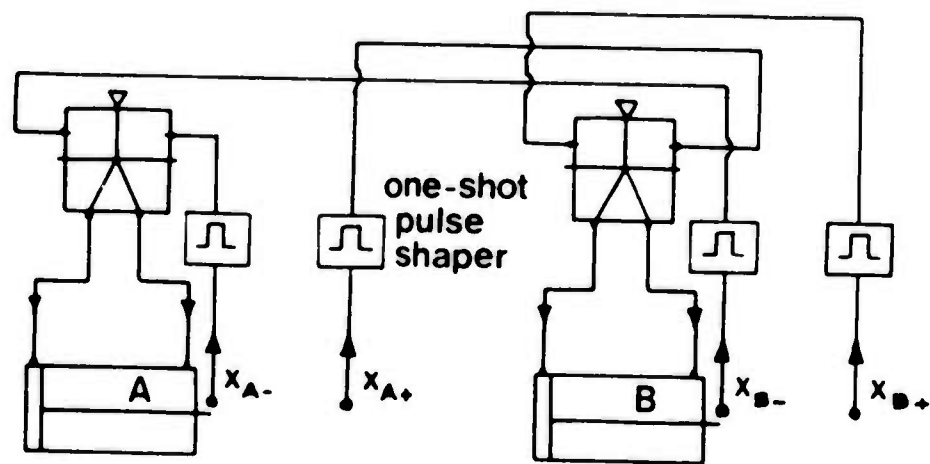
Fig. 12. Circuit for the sequence A+, B+, B-, A- using fluidic one-shot pulse shaper elements in the feedback from the limit switches.
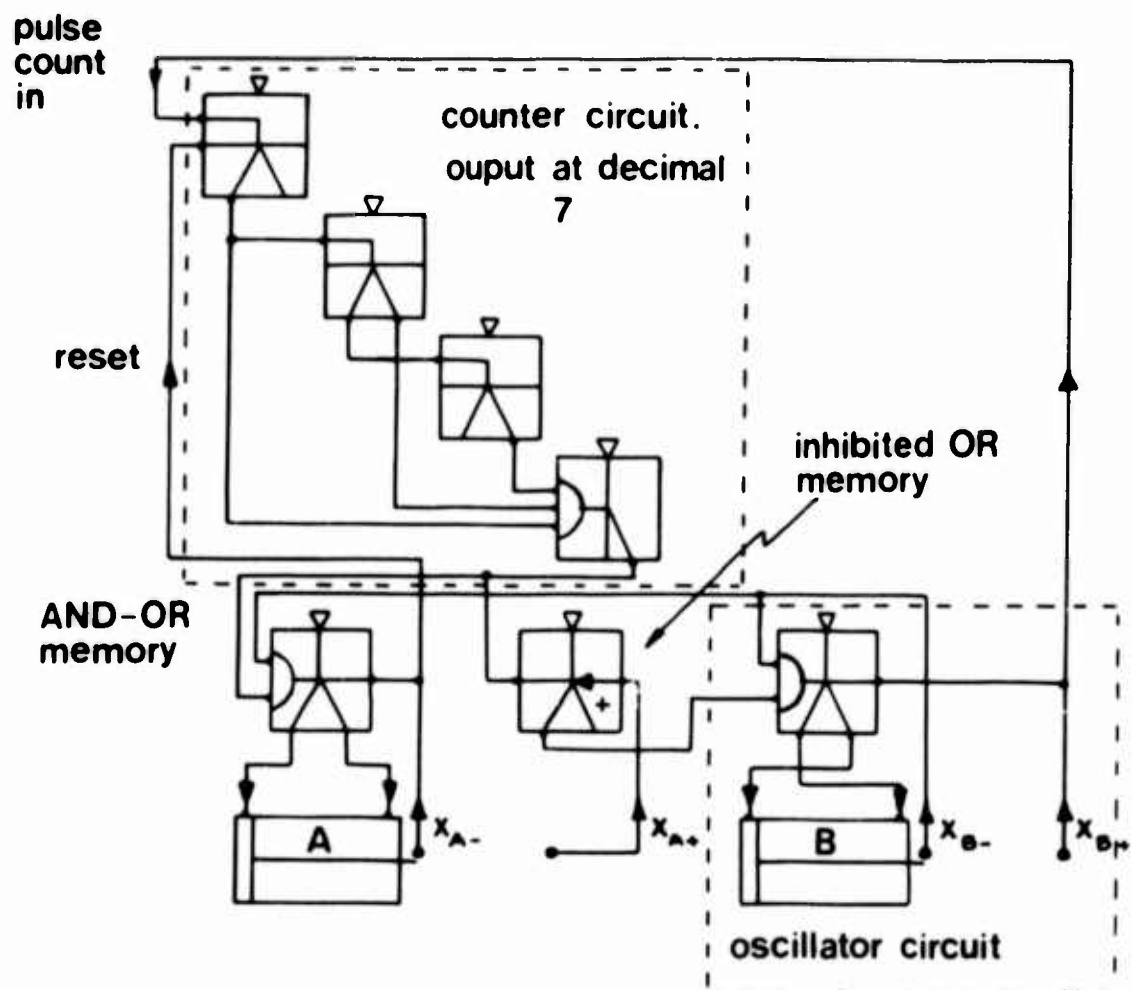
Fig. 13 Circuit for the repeated sequence A+, (B+, B-) x 7
A- using a counter circuit and composite memory
elements. (Ref. 29).

Digital-Analog Hybrid Fluidic Feedback Systems

Charles K. Taft, Professor

University of New Hampshire

In recent years digital fluidic elements have been used to process analog signals. In addition, pulse-width modulated analog amplifiers have also been constructed and developed which use digital power elements to process analog information. Compensators to provide lead compensation can be placed in the error signal path of an otherwise analog system. Lead compensators which are very useful in the compensation of resonant systems have been constructed.

Basic Concepts

Feedback systems can be controlled by rather coarsely quantized information. The advantage of this approach is that it allows on/off elements to control the power in a feedback system. Often there are many devices such as power transistors and fluidic power amplifiers which operate best in an on/off mode. On the other hand the use of such devices in a feedback system necessitates the analysis and design of a highly nonlinear system. Looking at a basic feedback system with an on/off element in its forward path processing the error signal, as shown in Figure 1, we see that the levels of effort which can be applied to the continuous part of the system are limited to a finite number. In this case two levels of information are fed to the continuous part of the system. For the moment let us assume that the continuous part of the system has one integration since this describes a very interesting class of fluid control problems. If two levels of control are available, ± 1 [it is always possible to normalize a quantizer like this and include its gain K in $G(s)$] then the system is forced to oscillate continually between one level and the other, unless the error signal $e(t)$ is always positive or negative because input $r(t)$ is changing too fast for the output to follow.

If the input to this system is a step, then the output will also be a step. Superimposed on the step will be a steady state oscillation or limit cycle. The frequency of the limit cycle is determined largely by the dynamics of the continuous part of the system. The amplitude of the limit cycle is determined by the same dynamics and the magnitude of the system gain K. It can be shown that such a device must always exhibit a steady state oscillation to step inputs of any size and further that the magnitude of the limit cycle will be smaller as the gain or maximum corrective rate K decreases.

It should be mentioned that very satisfactory control systems can be constructed using this concept. However, such systems always exhibit a steady state oscillation or limit cycle.

41

By adding another level to the error signal we construct a three-level quantized control as shown in Figure 2 which can exhibit several response forms to step inputs. Again, assuming that the continuous part of the system has an integration, this system can exhibit a step response with no oscillation. A response which is the least oscillatory kind of response that the system can exhibit has been classified as two-step response.[1] With this type of response, the system will exhibit a response for a step of any magnitude which has only two changes in level of the error signal. This response is shown in Figure 2b. In Figure 3 is a design chart which relates the parameters' a_o and K to obtain two step response.[2] Figure 3 applies to systems of the form shown in Figure 2 in which the continuous part of the system has dynamics which we might classify as being overdamped. This can be stated mathematically by requiring that the continuous part transfer functions have the form

$$G(s) = \frac{Ke^{-t_d s} \sum_{m=0}^{M} A_m s^m}{s \prod_{n=0}^{N} (T_n s + 1)} \quad \text{and} \quad \frac{dg(t)}{dt} > 0 \text{ for } t > 0$$

where $g(t)$ is the continuous part impulse response

This so-called two-step response forms a lower bound or least oscillatory response for the response of a system of the form shown in Figure 2. In a like way as the maximum corrective rate K is increased or the dead zone $2a_0$ decreased, the system response will become more oscillatory exhibiting four, six, or more steps until finally it exhibits a limit cycle similar to that of the two level quantizer, figures 2c, d, e. The nature of the system response depends upon a_0/K, the ratio of one half the width of the error region in which no signal is applied to the output (a_0), divided by the maximum output rate in the steady state (K). This so-called characteristic time is very useful in the design of digital feedback systems. Furthermore, other response forms can also be related to this same number. For example, if a system of the form shown in Figure 2 is subjected to a ramp input it can be shown that it will exhibit a limit cycle and the magnitude of the limit cycle can be determined by a describing function analysis; this has been demonstrated by Limbert and Taft.[3] The magnitude of the limit cycle depends on a_0/K, the magnitude of the ramp and the system parameters. Increasing the number of levels of the error quantizer to 5, 7, and so on, does little to change the basic notions that we have outlined here. There are least oscillatory response forms which depend upon the size of the input step, and the system can be designed in general to have a least oscillatory system response for step inputs of any size. However, it will always exhibit a steady state oscillation or limit cycle for ramp inputs.

42

Pulse-Width Modulated Amplifiers

There are several advantages in control in using systems of the type shown in Figure 1 in a steady-state oscillation mode. This mode can be induced by adding to the error a sinusoidal signal or a periodic signal of some other waveform. If this injected periodic signal is of high enough frequency, it is effectively filtered by the continuous part of the system, and so does not appear in the feedback signal $e(t)$. A missile control system was constructed by Campagnuolo and Sieracki using this approach.[4]   It is useful to examine the spectrum of the signal entering the quantizer, whether it be 2, 3, or n levels. If it contains a dc level component, and a high frequency dither component the output will also contain a dc level and harmonics of the dither. These high frequency components, if they are high enough in frequency, will essentially be greatly reduced in amplitude by the continuous part of the system. So, effectively they can be ignored. It is useful, therefore, to examine the spectrum of the output of the quantizer when the input is a dc signal applied along with a dither, or high frequency signal as shown in Figure 4. The relationship between the dc level of the output E^1_o and the dc level of the input E_o provides a low frequency picture of the system. Much more complex methods can be employed to analyze such systems in which two frequencies exist.[5]   However, great insight into the response of a system with a dither signal can be obtained by simply looking at the relationship between dc signal in and the dc signal out. This relationship is known as the "altered characteristic." For example, in Figure 4 we see a two level quantizer subjected to a dc level and a sinusoidal dither signal. Take the Fourier series representation of the output of the quantizer operating under such conditions, and look at the dc level component, ignoring the component due to the high frequency dither. Then plot the relationship between the dc level E^1_o out and the dc level in E_o in Figure 5a.   In Figure 5b the altered characteristic measured for a fluidic Schmitt trigger is shown. Notice that in this situation, the altered characteristic is nearly linear over a wide range of input dc levels, and that this range of input dc levels depends upon the amplitude of the dither signal. The effect of the dither amplitude B upon the behavior of this on/off element has been to control the gain and range of proportioned operation. If the dither signal were a saw tooth wave, then the resulting normalized (E_o/B) characteristic would be shown in Figure 6. The same result could be obtained with a triangular wave. Further, a square wave has the effect of altering the characteristic of a two level quantizer to make it appear as a three level quantizer. In this way a high frequency periodic dither signal can be used to alter the behavior of a quantizer Lastly, a two-level quantizer with hystersis can also be examined and the altered characteristic developed as shown in Figure 7. Notice the effect of hystersis up to 40 percent of the dither is minimized for inputs E_o which are 40 percent of the dither amplitude. The effect of the high frequency dither signal has been to linearize the highly nonlinear quantizers. Hanafusa, and Miyata postulated a pulse-width modulated amplifier in which the dither signal was triangular.[6]

43

A further refinement of this approach results when a feedback loop is closed around the basic amplifier element to provide a high frequency limit cycle. This is shown in Figure 8 where the transfer function H(s) describes feedback dynamics. If this loop is closed so that the frequency of the limit cycle is large compared to the natural frequency of the continuous parts of the system that is being controlled, then it is possible to provide the dither signal internally by a self-induced oscillation. This basic notion has been used to build up amplifiers which operate with digital elements to provide analog-like behavior. Bermel and Limbert described a fluidic operational amplifier which was constructed by Corning Glass Works.[7] Lloyd also constructed a proportional amplifier using digital elements.[8] The model for the Bermel amplifier is shown in Figure 9 and the resulting input-output altered characteristic measured on the Bermel power amplifier as shown in Figure 10. This approach has some advantages although the frequency of the limit cycle tends to change with the input amplitude $r(t)$ and it is fairly low for small or large inputs. On the other hand, if the rest of the system contains an integration, this effect is hardly noticeable except during large transients. This approach makes the power amplifier very useful as its behavior is independent of the amplitude of some external dither signal. As was shown, when the external dither signal is provided, its amplitude must remain nearly constant, otherwise changes will result in the "altered characteristic." In this way a very effective pulse-width modulated power amplifier can be constructed.

There are some difficulties with this approach, which lie in the fact that we have assumed that the frequency of the dither is large compared to the natural frequency of the rest of the system. As the frequency of the dither approaches the natural frequency of the system, several problems begin to arise. The first, and most pronounced of these is that the dither signal begins to appear in the output of the system, in many systems this is objectionable behavior. It results because the filtering action of the system upon the dither is reduced as the frequency of the dither approaches the natural frequency of the system. But more important, as this happens, the subharmonics can be generated. If the input to a PWM amplifier is a sinusoidal signal, whose frequency is a ratio of integers times the dither frequency, it is possible for the output $e'(t)$ to have subharmonics. That is, harmonics which are of lower frequency than the dither signal (β), or a signal being applied (ω) this is illustrated in Figure 11. The magnitudes of these subharmonics are usually small unless the frequency of the dither and the frequency of the sinusoidal signal approach one another. As they do, the magnitude of the subharmonic component becomes larger and larger. Of course the system will have difficulty in filtering the subharmonic signals. The answer to this is, of course, that the dither frequency must be large compared to the natural frequency of this system. As long as this situation is maintained then problems with subharmonics are not likely to occur and the dither is likely to be filtered. A rule of thumb which can be used is to keep the dither frequency five to ten times the natural frequency of the system.

The dual input describing function can be used to further investigate the effects as $\omega \to \beta$, however, the computational problems with this approach are quite severe as there are a large number of parameters associated with the response.[5]

Pulse Compensators

We have shown how analog information can be handled by relatively coarse quantizers of two levels. A further refinement exists in the ability to construct compensators which provide lead compensation in control systems. Whenever information is processed in a control system by a quantizer, the output of the quantizer can be decomposed into a sum of steps. If this signal is to be compensated by a lead compensator, such as is often used in a control system, then the resulting signal out of the lead compensator should be the original step plus an impulse as shown in Figure 12a. Obvious limitations on signal magnitude, and band width limit the magnitude and duration of this pulse to the finite values. If one were to recognize that whenever a uniform quantizer changes from one state to another, it produces a step of fixed magnitude, then an approximation could be made to this lead compensator which consisted of an impulse of fixed magnitude (α_1) and duration (T'_1) added to this step. Indeed, as the magnitude of this pulse (α_1), is increased and its duration decreased (T'_1), this approximation becomes quite good. To investigate this, suppose that we look at the step response of such a compensator. A step applied to such a compensator produces a step plus an impulse as shown in Figure 12b, Figure 12c shows how it could be mechanized. We can write a Laplace transform for each of these two signals. Because the type of signal we are inputing to the conpensator is fixed, we can develop a transfer function for the device, even though it is operating with nonlinear elements. This transfer function can be obtained by simply dividing the Laplace transform of the output by the transform of the input. The resulting equation is shown below:

$$e'(s) = \frac{1}{s} \quad , \quad e''(s) = \frac{1+\alpha_1}{s} - \frac{\alpha_1 e^{-T'_1 s}}{s}$$

$$G_c(s) = \frac{e''(s)}{e'(s)} = 1 + \alpha_1 - \alpha_1 e^{-T'_1 s}$$

This transfer function can be examined further to show its relationship to a conventional lead compensator. If a sinusoidal signal is applied to a two level quantizer, the output is a square wave. If this square wave is in turn applied to the pulse compensator described

45

above which produces a pulse of fixed amplitude and duration each time that the square wave input to it changes level, then the output of the compensator will appear as shown in Figure 13. If we expand the input to the compensator and the output of the compensator in a Fourier series, and look at the fundamental components of this series, it can be shown that fundamental component of the compensator output has phase lead and that the lead is determined by input frequency ω, pulse height α_1, and pulse direction T'_1.

if $\quad e(t) = E_1 \sin\omega t$

then $\quad e'(t) = \frac{4}{\pi} \sin\omega t + harmonics$

and $\quad e''(t) = \frac{4}{\pi}\left[1 + \alpha_1 - \alpha_1 \cos\omega T_1'\right] \sin\omega t + harmonics$

$$+ \frac{4}{\pi}\alpha_1 \sin\omega T_1' \cos\omega t$$

A describing function for the output e'(t) relative to the input e(t) can be shown to be

$$G_{dc} = \frac{4}{\pi E_1}\left[1 + \alpha_1 - \alpha_1 e^{-T_1' j\omega}\right]$$

However, the describing function of the two level quantizer is:

$$G_d = \frac{4}{\pi E_1}$$

This implies that the frequency response function for the compensator operating on the fundamental of the quantizer output is:

$$G_c(j\omega) = 1 + \alpha_1 - \alpha_1 e^{-T_1' j\omega}$$

So for the configuration shown in Figure 13, a quantizer followed by a pulse compensator, the describing function can be written as

$$G_{dc} = G_d G_c(j\omega)$$

46

It can be shown that for a more complex quantizer this same relationship is valid. Therefore, the frequency response function for the pulse compensator $G_c(j\omega)$ can be used for design purposes and combined with the system dynamics in the normal way using polar, Nichols or Bode plots as if it were a linear device.

However, this same frequency response function $G_c(j\omega)$ would result by allowing: $s = j\omega$ in the transfer function just as is done in linear systems. For this reason it can be shown that the frequency response function for a pulse compensator can be determined from its transfer function. The polar plot of this frequency response function is quite useful in designing the compensators and evaluating the effect of the compensator on any given system. In a similar way Bode or Nichols plots can also be used for design. For example, the frequency response function can be plotted for a single pulse compensator by normalizing the frequency response function. This can be accomplished by setting: $\Omega = T_1'\omega$. This relationship normalizes the frequency of the frequency response function. A further normalization can be performed:

$$ G_c(j\Omega) = 1 + \alpha_1 - \alpha_1 e^{-j\Omega} $$

or

$$ G_c(j\Omega) - 1 = \alpha_1 (1 - e^{-j\Omega}) $$

finally

$$ \frac{G_c(j\Omega) - 1}{\alpha_1} = 1 - e^{-j\Omega} = \overline{G_c(j\Omega)} $$

The resulting function $\overline{G_c(j\Omega)}$ is a normalized frequency response function in the complex plane. It is a circle which is the basic shape of the polar frequency response function plot. The actual plot for a given α_1, T_1' is shifted to the right by one and has a radius of α_1 in the complex plane as shown in Figure 14. Thus all single pulse compensators have a frequency response function which has a circular shape. The effect of pulse height can be easily shown since when the height of the pulse is increased the amplitude of the vector in the frequency response function polar plot increases which increases the size of the circle in the complex plane. Obviously as the height of the pulse reaches infinity the circle approaches a vertical line located at +1 and the effect of the frequency response of the pulse compensator is identical to $G_c(j\omega) = 1 + j\omega$, or proportional plus derivative control. The effect of the pulse duration time T_1' on the frequency response function is to cause the frequency at which a vector from the origin to the point on the frequency response function plot occurs to be larger as T_1' decreases.

Notice further that the frequency response function plot is a periodic function of frequency with period $2\pi = T_1'\omega = \Omega$. This can be shown in a bode plot of the frequency response function for a single pulse compensator which is shown in Figure 15. Since a Bode plot is a log plot, the magnitude and phase angle of the frequency response function becomes compressed at high frequencies.

Single pulse compensators are useful in the compensation of the overdamped systems. However, many significant control systems are lightly damped, in particular pneumatic and hydraulic systems which are required to move large masses are often very lightly damped. Therefore a compensator which would be capable of handling more complex systems is useful. Such a compensator results if two pulses are used for compensation purposes. This kind of compensator is shown in Figure 16. On each transition of the quantized signal the two pulses are produced rather than one. The pulse heights and durations are described by the parameters α_1 and α_2 and T_1' and T_2' where the senses of α_1 and α_2 are shown in the figure. In a like way it can be shown that the transfer and frequency response functions for this compensator are:

$$\theta_c(s) = 1 + \alpha_1 - (\alpha_1 + \alpha_2)e^{-T_1's} + \alpha_2 e^{-T_2's}$$

$$\text{let } s = j\omega$$

$$\theta_c(j\omega) = 1 + \alpha_1 - (\alpha_1 + \alpha_2)e^{-T_1'j\omega} + \alpha_2 e^{-T_2'j\omega}$$

$$\text{let } \Omega = T_1'\omega$$

$$G_c(j\Omega) = 1 + \alpha_1 - (\alpha_1 + \alpha_2)e^{-j\Omega} + \alpha_2 e^{-\frac{T_2'}{T_1'}j\Omega}$$

The frequency response function shape depends upon α_1, α_2 and T_2'/T_1'. First let us examine the effect of the T_2'/T_1'. It can be shown that the frequency response function for a two pulse compensator will contain cusps or loops and the number of these cusps or loops will be equal to $T_2'/T_1' - 1$. If T_2'/T_1' is not an integral quantity then the frequency response function will have a period in the complex plane which is $2\pi \times$ (the denominator of the T_2'/T_1' ratio when expressed as a reduced fraction). For example $T_2'/T_1' - 5/2$ repeats in frequency with period of $\Omega = 4\pi$. Several examples of this are shown in Figure 17. The most useful of these compensators appears to be the one in which T_2'/T_1' is equal to two. For a fixed T_2'/T_1' (in this case, 2) the effect of α_1, α_2 is shown in Figure 18. α_2 is plotted versus α_1 and this plane is divided into regions in which a particular form or shape of the frequency response function results. The dots in each of

these sketches is the +1 point where $\Omega = O$. The arrow shows the direction of increased Ω. A number of useful compensators can be developed. The dotted lines in this plane represent compensators which are zero-pass, that is, which have a frequency response function that is zero at some frequency, either at $\Omega = \pi$ or at some lower value of Ω. Two of these compensators from this infinite set of zero-pass compensators are of particular interest as they were postulated by Q.J.M. Smith in his posicast concept.[9] They are indicated on the plot. One of the compensators of this infinite set is very interesting as it is a zero-pass compensator which requires no new signal levels. That is the case where $(\alpha_1 = 0, \alpha_2 = 1$). The frequency response function in this case is shown in detail in Figure 19 as a polar plot and in Figure 20 in a Bode plot. Furthermore, the mechanism by which this compensator operates can be shown quite easily. Suppose, for example, a sine wave of frequency $\omega = \frac{\pi}{3T_1}$, is fed to a two level quantizer to produce a square wave as shown in Figure 21. This signal then is fed to the zero-pass filter with $T'_2 = 2T'_1$. Because of the filter configuration, the output of the filter is a square wave signal of frequency 3ω. Consequently, the zero-pass effect is accomplished by frequency multiplication in this case. This form of filter is particularly useful in the compensation of resonant systems. However, there are problems in its use. These problems result from the fact that at low frequencies the compensator introduces a phase lag while the amplitude of the compensator is decreasing as shown in Figure 21. Above the zero-pass frequency the compensator provides phase leads of as much as 130° and its amplitude is increasing. When applied to a resonant system it moves the imaginary axis crossing to a much higher frequency. However, because of the phase lead, the system and compensator frequency response function will exhibit loops in the complex plane requiring careful design at high frequency. This is shown in Figure 22. A more effective approach to the resonant system compensation problem is to use compensators which are in the sector of the α_2, α_1 plane which is enclosed by the $\alpha_2 = 0$, $\alpha_1 = \alpha_2$ lines in the first quadrant. In these compensators, it is possible, as shown by Foster and Taft,[10] to produce compensators which are capable of compensating a resonant system and providing a large increase in system gain at no increase in system overshoot or decrease in system stability. Foster investigated a system of the form shown in Figure 23. He chose $\alpha_1 = \alpha_2 = n$ and $T'_2/T'_1 = 2$. For various values of open loop damping ratio ζ and closed loop maximum frequency response function magnitude M_m, he chose a compensator specified by n and T_1 and compared compensated and uncompensated responses. Examples of the results are shown in Figures 24-29. As with the single pulse compensator the larger the magnitude of the compensation pulse the more effective it will be. Foster demonstrated for this digital system how the compensator could be mechanized and produce exceedingly effective compensation for resonant systems. Bermel and Taft also demonstrated that the zero-pass filter could be used for compensating resonant systems.[11]

It is obviously possible to add additional compensation pulses and three pulse compensators have been classified. It has been shown that when the three pulses have equal duration their polar plots will exhibit two cusps or loops and that the shape of these frequency response functions is considerably more complex than those for the two pulse compensator. As yet no applications have been made of this three pulse compensation method, however Porter did classify the forms of response which were possible.[12] Typical frequency response function polar plot shapes for the three pulse compensator are shown in Figure 30. Note that these have been mormalized and so for the actual polar plot the small circle represents $\Omega = 0$ at +1.

Dithered Pulse Compensation

The notions of the altered characteristic, the use of quantizers with dither to provide proportional behavior and the idea of pulse compensation can be combined to produce compensators which can be added to otherwise analog systems to provide lead compensation or resonant system compensation. This approach essentially uses a combination of the two ideas presented so far. The notion as originally developed by Taft and Hamlin[13] is shown in Figure 31a. The system error signal $e(t)$ would be added to a dither signal. The resulting signal would be processed by a two level quantizer and the output operated on by a pulse compensator. The resulting pulse compensated signal would then be applied to the system.

This notion can be illustrated by examining the waveform of signals in a compensation circuit of this type. In Figure 32 assume that the input to the compensator $e(t)$ is a sine wave as shown. It is further assumed that triangular wave dither $b(t)$ is added to the signal to produce the wave form shown. This signal is fed to a two level quantizer which produces a pulse-width modulated signal $e'(t)$. At each transition of the pulse-width modulated signal a pulse of height $2\alpha_1$ and duration T_1' is produced. These compensation pulses are shown as $e''(t)$. These pulse trains are periodic with the same fundamental frequency as the original signal $e(t)$. The fundamental and DC level of the positive and negative pulses is shown. Notice that the sum of these two signals or the total low frequency effect of the pulses is a sine wave which leads $e(t)$ by 90°. The magnitude of this sine wave increases with α_1 and T_1'. These waveforms illustrate how the dithered quantizer and pulse compensator produce a phase lead signal, they also show how compensation can be accomplished by only applying the positive or the negative compensation pulses. This approach was used by Bermel and Taft in a resonant system compensator.[11] The difficulty with this approach, of course, is that it requires that the signal must be

50

quantized in order to provide the pulse compensation and several difficulties result from this. The first of these is that dither and the higher harmonics generated by the quantizer show up as ripple in the output.

A further step was taken to reduce the ripple in the compensated system. This was accomplished by operating on the error signal, leaving the original error signal path present in the feedback system as shown in Figure 31b. The error signal is mixed with the dither and fed to a quantizer then compensation pulses are produced from this signal which are added to the analog error signal. This approach greatly reduced the ripple in the output due to the compensator. In addition it allows the compensator to be inserted in the existing system as a parallel path so that very little modification needs to be made in the existing system to add the compensator. This approach has advantages, for the application of this notion to the control fluid systems since it allows an easy addition of the compensator to an existing system. The effective transfer function of the compensator is determined by the magnitude of the compensator pulses $2M\alpha_1$, the magnitude of the dither B and the output level of the quantizer M.

The system shown in Figure 31b can be replaced by an equivalent low frequency system where the dither and quantizer are replaced by the altered characteristic as shown in Figure 31c. For error signals less than .7B, the altered characteristic is very nearly linear with gain $2M/\pi B$. Therefore since the pulses are added to the error signal the overall transfer function between error e(s) and system input e"(s) is:

$$G_c(s) = \frac{2M\alpha_1}{\pi B}\left(1 - e^{-T_1's}\right)$$

Notice that either quantizer output in or dither amplitude B can be controlled to provide simple adaption control of the compensator. Another problem in the use of the compensator results because as compensator pulse duration T_1' is made larger and larger the possibilities of pulse overlap begin to occur. That is, it is possible for a second or third compensation pulse to be called for before the original pulse is over. This would, in effect, require memory in the pulse compensator and increases the amount of hardware necessary to mechanize the pulse compensation concept. Nawaz developed fluidic circuitry to accomplish this but it does require more hardware.[14]

The finite operating times of fluidic elements and the desire to keep dither frequency high and pulse duration low puts limitations on the application of the compensator. Further the operating time of the fluidic digital elements can be of the order of the compensation pulse duration. This has the effect of degrading compensator effectiveness.

For example consider the system shown in Figure 33 with a two pulse compensator whose transfer function is $G_c(s)$. The fluidic elements used to produce the compensation pulses have switching times of t_d which is equivalent to a transport delay as shown. For $\alpha_1 = \alpha_2 = 5$ and $T_2' = 2T_1'$ the resulting effect of various transport delays on the first two quadrants of the compensator frequency response function $G_c(j\omega)e^{-t_d j\omega}$ are shown in Figure 34. As would be expected, the time delay causes less phase lead to be contributed by the compensator and considerably less compensator magnitude. The former effect is detrimental, however, the latter effect may actually be beneficial.

Bermel and Taft[11] used the compensator form shown in Figure 32b in the construction of a very resonant pneumatic positioning system. In addition, no dither was used and only positive pulses were applied. An all-fluidic system was built by Bermel which positioned a mass using pneumatic cylinder and vortex sensor as the position feedback element. The resonant compensator used in the system has the form shown in Figure 35. Furthermore these compensation pulses were added at the high power levels directly into the actuating cylinder. The approach proved quite effective although Bermel did not use a dither signal and operated the system with only pulses in one direction which meant that the compensation was highly nonlinear. The resulting response of the system was considerably less oscillatory than the one without compensation. The results of this approach are shown in Figure 56.

SUMMARY AND CONCLUSIONS

Digital fluidic elements can be used to process analog signals. By adding a sinusoidal or periodic signal to an analog signal and then processing the result by two or three level quantizers it is possible to produce an output whose low frequency components are nearly proportional to the input over a range of inputs. This in effect alters the characteristic of the quantizer. This "altered characterisitc" demonstrates analytically the linearizing effect of a dither signal. The dither signal may in fact be generated internally by closing a feedback loop around the quantizer itself. This process is producing the dither by causing the system to exhibit a limit cycle. Pulse-width modulated amplifiers are the result of an approach like this and can be used for proportional control.

A further refinement results if one notices that the output of any quantizing processes is a sum of steps. The resulting signals can be compensated by adding pulses whenever these steps occur. The added pulses can be produced by digital elements and so a digital compensation results. The resulting compensators can be analyzed by linear methods. A transfer function can be developed for these devices and a frequency response also developed. This allows compensators which

52

result from one, two and three pulses to be designed. The design of
these compensators also involves problems associated with the overlap
of pulses which can occur when pulse durations are long and signals
are changing rapidly. Furthermore, these compensators tend to produce
a ripple in the output due to the high frequency components of the
dither, which are accentuated by the compensation pulses. Some of
these effects can be reduced by producing the compensation pulses alone
rather than processing the signal with the quantizer in order to allow
the use of the compensation pulses. This approach involves applying a
parallel error path in a fluid system through which signals are pro-
cesses and compensation pulses produced to provide system compensation.
This approach should offer considerable advantages in many fluid sys-
tems especially those which are very resonant. In this way fluidic
elements can be used to provide rather sophisticated forms of com-
pensation without any moving parts nor any signal conversions. The
advantages of using fluidic devices for this purpose show promise.

BIBLIOGRAPHY

1. Gaither, P.H., Taft, C.K. "Digital Lead Compensation of Pulse-Data Control Systems" ASME paper 63-WA-183, Winter Annual Meeting Philadelphia, November 1963.

2. Taft, C.K., Pokoski, J.L., Wochholz, H.E. Digital Control System Design. Notes for short course at University of New Hampshire, 1969.

3. Limbert, D.E., Taft, C.K. "Limit Cycle Behavior in Systems with Quantized Error Signals" IFAC Symposium on Pulse Control, Budapest, Hungary, April 1968.

4. Canpaynuolo, Carl J., Sieracki, Leonard M. "A Digital-Proportional Fluic Amplifier for a Missile Control System" p 131-159, Vol. III, Proceedings of the Fluid Amplification Symposium, October, 1965.

5. Gibson, J.E. Nonlinear Automatic Control, McGraw-Hill, 1963, Chapter 9.

6. Hanafusa, H., Miyata, K. "Fluidic Servo Amplifier Operated in PWM Mode" Fluidics Quarterly, No. 13, p. 30-44, October 1971.

7. Bermel, T.W., Limbert, D.E. "Digital Fluidic Operational Amplifier" Joint Automatic Control Conference, August 1971, Conference proceedings.

8. Lloyd, G.F.H., "A Fluidic Proportional Amplifier Using Pulse-Width Modulation Techniques" Paper H4 Fourth Cranfield Fluidics Conference, March 1970, Coventry, England.

9. Smith, O.J.M. Feedback Control Systems, McGraw-Hill, 1958, pp 331-345.

10. Foster, A.M., Taft, C.K. "Discontinuous Compensation for Quantized Systems" ASME Winter Annual Meeting Pittsburgh, ASME-67-WA-AUT-9, November 1967.

11. Bermel, T.W., Taft, C.K. "Compensation of an Underdamped Fluidic Position Control System by a Digital Pulse Compensator" Paper G4 Fifth Cranfield Fluidics Conference Proceedings, June 1972, Upsala, Sweden.

12. Porter, J. "Frequency Response Characteristics of Triple Delay Digital Compensators" M.S. Thesis Case Institute of Technology, November 1967.

54

Bibliography - (Continued)

13. Hamlin, D.R., Taft, C.K. "A Simple Digital Compensator for Continuous Control Systems" Joint Automatic Control Conference Preprints pp 557-565, June 1967.

14. Nawaz, S., Taft, C.K. "Fluidic Digital Compensators for Analog Systems" Proceedings of Fourth Cranfield Fluidics Conference, Coventry, England, March 1970.

Symbols

a_0	One half of deadzone
Am	Coefficient of mth power of s in inumerator of $G(s)$
$b(t)$	Dither signal
B	Nonsinusoidal dither amplitude
Bn	Coefficient of $(n+1)^{th}$ power of s in denominator of $G(s)$
$c(t)$	Output
$e(t)$	Error (input minus feedback)
$e(s)$	Laplace transform of $e(t)$
$e'(t)$	Output of quantizer
$e'(s)$	Laplace transform of $e'(t)$
$e''(t)$	Compensator output
$e''(s)$	Laplace transform of $e''(t)$
$e_1''(t)$	Fundamental frequency component of compensator pulse output
E_0	Dc level of $e(t)$
E_0'	Dc level of $e'(t)$
E_1	Fundamental frequency component of $e(t)$
E_1'	Fundamental frequency component of $e'(t)$
$g(t)$	Inverse transform of $G(s)$ - impulse response
$G(s)$	Continuous part forward loop transfer function
$G_c(s)$	Compensator transfer function
$G_c(j\omega)$	Compensator frequency response function
$\overline{G_c(j\Omega)}$	Dimensionless frequency response function
G_d	Describing function for $e'(t)$ relative to $e(t)$
G_{dc}	Describing function for $e''(t)$ relative to $e(t)$

56

Symbols - (Continued)

H(s)	Feedback transfer function
j	$\sqrt{-1}$
k	Loop gain
M	2 level quantizer output
M_m	Maximum magnitude of closed loop frequency response function
n	$_1 = _2$ pulse height when both pulses =
po	Input differential pressure
po'	Output differential pressure
r(t)	Input
R	Magnitude of step input
S	Laplace operator
t	Time
t_d	Time delay
$t_1, \ldots t_5$	Times at which e'(t) changes
T	Time constant
T_n	n^{th} time constant
T_1', T_2', T_3'	Compensation pulse times
u(t)	Unit step = 1 t 0, = 0m t 0
$_1\ _2\ _3$	Compensation pulse heights
β	Dither frequency
Δ	Hystersis
ω	Signal frequency
Ω	Dimensionless frequency $T_1'\omega$
$\int$	Damping ratio

57
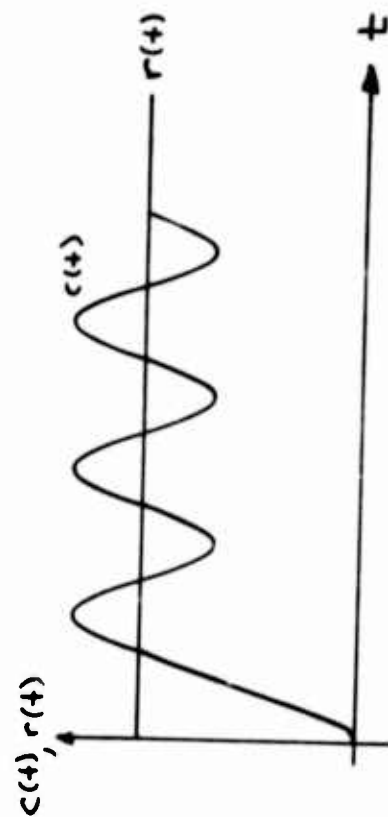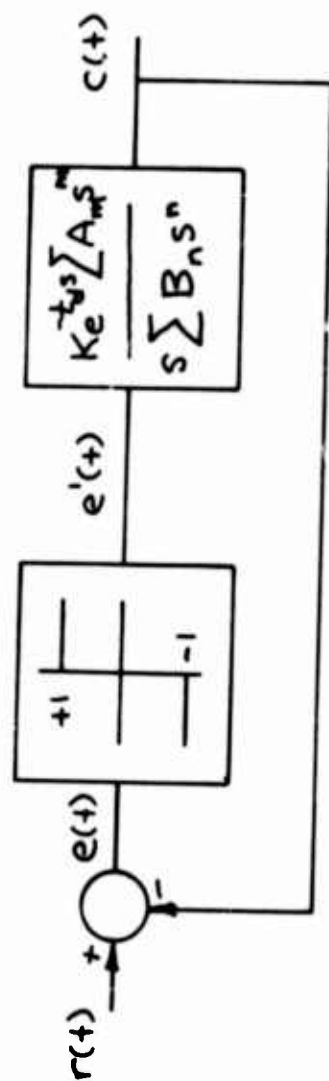
1. ON-OFF FEEDBACK SYSTEM

For $G(s) = \dfrac{Ke^{-t_d s} \sum\limits_m A_m s^m}{s \prod\limits_n (T_n s + 1)}$

WHEN $\dfrac{dg(+)}{dt} > 0$, $t > 0$

2 STEP

MULTISTEP

$\dfrac{a_0}{K}$ sec

$t_d + \sum\limits_n T_n - A_1$
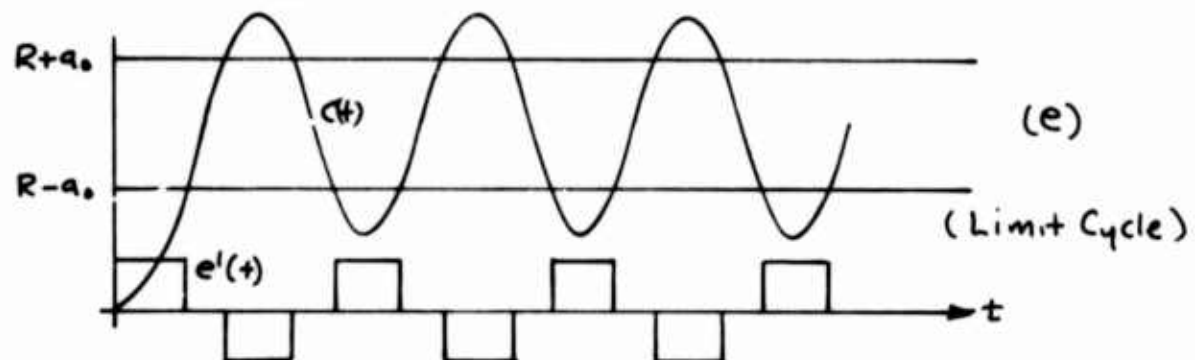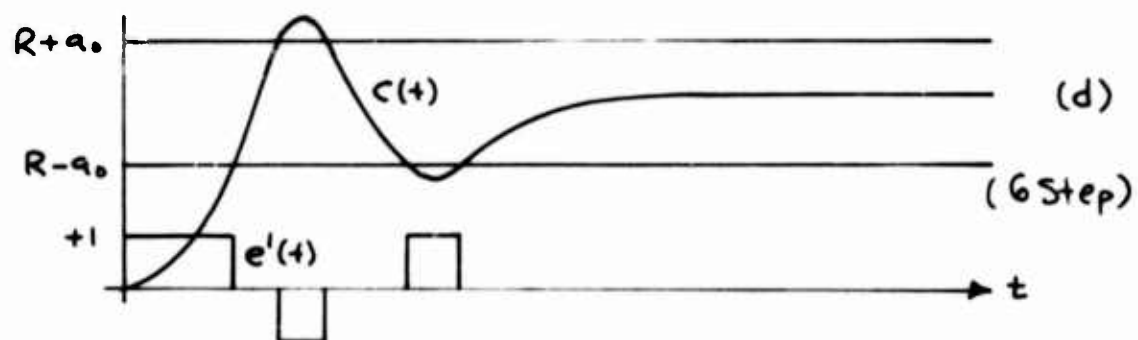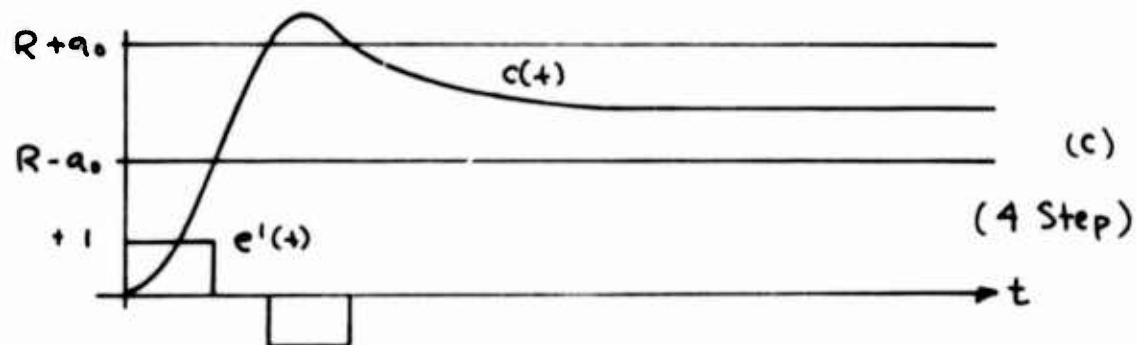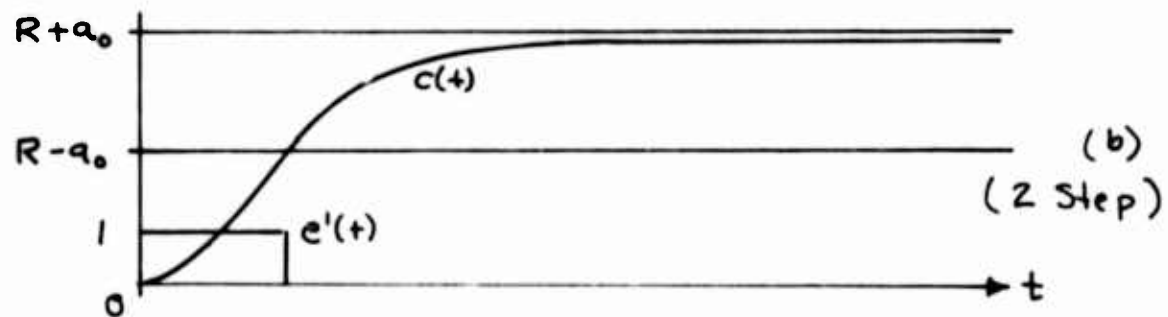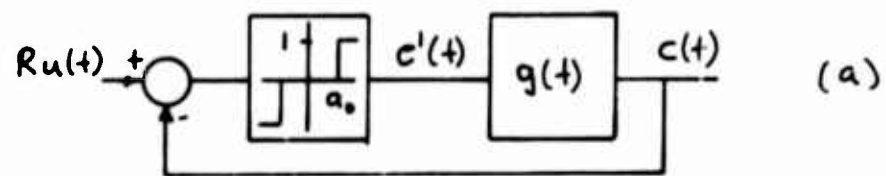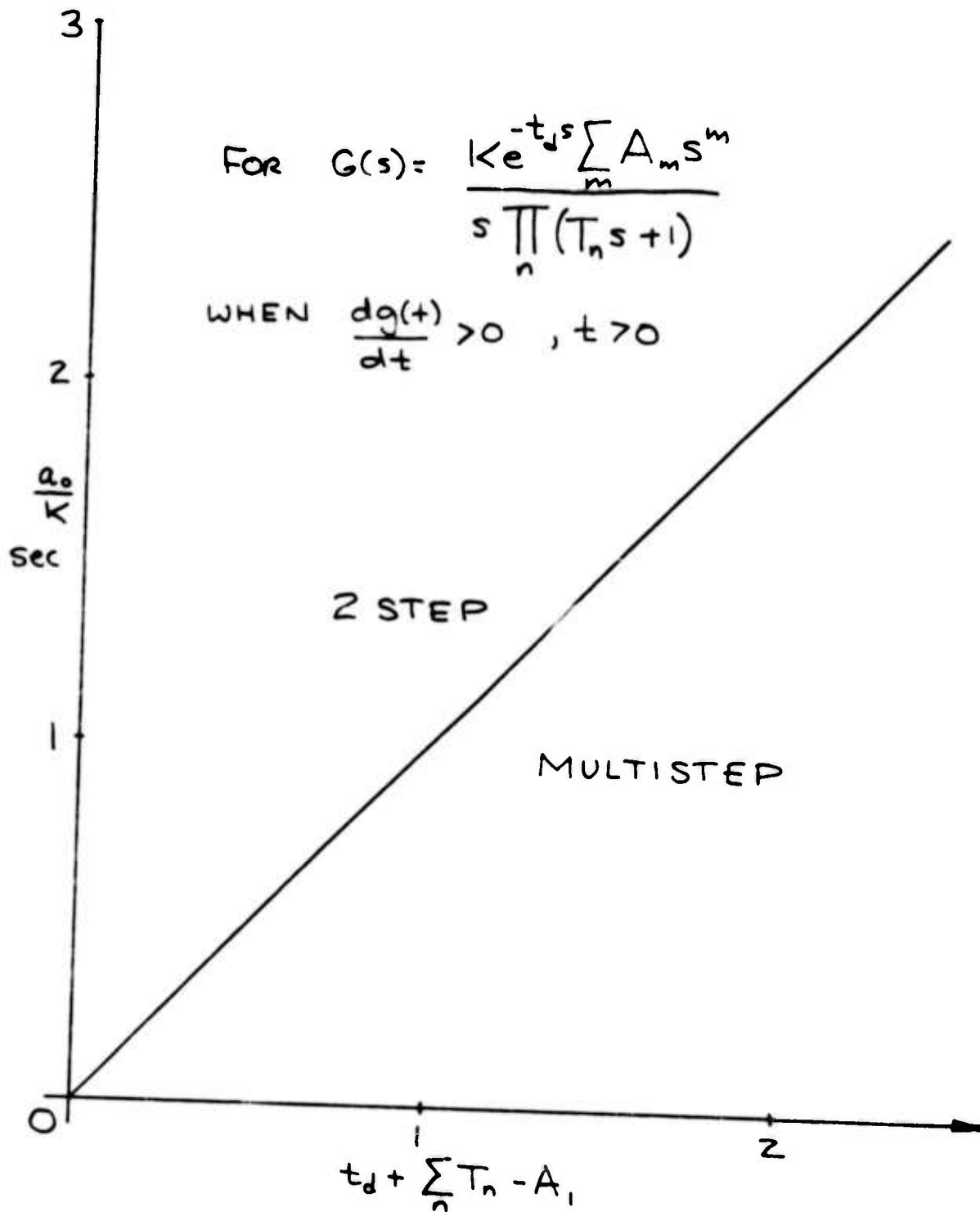
3. THREE-LEVEL QUANTIZED SYSTEM DESIGN CHART BASED ON STEP RESPONSE

60
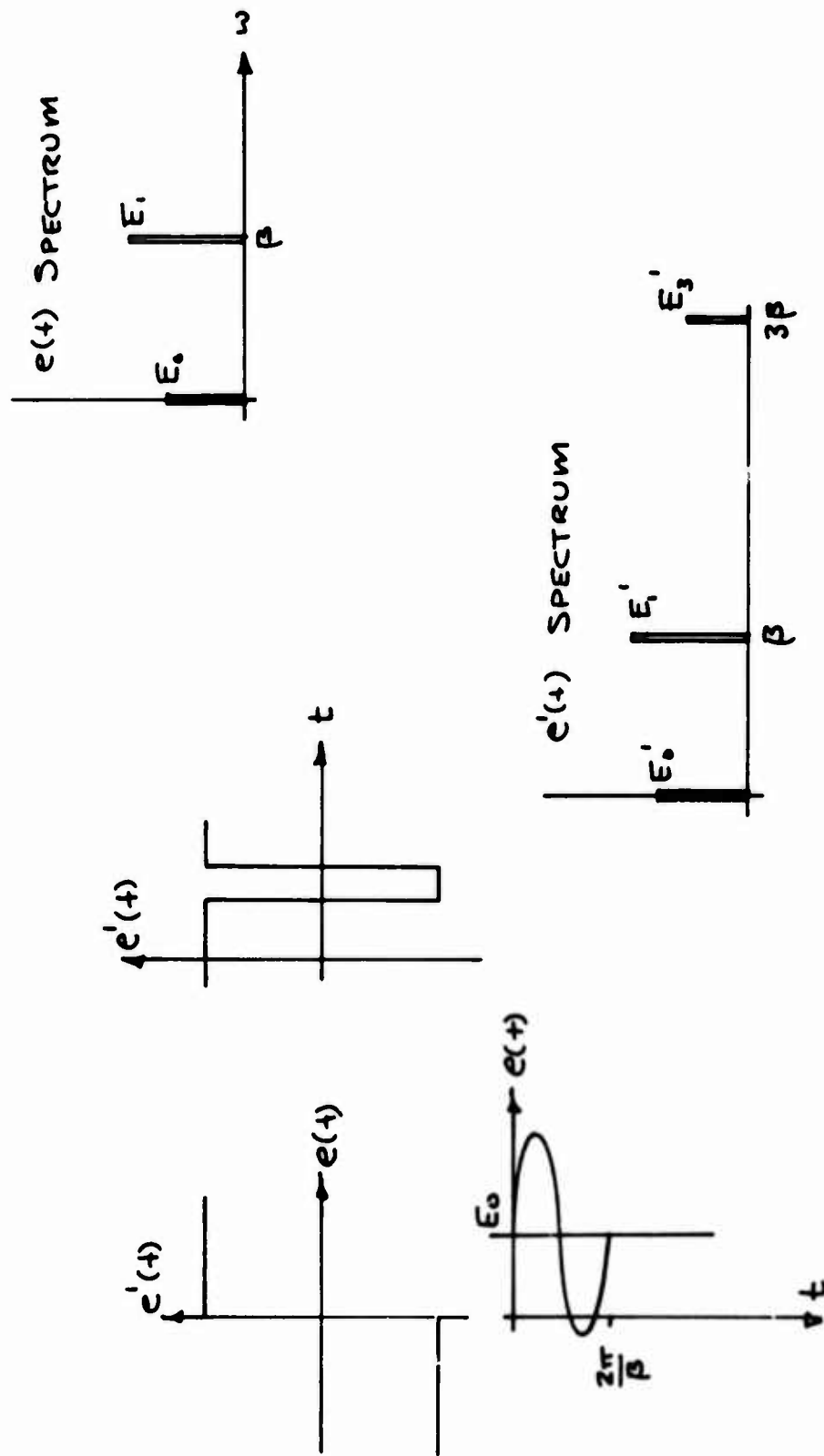
4. TWO-LEVEL QUANTIZER INPUT-OUTPUT WAVEFORMS AND SPECTRA

61
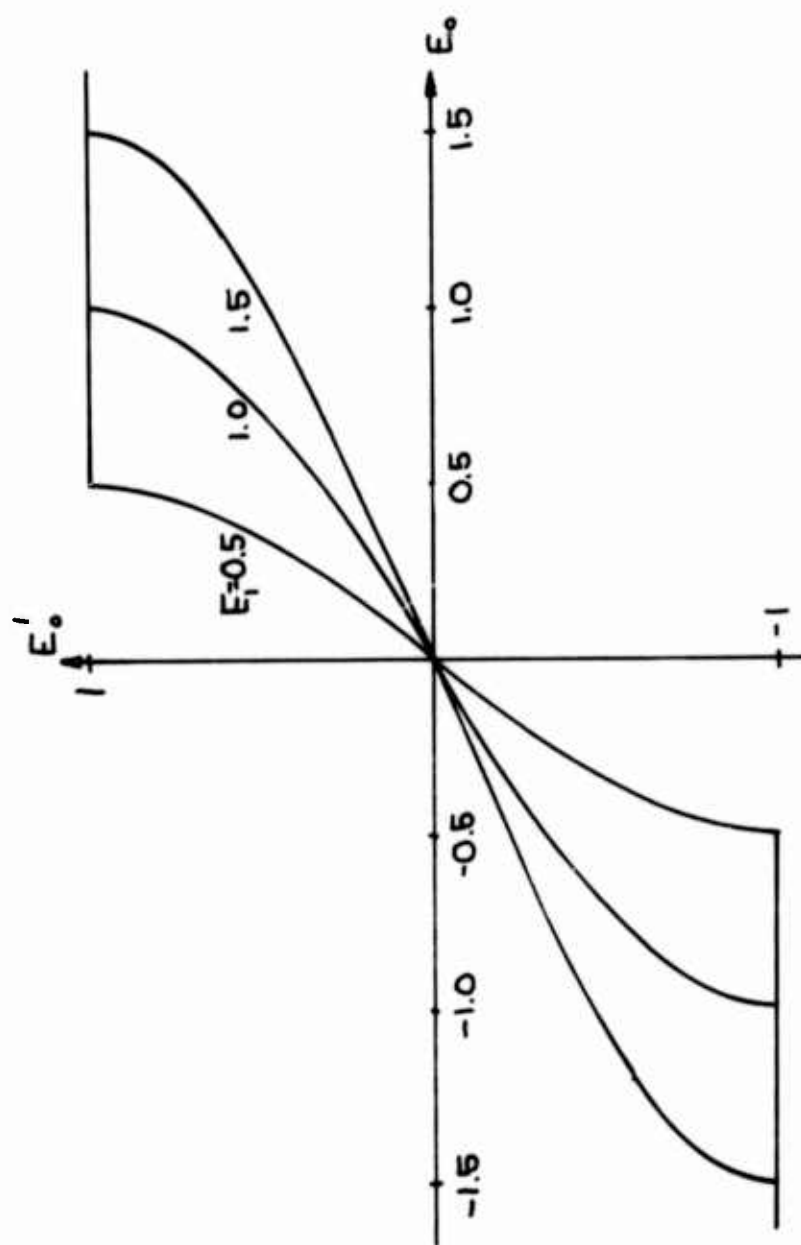
5a. ALTERED CHARACTERISTIC FOR TWO-LEVEL QUANTIZER AND SEVERAL DITHER AMPLITUDES

62
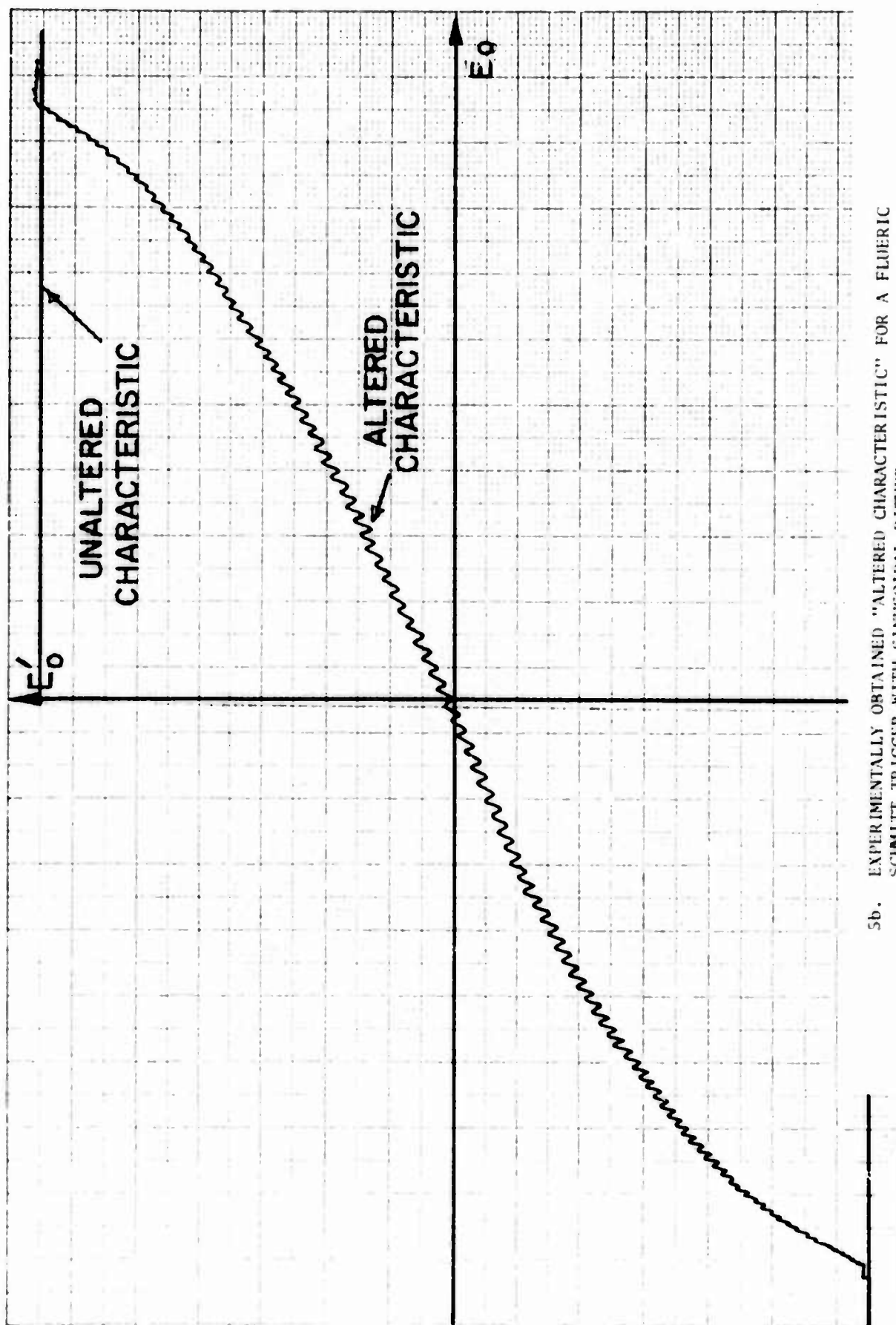
5b. EXPERIMENTALLY OBTAINED "ALTERED CHARACTERISTIC" FOR A FLUERIC SCHMITT TRIGGER WITH SINUSOIDAL DITHER
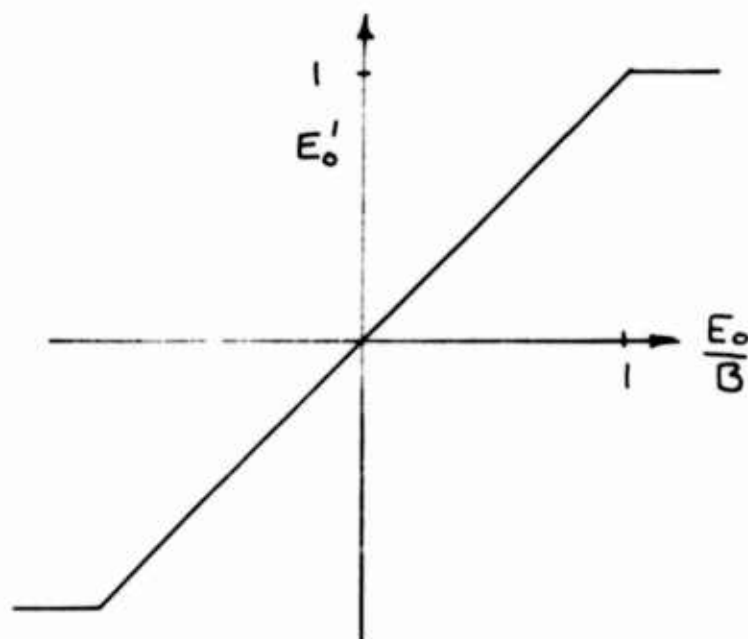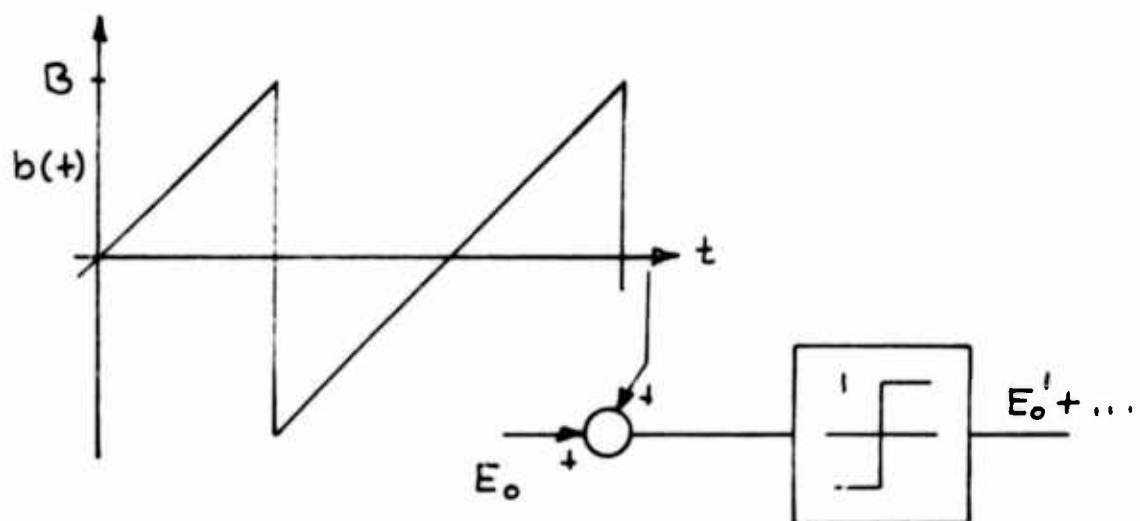
6. ALTERED CHARACTERISTIC FOR TWO-LEVEL QUANTIZER WITH SAWTOOTH DITHER
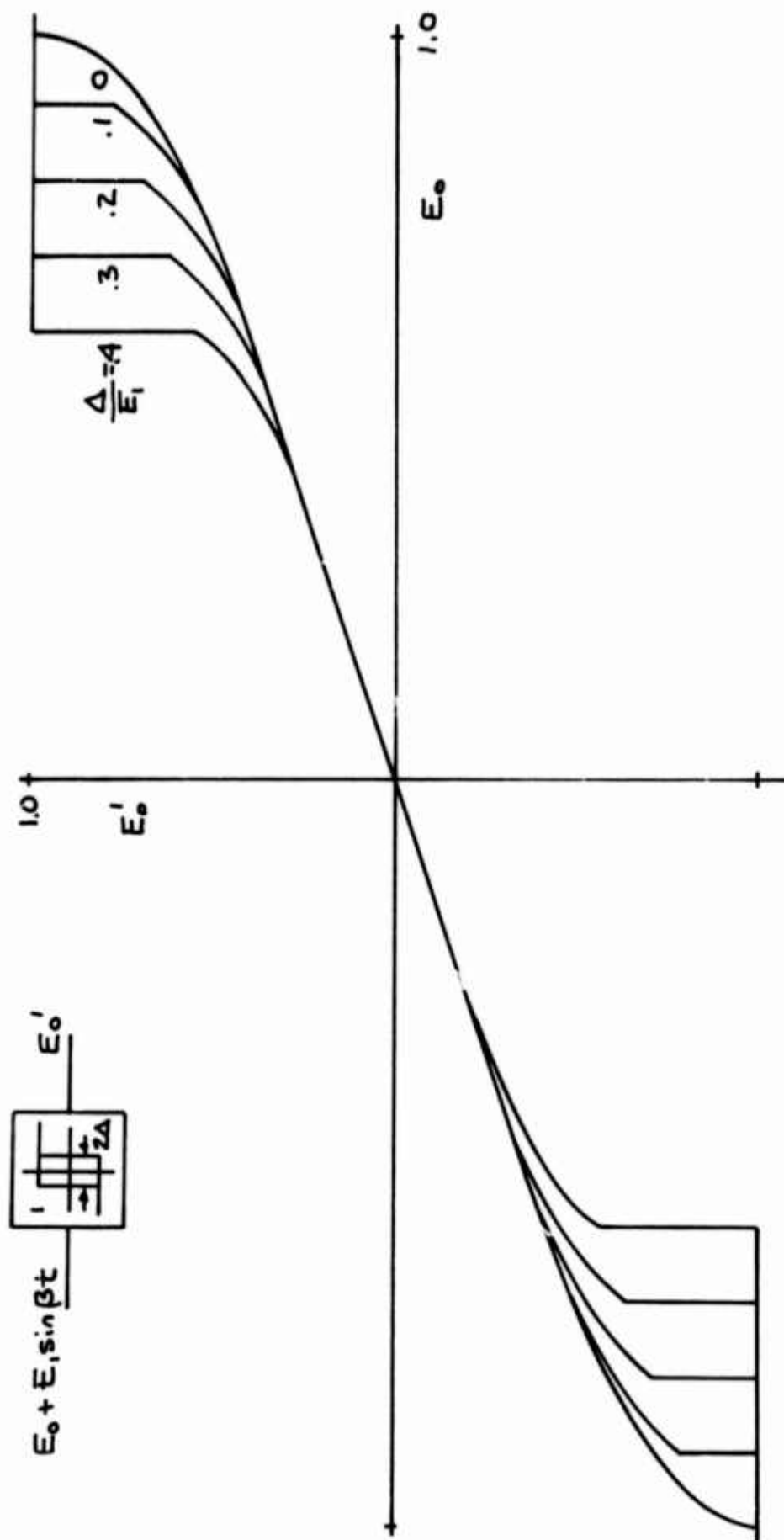
7. ALTERED CHARACTERISTIC FOR TWO-LEVEL QUANTIZER WITH HYSTERSIS AND SINUSOIDAL DITHER

65
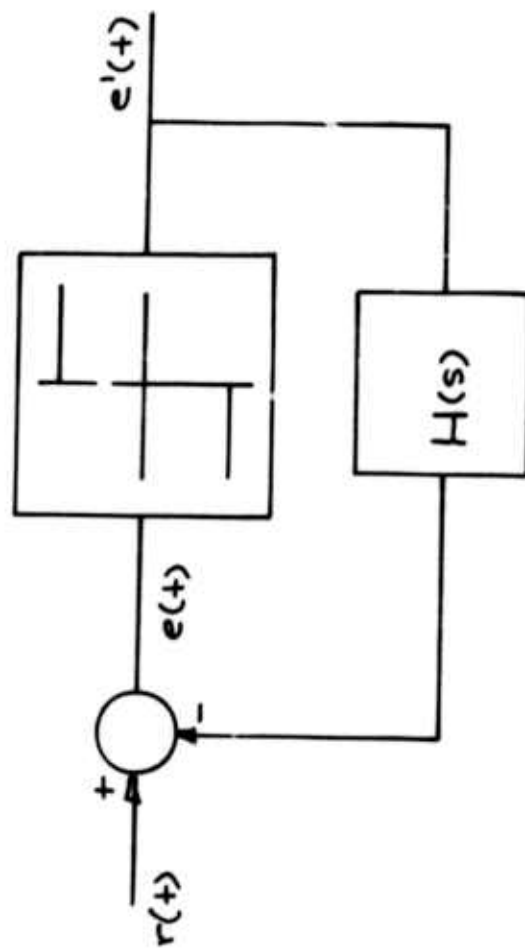
8. PULSE-WIDTH MODULATED AMPLIFIER WITH FEEDBACK

66
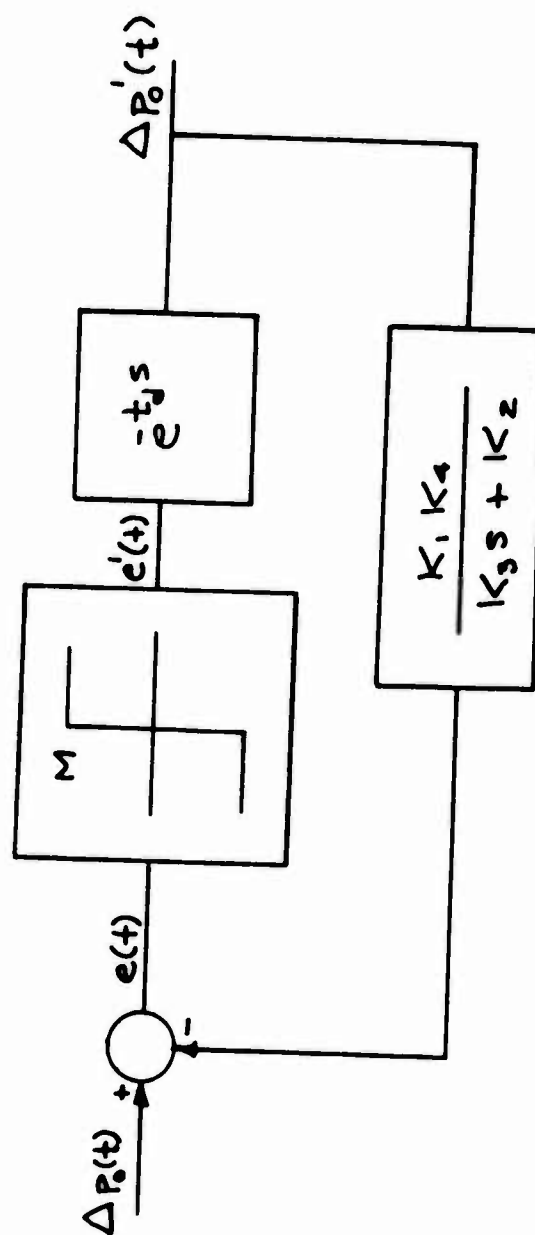
9. BLOCK DIAGRAM BERMEL FLUIDIC POWER AMPLIFIER

10. $\Delta P_o'$ OUTPUT VS ΔP_o INPUT FOR FLUIDIC POWER AMPLIFIER

$E_1 \sin \omega t$

DITHER

$c'(t)$

DITHER
PERIOD $= \dfrac{4\pi}{5\omega}$

t

$e'(t)$

NOTE
OUTPUT
PERIOD $= \dfrac{4\pi}{\omega}$

t
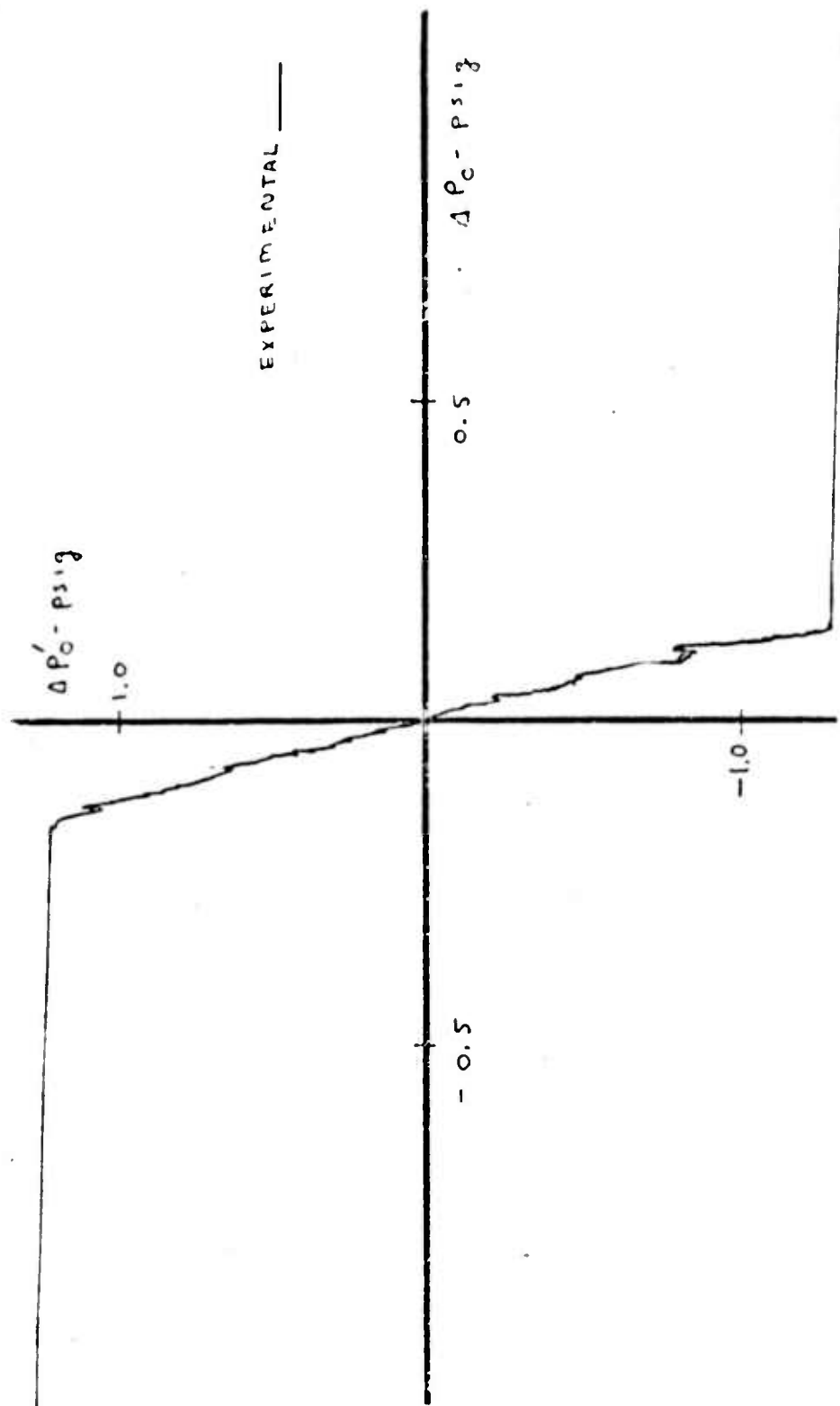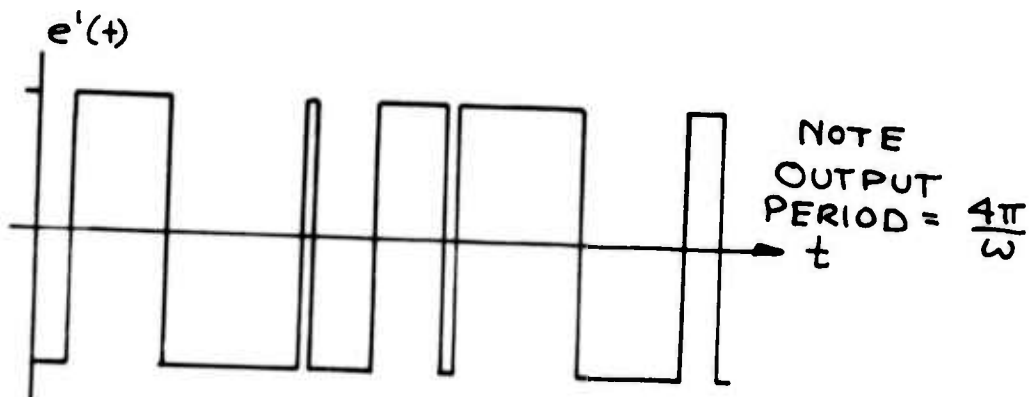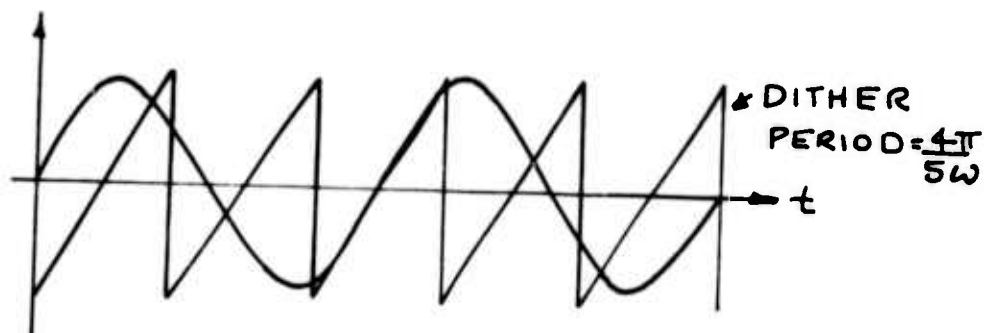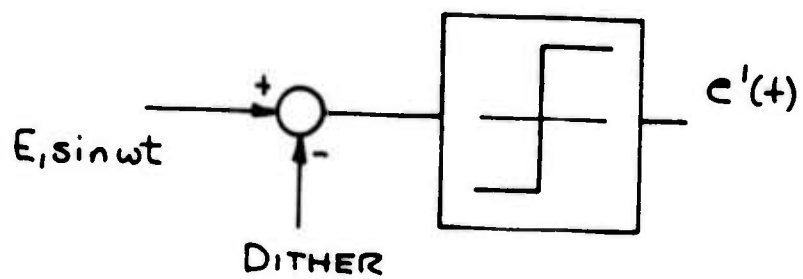
11. SUBHARMONICS IN PULSE-WIDTH MODULATED AMPLIFIER
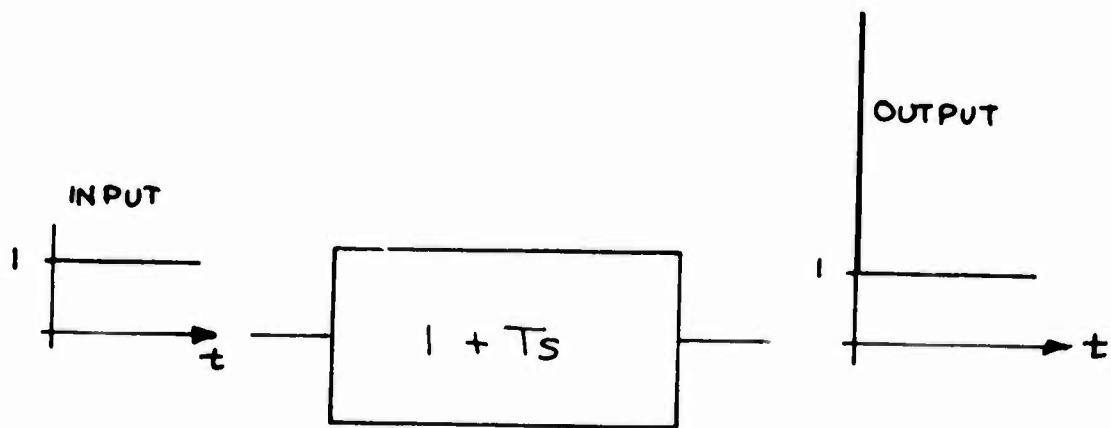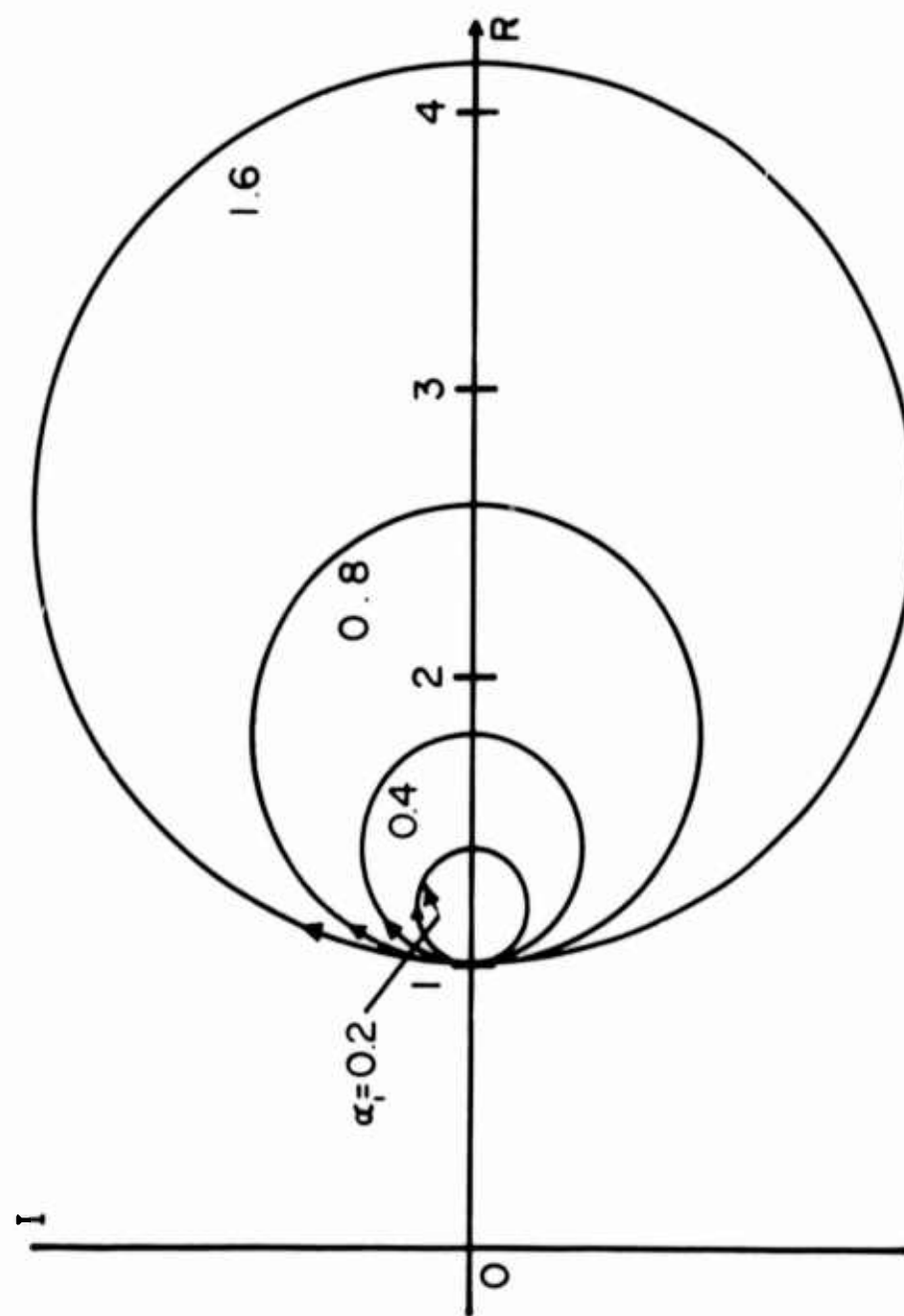
(a) PROPORTIONAL PLUS DERIVATIVE
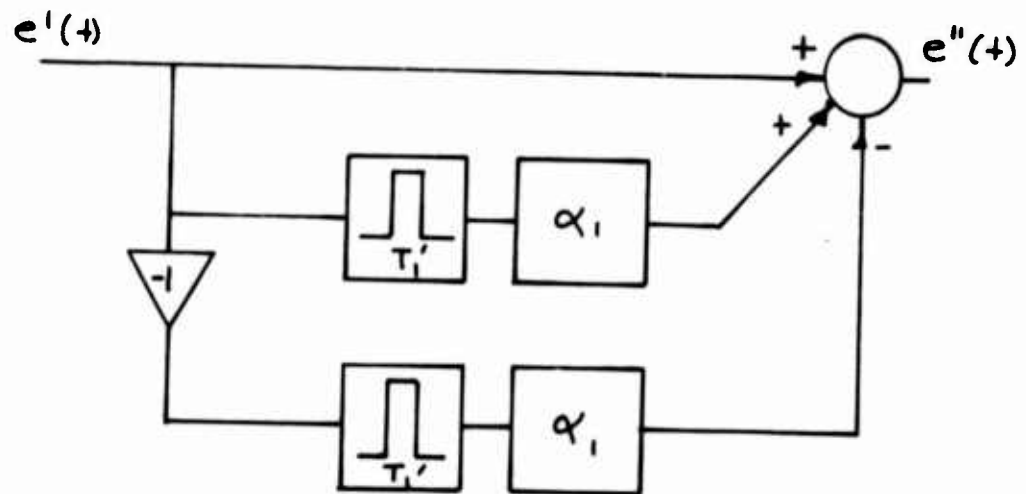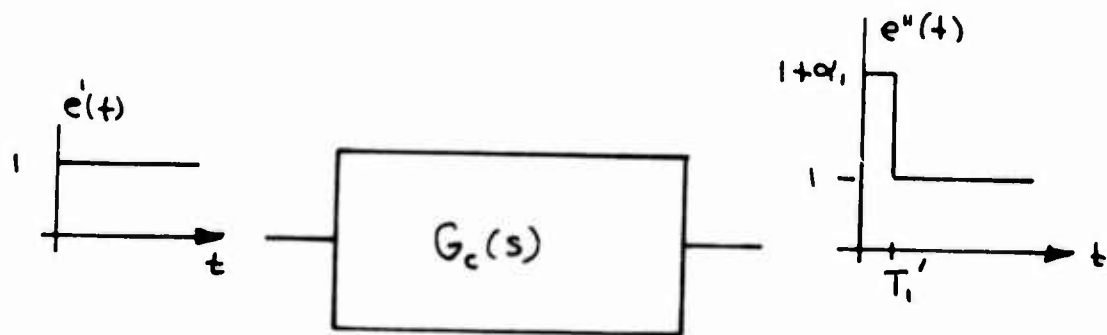
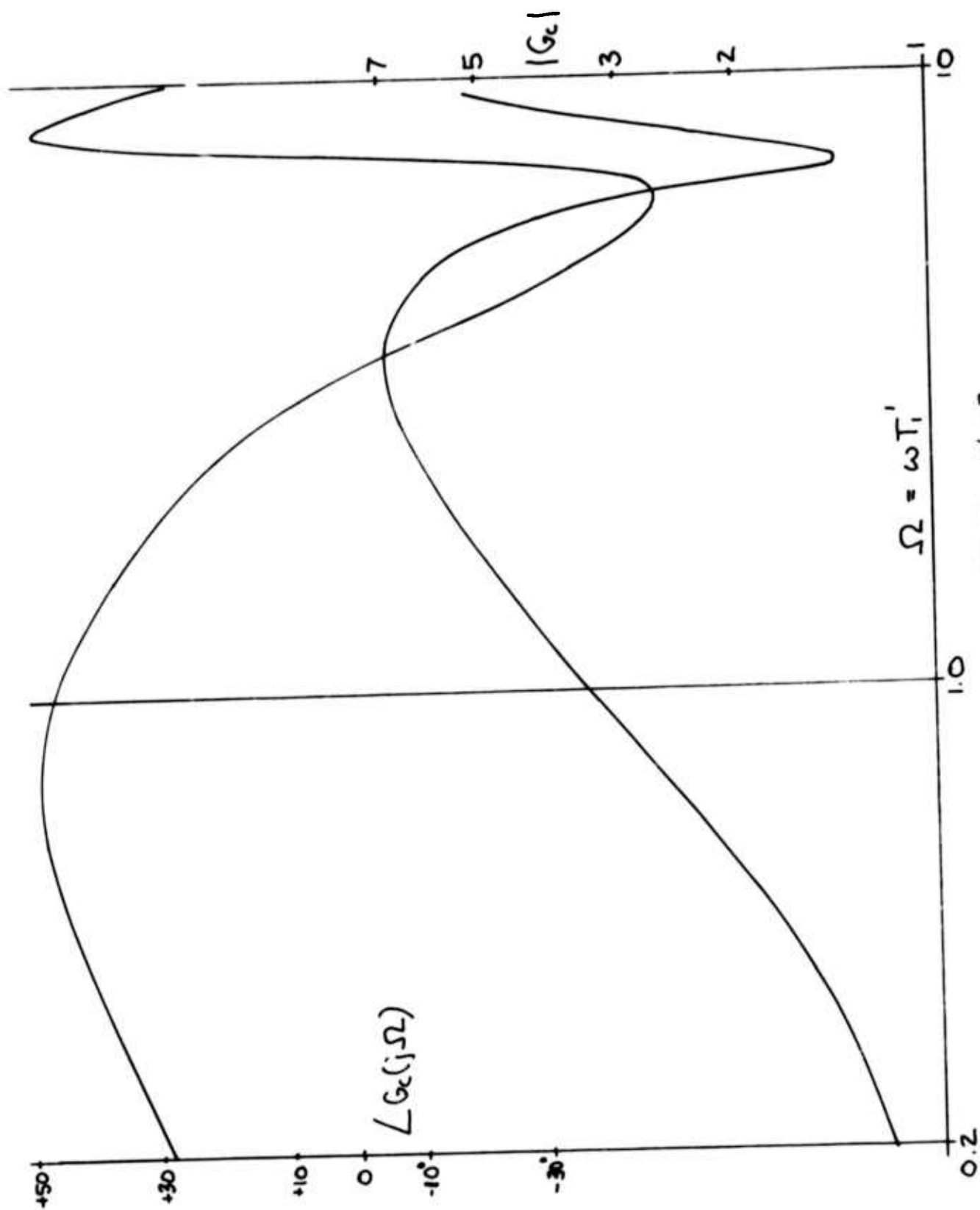12. EVOLUTION OF DIGITAL LEAD COMPENSATION
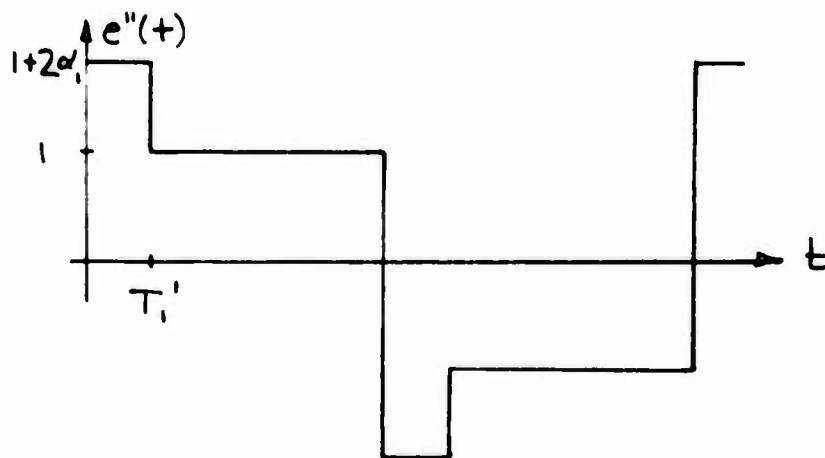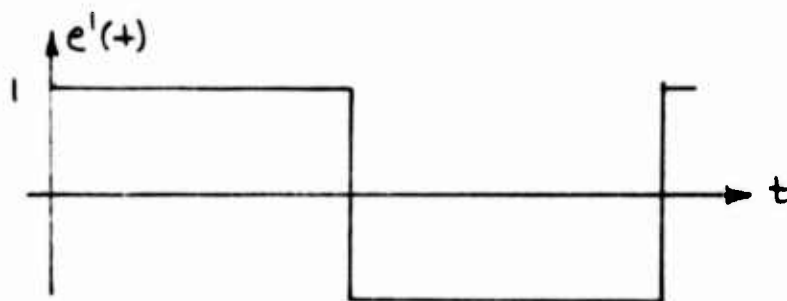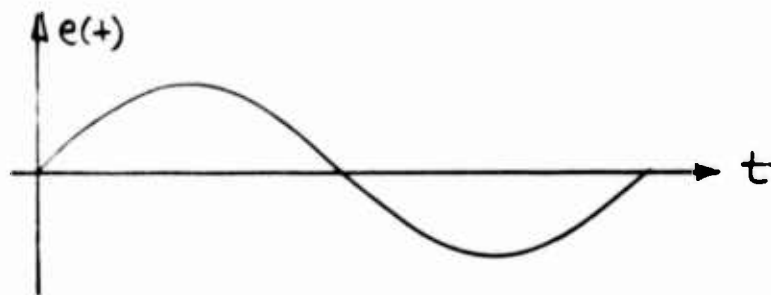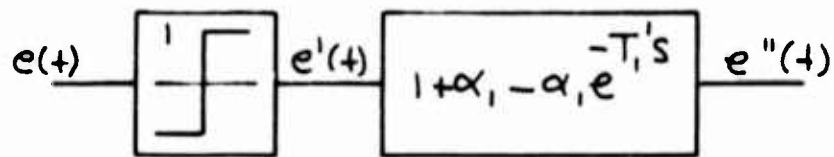
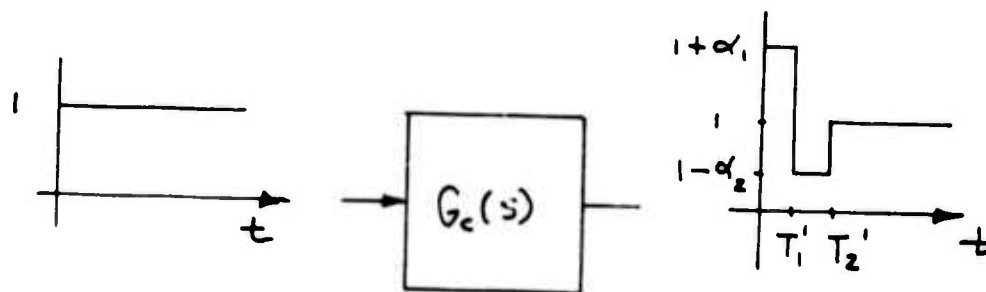13. QUANTIZER AND SINGLE PULSE COMPENSATOR WAVEFORMS FOR SINUSOIDAL INPUT

71

14. FREQUENCY RESPONSE FUNCTION FOR SINGLE PULSE COMPENSATOR $\alpha_1 > 0$
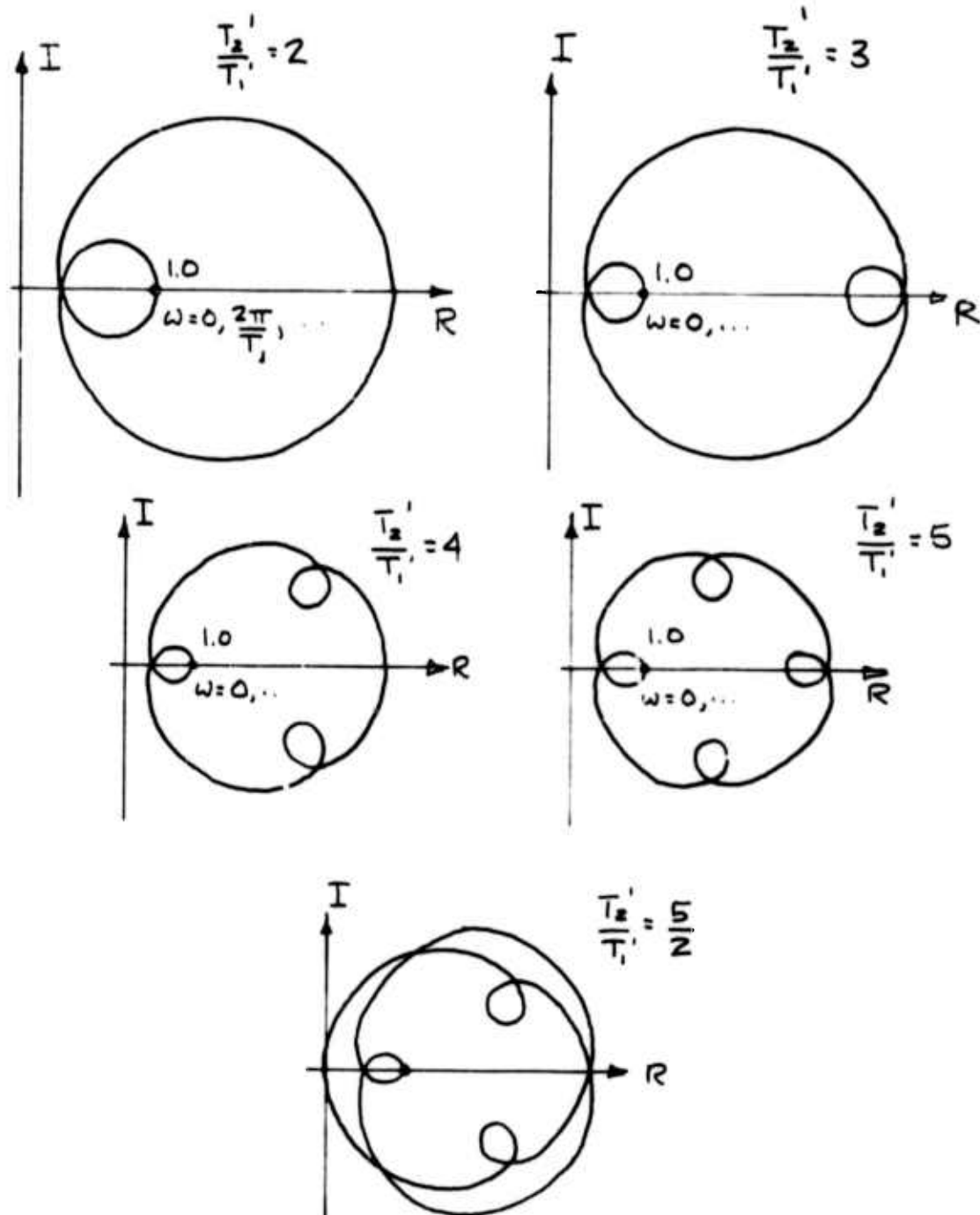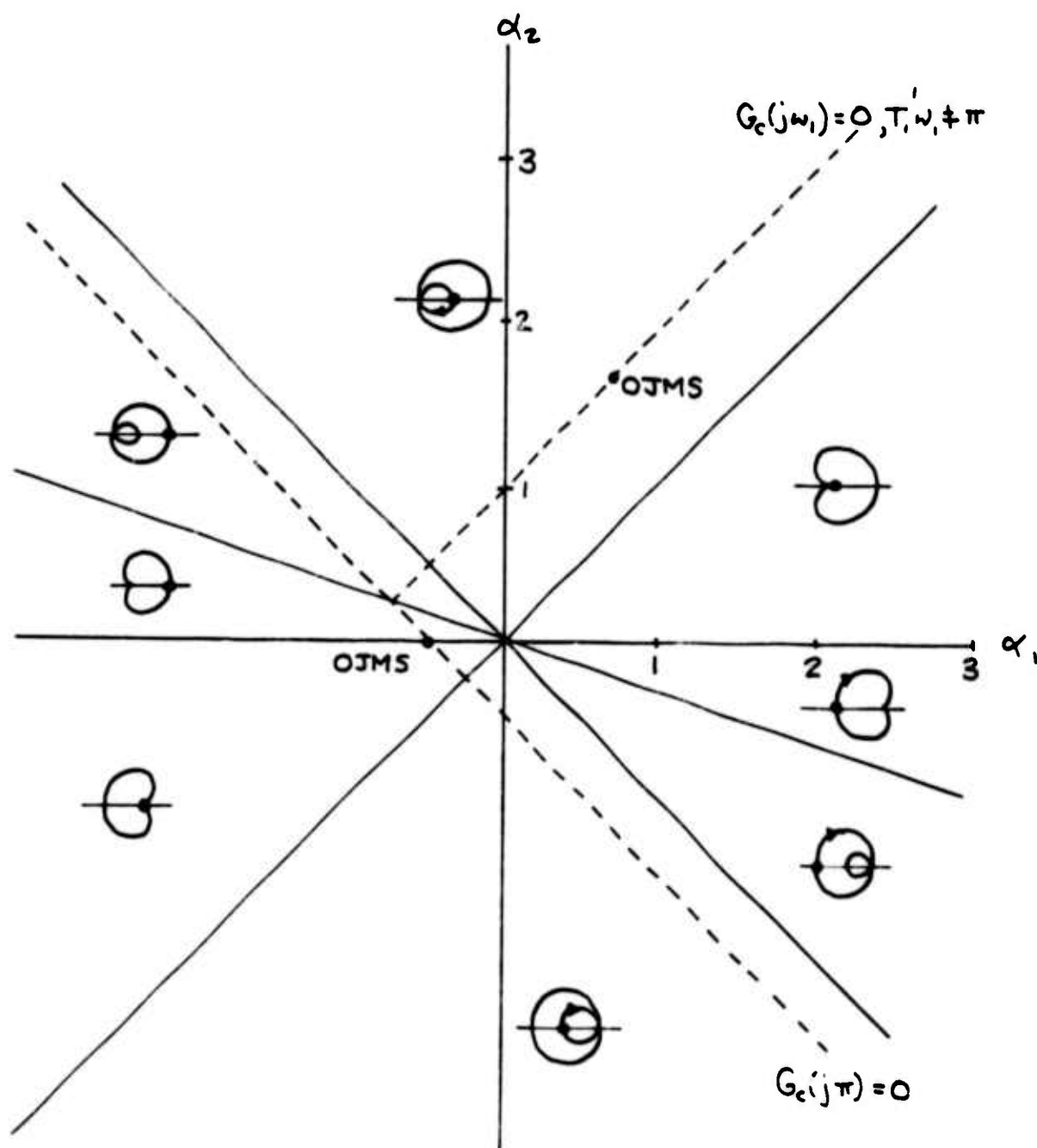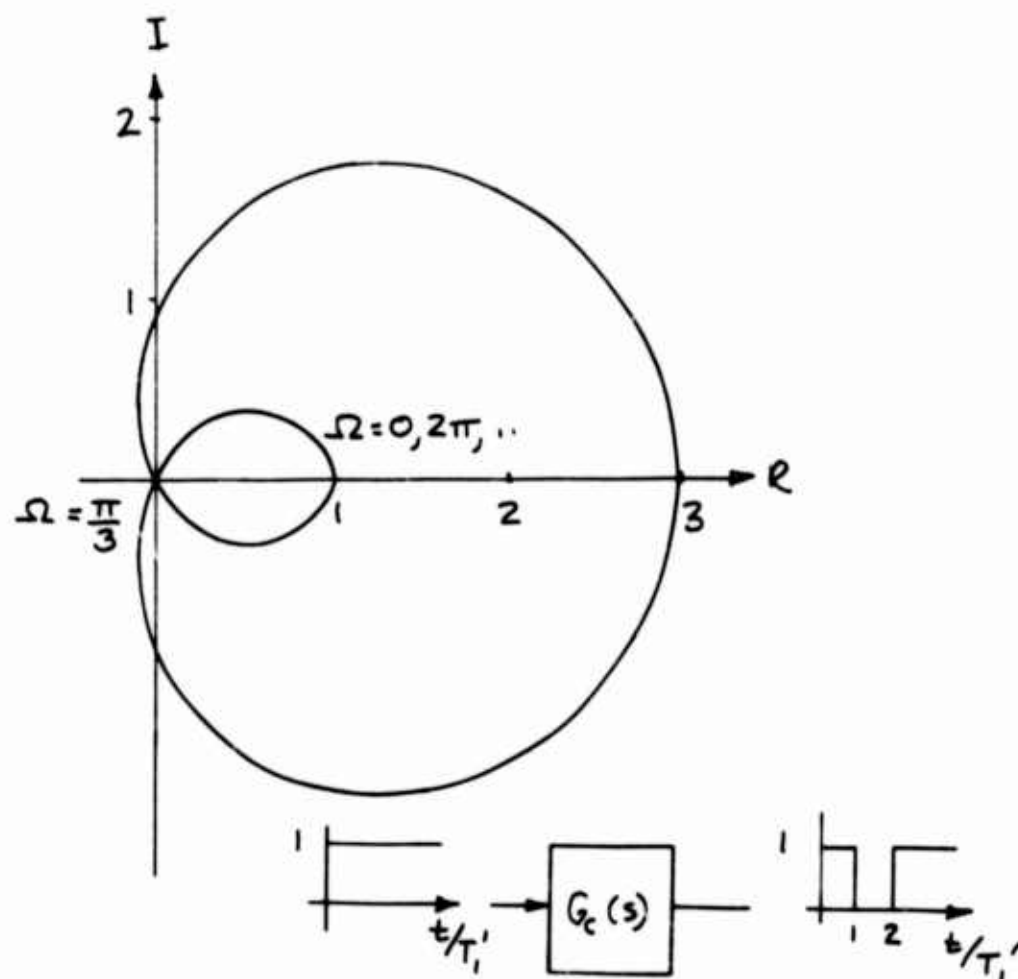
15. DIGITAL COMPENSATOR BODE PLOT FOR $\alpha_i = 3$

16. TWO PULSE COMPENSATOR
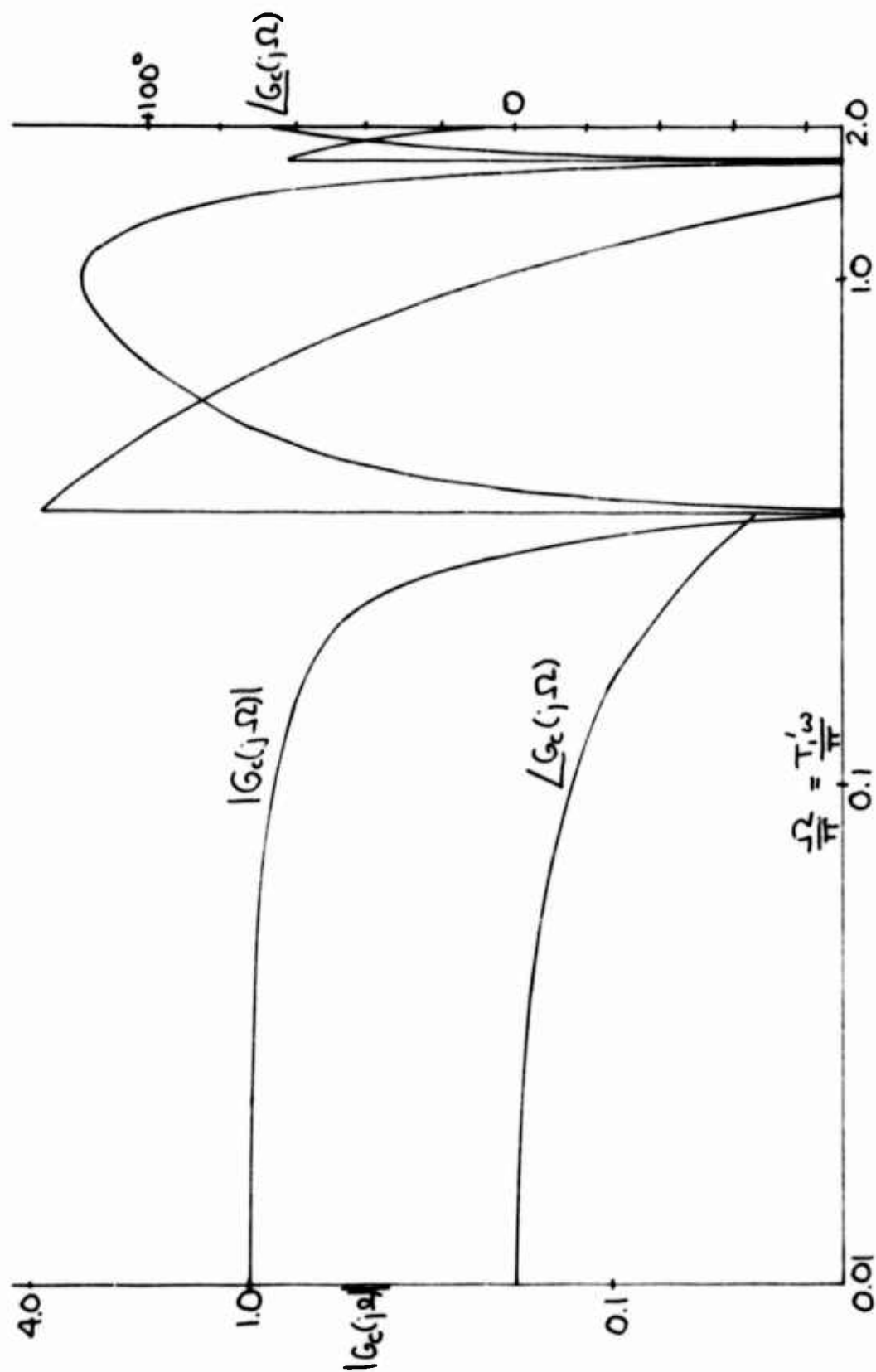
17. EFFECT OF T_2'/T_1' ON COMPENSATOR FREQUENCY RESPONSE FUNCTION POLAR PLOT

18. TWO PULSE COMPENSATOR FREQUENCY RESPONSE FUNCTION AS A FUNCTION OF α_1, α_2 WITH $T_2'/T_1' = 2$.

19. ZERO-PASS TWO PULSE COMPENSATOR FREQUENCY RESPONSE FUNCTION POLAR PLOT

77

20. BODE PLOT FOR TWO PULSE ZERO-PASS COMPENSATOR

78
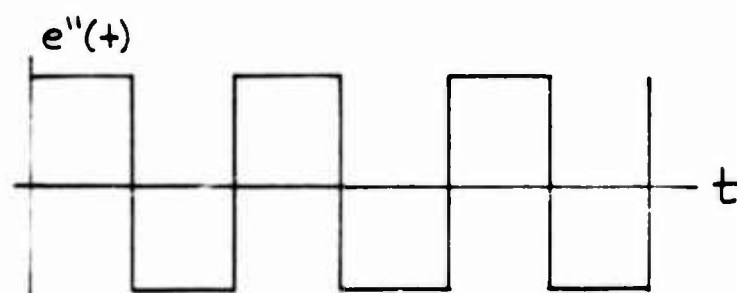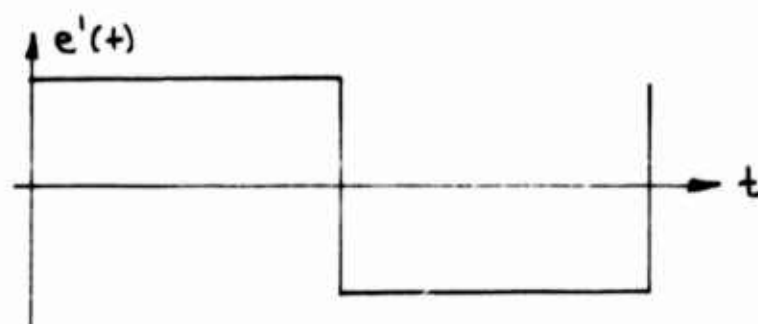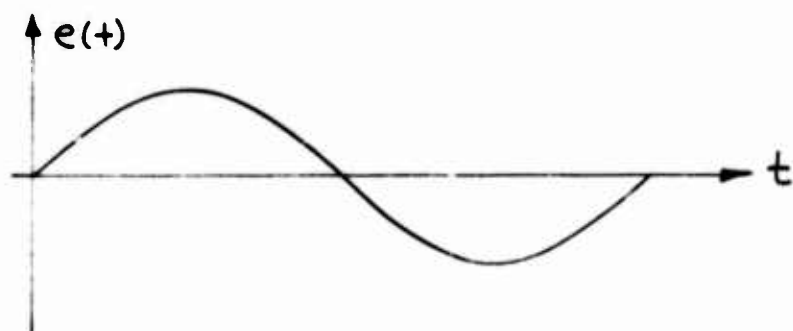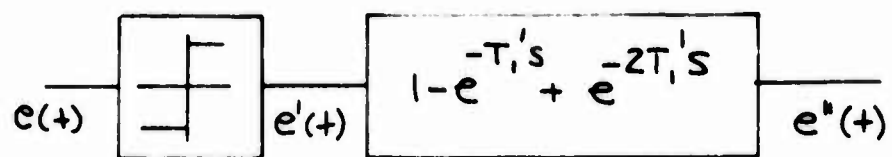
21. ZERO-PASS COMPENSATOR WITH INPUT AT ZERO-PASS FREQUENCY

$G(j\omega) G_c(j\omega)$
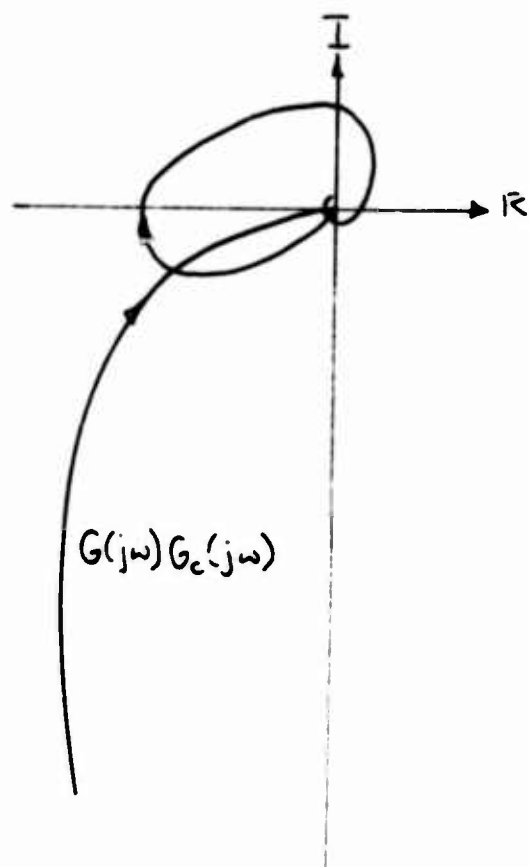
22. OVERALL SYSTEM FREQUENCY RESPONSE FUNCTION WITH ZERO-PASS COMPENSATION
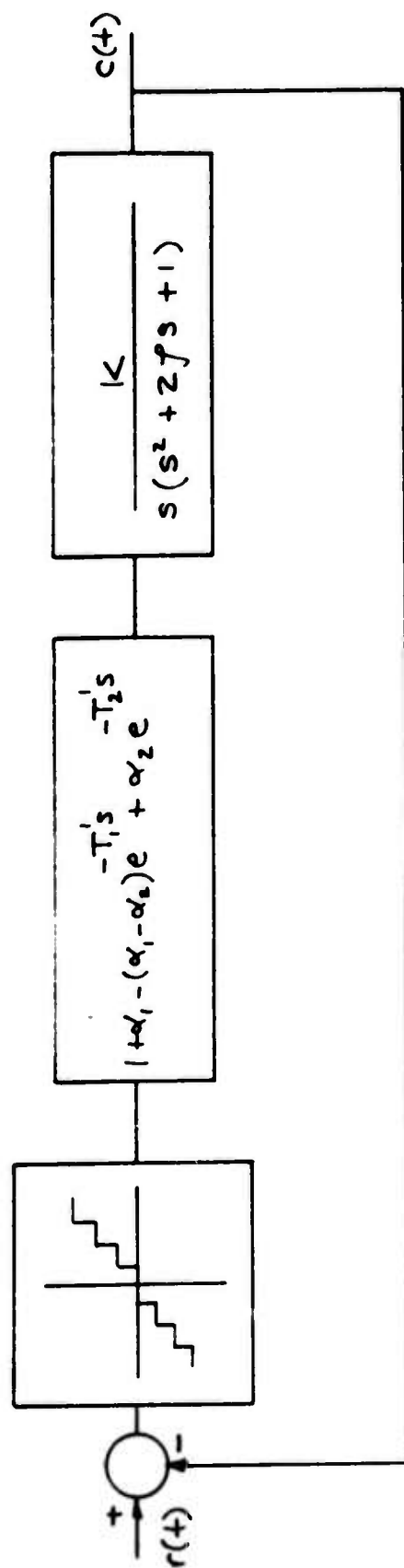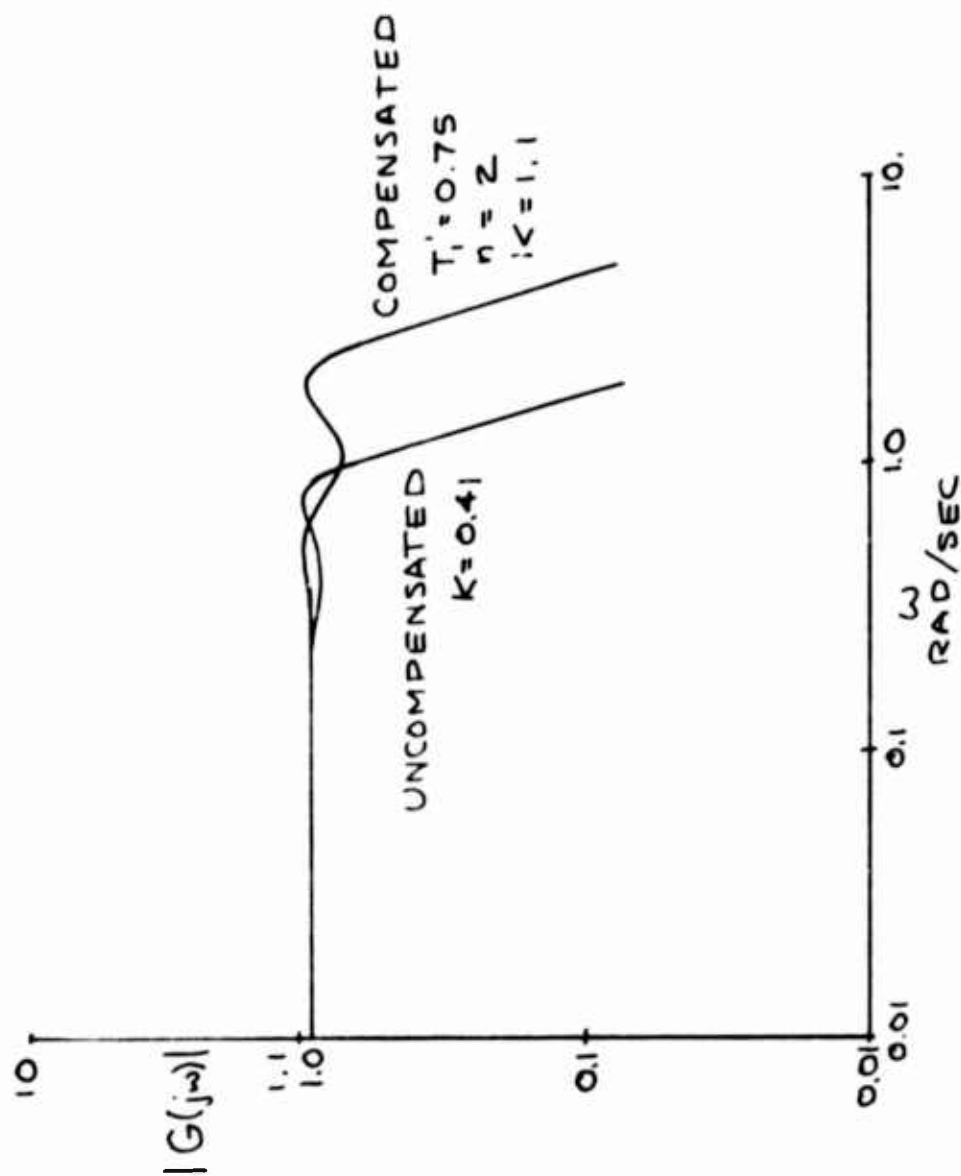
23. RESONANT THIRD ORDER SYSTEM WITH COMPENSATION

24. CLOSED LOOP AMPLITUDE BODE PLOT OF THIRD ORDER SYSTEM - PULSE HEIGHT OF 2 TIMES QUANTIZER STEP SIZE (n=2)
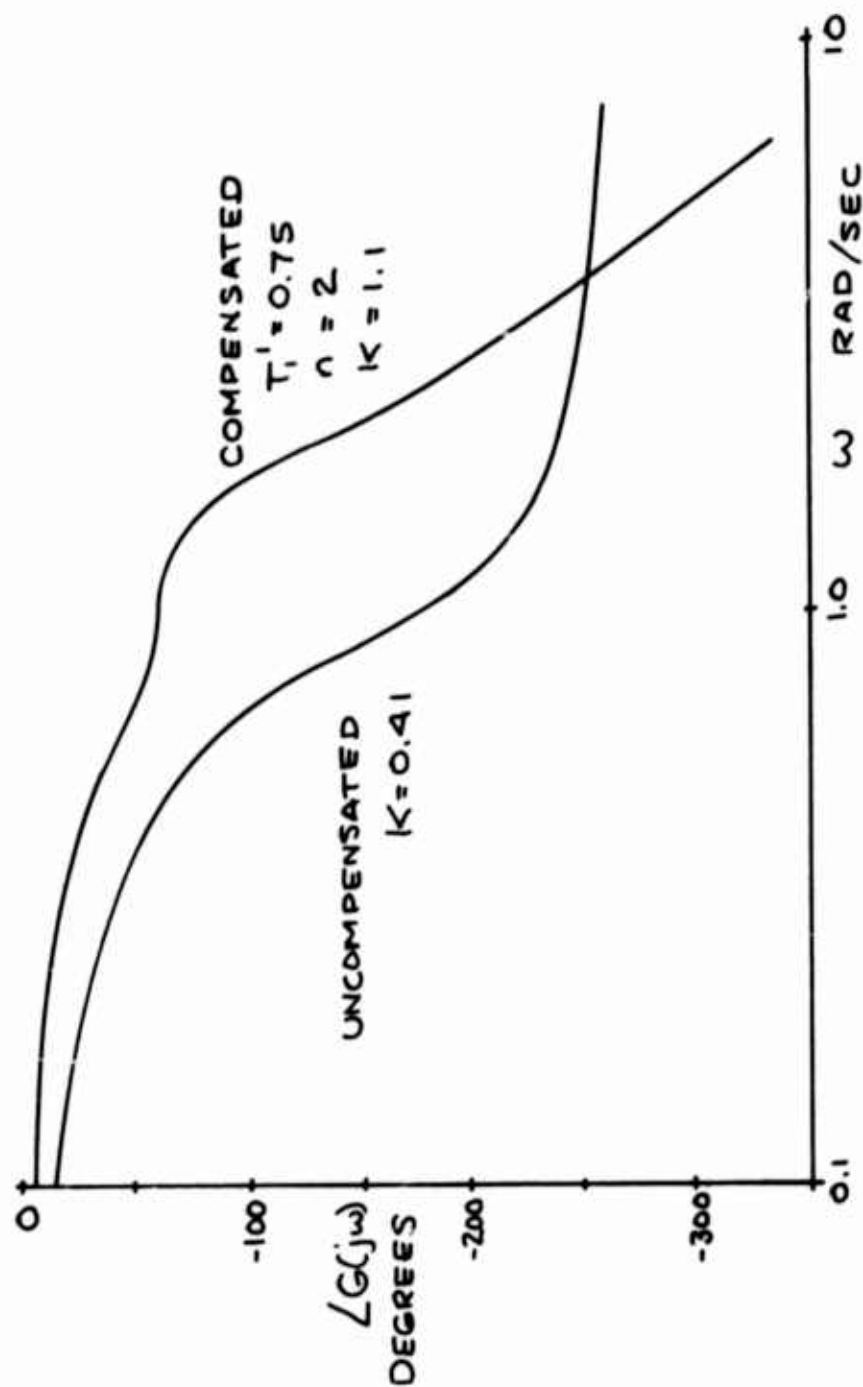
25. CLOSED LOOP PHASE ANGLE BODE PLOT OF THIRD ORDER SYSTEM-PULSE HEIGHT
OF 2 TIMES QUANTIZER STEP SIZE (n=2)
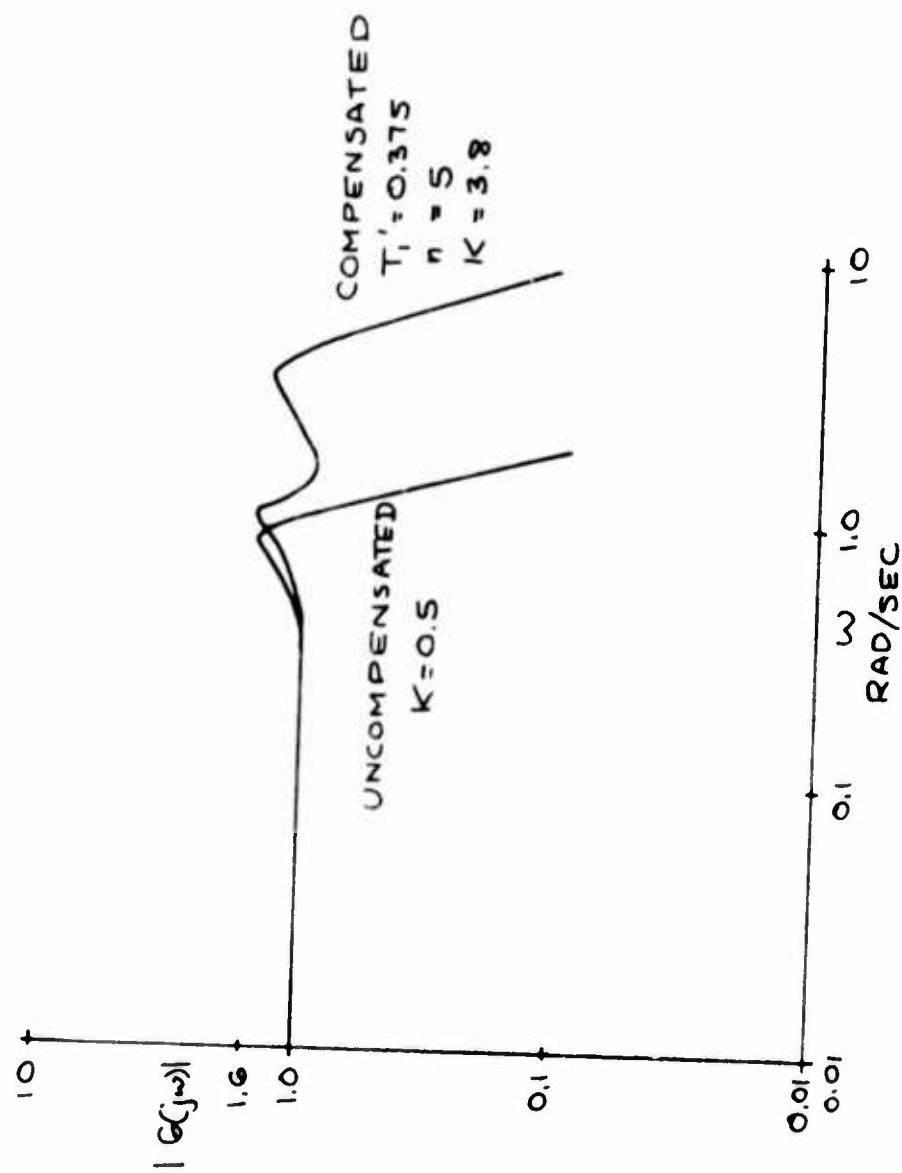
26. CLOSED LOOP AMPLITUDE BODE PLOT OF THIRD ORDER SYSTEM—PULSE HEIGHT OF
5 TIMES QUANTIZER STEP SIZE (n=5)
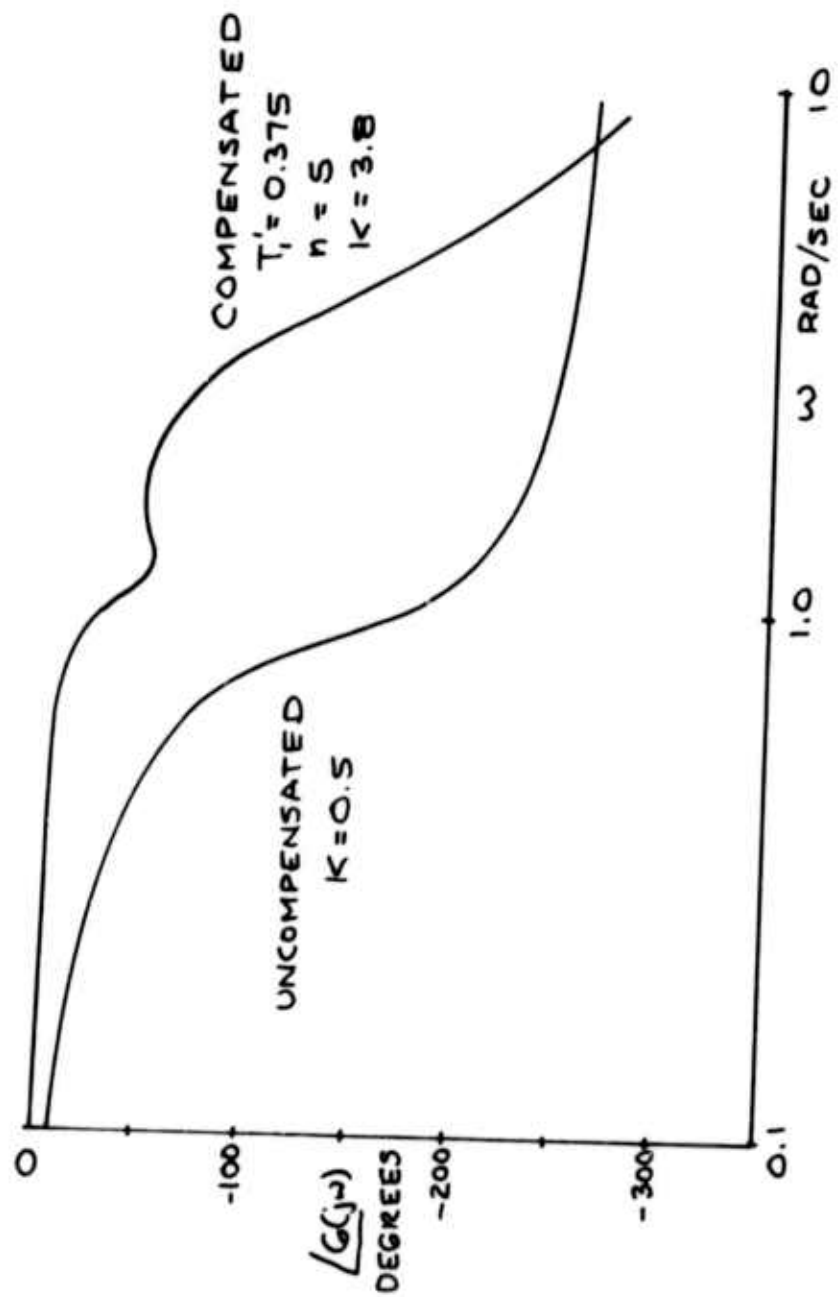
27. CLOSED LOOP PHASE ANGLE BODE PLOT OF THIRD ORDER SYSTEM-PULSE HEIGHT OF 5 TIMES QUANTIZER STEP SIZE (n=5)

28. CLOSED LOOP AMPLITUDE BODE PLOT OF THIRD ORDER SYSTEM-PULSE HEIGHT OF 20 TIMES (MANTISSA STEP SIZE (n=20)
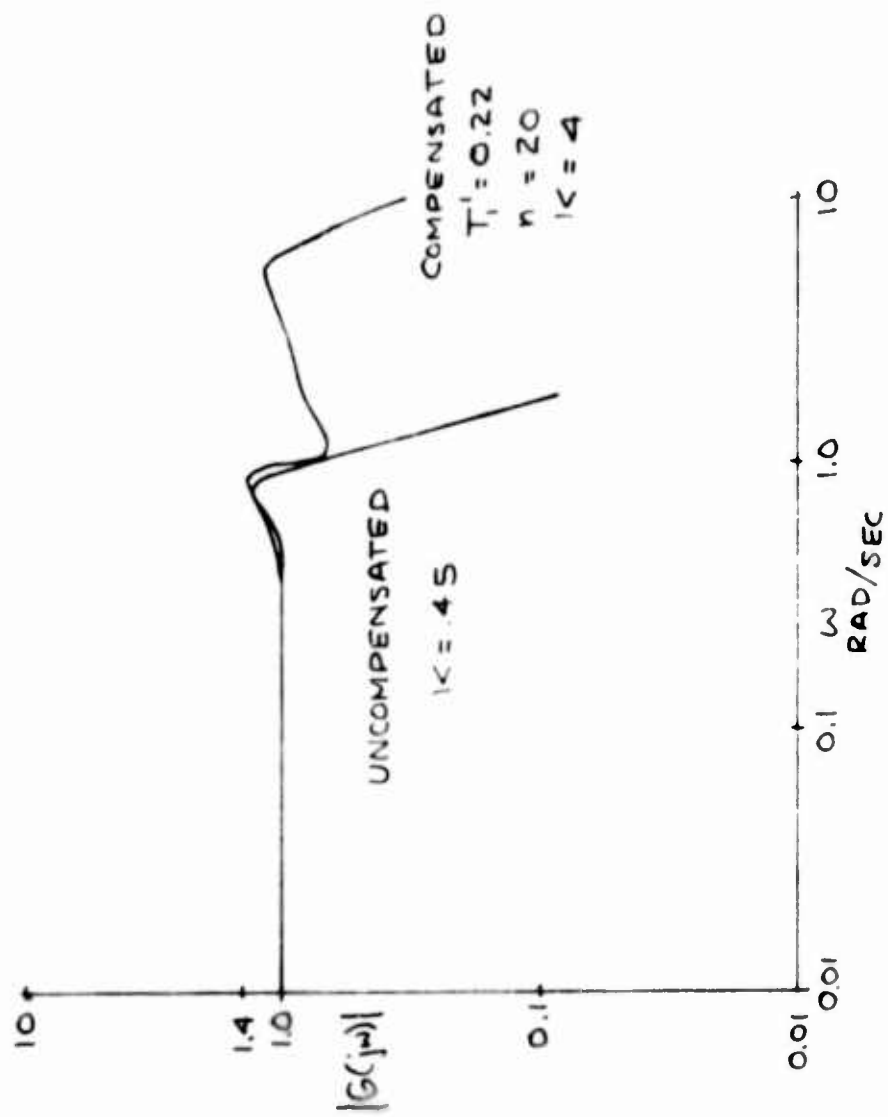
29. CLOSED LOOP PHASE ANGLE BODE PLOT OF THIRD ORDER SYSTEM-PULSE HEIGHT
OF 20 TIMES QUANTIZER STEP SIZE (n=20)
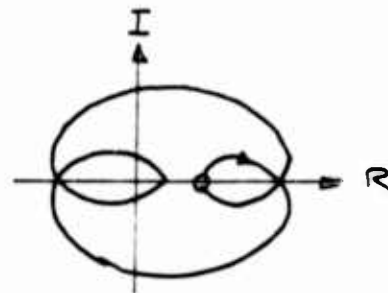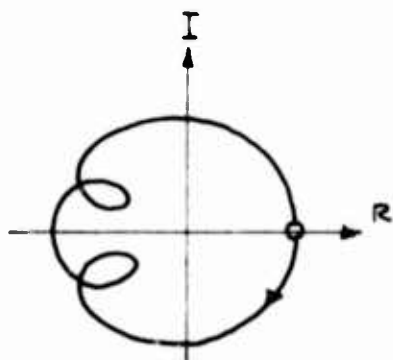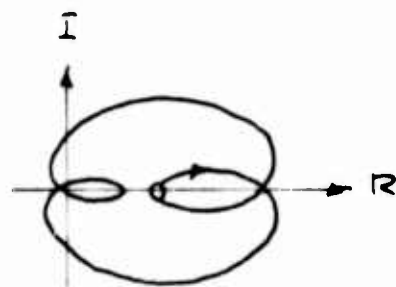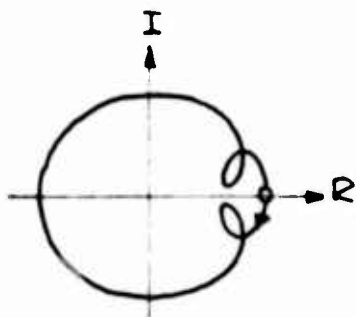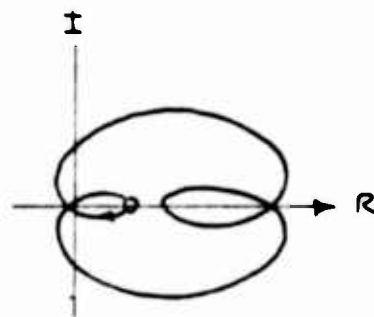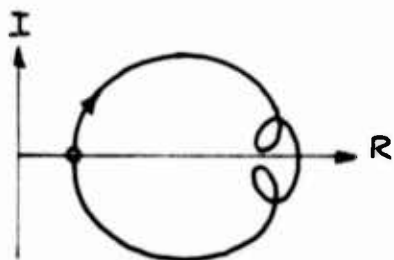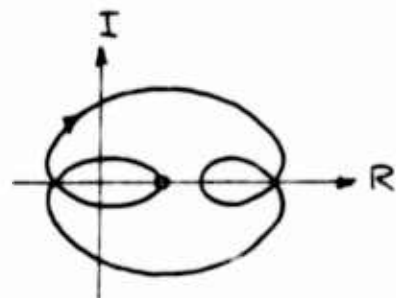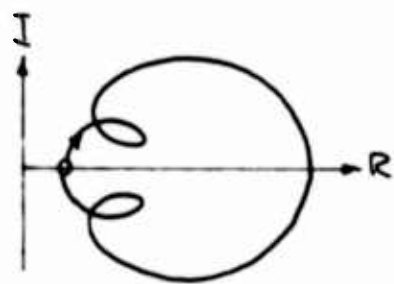
30. FREQUENCY RESPONSE FUNCTION POLAR PLOT FORMS FOR THREE PULSE COMPENSATOR
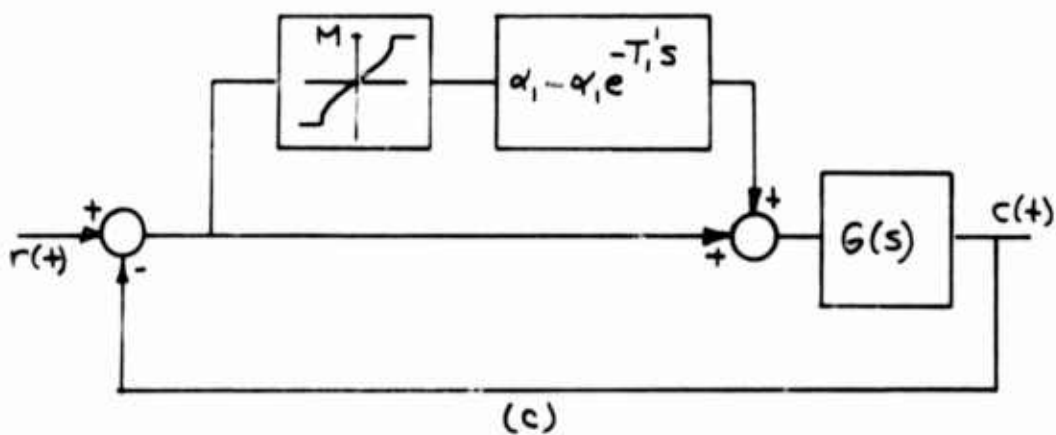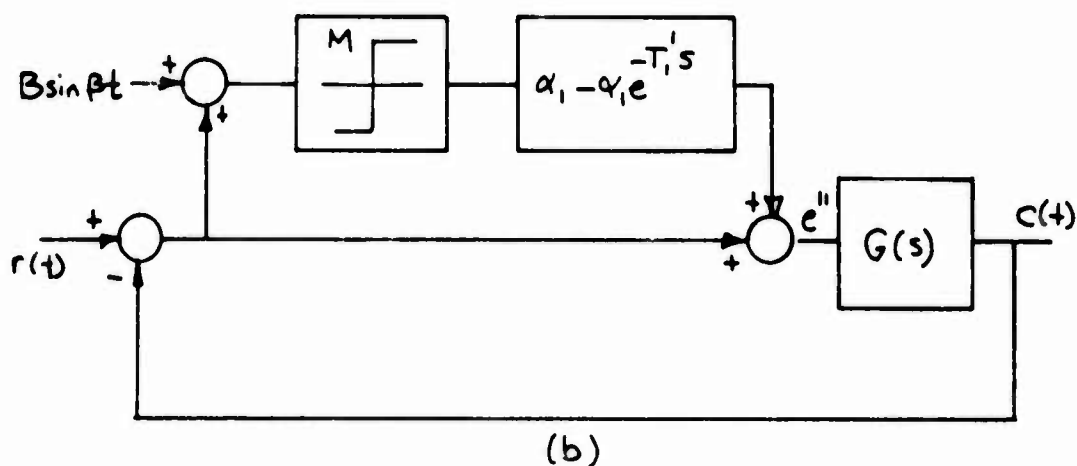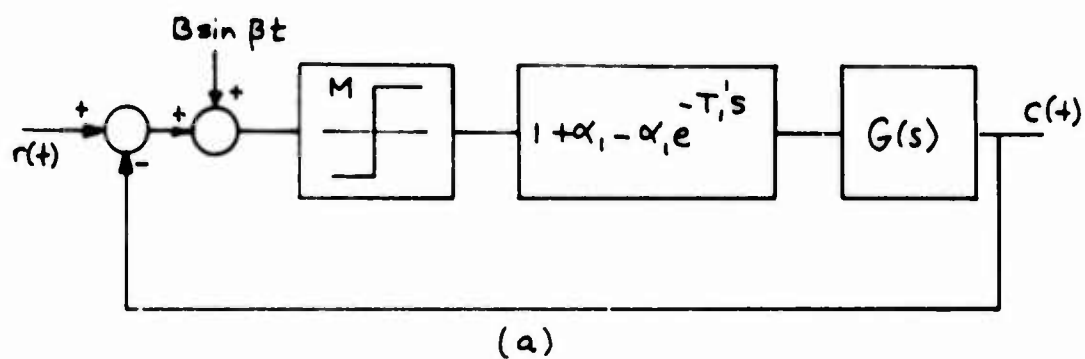
31. EVOLUTION OF COMPENSATOR WITH REDUCED OUTPUT RIPPLE
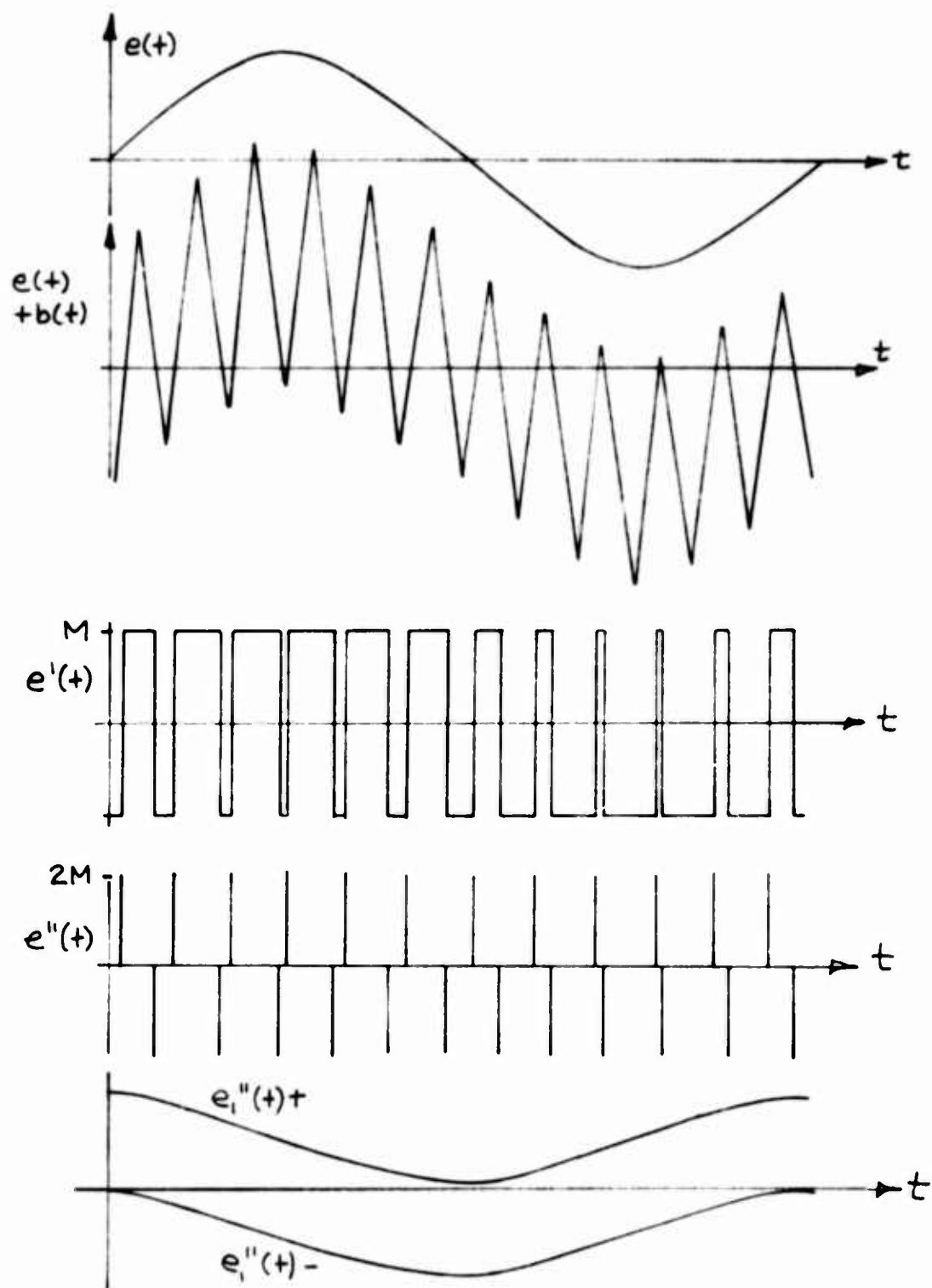
32. DITHERED QUANTIZER AND COMPENSATOR WAVEFORMS WITH SINUSOIDAL INPUT
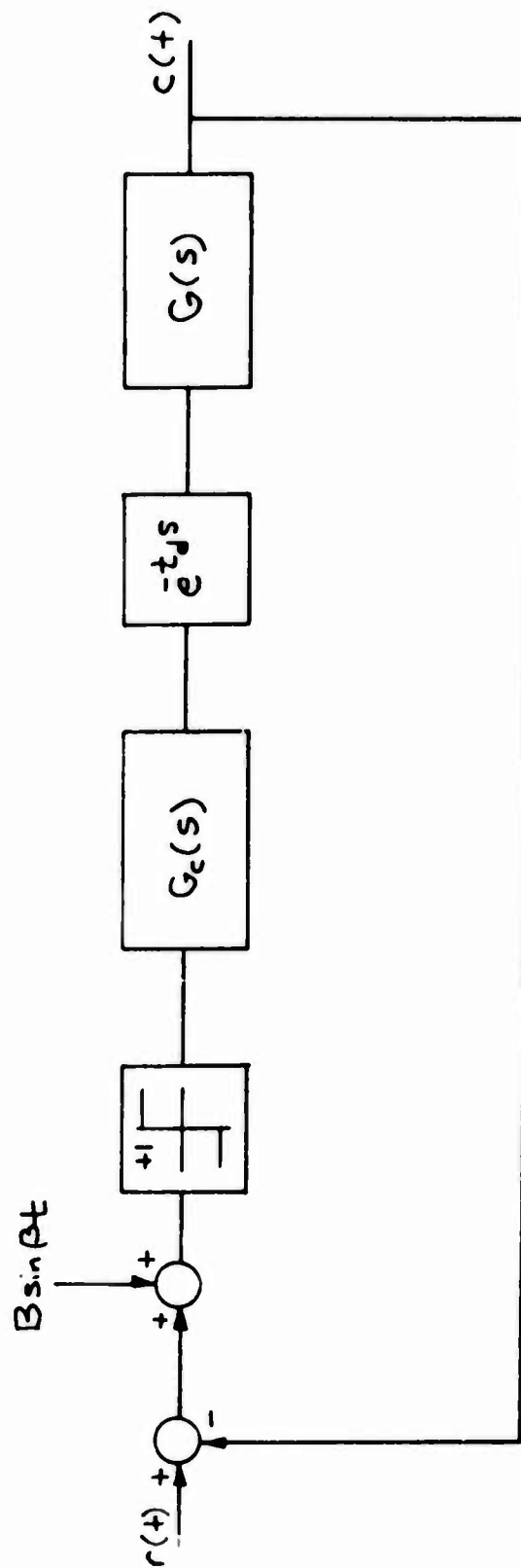
33. COMPENSATED SYSTEM SHOWING TRANSPORT DELAYS DUE TO COMPENSATOR HARDWARE

$$G_c(j\Omega) = e^{-j t_d \Omega / T_1'} \left[1 + \alpha_1 - (\alpha_1 + \alpha_2) e^{-j\Omega} + \alpha_2 e^{-j T_2' \Omega / T_1'} \right]$$

$$\text{WHERE}: \quad T_2' = 2T_1', \quad \alpha_1 = \alpha_2 = 5$$
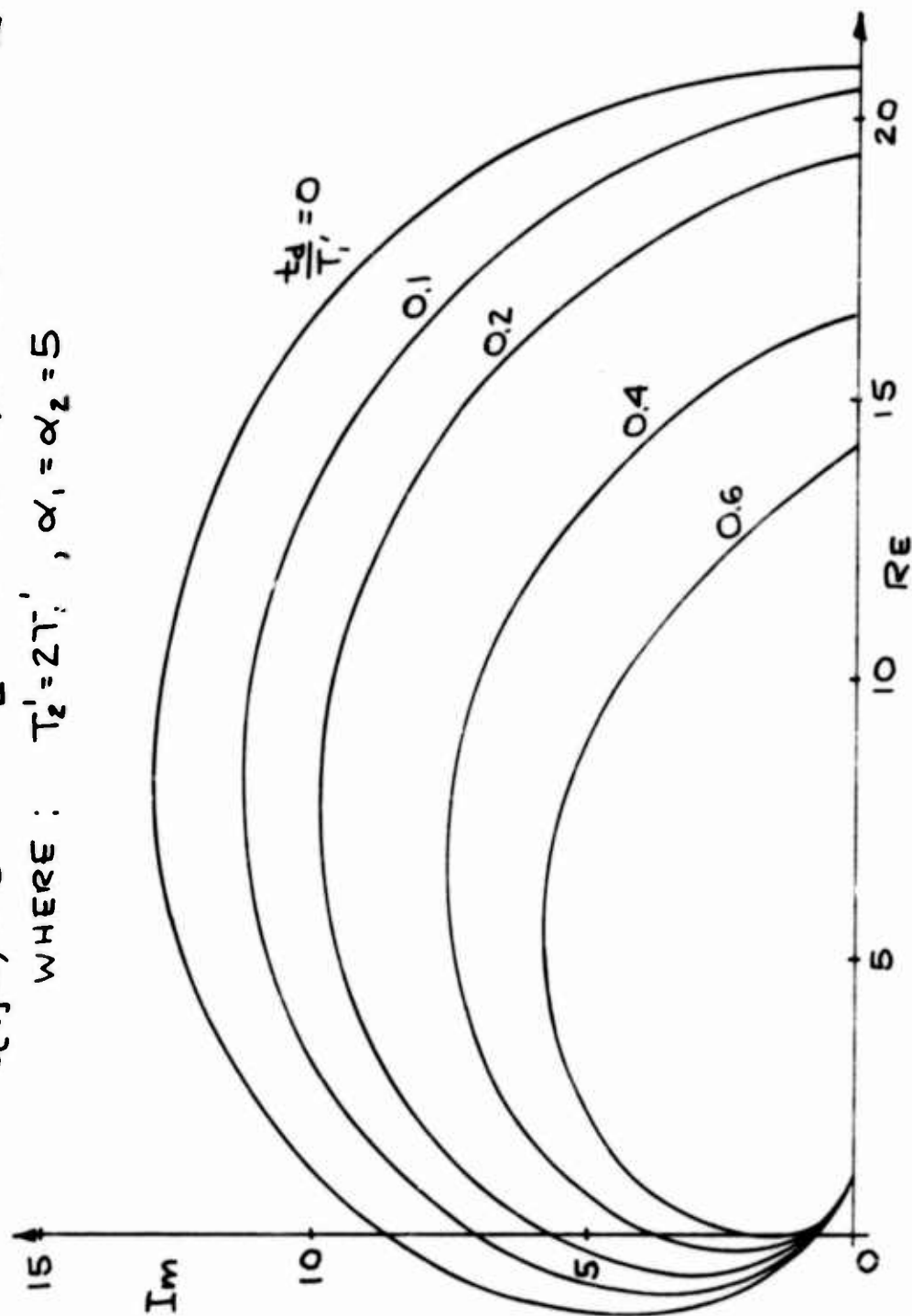
34. EFFECT OF TRANSPORT DELAY ON TWO PULSE COMPENSATOR POLAR PLOT

92
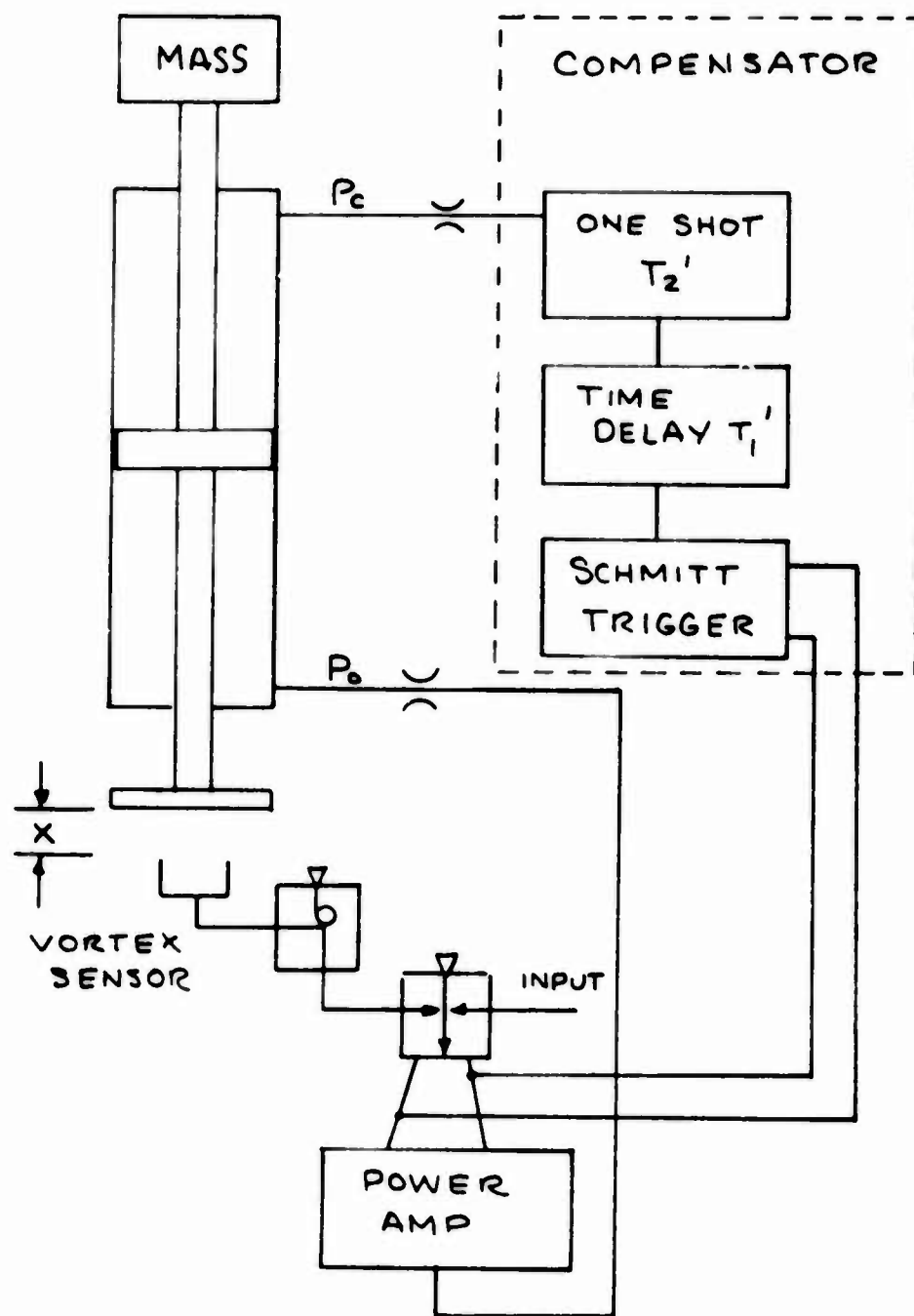
35. FLUIDIC POSITION CONTROL SYSTEM WITH RESONANT COMPENSATOR
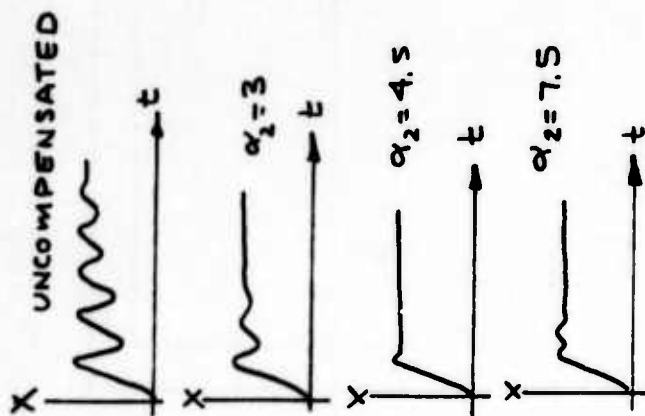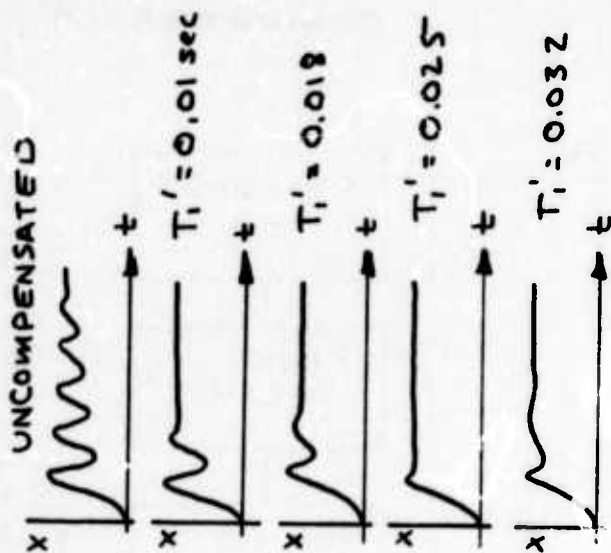
36. RESONANT SYSTEM STEP RESPONSES WITH CHANGES IN SECOND PULSE AMPLITUDE α_2 AND FIRST PULSE DURATION T_1'

Regenerative Process-Fluid Switching Circuits

J.R. TIPPETTS, B.Sc.Eng. Ph.D.

Department of Chemical Engineering and Fuel Technology,
University of Sheffield, Sheffield.

Summary

Useful new hardware and theoretical insight have evolved from the study of process-fluid switching in "regenerative circuits". Such circuits may be applied in furnace air supply systems in which hot waste gas and cold incoming air flow alternately over regenerative heat-exchangers. Other potential applications are in toxic fluid pumping or filtration.

The circuit incorporates two sub-circuits:

1) an "alternator" (or inverter), and 2) a rectifier (full-wave bridge rectifier). In heat-exchange systems the rectifier must not allow flow to bypass the load (furnace) and several new devices have been constructed to meet this requirement. Six distinct types of active node-elements are identified which correspond to the six types of 3-terminal junctions in these circuits. 24 basic circuits are listed which result from combining these devices in different ways; many more circuits can be derived from the basic list. A form of duality is shown to relate alternators and rectifiers; in general an item of alternator-type is matched by a rectifier-type.

These topics give rise to questions of a general theoretical nature and within the confines of what may be termed "theory of Eulerian networks" certain definite answers are given. The power transmitting properties of 3-terminal elements are emphasized and an "indefinite" characterisation scheme is defined which concisely relates these elements to ideal network devices, such as gyrators and transformers, and to fluid systems such as pumps and aerofoils. Circuit design procedures are put in terms of "data transformations" which are analogous to matrix operations in linear circuit analysis.

Nomenclature

A, B, & C	Performance Parameters (Ratios of pressures).
a, b, c, & d	nodes in lattice network, Fig. 18.
C_p	pressure coefficient (Euler number).
d	diameter.
E	Non-dimensional pressure, Performance parameter of FJ and Bistable Amplifier.
$\overrightarrow{e}$	pressure difference, arrow goes from high to low.
F	function.
f	function.
G	Performance parameter (Ratio of pressures).
k	resistance coefficient of the form e/q^2.
K	ratio of resistance coefficients.
Q	non-dimensional flow.
q	flow.
Re	Reynolds number.
r	radius (independent polar coordinate).
s	radius (dependent polar coordinate).
T	Turndown ratio (Flow ratio).
u, v, & w	dependent terminal variables.
v	velocity.
X	Performance parameter for VA and RFVA.
x, y & z	independent terminal variables.
Z-state	Flow state in which all-but-two flow variables are zero.
α	Angle (independent polar coordinate).
β	Angle (dependent polar coordinate).
Θ	Angle (independent polar coordinate in an indefinite system).
$\emptyset$	Angle (dependent polar coordinate in an indefinite system).
μ	Multiplier.
υ	kinematic viscosity.
ρ	density.
η	efficiency (ratio of powers).

Subscripts

a, b & c) x, y & z)	terminals of a 3-terminal device).
L	load.
m	maximum.
o	reference value. Output.
r	function defining r.
s	supply. Function defining s.
β	function defining β.

Abbreviations

A-RFD	Alternator type Reverse Flow Diverter.
CSV	Coanda-Switched Vortex device.
CSVRFD	a specially designed vented CSV.

96

DT	Tee joint connecting two diodes.
FJ	Flow Junction, a special Y-joint.
JPD	Jet-pump-diode, a jet pump with a diode.
R-RFD	Rectifer-type Reverse Flow Diverter.
RFDVA	Reverse Flow Diverting Vortex Amplifier, a specially designed vented VA.
VA	Vortex Amplifier.

Introduction

This paper concerns the application of fluidic (no-moving-part) techniques to the control of flow in networks. The fluidic devices are regarded primarily as process-fluid handling valves and this role makes special demands of theory and hardware that are not encountered in pure information-switching systems (logic). In this context, fluidics can be related to electronics and it is to be expected that a theory of fluidic networks must exist which is, to some extent, distinct from fluid dynamics in the same way that electrical network theory is distinct from electron dynamics. There is some justification for this because there are relationships and techniques of design and analysis which are uniquely useful in fluidic circuits but which depend only on the most elementary aspects of fluid mechanics. Needless to say, the comprehensive design of a fluidic (or any) system requires a wide range of already well-understood engineering science; here only the special factors which apply to fluidics are emphasized.

These topics arise almost inevitably in connection with "regenerative circuits", the study of which has resulted in new devices and general design methods which are already being used in a wider field.

Regenerative Networks

The network shown in Fig. 1. represents the path taken by process fluid in a regenerative system. Its significance is made clear by considering a furnace air supply system with regenerative pre-heating. The "regenerators" are regenerative heat exchangers, which could be stacks of metal plates. The "load" is a furnace in which the heated air is burnt with fuel (not shown) and hotter waste gases are produced; the flow in the furnace is steady and unidirectional. The "source" represents a steadily operating air blower; it also represents the chimney and the "connection", by way of the atmosphere, to the blower. The "alternator" and the "rectifier" are flow switching circuits which cause hot waste gases and cold incoming air to alternate in the regenerative heat exchangers.

This application of fluidic switching was envisaged by Swithenbank and Taylor (Ref. 1.) and various aspects of the design of such systems have been described in Refs. 2, 3 and 4. The advantages to be gained with fluidic switching are:-

1) Valves which do not wear out at high operating frequencies.

2) Reduced size of heat exchangers resulting from 1.

3) Reduced cost resulting from 1 and 2.

4) More applications, thus saving heat.

Regenerative flow switching circuits of this type may have many other applications however:

The alternator is equivalent to a directional control valve; it is a circuit able to cause a piston to reciprocate.

The rectifier ideally acts as a full-wave bridge-rectifier converting alternating source flow into unidirectional load flow.

The alternator and rectifier can be used separately or in conjunction with conventional (moving part) circuits. A method of pumping abrasive or "difficult" fluid with air is shown in Fig. 2. Here the switching circuits are represented as 4-terminal networks and the load is simply the head difference between the two reservoirs. The regenerative elements are "gas-pistons" - simply vertical cylinders in which alternating gas pressure drives the liquid up and down. Hence, the circuit enables a steadily flow-ing easily-pumped fluid to induce a relatively steady flow of a hard-to-pump fluid.

A pumping system in which all of these elements are identifiable was described by Walkden and others Refs. 5. and 6. and it enabled molten salt at 1500°K to be pumped by air pressure. Walkden's "Alternator" was electromechanical but the "rectifier" was basically a jet-pump with two driving jets to which the alternating flow was applied.

Various other applications for these systems can be envisaged depend-ing on the type of regenerative elements used, several types of which are shown in Fig. 3. The diaphragm, or a series of gas-pistons, allows pumping energy to be communicated through a pressure vessel. A pressure amplifying system results from the double-area rams, and a self-cleaning filtration system can be devised by using filterscreens which are washed-clean by reverse flow.

Criteria of Merit

Many types of circuit can be made so it is useful to have criteria by which they can be judged.

"Flow control" implies that the fluid must take a prescribed path; such is the case in the rectifier used in the furnace system. Here, no heat-carrying air must by-pass the load (furnace) nor must flow be recycled through it, as can happen in some fluidic circuits. This can be described as a "no-leakage" criterion.

The running cost of a circuit is determined by a suitably defined "efficiency" η. In some cases it is possible to maximise the efficiency by judicious circuit design. In the case of a pump supplying a known, fixed load, efficiency can be simply defined and it is a direct measure of the merit of the circuit, but if the load is variable or unknown the merit will depend on various characteristics of the circuit.

Scope of the Analysis

The analysis concerns the steady-state operation of systems of chara-cterised devices with incompressible non-cavitating flow. It is, therefore, subject to some obvious, but quantifiable, restrictions, however, recent experience has shown that such analysis is useful. As a result, the cir-cuits are considered to be "Kirchhoffian non-linear networks" which have been studied extensively, for example by Chua (Ref. 7.). Such studies are

comprehensive and very general but they are mainly carried out in the context of electrical networks. Fluidic networks are distinct, however, in that a "similarity" condition (described later) applies which can greatly simplify the analysis. Also many fluidic devices are "active" in a special sense which distinguishes them from pipe-networks and from many circuits using semi-conductor electronic devices.

These special features can be conveniently described in terms of an idealized "3-terminal device" which can represent a vortex amplifier, tee-joint, or a large number of fluidic devices. The following discussion is therefore slightly abstract, but this is necessary in order to derive concise general statements which apply to the numerous devices and circuits which are useful in controlling flows.

3-terminal Devices

A 3-terminal device, having 3 pipe-connections, is representative of many fluidic devices and it may also be used as a basic unit of sub-division for more complex circuits.

The objective considered here is the determination of the device operating point from characteristics defined by the continuous variables. Boolean or logical variables are sometimes necessary in characterising devices with multi-valued characteristics such as bistable amplifiers but a change in the value of the logical variable simply means a repetition of the procedures described in the following.

In finding the operating point these factors are important:

Three flows (q) and three pressure differences (e) are the terminal variables as shown in Fig. 4a.

If it is Kirchhoffian (using the "zero-sum" allocation of variables):

$$q_a + q_b + q_c = 0$$
$$e_a + e_b + e_c = 0$$

...... (1)

also the power dissipated in the device is given by any of these expressions.

$$\begin{vmatrix} e_a & q_a \\ e_b & q_b \end{vmatrix} = \begin{vmatrix} e_b & q_b \\ e_c & q_c \end{vmatrix} = \begin{vmatrix} e_c & q_c \\ e_a & q_a \end{vmatrix} \quad ...... (2)$$

A single operating point can be described adequately by a minimum of four suitably chosen "characterisation variables" which are denoted by x, y, u and v. These can be allocated in 21 ways. x and y denote independent variables and these can be allocated in 30 ways, 6 of which are homogeneous allocations (x and y both pressures or both flows). Any 2 variables can identify uniquely an operating point. At any operating point, four partial differentials completely describe a local linearization of the characteristics:

$$\left.\frac{\partial u}{\partial x}\right|_y \qquad \left.\frac{\partial u}{\partial y}\right|_x \qquad \left.\frac{\partial v}{\partial x}\right|_y \qquad \left.\frac{\partial v}{\partial y}\right|_x \qquad \cdots\cdots (3)$$

(representing gains, impedances, admittances, etc. depending on how x, y, u and v are allocated to flow and pressure variables)

The characteristics can be regarded as a useful range of operating points listed systematically by imposing constraints on the independent variables. Consequently the operation of a device may be described in many different but equally valid ways dependent on these artificially imposed allocations of:

1. Signs to variables.

2. Characterisation variables.

3. Independent variables.

4. Constraints.

The effect of changing any of these allocations greatly affects the appearance and utility of the characteristics but the effect is always predictable.

The re-allocation of **signs** and of certain characterising variables depends on simple linear relationships. For example, the zero-sum designation of pressures is useful in emphasising certain general features and in programming but for many purposes it is convenient to use a "2-port" format as shown in Fig. 4b. in which one terminal is chosen as a datum. The datum terminal can be chosen in three ways and Table 1. shows the values of the pressure variables (primed) in the 2-port format in terms of those in the zero-sum format (entries in the table)

		2-port variables		
		e'_a	e'_b	e'_c
datum	a	$*$	$-e_c$	e_b
terminal	b	e_c	$*$	$-e_a$
	c	$-e_b$	e_a	$*$

Table 1.

The ability to determine easily the effect of re-allocations 3 and 4 can be regarded as the essence of circuit analysis. In a linear system this is accomplished by standard matrix methods. Thus, device characteristics in one format (impedance, admittance or hybrid) can be converted into any other format to suit the circuit topology (series, parallel or hybrid). This applies, of course, to local linearization of non-linear systems and Shekel, Ref. 8, has described simply-applied routine methods.

The significance of "constraints" can be understood by analogy: consider linear dynamic systems; these are usually characterised by their response to sinusoidal functions, i.e. one of the independent variables is constrained by a sine function. The Laplace transform determines the effect of changing the constraint algebraically.

In fluidic systems subject to Eulerian similarity, the analysis can be partly accomplished algebraically by formulas ("data transformations") that apply to all devices. Also, certain characterising functions can be defined which are invariant with respect to the constraints and concise "large signal" parameters can be defined which complement the small signal linearizations which feature so much in electrical circuit analysis.

These topics are next discussed in detail for conditions of ideal Eulerian similarity. The results also apply to quasi-steady dynamic conditions; also quickly converging iterative solutions can be deduced in terms of the ideal even when only moderate similarity applies. When similarity does not apply and the system is completely non-linear or if detailed dynamic response must be predicted, the analysis becomes the province of programming and mathematical modelling - subjects which are receiving much attention elsewhere.

Eulerian Similarity

The consequences of similarity can be explained easily by using an extension of Paynter's (Ref. 9.) characterisation of turbo-machines (pumps and turbines). For this it is simplest to consider a device characterised by two homogeneous independent variables x and y. An operating point is represented by a point in the x y plane and a corresponding point in the u v plane. These points can also be located by polar coordinates αr and βs as shown in Fig. 5. The polar representation and associated functions are useful for conceptual purposes but ultimately they must be put in cartesian form.

Characterisation concerns the mapping of points in the x y plane to points in the u v plane. To simplify the representation of the mapping, constraints may be imposed on x and y by means of a functional relationship which may be defined by $r = f_r(\alpha)$; also an auxilliary function $\beta = f_\beta(\alpha)$ may be defined. A curve $r = f_r(\alpha)$ in the x y plane therefore maps into a curve $s = f_s(\beta)$ in the u v plane and the point-by-point correspondence is specified by the function $\beta = f_\beta(\alpha)$.

Eulerian similarity is characterised by

1. Radial lines in the x y plane map into radial lines in the u v plane.

2. Two points αr_1 and αr_2 on the same radial line in the x y plane map into two points βs_1 and βs_2 on the same radial line in the u v plane. and their radial positions are related by

$$\frac{s_2}{s_1} = \left(\frac{r_2}{r_1}\right)^n \qquad (4)$$

where n = 2 if r represents flow (and s pressure); and n = $\frac{1}{2}$ if r represents pressure (and s flow).

Also, if there is a change in the fluid density or the size of the device, for a fixed value of α, the effect is easily predictable.

This form of similarity is expected in ideal flows dominated by inertial forces as considered by Euler in his conception of turbomachines. But it is a fortuitous characteristic of many flows that turbulent shear stress is generated in such a way that the same form of similarity still prevails in real systems. The extent to which this is true must, however, be determined by experiment. (The range of validity can be put in terms of Reynolds number, Mach number, Cavitation number, etc.).

Three fluid systems which are subject to Eulerian Similarity may be compared:

	System	Representative of	
1	Centrifugal pump	2-port elements	} internal
2	Vortex amplifier	3-terminal network elements	} flows
3	Aerofoil	Field-controlled elements (external flows)	

Characterising variables may be allocated as follows:

	Independent variables		Dependent variables	
	x	y	u	v
pump	flow	shaft speed	pressure	shaft torque
VA	control pressure	supply pressure	control flow	supply flow
	α	r	u	v
Aerofoil	angle of attack	air velocity	lift force	drag force

The three systems have a basic feature in common: they depend on two flow-like and two pressure-like variables. There are differences in detail: for the aerofoil, "air velocity" is idealized as "velocity at infinity v_∞"; for the pump or the VA the idealization applies instead, to the pressures, which must be measured under well-defined conditions. (Variables appropriate to fields are different from those appropriate to networks).

Also, in a pump the shaft and the pipe connections cannot be interchanged, so although it has two energy-transmitting ports it cannot be represented as a 3-terminal device. Its characterisation is therefore subject to fewer "allocations" of variables.

Consequences of Similarity

When similarity prevails, the mapping of a single curve in the x y

plane is sufficient to determine the mapping of all points. Characteris-ation therefore involves three functions which in polar form are f_r, f_β and f_s. But it is the shape of these functions, not the magnitude, which is distinctive since the effect of changing r is easily predictable and is the same for all devices but the effect of changing α is a unique characteristic of a particular type of device. It is therefore convenient to standardize the magnitude in some way.

Numerous methods can be devised; for example, simple graphical tech-niques result from plotting virtually raw data on a double logarithmic flow-pressure plane as described in Ref. 10. For more general use it is convenient to define non-dimensional characteristics as in the following.

The function f_β is dimensionless already. The functions f_r and f_s can be represented as the products of non-dimensional functions F_r and F_s and certain characteristic reference magnitudes r_o and s_o:

$$f_r = r_o F_r$$
$$f_s = s_o F_s$$

(5)

The reference magnitudes r_o and s_o can be defined as the values of the functions f_r and f_s in a certain selected "non-dimensional reference states" denoted by α_o and β_o.

Characteristic Reynolds and Euler numbers (Re and C_p) can be defined in terms of r_o and s_o. Suppose, for example, that r represents flow and s pressure and d a characteristic diameter of a nozzle, say:

$$Re = \frac{vd}{v} \qquad C_p = \frac{2 s_o}{\rho v^2} \qquad \text{and } v = \frac{4 r_o}{\pi d^2}$$

(6)

A resistance coefficient k may also be defined which can be used to describe the effective size of a device in terms of the fluid variables:

$$k = \frac{s_o}{r_o^2}$$

(7)

k is simply a convenient combination of other more basic characteristics.

Obviously, non-dimensionalization is a further source of artifici-ally introduced complexity, however, the basic characteristics of a partic-ular device can be related to these non-dimensional functions:

1) $r = r_o F_r(\alpha)$ an independent constraint

2) $\beta = f_\beta(\alpha)$ a characteristic independent of F_r

3) $s = s_o F_s(\beta)$ a dependent characteristic

(8)

The distinctive characteristics of a device are therefore functions of a single variable α, and there are certain "invariant" characteristics f_β which are independent of the artificially imposed constraints.

The same factors can be observed in local linearizations which can be based on these partial differentials:

$$\frac{\partial \beta}{\partial \alpha} \qquad \frac{\partial \beta}{\partial r} \qquad \frac{\partial s}{\partial \alpha} \qquad \frac{\partial s}{\partial r} \qquad (9)$$

The first of these differentials is the gradient of $_1\beta$, the second is zero, the third can be put in terms of the gradients of f_β and F_s and the fourth is calculable from the similarity property.

Relationship to Cartesian Characterisation

The polar relationships emphasise some basic features but, in general, characteristics are most useful in cartesian form plotted on a flow-pressure plane.

Consider, for example, the vortex amplifier. The variables are defined in Fig. 6. A convenient reference state is when $q_c = 0$, and constraint: $e_s = \text{cons'ant} = e_{so}$ (represented by a horizontal line in the x y plane, Fig. 5.). Non-dimensional variables may be defined by

$$E_c = \frac{e_c}{e_{so}} \qquad Q_s = \frac{q_s}{q_{so}} \qquad Q_c = \frac{q_c}{q_{so}} \qquad (10)$$

and the two non-dimensional characteristics are F_s and F_c:

$$Q_s = F_s(E_c) \qquad \text{a transfer characteristic}$$

$$Q_c = F_c(E_c) \qquad \text{a driving-point characteristic.} \qquad (11)$$

These functions are shown in Fig. 6.

The polar functions are implicit in these characteristics, thus E_c is representative of α since $E_c = \cot \alpha$, also $\cot \beta = Q_c/Q_s$. A graph of ^cE_c against Q_c/Q_s is representative of the invariant function f_β. The partial differentials can similarly be inter-related and these are described in Ref. 11; here, however, the main objective is large signal analysis.

Performance Parameters

The "large signal" properties of a device can be concisely given by "performance parameters" defined in a few self-evidently significant states. The turndown ratio T and control pressure ratio G of a VA, defined as follows, are typical:

Name of State	Q_s	Q_c	E_s	E_c
"Normal" (N in Fig.)	1	0	1	X
"Vortex" (V in Fig.)	0	$\frac{1}{T}$	1	G

The entries in the table denote values of the variables non-dimensionalized in terms of Q_s and E_s in the normal state. X is a necessary, but less important, characteristic for the VA; also the ratio: T/G is an important

"power index".

Z-states

The normal and vortex states are "Z-states", defined when all-but-two terminals carry flow. The direction of flow is significant so a 3-terminal device has 6 Z-states.

In flow control circuits it may be necessary that all devices operate in Z-states, in which case analysis is simplified (see Ref. 12.). Furthermore, circuit operation may still be calculable if fluids of different densities flow in the circuit.

Parametric Characterisations

For theoretical or computational analysis it is interesting to consider various constraint functions.

Consider this constraint defined in terms of the parameter Θ:

$$x = r_0 \, \text{Sin} \, \Theta \qquad y = r_0 \, \text{Sin}(\Theta + \frac{2\pi}{3}) \qquad (12)$$

This is an ellipse in the x y plane. This subjects all independent variables to the same sequence of magnitudes. Furthermore, a change in Θ by $\frac{2\pi}{3}$ represents a re-orientation of the device in a network. This suggests another polar coordinate system in terms of Θr and ϕs in which 3 radial axes, one for each independent variable, intersect at $120°$ as shown in Fig. 7. The constraint is then a circle and Θ and ϕ take the place of α and β. If the zero-sum allocation of variables is used, certain general characteristics can be simply stated. For example, if $\varsigma = \phi$ or $\phi - \pi$ the device is lossless; also the characterising function s = constant (a circle) represents a 3-terminal gyrator, a device with useful general properties described later.

Other functions can be considered; for example, by an iterative computation the independent constraint function could be made identical to the dependent function, i.e. Fr = Fs. It could be argued that the resulting function is least dependent on changes of magnitude (which are predictable).

Also, for each device there may be a particular constraint Fr for which the characteristics are least affected by change of Re.

Data Transformations

The effect of changing the independent function can be determined by a "data transformation".

The characteristics can be regarded as a list of operating points and the basis of the "data transformations" are described here by operations on a single operating point.

The most important operation represents a radial shift of points in the x y and u v planes specified algebraically by:

106

original values	q_a	q_b	e_a	e_b
new values	μq_a	μq_b	$\mu^2 e_a$	$\mu^2 e_b$

Suppose the "original values" correspond to characteristics with q_a = constant = q_o and the "new values" are required for which e_a = constant = e_o. The multiplier must be such that $\mu^2 e_a = e_o$. This multiplication is carried out for each operating point, and, as a result, the characteristics can be said to have been converted from an impedance format to an admittance format. To regenerate the old values, μ is defined by $\mu q_a = q_o$. In the parametric representations, μ is a function of both q_a and q_b or e_a and e_b.

Other operations described in Refs. 4. and 11. determine the effect of resistances in series or parallel with a device.

Circuit Analysis

These types of relationship apply to Eulerian 3-terminal devices:

1) Linear (Kirchhoffian)

2) Square-law ("Eulerian")

3) Non-linear (two characterising functions of one variable, e.g. θ.

Only relationship (3) is different in different devices.

As fluid mechanics, these facts are unremarkable, but in circuit analysis they are highly significant. The two characterising functions can easily be stored (or, sometimes, calculated as described by Wormley, Ref. 13.) and manipulated by computer. For example, programs have been written in an interactive language (FOCAL) implementing various data transformations which analyse circuits simply and indicate the degree of extrapolation from test conditions implied by the analysis.

Also numerous graphical methods can be devised as described in Ref. 4.

Needless to say, the utility of this generalized analysis depends on the availability of hardware; this is now discussed.

The Existence and Non-Existence of Basic Network Elements

The regenerative elements shown in Fig. 3. are equivalent to certain basic network elements; the diaphragm is equivalent to series capacitance; the pressure amplifying ram is equivalent to a transformer. These two elements, and a third called a "gyrator", are frequently desirable but they are difficult or impossible to construct without using moving parts. Their elusive character can be explained as follows:

Series Capacitor

A rotating ring of fluid resists compression "elastically". Such a

ring, confined in a cylinder, would act as an elastic membrane separating a central terminal from a peripheral terminal.

Unfortunately, this has obvious shortcomings.

Pressure Amplifying "Transformer"

The essential characteristic of a flow amplifying transformer is also a characteristic of a jet-pump as indicated in Fig. 8. But, the jet-pump is non-reciprocal: it cannot be used as a pressure amplifier.

The existence of a complementary device to the jet-pump is discussed in Ref. 14. and it is concluded that it must depend on a rotating flow field maintained by the radial spread of vorticity from a central line-source. At increasing radial distance, pressure increases. This effect contrasts with that in a jet-flow in which flow increases at increasing downstream distance.

A practical embodiment of this effect has yet to be demonstrated.

Gyrator

The gyrator is a two-port element by which the roles of pressure and flow variables are interchanged. For example, a short-circuit at the output port is "seen" as an open-circuit in the input port.

As a 3-terminal element it has a flow-pressure modulating function which is basic in the same way that certain logic functions are basic (e.g. NOR, NAND, etc.) i.e. a large number of flow control networks can be synthesised with gyrators alone. It is therefore a desirable element.

In a vortex flow the orthogonal relationship of tangential velocity and radial force is a "gyrational" effect and as Paynter Ref. 9. has emphasized, it is strongly apparent in the characteristics of turbo-machines. The effect is also available to fluidics but peripheral jets seem to be the only practicable source of vorticity and these jets are therefore subjected to the vortex-generated pressure. This is analogous to an inevitable feedback which dominates the otherwise gyrator-like quality of vortex devices. (A simple model vortex device is represented in Table 2. by a gyrator plus losses and feedback). Clearly, a range of devices is needed since no single one corresponds to the ideal represented by the gyrator.

Two Distinctive Fluid-Dynamic Phenomena

Despite the elusiveness of "Pressure amplification", there is great scope for the evolution of new devices and in this context these two effects are noteworthy:

1) Jet-pump action occurs in many fluidic devices and this distinguishes them from simple electronic elements. The effect can be re-stated: a jet-pump can only be represented by interconnected branch-elements if one of these is "active" (i.e. acts as a pump).

2) Non-reciprocity is idealized mathematically in the gyrator, physically, however, it is strongly apparent in the difference between sink-flow into a nozzle and jet-flow from a nozzle as emphasized by Walkden, Ref. 6 .

Development and Classification of Devices

The development of new devices can be guided by some criteria which may be stated concisely in terms of the Θ-$\emptyset$ parameters. (Θ being used to denote a flow state, and $\emptyset$ for pressure).

It is desirable to have devices which are efficient for a wide range of Θ. The angular difference between Θ and $\emptyset$ is a measure of inefficiency and over certain ranges of Θ the "best device" is the one for which this is least. So, for operation over such ranges, optimality is easily defined, but, for operation over a wider range covering the "territory" of several devices, no simple generalization can be made.

A characteristic operating range (of Θ) may also provide a form of classification of devices, for example: a jet-pump belongs to the class of devices which carry out a useful function even when their "range" of operation is confined to a single value of Θ.

It would be premature to carry out an elaborate "classification" at present but the list of comparative performance parameters, shown later, is a step towards this objective.

Special-Purpose Flow Control Devices

Some special-purpose devices are next described. Their names emphasize their specific role, thus a "reverse flow diverter" is like a vent but must have very special properties. In many cases the devices were constructed from a "kit of parts": diffusers, housings, nozzles, etc. and further development would be justified. Also, planar and axi-symmetric configurations can be considered.

Some devices result from "merging" two existing devices to obtain a beneficial interaction.

Only the basic "Θ-dependent" characteristics are described. Eulerian similarity certainly prevails over a useful range but the detailed effects of Re variation have not been determined. "Pressure" represents total-pressure measured at points where the dynamic component is small compared with the greatest terminal pressure difference.

In the following "port" means pipe-connection (i.e. "terminal").

Flow Junction (FJ, Figs 9. and 28.)

The FJ is a symmetrical Y-joint specially designed for high efficiency in the two Z-states when flow enters ports a or b and all emerges from port o. Characteristics are shown in Fig. 10. with q_a constant. Non-dimensional variables, denoted by capitals, are defined in terms of

the values of e_a and q_a in the Z-state for which $q_b = 0$. A single performance parameter E is defined as e_o/e_a in this state. It is advantageous for E to be large and the best value so far is .67.

For a symmetrical device the characteristics apply also when a and b are interchanged, also, as a consequence, characteristics for which $Q_o > 2$ are redundant. The parameter E applies, therefore, to two states.

Reverse Flow Diverters (RFDs) Fig. 11.

RFDs operate in a "forward" and a "reverse" state; in the reverse state, flow in one port is reversed and the flow path through the device is different from that in the forward state.

Several types of RFD can be constructed to suit different circuits. Some of these are shown in Fig. 11. The desired performance of each type can be described in terms of the performance parameters A, B and C as defined in this table.

Type	State	q_a	q_b	e_a	e_b
X	Forward	1	1	1	A
	Reverse	0	-1	-C	B
A	Forward	1	1	1	A
	Reverse	0	-1	C	B
R	Forward	1	1	1	A
	Reverse	-1	0	-B	-C

For all RFDs, A, B and C are positive pressure ratios between 0 and 1; also A should be large and B should be small.

X-type RFD

In this RFD, the pressure at port a should be low in the reverse state, this simplies that C should be large. These requirements are consistent with this hypothetical application:

A pump supplies flow to a pressure vessel via an X-RFD operating in the forward state; if the pump fails, the RFD diverts the reverse flow from the vessel without impeding it but without applying back-pressure to the pump.

It may be useful in certain alternator circuits and several designs were tested by Holmes (Ref. 2.). In two of these, swirling flow and recovery in a radial diffuser was used as a diverting mechanism (not an impeding one).

Typical values of the performance parameters are

$$A = .41 \qquad B = .22 \qquad C = .3$$

however improved designs could undoubtedly be made.

Alternator Type RFD

This RFD is useful in alternators and the pressure at port a should be high in the reverse state so C should be large. An axi-symmetric design is shown in Fig. 11 (without swirl vanes); the radial diffuser helps to reduce pressure loss in the reverse state. The design and characteristics of an effective device are given in Ref. 2., typical performance parameters are

$$A = .66 \qquad B = .165 \qquad C = .15$$

Rectifier Type RFD (Fig 11.)

This RFD is useful in rectifiers; in the reverse state the pressure at port b should be high implying that C should be small. It consists basically of two diffusers; for optimum performance in Z-states the diffuser consituting port b should be the larger of the two.

Characteristics non-dimensionalized in terms of the forward Z-state are shown in Figs. 12. and 13. The forward Z-state occurs when $Q_b = 1$ in the forward characteristics, and the reverse Z-state occurs when $Q_a = 1$ in the reverse characteristics. The best parameters measured so far are

$$A = .69 \qquad B = .19 \qquad C = .01$$

Symmetrical R Type RFD

An R-RFD with equal diffusers is useful in rectifiers and pumping circuits but it is not primarily intended for Z-state operation and its Z-state parameters are worse than those of the R-RFD. The two diffusers can be regarded as two rather inefficient diodes but when they are embodied in the R-RFD they interact so that their diode-like action is enhanced.

Jet-Pump-Diode (JPD) Fig. 14.

The JPD (see Ref. 11.) is a merger of a jet-pump, designed like an R-RFD, and a diode. It is not intended for Z-state operation but it is able to operate at nodes b and c in rectifiers (see Fig. 18.) and may be compared with two interconnected diodes.

Coanda-Switched-Vortex Device + A Type RFD (CSVRFD) Fig. 14.

The CSVRFD is a specially designed vented CSV created by merging an A-RFD into the outlet of the vortex chamber of a CSV. It is not primarily intended for Z-state operation but it can be used at nodes b and c in alternators.

Only moderate performance has been proven but no special development has been carried out.

Reverse Flow Vortex Amplifier (RFVA) Fig. 15.

The RFVA, described in Refs. 15, 16, 17, is a VA designed to give

minimum resistance to flow passing the wrong way through it. It is useful in the branches of rectifiers; its Z-state performance parameters are defined by

State	Q_a	Q_c	E_a	E_c
Normal	1	0	1	-X
Vortex	$-\dfrac{1}{T}$	$\dfrac{1}{T}$	-1	G

T, G, (1-X) and the ratio T/G, have the same significance as for the VA. It can be expected that comparable values can be achieved for the RFVA.

Vented RFVA Figs. 15. and 28.

The swirling control flow can be extracted, with some pressure recovery, from the RFVA by adding a vent in the form of a radial diffuser. A main stream can therefore be halted without a large volume of control fluid entering the system and, in principle, with the least loss of energy. In this respect, the vented RFVA is potentially superior to other comparable sub-circuits in which control flow is substituted for main flow. (This applies, by analogy, to vented VAs).

The main attributes of this device have been proven but further development would be worth while.

Vortex Amplifier + A-RFD (RFDVA) Figs. 16. and 28.

The RFDVA is a specially designed vented VA created by merging an A-RFD and a VA. A usefully effective design is described in Ref. 15. but it could be improved by incorporating a well designed VA section (such as Saunders' design Ref. 18.).

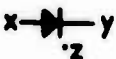Two Parallel-Connected Turn-up Vortex Amplifiers (Fig. 17.)
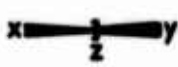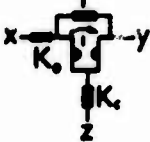
A special type of vortex amplifier can be constructed in which control flow cancels-out a vortex which is normally created by the main flow. Two such "turn-up vortex amplifiers" can be connected in parallel, as proposed by Boucher et al (Ref. 19.) to form a 3-terminal sub-circuit with uniquely useful characteristics. The combined devices can be used at one node in alternator circuits and for this application the following characteristics are important:

when the pressure at terminal a is high, the resistance to inflow at b is low (and vice-versa when a and b are interchanged) outflow is from o.

Comparative Performance Parameters

The "large-signal performance parameters" of several devices in one or two operating states are listed in Table 2. Each row describes a single operating point in terms of variables non-dimensionalized in terms of reference-state values. For each device, the reference state is the first state listed. The objective is to show concisely the relationship

Device	State	FLOW (q)			PRESSURE (e)			CURRENT FEASIBLE VALUES
		x	y	z	x	y	z	
Coanda Switched Vortex Device	normal	T	-T	0	0	-1	1	T = 5
	vortex	1	-1	0	0	-1	1	
Diode	forward	T	-T	0	0	-1	1	T = 10
	reverse	-1	1	0	0	1	-1	
Vortex Amplifier	normal	-T	T	0	1-X	X	-1	$\frac{T}{G}$ = 12
	vortex	-1	0	1	1-G	G	-1	
Reverse Flow Vortex Amplifier	normal	T	-T	0	X-1	-X	1	$\frac{T}{G}$ = 7
	vortex	-1	0	1	1-G	G	-1	
Bistable Amplifier	right	1	-1	0	E	-1	1-E	E = .47
	left	1	0	-1	-E	E-1	1	
Flow Junction	right	-1	1	0	1	E-1	-E	E = .67
	left	-1	0	1	-1	E	1-E	
A-type Reverse Flow Diverter	forward	-1	1	0	1	-A	A-1	A = .66 B = .165 C = .15
	reverse	1	0	-1	C	-B	B-C	
R-type Reverse Flow Diverter	forward	1	-1	0	A	-1	1-A	A = .69 B = .19 C = .01
	reverse	-1	0	1	-C	B	C-B	
CSVRFD	normal	-T	T	0	1	-A	A-1	T = 3 A = .5 B = .15
	vortex	T	1	-T-1	1	-B	B-1	
Jet Pump Diode	forward	T	-T	0	A	-1	1-A	T = 5 A = .5 B = .2
	reverse	-T	1	T-1	A	B	-1-B	
2 Parallel Connected TUVAs	right	-T-1	T	1	B-1	1	-B	
	left	-T-1	1	T	1-B	B	-1	
Symmetric R-RFD	right	T	1	-T-1	1	-B	B-1	T = .7
	left	T	-T-1	1	-1	1-B	B	B = 0
Ideal Transformer		1	-n	n-1	1	-n	n-1	n=turns ratio
		-1	n	1-n	1	-n	n-1	
Ideal Gyrator		-g	g	0	1	-1	0	g=conductance
		-g	0	g	1	0	-1	
Eulerian gyrator + losses and feedback (compare with VAs		-T	T	0	1-X	X	-1	$T=\sqrt{1/K_o +1}$ $G=1+K_c/(1+K_o)$ $X=1-1/K_o$
		-1	0	1	1-G	G	-1	

Signs and subscripts conform with zero sum format.

Comparative Large-Signal Performance Parameters.

Table 2.

113
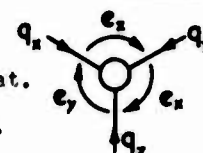
between flow and pressure states, so the zero-sum format is used for subscripts and signs.

Certain parameters have the same significance and the same ideal values for all devices as indicated here: T (∞), A and E (1), B (o) and G (1 or less, less implies pressure amplification).

Ideally for flow control applications a range of devices should be available which generate useful pressure states at various pairs of Z-states but because "pressure amplification" is unattainable this cannot entirely be achieved. The last four fluidic devices listed in Table 2. are subject to this restriction but they represent those devices which come closest to the ideal.

Included also in the table are the distinctive characteristics of the ideal transformer and gyrator.

Alternators and Rectifiers

These circuits can be considered separately, since they are only connected at two points in the regenerative circuit. They have an interesting dual relationship which may be observed in two electronic circuits: a 4-diode bridge rectifier and an inverter (i.e. alternator) using four semiconductor-controlled-rectifiers (TRIACs). The corresponding fluidic devices are diodes and CSVs but the dual relationship extends to other devices as shown in this list.

Class No.	Alternator Types	Rectifier Types
1	Coanda-Switched Vortex Device	Diode
2	Vortex Amplifier	Reverse Flow Vortex Amplifier
3	Bistable Amplifier	Flow Junction
4	A-type Reverse Flow Diverter	R-type Reverse Flow Diverter
5	CSV RFD	Jet Pump Diode
6	2-Parallel Connected Turn-up Vortex Amplifiers	Symmetrical R-type Reverse Flow Diverter
Integrated Circuits	Vented Bistable Amplifier and Pressure-Switch (Rimmer, Ref. 20.)	Integrated FJ-2-RFD Rectifier and Reciprocating Jet-Pump (Walkden, Ref. 6 .)

Other devices can be conceived by merging the listed devices; the integrated circuits represent the end result of certain mergers. One of these, described by Rimmer, Ref. 20., is notable because it has a very small pressure loss.

The devices are classified with a number to faciliate a concise listing of basic circuits from which any such mergers may be considered. The circuit list represents different allocations of devices to the

114

nodes and branches of the 4-terminal lattice network shown in Fig. 18. A steady pressure difference occurs across terminals a and d and alternating pressure across b and c. The circuit represents an alternator or a rectifier according to which types of devices are used.

Circuit Number	NODES			BRANCHES		Notable for
	a	b & c	d	1 & 2	3 & 4	
1				1	1	4-diode rectifier
2				1	2	
3				2	1	
4				2	2	4-VA Alternators
5	3	4				Simple no-leakage rectifier
6	3		6			FJ-Symmetrical-R-RFD rectifier
7		5				JPD pumping circuits
8	3				1	FJ-2-Diode rectifier
9	3				2	
10		4		2		RFDVAs for efficient alternators
11			6	1		
12			6	2		

List of Alternators and Rectifiers

Only symmetrical circuits with some special practical or academic significance are listed. An infinite number of circuits could be made by parallel or series combination of the listed circuits and devices, but it can be suspected that some of these are redundant. Hence, there is scope for theory to investigate the suspicion.

The main characteristics of the circuits can be expressed in terms of "supply" and "load" variables denoted by subscripts s or L. Also the efficiency η is important: $\eta = e_L q_L / e_s q_s$

and a load resistance coefficient k_L: $k_L = e_L/q_L^2$.

$$(13)$$

Branch-Element Circuits

The effectiveness of circuits of type 1, using four diodes or CSVs, depend entirely on the performance parameter T of the devices. For a fixed load, k_L, there is an optimum size for all four devices in order to maximise the efficiency. The maximum efficiency η_m and the optimum size ratio denoted by K are functions only of T as shown in Fig. 19. K is the low-resistance-state resistance coefficient divided by k_L. The flow ratio Q_1 plotted in Fig. 19. represents the flow leaking past the load via one of the high resistance devices divided by q_L; $2 Q_1$ represents the total leakage.

The maximum value of T for current CSVs is about 5 and the corresponding value of η (25%) represents a very poor alternator. The potential efficiency of rectifiers however is much better, but as one would expect, high efficiency is paid for in increased complexity: the best diodes appear to be "cascade" diodes (employing a series of swirl vanes in a pipe) and even using four of these, it seems that an efficiency of 50% would be difficult to achieve.

McGuigan and Boucher, Ref. 21., have obtained results for a rectifier using 4 vortex diodes which had a measured η_m equal to 30% and a potential η_m (at high Reynolds number) of about 40%.

In this type of rectifier, leakage must always occur for all practical designs of the diodes so it cannot be used directly in the heat exchanger circuit, however, it has a characteristic which makes it suitable in pumping applications when the load may be unknown or varying: when q_L diminishes to zero the value of e_L increases steadily to within a small fraction of e_s. The circuit serves as a "fluid coupling with a high stall torque".

Controlled Rectifiers with No-Process-Fluid Leakage

By adding tee-joints on either side of each diode in circuit 1 and supplying a suitable set of control flows, the "leakage flow" in each high-resistance branch can be substituted by control flow. The circuit therefore offers no leakage path for process fluid.

Here, it is useful to represent the circuits by rectangle diagrams (see Refs. 22. and 23.) as shown in Figs. 20. and 21. The height, width and area of each rectangle represent the pressure-drop, flow and power-loss in each branch of the circuit. The circuit in one state together with the rectangle diagram is shown in Fig. 21. and it is interesting to note that the missing "corners" of the diagram indicate that it has a potentially higher efficiency than the original 4-diode circuit. An efficient control circuit would be needed to take advantage of this.

The two-tee-joint-diode combinations can be replaced by vented RFVAs and, with well designed devices, both zero-effective-leakage and high efficiency (at least 50%) may be expected. The control flow circuitry is a complication but it would allow a degree of "adaptation" to take place to cope with varying load, (in order to maintain the no-leakage condition).

Alternators using Vortex Devices

The alternator of circuit 4 consisting of four VAs is of practical importance because an η_m of about 50% can be expected with current devices. This estimate is based on Z-state analysis described in Ref. 3. It would appear, however, that a well designed RFDVA would yield a simpler but efficient circuit. Two RFDVAs are needed and, in fact, circuits equivalent to this, using two vented VAs, have been investigated by other workers.

116

Flow Junctions in Rectifiers

An FJ can be located at node a and, if it is the correct size, and if the load is fixed, the leakage in the upstream branches of the rectifier can be eliminated. Another attribute is that the FJ is much simpler than the branch elements which it can replace so it is interesting to determine the effect of this replacement solely in terms of efficiency. A simple example is described next.

Redundancy of Circuits

The FJ is comparable to two other devices shown in Fig. 9: 1) a two diode tee-joint (DT) and 2) an FJ with diodes connected in series with its upstream terminals (FJD). By comparing the invariant functions of each of these devices, some of them can be shown to be redundant under certain conditions.

A suitable representation of the invariant function is a plot of $\frac{e_o}{e_a}$ against $\frac{q_o}{q_a}$ and this is shown for the FJ and for the DT (with various diodes characterised by T) in Fig. 22. Only symmetrical DTs are considered and their characteristics are calculated assuming ideal square-law resistance with T representing the forward-reverse flow ratio with a constant pressure drop.

The corresponding invariant function for the FJD can be put in terms of those of the DT and the FJ:

$$\left(\frac{e_o}{e_a}\right)_{FJD} = \frac{\left(\frac{e_o}{e_a}\right)_{FJ}}{1 + K} + \frac{\left(\frac{e_o}{e_a}\right)_{DT}}{1 + 1/K} \tag{14}$$

where $K = (e_a)_{DT}/(e_a)_{FJ}$

The factor K depends on the characteristics of the DT and the FJ, and on the relative sizes of the diodes and the FJ. This means that a range of FJD devices can be constructed by changing the relative size but the value of e_o/e_a for the FJD must always lie between the values of this ratio for the DT and the FJ. As the diodes are made relatively smaller, so their characteristics predominate in the FJD; if the DT had been connected in parallel with the FJ instead of the series connection the opposite effect would have occurred.

The redundancy of these circuits can now be stated:

For a fixed operating point-pair, denoted by a single value of q_o/q_a, an FJ or a DT should be chosen according to which has the higher value of e_o/e_a. Under these conditions a device such as the FJD is redundant.

When a _range_ of operating points must be covered, an FJD may be

useful. A judicious choice of relative diode size may yield an FJD optimally matched to the operating range.

Comparison of the characteristics on Fig. 22. shows, in particular, that the FJ is superior to <u>all</u> diodes for $q_0/q_a > 1$, over this range it exhibits the transformer-like action which is the special "active" feature of fluid-dynamic circuit elements. This type of analysis shows that it is advantageous to use an FJ-2-diode rectifier (Circuit 8) rather than a 4-diode rectifier if T for the diodes is less than about 8.

Comparison of Diode-Tee-Joint and a Symmetrical R-RFD

The invariant functions of the RFD and the comparable diode-tees are shown in Fig. 23., in terms of $\frac{e_y}{e_x}$ against $\frac{q_y}{q_x}$. In this representation, $\frac{e_y}{e_x}$ should be as small as possible and it is obvious that the embodiment of the diffusers into the RFD yields significantly better characteristics than the equivalent "diode"-tee using conical diffusers (for which T is about 2.5).

The FJ-Symmetrical-R-RFD Rectifier

This circuit (No. **6**.) shown in Fig. 24., is the simplest with which to describe some useful techniques of design and analysis.

Analysis

The characteristics of the circuit can be determined by using the data-transformations to put the FJ and RFD characteristics into a suitable form. These steps indicate the method.

1) The topology of the circuit means that a particular hybrid format is needed. A suitable allocation of variables is:

	independent		dependent	
	x	y	u	v
FJ	q_o	e_a	q_a	e_o
RFD	q_y	e_x	q_s	e_y
Circuit	q_L	e_s	q_s	e_L

2) The characteristics are put into the desired format. A suitable constraint is $y = \text{constant} = e_s$.

3) For each value of q_L (equal to q_o for the FJ and q_y for the RFD) find e_L and q_s by summation:

$$e_L = e_o - e_y$$

Graphs of e_L and q_s against q_L constitute the main circuit characteristics. At a certain value of q_L, the efficiency will be maximum for a given circuit; repetition of the procedure for different relative sizes of FJ and RFD would enable an overall optimum circuit design to be found.

Optimum Circuit Design

The circuit with maximum efficiency can be determined solely by considering the invariant functions of the two devices as shown here:

The efficiency can be expressed in terms of the device variables by

$$\eta = \frac{q_o (e_o - e_y)}{e_a (q_a + q_x)} \tag{15}$$

Noting that $e_a = e_x$ and $q_o = q_y$

$$\eta = \left(\frac{e_o}{e_a} - \frac{e_y}{e_x}\right)\left(\frac{q_a}{q_o} + \frac{q_x}{q_y}\right)^{-1} \tag{16}$$

Hence, η has been put explicitly in terms of the ratios which constitute the invariant functions and so η can be regarded basically as a function of the two dimensionless flow states of the FJ and RFD. By partial differentiation, the optimum states can be put in terms of the gradients of the invariant functions. The resulting maximum efficiency is about 28% with current devices.

Circuit 5

Vented Bistable Amplifier Alternator

The devices constituting this circuit can be merged to form a familiar form of Alternator: a vented bistable amplifier. The potential efficiency of an un-merged circuit operating in Z-states with no-leakage is simply determined as explained in Ref. 2., η equal to 24% was feasible. A measured maximum efficiency of 26% was obtained for a demonstration circuit not confined to Z-state operation. It is to be expected that by a careful merger of the three devices a more efficient integrated circuit would result.

No-Leakage-Rectifier (FJ-2-RFD Rectifier), Fig. 25.

This rectifier, supplying a fixed load, can be designed for Z-state operation (with no-leakage) and it simultaneously can have a relatively high efficiency as determined here.
Z-State Analysis

Consider a unit flow passing through the circuit. The resulting pressures are indicated in Fig. 25. in terms of the RFD performance parameters and the unknowns e_s, e_a, and e_L. By summing pressures in Fig. 25.

$$e_s = 1 + B \qquad e_a = A + C \qquad e_L = e_o - C \qquad (17)$$

By definition for the FJ $\qquad E = e_o/e_a \qquad (18)$

so the circuit efficiency is given by

$$\eta \;=\; \frac{e_L}{e_s} \;=\; \frac{E(A + C) - C}{1 + B} \tag{19}$$

This implies an efficiency of 38.6% using current devices.

Integrated FJ-2-RFD Rectifier

By merging together the two RFDs and the FJ, the second diffusers in the RFDs can be eliminated and increased efficiency can be expected. A planar form of this integrated circuit is shown in Fig. 26. An optimum circuit would have rounded channels but since a planar device is very simply constructed it is worthwhile determining a good planar design.

A prototype planar rectifier was tested and yielded the characteristics shown in Fig. 27. The supply flow q_s is constant, the reference state is when the load flow is zero and dimensionless variables denoted by capitals are derived in terms of e_s and q_s in this state. The efficiency is 34% at the zero-leakage point $(Q_L = 1)$ and the peak efficiency is about 37% at a slightly reduced load flow.

An improved planar rectifier, shown in Fig. 28. and undergoing development, has a peak efficiency of 40%.

An air powered liquid circulating pump using a planar rectifier and a vented bistable amplifier is shown in Fig.29.

A range of rectifiers can be considered which depend on similar principles as shown in Fig. 26. This includes a 3-phase rectifier, which avoids the discontinuous acceleration occurring in 2-phase rectifiers, and Walkden's reciprocating jet-pump which represents the end result of merging the FJ-2-RFD rectifier.

Conclusions

New flow control devices and useful theoretical insight have resulted from the study of regenerative circuits. The theory has been based on ideal similarity in steady-state networks. This involves the very simplest fluid mechanics but it has useful and interesting consequences in the design of flow switching circuits. When exact similarity does not prevail, analyses based on the ideal still describe effects which largely predominate in many real systems. If these are not calculable, they obscure the really distinctive features of a particular device.

The fluid devices can be combined to form many types of flow and power control circuits and in particular a range of regenerative circuits are feasible and could be applied to furnace systems or the pumping of "difficult" fluids.

Acknowledgement

References

1. Swithenbank, J. and Taylor, D.S.: Unpublished work in Dept. of Chemical Engineering and Fuel Technology, University of Sheffield, 1968.

2. Holmes, B.A., Swithenbank, J. and Tippetts, J.R.: Fluidic Process Fluid Switching in Regenerative Heat Exchangers, Paper B6, Proc. 5th. C.F.C. BHRA, June, 1972.

3. Tippetts, J.R. and Swithenbank, J.: Fluidic Flow Control Circuits for General Regenerative Systems, Proc. Symposium Power Fluidics for Process Control, pp. 119-130, Organised by the Institute of Measurement and Control, April, 1973.

4. Tippetts, J.R.: General Design Methods Applied to Circuits Associated with Regenerative Systems. Proc. 6th. C.F.C., BHRA , March, 1974.

5. Walkden, A.J. and Kell, R.C.: A Reciprocating Jet Pump for Hot Corrosive Fluids, pp. 901 , G E C Journal $\underline{34}$ General Electric Co. Ltd., London, 1967.

6. Walkden, A.J. and Eveleigh, B.D.: Experimental and Theoretical Study of a Reciprocating Jet Pump Using Pneumo-hydraulic Drive. Trans. Inst. Chem. Engrs. $\underline{48}$, pp. T121-T128, July, 1970.

7. Chua, L.O.: Introduction to Non-Linear Network Theory, McGraw-Hill, 1969.

8. Shekel, J.: Matrix Representation of Transistor Circuits Proc. Inst. Radio Engineers, 40, 1493-1497, November, 1952.

9. Paynter, H.M.: The Dynamics and Control of Eulerian Turbo Machines. Journal of Dynamic Systems, Measurement and Control, ASME, pp. 198-205, Sept. 1972.

10. Tippetts, J.R. and Royle, J.K.: Design of Flow Control Circuits involving Unvented Bistable Fluid Amplifiers, Fluidics Quarterly, $\underline{3}$, 4, pp. 1-15, Oct. 1971.

11. Tippetts, J.R., Syred, N., Grant, J. and Strong, R.E.: Flow Control Circuits for Toxic Fluids. Proc. Harry Diamond Labs. State of the Art Symposium on Fluidics, October, 1974.

12. Tippetts, J.R.: Minimisation of Power Loss in Fluidic Flow Control Circuits. J. Mech. Eng. Science. Inst. Mech. Eng., Vol. 15 No. 6, Dec.1973.

13. Wormley, D.N.: A Design Basis for Vortex-Type Fluid Amplifiers Operating in the Incompressible Flow Regime. Trans. ASME J. Basic Eng. pp. 369-376, June, 1970.

14. Tippetts, J.R.: The Fluidic Hydraulic Ram and a Conjectured Pressure Amplifier, To be published Fluidics Quarterly, 1974.

15. Tippetts, J.R.: A Survey of Fluidic Flow Control Devices, Proc. Symposium: Power Fluidics for Process Control, Inst. Measurement and Control. April, 1973.

16. Syred, N. and Tippetts, J.R.: The Coupling of a Fluid Amplifier and a Naturally Aspirated Pulsating Combustor. Proc. Symposium: Power Fluidics for Process Control, Inst. Measurement and Control. April, 1973.

17. Syred, N. and Tippetts, J.R.: A High Gain Active Diode- - The Reverse Flow Vortex Amplifier, Proc. 6 th. C.F.C. BHRA, March, 1974.

18. Saunders, D.H.: The Development of a Vortex Valve for use as a Flow Control Valve, Proc. Symposium: Power Fluidics for Process Control, Inst. Measurement and Control, April, 1973.

19. Boucher, R.F., Asquith, R.W. and Royle, J.K.: Vortex Flow Controllers: Design, Stability and Applications. Proc. Symposium on Power Fluidics for Process Control, Inst. Measurement and Control, April, 1973.

20. Rimmer, R.: A Fluidic Pressure Ratio Sensor for Gas Turbine Engine Control, Paper C3, Proc. IFAC Symposium on Fluidics, London, November, 1968.

21. McGuigan, J.A.K. and Boucher, R.F.: A Fluidic Rectifier for Pumping, Proc. Symposium: Power Fluidics for Process Control Inst. Measurement and Control, April, 1973.

22. Cherry, C.: Some General Theorems for Non-linear Systems Possessing Reactance, Phil. Mag. 42, pp. 1161-1177, Oct. 1951.

23. Millar, W.: Some General Theorems for Non-linear Systems Possessing Resistance Phil. Mag. 42, pp. 1150-1160, Oct. 1951.

Figure Captions

Fig. No.

1   Regenerative network.

2   Regenerative circuit used as a pump for toxic liquids.

3   Mechanical regenerative elements.

4   3-terminal element and variables.

5   Polar representation of characterisation.

6   Typical cartesian characteristics of a vortex amplifier.

7   Indefinite parametric characterisation for Eulerian
    3-terminal devices.

8   Active property of transformers and jet-pumps.

9   The flow junction and related synthetic devices.

10 Characteristics of a flow junction.

11 Reverse flow diverters.

12 Forward characteristics of an R-RFD.

13 Reverse characteristics of an R-RFD.

14 Typical merged devices.

15 Diode-like active branch elements.

16 Reverse-flow-diverting vortex amplifier (RFDVA).

17 Parallel connected turn-up vortex amplifiers (Boucher et al).

18 4-terminal network representing alternators and rectifiers.

19 Optimum characteristics of 4-diode and 4-CSV bridge circuits

20 Bridge circuit and rectangle diagram.

21 4-diode rectifier with no process-fluid leakage.

22 Comparison of a flow junction and equivalent diode-tees.

23 Comparison of a symmetrical-R-RFD and equivalent diode-tees.

24 Flow-junction-symmetrical-R-RFD rectifier.

25 FJ-2-RFD rectifier shown operating with one unit of flow
    and no leakage.

26 Integrated fluidic bridge-rectifier circuits.

27 Characteristics of a planar integrated FJ-2-RFD rectifier.

28 a) Reverse-flow-diverting vortex amplifier b) Vented reverse
    flow vortex amplifier c) Flow junction d) Integrated planar
    FJ-2-RFD rectifier.

29 a) Regenerative circuit consisting of a bistable amplifier,
    two A-type RFDs, two vortex diodes and a flow junction
    b) Air-driven liquid pumping circuit consisting of a vented
    bistable amplifier and an integrated planar rectifier.
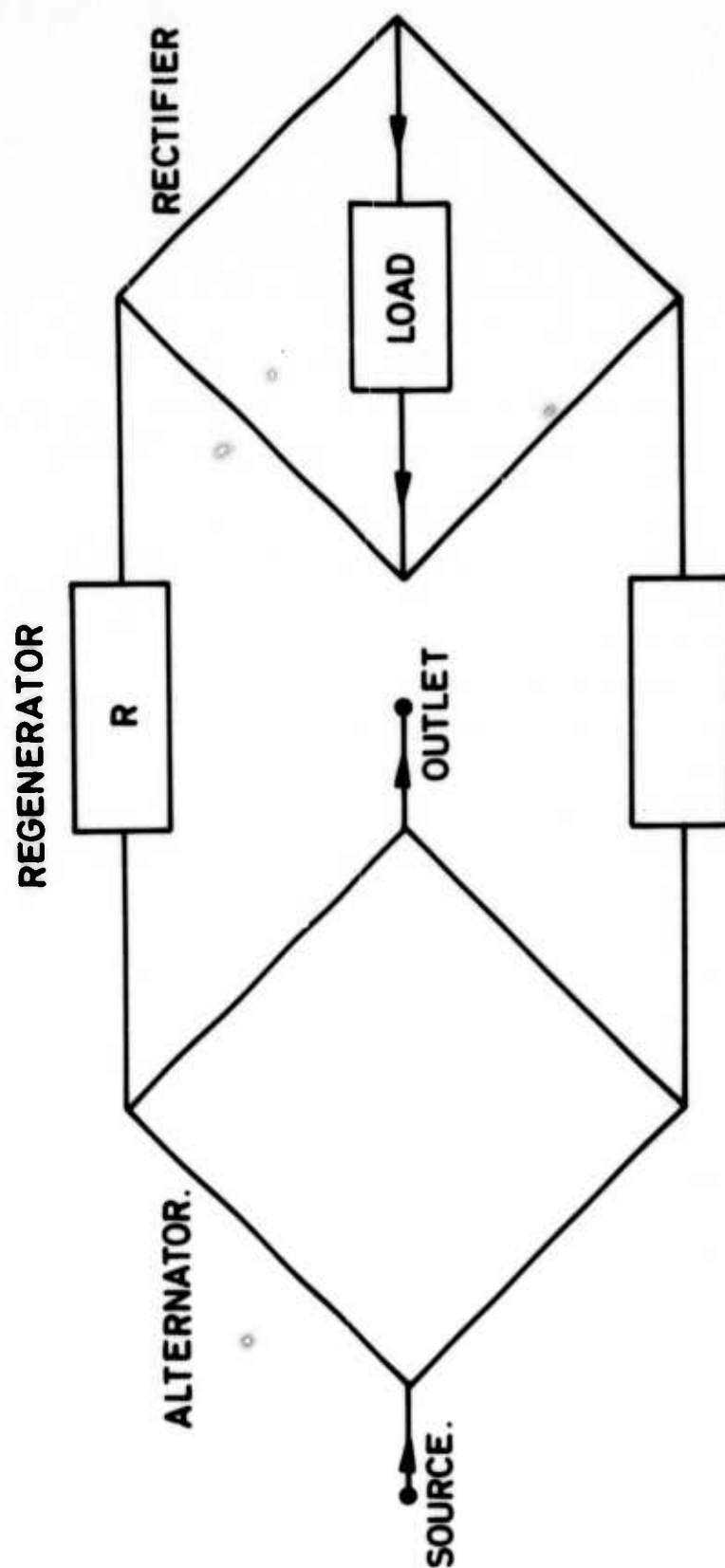   Both circuits controlled by a fluidic oscillator.
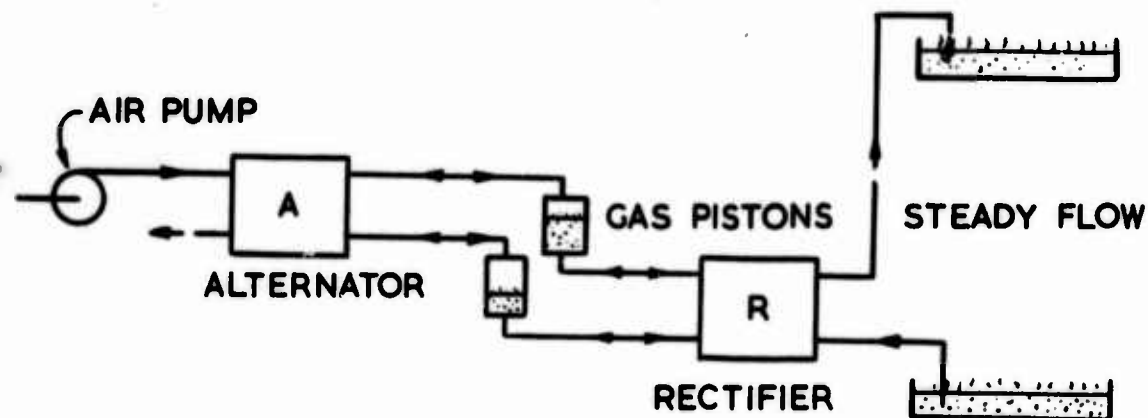
FIGURE 1. REGENERATIVE NETWORK

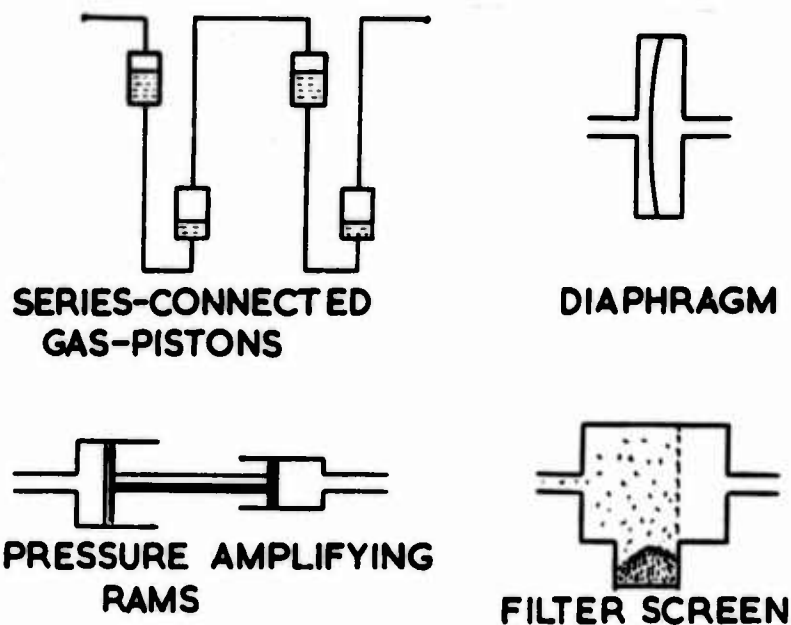FIGURE 2 **REGENERATIVE CIRCUIT USED AS A PUMP FOR TOXIC LIQUIDS**

FIGURE 3 **MECHANICAL REGENERATIVE ELEMENTS**
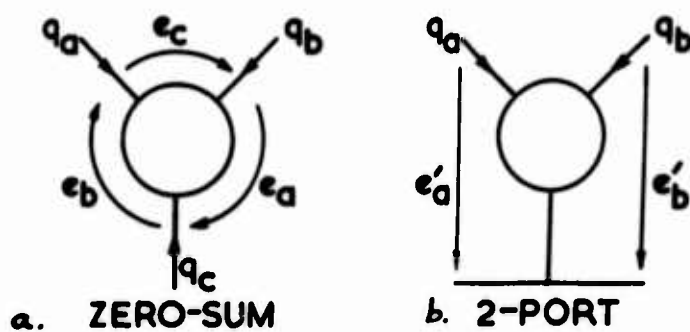
FIGURE 4 **3-TERMINAL ELEMENT AND VARIABLES**

125

INDEPENDENT   INVARIANT   DEPENDENT
CONSTRAINTS   FUNCTIONS   FUNCTIONS
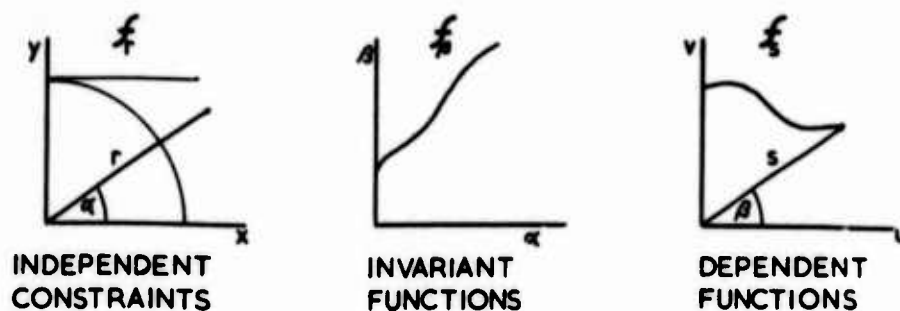
FIGURE 5 POLAR REPRESENTATION OF CHARACTERIZATION
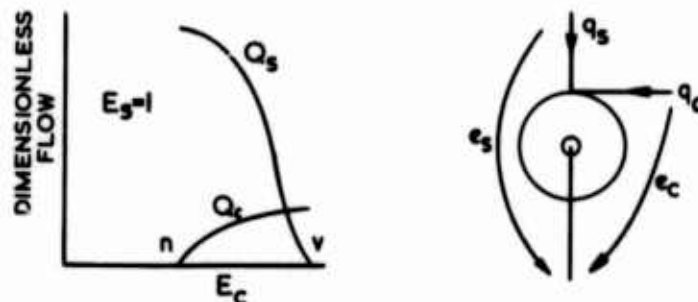
FIGURE 6 TYPICAL CARTESIAN CHARACTERISTICS OF A   VA

CONSTRAINT: INVARIANT   DEPENDENT
r = constant   FUNCTION   FUNCTION
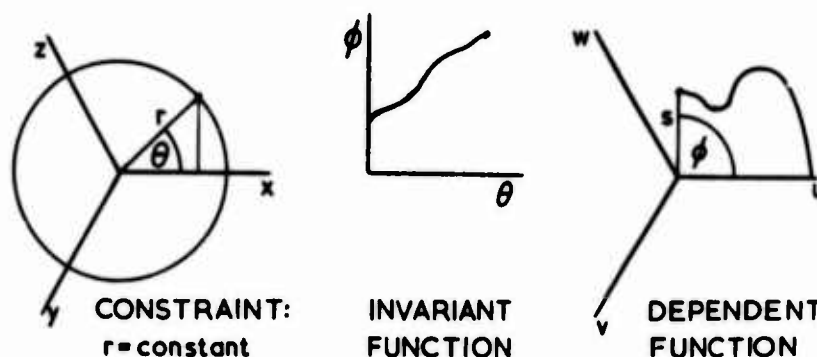
**FIGURE 7 INDEFINITE PARAMETRIC CHARACTERIZATION FOR
EULERIAN 3-TERMINAL DEVICES**
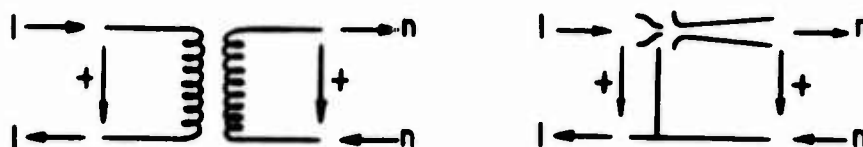
FIGURE 8 ACTIVE PROPERTY OF TRANSFORMERS AND JET PUMPS
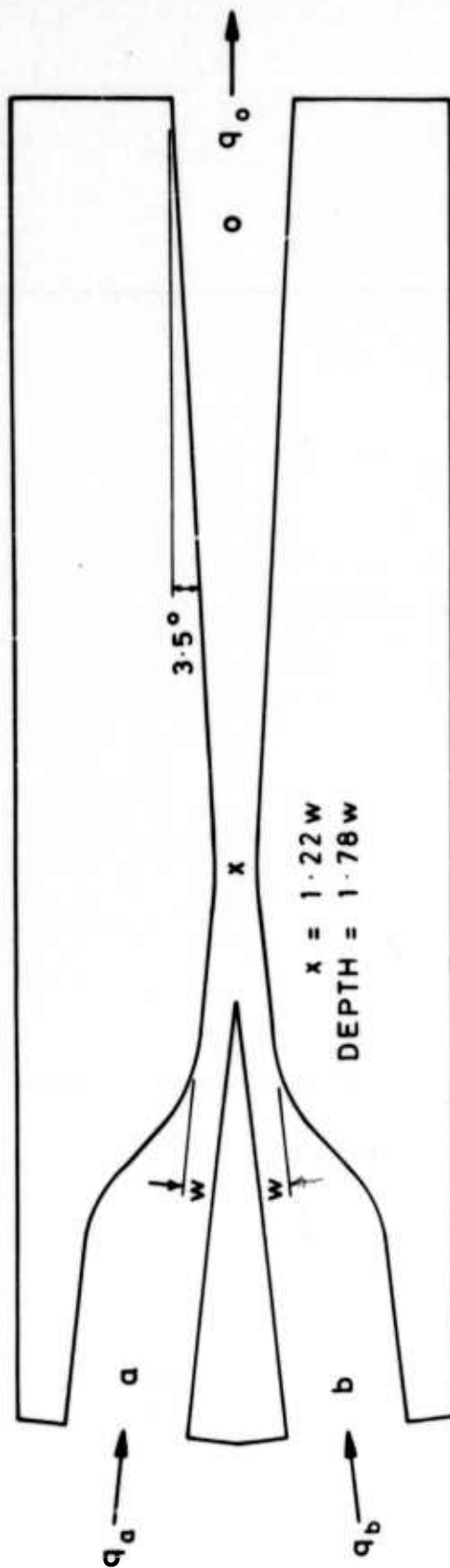
ALL CHANNELS RECTANGULAR.
THE FLOW JUNCTION.

$x = 1.22w$
DEPTH $= 1.78w$

DIODE TEE   F J + DIODES

COMPARABLE DEVICES

SYMBOL AND
VARIABLES
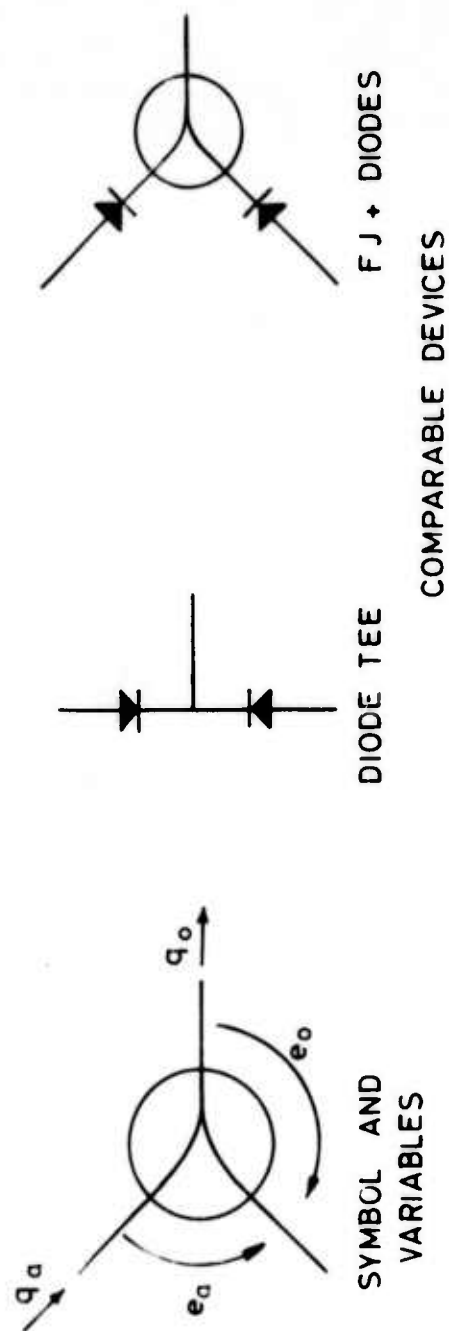
FIGURE 9. THE FLOW JUNCTION AND RELATED SYNTHETIC DEVICES

127

CHARACTERISTICS OF A FLOW JUNCTION.

FIGURE 10

ANNULAR WALL-JET

X-TYPES

RADIAL DIFFUSER

SWIRLER

A-TYPE (WITHOUT SWIRLER)
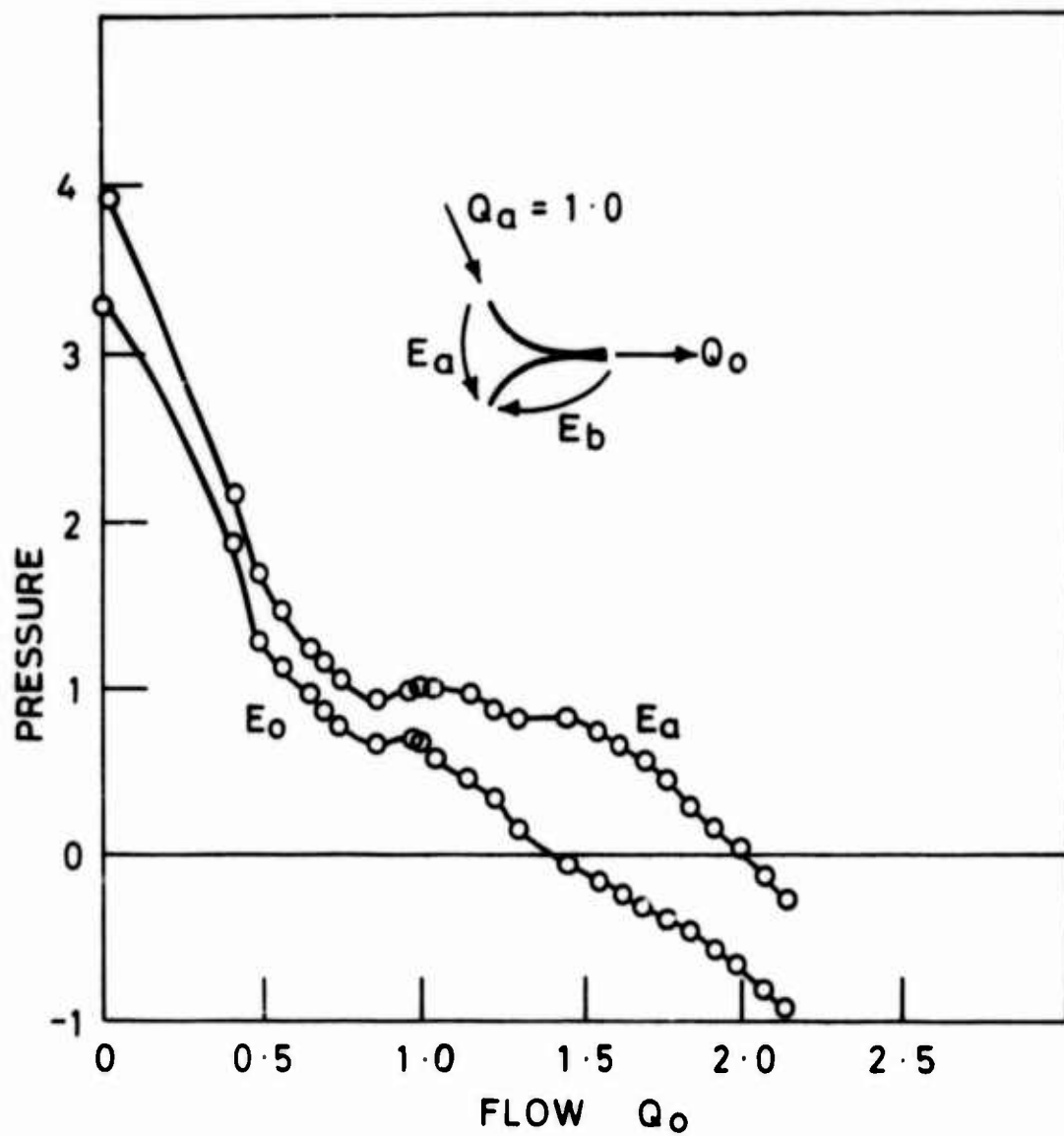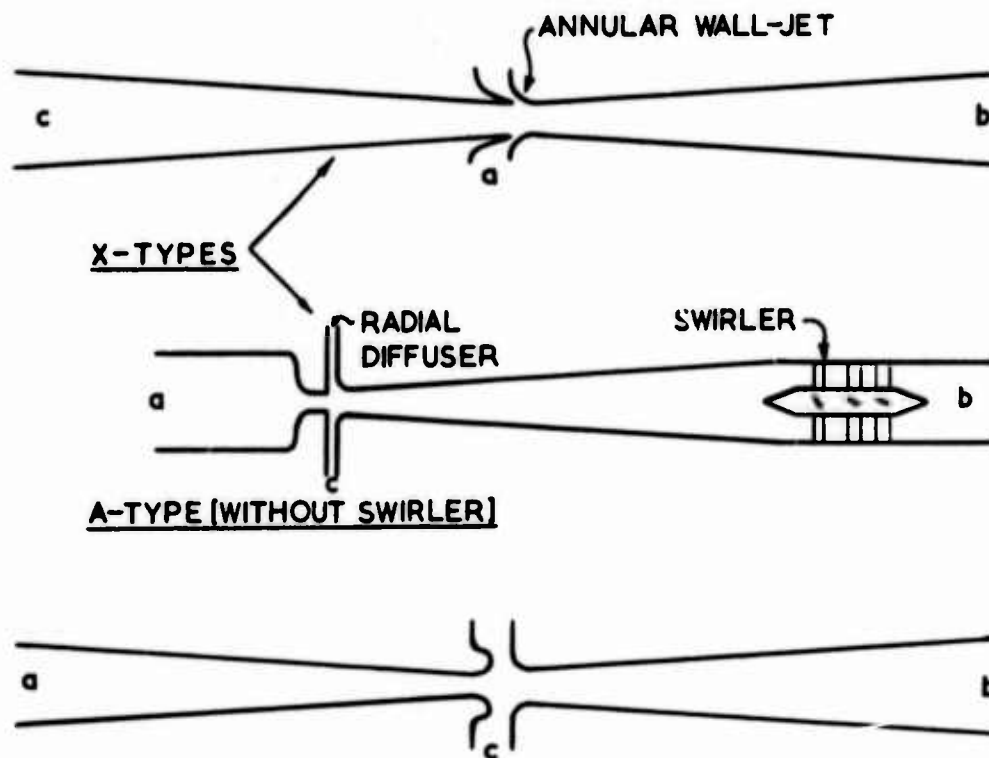
R-TYPE

ALL AXI-SYMMETRIC
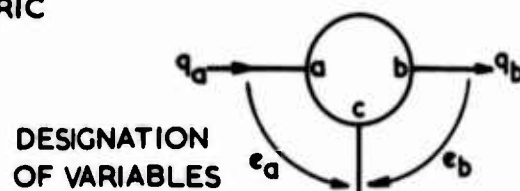
DESIGNATION OF VARIABLES

REVERSE FLOW DIVERTERS

FIGURE 11

129
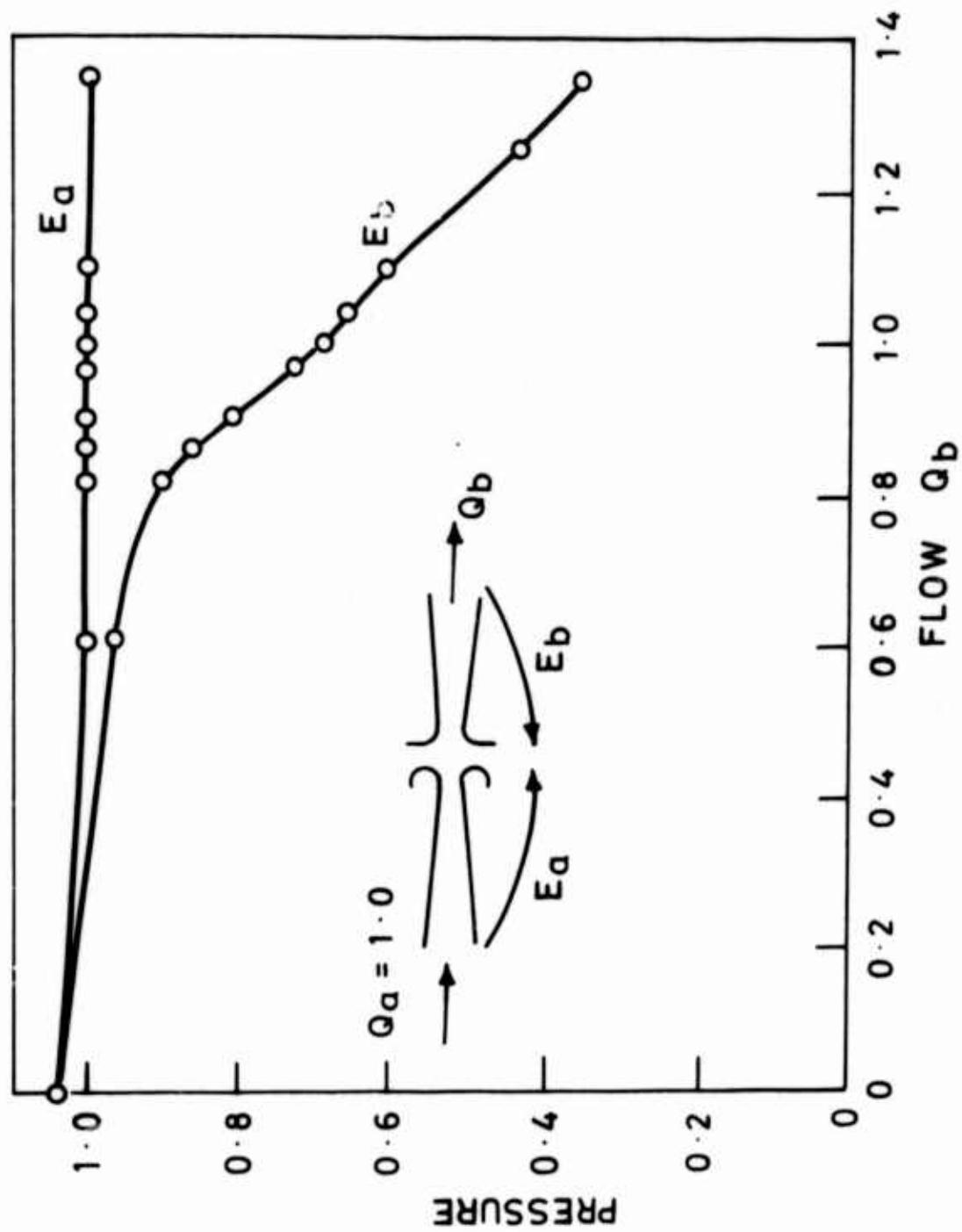
FORWARD CHARACTERISTICS OF A R - RFD

FIGURE 12

REVERSE CHARACTERISTICS OF A R-RFD.

FIGURE 13

131

RADIAL DIFFUSER

CSV

COANDA-SWITCHED VORTEX
DEVICE MERGED WITH AN A-RFD

VORTEX
DIODE

JET-PUMP-DIODE
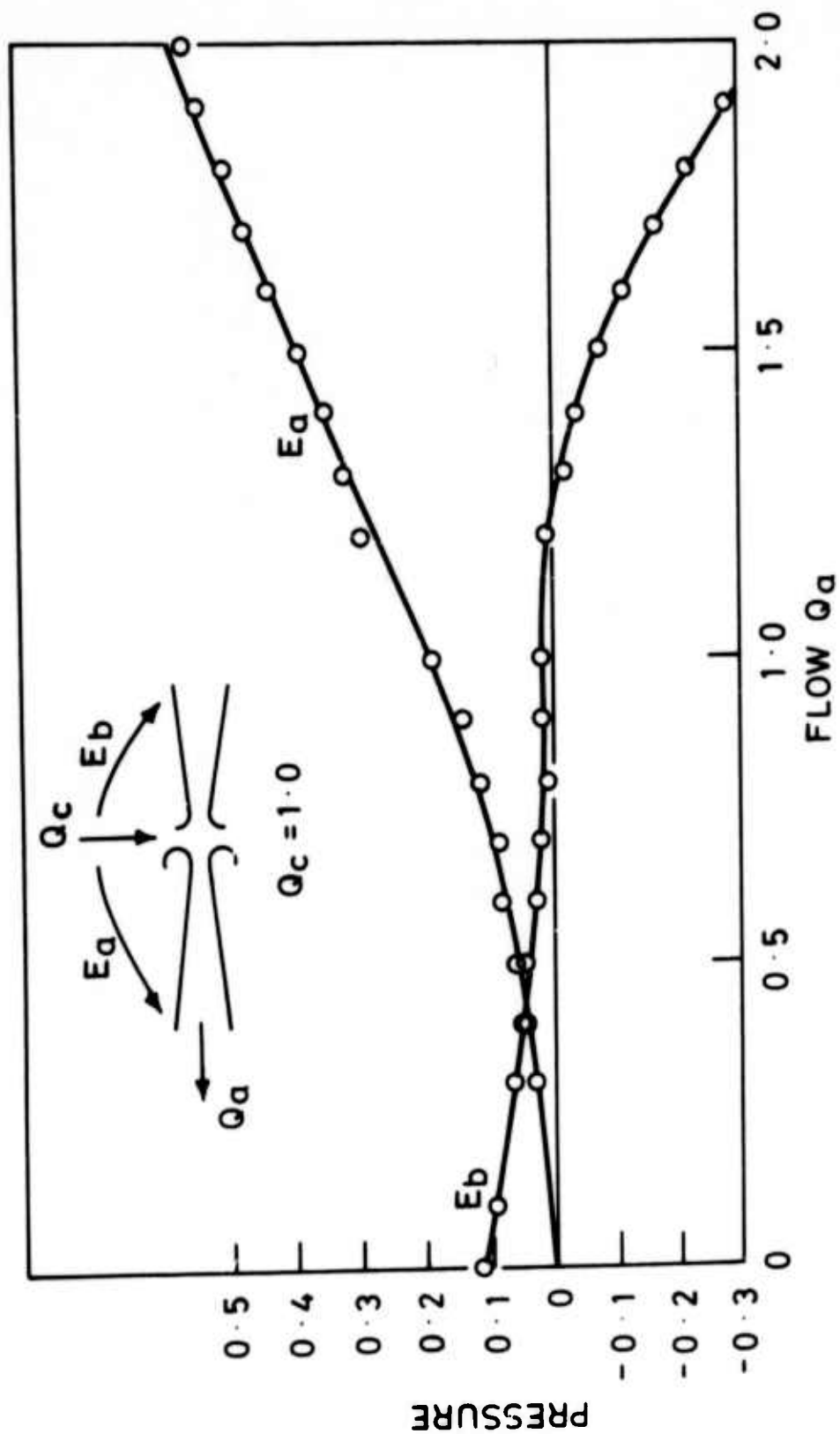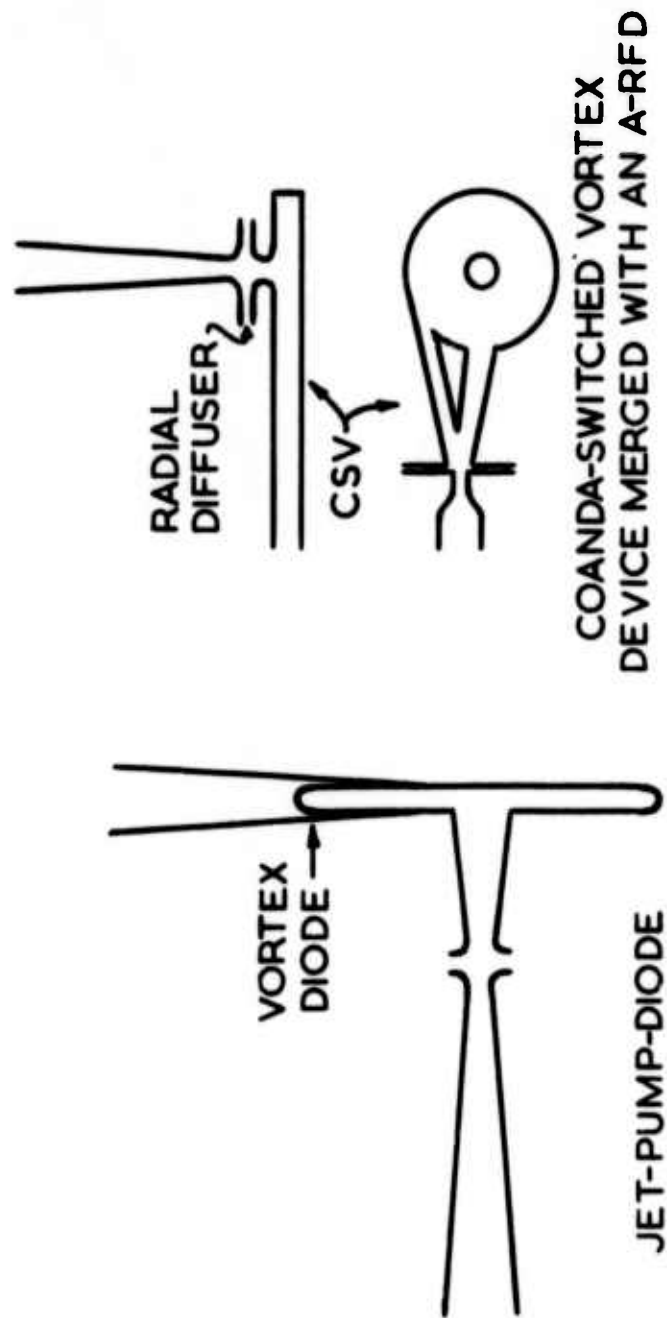
TYPICAL MERGED DEVICES

FIGURE 14

132
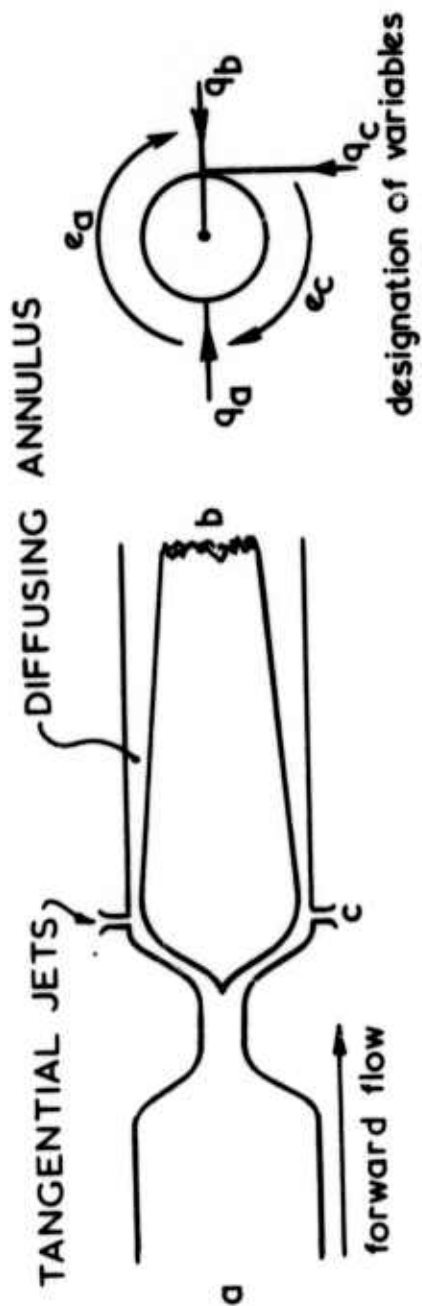
REVERSE FLOW VORTEX AMPLIFIER (RFVA)
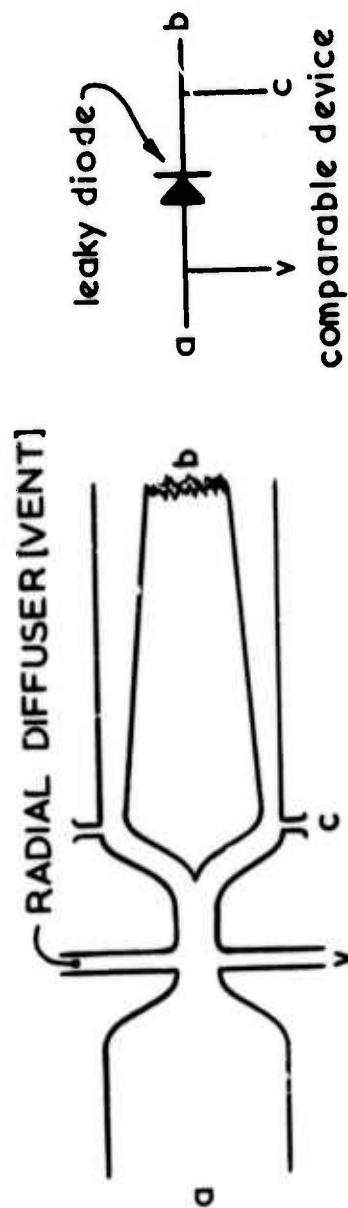
VENTED RFVA

DIODE-LIKE ACTIVE BRANCH ELEMENTS

FIGURE 15

133

TANGENTIAL JETS

RADIAL DIFFUSER

REVERSE FLOW

CONTROL FLOW
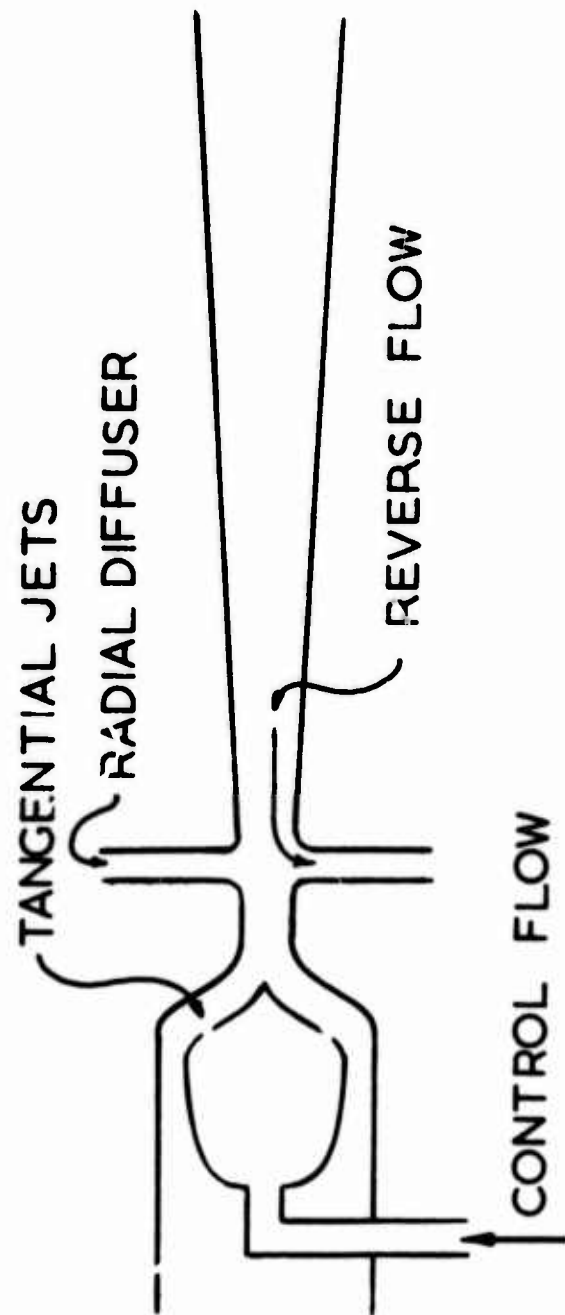
REVERSE-FLOW-DIVERTING VORTEX AMPLIFIER [RFDVA]

FIGURE 16

134
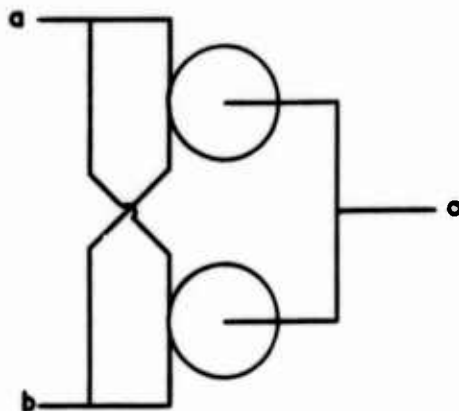
PARALLEL CONNECTED TURN-UP
VORTEX AMPLIFIERS [Boucher et al]

FIGURE 17
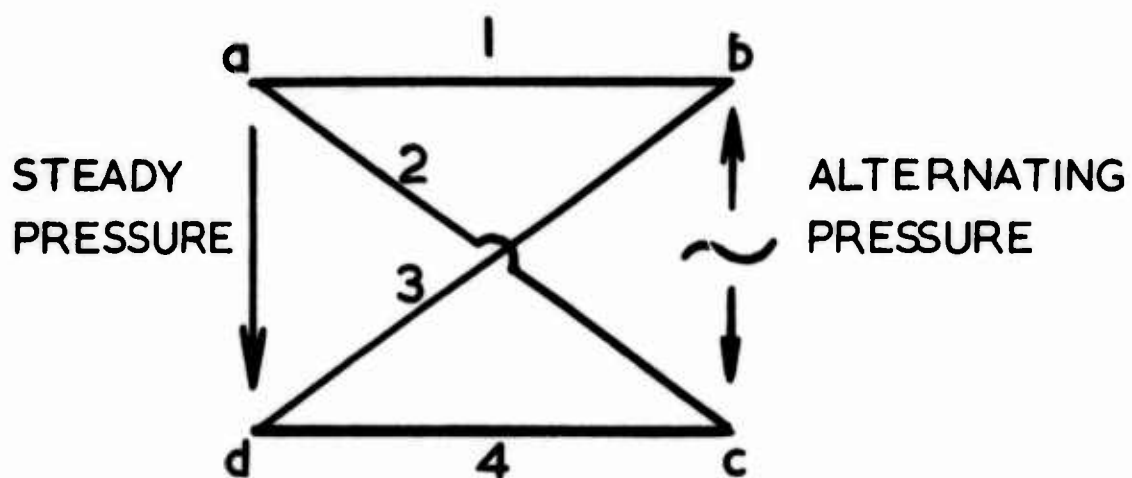
4-TERMINAL NETWORK REPRESENTING ALTERNATORS AND RECTIFIERS

FIGURE 18
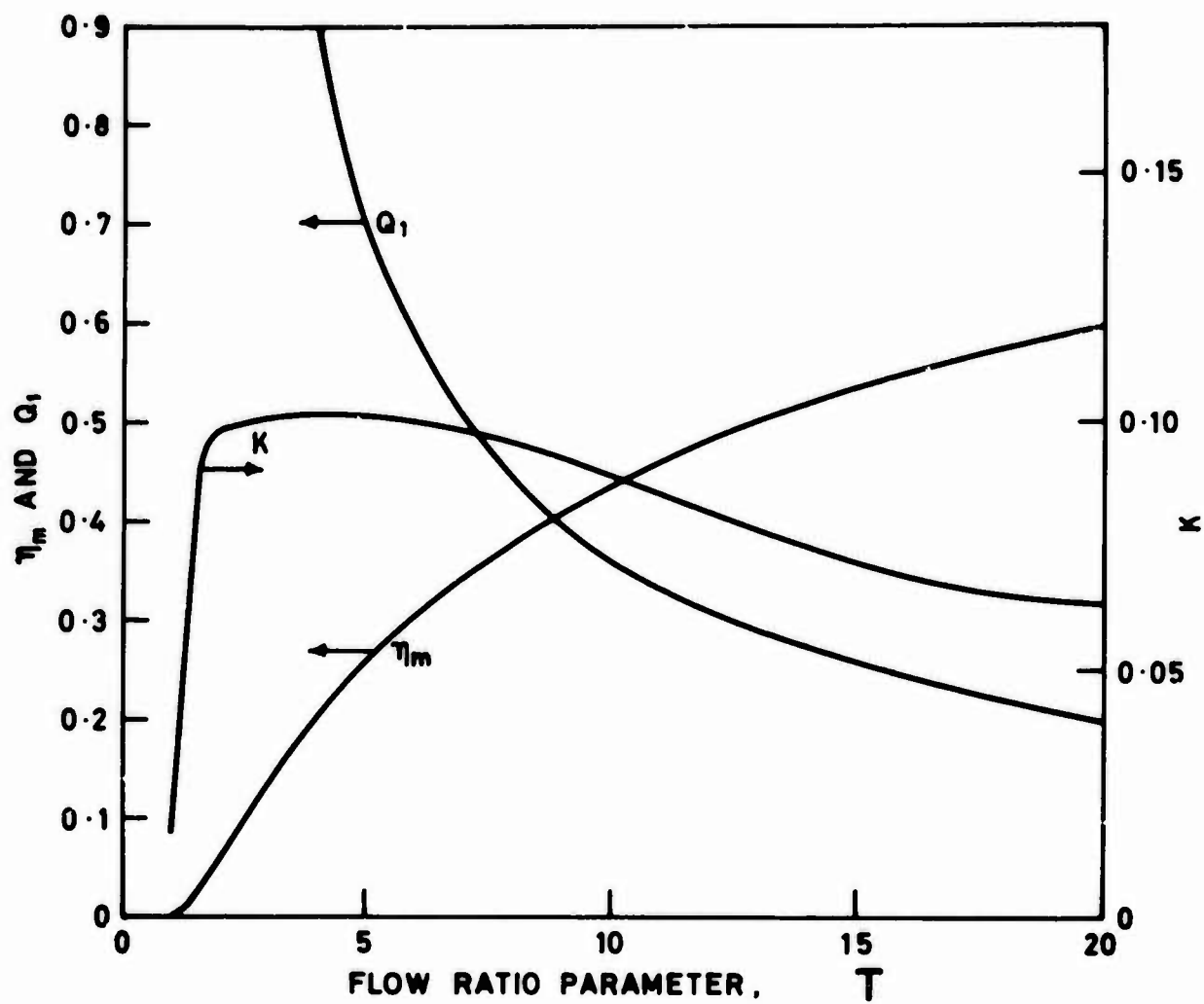
FIGURE 19. OPTIMUM CHARACTERISTICS OF 4-DIODE AND 4-CSV BRIDGE CIRCUITS

136
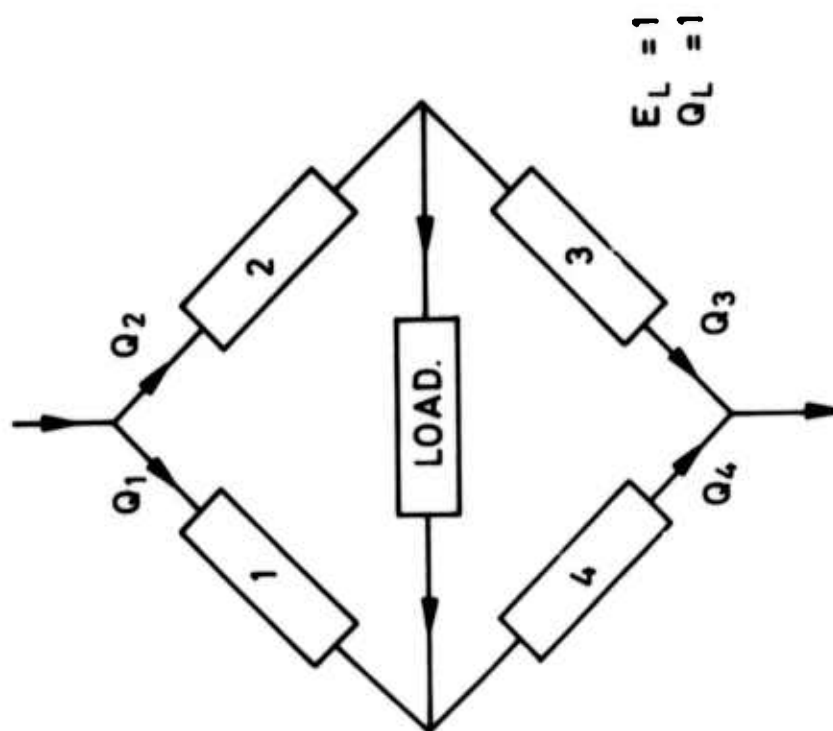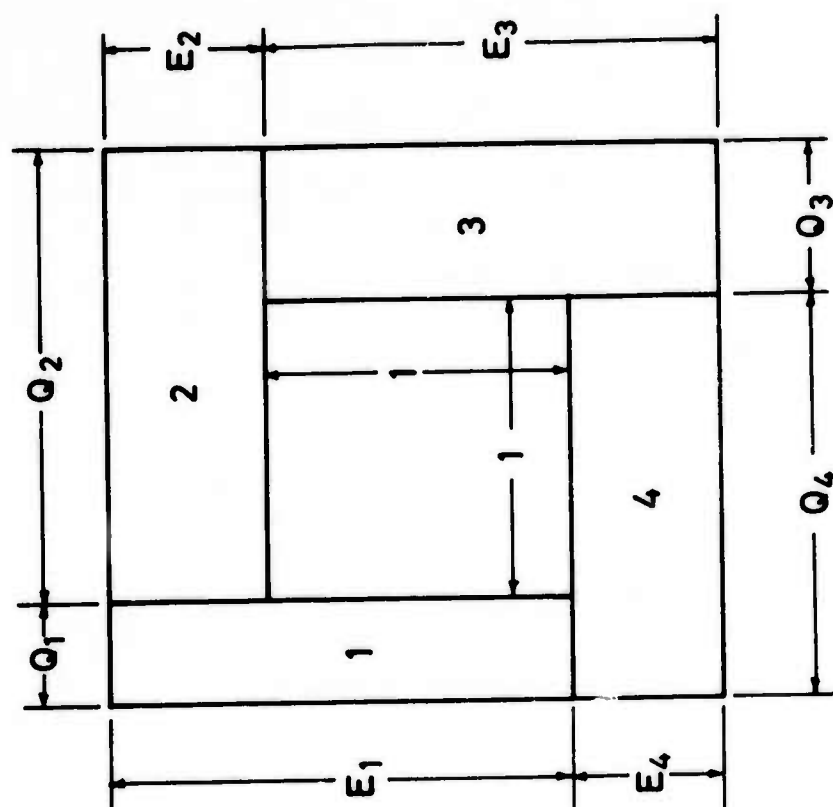
DIMENSIONLESS VARIABLES.

FIGURE 20. BRIDGE CIRCUIT AND RECTANGLE DIAGRAM

$E_L = 1$
$Q_L = 1$

137
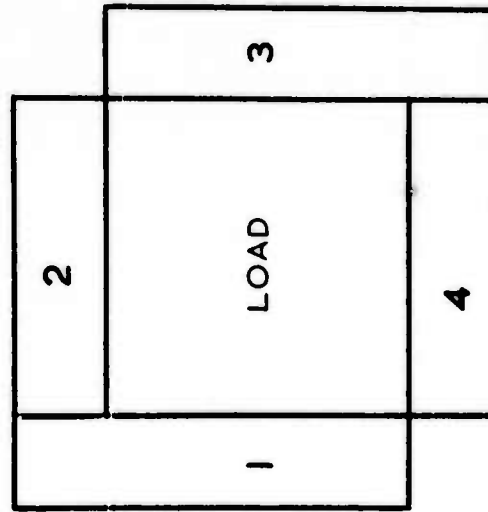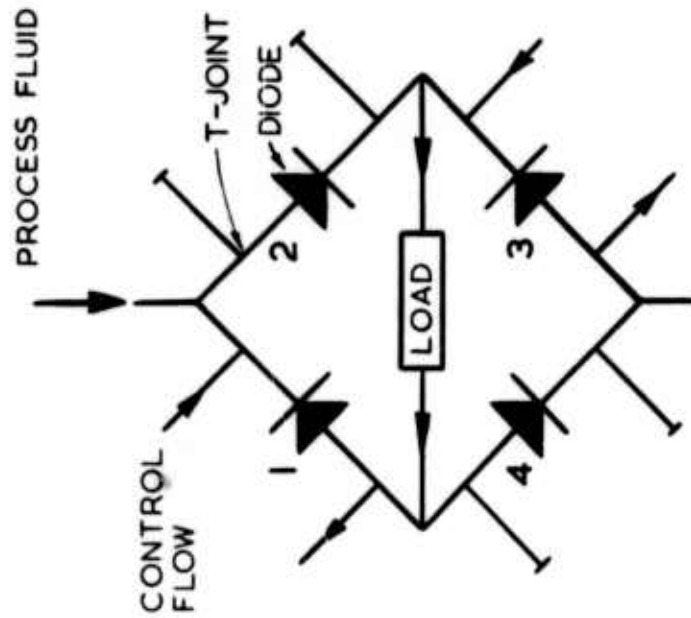
RECTANGLE DIAGRAM

4-DIODE RECTIFIER WITH NO PROCESS FLUID LEAKAGE

FIGURE 21

138
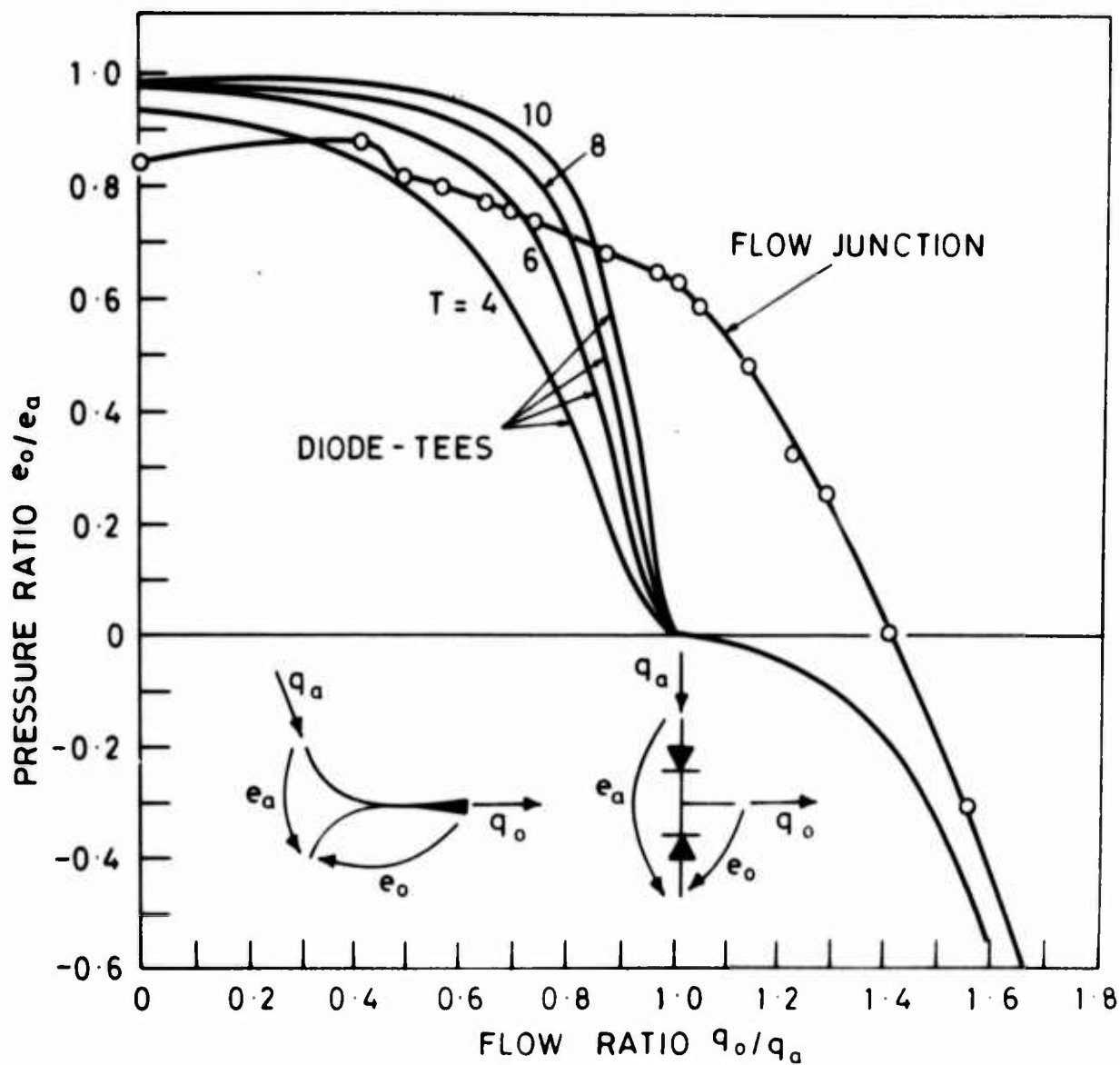
COMPARISON OF A FLOW JUNCTION AND EQUIVALENT
DIODE - TEES.

FIGURE 22
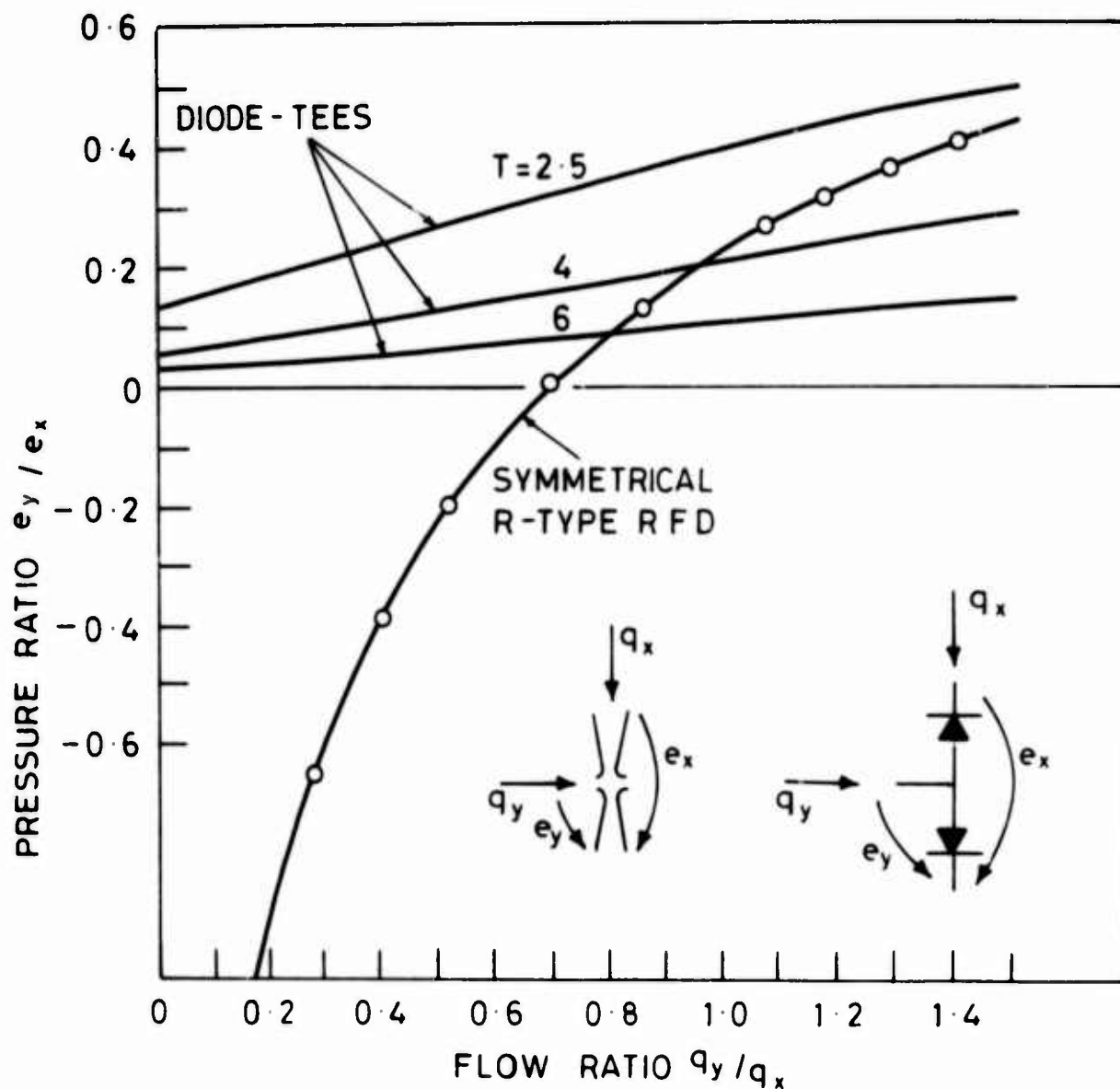
COMPARISON OF A SYMMETRICAL - R-RFD AND
DIODE - TEES.

FIGURE 23

140
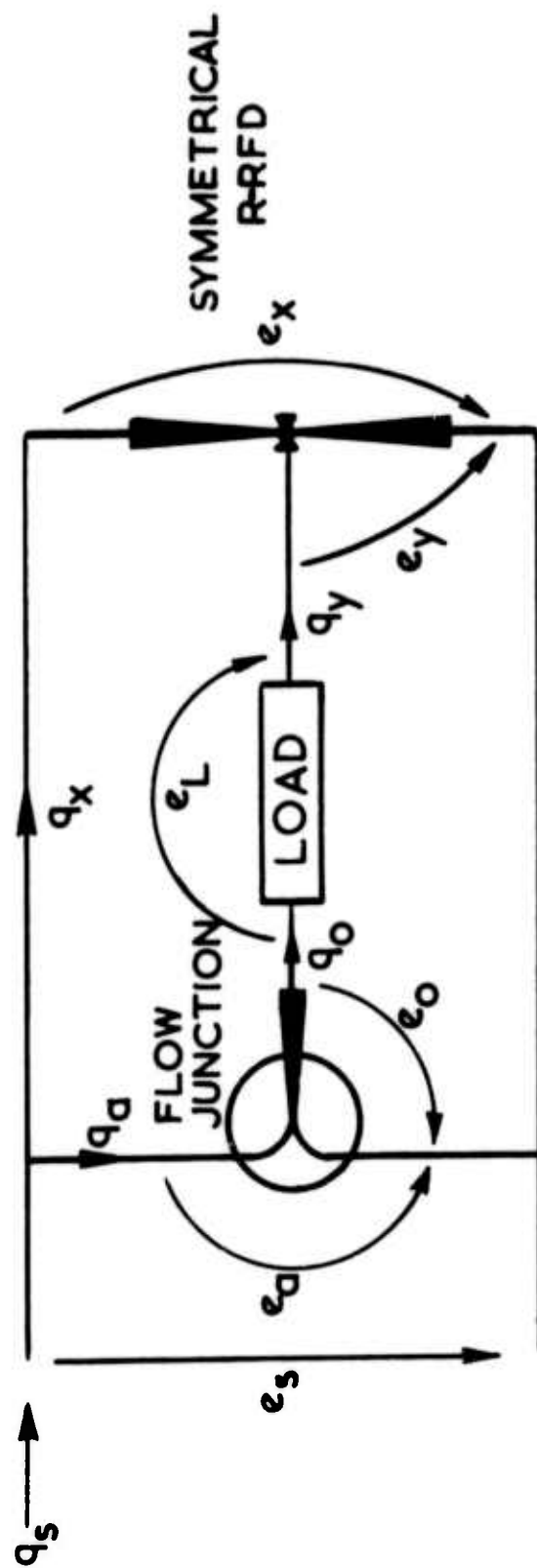
FLOW-JUNCTION-SYMMETRICAL-R-RFD RECTIFIER

FIGURE 24

141
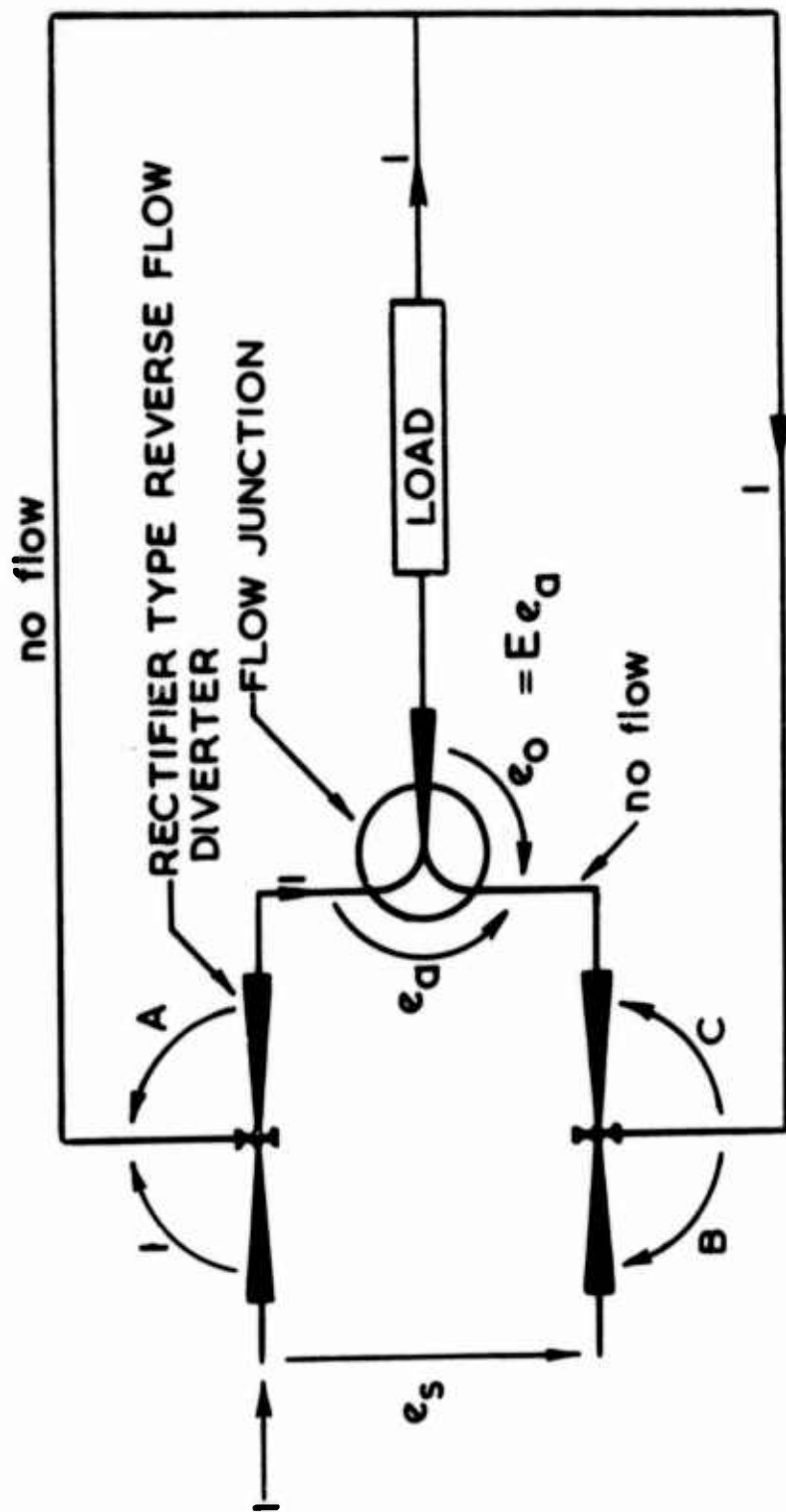
A,B,C & E: performance parameters of RFDs and FJ.

FJ-2-RFD RECTIFIER SHOWN OPERATING WITH ONE UNIT
OF FLOW AND NO LEAKAGE

FIGURE 25

142

FJ-2-RFD RECTIFIER

PLANAR DESIGN

3-PHASE RECTIFIER

LOAD

DESIGN WITH ROUNDED
CHANNELS

RECIPROCATING
JET PUMP
[WALKDEN et al.]
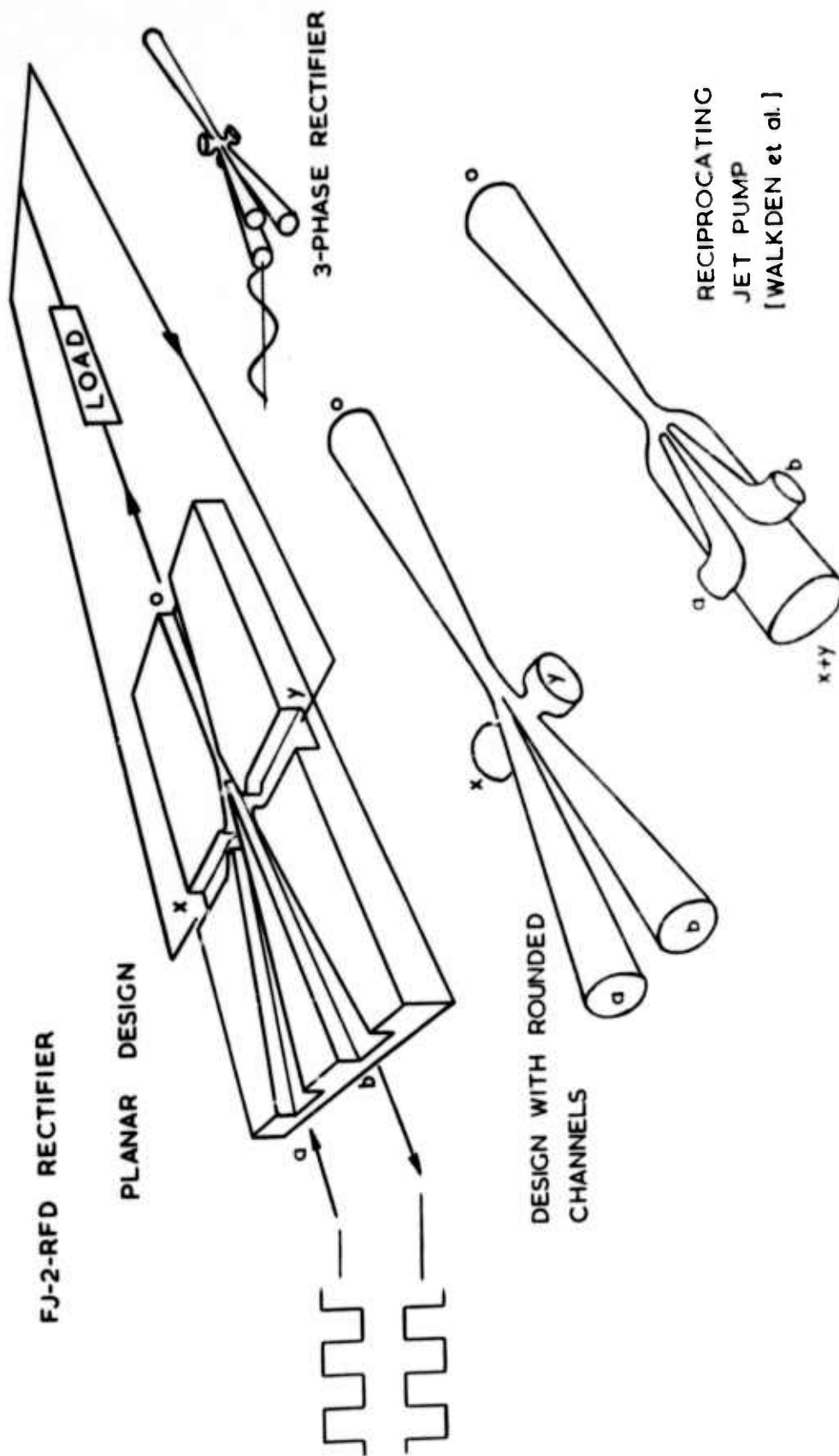
INTEGRATED FLUIDIC BRIDGE-RECTIFIER CIRCUITS

FIGURE 25

143

FIGURE 27. CHARACTERISTICS OF A PLANAR INTEGRATED FJ-2-RFD RECTIFIER
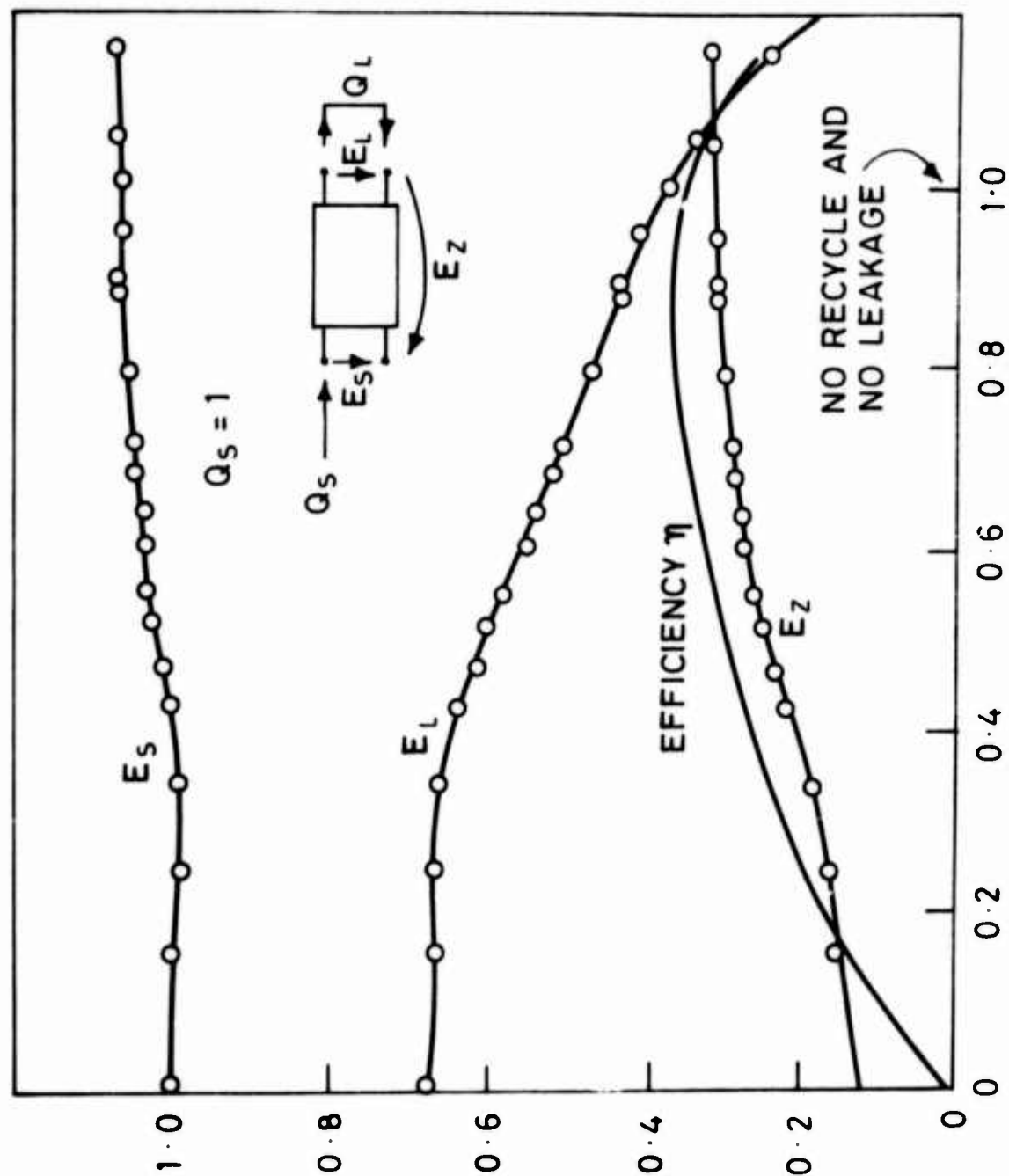
NON - DIMENSIONAL LOAD FLOW Q_L
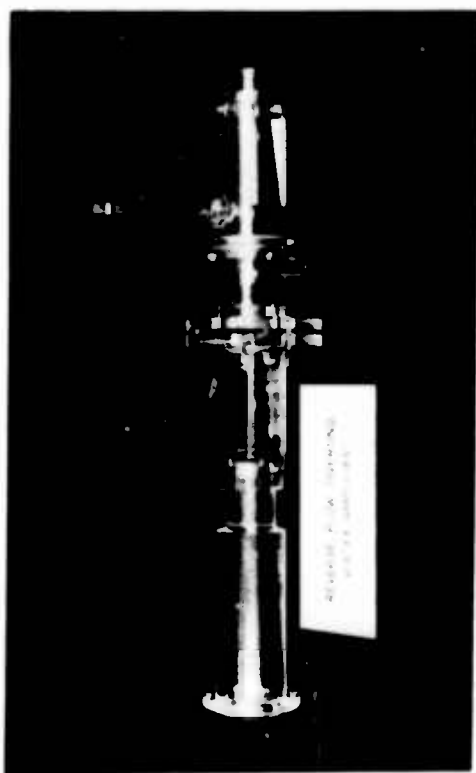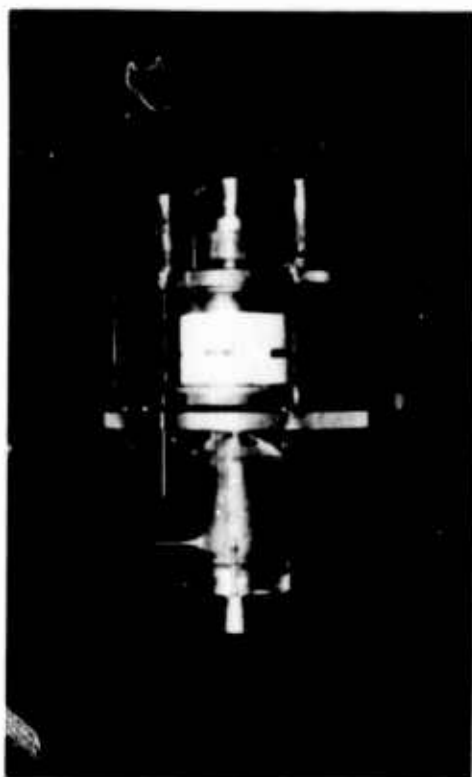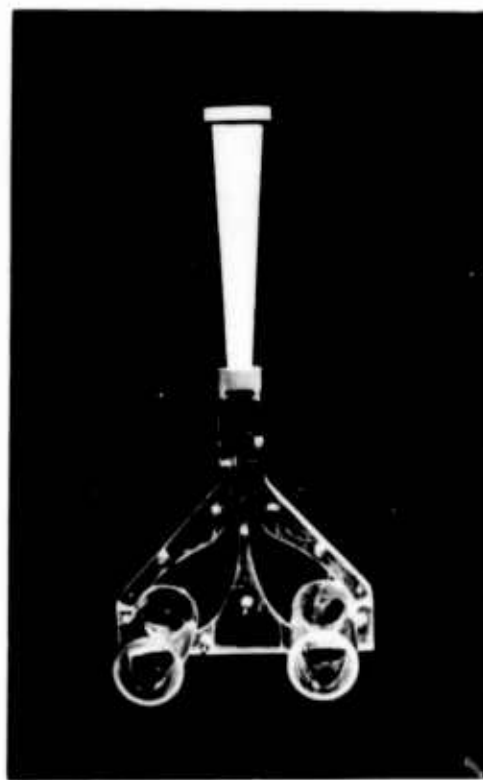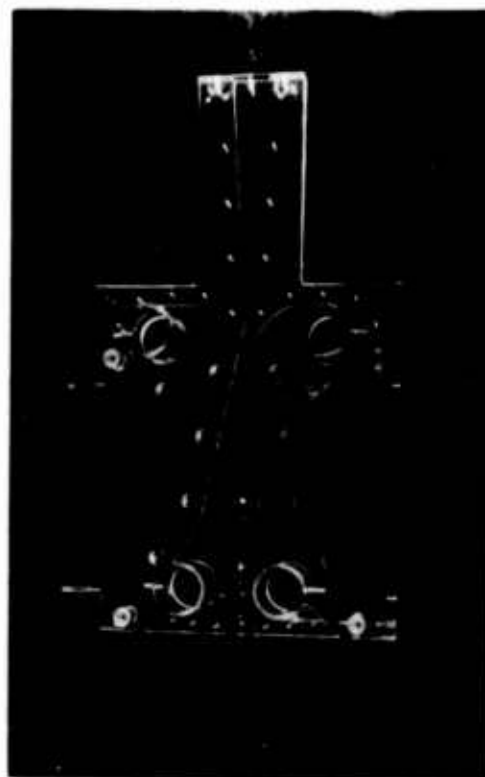
FIGURE 28a. REVERSE-FLOW-DIVERTING VORTEX AMPLIFIER; b. VENTED REVERSE FLOW VORTEX AMPLIFIER; c. FLOW JUNCTION; d. INTEGRATED PLANAR FJ-2-RFD RECTIFIER

145
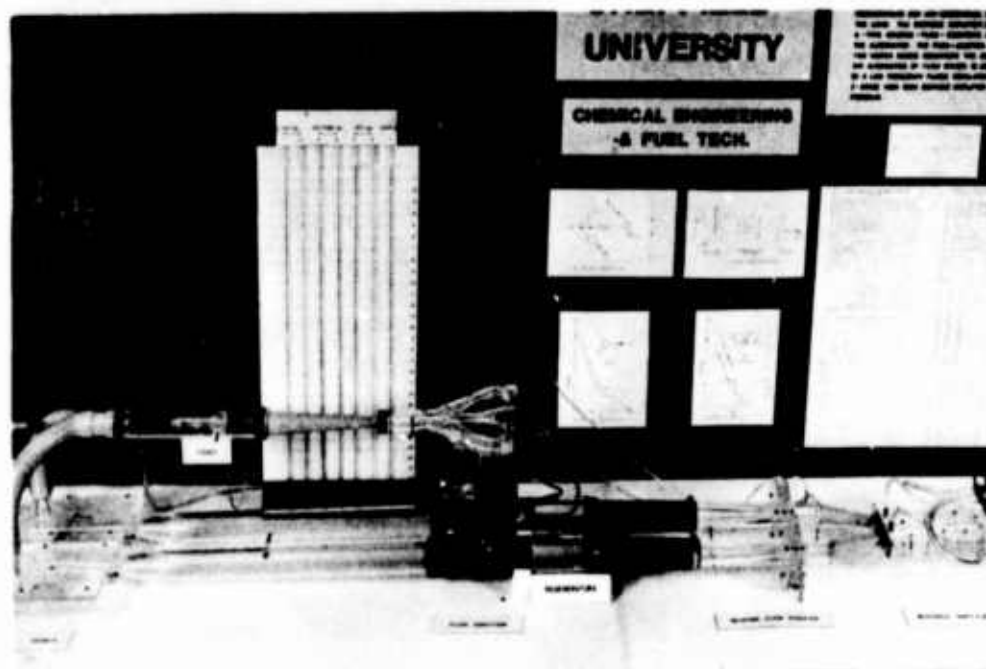
FIGURE 29a. REGENERATIVE CIRCUIT CONSISTING OF A BISTABLE AMPLIFIER, TWO A-TYPE RFDs, TWO VORTEX DIODES AND A FLOW JUNCTION
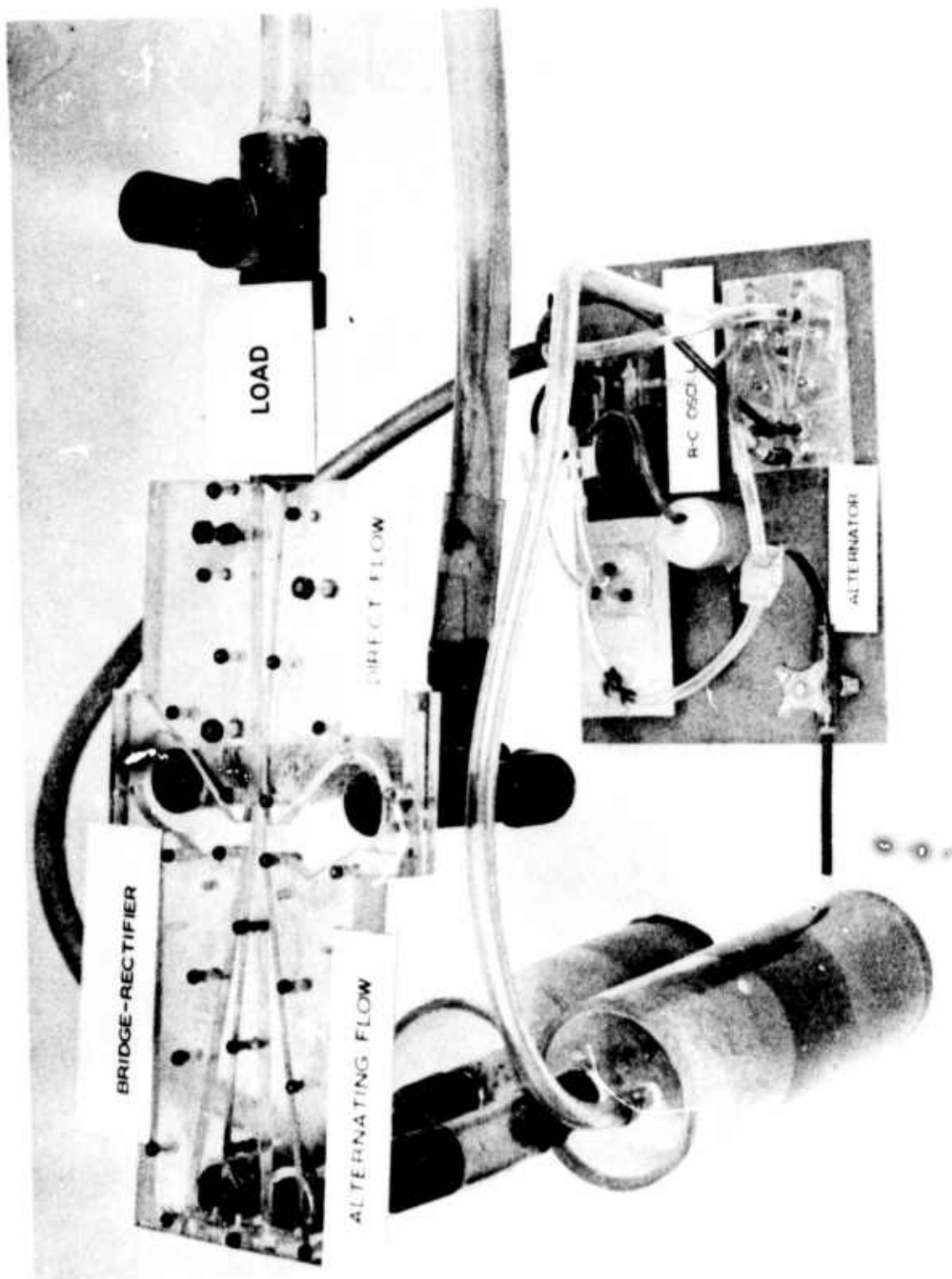
FIGURE 29b. AIR-DRIVEN LIQUID PUMPING CIRCUIT CONSISTING OF A VENTED BISTABLE AMPLIFIER AND AN INTEGRATED PLANAR RECTIFIER. BOTH CIRCUITS CONTROLLED BY A FLUIDIC OSCILLATOR.

147

CONCEPTUAL MODELS FOR FLUID LOGIC NETWORKS

J. H. Cole
Associate Professor
Department of Mechanical Engineering
University of Arkansas
Fayetteville, Arkansas

CONCEPTUAL MODELS FOR FLUID LOGIC NETWORKS

ABSTRACT

Conceptual models are important to control designers because the "model" is really a definition or visualization of the problem. The problem definition usually dictates the solution method; and this is especially true for switching networks. This paper describes existing conceptual models for fluid logic networks and points out that the use of one of these models provides an opportunity for the development of new fluidic devices.

INTRODUCTION

A common statement among design engineers is that a problem well defined is already half solved. However, because of the emphasis placed on analysis, an inexperienced designer often makes the mistake of plunging into a problem solution without first carefully defining what the problem should be. Definition is highly important because it usually establishes the solution method to be followed. Sometimes, the best way out of an impasse is to simply redefine the unsolvable problem into one that can be solved.

In controls work, conceptual models are used to help define and visualize problems. For example, in modern control theory, the "state space" model is used to mathematically represent continuous control systems.

Models are also used in defining digital control systems. A digital system processes information consisting of physical quantities constrained to have only discrete values. These quantities are called variables or, more often, signals. Most digital systems work with signals which take on only two discrete values. Such signals are termed as binary.

Switching circuits or networks perform the logical functions required in digital systems. This paper describes the conceptual models which are available to help define logic networks using fluidic devices.

GENERALIZED SWITCHING NETWORK

A generalized switching network is indicated by Figure 1. The x's collectively represent a set of binary input signals and the z's represent a set of binary output signals. If there are n input signals, the set of input signals may be thought of as an ordered n-tuple or vector consisting of n binary variables. When all of the variables are in a stable condition (not changing), at some time interval i, then the n-tuple may be represented by the input state vector, $\vec{x}_i$. The stabilized

150

k-tuple, consisting of the k output variables, can similarly he represented at time interval i by the state vector $\vec{z}_i$.
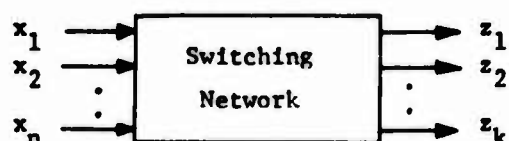
Figure 1. Generalized switching network.

A switching network with input terminals and output terminals accepts a time sequence of input states and as a result, produces a time sequence of output states. When the input state at time i uniquely determines the output state at time i, for every i, the network is called combinational. That is, the output state is always a function of the combination of input variables. However, if the output state $\vec{z}_i$ depends not only on $\vec{x}_i$, but also on previous input states, the network is called sequential. The sequential network must possess a logical memory, enabling it to keep a record of what has happened preceding the time interval i. If a clock pulse is not used to synchronize the switching operation, the sequence is called asynchronous.

Fluid logic networks almost always operate in the asynchronous mode. Synchronous operation is, in general, not feasible because of the difficulty in generating suitable clocked pulses and the problem of maintaining pneumatic pulse shapes as the signals travel through the transmission lines. Then too, many processes are ideally suited for control by asynchronous fluid logic networks.

COMBINATIONAL NETWORKS

The combinational network is adequately represented by Figure 1. Output equations, expressed in Boolean algebra notation, are easily obtained. The main task in designing combinational networks is to minimize the complexity of the output equations; and is readily accomplished through the use of Karnaugh maps or by tabular techniques.

Or :e minimized equations are obtained, the physical network can be implemented by replacing the Boolean algebra connectives with fluid logic gates which perform such functions as "AND", "OR", "NOT", "NOR", and "NAND".

SEQUENTIAL NETWORKS

As previously stated, output equations for a sequential network cannot be obtained by simply combining input signals as in the manner of combinational networks. Memory must be included, and the synthesis problem is generally regarded as much more difficult.

Two basic approaches may be taken in defining the sequential problem, and conceptual models are used to help in the visualization.

PSEUDO-COMBINATIONAL MODEL

This approach effectively converts the problem from sequential to combinational by adding auxiliary inputs to the network. These auxiliary inputs must be produced by the switching network itself. The chief task is to assign the minimum number of auxiliary inputs and to obtain equations to produce the assigned inputs. Once this is done, the problem is reduced to that of minimizing the output expression in the same manner as for combinational networks.

Two equivalent forms of this model are used. The first is shown in Figure 2. Here, the network is made up of gate elements (AND, OR, NOR, etc.). Memory is provided by inserting delay elements in the feedback paths. The x's and y's, combined together, form the network inputs. The system may now be treated as combinational, because for each unique input combination, or state, there corresponds one and only one unique output state. An alternative is to use flip flop elements for the memory function, as shown in Figure 3. E_1, E_2, $\cdots$, E_m are the flip flop excitation signals. The y's are the flip flop output signals and become inputs to the combinational network.
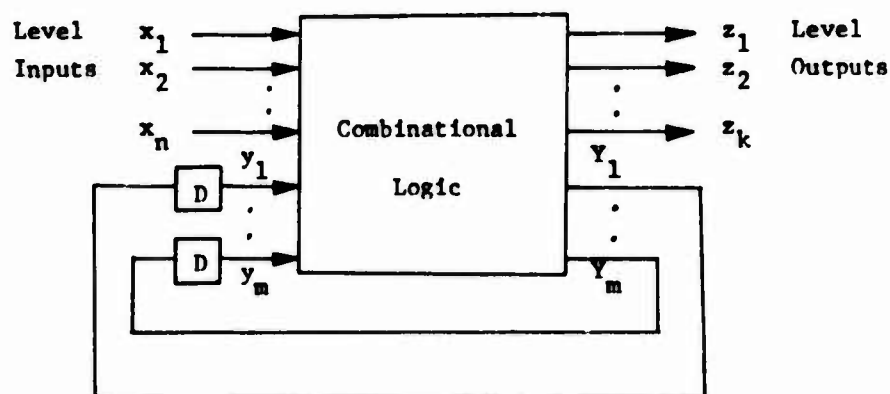
Figure 2. Sequential network model.

152
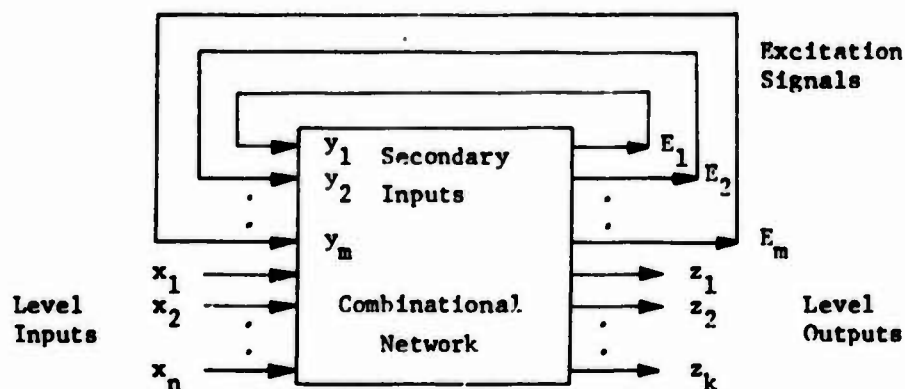
Figure 3. Sequential model with flip-flop memory.

Methods for assigning the auxiliary inputs and for obtaining Boolean algebra expressions for assigned inputs are presented in numerous modern textbooks on switching theory. Marcus(1)[1] has a clear, easy-to-follow presentation. Although these synthesis procedures were developed for electrical and electronic switching networks, Fitch (2) has shown that the procedures can be applied equally well to fluid logic networks. Some recent papers present minor variations in the method of assignment of auxiliary inputs, but the basic approach is the same.

The synthesis technique associated with the pseudo-combinational model is sometimes called the "classical" method because it was the first procedure which was totally rational, and did not depend on intuition.

While, intuition is avoided, the classical method is limited in usage by the number of variables it can handle. Network equations are obtained by constructing and interpreting a series of rectangular matrices, known as Karnaugh maps. These maps provide a cell space for

[1]Numbers in parentheses refer to references a the end of this paper.

153

each possible combination of the input variables. Three variables call for a map having 2^3 or 8 cells. Four variables require 2^4 or 16 cells, etc. As the number of variables increases the map size grows exponentially. After 5 or 6 variables, the maps become difficult to interpret and digital computers must be used to aid in the reduction.

STEERING GATE MODEL

This model of a sequential network is made possible by the concept of a steering gate as a logical memory device. The steering gate is a passive device without an output of its own. Its function is to direct or distribute an incoming signal to different destinations within the network. Its role is much like that of a switch in a railroad yard, with the train being thought of as the signal to be directed.

The steering gate is also called a "Y-gate" because it acts as a "Y" in the signal path and can direct the signal in either one of two directions. Figure 4 is a symbolic representation of a Y-gate. When the input signal x is absent, the gate has no output. That is, terminals labeled xy and x$\bar{y}$ both have a logical value of zero. When input signal x appears, it is steered in one of two directions, depending on the state of the Y-gate. If the gate is in the set state, signal x will cause terminal xy to have a logical value of 1 while terminal x$\bar{y}$ remains zero. Conversely, if the Y-gate is in the reset state, signal x will cause terminal x$\bar{y}$ to become 1 while terminal xy remains zero. The state of the gate is established before the arrival of signal x and the state is not changed again while signal x is present.

Input signal
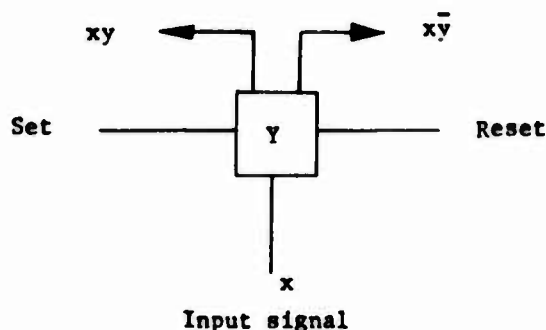
Figure 4.   Steering gate symbol.

154

A signal may be distributed in as many directions as desired simply by cascading Y-gates. Three-way distribution is accomplished by two Y-gates as shown in Figure 5. Note that the signal output labeled $x\bar{y}_1$ is independent of the state of gate Y_2. If four way distribution were required, signal xy_1y_2 would be used as the input to a third Y-gate, Y_3. In general, if an input signal is to be distributed in n directions, (n-1) gates are needed.
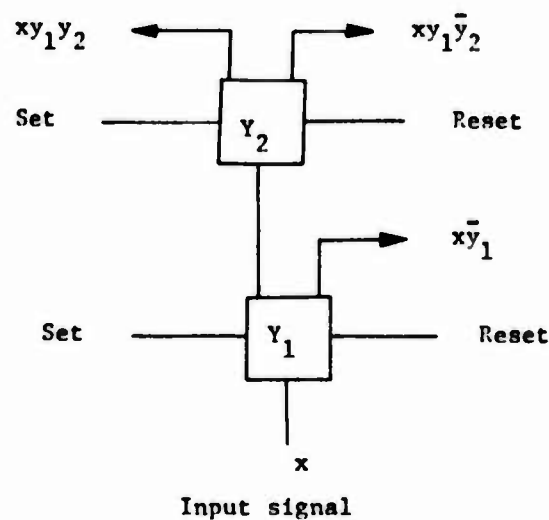
Figure 5. Three-way signal distribution using steering gates.

The concept of the steering gate has permitted the formulation of a second basic model of the generalized switching network. This model is illustrated in Figure 6. Note that only the input variables enter the combinational logic section, producing discrete input vector states that depend on the values of the input variables.

Now, the switching network can be defined as a memory operator which translates the input vector states into corresponding output states as defined by the machine specification. If the specification is combinational, the operator simply has zero memory. When the specification is sequential, the operator must apply memory modification to those input states which do not produce unique output states. If an input state always corresponds to a unique output state, then the operator will perform no memory modification on that input state. Only input states corresponding to multiple output states will receive memory modification. Thus a switching network may be completely combinational, completely sequential or anywhere in between.

155
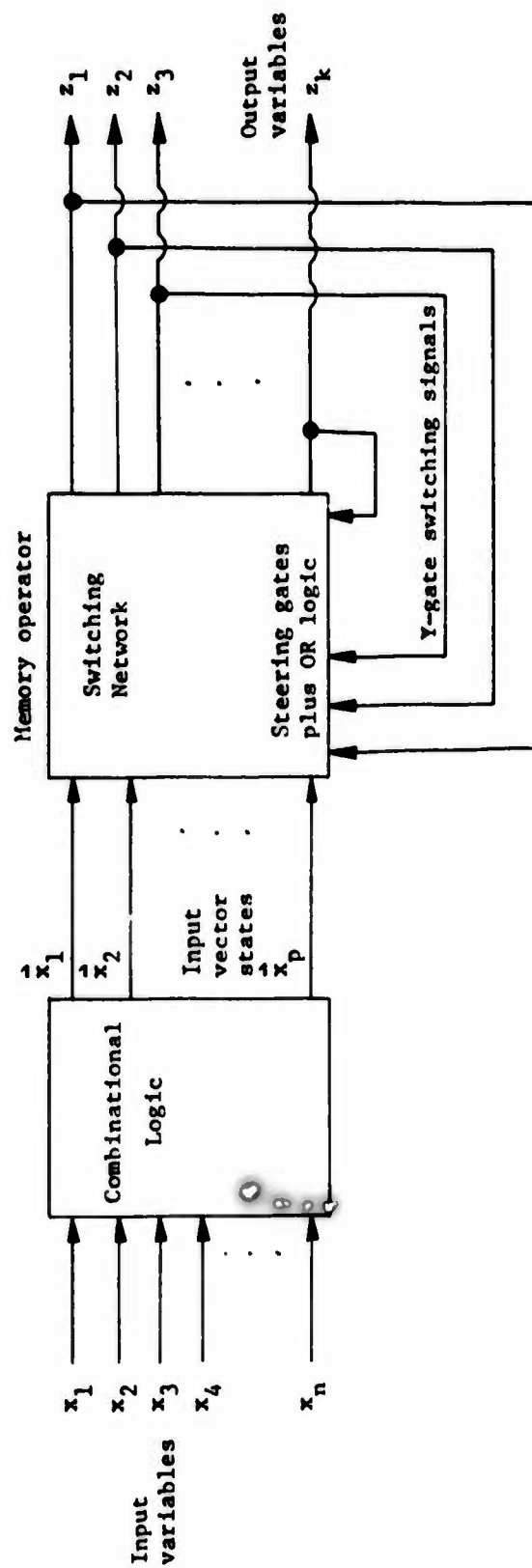
Figure 6. Steering gate model for sequential network.

156

Relatively new synthesis techniques are used to derive working networks based on the steering gate model. Reference (3) presents a method for deriving network equations when the sequence of input states is constrained to always occur in a specific order. References (4, and 5) treat the case where alternate transitions between input states are allowed to occur. Since Y-gates and their switching signals can be chosen without the use of Karnaugh maps, the procedures are more direct and it is easier to synthesize large networks than with the classical method.

References (3, 4, and 5) also show how Y-gates can be made from existing fluid logic devices. A miniature pilot operated, detented spool valve can be used directly as a Y-gate. Also, two "AND" gates combined with an active flip flop can make up a Y-gate. A third way is to use a passive flip flop cascaded with an active flip flop; but special care must be taken in the design.

When all NOR logic is used, the steering gate suffers in economy of components; for it requires eight NOR gates to make one Y-gate.

There is a real need to develop a new fluidic Y-gate to enhance the attractiveness of using the steering gate model. Perhaps a unit consisting of 3 Y-gates in cascade, with the option of using all or part of it, would be an optimum configuration.

SUMMARY

Basic conceptual models of fluid logic networks have been presented. Designers are encouraged to become familiar with these concepts and the synthesis procedures associated with each, in order to achieve maximum versatility in design capability.

The model selected should be determined by the complexity of the problem and by the hardware to be used in implementing the network.

REFERENCES

1. Marcus, M. P., _Switching Circuits for Engineers_. Englewood Cliffs, N. J.; Prentice-Hall, Inc., 1967.

2. Fitch, E. C., Jr., _Fluid Logic_, Oklahoma State University, Stillwater, Oklahoma, 1966.

3. Cole, J. H. and E. C. Fitch, Jr., "Synthesis of Fluid Logic Circuits with Combined Feedback Input Signals." _Fluidics Quarterly_, Vol. 2, No. 5, pp 14-21 (1970).

4. Woods, R. L., "The State Matrix Method for the Synthesis of Digital Logic Systems." (M.S. Thesis, Stillwater: Oklahoma State University, 1970).

5. Cole, J. H. and E. C. Fitch, Jr., "Synthesis of Fluid Logic Networks with Optional Input Signals," ASME Paper 70-Flcs-19. _Fluidics Quarterly_, Vol. 2, No. 5, pp 22-29 (1970).

Fluidic Threshold Logic - State of the Art

by

Charles A. Martin
General Motors Institute
Flint, Michigan

Abstract

The state of the art of fluidic, threshold logic is perhaps more de-
veloped than is commonly known. Threshold logic is not just another tech-
nique used to simplify the complex problem of digital design. It is a new
philosophy, for it involves not only the mere presence of a signal but al-
so its relative strength.

With threshold logic, logic functions may be implemented with fewer
gates than the usual AND, OR/NOR combinations. Thus, the possibility
exists for increases in system speed and savings in equipment by the proper
use of threshold elements.

This paper will summarize the present state of development of fluidic
threshold logic from synthesis to implementation, with single thresholds,
variable thresholds and multi-thresholds.

Introduction

The synthesis of digital control systems involves the proper interconnection of elementary building blocks or elements to realize specific outputs from a given set of inputs. Classes of elements vary in richness, that is in the ability of a single element of one class to realize more output functions than an element of a poorer class from a given set of inputs. One class of elements consists of AND, OR, and NOT gates. Another richer class consists of NAND and NOR elements. A still richer class consists of THRESHOLD ELEMENTS.

In digital fluidic control systems, NOR, OR, and sometimes AND gates form the usual basic building blocks. These building blocks are connected to one another in one way or another so that specific combinations of system ON-inputs result in particular ON-outputs, such as in the construction of adders, counters, etc. With these blocks or elements, any digital logic function may be implemented.

This approach, however, can be too diffuse, that is, it accomplishes its ends with too many devices and in too many steps. Long ago, manufacturers and merchants learned that the weighing of small objects was faster and cheaper than the counting of each one. The same principle is used in threshold logic and with threshold gates.

Since the logic function realized by a single threshold element is relatively complex in comparison to that realized by the usual AND, OR, or NOR gates, a given function can, in general, be implemented with fewer threshold elements. Thus, the possibility exists for increases in speed and savings in equipment by the proper use of threshold elements in logic circuits.

Threshold elements, probably the most potentially powerful, logic elements currently being studied and used in logic circuits, were first theoretically discussed in 1943 by McCulloch and Pitts and later by von Neumann, with emphasis on reliability. These authors regarded such logic elements as mathematical models of neurons, used for the processing of neurological data in living organisms (Ref. 1 and 12). Since then, logic elements based on the threshold principle have been used in both electrical and fluid circuits.

Threshold elements may be placed in three general categories:

      a. Single threshold elements
      b. Multi-threshold elements
      c. Variable threshold elements.

Single Threshold Elements

A threshold element (T.E.) is a device with at least one two-valued output and a number of two-valued inputs. Associated with each input is a real number called the weight. The output of the device is a constant denoted by the logic value ZERO (off) unless the weighted sum of the inputs equals or exceeds a real number called the threshold, in which case the output assumes a distinctly different constant value denoted by the

logic value ONE (on). In threshold logic, this is the basis for the definition of a single threshold element and may be stated as (Ref. 1):

$$f = 0 \quad \text{iff} \quad T > \sum_{i=1}^{n} w_i x_i$$
(OFF)

$$f = 1 \quad \text{iff} \quad T \leq \sum_{i=1}^{n} w_i x_i$$
(ON)

where f is the logic function realized
 T is the threshold value
 w_i is the weight factor
 x_i is the logic input values for the ith terms, 1 or 0
 iff means "if and only if"   (1)

This is shown graphically in Figure 1.

The sum and product operations used in Eq. (1) are the usual arithmetic ones. The notation

$$f = \sum_{i=1}^{n} w_i x_i \quad T$$
(2)

is sometimes used to represent Eq. (1). The function f may also be thought of as a Boolean-function representation,

$$f = F (x_1, x_2, \ldots x_n)$$
(3)

in which the value of the function is expressed in terms of only the independent variable x_i and the Boolean operators, +, OR; ·, AND; and —, NOT.

Figure 2 shows diagrammatically a single threshold, threshold element with two binary inputs, the independent variables x_A and x_B, and a single output.

The translation from the function representation in terms of threshold notation, Eq. (2), to the Boolean-function representation, Eq. (3), is straightforward. The problem is to translate from the Boolean-function to the threshold representation.

Multi-threshold Elements

The multi-threshold element is a generalization of the conventional threshold element in which k thresholds (k = 1, 2, 3...), rather than the usual single threshold, are used to separate the true inputs from the false inputs. The following is a definition of a k-threshold T.E. (Ref. 2):

$$f = 1 \quad \text{iff} \quad T_1 \leq \sum_{i=1}^{n} w_i x_i$$

$$\text{or} \quad T_{2j} \geq \sum_{i=1}^{n} w_i x_i \geq T_{2j+1} \quad (j = 1, 2, 3...)$$
(4)

161
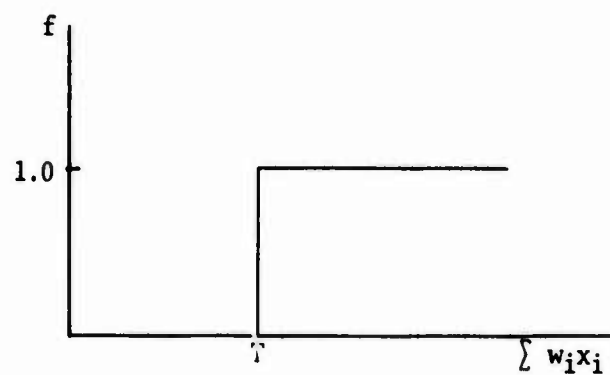
Figure 1. Definition of a threshold function.
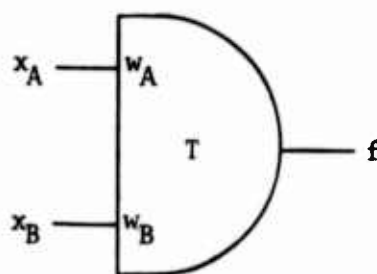
Figure 2. The symbol for a single threshold element with two inputs.
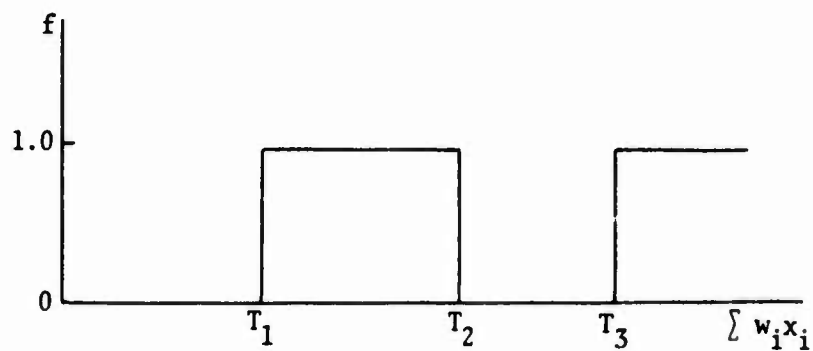
Figure 3. Definition of a multi-threshold function.

162

f = 0 otherwise,

where n is the total number of inputs
k is the total number of thresholds.

The multi-threshold, threshold element with a number k different threshold levels (Figure 3) will switch ON and OFF as the weighted input is increased. Any arbitrary logic function can be realized, theoretically, by a single k-threshold, threshold element having sufficiently large k (Ref. 2).

Variable Threshold Elements

The variable threshold element has a variable threshold, fixed input weights and a variable output logic function (Ref. 5). The output logic function is variable with a variable threshold element because as the threshold is varied a set of logic functions is produced. This is best demonstrated with an example.

In Figure 2 is shown a representation of a single threshold element with two inputs, x_A and x_B. If some arbitrary value of an input control variable q is chosen to be a basic unit, then let the threshold level be set at Tq. Let the weighted input $w_A x_A$ be a value of either 2q or 0. Let the weighted input $w_B x_B$ have a value of either 1q or 0. Let the element be ON when the input is greater than or equal to Tq, where in this case we set $1 \geq T > 0$. When $w_A x_A$ is 0 and $w_B x_B$ is 1q, the element is ON. When $w_B x_B$ is 0 and $w_A x_A$ is 2q, the element is ON. When $w_A x_A$ is 1q and $w_A x_A$ is 1q, the element is ON. When $w_A x_A$ is 0 and $w_B x_B$ is 0, the element is OFF.

A truth table and a Karnaugh map will be used to see what function is realized. When an input is ON, it will have a logic value of 1, and when OFF, it will have a logic value of 0.

x_A	x_B	Element State	f
0	0	OFF	0
0	1	ON	1
1	0	ON	1
1	1	ON	1

The function realized is then A + B, A OR B, (a logic OR function).

The switching setup is now modified by increasing the element's threshold level. Using this modification with several threshold levels, the functions that will be realized may be found by using a tabular technique.

163

Threshold	$w_A x_A$	$w_B x_B$	Element Effective Input
T	0	0	-T
T	0	1	1-T
T	2	0	2-T
T	2	1	3-T

(In the form of a truth table when an ON condition occurs, the effective input is non-negative.)

Let the threshold be set so that $2 > T > 1$. Using a Karnaugh map, it is seen that the function realized is then logically A.

When the threshold is set so that $3 > T > 2$, the function generated is then AB, A AND B, (a logic AND function). If the threshold is more positive than three, the element will never be turned ON, $f = 0$. If it is negative, the element will never be OFF, $f = 1$.

Thus, by varying the threshold level, one two-variable input configuration can realize at least five logic functions. If the output complement is also available, eight different functions are realized.

Input Weights	Threshold Values	f	$\overline{f}$
$w_A = 2$	$T < 0$	1	0
$w_B = 1$	$0 < T \leq 1$	$A + B$	$\overline{A}\ \overline{B}$
	$1 < T \leq 2$	A	$\overline{A}$
	$2 < T \leq 3$	A B	$\overline{A} + \overline{B}$
	$3 < T$	0	1

To demonstrate the power and versatility of threshold logic elements, a two input, single threshold element can be used, ideally, to realize fourteen of the sixteen logic functions that it is possible to realize. It cannot realize the EXCLUSIVE OR function or its complement.

The Threshold Element

Essentially, a threshold element consists of weights with corresponding binary inputs (which may be OFF, logic ZERO, or ON, logic ONE) a device to sum each input weight-product and a quantizer to dichotomize the analog sum into a binary output. (See Figure 4.)

From an analysis of work in the field, there seems to be three basic possible approaches to weights in fluidic threshold logic design.

1) Pressure: Each weighted input could correspond to a given input pressure.
2) Restriction, resistance, flow: Each weighted input could correspond to a given restriction value or flow value.
3) Momentum flux, jet positioning: In this method, jet streams interact so that the resultant stream is positioned according to relative momentum flux strengths.

164
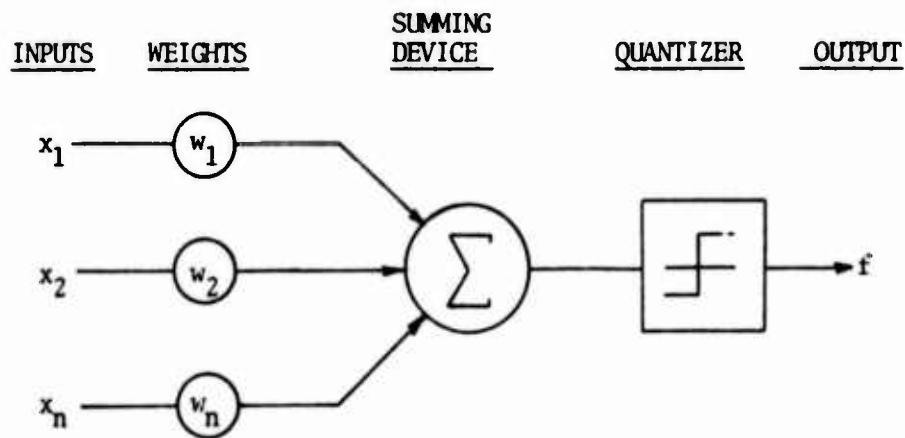
Figure 4. A threshold logic element.

$P_{o1} = P_{o2} = \ldots = P_{oi}$

$R_1 = R_2 = \ldots = R_n =$ Forward resistance

$R_1' = R_2' = \ldots = R_n' =$ Reverse resistance

$P_o =$ Const.
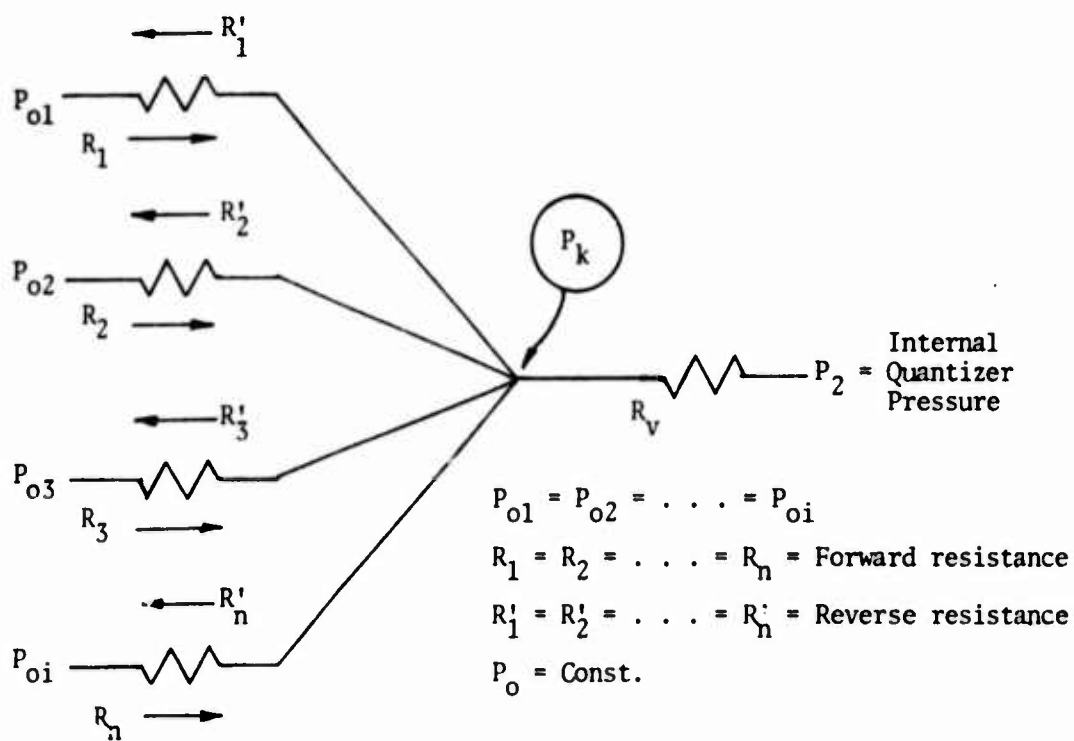
Figure 5. Idealized summing junction model.

165

Figure 7. Summing chamber characteristics for turbulent restrictions

$$q_i = K_i \sqrt{P_i - P_k}$$

$$K_1 = K_2 = K_3 = K_4$$

1. $K_1' = K_2' = K_3' = K_4' = 0$ $K_v = K_1$ (diodes)

2. $K_1' = K_2' = K_3' = K_4' = K_v = K_1$

3. $K_1' = K_2' = K_3' = K_4' = K_1 = \dfrac{K_v}{2}$

Normalized summing pressure $\dfrac{p_k}{p_{k\ max}}$

Weighted input sum $\sum\limits_{i=0}^{4} w_i x_i$

Figure 6. Summing chamber characteristics for laminar restrictions

$$q_i = G_i(P_i - P_k)$$

$$G_1 = G_2 = G_3 = G_4 = G_v$$

1. $G_1' = G_2' = G_3' = G_4' = 0$ (diodes)

2. $G_1' = G_2' = G_3' = G_4' = G_1$

3. $G_1' = G_2' = G_3' = G_4' = 2G_1$

Normalized summing pressure $\dfrac{p_k}{p_{k\ max}}$

Weighted input sum $\sum\limits_{i=0}^{4} w_i x_i$

166

"Summation" may be accomplished in two ways:

A) Continuity: The sum of the mass flows into a fluid junction, under steady flow conditions, is zero.

B) Momentum flux vector summation: The sum of the input momentum flux vectors equals the output momentum flux vector.

Of the summation techniques described, "continuity" is perhaps the most useful and the most versatile. With this approach, a manifold summing chamber is used.

The first question that may come to mind with a summing chamber is, what is it that is being summed? Looking at the basic fluid relations of continuity or energy, it could be either mass flow or energy flux. Energy flux is, however, a function of mass flow and the total mass flow is a function of the energy losses. Whatever the "actual" summed parameter, since all fluid control devices may be considered pressure controlled devices, pressure may be considered as the summed parameter in the summing chamber.

Pressure summation in a manifold type chamber is generally not a linear summation. Fortunately linear summation in connection with threshold logic is not necessary and in many situations it is not desirable. All that is necessary is a repeatable, known relation between the pressure "sum" (the chamber pressure) and the inputs present. This means that the variation in chamber pressure may not even resemble a summation in the usual sense. However, since the basic intent is to bring together or sum the input signals, the term "sum" may be used to denote this intent.

The manifold summer is a versatile device, as it can be used in conjunction with dead ended input devices such as spool valves, or with flow input devices such as fluidic units. A wide variety of summing characteristics may be obtained by varying restriction and input pressure values and relative vent conditions, even multi-threshold characteristics can be obtained. Figure 5 shows an idealized manifold summing model. Figures 6 and 7 show some manifold summing characteristics.

Existing Fluidic Threshold Elements

Figures 8 through 11 show examples of fluidic devices that have been used in a threshold logic manner. These devices will now be examined in light of the past discussion.

In Figure 8 is shown a threshold gate which consists of four basic elements (Ref. 3). This unit has three summing devices. Two identical devices, which operate on somewhat of a momentum principle, are used to sum pressure signals on either side of a proportional amplifier. The proportional amplifier then sums the two summed signals. The bistable device is the quantizer.

This gate which was used as a single threshold element in a fluidic binary comparator may also be used as a two threshold element, if the proportional amplifier is overdriven.

167

In Figures 9 and 10 are shown examples of momentum flux operated threshold gates (Ref. 4). The unit in Figure 9 realizes a one threshold function and the unit in Figure 10 realizes a two threshold function.

Shown in Figure 11 is probably the most versatile of the threshold units (Ref. 10). This unit, using a manifold summing chamber, can be made to have a variety of characteristics. It can be used to realize a still undetermined number of different logic functions. It can easily be used in a variable threshold mode. It can also, with proper summing input conditions, be used in a multi-threshold mode.

Threshold Logic Synthesis

As stated earlier, the problem is how to realize the threshold representation of a given Boolean-function. If the Boolean function is realized by one single threshold element, this is not a difficult problem (Ref. 8).

For the synthesis of these Boolean-functions, the first thing that must be done is to limit the problem to one of single thresholds. This may be done by using the criteria as stated by Winder (Ref's. 8, 12).

Using the technique outlined in Reference 8, the magnitudes of input weights and relative threshold values may be easily calculated. The keys to this method are the application of the definition of a single threshold function, Eq. 1, and the use, for weight values, of a base number raised to integer powers N^0, N^1, N^2, etc. $N! \neq 1$.

Conclusion

Fluid threshold logic offers the designer a new tool for implementing control systems. Individual threshold gates may cost more but they'll produce savings because fewer will be needed for specific control functions and some will be able to realize different functions at different times, perhaps resulting in further circuit simplifications. It is hoped that the system reliability will increase and the price will decrease with the prudent use of threshold logic. With these elements previously unusable, design approaches are now possible. Threshold logic should prove to be a big step forward in fluidic technology.
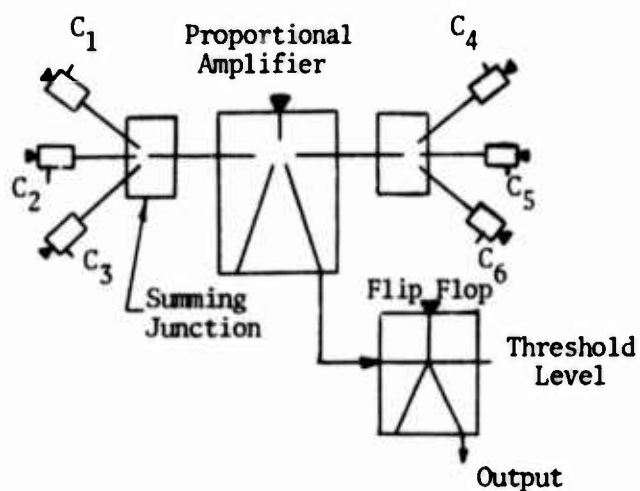
Figure 8. Threshold device designed by Eckerlin and Bell (Ref. 3).
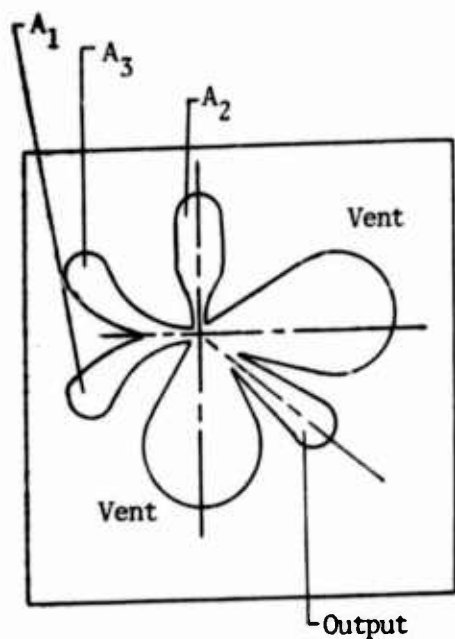
Figure 9. Fluidic threshold gate for function, $F = A_1(A_2+A_3)$ (Ref. 4).
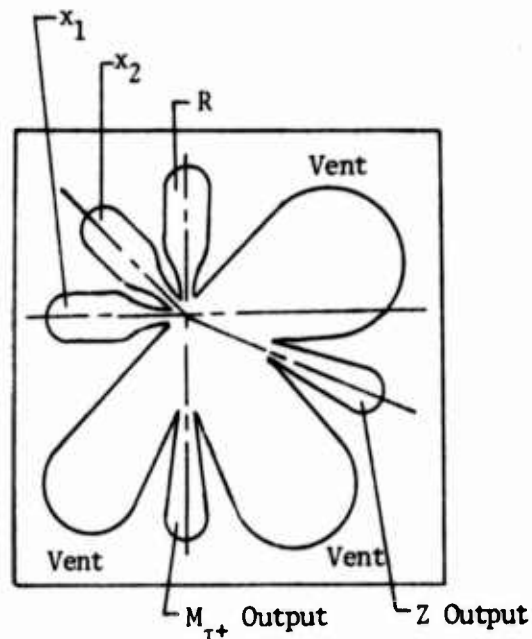
Figure 10. Threshold gate for two-hand security system (Ref. 4).
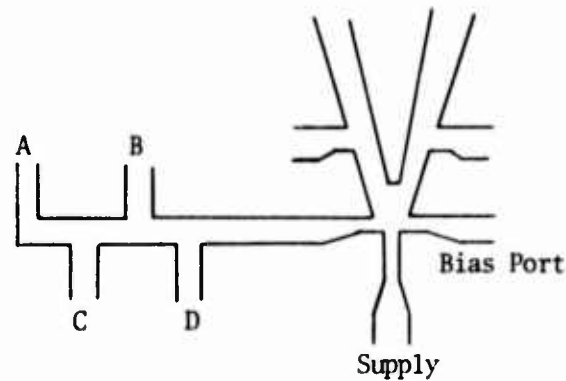
Figure 11. A four variable, single threshold logic element (Ref. 10).

References

1. Dertouzos, M.L., Threshold Logic, Cambridge, Mass., The M.I.T. Press, (1965).

2. Haring, D.R., Multi-Threshold Threshold Elements, IEEE Trans. Elec. Computers, pp. 45-65 (February 1966).

3. Eckerlin, H.M. and Bell, N.R., Fluidic Realization of Threshold Logic, ASME, 68-WA/FE-28 (December 1968).

4. Jaskolski, E.P. and Camp, D.T., Fluidic Threshold Logic, ASME 71-WA/Flcs-5 (December 1971).

5. Meisel, W.S., Variable-Threshold Threshold Elements, IEEE Trans. Computers, pp. 656-667 (July 1968).

6. Lewis, P.M. and Coates, C.L., Threshold Logic, New York: John Wiley and Sons (1967).

7. Martin, C.A., Threshold Logic and Fluidics, Fluidic Symposium, Amer. Soc. Tool & Mfg. Eng., MS69-586 (June 1969).

8. Martin, C.A., Examples of Threshold Logic, Soc. of Mfg. Eng., NE Eng. Conf., MS70-529 (October 1970).

9. Martin, C.A., Threshold Logic, Machine Design, pp. 102-105 (January 25, 1973).

10. Martin, C.A., Threshold Logic and Existing Fluidic Devices, 6th Cranfield Fluidics Conference, March 1974.

11. von Neumann, J., Theory of Self-Reproducing Automation, Urbana, University of Illinois Press, 1956.

12. Winder, R.O., Threshold Logic Will Cut Costs, Especially with Boost from LSI, Electronics, pp. 94-103 (May 27, 1968).

STATE DIAGRAM SYNTHESIS FOR FUNDAMENTAL MODE SEQUENTIAL
FEEDBACK CONTROL CIRCUITS

P. I. Chen
Applied Science and Engineering Department
Portland State University

Y. H. Lee
Physiology Department
University of Oregon Medical School

Portland, Oregon

The authors present their state diagram method for designing fluidic
sequential feedback control circuits of the fundamental mode. To illus-
trate this method, two hypothetical systems are used. They consist of a
series of events characterized by the piston positions of some double-
acting cylinders. Each extension or retraction of a piston provides a
feedback signal which can initiate the next action through a fluidic
circuit. If different control signals are resulted from a unique com-
bination of feedback signals, the circuit design is straight forward.
Otherwise, secondary variables are required in order to avoid ambiguities.
Two kinds of ambiguous pairs are defined and their implication in ob-
taining the secondary variables are described. When a sufficient number
of secondary variables are achieved they are shown graphically along with
the feedback and the control signals to form a state diagram. On this
diagram, "don't cares" and bistable conditions are identifiable which,
when fully utilized, a set of final control equations for circuit implemen-
tation can be obtained. Possible signal hazards can also be detected from
the state diagram.

INTRODUCTION

This paper presents a newly developed method for designing fluidic
sequential feedback control circuits of the fundamental mode. A general
model of such a circuit with feedbacks is shown in Figure 1. In this
figure, X1, X2,..., and Xm stand for external control signals, or the
external inputs; L1, L2,..., and Ln express the feedback signals, or the
feedback circuit inputs; Y1, Y2,..., and Yp indicate the secondary variables;
and C1, C2,..., and Cp are the circuit outputs, or the control signals. If
a change in one input occurs while there is no change in other inputs until
the transition of each secondary variable and each output signal is stabil-
ized, the circuit is said to be operating in the fundamental mode.

To illustrate this method, two hypothetical systems containing a series
of events characterized by the positions of two pneumatic (or hydraulic)
cylinders are used. Each extension or retraction of a piston provides a
feedback input signal as a base for logic decision to initiate the next
action through the fluidic circuit that is to be designed.

When an operating function of a system has been selected, the logic
condition of each feedback signal and each control signal at every state is

171

determined. A logic relationship between these two classes of signals can be established. According to this relationship, a control circuit may be designed by using the feedback signals as inputs to obtain a proper control signal for each state. However, if there are two states in the operating sequence which possess a same combination of feedback signals but different control signals, a secondary variable is needed to differentiate between the same appearance of the ambiguous feedback combination. These two states are said to be an ambiguous state pair.

In this method, a secondary variable is obtained by set-reset of a flip-flop element with a pair of feedback signal combinations. If any two states in a system possess a same feedback signal combination but different control signals, these two states are called an ambiguous pair of the first kind. If two states with a same feedback combination and their respective following states are ambiguous, they are called an ambiguous pair of the second kind. A secondary variable must first be found for the ambiguous pair of the second kind. This variable together with the feedback signals if used to set-reset of a flip-flop, another secondary variable can be obtained for the ambiguous pair of the first kind. Now with the aid of a secondary variable two ambiguous states can be made differentiable between each other. Therefore, if enough secondary variables are obtained, an ambiguous system may become non-ambiguous. These variables are then shown graphically along with the feedbacks and the control inputs as a state diagram. On this diagram, "don't cares"and bistable conditions are easily identifiable which when fully utilized a set of control equations for circuit implementation can be obtained. These control equations may be combined with other system requirements, such as start and stop, to form a complete circuit.

ILLUSTRATIVE EXAMPLES

In order to illustrate the synthesis technique, two simple control systems involving the extension and retraction of two pneumatic cylinders are provided.

Each system requires also a start button that will initiate the operation, a stop button that will stop the operation at the end of its cycle, and an emergency stop which will halt the operation immediately and retract both cylinders fully. Assume the cylinders are double-acting, the power valves controlling the cylinders with fluidic interface valves connected at each end and the remainder of the system fluidic. The piston positions are detectable by fluidic touch sensors which are installed at the extremes of the piston stroke. When a sensor is tripped by each extension or retraction of a piston, it delivers a feedback signal to initiate the next action through the fluidic circuit to be synthesized.

A schematic diagram of the hypothetical system is shown in Fig. 2, in which we have used Ci for control signals and Li for feedback signals.

Example 1: A certain industrial automation consists of two pneumatic cylinders which will perform one event at each step in the following order:

> Step 1   Cylinder 2 extends
> Step 2   Cylinder 2 retracts
> Step 3   Cylinder 1 extends
> Step 4   Cylinder 2 extends
> Step 5   Cylinder 2 retracts
> Step 6   Cylinder 1 retracts
>   Operation begins again or stops

Let us begin with the formulation of a table of the logic output form for the complete cycle of the event. From the table we may investigate whether additional variables are required in order to identify each unique combination of outputs for certain specified inputs. In Table 1, the first column represents the state of event, the second column, the feedback signal combinations and the third column, the appropriate control signal for initiating the next action.

The function of control signal Ci is to extend or retract the piston as soon as it receives a proper feedback signal generated from the actuation of the piston movement. From columns 2 and 3, a relationship between Ci and Li can be found, for examples,

$$C3 = L1L3 \text{ at state } 0$$

$$C4 = L2L4 \text{ at state } 4$$

By examining the feedback signal combinations, we notice that there are some combinations that appear more than once during the whole cycle, such as L1L3 at state 0 and 2. This combination will activate C3 at state 0 and C1 at state 2. However, only C3 is permitted to go "on" at state 0, while C1 must be "off"; in the same manner, C1 must be "on" while C3 must be "off" at state 2. Same situations exist for L2L3 at states 3 and 5.

Since there is not enough information available in all these cases on which a logical decision can be made, secondary variables must be introduced in order to differentiate each of these appearances of ambiguous feedback signal combinations. We can see that there are two secondary variables X and Y present in column 4. From previous definition, these variables are used to differentiate the ambiguous pairs of the first kind. With these new variables, one can obtain a new set of relationships between C1 and C3 as,

$$C3 = L1L3X \text{ at state } 0$$

$$C1 = L1L3\overline{X} \text{ at state } 2$$

SECONDARY VARIABLES

A way to generate the secondary variables is through the use of the feedback signals to set and reset the memory flip-flop elements.

By examining the condition of the feedback signals at each state, along with the required condition of the secondary signals at certain states (shown by the solid segments), one can assign a pair or a number of pairs of set and reset conditions for each of the secondary variables (as shown in Fig. 3). Once these conditions are assigned, the states of secondary signals are determined after connecting the solid and the dotted segments.

Frequently, there are multiple pairs of set and reset conditions which meet the requirement of each secondary variable. And, among these secondary variables, there may be some redundancy, i.e., variables having the same output forms. These variables, often referred to as pseudo-equivalent variables, should be combined for the sake of circuit simplicity. In this example, a variable Z can meet the required conditions of the secondary variable X,

while $\overline{Z}$ can meet the required condition of the secondary variable Y. So, we can reduce two variables X and Y to simply Z.

STATE DIAGRAM AND CONTROL EQUATIONS

The secondary variable Z can be combined with the feedback signals L1 and L3 and the control signals, C1, C2, C3, and C4 to form a state diagram as shown in Fig. 4. Since $L2 = \overline{L1}$ and $L4 = \overline{L3}$, only L1 and L3 are needed on the diagram. For the control signals, solid segments represent the required conditions, while dotted segments stand for the "don't cares."

The control signal, C1, requires "on" at state 2 and "don't cares" at states 3 and 4. This requirement can be met by using a combination of the secondary variables and the feedback signals as follows,

$$C1 = L3\overline{Z} + \underline{\overline{L1L3}}$$

where we have underlined the "don't cares."

Similarly, control signal C2 must be "on" at state 5, and "don't cares" at states 3 and 4. It can be expressed as,

$$C2 = L3Z + \underline{L1\overline{L3}}$$

We can also express C3 and C4 as,

$$C3 = L1Z + \overline{L1}\overline{Z}$$

$$C4 = L1\overline{Z} + \overline{L1}Z$$

The foregoing logic equations obtained intuitively can also be obtained by using Karnaugh Maps. However, for a problem involving more than six variables, the use of Karnaugh Maps becomes rather tedious and, therefore, not recommended. The control signals, C1, on the state diagram indicated that if each control signal covers not only the "on" conditions but also the "don't cares," then there exists a bistable condition between C1 and C2, also between C3 and C4. There are three possible selections for C1 and C2:

$$(1) \quad C1 = L3\overline{Z}$$

$$C2 = L3Z$$

$$(2) \quad C1 = L3\overline{Z} + \overline{L1}\overline{L3}$$

$$C2 = \overline{C1}$$

$$(3) \quad C1 = \overline{C2}$$

$$C2 = L3Z + L1\overline{L3}$$

Also, there are three possible selections for C3 and C4:

$$(1) \quad C3 = L1Z + \overline{L1}\overline{Z}$$

$$C4 = L1\overline{Z} + \overline{L1}Z$$

174

$$(2) \quad C3 = L1Z + \overline{L1}\overline{Z}$$

$$C4 = \overline{C3}$$

$$(3) \quad C3 = \overline{C4}$$

$$C4 = L1\overline{Z} + \overline{L1}Z$$

Based on the criterion of using minimum number of components, we have chosen the first selection for C1 and C2 and the third selection for C3 and C4 for circuit implementation.

START AND STOPS

Since the system requires start, stop, and emergency stop controls, they must all be integrated into the circuitry.

The start action is generated by activating S1, so that C3 will be on and the operation begins. The start pulse is also used to set the flip-flop to ensure that the secondary variable Z will go "on" at state 0; therefore, every operation will begin at state 0. In order to terminate the operation, we may deactivate C3 at state 0. This is accomplished by using the start-stop circuit as shown in Fig. 5. The control signal, C3, can then be expressed as

$$C3 = \overline{C4} \; (S1 + \overline{Z})$$

A stop pulse which can turn S1 to "off" will terminate the operation when it reaches the 0th state.

All that remains to complete the system requirements is the addition of any emergency stop button, S2, which when pressed will stop the cylinders movements at any state and retract all cylinders instantaneously. This is carried out by using a flip-flop to activate C2 and C4. The logic equation for control signals are now changed to

$$C1 = L3\overline{Z}S2$$

$$C2 = L3Z + S2$$

$$C3 = \overline{C4} \; (S1 + \overline{Z})$$

$$C4 = L1\overline{Z} + L2Z + S2$$

As soon as C2 and C4 are activated, the respective interface valves are energized which accordingly will retract all cylinders. At this time, power supply to the system is ready for shut down.

PHYSICAL IMPLEMENTATION

The final control equations when implemented by using fluidic elements is as shown in Fig. 6. We notice that the bistable characteristics between C3 and C4 has been utilized in the control equations.

In the final circuit, all components except that of interface valves and

175

cylinders are fluidic. The subcircuit shown in the dotted enclosure represents the control signals generated by the control equations, the subcircuit above the enclosure is for the start-stop controls, while the subcircuit on the left is for the secondary variables.

Example 2: An industrial operation requires the action of two pneumatic cylinders according to the following steps:

Step 1   Cylinder 2 extends
Step 2   Cylinder 1 extends
Step 3   Cylinder 1 retracts
Step 4   Cylinder 2 retracts
Step 5   Cylinder 2 extends
Step 6   Cylinder 1 extends
Step 7   Cylinder 2 retracts
Step 8   Cylinder 1 retracts
Operation begins again or stops

With the background of the synthesis technique as provided in Example 1, we can immediately establish Table 2. On this table, three secondary variables, namely X, Y and Z are obtained such that states 1 through 6 can be made non-ambiguous. Also, from previous definition, we know that the states 2 and 6 belong to the first kind ambiguous pair, thus make states 1 and 5 an ambiguous pair of the second kind. Also, state 0 and 4 become an ambiguous pair of the second kind. After identifying the nature of each ambiguous pair we can proceed to find the set-reset pairs for both secondary variables X and Y first before employing Y to obtain secondary variable Z. This has been shown in Fig. 7.

It must be mentioned here that there is no need to find all possible set-reset pairs for secondary variables whose function is to differentiate the ambiguous pair of the second kind. Also, it must be noted that there are cases in which more than one additional variable must be sought in order that they may be employed along with proper feedback combinations to obtain the secondary variable for differentiating the ambiguous pair of the first kind.

We shall now form the state diagram from the feedback signals L1 and L3, and secondary variables X and Z together with the four controls C1, C2, C3 and C4   (see Fig. 8). According to the previous process, following control equations are obtained:

$$C1 = \overline{L3}X + \overline{L3Z}$$

$$C2 = \overline{XZ} + L3$$

$$C3 = X + \overline{L1Z}$$

$$C4 = L1\overline{X} + \overline{X}Z$$

Similar to that in Example 1, we shall incorporate the start-stop controls as well as utilize the bistable characteristics between C1 and C2, also between C3 and C4 to obtain the final control equations as follows:

$$C1 = \overline{C2}$$

$$C2 = \overline{X}\overline{Z} + L3 + S2$$

$$C3 = (X+\overline{L1}\overline{Z})\ \overline{S2}\ (S1+Z)$$

$$C4 = \overline{(X + \overline{L1}\overline{Z})}$$

The fluidic circuit based on these equations are shown in Fig. 9. Again, the subcircuit in the dotted enclosure represents the control signals; the one above it is for the start-stop controls; while the subcircuit on its left is for the secondary variables.

POSSIBLE SIGNAL HAZARDS AND THEIR REMOVAL

By having the state diagram, one can detect all possible signal hazards in the control equations before he proceeds to construct the circuit. This is done by examining the control output form along with its input signal characteristics on the state diagram.

There exists two possible signal hazards in the final control equations in Example 1. In the equation for C1, the hazard may occur between states 0 and 1, while in C2 it may occur between states 3 and 4. These hazards can be removed by a delay of $\overline{Z}$ and Z respectively. There is no possible hazard for C3 and C4.

In Example 2, the only possible hazard is located between state 3 and state 4 for control equation C2. It can be removed by delaying the $\overline{X}\overline{Z}$ signal. The delay of each signal as stated above can be accomplished by sending that signal through a series of capacitor and resistor prior to entering its immediate following logic element as an input.

CONCLUSION

A digital circuit synthesis technique using the state diagram is presented in this paper by example of two simple two-cylinder systems. This technique provides a systematic procedure in obtaining the simplified final control equations. By using the state diagram, a circuit designer may select proper set-reset conditions to reduce the number of the secondary variables needed, he may detect possible circuit hazards as well as visualize the "don't cares" and the bistable conditions associated with the control variables. This semi-graphical method pertains not only to fluidic circuit synthesis, but is also equally applicable to analysis of digital feedback circuits to be implemented by pneumatic, hydraulic, and electronic components. In each case, considerations must be given to relate the physical characteristics of inputs and outputs with respect to the equations of control variables for proper system implementation. The power supply to the control elements and that of the actuators must be scaled to certain required levels of operation.

By this new technique, one can easily identify the state of each signal on the state diagram so that he can obtain the final control equations intuitively. When the complexity of the system increases, the complete procedure of our outlined technique can be programmed on a digital computer to facilitate the seeking of the final control equations. Therefore, as compared to other available methods, this technique offers in addition to the aforementioned advantages, a means for designing control systems of varying degrees of complexity.

REFERENCE

Chen, P.I., Lee, Y.H., "State Diagram Synthesis of Fluidic Feedback
   Circuits", ASME Paper 73-WA/Flcs-2, 1973.

Table 1   Table for Determining the Requirement of Secondary Variables

State	Feedback Signal Combination	Control Signal	Secondary Variables
0	L1L3	C3	X
1	L1L4	C4	
2	L1L3	C1	$\overline{X}$
3	L2L3	C3	Y
4	L2L4	C4	
5	L2L3	C2	$\overline{Y}$

Table 2   Table for Determining the Requirement of Secondary Variables

State	Feedback Signal Combination	Control Signal	Secondary Variables
0	L1L3	C3	$\overline{Y}$
1	L1L4	C1	X
2	L2L4	C2	$\overline{Z}$
3	L1L4	C4	$\overline{X}$
4	L1L3	C3	Y
5	L1L4	C1	X
6	L2L4	C4	Z
7	L2L3	C2	

CAPTIONS

Fig. 1   A model of the fundamental mode circuit

Fig. 2   The physical arrangement of a two-cylinder system

Fig. 3   The state diagram of secondary variables
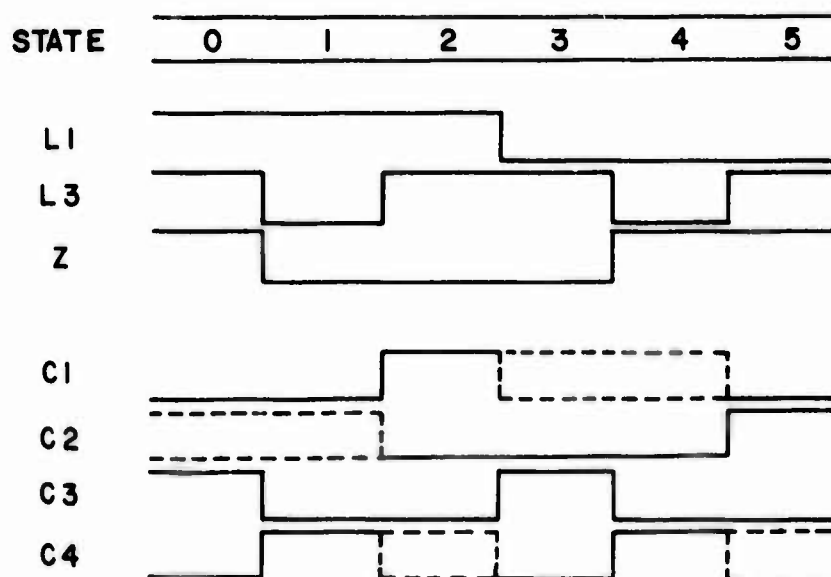
Fig. 4   The state diagram
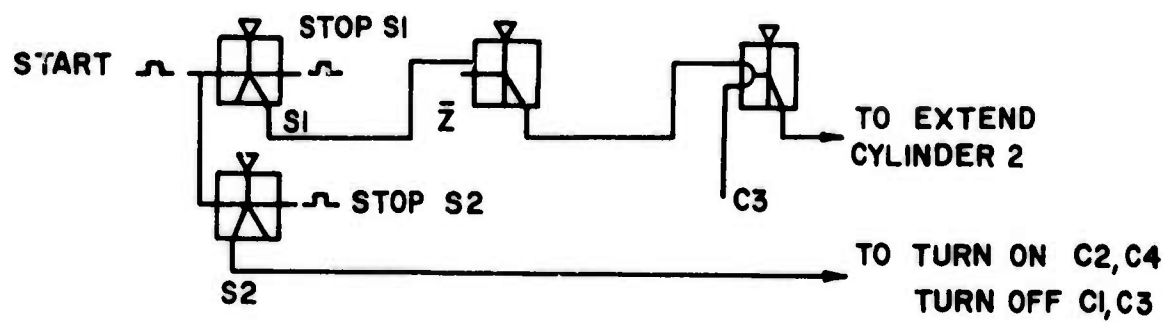
Fig. 5   The start-stop circuit
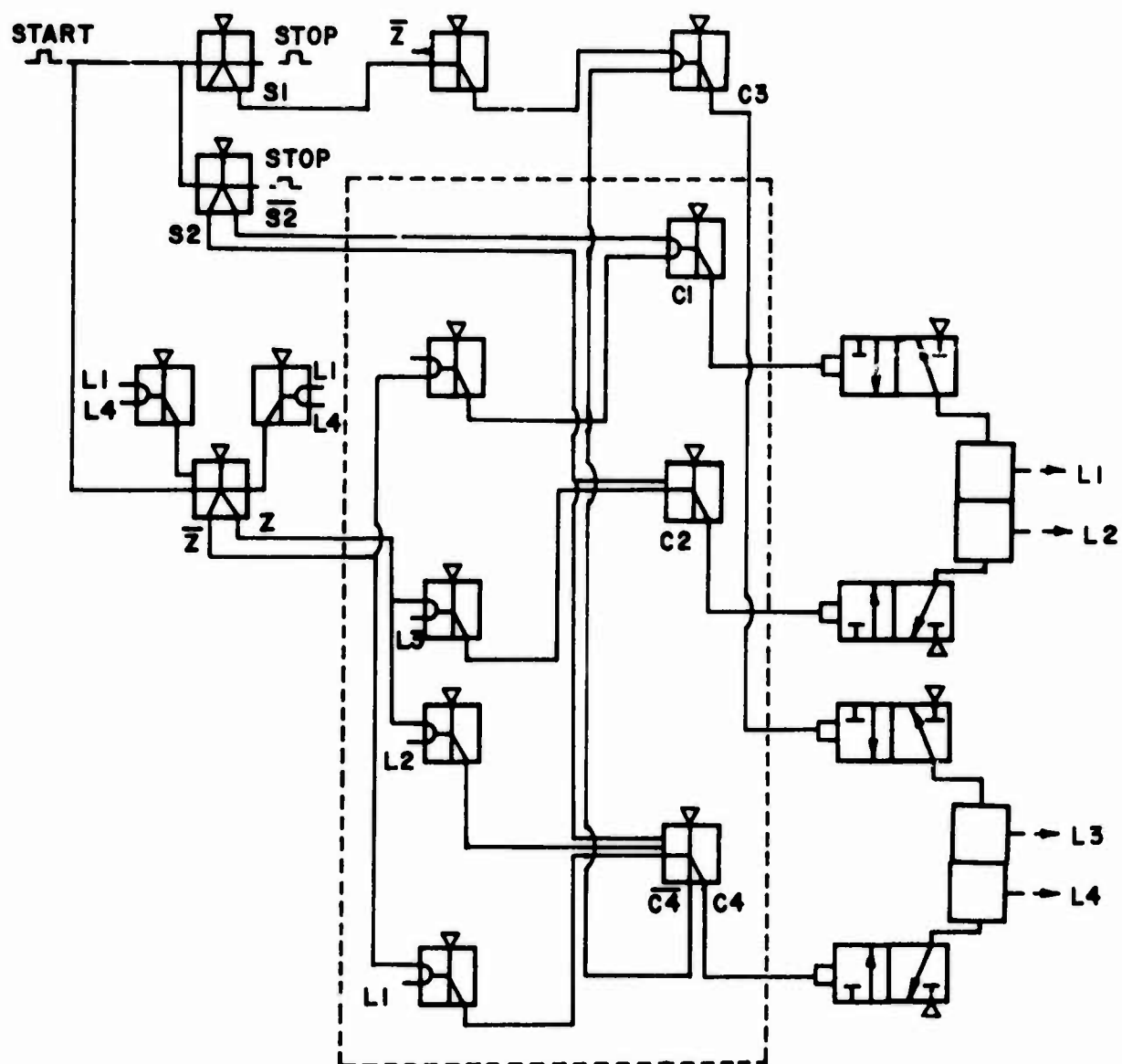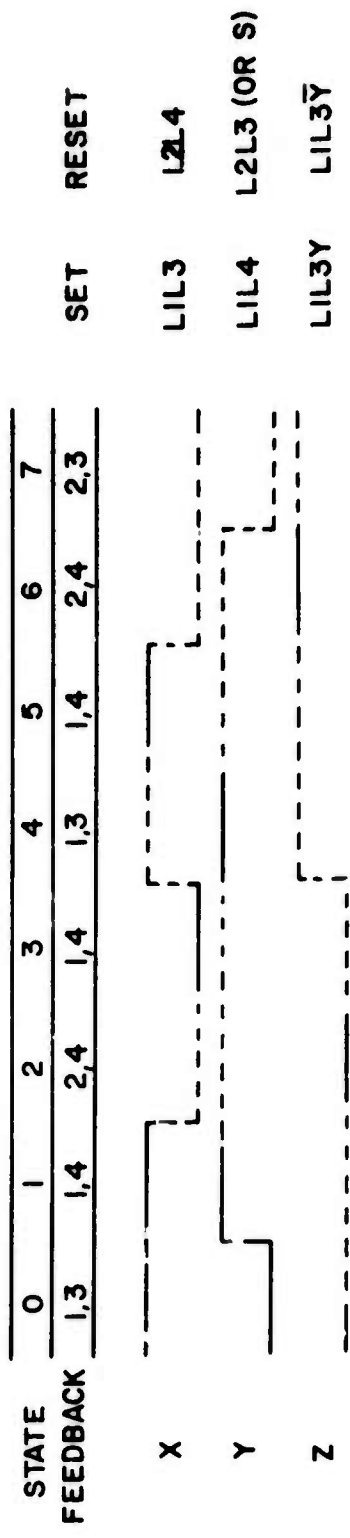
Fig. 6   The fluidic control circuit for the system in Example 1

Fig. 7   The state diagram of secondary variables
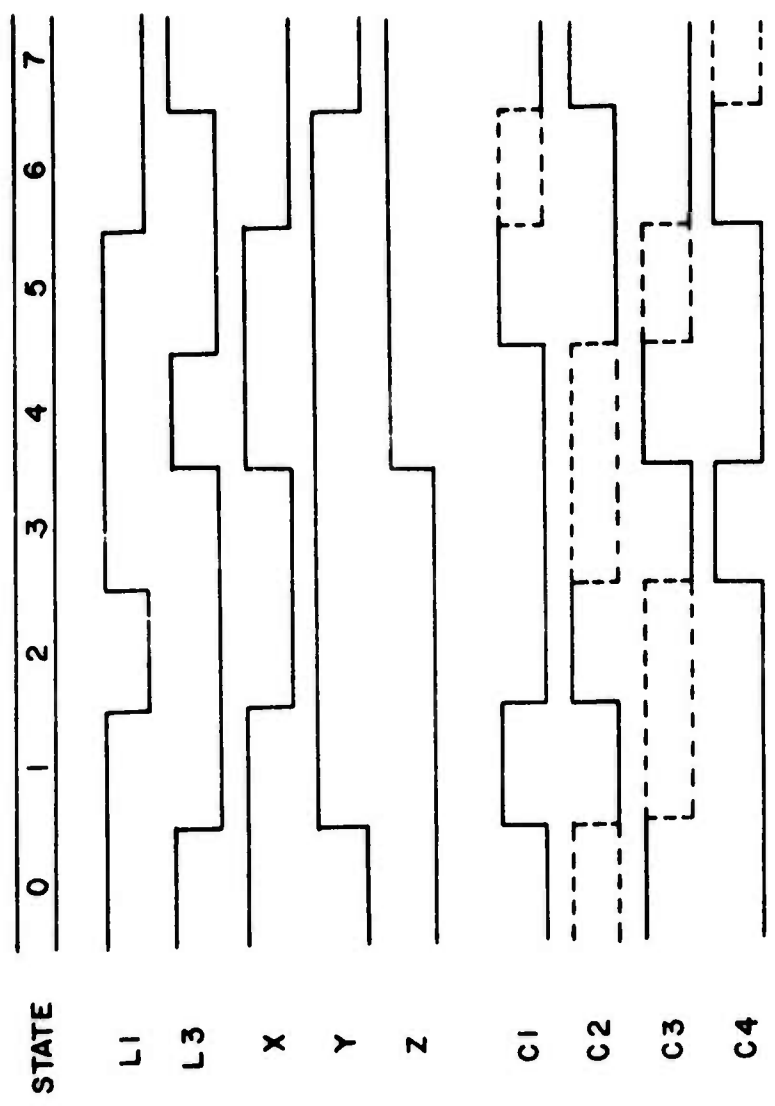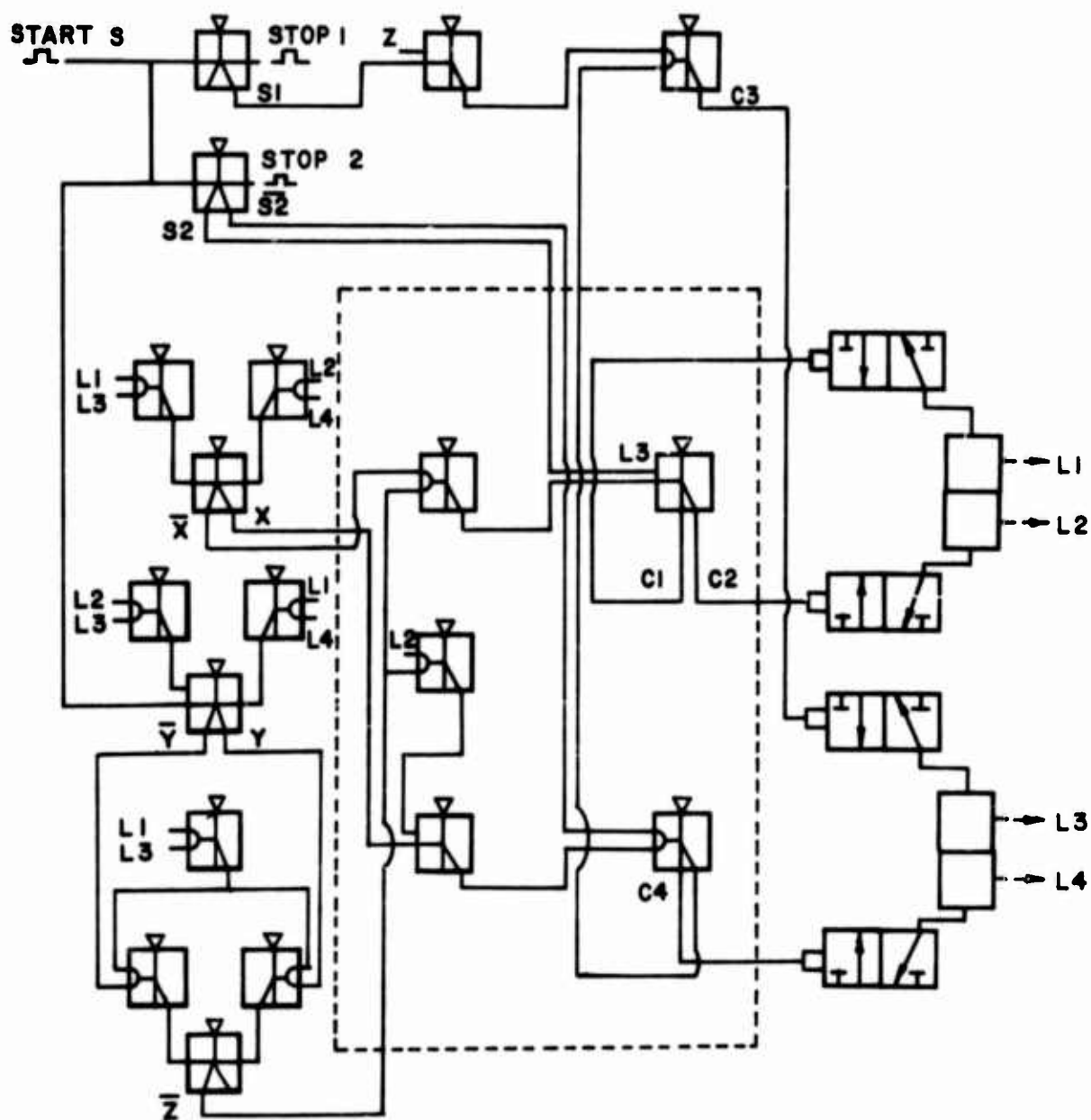
Fig. 8   The state diagram

Fig. 9   The fluidic control circuit for the system in Example 2

Fig. 1   A model of the fundamental mode circuit

Fig. 2   The physical arrangement of a two-cylinder system

182

Fig. 3   The state diagram of secondary variables

Fig. 4   The state diagram

183

Fig. 5   The start-stop circuit

Fig. 6   The fluidic control circuit for the system in Example 1

185

Fig. 7 The state diagram of secondary variables

Fig. 8 The state diagram

Fig. 9   The fluidic control circuit for the system in Example 2

187

Fluidics State-of-the-Art Symposium

꘰th Sept.-3rd Oct. 1974

Adelphi (Maryland) USA

Signal Analysis of Fluidic Networks

by

H. M. Schaedel

Fachhochschule Köln

German Federal Republic

189

Fluidic circuit theory
========================

Contents

Nomenclature

A	work in equ. (2.17)
A	area
a	aspect ratio $= h/b$
a	four pole parameters in equ. (4.25)
b	width
c	speed of sound
c_a	speed of sound in free air
C	capacitance
C_{pr}	pressure recovery coefficient
C_{pri}	ideal pressure recovery coefficient
C_R	resistance coefficient for the rectangular duct
c_p	specific heat at constant pressure
c_v	specific heat at constant volume
D	diameter
D_{nr}	radial damping number
e	mechanical potential
f	frequency
f	friction coefficient in equ. (3.7)
F_{nr}	radial frequency number
G	conductance
h	height
h,H	pressure head in equ. (2.16) and chapter 3.3 and 3.4
k	correction coefficient
l	length
L	inductance
m	mass
$\dot{m}$	massflow rate
n	gas process constant
P	power
p	overpressure
$\bar{p}$	average overpressure
p^*	absolute pressure $= p + p_0$
p_0	reference pressure (e.g. atmospheric pressure)
Pr	Prandtl number
Q	energy factor
r	dynamic resistance
$\bar{R}$	resistance
Re	Reynolds number
Rg	gas constant in equ. (2.15) and equ. (5.10)
s	entropy
T	temperature in $°K$
t	time
V	volume
v	velocity
W	complex input impedance
x	coordinate
Y	admittance
y	coordinate
z	coordinate
Z	impedance
Z_0	surge impedance
Z_{so}	surge impedance of the lossless line

α	angle
α_1	attenuation factor
α_i	eigenvalue in equ. (4.41)
β_1	wave number
γ_1	propagationfactor $= \alpha_1 + i\beta_1$
	reflection coefficient
ε	coefficient
η	efficiency
θ	angle
κ	specific heat ratio $= c_P/c_V$
λ	wave length
λ	loss coefficient in chapter 3.3 and 3.4
μ	dynamic viscosity
ν	kinematic viscosity
ν_T	thermal diffusity
ρ	density
τ	propagation time
ω	angular frequency
ω_γ	characteristic angular frequency

Subscripts

a	adiabatic
ap	apparent
d,diff	diffuser
e	effective
fd	fully developed
i	internal
irr	irreversible
l	loss
L	load
lam	laminar
m	mechanical
n	nozzle
Q	source
s	sectional
st	steady state
turb	turbulent
v,ν	viscous

Introduction

Problems of signal processing in fluidic networks are very
similar to those in electrical communication engineering.
Because we have in communication engineering excellent methods
for treating networks it is convenient to modify the basic
equations of flow mechanics and thermodynamics in such a way
that it is possible to apply those methods to fluidic networks.

Due to its linearity electrical circuit theory can be handled
with relative ease. The equations of motion in flow mechanics,
however, are nonlinear, involve momentum, temperature and tur-
bulence effects. To find a general fluid circuit theory therefore
seems to be hopeless.

In we restrict our considerations to small signals the problem
turns out to be not so serious. The governing equations then
can be linearized thus admitting a linear circuit theory for
application. The most important step therefore will be to derive
equivalent circuits for the single fluidic components.

For dc-behaviour, we mostly will have nonlinear components even
if compressibility is neglected. The linear ac equivalent then
is derived on the basis of small changes of pressure and flow
from a given operating point.

Although the assumption of small signals restricts the appli-
cation to fluid circuits it seems that results obtained in
optimizing fluidic circuits are promising.

Anyway, solving the set of fluid equations for each particular
circuit will not be possible or at least extremely cumbersome.
Therefore as long as we are concerned with signal processing in
fluidic networks a small signal circuit theory will be of great
help. In this case the whole circuit theory of communication
engineering, a powerful tool for complicated system design,
will be available to the system engineer. However, this will
only be possible if we make use of equivalent circuits, where
we consider the peculiarities of flow mechanics and thermody-
namics. We may not forget that these equivalent circuits are
only an interpretation of the basic equations under certain
assumptions.

2. The electric-fluidic analogy

In order to describe the behaviour of fluidic networks using
the methods of communication engineering we need two quantities
analogous to current and voltage.

Mass flow rate $\dot{m}$ as analog to current i is easily found because
mass flow is conserved. The node theorem in fluidic circuits
therefore will be $\sum \dot{m} = 0$. To find an analog for the electric
potential is more difficult. Mostly the pressure p is taken as

fluidic potential. The advantage is that it can easily be
measured. But the product of mass flow rate and pressure does
not yield a power term directly. In order to find a compatible
potential Kirshner (ref.1) derived a mechanical potential out
of the energy equation. He finds that the change in mechanical
power Pm is equal to the change of entropy along a streamline

$$(2.1) \quad dP_m = \dot{m} \, d \left(\int \frac{dp^*}{\rho} + \frac{v^2}{2} \right) = -d \left(T \int d s_{irr} \right).$$

For convenience in measurement the pertinent quantities are
averaged over the cross-sectional area. The losses in a fluidic
circuit are due to irreversible process the working medium
undergoes.

From equation (2.1) the mechanical potential is found as

$$(2.2) \quad de = d \left(\int \frac{dp^*}{\rho} + \frac{v^2}{2} \right).$$

p^* is denoted as absolute static pressure and p as pressure
above a reference pressure, especially above atmospheric
pressure p_o. This mechanical potential can also be enterpreted
as mechanical energy per unit mass. In a lossless duct the
mechanical energy per unit mass is constant. This is expressed
by the BERNOULLI-law for a nonuniform duct along a streamline

$$(2.3) \quad \int \frac{dp^*}{\rho} + \frac{v^2}{2} = const$$

The BERNOULLI-law therefore expresses that the mechanical
potential in a lossless duct does not change. That means de = C.

2.1 The mechanical potential for incompressible or low compressible flow

For incompressible or low Machnumber compressible flow the
mechanical potential becomes

$$(2.4) \quad e = \frac{p^*}{\rho} + \frac{\bar{v}^2}{2}.$$

This again is identical with the BERNOULLI-law for incompressible
flow

$$(2.5) \quad \frac{p^*}{\rho} + \frac{\bar{v}^2}{2} = const$$

The energy per mass unit is found to be the sum of potential (p^*/ρ) and kinetic $(\bar{v}^2/2)$ energy per mass unit. In a lossless duct the sum remains constant whereas the single portions can change rather strongly depending on the cross-sectional area.

One serious disadvantage of the mechanical potential, however, is the fact, that it cannot be measured directly. It must be calculated out of pressure, flow and density measurements.

For ac flow this will be rather difficult, because pressure and flow in general are not in phase.

2.1.1 The interpretation of the BERNOULLI-law by an equivalent circuit

To avoid these measuring problems we will define a so called cross-sectional resistance (ref.2). The mechanical potential can be written as follows

$$(2.6) \quad e = \frac{p^*}{\rho} + \frac{\bar{v}^2}{2} = \frac{1}{\rho}\left(p^* + \rho\,\frac{\bar{v}^2}{2}\right).$$

If we only use the pressure p as fluidic potential we can interpret the term $\rho\bar{v}^2/2$, representing the kinetic portion, as pressure drop across a nonlinear cross-sectional resistance

$$(2.7) \quad R_s = \frac{\dot{m}}{2\rho A^2}$$

where A is the cross-sectional area.

we find the following relation

$$(2.8) \quad e = \frac{1}{\rho}\left(p^* + R_s\,\dot{m}\right).$$

For small changes the dynamic cross-sectional resistance

$$(2.9) \quad r_s = \frac{\dot{m}}{\rho A^2}$$

must be taken into account

$$(2.10) \quad de = \frac{1}{\rho}\left(dp^* + d\left(\rho\,\frac{\bar{v}^2}{2}\right)\right) = \frac{1}{\rho}\left(dp + \frac{\dot{m}}{\rho A^2}\,d\dot{m}\right) = \frac{1}{\rho}\left(dp + r_s\,d\dot{m}\right).$$

As long as the pressure variations are small enough to neglect compressibility we can use the pressure p as fluidic potential, if we take into account the cross-sectional resistance.

The expression for power then will be

$$(2.11) \quad P_m = \dot{m}\,e = \frac{1}{\rho}\,\dot{m}\left(p^* + \dot{m}\,R_s\right) = \frac{1}{\rho}\,\dot{m}\,p_{tot}$$

where

$$p_{tot}^* = p^* + \dot{m}\,R_s$$

is a sort of source pressure. Pressure p will be equal to p_{tot} if the massflow rate is zero. If the massflow rate increases, the pressure drop across the cross-sectional resistance increases, so that p decreases.

We will now establish the equivalent circuit for a lossless nonuniform duct shown in Fig. 2.1.

Referring to the two cross-sections 1 and 2 we can write the BERNOULLI-law as

$$(2.12) \quad p_1^* + \rho\frac{\bar{v}_1^2}{2} = p_2^* + \rho\frac{\bar{v}_2^2}{2} = p_{tot}^* = const.$$

where we refer p to the atmospheric pressure

Introducing the cross-sectional resistances

$$(2.13) \quad R_{s_1} = \frac{\dot{m}}{2\rho A_1^2} \quad and \quad R_{s_2} = \frac{\dot{m}}{2\rho A_2}$$

we find a mesh theorem

$$(2.14) \quad p_1^* + R_{s_1}\,\dot{m} = p_2 + R_{s_2}\,\dot{m} = p_{tot}^*$$

which can be interpreted by the equivalent circuit in Fig. 2.2

The change in pressure between the areas 1 and 2 becomes

$$(2.15) \quad p_1^* - p_2^* = \dot{m}\left(R_{s_2} - R_{s_1}\right).$$

The change in pressure which is caused by a change in cross-section can therefore be described by the pressure drop across a nonlinear positive resistance

$$R_{s_2} = \frac{\dot{m}}{2\rho A_2^2}$$

and a nonlinear negative resistance
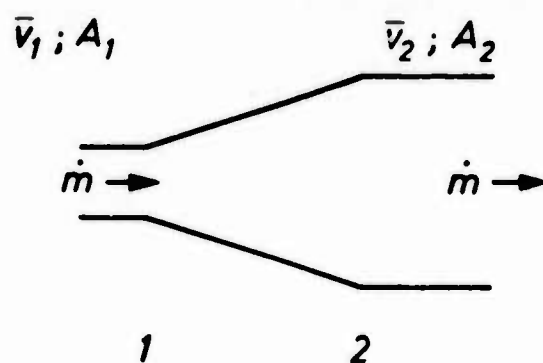
Fig. 2.1   Nonuniform duct
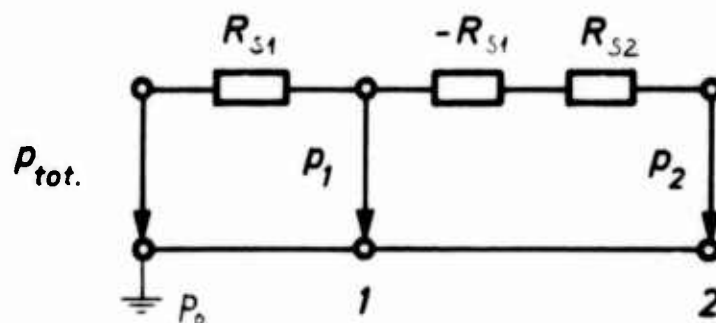
Fig.2.2   Interpretation of Bernoulli law by a network
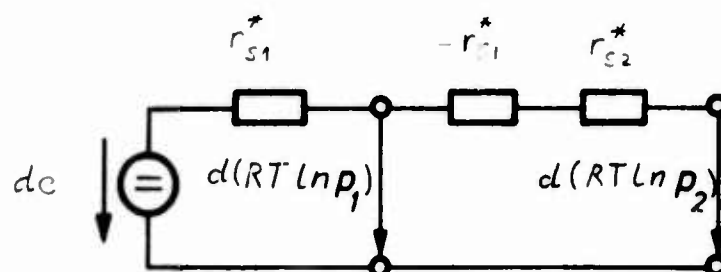
Fig.2.3   Interpretation of the mechanical potential
by a network

198

$$-R_{S_1} = -\frac{\dot{m}}{2\rho A_1^2} \,.$$

The positive resistance is responsible for the pressure decrease and the negative resistance for the pressure increase.

The geometrical relations determine which resistance is dominating. An increase in cross-sectional area causes a pressure-increase, a decrease in cross-sectional area causes a pressure-decrease.

It must be emphasized that the cross-sectional resistances have no dissipative nature. In those cross-sectional resistances static pressure is transformed into dynamic pressure and inverse. As long as pressure and flow are taken as measuring quantities one can not determine whether a pressure drop is caused by friction or change in area.

So using the idea of cross-sectional resistance we are working in reality with a potential

$$(2.14) \quad P_{tot}^* = \frac{e}{\rho} \,.$$

2.2 A fluidic potential for high pressure and density variations

Taplin (ref.3) takes the work of an irreversible steady flow machine to define a compatible force.

The total power available for work by processing from pressure p_1 to pressure p_2 can never be larger than

$$(2.15) \quad P_m = \dot{m}\, R_g\, T_1\, \ln \frac{P_1^*}{P_2^*} \,.$$

For the case of perfect throttling all energy is made unavailable and we can define a potential

$$(2.16) \quad H = R_g\, T_1\, \ln \frac{P_1^*}{P_2^*} \,.$$

We come to the same conclusion if we take the change of entropy to calculate the expression for unavailable work.

$$(2.17) \quad A_{irr} = T_1\, \Delta S = \frac{m\, R_g\, (\kappa - 1)}{n\,(\kappa - 1)}\, \ln \frac{P_1^*}{P_2^*}$$

from this we find the unavailable power to be

199

$$(2.18) \quad P_{irr} = \frac{dA_{irr}}{dt} = \dot{m} \, R_g T \, \frac{\kappa-n}{n(\kappa-1)} \, \ln \frac{p_1^*}{p_2^*} = P_m.$$

For isothermal conditions this expression will become maximal

$$(1.19) \quad P_{irr} = \dot{m} \, R_g T \, \ln \frac{p_1^*}{p_2^*}$$

or

$$(1.19b) \quad dP_{irr} = \dot{m} \, d\left(RT \int \frac{dp^*}{p} \right)$$

and using the state equation for a perfect gas

$$(2.19c) \quad dP_{irr} = \dot{m} \, d \int \frac{dp^*}{\rho}.$$

The mechanical potential defined by Kirshner

$$de = d\left(\int \frac{dp^*}{\rho} + \frac{\bar{v}^2}{2} \right)$$

therefore differs from the potential defined by Taplin

$$dH = d\left(R_g T \, \ln \frac{p_1^*}{p_2^*} \right)$$

in the term for kinetic energy $\frac{\bar{v}^2}{2}$.

Taplin shows that this potential can be used with sufficient accuracy up to pressure ratios of $p_1^*/p_2^* \leq 2$.

So this potential seems to be of great value for circuit design if compressibility cannot been neglected.

In order to find a complete mechanical potential using the ideas of Kirshner, Taplin and Schaedel would be to complete the potential of Taplin by a term considering the change of potential on a cross-sectional resistance.

$$(2.20) \quad de = d\left(R_g T \, \ln \frac{p_2^*}{p_1^*} \right) + r_s^* \, d\dot{m}$$

where

(2.21) $r_s^* = \dfrac{d(\bar{v}^2/2)}{d\dot{m}} = \dfrac{d}{d\dot{m}}\left(\dfrac{\dot{m}^2}{2\varsigma^2 A^2}\right) = \dot{m}\,\dfrac{R_g^2 T^2}{A^2 p^{*2}} = \dfrac{\dot{m}}{A^2\,\dfrac{p^{*2}}{R_g^2 T^2}}$

is the dynamic cross-sectional resistance.

The dc-resistance is found to

(2.22) $R_s^* = \dfrac{r_s^*}{2} = \dot{m}\,\dfrac{R_g^2 T^2}{2 A^2 p^{*2}}$.

The modified BERNOULLI-law will then be

(2.23) $d(R_g T \ln p_1) + r_{s_1}^* d\dot{m} = d(R_g T \ln p_2) + r_{s_2}^* d\dot{m}$.

The equivalent circuit is shown in Fig. 2.3.

So the mechanical potential e appears as the source potential in the network. It differs from the logarithmic potential after Taplin by the potential drop across the nonlinear cross-sectional resistance.

In our further considerations we will refer to the network theory where p is used as fluidic potential as small density variation theory and where we use the logarithmic potential $H = R_g T \ln(p_1^*/p_2^*)$ we will refer to large density variation theory.

2.3 Fluidic resistance, capacitance and inductance

Using pressure as fluidic potential the fluidic resistance is defined as ratio of pressure drop to massflow

(2.24) $R = \dfrac{p_1 - p_2}{\dot{m}} = \dfrac{\Delta p}{\dot{m}}$

where the pressure drop for dc can be caused by friction losses as well as by change in cross-section.

Fluidic networks also have the ability of storing potential and kinetic energy. Accordingly one defines fluidic capacitance and inductance.

In a volume with the dimensions shown in Fig. 2.4 the mass $m = \varsigma l A$ can be stored. Massflow into the volume then is proportional to the change in density per time unit

(2.25) $\dot{m} = l A \dfrac{d\varsigma}{dt}$.
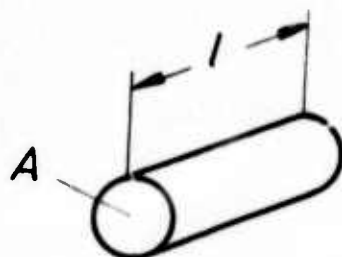
Fig.2.4   Volume
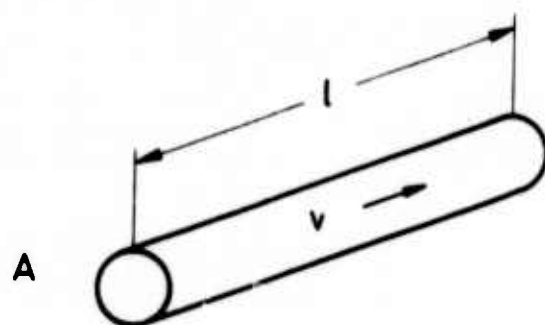
Fig.2.5   Tube

Assuming adiabatic conditions massflow in dependence of
change in pressure per time unit follows as

$$(2.26) \quad \dot{m} = lA \frac{d\varrho}{dp^+} \frac{dp^+}{dt} = \frac{lA}{c_a^2} \frac{dp}{dt}$$

where

$$(2.27) \quad c_a = \sqrt{\frac{dp^+}{d\varrho}} \qquad \text{velocity of sound}$$

According to the electric analogy $\left(i = C \frac{du}{dt} \right)$ the adiabatic
capacitance is defined as

$$(2.28) \quad C_a = \frac{A \cdot l}{c_a^2} = \frac{V}{c_a^2} \, .$$

In a tube shown in Fig. 2.5 a change in pressure can be caused
by accelerating the mass $m = \varrho l A$ in the tube.

The force acting on the cross-section A is

$$(2.29) \quad F = \frac{d}{dt} \left(m \bar{v} \right) .$$

From this the pressure follows as

$$(2.30) \quad p = \frac{1}{A} \frac{d}{dt} \left(\varrho l A \bar{v} \right) .$$

The pressure induced by change in massflow then becomes

$$(2.31) \quad p = \frac{l}{A} \frac{d\dot{m}}{dt} .$$

According to the electric analogy $\left(u = L \frac{di}{dt} \right)$ the adiabatic
inductance is defined as

$$(2.32) \quad L_a = \frac{l}{A} \, .$$

3. DC - Circuits

3.1 Uniform ducts

3.11 The laminar resistance

In the case of laminar velocity distribution the uniform duct
may be described by a dc-resistance R_{lam}. The pressure drop
along the line is

$$(3.1) \quad p = R_{lam} \, \dot{m} .$$

$$\frac{2}{a}\left(\sum_{i=1}^{\infty}\frac{a}{\alpha_i 5}\left(\frac{\alpha_i}{a}-\tanh\frac{\alpha_i}{a}\right)\right)^{-1}$$

$$\frac{8(1+a)^2}{a}$$
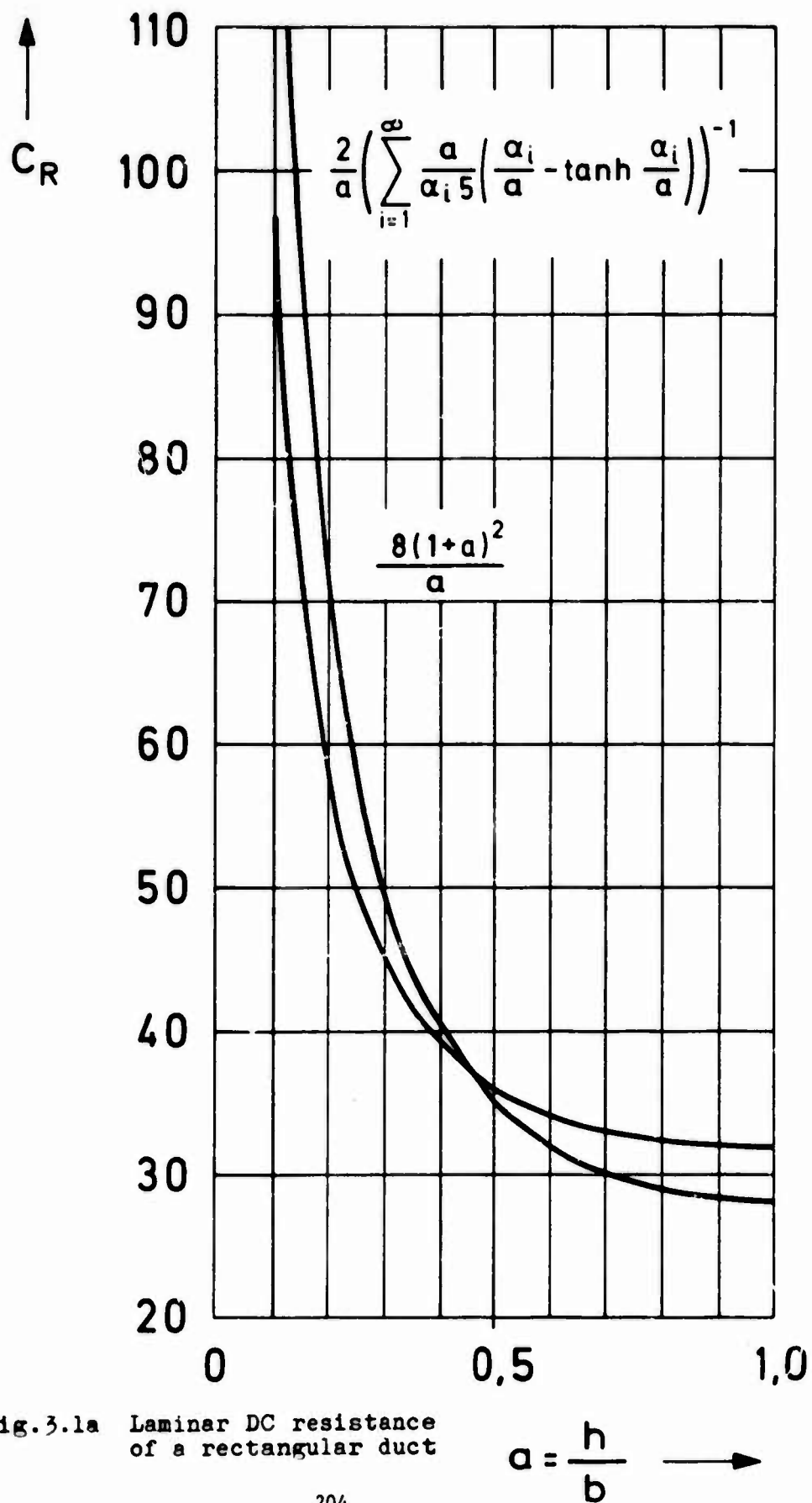
Fig.3.1a Laminar DC resistance of a rectangular duct

$$a = \frac{h}{b}$$

204

The dc resistance of a uniform line with circular cross-section is

(3.2) $R_{lam} = \dfrac{8\pi\nu l}{A^2}$.

For rectangular cross-section the dc-resistance becomes

(3.3) $R_{lam} = \dfrac{\nu l}{A^2} C_R$

where

(3.4) $C_R = \dfrac{2}{a} \left(\sum_{i=1}^{\infty} \dfrac{a}{d_i^5} \left(\dfrac{d_i}{a} - \tanh \dfrac{d_i}{a} \right) \right)^{-1}$

with

$a = \dfrac{\text{depth}}{\text{width}}$ aspect ratio of the duct

and $d_i = \dfrac{2i-1}{2}\pi$ eigen values

A good approximation for C_R is given by

(3.5) $C_R = \dfrac{8(1+a)^2}{a}$.

In Fig. 3.1a C_R is plotted as a function of a.

3.1.2 Turbulent resistance

For turbulent flow the Blasius law gives the friction factor f_{turb} as

(3.6) $f_{turb} = \dfrac{0{,}3164}{\sqrt[4]{Re}}$.

Introducing this into

(3.7) $\dfrac{\Delta P}{\rho \frac{\bar{v}^2}{2}} = \dfrac{l}{De} f$

where De $= \dfrac{4 \ \text{area}}{\text{circumference}}$ is the hydraulic diameter, we find the tubulent resistance as

(3.8) $R_{turb} = R_{lam} \cdot R_e^{3/4} \dfrac{0{,}3164}{64} = R_{lam} \left(\dfrac{Re}{1185} \right)^{3/4}$.

205

This formula is valid in the range of Reynolds number
$$2300 < R_e < 80,000.$$

The Reynolds number may be calculated from massflow by

$$(3.9) \quad R_c = \frac{\tilde{\pi}}{4} \frac{\dot{m}}{D_e \cdot \mu} .$$

3.1.3 Resistance_due_to_flow_development

A fluid entering a duct with an initially uniform velocity
profile undergoes a hydrodynamic development until the fully
developed laminar profile is achieved. This flow development
in the entrance region results in an increment in pressure
drop. Using ref. 4 and 5 the resistance of a channel including
the pressure drop resulting from entrance effects follows
out of

$$(3.10) \quad \frac{p(0) - p(l)}{\rho \frac{\bar{v}^2}{2}} = f \frac{l}{D_e} + k(l)$$

as a series connection of the known laminar resistance and a
nonlinear resistance $K(l) \frac{\dot{m}}{2\rho A^2}$ to

$$(3.11) \quad R_v = R_{lam} + k \frac{\dot{m}}{2\rho A^2} .$$

The distance necessary for fully developed laminar flow can
approximately determined by

$$(3.12) \quad l_{fd} = 0.02 \, R_e \, D_e .$$

For a duct length $l \geq l_{fd}$ the profile will be fully developed
and k is constant. For circular cross-sections one finds $k_{fd} = 4/3$.
For rectangular cross-sections k_{fd} is plotted in Fig.
3.1b.
For a duct length $l \leq l_{fd}$ HAN gives the following approximation
(ref.6)

$$(3.13) \quad \frac{p(0) - p(l)}{f \frac{\bar{v}^2}{2}} \approx C_{ap} \frac{l}{D_e \cdot R_e}$$

with

$$(3.14a) \quad C_{ap} = 15.2 \left(\frac{D_e R_e}{l} \right)^{1/2} \qquad \text{rectangular cross-section}$$

$$(3.14b) \quad C_{ap} = 13.8 \left(\frac{D_e R_e}{l} \right)^{1/2} \qquad \text{circular cross-section.}$$

Combining equ. (3.13) and (3.14) we find

206

$$R_{fd} = K_{fd} \cdot \frac{\dot{m}}{2\rho A^2}$$
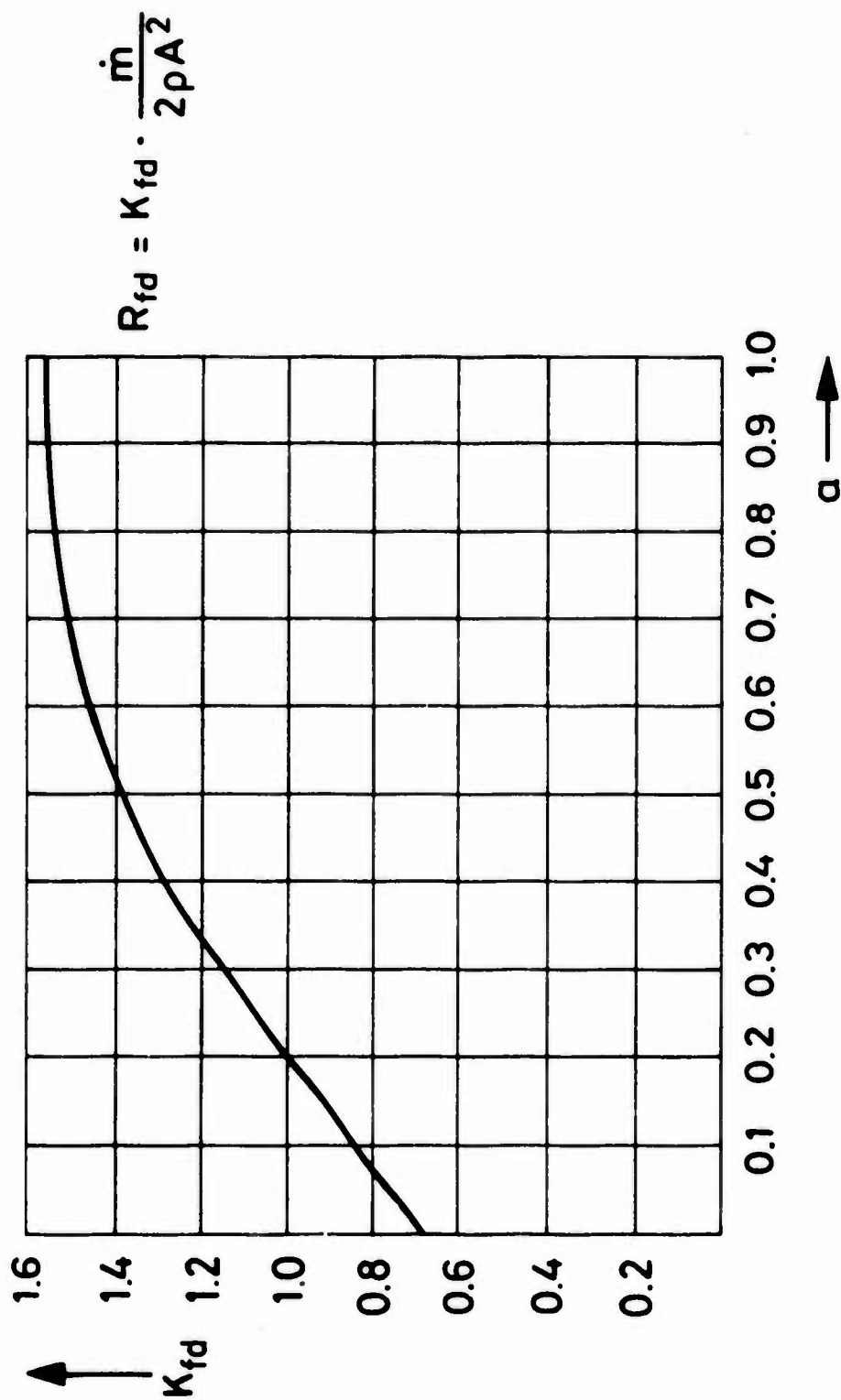
Fig.3.1b DC resistance of a rectangular duct due to flow development

207

(3.15a) $\dfrac{p(0)-p(l)}{\dfrac{\dot{m}^2}{2\varsigma A^2}} = 12.2\left(\dfrac{\dot{m}}{l\mu}\right)^{-1/2}$ circular cross-section

(3.15b) $\dfrac{p(0)-p(l)}{\dfrac{\dot{m}^2}{2\varsigma A^2}} = 7.6\,\dfrac{a+1}{\sqrt{a}}\left(\dfrac{\dot{m}}{l\mu}\right)^{-1/2}$ rectangular cross-section.

In terms of massflow rate the length for flow development is found as

(3.16a) $l_{fd} = 0.025\,\dfrac{\dot{m}}{\mu}$ circular cross-section

(3.16b) $l_{fd} = 0.08\,\dfrac{\dot{m}}{\mu}$ rectangular cross-section.

3.2 Nonuniform ducts

In chapter 2 we have already derived an equivalent circuit for a nonuniform duct introducing nonlinear cross-sectional resistances (Fig.3.2), assuming an incompressible and lossless medium

(2.14) $p_{tot} = p_1 + R_{S1}\,\dot{m} = p_2 + R_{S2}\,\dot{m}.$

3.2.1   Nozzles

From equ. (2.14) and Fig. 3.2 the nozzle resistance is found as

(3.17) $R_n = \dfrac{p_1-p_2}{\dot{m}} = \dfrac{\dot{m}}{2\varsigma A_2^2}\left(1 - \left(\dfrac{A_2}{A_1}\right)^2\right)$

assuming that there is not jet contraction.
For $A_2 = 0$ R_n becomes infinite (no flow) and for $A_2 = A$ R_n becomes zero (short circuit).

Expressing the flow through the nozzle by pressure difference across the nozzle we have

(3.18) $\dot{m} = A_2 \sqrt{\dfrac{2\,\varsigma\,(p_1-p_2)}{1 - \left(A_1/A_2\right)^2}}.$

Considering compressibility at higher pressures for adiabatic conditions we find

(3.19) $\dot{m} = A_2 \varsigma_1\, c_a \left(\dfrac{p_2^{\divideontimes}}{p_1^{\divideontimes}}\right)^{1/\kappa} \sqrt{\dfrac{2\kappa}{\kappa-1}} \sqrt{\dfrac{1 - \left(\dfrac{p_2^{\divideontimes}}{p_1^{\divideontimes}}\right)^{\frac{\kappa-1}{\kappa}}}{1 - \left(\dfrac{A_2}{A_1}\right)^2\left(\dfrac{p_2^{\divideontimes}}{p_1^{\divideontimes}}\right)^{2/\kappa}}}.$
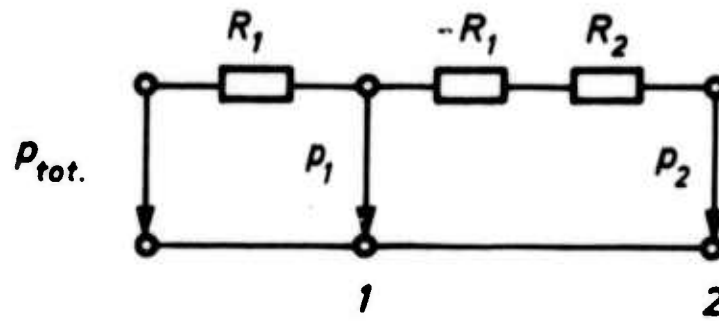
Fig.3.2   Equivalent circuit of a nonuniform duct
           without losses
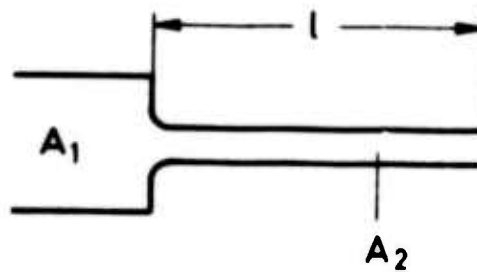
Fig.3.3   Nozzle geometry
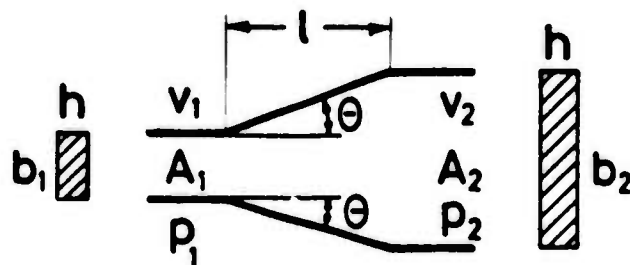
Fig.3.4   Diffuser geometry

For nozzles exits with several nozzle widths as shown in Fig. 3.5 the entrance losses due to flow development have to be considered (see 3.1.3).

3.2.2 Diffusers

Using equ. (2.14) the pressure drop in an ideal diffuse may be written as

$$(3.20) \quad P_1 - P_2 = \dot{m}\left(R_{S2} - R_{S1}\right) = -\frac{\dot{m}}{2 \varsigma A_1{}^2}\left(1 - \left(\frac{A_1}{A_2}\right)^2\right).$$

Because the cross-section A_2 in any case is larger than A_1 the negative resistance is dominating. The pressure drop turns out to be negative, the diffuser therefore causes a pressure increase. Using the ideal pressure recovery coefficient.

$$(3.21) \quad C_{pri} = 1 - \left(\frac{A_1}{A_2}\right)^2$$

the diffuser resistance of an ideal diffuser becomes

$$(3.22) \quad R_{d,ideal} = -R_{S1}C_{pri}.$$

The diffuser resistance of a real diffuser becomes

$$(3.23) \quad R_{d,real} = \eta_d R_{d,ideal} = -C_{pr}R_{S1}$$

where

$$\eta_d = \frac{C_{pr}}{C_{pri}} \qquad \text{diffuser effectiveness}$$

and

$$C_{pr} \qquad \text{pressure recovery coefficient of a real diffuser.}$$

Detailed data on the performance of straight-walled diffusers are found in ref. 7 and 8. It should be pointed out that investigations of diffusers in flow mechanics were carried out at configurations which were large compared to those of fluidic elements. The results of diffuser design of energy flow mechanics can therefore not be directly transfered to fluidics. The common methods assume that the boundary layer is small compared with the cross-sectional dimensions. For the large dimensions of the

flow mechanical energy technique this is nearly always valid. In fluidic circuits, however, the boundary layer is of the order of the cross-sectional dimensions. Investigations of fluidic jet deflection amplifiers showed that the pressure recovery of the diffusers is strongly dependent on mass flow and sometimes extremely pocr (ref.9).

Gibson found in 1911 (ref.10) that the losses in a diffuser compared with an ideal diffuser can be expressed as a function of the carnot-losses and the total angle 2Θ (Fig. 3.4)

$$(3.24) \quad P_l = k(\Theta) \frac{\dot{m}}{2 \rho A_1^2} \left(1 - \frac{A_1}{A_2} \right)^2$$

where $k(\Theta)$ can be expressed in the range $0 < 2\,\Theta < 35^\circ$ by the relation

$$(3.25) \quad k(\Theta) = 5.3 \left(\tan \Theta \right)^{1.4}.$$

The experimental results from Gibson show that his formula only describes the losses in the range $10^\circ < 2\,\Theta < 35^\circ$ with sufficient accuracy. Below $2\,\Theta \approx 7^\circ$ the losses in these experiments again increased. It seems therefore to be convenient to interprete these losses by friction losses. If we assume that the flow is laminar and does not significantly change the velocity profile, the laminar resistance of a small fluidic diffuser (ref.9) becomes

$$(3.26) \quad R_{d,lam} = 8\nu \int_0^{l_d} \frac{(a(x)+1)^2}{a(x)\,A(x)^2} \, dx.$$

Inserting the geometrical conditions for a straight-walled diffuser we obtain

$$(3.27) \quad R_{d,lam} = \frac{8\pi\,\nu}{A_1^2} \, l_e$$

with an effective diffuser length

$$(3.28) \quad l_e = l_d \, \frac{2a_1\left(1 - \frac{A_1}{A_2}\right) + \frac{a_1^2}{2}\left(1 - \left(\frac{A_1}{A_2}\right)^2 + ln\left(\frac{A_2}{A_1}\right)\right)}{\left(\frac{A_2}{A_1} - 1\right)\left(a_1 + 1\right)^2}.$$

Combining equ. (3.27) and (3.28) with the equation for the ideal diffuser the pressure increase in a real diffuser becomes

$$(3.29) \quad P_2 - P_1 = \frac{\dot{m}^2}{2\rho A_1^2} \left[1 - \left(\frac{A_1}{A_2}\right)^2 - k(\Theta)\left(1 - \frac{A_1}{A_2}\right)^2 - 16 \frac{(1+a_1)^2/a_1}{\dot{m}/(\mu\,l_d)} \frac{l_e}{l_d} \right].$$
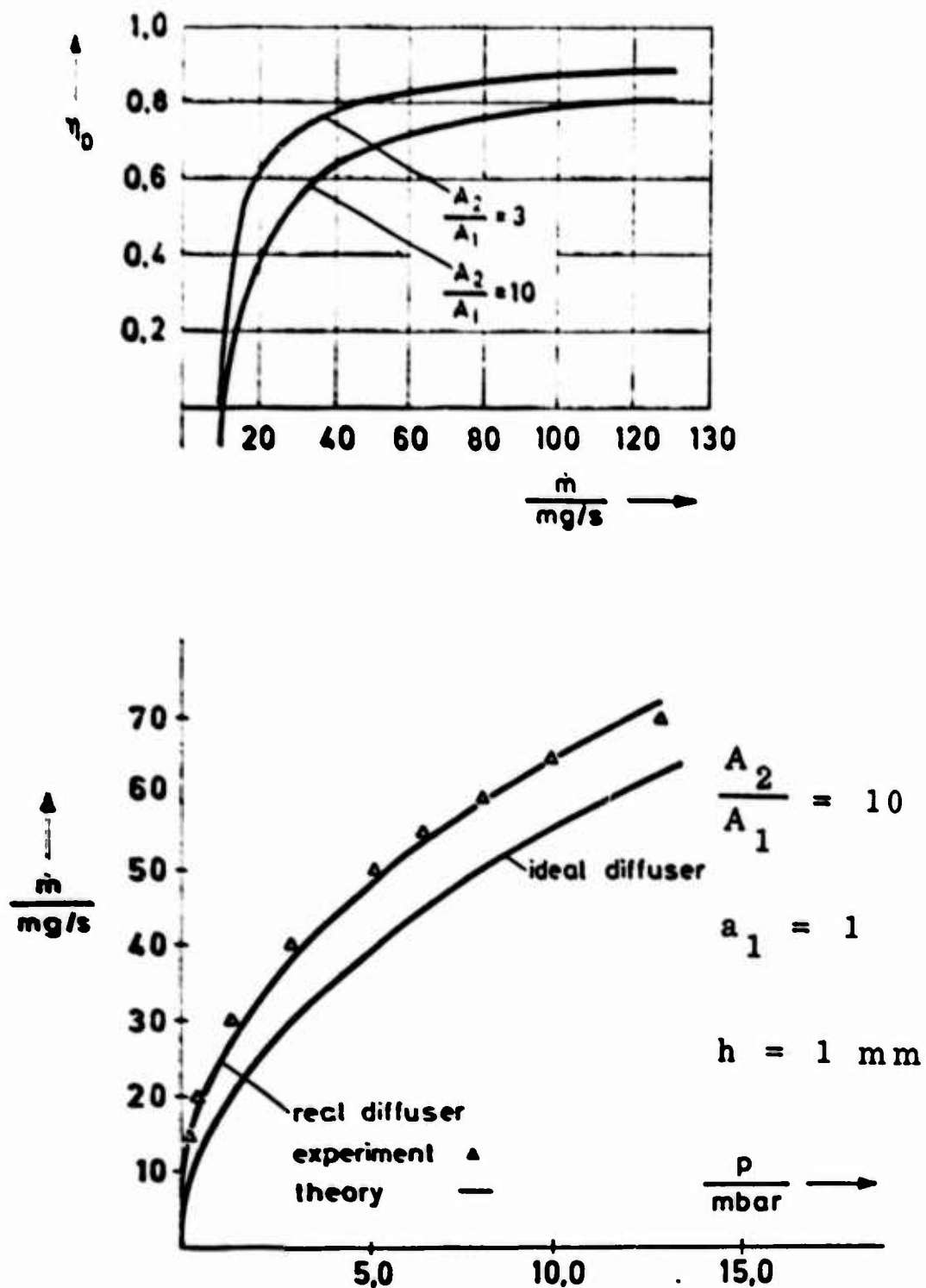
Fig.3.5   Diffuser efficiency

and from this the diffuser efficiency

$$(3.30)\ \eta_d = 1 - \frac{k(\theta)\left(1 - \frac{A_1}{A_2}\right)^2 - \frac{16(1+a_1)^2/a_1}{\dot{m}/(\mu\,l_d)}\frac{l_e}{l_d}}{1 - \left(\frac{A_1}{A_2}\right)^2}.$$

Fig. 3.5 shows the diffuser efficiency η_d plotted against the massflow rate. The dimensions of the diffuser are $b_1 = 1$ mm, $h = 1.05$ mm, $2\theta = 8^\circ$.
For further information see ref. 9.

The diffuser resistance now will be

$$(3.23a)\ R_{d,real} = -\frac{\dot{m}}{2\rho A_1^2}\left[1 - \left(\frac{A_1}{A_2}\right)^2 - k(\theta)\left(1 - \frac{A_1}{A_2}\right)^2\right] + R_{d,lam}.$$

Equ. (3.23a) very accurately describes a diffuser with an
approximately uniform velocity profile at the diffuser inlet.
This is nearly always given for jet deflection amplifiers,
where the receiver takes a small part out of the jet profile.
In wallattachment amplifiers the assumption will not hold
any longer because of the nonuniform velocity distribution at
the receiver inlet. Nevertheless equ. (3.23a) will give a cer-
tain guide to estimate the losses which mostly are higher than
predicted by energy flow mechanics.

'.3 Jet receiver nozzle

..t of a supply nozzle a jet emerges which is received by a
nozzle as indicated in Fig. 3.6.
If we block the nozzle we obtain the maximum pressure which we
call source pressure p_Q. If we load the receiver channel by a
finite resistance the static pressure at the nozzle mouth
decreases by $1/2 \cdot \rho \bar{v}_1^2$. The pressure in the receiver mouth
therefore becomes

$$(3.31)\quad p_1 = p_Q - \frac{1}{2}\rho \bar{v}_1^2 = p_Q - R_i\,\dot{m}$$

where $\quad R_i = R_{s1} = \dfrac{\dot{m}}{2\rho A_1^2}.$

The equivalent circuit for the nozzle mouth is found as a
pressure source p_Q with a nonlinear internal resistance R_i.
At this internal resistance we find the pressure drop
$R_i \dot{m}$. The difference between source pressure p_Q and pressure
drop at the internal resistance R_i is the pressure in the
mouth of the nozzle. In reality the source pressure p_Q will
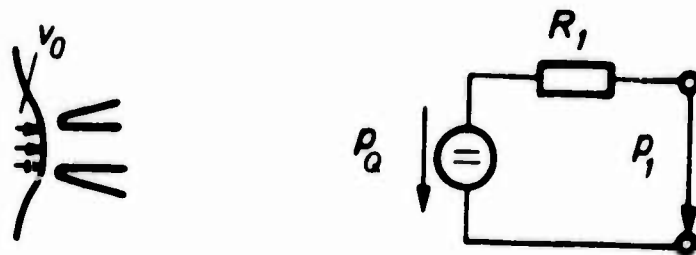
Fig.3.6   Jet receiver nozzle
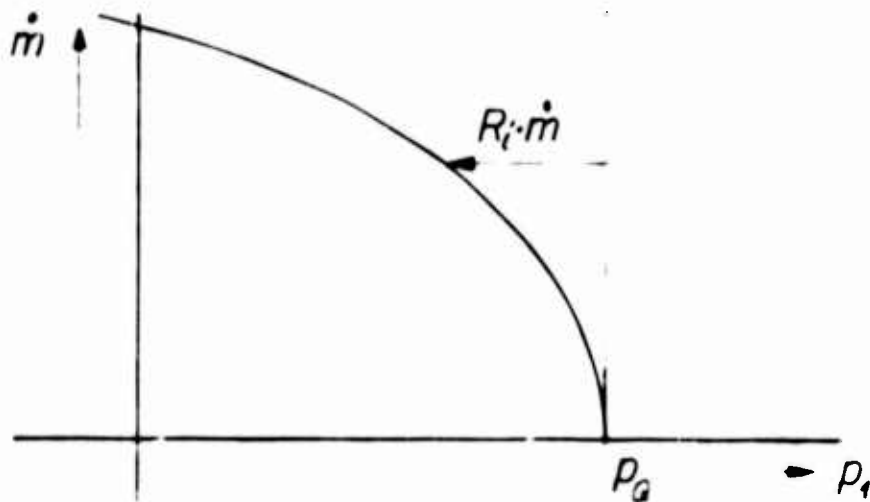
Fig.3.7   Typical jet receiver characteristic
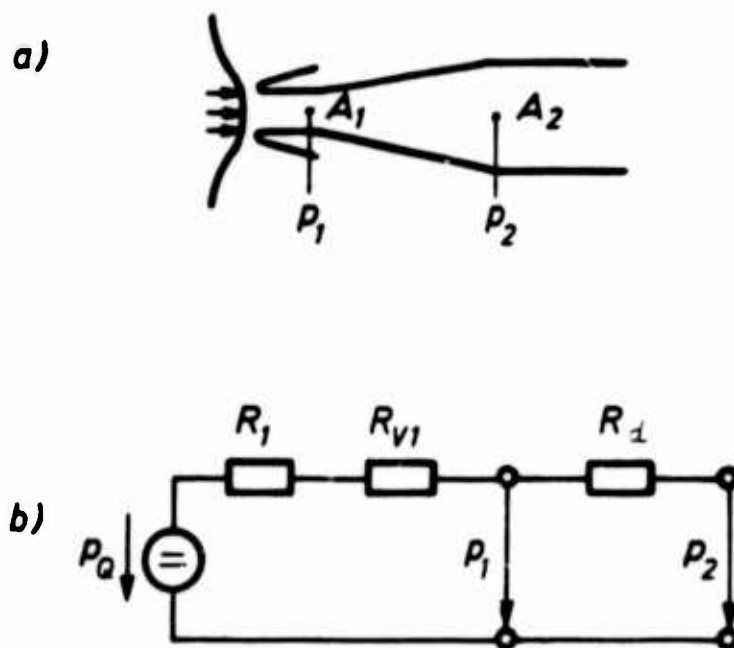
Fig.3.8   Jet receiver nozzle with diffuser

not remain constant for different loading because of changes
in the velocity profile. The equivalent circuit could therefore
be changed by introducing a load depending pressure source.
This again can be interpreted by an additional internal
resistance.

In ref. 11 Kessel has calculated the pressure source and this
additional internal resistance of the receiver source pressure
for a jet deflection amplifier.

For fluidic wall-attachment amplifiers the calculation of the
internal resistance will be very difficult. Nevertheless the
equivalent circuit for the receiver as a pressure source with
nonlinear internal resistance is valid, even if the single
quantities have to be determined out the pressure-flow
characteristics.

A typical pressure-flow characteristic shows fig.3.7.

If we now combine a receiver nozzle with a diffuser we can
directly draw the equivalent circuit for the whole con-
figuration (Fig. 3.8). The viscous losses in the nozzle are
considered by a resistance R_v which is calculated by equ.
3.11.

3.3   The fluidic line branching (ref.12)

Unlike in electronics line branchings in fluidic networks are
of very complicated nature even for dc. Whilst the electrical
line branching is fully described by the node theorem
we find potential jumps in the fluidic lines branching off
caused by different velocities in the branches (Fig.3.9).
A further influence factor is the vector characteristic of
the velocity which results in a preference of lines depending
on geometry.

3.3.1   The equivalent circuit of the 'ideal' line branching

Consideration is to be limited only to the change at sectional
areas that are marked by the dotted lines shown in Fig. 3.10.
We assume that the medium is incompressible or at least that it
has low compressibility. Considering the losses, we form the
BERNOULLI equation for the streamlines from branch 1 to 2 and
from branch 1 to 3.

$$(3.32a) \quad P_1 + \frac{1}{2} \rho \bar{V}_1^2 = P_2 + \frac{1}{2} \rho \bar{V}_2^2 + H_{12}$$

$$(3.32b) \quad P_1 + \frac{1}{2} \rho \bar{V}_1^2 = P_2 + \frac{1}{2} \rho \bar{V}_3^2 + H_{13}.$$

The total losses H_{12} and H_{13} in the branches 1 to 2 and 1 to 3,
respectively, can be divided into the mixing loss h_{ij} and the
frictional losses. By introducing the mass flow rate we obtain

$$(3.33a) \quad P_1 + R_1 \dot{m}_1 = P_2 + R_2 \dot{m}_2 + H_{12}$$

$$(3.33b) \quad P_2 + R_2 \dot{m}_2 = P_3 + R_3 \dot{m}_3 + H_{13}$$

215
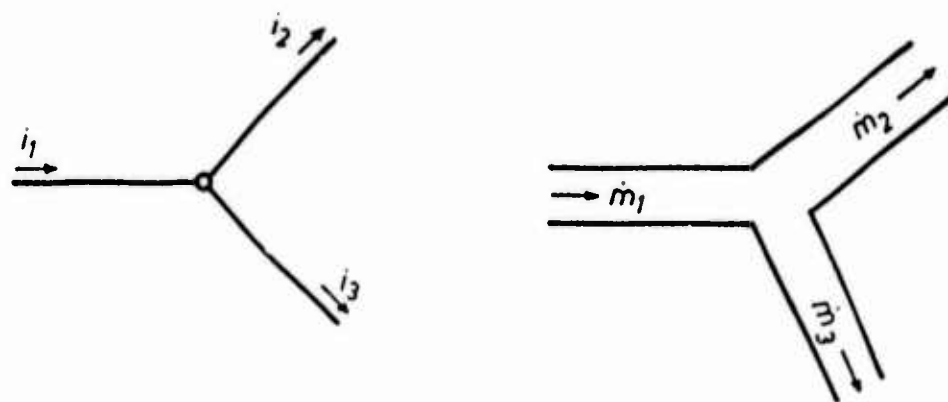
Fig.3.9   Electric and fluidic line branching
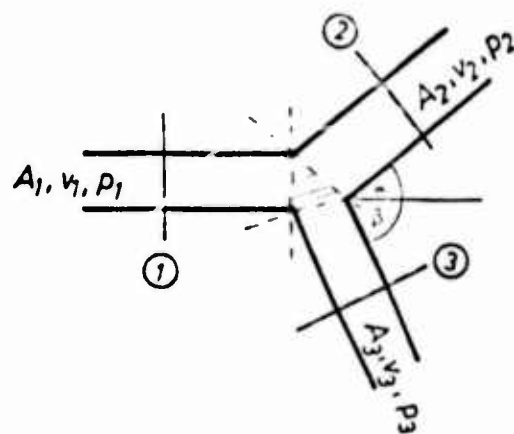
Fig.3.10   Dimensions of a fluidic line branching
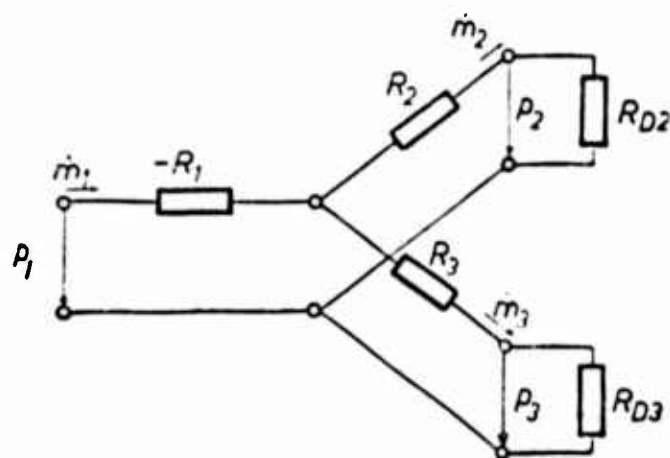
Fig.3.11   Equivalent circuit for the "ideal" line branching

where R_1, R_2 and R_3 are the nonlinear cross-sectional resistances

$$(3.34) \quad R_1 = \frac{\dot{m}_1}{2 \rho A_1^2} \qquad R_2 = \frac{\dot{m}_2}{2 \rho A_2^2} \qquad R_3 = \frac{\dot{m}_3}{2 \rho A_3^2} \ .$$

We shall designate R_{n1} and R_{n2} as arbitrary terminating resistances, eg. nozzles.

Using the mash-theorem we obtain two equations to describe the line branching. In addition we have the continuity equation for use here. Neglecting the losses the equivalent circuit for the 'ideal' line branching in Fig. 3.11 can be found. This equivalente circuit is used as reference for the real ('lossy') line branching that considers the losses.

3.3.2 The lossy line branching

In ref. 13 Vazsonyi finds a mathematical approach for losses in duct branches. His calculations were based on the extensive tests at the Hydraulic Institute of the Technical University of Munich (ref.14 and 15).

The losses can be devided into pressure losses caused by the frictional losses in the ducts, the hydromechanical development of the velocity profile and the mixing losses in the region of flow division.

The mathematical approach of Vazsonyi for the mixing losses is given as

$$(3.35) \quad 2 h_{12} = \rho \left[\lambda_1(\alpha) \bar{v}_1^2 + \left(2 \lambda_1(\alpha) - \lambda_2(\alpha) \right) \bar{v}_2^2 - 2 \lambda_2(\alpha) \bar{v}_1 \bar{v}_2 \cos \alpha' \right]$$

$$(3.36) \quad 2 h_{13} = \rho \left[\lambda_1(\beta) \bar{v}_1^2 + \left(2 \lambda_1(\beta) - \lambda_2(\beta) \right) \bar{v}_2^2 - 2 \lambda_2(\beta) \bar{v}_1 \bar{v}_3 \cos \beta' \right].$$

The loss coefficients λ_1 and λ_2 and the effective angles in equ. (3.35) and (3.36) can be taken form Fig. 3.12 and 3.13.

Considering the mixing losses the equations for the real line branching can be written as

$$(3.37) \quad p_1 - p_2 = - R_1 \dot{m}_1 + R_2 \dot{m}_2 + h_{12}$$

$$(3.38) \quad p_1 - p_3 = - R_1 \dot{m}_1 + R_3 \dot{m}_3 + h_{13} \ .$$

From equ. (3.35) through (3.38) we obtain the equivalent circuit shown in Fig. 3.14, where

$$(3.39) \quad R_{11} = - R_1 K_{11} \qquad\qquad \Delta p_{11} \sim \dot{m}_1^2$$

$$R_{12} = R_1 K_{12} \left(\frac{\dot{m}_2}{\dot{m}_1} \right)^2 \qquad\qquad \Delta p_{12} \sim \dot{m}_2^2$$

$$R_{13} = R_1 k_{13} \frac{\dot{m}_2 \dot{m}_3}{\dot{m}_1^2} \qquad \Delta P_{13} \sim \dot{m}_2 \dot{m}_3$$

$$R_{21} = R_2 k_{21} \qquad \Delta P_{21} \sim \dot{m}_2^2$$

$$R_{31} = R_3 \cdot k_{31} \qquad \Delta P_{31} \sim \dot{m}_3^2$$

$$R_{32} = R_3 \frac{\dot{m}_2}{\dot{m}_3} \qquad \Delta P_{32} \sim \dot{m}_2 \cdot \dot{m}_3 .$$

The correction terms k only depend on geometry, for a given branching they are constant.

$$(3.40) \qquad K_{11} = 1 - \lambda_1(\alpha)$$

$$K_{12} = \lambda_1(\beta) - \lambda_1(\alpha)$$

$$k_{13} = -2 \frac{A_1}{A_2} \lambda_2(\alpha) \cos\alpha'$$

$$k_{21} = 2\lambda_1(\alpha) - \lambda_2(\alpha) + 1 - 2 \frac{A_2}{A_1} \lambda_2(\alpha)\cos\alpha' + \left(\frac{A_2}{A_1}\right)^2 \left(\lambda_1(\alpha) - \lambda_1(\beta)\right)$$

$$k_{31} = 2\lambda_1(\beta) - \lambda_2(\beta) + 1 - 2 \frac{A_3}{A_1} \lambda_2(\beta)\cos\beta' + \left(\frac{A_3}{A_1}\right)^2 \left(\lambda_1(\beta) - \lambda_1(\alpha)\right)$$

$$K_{32} = 2\left(\frac{A_3}{A_1}\right)^2 \left(\lambda_1(\beta) - \lambda_1(\alpha)\right) + 2 \frac{A_3^2}{A_1 A_2} \lambda_2(\alpha)\cos\alpha' - 2 \frac{A_3}{A_1} \lambda_2(\beta)\cos\beta' .$$

The resistances R_{v_1}, R_{v_2} and R_{v_3} consider the pressure losses in the single branches caused by friction and the development of the velocity profile. The resistances R_{11}, R_{21} and R_{31} only depend on the mass flow rate through the branch that they are appointed to in the equivalent circuit. The resistances R_{12}, R_{13} and R_{32} depend on the several flows simultaneously. In order to describe them in a network a parametric representation with respect to flow is necessary.

Using flow-controlled resistances it could be possible to find other constellations of resistances in the equivalent circuit. However, in ref. 12 it is shown that the chosen configuration is convenient for the measuring techniques used.

Combining the single resistances in the branches we find the equivalent circuit using the branch resistances (see Fig. 3.15).

$$(3.41) \qquad R_{10} = k_{10} R_1$$

$$R_{20} = k_{20} R_2$$

$$R_{30} = k_{30} R_3$$

which are related to the cross-sectional resistances shown in Fig.3.11, where
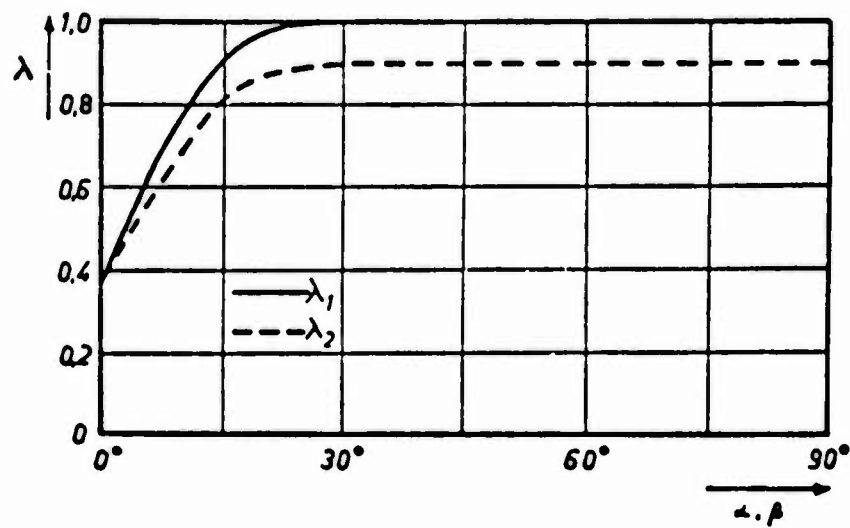
Fig.3.12   Loss coefficient as function of angle of deflection
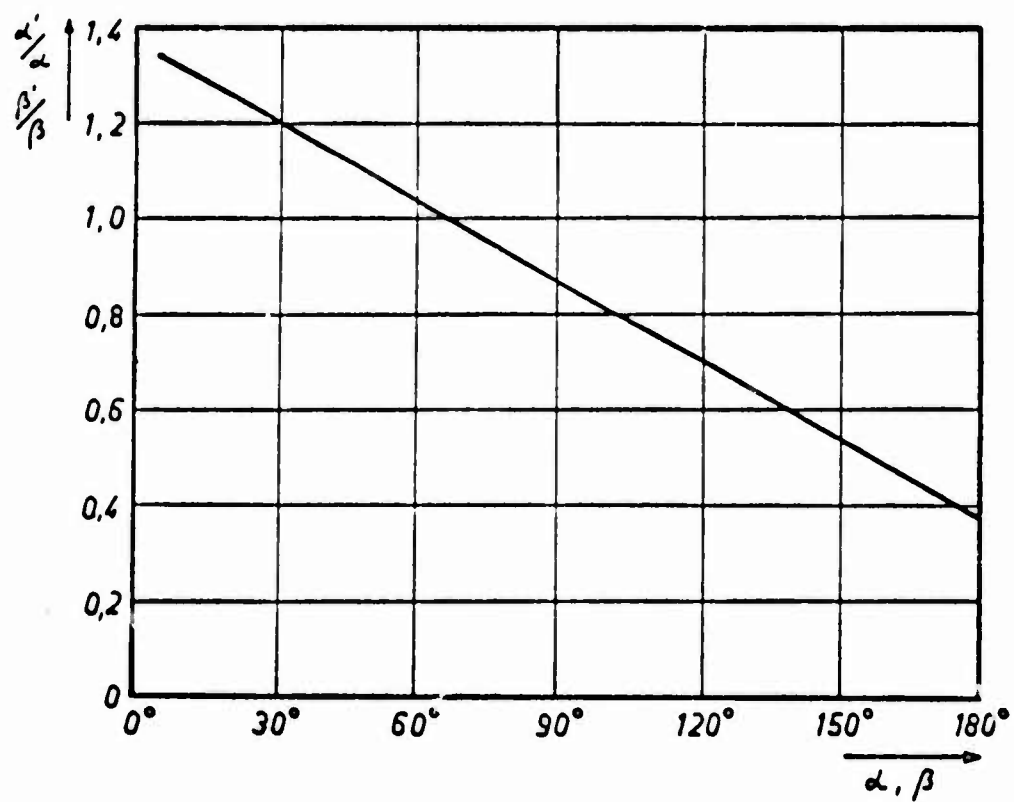
Fig.3.13   Effective angle of deflection as function of
angle of deflection

Fig.3.14   Equivalent circuit of a general line branching

Fig.3.15   Equivalent circuit with branch resistances
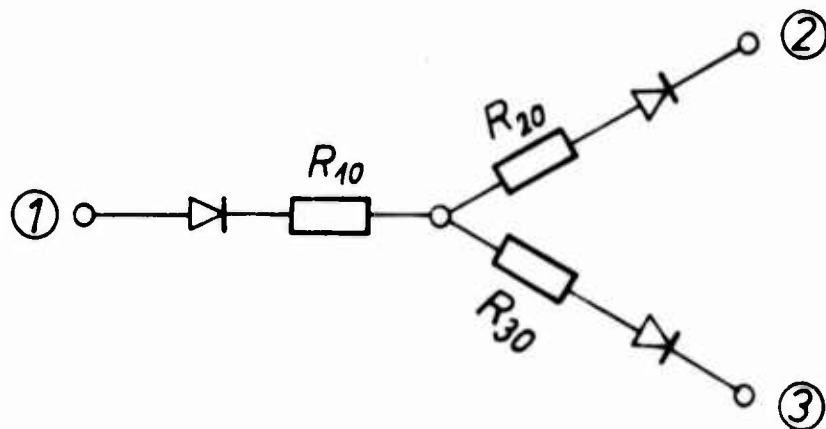
Fig.3.16   Equivalent circuit of a line branching
with flow diodes showing flow direction

$$(3.42) \quad K_{10} = K_{11} + K_{12}\left(\frac{\dot{m}_2}{\dot{m}_1}\right)^2 + K_{13}\frac{\dot{m}_2\,\dot{m}_3}{\dot{m}_1^2}$$

$$K_{20} = K_{21}$$

$$K_{30} = K_{31} + K_{32}\frac{\dot{m}_2}{\dot{m}_3}\ .$$

It should be emphasized that a topological agreement of the equivalent circuit with the test model is only valid for the three terminating points 1, 2 and 3, because the equivalent circuit merely describes the pressure transfer for the hatched region in Fig.3.10 if the viscous resistances R_v take into account the losses in the lines. In addition the equivalent circuit depends on the direction of the input flow.
In order to show for which flow direction the equivalent circuit has been developed flow diodes can be introduced as shown in Fig. 3.16.

3.3.2.1 Equivalent circuit for symmetrical line branching

The branching is defined to be symmetrical if the cross sections A_2 and A_3, and the angles α and β are equal. For this case the equivalent circuit can be simplified to that of Fig. 3.17. The resistances R_{12} and R_{32} disappear.

For equal lengths in the output branches the total resistances for the branch 2 and 3 have the same flow characteristic. The single resistance can be described by

$$(3.43) \quad R_{11} = R_1\left(1 - \lambda_1(\alpha)\right)$$

$$R_{13} = R_1\left(-2\frac{A_1}{A_2}\lambda_2(\alpha)\cos\alpha'\right)\frac{\dot{m}_2\,\dot{m}_3}{\dot{m}_1^2}$$

$$R_{21} = R_{31} = R_2\left(2\lambda_1(\alpha) - \lambda_2(\alpha) + 1 - 2\frac{A_2}{A_1}\lambda_2(\alpha)\cos\alpha'\right)$$

3.4 The fluidic line junction

Problems in fluidic line junctions are very similar to those in fluidic line branchings. In ref. 16 therefore Kohl derives an equivalent circuit in analogy to that of the line branching, using the results from Vazsonyi (ref.13) for the mixing losses.

221
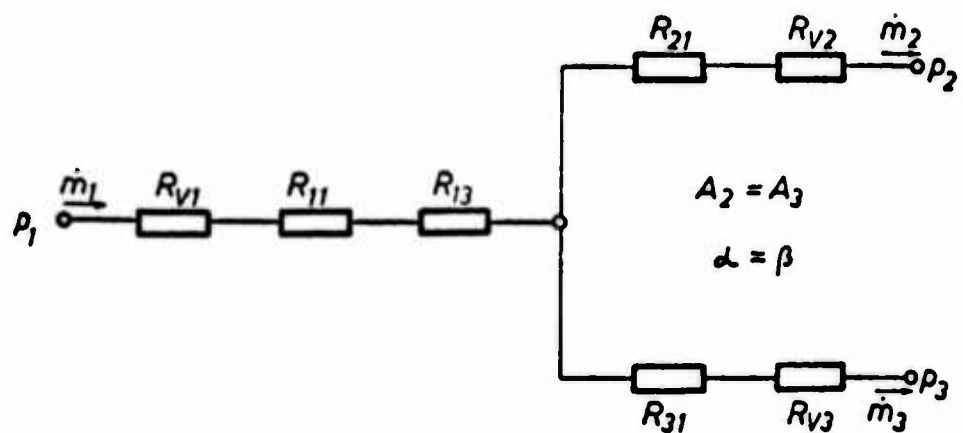
Fig.3.17 Equivalent circuit for the symmetrical line branching

3.4.1 The equivalent circuit of the 'ideal' line junction

Assuming that the medium is incompressible or at least that it has low compressibility, we form the PERNOULLI-equation for the streamlines from branch 1 to 3 and from branch 2 to 3 (Fig. 3.18)

$$(3.44a) \quad p_1 + \frac{1}{2} \rho \bar{v}_1^2 = p_3 + \frac{1}{2} \rho \bar{v}_3^2 + H_{13}$$

$$(3.44b) \quad p_2 + \frac{1}{2} \rho \bar{v}_2^2 = p_3 + \frac{1}{2} \rho \bar{v}_3^2 + H_{23} .$$

The total losses H_{13} and H_{23} can be devided into the mixing losses h and the frictional losses.

By introducing the massflow rate we obtain

$$(3.45a) \quad p_1 + R_1 \dot{m}_1 = p_3 + R_3 \dot{m}_3 + H_{13}$$

$$(3.45b) \quad p_2 + R_2 \dot{m}_2 = p_3 + R_3 \dot{m}_3 + H_{23} .$$

where R_1, R_2 and R_3 are the cross-sectional resistances

$$(3.46) \quad R_1 = \frac{\dot{m}_1}{2\rho A_1^2} \qquad R_2 = \frac{\dot{m}_2}{2\rho A_2^2} \qquad R_3 = \frac{\dot{m}_3}{2\rho A_3^2} .$$

Neglecting the losses the equivalent circuit for an 'ideal' line junction is found in Fig. 3.19.
This equivalent circuit is used as reference for the real ('lossy') line junction that considers the losses.

3.4.2 The equivalent circuit of the real line junction

The mathematical approach of Vazsonyi for the mixing losses is given as

$$(3.47) \quad 2 h_{13} = \rho \left[\lambda_3(\alpha) \bar{v}_1^2 + \bar{v}_3^2 - 2 v_3 \left(\frac{\bar{v}_1 \dot{m}_1}{\dot{m}_3} \cos\alpha' + \frac{\bar{v}_2 \dot{m}_2}{\dot{m}_3} \cos\beta' \right) \right]$$

$$(3.48) \quad 2 h_{23} = \rho \left[\lambda_3(\beta) \bar{v}_2^2 + \bar{v}_3^2 - 2 \bar{v}_2 \left(\frac{\bar{v}_2 \dot{m}_2}{\dot{m}_3} \cos\beta' + \frac{\bar{v}_1 \dot{m}_1}{\dot{m}_3} \cos\alpha' \right) \right] .$$
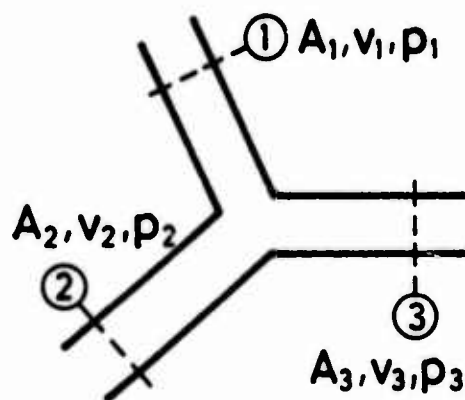
Fig.3.18   Fluidic line junction
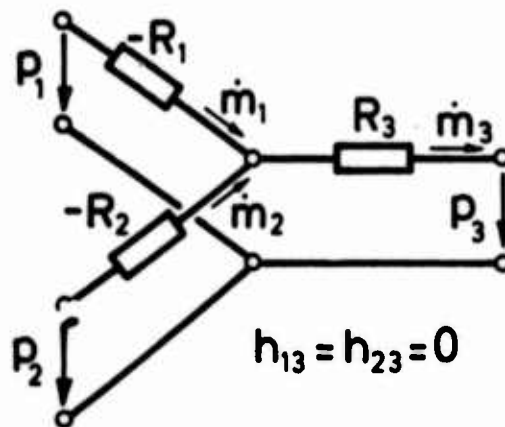
Fig.3.19   Equivalent circuit for the "ideal" line junction
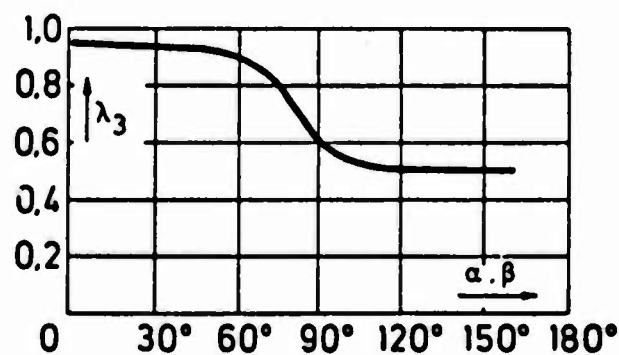
Fig.3.20   Loss coefficient as function of angle of deflection

The loss coefficient λ_3 can be taken from Fig. 3.20 and the effective angles can be taken from Fig. 3.13.

Considering the mixing losses the equation for the real line junction we obtain the equivalent circuit shown in Fig. 3.21, where

(3.49)
$$R_{11} = R_1 K_{11} \qquad\qquad \Delta p_{11} \sim \dot{m}_1^2$$

$$R_{12} = R_1 K_{12} \left(\frac{\dot{m}_2}{\dot{m}_1}\right)^2 \qquad \Delta p_{12} \sim \dot{m}_2^2$$

$$R_{13} = R_1 K_{13} \frac{\dot{m}_2}{\dot{m}_1} \qquad\quad \Delta p_{13} \sim \dot{m}_1 \dot{m}_2$$

$$R_{21} = R_2 K_{21} \qquad\qquad \Delta p_{21} \sim \dot{m}_2^2$$

$$R_{22} = R_2 K_{22} \left(\frac{\dot{m}_1}{\dot{m}_2}\right)^2 \qquad \Delta p_{22} \sim \dot{m}_1^2$$

$$R_{23} = R_2 K_{23} \frac{\dot{m}_1}{\dot{m}_2} \qquad\quad \Delta p_{23} \sim \dot{m}_2 \dot{m}_1 .$$

The correction terms k only depend on geometry, for a given line branching they are constant.

(3.50)
$$K_{11} = \lambda_3(\alpha) - 1 - 2\frac{A_1}{A_3}\cos\alpha' + 2\left(\frac{A_1}{A_3}\right)^2$$

$$K_{12} = 2\left(\frac{A_1}{A_3}\right)^2 - 2\frac{A_1^2}{A_2 A_3}\cos\beta'$$

$$K_{13} = 4\left(\frac{A_1}{A_3}\right)^2$$

$$K_{21} = \lambda_3(\beta) - 1 - 2\frac{A_2}{A_3}\cos\beta' + 2\left(\frac{A_2}{A_3}\right)^2$$

$$K_{22} = 2\left(\frac{A_2}{A_3}\right)^2 - 2\frac{A_2^2}{A_1 A_3}\cos\beta'$$

$$K_{23} = 4\left(\frac{A_2}{A_3}\right)^2 .$$

The resistances R_{v1}, R_{v2} and R_{v3} consider the pressure losses in the single branch caused by friction and flow development.
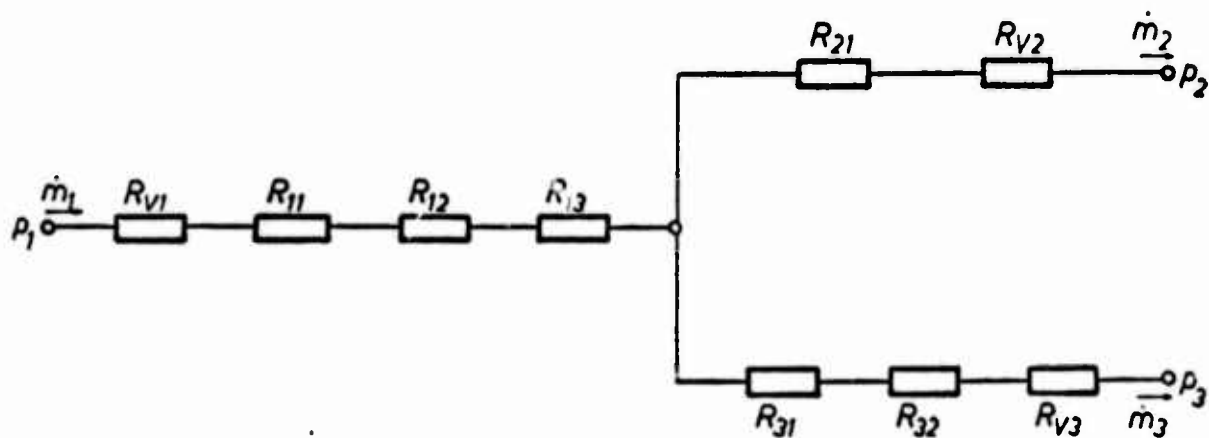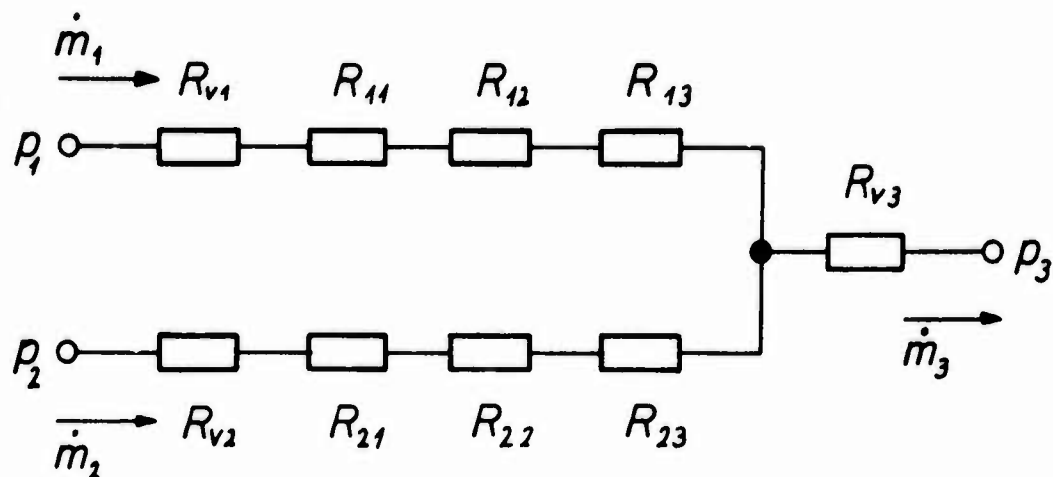
Fig.3.21   Equivalent circuit of a general line junction
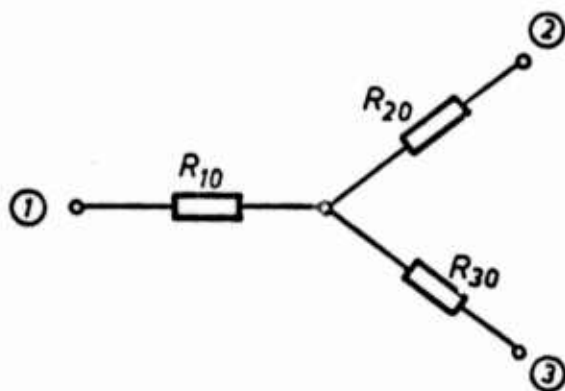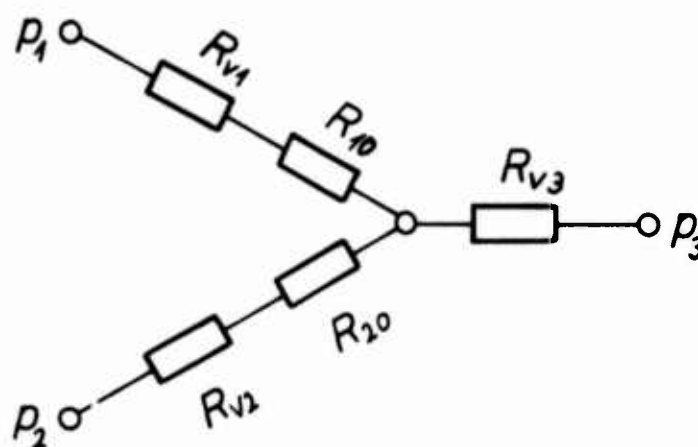

Fig.3.22   Equivalent circuit with branch resistances
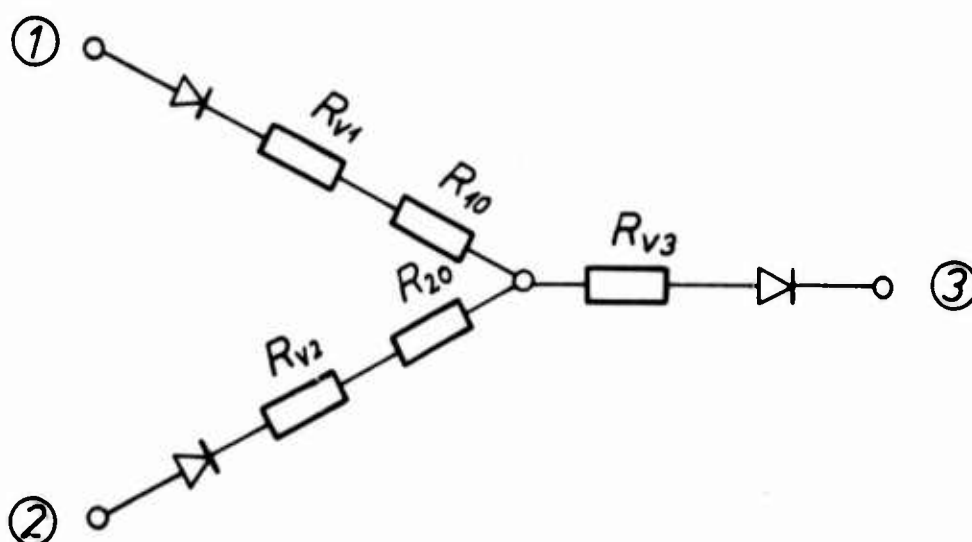
Fig.3.23   Equivalent circuit of a line junction with flow
diodes showing flow direction

Similar to the equivalent circuit of the line branching the resistances R_{11} and R_{21} only depend on the massflow rate through the branch they are appointed to in the equivalent circuit. The resistances R_{12}, R_{13}, R_{22} and R_{23} depend on the ratio of the flow rates $\dot{m}_1$ and $\dot{m}_2$. In order to describe them in a network a parametric representation with respect to flow is necessary.

Combining the single resistances in the branches we find the equivalent circuit using the branch resistances (see Fig. 3.22).

$$(3.51) \quad R_{10} = k_{10} R_1$$

$$R_{20} = k_{20} R_2$$

which are related to the cross-sectional resistances, where

$$(3.52) \quad k_{10} = k_{11} + k_{12} \left(\frac{\dot{m}_2}{\dot{m}_1} \right)^2 + k_{13} \frac{\dot{m}_2}{\dot{m}_1}$$

$$k_{20} = k_{21} + k_{22} \left(\frac{\dot{m}_1}{\dot{m}_2} \right)^2 + k_{23} \frac{\dot{m}_1}{\dot{m}_2} .$$

As already said above for the line branching the equivalent circuit depends on the direction of the input flows. In order to show for which flow direction the equivalent circuit has been developed flow diodes can be introduced as shown in Fig. 3.23.

3.4.2.1 Equivalent circuit for a symmetrical line junction

For a symmetrical line junction ($A_1 = A_2$ and $\alpha = \beta$) we obtain

$$(3.53) \quad k_{11} = k_{21}$$

$$k_{12} = k_{22}$$

$$k_{13} = k_{23} .$$

4.   Transmission Lines

Contrary to processes in fluidic networks with lumped com-
ponents pressure and flow depend on time as well as on space.
Comparing the pneumatic and the electric transmission line
we find that the velocity of sound in air is about the factor
10^6 smaller than the velocity of light. We therefore obtain
in fluidic engineering the same wave lengths at frequencies
which are about 10^6 lower than in electrical engineering.
For instance 600 Hz in fluidic engineering (medium air) may
be compared with 600 MHz in electrical engineering. The wave
length λ in both cases is 50 cm. In Table 1 the frequency ranges
of electronics and fluidics (medium air) are compared.

Frequency range _____ wave length range

Electronics	Fluidics (air)				
0,3 – 3MHz	0,3 – 3Hz	MF	1000	–	100 m
3 – 30MHz	3 – 30Hz	HF	100	–	10 m
30 –300MHz	30 – 300Hz	VHF	10	–	1 m
0,3 – 3kHz	0,3 – 3kHz	UHF	10	–	1 dm
3 – 30kHz	3 – 30kHz	SHF	10	–	1 cm

Table 1

The above mentioned frequencies of 600 Hz therefore belong to
microwave range. But even for frequencies of 30 Hz we must be
aware of handling ultra short waves.

4.1   The equivalent circuit for a short length of fluidic transmission line

Analogous to the electric transmission line an equivalent
circuit for a short length of the uniform fluidic transmission
can be derived as shown in Fig. 4.1,

where

R'   resistance per unit length
L'   inductance (inertia) per unit length
C'   capacitance per unit length
G'   conductance per unit length

Uniform means that the transmission line characteristics do not
change along the line (same geometry and flow conditions).
Putting up the mesh theorem for the pressure

$$(4.1) \quad \sum p = 0$$

and the node theorem for the massflow

$$(4.2) \quad \sum \dot{m} = 0$$
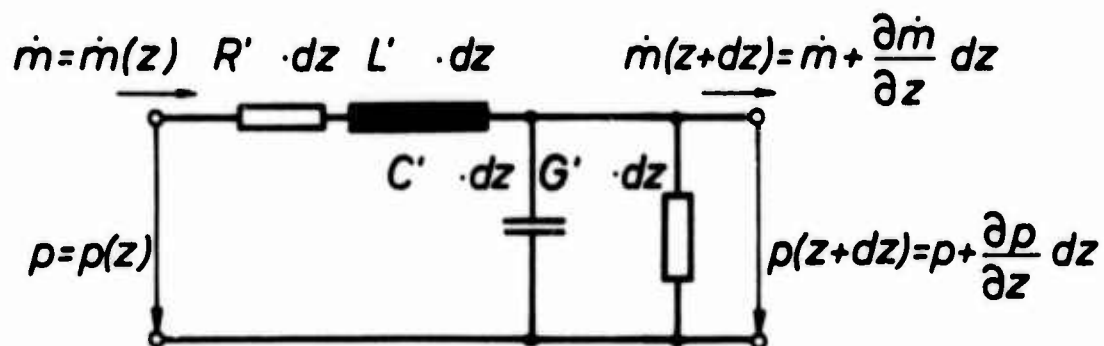
Fig.4.1   Equivalent circuit for a short length of a fluidic
transmission line
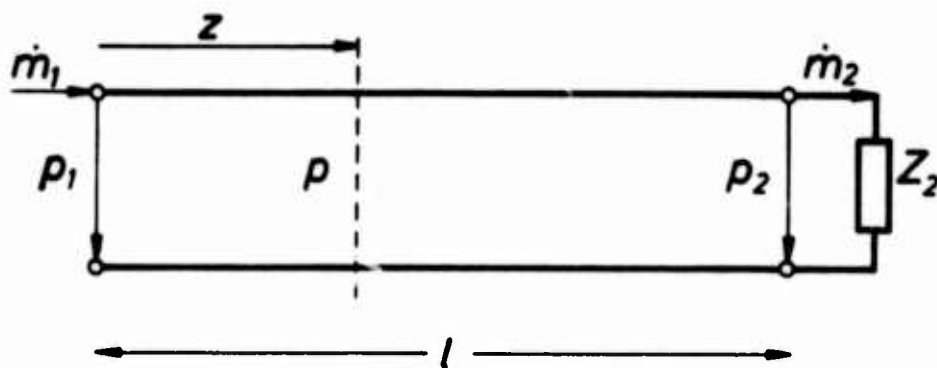
Fig.4.2   Fluidic transmission line with arbitrary load
impedance
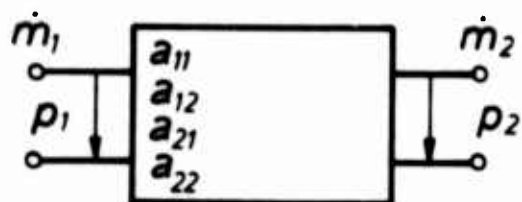
Fig.4.3   Fluidic transmission line as four pole

we find the following relations

$$(4.3) \quad -\frac{\partial p}{\partial z} = \left(R' + j\omega L' \right) \dot{m} = z_1' \cdot \dot{m}$$

$$(4.4) \quad -\frac{\partial \dot{m}}{\partial z} = \left(G' + j\omega C' \right) p = Y_1' p$$

where

$(4.5) \quad z_1' = R' + j\omega L'$ series impedance per unit length

$(4.6) \quad Y_1' = G' + j\omega C'$ shunt admittance per unit length.

4.2   The uniform transmission line of arbitrary length

4.2.1 Surge impedance and propagation factor

Out of the equations for the series impedance per unit length
and shunt admittance per unit length the differential equation
for the pressure is obtained as

$$(4.7) \quad \frac{\partial^2 p}{\partial z^2} = \left(R' + j\omega L' \right)\left(G' + j\omega C' \right).$$

This linear differential equation can be solved by

$$(4.8) \quad p = a\, e^{\gamma_1 z}$$

where

$$(4.9) \quad \gamma_1 = \sqrt{\left(R' + j\omega L' \right)\left(G' + j\omega C' \right)}.$$

From equ. (4.8) the general solution is found as

$$(4.10) \quad p = a_1 e^{-\gamma_1 z} + a_2 e^{+\gamma_1 z}.$$

γ_1 is called propagation factor, with

$$(4.11) \quad \gamma_1 = \alpha_1 + j\beta_1$$

where

α_1 attenuation factor

β_1 wave number.

The solution of the differential equation for the massflow rate gives

$$(4.12) \quad \dot{m} = \frac{a_1}{Z_0} e^{-\gamma_1 z} - \frac{a_2}{Z_0} e^{+\gamma_1 z}$$

where

$$(4.13) \quad Z_0 = \sqrt{\frac{R' + j\omega L'}{G' + j\omega C'}} \; .$$

Z_0 has the dimensions of a fluidic resistance and is called 'surge impedance' or 'characteristic impedance' of the line.

Using the conventional complex time notation one obtains

$$(4.14) \quad \hat{p} \, e^{j\omega t} = \hat{a}_1 e^{-\alpha_1 z} e^{j(\omega t - \beta_1 z)} + \hat{a}_2 e^{\gamma_1 z} e^{j(\omega t + \beta_1 z)}$$

$$(4.15) \quad \hat{m} \, e^{j\omega t} = \frac{\hat{a}_1}{Z_0} e^{-\alpha_1 z} e^{j(\omega t - \beta_1 z)} + \frac{\hat{a}_2}{Z_0} e^{\alpha_1 z} e^{j(\omega t + \beta_1 z)} .$$

Pressure and flow along the line result out of the super-position of a wave travelling in positive z-direction and a wave travelling in negative z-direction.

The amplitudes decrease with increasing direction of propagation according $e^{-\alpha_1 z}$. The phase changes with ωt and in addition along the propagation coordinate with $\beta_1 z$.
The phase velocity is

$$(4.16) \quad c = \frac{\omega}{\beta_1} \; .$$

The phase velocity in general is smaller than the velocity of sound c_a in free space (or lossless transmission line).
The relation between frequency and wavelength is given by

$$(4.17) \quad c = \lambda \cdot f \; .$$

4.2.2 The characteristic equations for the transmission line

Calculating the constants a_1 and a_2 out of the boundary con-ditions we find the characteristic equations for the trans-mission line which gives the correlation between pressure p_1 and mass flow rate $\dot{m}_1$ at the beginning of the line and pressure p_2 and massflow rate $\dot{m}_2$ at the end of the line.

231

$$(4.18) \quad p_1 = p_2 \cosh \Gamma_1 l + \dot{m}_2 Z_0 \sinh \Gamma_1 l$$

$$(4.19) \quad \dot{m}_1 = \dot{m}_2 \cosh \Gamma_1 l + \frac{p_2}{Z_0} \sinh \Gamma_1 l$$

Using

$$(4.20) \quad Z_2 = \frac{p_2}{\dot{m}_2}$$

for the load impedance of the line the transfer function for pressure and flow are

$$(4.21) \quad \frac{p_1}{p_2} = \cosh \Gamma_1 l + \frac{Z_0}{Z_2} \sinh \Gamma_1 l$$

$$(4.22) \quad \frac{\dot{m}_1}{\dot{m}_2} = \cosh \Gamma_1 l + \frac{Z_2}{Z_0} \sinh \Gamma_1 l.$$

4.2.3 Input impedance of a uniform line with arbitrary load impedance

The input impedance Z_{in} of a line loaded by an arbitrary impedance is found out of equ. (4.21) and (4.22) as

$$(4.23) \quad Z_{in} = \frac{1 + \frac{Z_0}{Z_2} \tanh \Gamma_1 l}{1 + \frac{Z_2}{Z_0} \tanh \Gamma_1 l} \, Z_2 .$$

Loading the line by its surge impedance $Z_2 = Z_0$, one finds that the input impedance is equal to its surge impedance

$$(4.24) \quad Z_{in} = Z_0 \qquad \text{with} \quad Z_2 = Z_0 .$$

The main wave is fully absorbed by the load impedance. The transmission line is 'matched'.

4.2.4 The four-pole equivalent circuit of the transmission line

The four-pole equivalent circuit of a line (Fig. 4.2) can be derived from the characteristic equations (4.18) and (4.19) which can be written as

(4.25)
$$\begin{pmatrix} p_1 \\ \dot{m}_1 \end{pmatrix} = \begin{pmatrix} a_{11} & a_{12} \\ a_{21} & a_{22} \end{pmatrix} \begin{pmatrix} p_2 \\ \dot{m}_2 \end{pmatrix}$$

where

$$a_{11} = \cosh \gamma_1 l$$
$$a_{12} = Z_0 \sinh \gamma_1 l$$
$$a_{21} = \frac{1}{Z_0} \sinh \gamma_1 l$$
$$a_{22} = \cosh \gamma_1 l.$$

For the T-type equivalent circuit in Fig. 4.4a we obtain

(4.26)
$$Z_{1T} = Z_{2T} = Z_0 \tanh\left(\frac{1}{2}\gamma_1 l\right)$$

(4.27)
$$Z_{3T} = Z_0 \frac{1}{\sinh \gamma_1 l}$$

and for the type equivalent circuit

(4.28)
$$Z_{1\pi} = Z_{2\pi} = Z_0 \frac{1}{\tanh\left(\frac{1}{2}\gamma_1 l\right)}$$

(4.29)
$$Z_{3\pi} = Z_0 \sinh \gamma_1 l.$$

For small argument $\gamma_1 l$ assuming

$$\frac{1}{6}\gamma_1^2 l^2 \ll 1$$

the transmission line can be described by the T-type or π -type equivalent circuit with lumped parameters in Fig. 4.5.
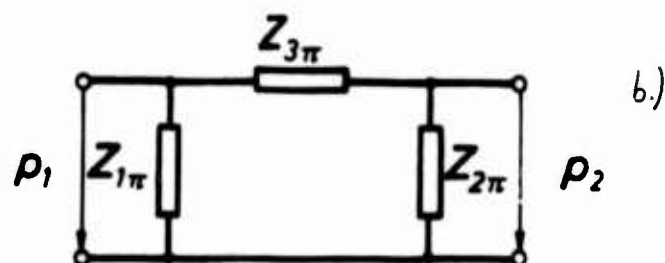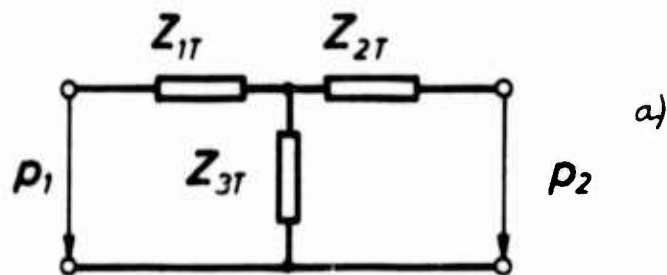
Fig.4.4a T-type equivalent circuit
      b π-type equivalent circuit
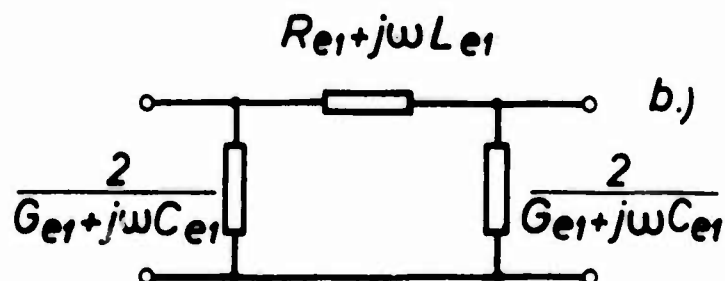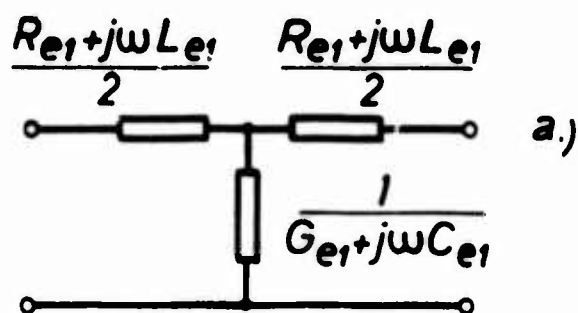
Fig.4.5   Four-pole equivalent circuit for a transmission
          line assuming $\frac{1}{4} r_i^2 l^2 \ll 1$
          a) T-type, b) π-type

234

A comparison between both lumped and distributed parameter models is given in ref. 17. In the same reference the various matrix presentations for the distributed parameter model forms are given.

4.3   The lossless uniform transmission line

Assuming that the losses of the transmission line can be neglected the series impedance and shunt admittance per unit length reduce to

$$(4.30) \quad Z_1' = j\omega L'$$

$$(4.31) \quad Y_1' = j\omega C'.$$

The equivalent circuit for a short length of the lossless transmission line is drawn in Fig. 4.6, where L' is represented by the adiabatic inductance per unit length L_a' and C' by the adiabatic capacitance per unit length C_a' (see chapter 2.3)

$$(4.32) \quad Z_{10}' = j\omega L_a' \qquad \text{where} \quad L_a' = \frac{1}{A}$$

$$(4.33) \quad Y_{10}' = j\omega C_a' \qquad\qquad C_a' = \frac{A}{c_a^2}$$

The surge impedance now becomes

$$(4.34) \quad Z_{so} = \sqrt{\frac{Z_{10}'}{Y_{10}'}} = \sqrt{\frac{L_a'}{C_a'}} = \frac{c_a}{A}.$$

The propagation factor γ_1 reduces to

$$(4.35) \quad \gamma_{10} = \sqrt{Z_{10}' Y_{10}'} = j\omega\sqrt{L_a' C_a'} = j\frac{\omega}{c_a} = j\beta_{10}.$$

Equ. (4.34) and (4.35) are mostly used in acoustics, where the diameters of lines are so large that the neglection of friction will not significantly influence the results. In fluidics the neglection of losses will not be permissible. Nevertheless those equations are of importance for fluidic circuit design. The surge impedance can be roughly calculated only with the knowledge of the cross-sectional area and the speed of sound, so giving an idea how to match the line (see chapter 5). Having only a real component the surge impedance Z_{so} can be used in graphical techniques (see chapter 6.2.1).
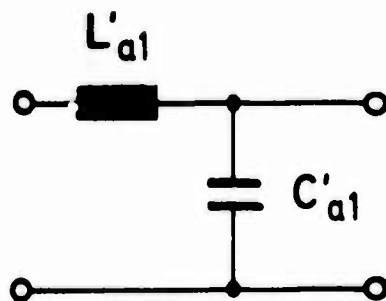
Fig.4.6   Equivalent circuit of a short length of lossless
fluidic transmission line
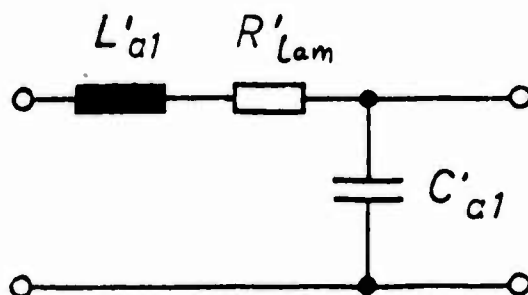
Fig.4.7   Equivalent circuit of a short length of fluidic
transmission line with frequency independent
line parameters

4.4 The lossy uniform transmission line with constant parameters

An improvement of transmission line theory is obtained by considering the dc-resistance per unit length (Fig. 4.7)

From this the surge impedance Z and the propagation factor are obtained as

$$(4.36) \quad Z_o = Z_{so} \sqrt{1 - j \frac{1}{\omega/\omega_p}}$$

$$(4.37) \quad \int_1 = j \frac{\omega}{C_a} \sqrt{1 - j \frac{1}{\omega/\omega_p}} .$$

The characteristic angular frequency is defined as

$$(4.38) \quad \omega_p = 2\pi f_p = \frac{R'_{lam}}{L'_a} = \frac{8\pi \nu}{A} .$$

This theory is also called constant parameter theory.

4.5 The lossy uniform transmission line with frequency dependent line parameters

The first descriptions of fluid transmission lines considering frequency dependence of the line parameters where carried out by Crandall already in 1927. In his work (ref.18) a frequency dependent resistance and reactance are calculated for the acoustic line with circular cross-section. Richardson presented measurements which showed the dependence of the profile in an acoustic line on frequency (annular effect) (ref.19). In ref. 20 Iberall gave the first general theory for fluid lines. The first comprehensive studies on frequency dependence of transmission line parameters have been done by Nichols (ref.21) and Brown (ref.22) solving the linearized flow equations for a transmission line with circular cross-section. In ref. 23 and 24 Schaedel presented a theory for transmission lines with rectangular cross-section.

The assumptions of Brown, Nichols and Schaedel are
1. Smal perturbations with small mean flow
2. Laminar flow
3. Retain only first order terms of equations
4. Wave length of signal $\gg$ cross-sectional dimensions
5. Isothermal walls
6. $\omega \ll \frac{3}{4} \cdot \frac{c^2}{\nu}$.

4.5.1 Transmission line with circular cross-section

Series impedance per unit length

$$(4.39) \quad Z_1' = j\omega L_a' \left(1 - \mathfrak{Z}\left(\frac{\omega}{\omega_\gamma}\right)\right)^{-1}$$

where

$$\mathfrak{Z}\left(\frac{\omega}{\omega_\gamma}\right) = \frac{2\mathfrak{J}_1(z_\nu)}{z_\tau \mathfrak{J}_0(z_\nu)}$$

$$z_\nu = \sqrt{8j^3 \frac{\omega}{\omega_\nu}}$$

$$\omega_\rho = \frac{8\pi\nu}{A}.$$

Shunt admittance per unit length

$$(4.40) \quad Y_1' = j\omega C_a' \left(1 + (\kappa - 1)\mathfrak{Z}\left(\frac{\omega}{\omega_T}\right)\right)$$

where

$$\mathfrak{Z}\left(\frac{\omega}{\omega_T}\right) = \frac{2\mathfrak{J}_1(z_T)}{z_T \mathfrak{J}_0(z_T)}$$

$$z_T = \sqrt{8j^3 \frac{\omega}{\omega_T}}$$

$$\omega_T = \frac{8\pi\nu_T}{A} = \frac{\omega_\rho}{P_r}$$

$$\nu_T = \frac{\nu}{P_r}$$

P_r = Prandtl number (= 0,708 for air)

$\mathfrak{J}_0(z)$ = Besselfunction of zero order
$\mathfrak{J}_1(z)$ = Besselfunction of first order

4.5.2 Transmission line with rectangular cross-section

Series impedance per unit length

$$(4.41) \quad Z_1' = \frac{2\nu}{aA^2} \mathfrak{S}\left(\frac{\omega}{\omega_\gamma}\right)^{-1}$$

where

238
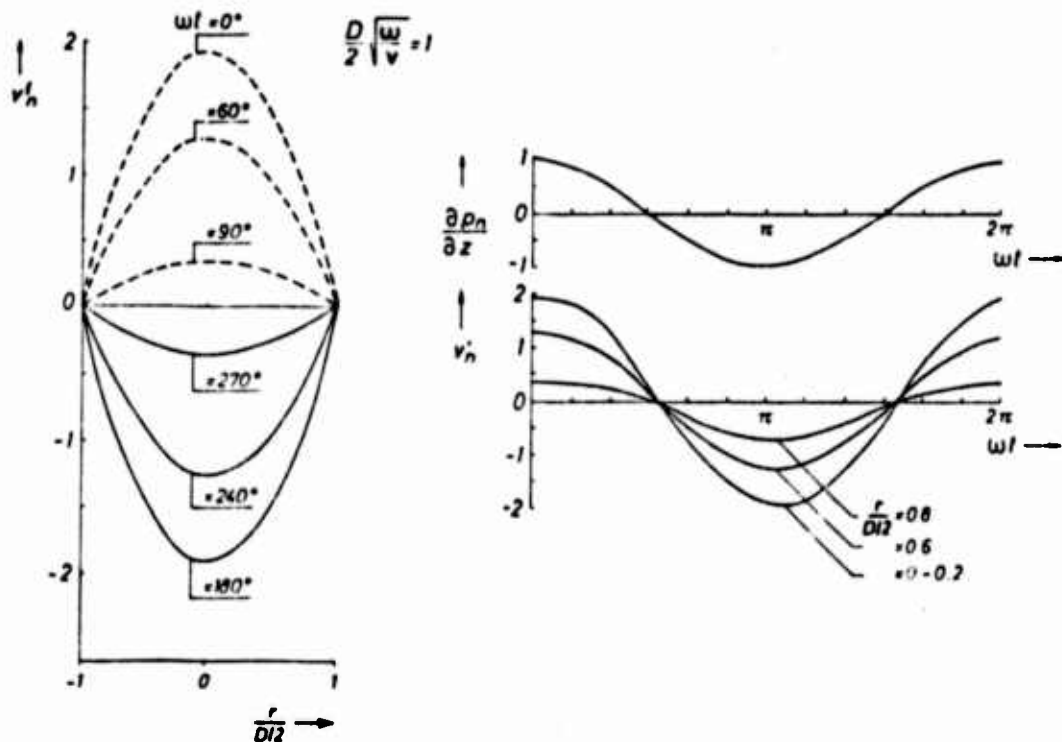
Fig.4.8 Velocity profiles for small frequencies in a circular duct
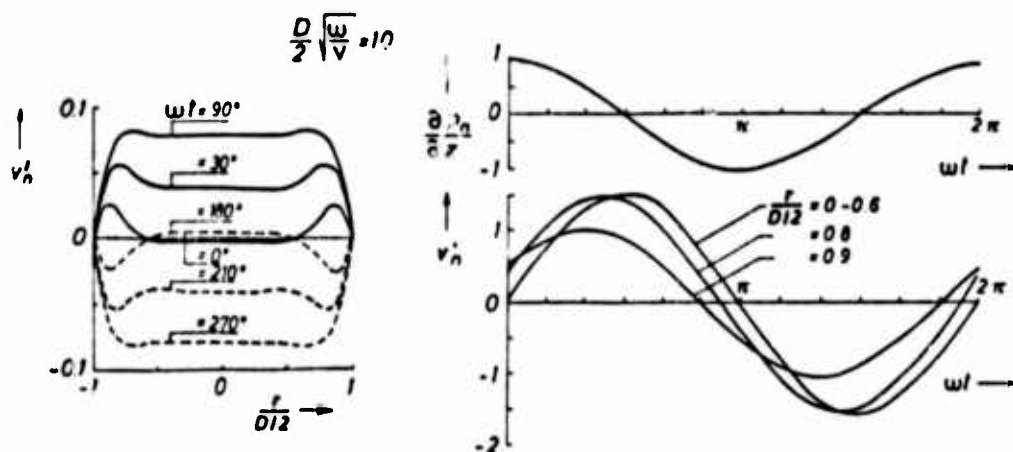
Fig.4.9 Velocity profiles for high frequencies in a circular duct

$$S\left(\frac{\omega}{\omega_\nu}\right) = \sum_{i=1}^{\infty} \frac{1 - \dfrac{\tanh\left(\frac{1}{a}\sqrt{d_i^2 + j\,2\pi a\,\frac{\omega}{\omega_\nu}}\right)}{\frac{1}{a}\sqrt{d_i^2 + j\,2\pi a\,\frac{\omega}{\omega_\nu}}}}{d_i^2\left(d_i^2 + j\,2\pi a\,\frac{\omega}{\omega_\nu}\right)}$$

$a = \dfrac{height}{width}$ aspect ratio, $d_i = \dfrac{2i-1}{2}\pi$ eigen values.

Shunt admittance per unit length

(4.42) $Y_1' = j\omega C_a'\left(\kappa - j(\kappa-1)\dfrac{\omega}{\omega_T}\,4\pi a\,S\left(\dfrac{\omega}{\omega_T}\right)\right)$

where $S\left(\dfrac{\omega}{\omega_T}\right) = \sum_{i=1}^{\infty} \dfrac{1 - \dfrac{\tanh\left(\frac{1}{a}\sqrt{d_i^2 + j\,2\pi a\,\frac{\omega}{\omega_T}}\right)}{\frac{1}{a}\sqrt{d_i^2 + j\,2\pi a\,\frac{\omega}{\omega_T}}}}{d_i^2\left(d_i^2 + j\,2\pi a\,\frac{\omega}{\omega_T}\right)}$.

4.5.3   The frequency dependence of the line parameters

For laminar dc flow the velocity distribution in a circular tube
is parabolic. The same parabolic distribution we find for small
frequencies. The magnitude varies in the same phase with that
of the pressure gradient (see Fig. 4.8). V_n' is the velocity
referred to the average velocity for dc flow. With increasing
frequency the amplitude diminishes. The maxima are found in the
neighbourhoud of the wall (see Fig. 4.9). The fluid in the center
of the tube flows with a phase lag of $90°$ to the pressure gradient
Only the fluid near the wall is in phase with the pressure gra-
dient. With increasing frequency the amplitude of the velocity
diminishes and the region in which the velocity and the pressure
gradient are in phase is getting smaller. The pure resistance
of the series impedance increases with increasing frequency.
This annular effect is very similar to the skineffect in elec-
trical engineering.

The following figures will show the frequency depence of the
single line parameters defined in the equivalent circuit for
lines with circular and rectangular cross-section. The frequency
f is referred to the viscous frequency $f_\nu = \dfrac{\omega_\nu}{2\pi} = \dfrac{4\nu}{A}$.

For small dimensionless frequencies, i.e. for small frequencies
and small cross-sections the ac-resistance is equal to the dc-
resistance. With increasing frequency and increasing cross-sec-
tion the ac-resistance may increase to a multiple of the dc-
resistance. (Fig. 4.10)

The inductance approaches the adiabatic inductance for large
cross-sections and high frequencies. For low frequencies and
small cross-sections it can grow about 30%. (Fig.4.11)

240
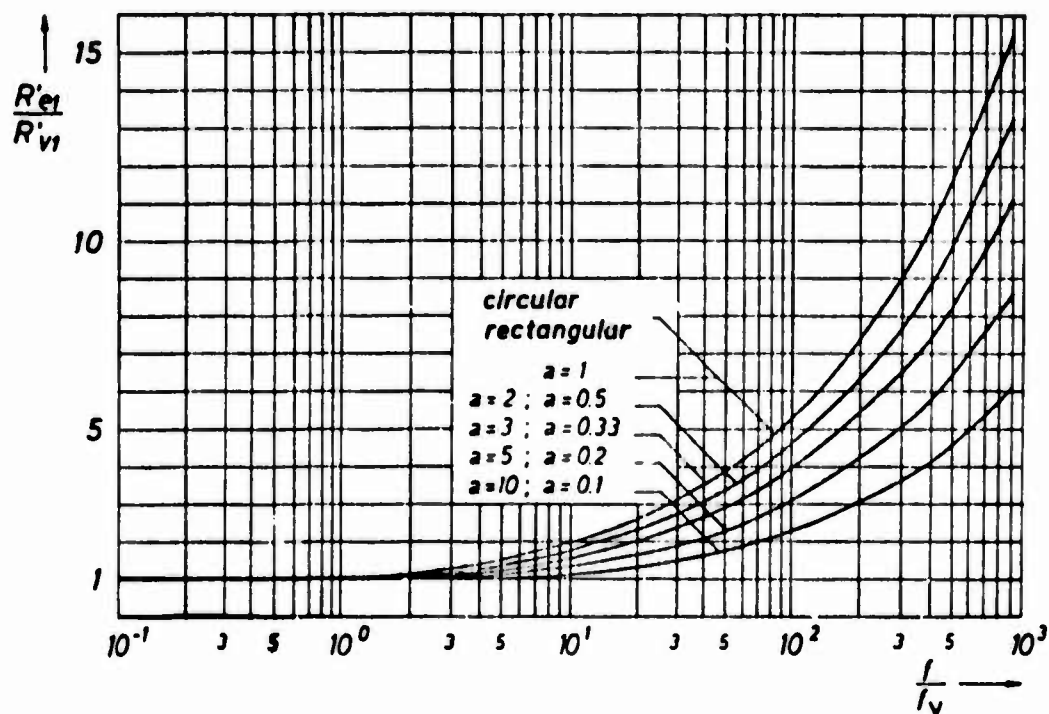
Fig.4.10   Frequency dependent resistance per unit length
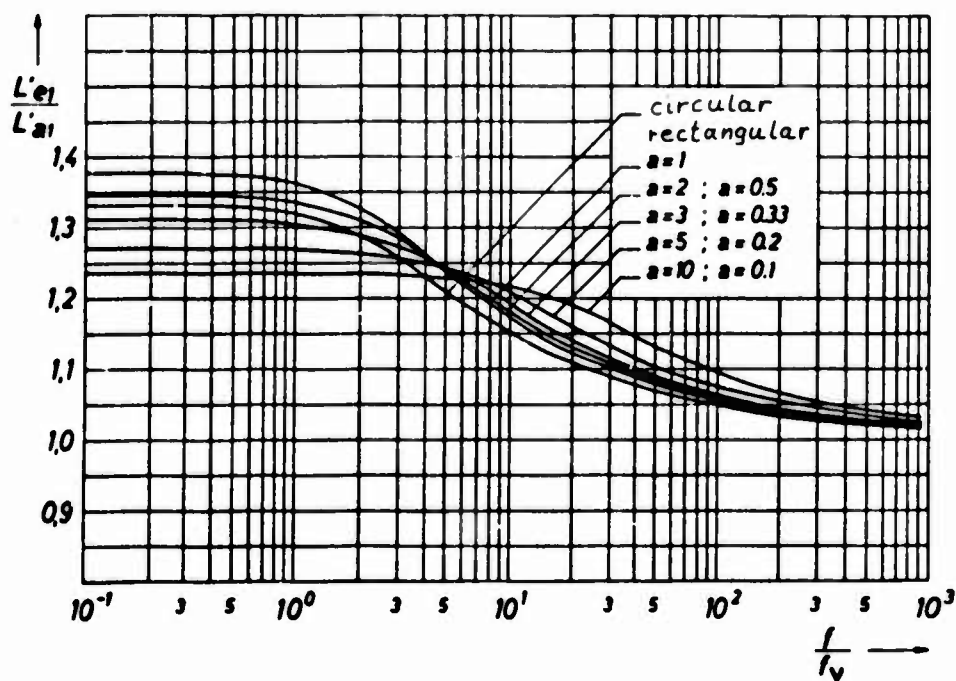
Fig.4.11   Frequency dependent inductance per unit length

241
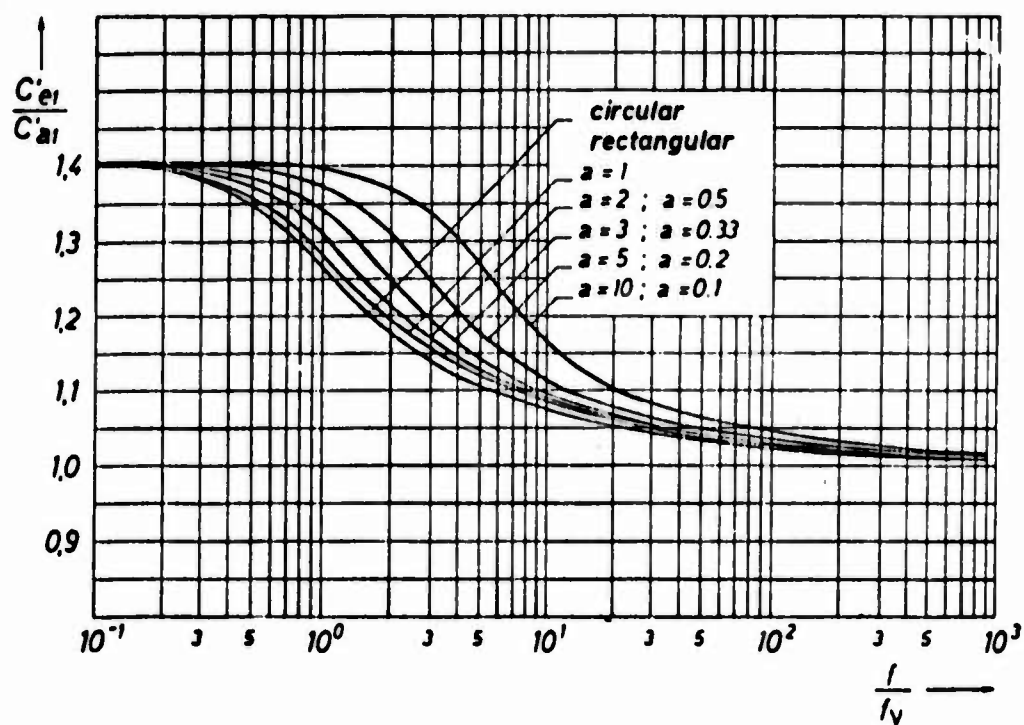
Fig.4.12 Frequency dependent capacitance per unit length
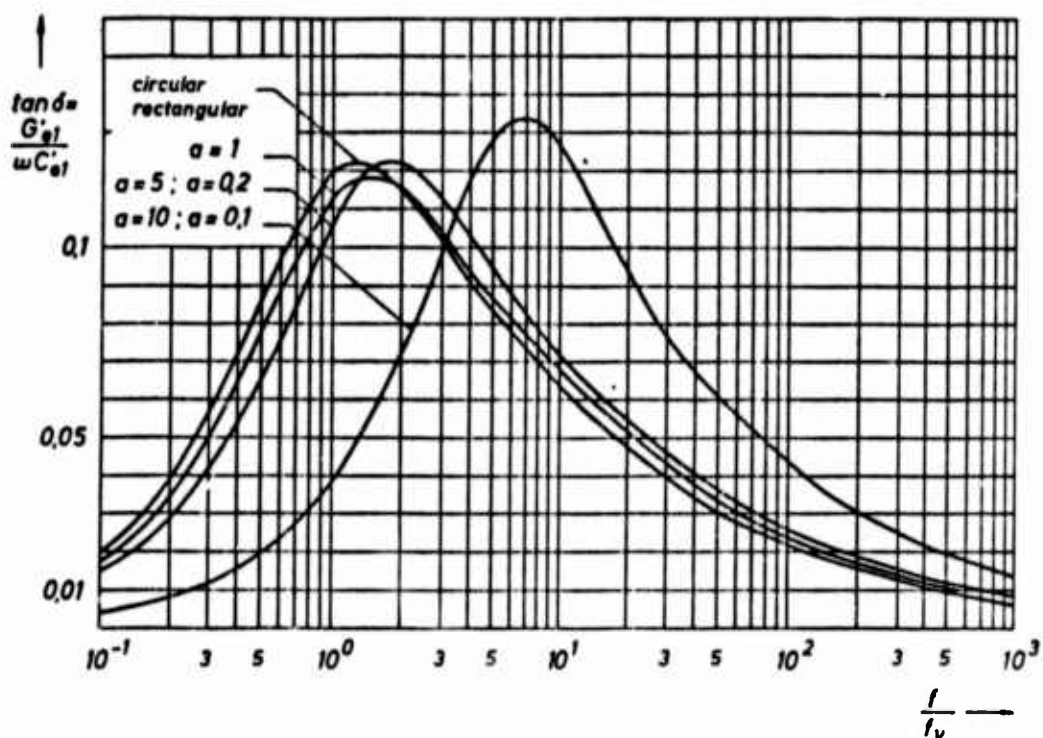
Fig. 4.13 Frequency dependent lossfactor of the
capacitance per unit length

242
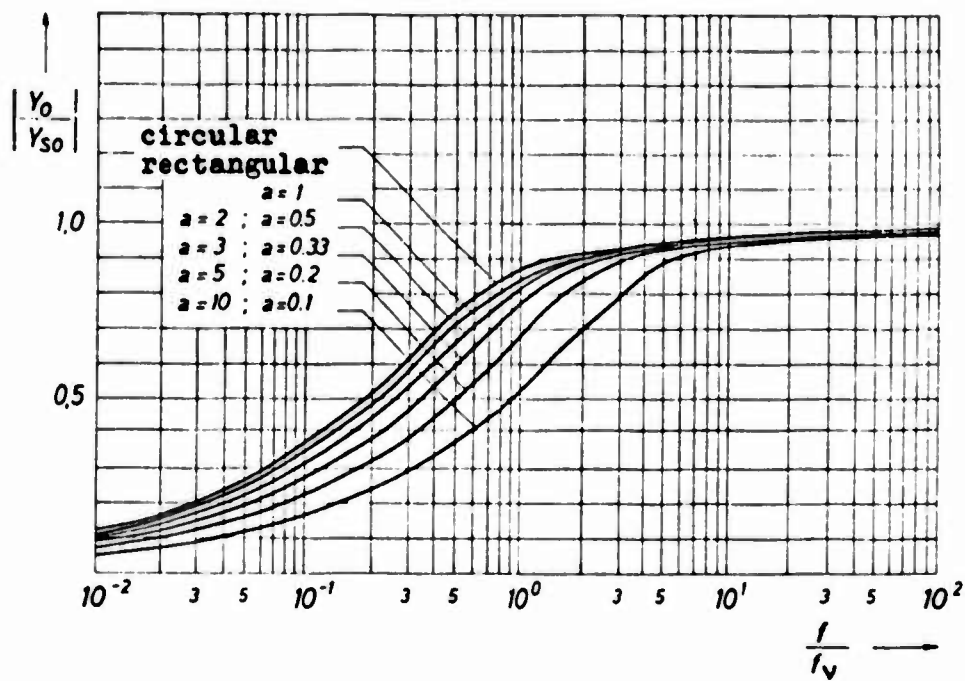
Fig.4.14   Magnitude of the surge impedance
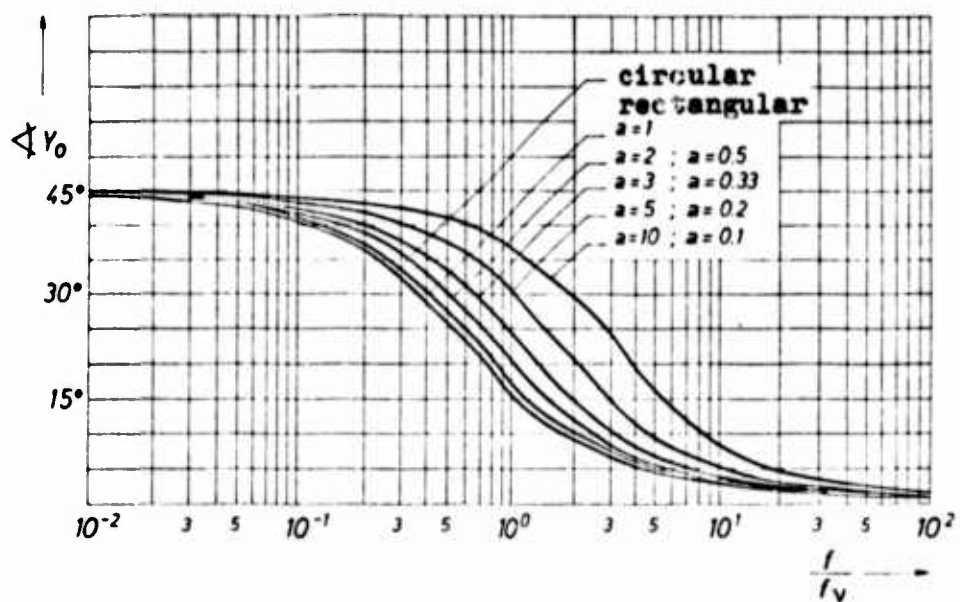
Fig.4.15   Phase angle of the surge impedance

243
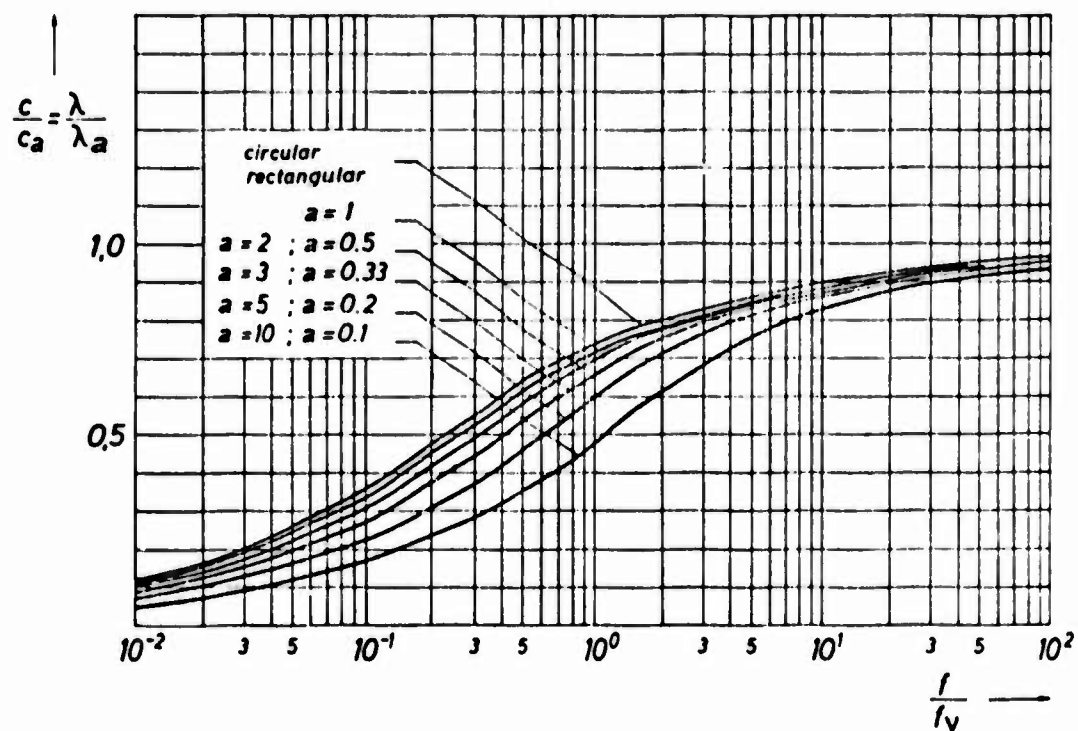
Fig.4.16   Phase velocity and wave length ratio
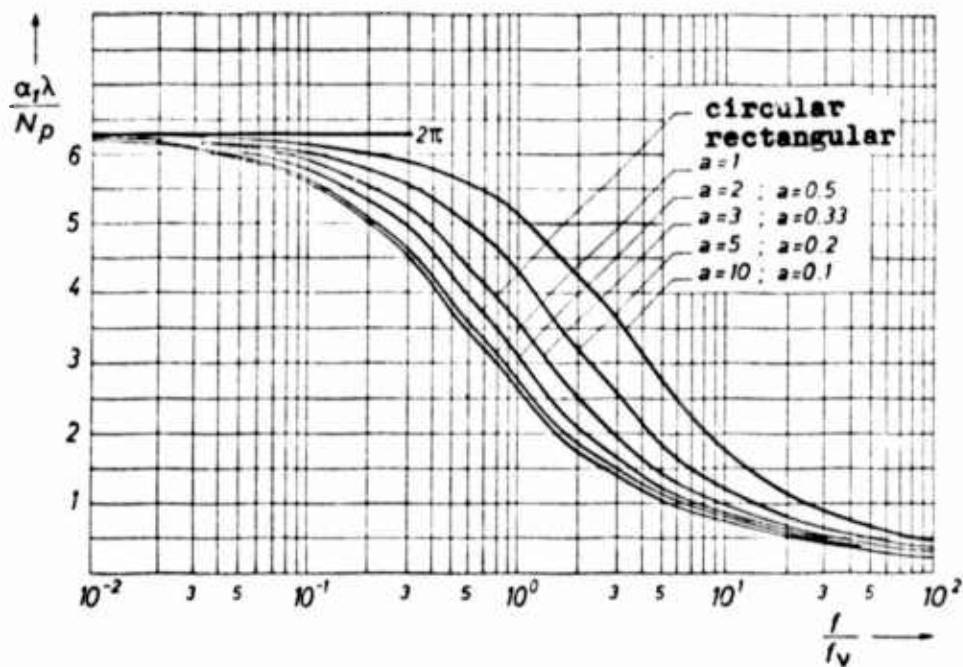
Fig.4.17   Attenuation per line wave length

244

The capacitance for high dimensionless frequencies f/f_ν behaves adiabatically. For small dimensionless frequencies it increases up to κ times the adiabatic capacitance. This is the value we calculate for isothermal conditions. Whether the capacitance behaves isothermally or adiabatically is not only determined by the operating frequency but also by the cross-section. Technical capacitors in nearly all cases behave adiabatically because of their large cross-sections even for frequencies of a few Hz. In transmission lines the behaviour mostly is polytropic. (Fig.4.12) The dissipation factor of the capacitance $\tan\delta = G'/\omega C'$ passes through a distinct maximum. The same phenomenon we find in electric capacitors using a dielectric with orientation polarised dipoles. It is caused by the inertia of the dielectric dipoles. (Fig.4.13) The dissipation in the fluidic capacitor is caused by the fact that the density variations do not follow the pressure variations with out inertia because of thermodynamic effects.

In Fig. 4.14-4.17 the surge impedance and the propagation factor are plotted as a function of the dimensionless frequency.

We see that only for high normalized frequencies the surge impedance approximates the value of the surge impedance of the lossless transmission line. The phase velocity also for high normalised frequencies only is approximately equal to the velocity of sound in free air. For low frequencies and small cross-sections the deviation from free air velocity may be considerable.

From this follows that the individual frequencies of a frequency mixture suffer different phase shifts and attenuation. This results in dispersion. Therefore the rise and decay times of pulses in fluidic transmission lines are increased.

In ref. 2, 24, 25 and 26 measurements have been carried out which show excellent accordance between theory and practice. In Fig. 4.18 and 4.19 pressure transfer functions are shown for a circular and rectangular duct for blocked load conditions.

For the line with circular cross-section Karam (ref.27) developed a high frequency model for $\omega \gg 2\omega_\nu$ that may be very helpful when a computer is not available. The line parameters in slightly modified notation are

$$R' = \frac{8\pi\nu}{A^2}\left[\frac{3}{8} + \frac{1}{2}\sqrt{\frac{\omega}{\omega_\nu}}\right] = R'_{lam}\left[\frac{3}{8} + \frac{1}{2}\sqrt{\frac{\omega}{\omega_\nu}}\right]$$

$$L' = \frac{1}{A}\left[1 + \frac{1}{2\sqrt{\omega/\omega_\nu}}\right] = L'_a\left[1 + \frac{1}{2\sqrt{\omega/\omega_\nu}}\right]$$

$$(4.43) \quad C' = \frac{A}{c_a^2}\left[1 + \frac{\kappa-1}{2}\left(\frac{1}{4}\frac{\omega}{\omega_T} + \frac{1}{\sqrt{\frac{\omega}{\omega_T}}}\right)\right] = C'_a\left[1 + \frac{\kappa-1}{2}\left(\frac{1}{4}\frac{\omega}{\omega_T} + \frac{1}{\sqrt{\frac{\omega}{\omega_T}}}\right)\right]$$

$$\frac{G'}{\omega C'} = \frac{\kappa-1}{2}\frac{1}{\sqrt{\frac{\omega}{\omega_T}}}.$$

Fig.4.18   Pressure transfer function

Fig.4.19   Pressure transfer function

246

From this the unit phase shift and attenuation become

$$\alpha_1 = \frac{1}{4}\left(1 + \frac{\kappa-1}{P_r}\frac{\sqrt{\omega\,\omega_p}}{c_a}\right)$$

(4.44)

$$\beta_1 = \frac{\omega}{c_a}$$

For the line with rectangular cross-section until now no approximations are available.

In ref. 25 Shearer, however, shows that the equations (4.39) and (4.40) for the line with circular cross-section can be applied to the line with rectangular cross-section using the hydraulic radius with good accuracy if the aspect ratio is in the range of about a = 2.0 to 1.0, resp. a = 0.5 to 1.0. It may be therefore possible to use the equations (4.43) and (4.40) for the high frequency approximation of the rectangular line in the range of aspect ratio mentioned above.

4.5.4   Higher modes in fluidic lines

All the information given up to here was concerned with the fundamental of longitudinal mode of propagation in a fluid line. In ref. 28 it is demonstrated, that other modes of propagation may exist in a fluid line. These additional modes which are called higher modes, are excited at the ends of the line, or at points of line discontinuity, because the fundamental mode alone is generally not capable of satisfying the end conditions, which occur at these locations. These modes are more prevalent as the fluid viscosity increases and for frequecies of engineering interest, do not propagate far from the point of exitation. For long transmission lines and low frequencies the effect of these modes may be generally neglected, for short lines, however, it may not be neglected.

Fig. 4.20 shows typical velocity profiles for four modes. In Fig. 4.21 and 4.22 the spatial attenuation factor as a function of radial frequency number is plotted,

where $F_{nr} = \dfrac{\omega\, r_0}{c_a}$ radial frequency number

$D_{nr} = \dfrac{\nu\, r_0^2}{c_a}$ radial damping number .

It is clearly to be seen that up to a critical frequency the attenuation factor of the higher modes is large compared to that of the 0th mode, so that the higher modes can be neglected. Above the critical frequency the attenuation factor of the higher modes becomes smaller than that of the 0th mode. This effect is similar to that in hollow wave guides in microwave techniques. For a transmission line with a diameter of 3 mm the critical frequency for the first mode is about 140 kHz, and for a line of D = 10 mm about 43 kHz. These considerations indicate the possibility of transmitting fluidic carrier frequency signals at higher modes with less attenuation than found

247
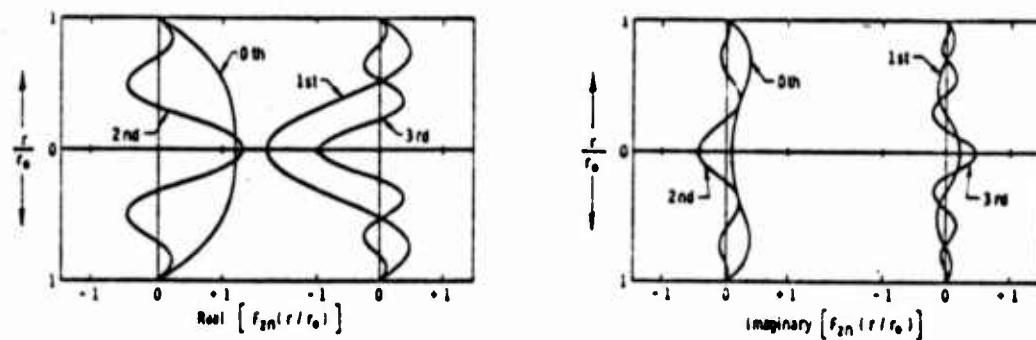
Fig. 4.20   Axial velocity profile function
for four modes
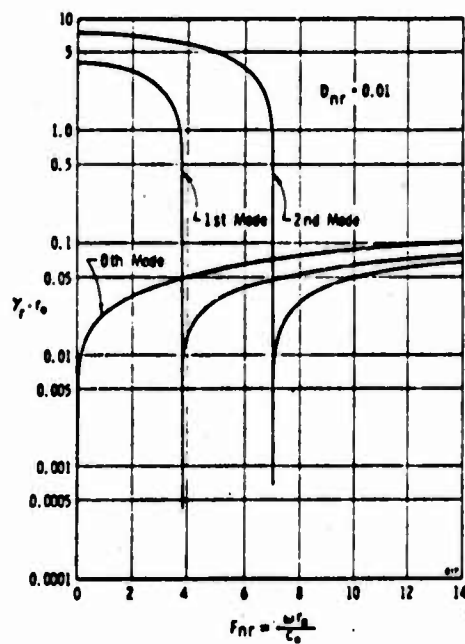
Fig.4.21

Spatial attenuation factor as a function of
radial frequency number for three modes
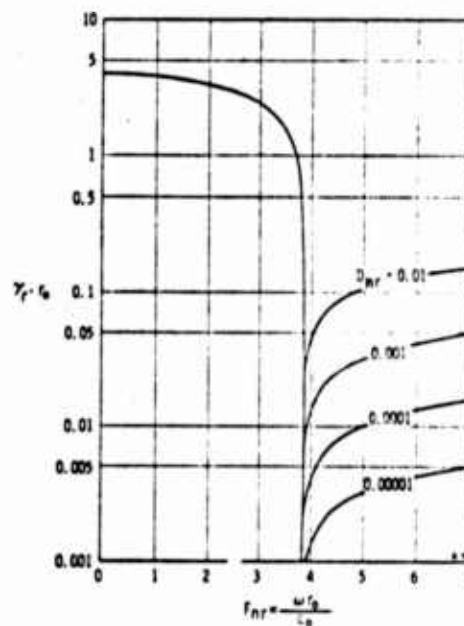
Fig.4.22

Spatial attenuation factor as a function of
radial frequency number for first mode

248

at the 0th mode.

4.4.5 Influence of superposed dc-flow

Little knowledge presently exists about the influence of signi-
ficant dc-flow on the frequency behaviour of a transmission line.
In ref. 30 Brown applies the method of characteristics to cal-
culate quasisteady wall shear on unsteady flowintubes. The
work is based on ref. 29 in which Zielke shows that the method
of characteristic can be adapted to handle frequency-dependent
wall shear. In ref.31 the investigations of ref. 30 are extended.
The results of semiempirical analytical and experimental studies
of the acoustic frequency response of circular tubes with a
mean turbulent flow are given.

The influence of dc-flow is considered by taking into account
the velocity profile for different Reynolds numbers. So a con-
stant parameter (I-R-C) model for frequencies considerably
below ω_ν is establishes with

(4.45) $\quad Z' = R_v' + j\omega L'$

(4.46) $\quad Y' = j\omega \kappa C_a'$.

The resistance R_v' is found from the widely established data
for the friction factor f (see chapter 3.1) as

(4.47) $\quad R_v' = \dfrac{\dot{m}}{2\rho A^2} \cdot \dfrac{f(R_e)}{D_e}$.

The incuctance L is calculated on the basis of the velocity
profile depending on Reynolds number.

(4.48) $\quad L' = k_L(R_e)L_a' = L_a' \dfrac{A\int v^2 dA}{\dfrac{1}{A}\left(\int_A v dA\right)^2}$

where $k_L(R_e)$ is given in Table 2.
The capacitance κC_a is the isothermal capacitance.

Reynolds number	$K_L = \dfrac{L'}{L'_a}$
Laminar flow	4/3
2500 (turbulent)	1.113
10^4	1.041
10^5	1.020
10^6	1.012
10^7	1.008
∞	1.000

Table 2

This low frequency model is extended for high frequencies.

4.6 Nonuniform transmission lines

Considerable work has been devoted to the nonuniform transmission
line in electronics and acoustics, where those tapered lines are
used as impedance matching elements between systems, filters
and puls transformers. A comprehensive collection of literature
can be found in ref. 32.

All these investigations are limited to lines with small taper
and negligible losses. For electrical and acoustical lines this
turns out to be sufficient. Because of dc-flow influence in
fluidic transmission lines solutions obtained can only be applied
to fluidic transmission lines with blocked load conditions or
no dc-flow. Until now there is no general solution for the loss-
less nonuniform transmission line with arbitrary shape. One of
the few nonuniform lines where a mathematical solution is possible
is the exponential line (exponential horn in acoustics).
Neglecting the losses we obtain for a short length of the non-
uniform line

$$(4.45) \quad \frac{\partial p}{\partial z} = -j \omega L'(z) \cdot \dot{m}$$

$$(4.46) \quad \frac{\partial \dot{m}}{\partial z} = -j \omega C'(z) p.$$

Assuming that the inductance and the capacitance change exponen-
tially

(4.47) $\quad L'(z) = L_0' e^{kz}$

(4.48) $\quad C'(z) = C_0' e^{-kz}$

the pressure and flow distribution along the .ossless exponential transmission line are found as

(4.49) $\quad p = a_1 e^{\frac{1}{2}kz - j\beta_k z} + a_2 e^{\frac{1}{2}kz + j\beta_k z}$

(4.50) $\quad \dot{m} = \frac{a_1}{Z_{01}} e^{\frac{1}{2}kz - j\beta_k z} + \frac{a_2}{Z_{02}} e^{\frac{1}{2}kz + j\beta_k z}$

where

(4.51a) $\quad Z_{01,2} = \dfrac{j\omega L_0' e^{kz}}{j\beta_k \mp \frac{1}{2}k}$

(4.51b) $\quad \beta_k = \sqrt{\beta^2 - \frac{1}{4}k^2} \quad$ with $\quad \beta = \dfrac{\omega}{c_a}$.

For

$$\frac{1}{2}k \ll \beta$$

or

$$\omega \gg c_a \frac{k}{2}$$

$Z_{0\,1,2}$ approximately is a pure resistance

(4.52) $\quad Z_{so} = \sqrt{\dfrac{L_0'}{C_0'}} \; e^{kz} = \dfrac{c_a}{A_i e^{-kz}} = Z_{oi} e^{kz}$

where A_i input cross-section of the line.
If the line is loaded at it end by a resistance

$$Z_2 = Z_{oi} e^{kl}$$

the main wave is fully absorbed and the line is matched. The input resistance then becomes

$$Z_{in} = Z_{oi} .$$

The line acts as a transformer that transforms the load resistance Z_2 to the resistance Z_{01}.

The line will be matched for frequencies which are about three times the cutoff frequency $f = \dfrac{c_a k}{4\pi}$.

251

Such an exponential horn has been used in ref. 33 for a fluidic
circuit in order to match the sending and receiving amplifiers
to a long transmission line with a diameter of 3.5 to 36.0 mm.

For nonuniform lines where no mathematical solution is known,
the line can be approximated by a number of uniform lines (ref.
34,35), as indicated in Fig. 4.23.

Experimental results show good agreement between theory and
practice for the acoustic case (no dc-flow, blocked load)
(ref.35).

For dc-flow the pressure increase or decrease caused by the
varying cross-section has to be considered. This is possible
by introducing the cross-sectional resistances $r_s = \dot{m}/\rho A_2^2)$

at the points where two uniform lines are connected. For the
acoustic case the cross-sectional resistances become zero $(\dot{m} = o)$.

In ref. 9 the transmission line parameters for a short length
of these equivalent uniform lines have been redefined for a
straightwalled tapered line (see Fig. 4.24), where

$$(4.53a) \quad r_e = R_{lam} - \frac{\dot{m}}{\rho A_1^2}\left[1 - \left(\frac{A_1}{A_2}\right)^2 - k(\Theta)\left(1 - \frac{A_1}{A_2}\right)^2\right]$$

$$(4.53b) \quad L_e = \frac{l}{A_1}\frac{A_1/A_2}{A_1/A_2 - 1}\ln\frac{A_1}{A_2}$$

$$(4.53c) \quad C_e = \frac{A_1}{C_a^2}\frac{A_1/A_2 + 1}{A_1/A_2}\frac{l}{2}.$$

The surge impedance for the lossless equivalent line follows as

$$(4.54) \quad Z_{so} = \frac{C_a}{A_1}\sqrt{\frac{2\left(\frac{A_1}{A_2}\right)^2\ln\frac{A_1}{A_2}}{\left(\frac{A_1}{A_2}\right)^2 - 1}} = \frac{C_a}{A_{eff}}$$

and the effective aspect ratio is defined as

$$(4.55a) \quad a_{eff} = \frac{h}{b_{eff}} = \frac{h^2}{A_{eff}} = \frac{h^2}{A_1}\sqrt{\frac{\left(\frac{A_1}{A_2}\right)^2 - 1}{2\left(\frac{A_1}{A_2}\right)^2\ln\frac{A_1}{A_2}}}.$$

In ref.9 a number of different straight-walled nonuniform lines
has been investigated under different load conditions and for
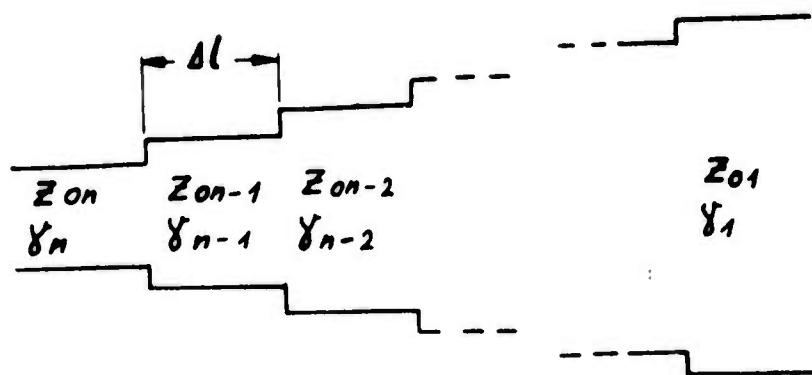
Fig.4.23   Approximation of a nonuniform transmission
line by uniform line segments
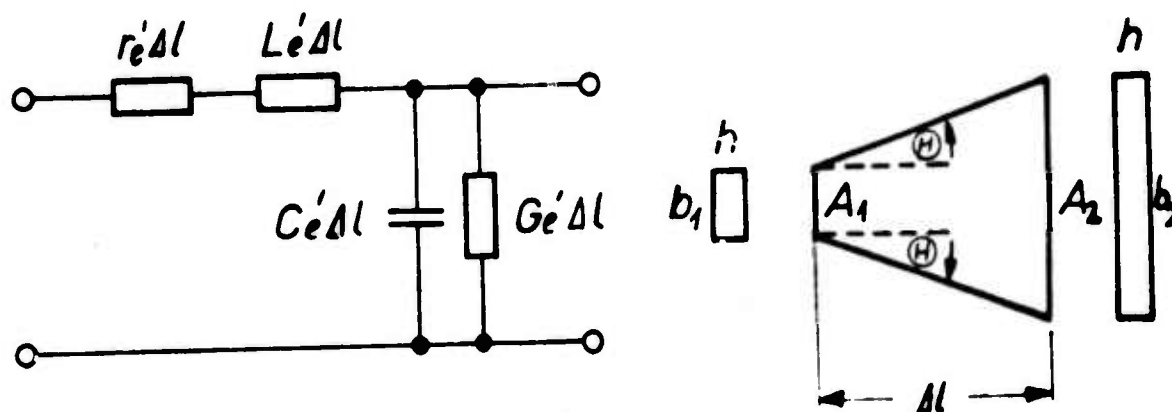
Fig.4.24   Equivalent circuit of a short length of
nonuniform transmission line

different dc-flow rates. Under blocked load conditions agreement
between theory and exp~iment was extremely good. Under finite
load conditions agreement differed rather much with the model.
It is supposed that number n of segments taken for simulation
has been too small. The highest number of segments has been 10.

In ref. 32 a numerical simulation of nonuniform electrical trans-
mission lines for a claimed calculation accuracy has been
evaluated. Results show that the number of segments necessary
may differ from some 10 to some 1000 for an accuracy of 10^{-3}
for the reflection coefficient. The number of segments necessary
is determined by the computer.
It should be therefore worthwhile to apply this computer simul-
tation of ref.32 to the problem of the nonuniform transmission
line using the equivalent circuit of Fig. 4.24.

5.   AC-Circuits

5.1   Signal transfer on a transmission line considering the reflection coefficients at the end and the beginning of the line

In real fluidic circuits the transmission line is fed by a
pressure source p_Q with an internal impedance Z_i. At its end
it is loaded by a load impedance Z_L (Fig. 5.1).[1]
The pressure and mass flow distribution along the line are
given by

$$(5.1) \quad p(z) = p_Q \, \frac{z_0}{z_i + z_0} \, e^{-\tilde{\gamma}_1 z} \, \frac{1 + \Gamma_2 e^{2\tilde{\gamma}_1(z-l)}}{1 - \Gamma_2 \Gamma_1 e^{-2\tilde{\gamma}_1 l}}$$

$$(5.2) \quad \dot{m}(z) = \frac{p_0}{z_i + z_0} \, e^{-\tilde{\gamma}_1 z} \, \frac{1 - \Gamma_2 e^{2\tilde{\gamma}_1(z-l)}}{1 - \Gamma_2 \Gamma_1 e^{-2\tilde{\gamma}_1 l}} \, .$$

Γ_1 and Γ_2 are the reflection coefficients at the beginning and
at the end of the transmission line

$$(5.3) \quad \Gamma_1 = \frac{z_i - z_0}{z_i + z_0} \quad ; \quad \Gamma_2 = \frac{z_L - z_0}{z_L + z_0} \, .$$

Pressure and massflow at the end of the line become
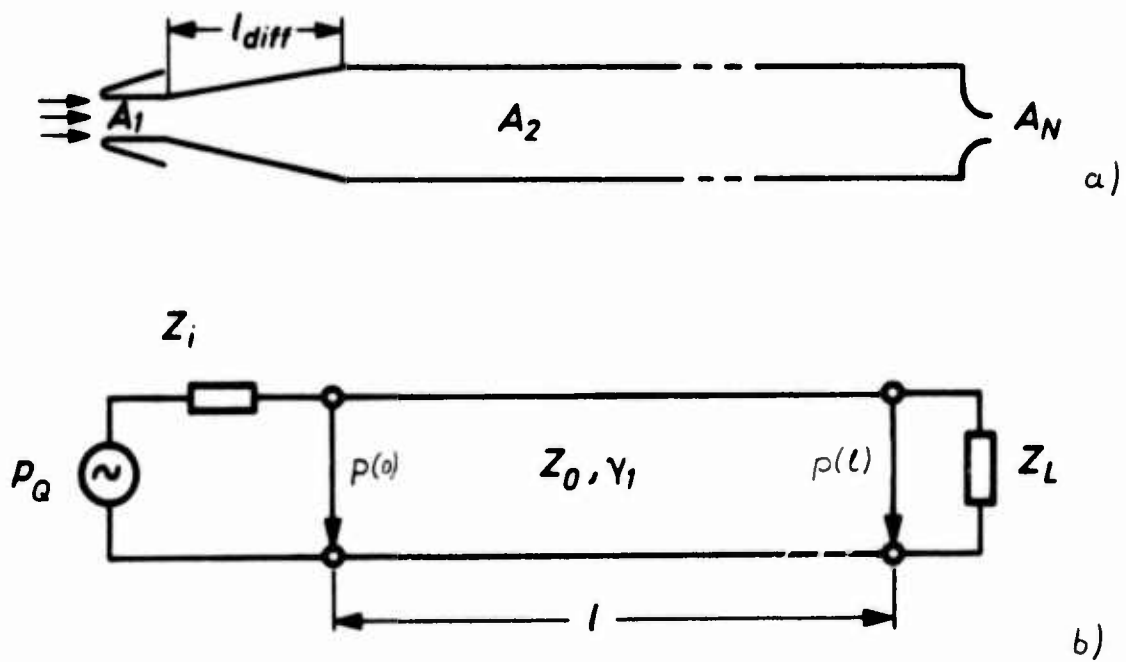
Fig.5.1   Loaded transmission line (a) and equivalent circuit (b)
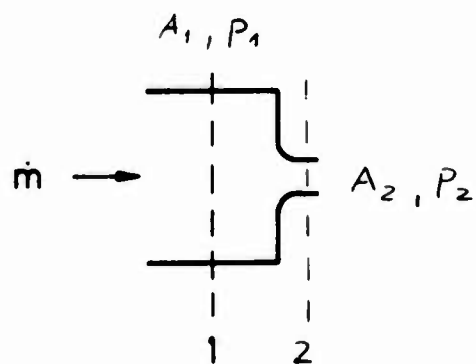
Fig.5.2   Nozzle

255

$$(5.4) \quad \hat{p}_E = p(\ell) = P_Q \frac{z_0}{z_i + z_0} e^{-\Gamma_1 \ell} \frac{1 + \Gamma_2}{1 - \Gamma_1 \Gamma_2 e^{-2\Gamma_1 \ell}}$$

$$(5.5) \quad \dot{m}_E = \dot{m}(\ell) = \frac{P_Q}{z_i + z_0} e^{-\Gamma_1 \ell} \frac{1 - \Gamma_2}{1 - \Gamma_1 \Gamma_2 e^{-2\Gamma_1 \ell}} .$$

If the line is matched at the end $\left(\Gamma_2 = 0\right)$ we see that pressure and massflow rate become

$$(5.6) \quad p(\ell) = P_Q \frac{z_0}{z_i + z_0} e^{-\Gamma_1 \ell}$$

$$(5.7) \quad \dot{m}(\ell) = \frac{P_Q}{z_i + z_0} e^{-\Gamma_1 \ell} .$$

If the line is matched at the beginning $\left(\Gamma_1 = 0\right)$ we obtain

$$(5.8) \quad p(\ell) = \frac{1}{2} P_Q e^{-\Gamma_1 \ell} \left(1 + \Gamma_2\right)$$

$$(5.9) \quad \dot{m}(\ell) = \frac{1}{2} \frac{P_Q}{z_0} e^{-\Gamma_1 \ell} .$$

5.2   Nonlinear components

5.2.1 AC-behaviour of nozzles

The dc-behaviour of nozzles is described in chapter 3.2.1.
In order to determine the ac-behaviour of the nozzle we assume
that the operating point is fixed by a certain dc-flow and that
a small ac-signal is superimposed. The resulting pressure and

256

flow variations determine the ac-resistance of the nozzle. We thus linearize the nonlinear resistance in its operating point. Out of equation (3.18) we have the relation between flow rate through a nozzle and the pressure difference across the nozzle for an incompressible or low compressible medium (see Fig. 5.2).

$$(3.18) \quad \dot{m} = A_2 \sqrt{\frac{2 \rho \, (\rho_1^* - \rho_2^*)}{1 - \left(\frac{A_2}{A_1}\right)^2}} \ .$$

The massflow $\dot{m}$ through a subsonic orifice is to a good approximation given by ref.3 as

$$(5.10) \quad \dot{m} = A_2 \sqrt{\frac{2\rho_2^* R_g T \, (\rho_1^* - \rho_2^*)}{1 - \left(\frac{A_2}{A_1}\right)^2}} = \frac{A_2 \sqrt{2 R_g T}}{\sqrt{1 - \left(\frac{A_2}{A_1}\right)^2}} \ \rho_2^* \sqrt{\frac{\rho_1^*}{\rho_2^*} - 1} \ .$$

Taking to total differentials

$$(5.11) \quad d\dot{m} = \frac{\partial \dot{m}}{\partial \rho_1^*} d\rho_1^* + \frac{\partial \dot{m}}{\partial \rho_2^*} d\rho_2^*$$

one finds similar to ref. 3

$$(5.12) \quad d\dot{m} = \dot{m}_0 \left\{ \frac{d\rho_2^*}{\rho_2^*} + \frac{d\rho_1^*/\rho_2^*}{2\left(\frac{\rho_1^*}{\rho_2^*} - 1\right)} - \frac{\rho_1^*}{\rho_2^{*2}} \frac{d\rho_2^*}{2\left(\frac{\rho_1^*}{\rho_2^*} - 1\right)} \right\}$$

where

$$(5.13) \quad \dot{m}_0 = \frac{A_2 \sqrt{2 R_g T}}{\sqrt{1 - \left(\frac{A_2}{A_1}\right)^2}} \ \rho_2^* \sqrt{\frac{\rho_1^*}{\rho_2^*} - 1}$$

is the dc-massflow rate.
Equation (5.12) can be written as

$$(5.14) \quad d\dot{m} = \frac{\dot{m}_0}{2(\rho_1 - \rho_2)} d\rho_1 - \frac{\dot{m}_0}{2(\rho_1 - \rho_2)} \left(2 - \frac{\rho_1^*}{\rho_2^*}\right) d\rho_2$$

which can be interpreted by the equivalent circuit in Fig. 5.3. The dynamic nozzle resistance in Fig. 5.3 is
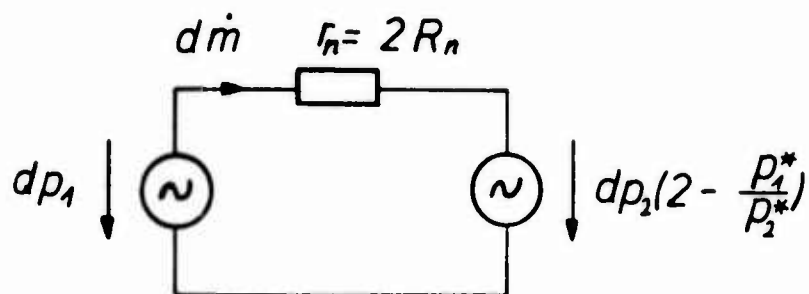
Fig.5.3   AC-equivalent circuit of the dynamic nozzle resistance
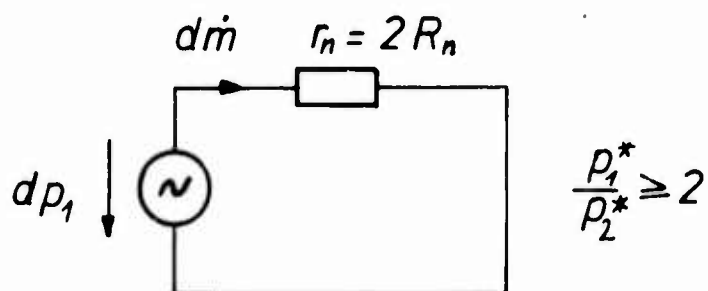
Fig.5.4   AC-equivalent circuit of a nozzle for the
            critical pressure ratio
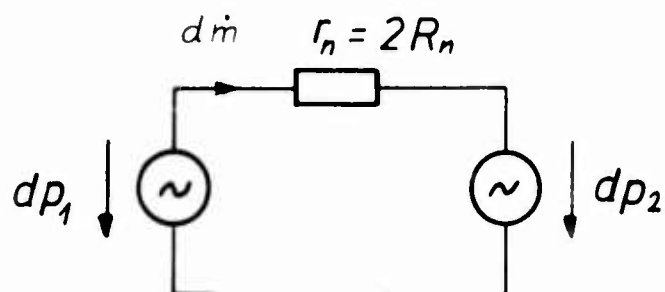
Fig.5.5   AC-equivalent circuit of a nozzle for small overpressures
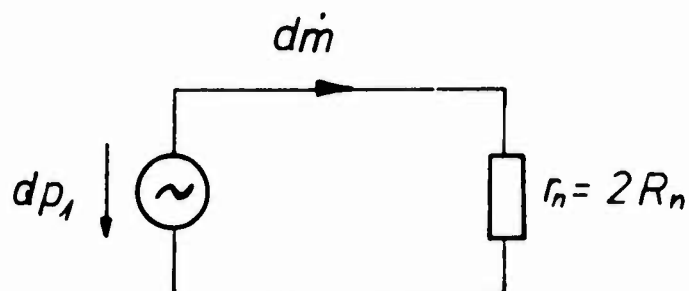
Fig.5.6   AC-equivalent circuit of a nozzle for constant
            exit pressure

$$(5.15) \quad r_n = 2\, \frac{p_1 - p_2}{\dot{m}_o} = 2\, R_n$$

which means that r_n is twice of the value of the dc-resistance in the operating point.

It should be noted that when $p_1{}^*/p_2{}^* \geq 2$, greater than the critical pressure ratio there is no influence of dp_2 on the flow rate. Flow changes are only effected by the upstream pressure dp_1. The equivalent circuit of Fig. 5.3 reduces to that in Fig. 5.4.

For small pressures above athmospheric pressure p_o

$$p_1 \approx p_2 \approx p_o \qquad \text{we obtain} \qquad \frac{p_1^*}{p_2^*} \approx 1$$

and the equivalent circuit reduces to that in Fig. 5.5.

For low pressure fluidic circuits the equivalent circuit of Fig. 5.5 will be sufficient.

5.2.1.1 Constant nozzle exit pressure

For constant nozzle exit pressure p_2 = const. the equivalent circuit further reduces to that in Fig. 5.6.
This for instance is the case where the flow of the terminating nozzle discharges into free atmosphere.
The dynamic nozzle resistance for this case can be expressed as

$$(5.15) \quad \frac{r_n}{c_a/A_1} = \frac{r_n}{z_{sol}} = \sqrt{\frac{2}{\kappa}}\ \frac{A_1}{A_2} \sqrt{1 - \left(\frac{A_2}{A_1}\right)^2}\ \sqrt{\frac{\bar{p}_1}{p_1^*}}$$

where
$$c_a = \sqrt{\frac{\kappa p_1^*}{\varrho_1}}$$

$$p_1^* = p_1 + p_o\ .$$

The dynamic resistance is referred to the surge impedance of the lossless transmission line.

For $\left(A_2/A_1\right)^2 \ll 1$ we obtain a very useful thumb rule

$$(5.16) \quad \frac{r_n}{z_{sol}} = \sqrt{\frac{2}{\kappa}}\ \frac{A_1}{A_2} \sqrt{\frac{\bar{p}_1}{p_o}}\ .$$

Considering the compressibility the expression becomes more complicated. For adiabatic condition follows

259
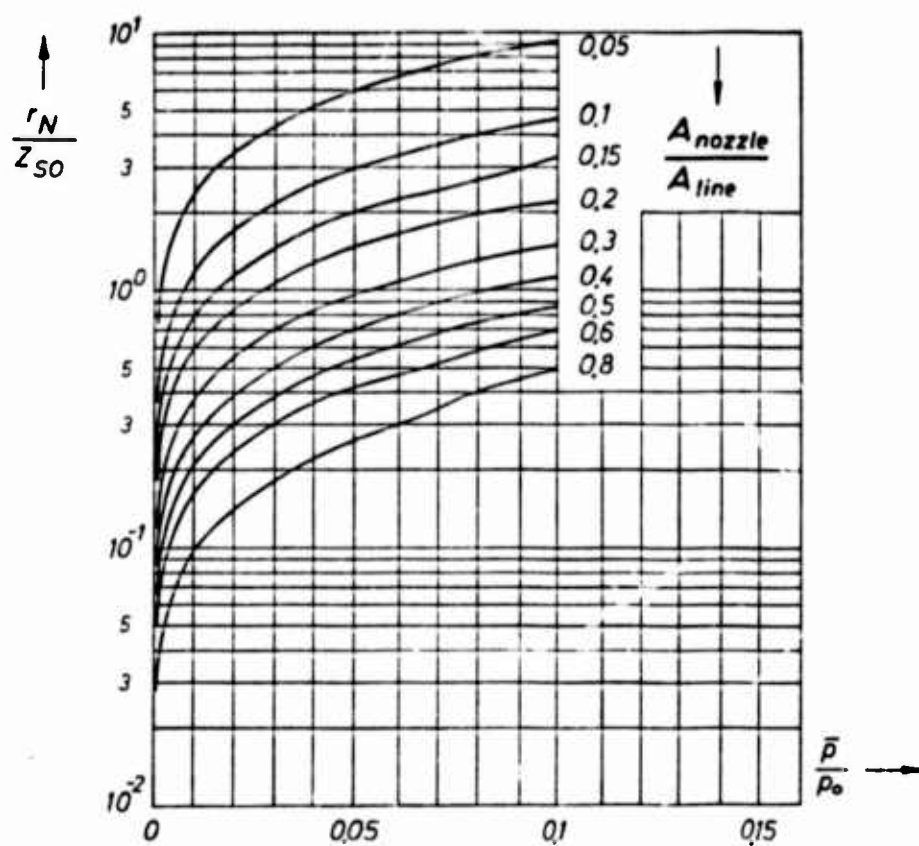
Fig.5.7   Dimensionless dynamic nozzle resistance
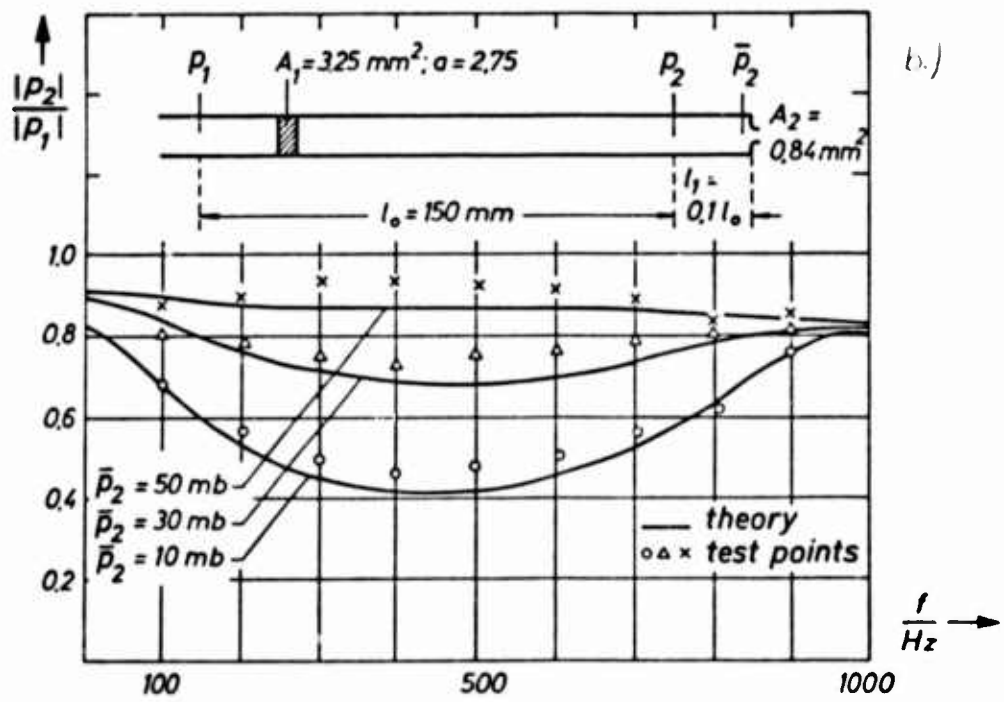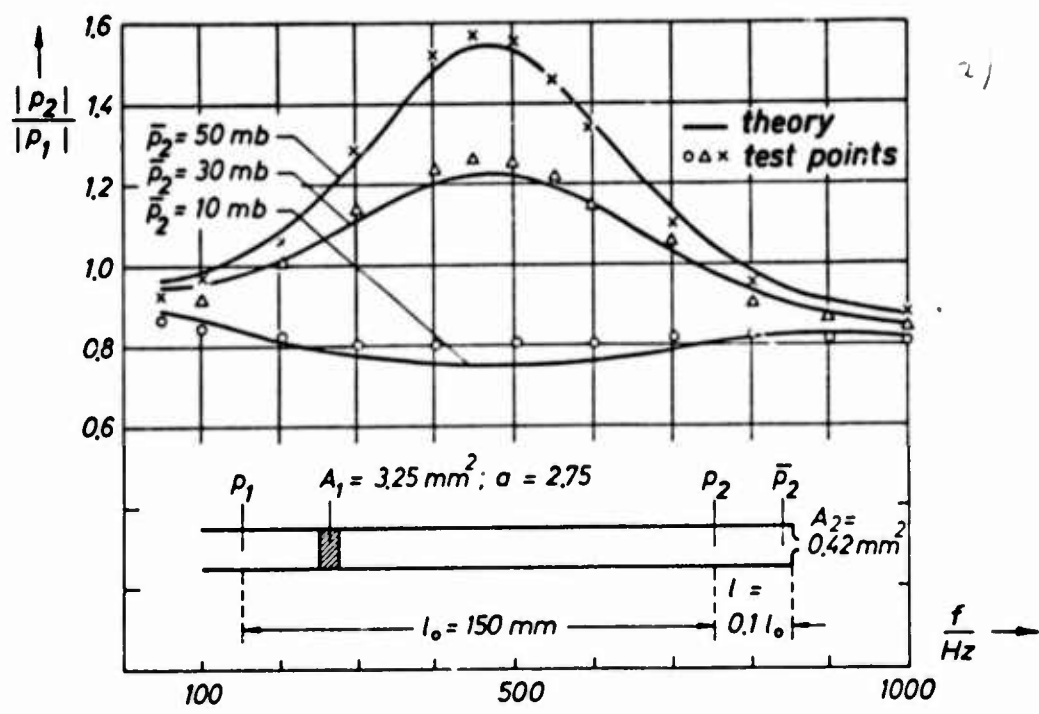
Fig.5.8   Pressure transfer functions of a transmission line
           loaded by a nozzle

261

$$(5.17) \ \frac{r_n}{z_{sol}} = \frac{\sqrt{2(\kappa-1)}}{\frac{A_2}{A_1}\frac{\rho_0}{\rho_1^*}} \frac{\left(1-\left(\frac{\rho_0}{\rho_1^*}\right)^{\frac{\kappa-1}{\kappa}}\right)^{1/2}\left(1-\left(\frac{A_2}{A_1}\right)^2\left(\frac{\rho_0}{\rho_1^*}\right)^{2/\kappa}\right)^{3/2}}{\kappa+1-2\left(\frac{\rho_1^*}{\rho_0}\right)^{\frac{\kappa-1}{\kappa}}-\left(\frac{A_2}{A_1}\right)^2(\kappa-1)\left(\frac{\rho_0}{\rho_1^*}\right)^{2/\kappa}} .$$

The evaluation of equ. (5.17) is shown in Fig. 5.7 (ref.2). The
dimensionless nozzle resistance is plotted against the dimension-
less dc-pressure. The ratio of the cross-sections is used as
parameter. It can be seen that for a given dc-pressure the line
is only matched $(r_n = z_{sol})$ at a distinct area ratio.
Fig. 5.8a and 5.8b show the results of experimental investigations
which are in high accordance with theory. (ref.2)

5.2.1.2   Varying nozzle exit pressure

A typical example for a nozzle with varying nozzle exit pressure
is the input nozzle of a beam deflection amplifier (Fig. 5.9).
With increasing pressure p_1 the beam is deflected and thus the
nozzle exit pressure decreases. If we assume a linear relation-
ship between dp_1 and dp_2 for small deflection angles

$$(5.18) \ dp_2 = -\varepsilon \, dp_1$$

the nozzle resistance is found as

$$(5.19) \ r_n = \frac{dp_1}{d\dot{m}} = \frac{2 R_{st}}{1+\varepsilon\left(2-\frac{\rho_1^*}{\rho_2^*}\right)}$$

where R_{st} is the steady state resistance.

For small overpressure equation (5.19) reduces to

$$(5.20) \ r_n = \frac{2}{1+\varepsilon} R_{st} .$$

Fig. 5.10 demonstrates the influence of ε on the dynamic
resistance. For constant exit pressure $(\varepsilon=0)$ the characteristic
of the resistance is represented by the tangent in the operating
point. With increasing ε the slope of the dynamic resistance
becomes steeper and for $\varepsilon=1$ the dynamic resistance is equal to
the dc-resistance.

The differential or dynamic input resistance of a beam deflection
amplifier in push-pull operation can be determined from the dc
input characteristics measured for constant input pressure dif-
ferences indicated in Fig. 5.11.

For pure push-pull operation we can seperate the input pressures
into a common mode pressure $\overline{p}_E$ and differential mode pressure
Δp_E, where
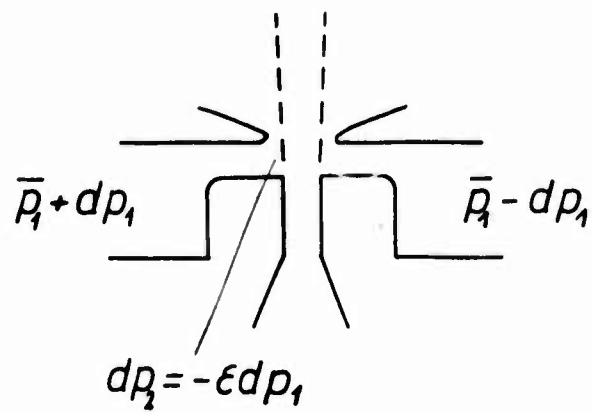
Fig.5.9   Input nozzle of a beam deflection amplifier
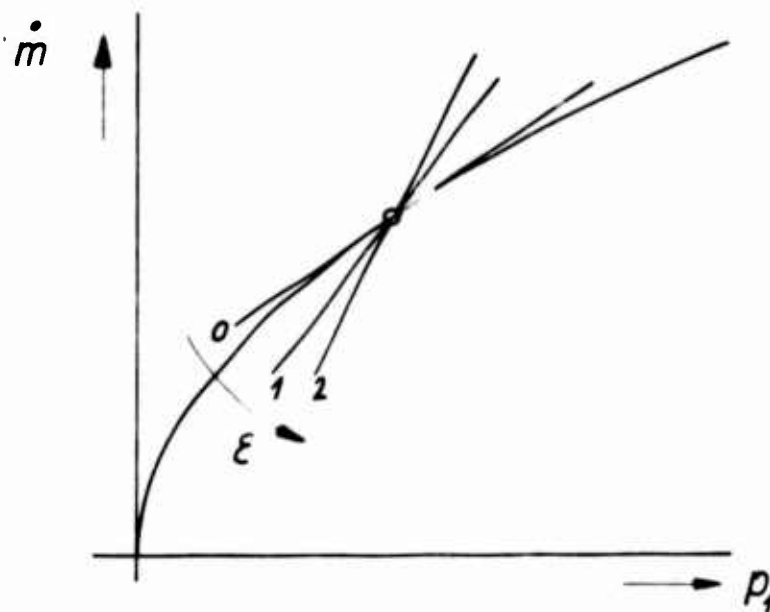
Fig.5.10   Input resistance of a nozzle with varying
           downstream pressure

263
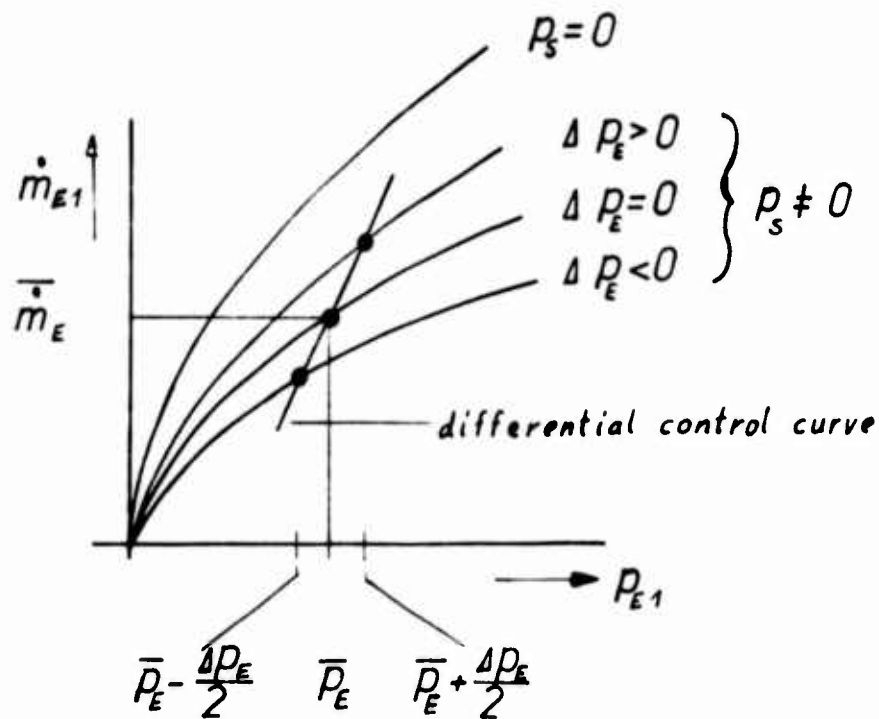
Fig.5.11 Input characteristics of a beam deflection amplifier
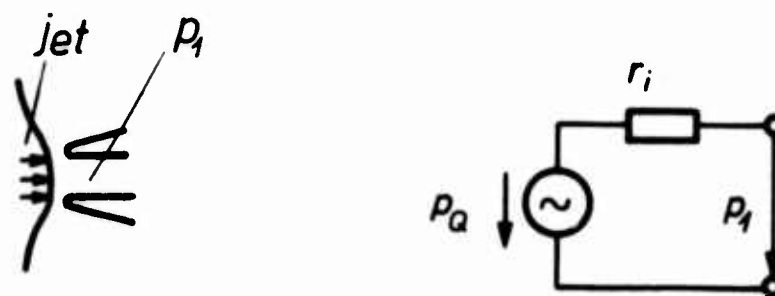
Fig.5.12 Jet receiver nozzle
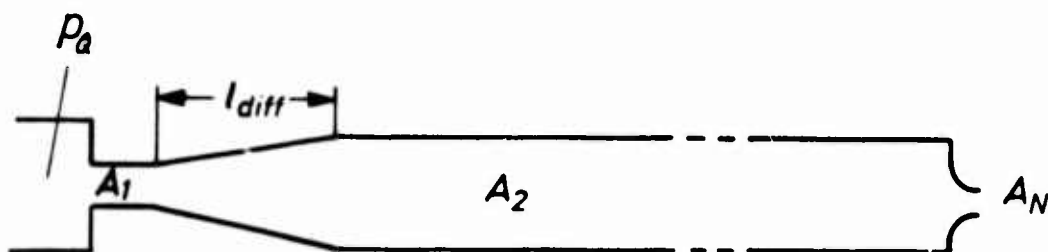
Fig.5.13 Simulation of a jet receiver nozzle

$$P_{E1} = \overline{P_E} + \Delta P_E / 2$$

(5.21)

$$P_{E2} = \overline{P_E} - \Delta P_E / 2$$

Care has to be taken that the common mode pressure $\overline{p_E}$ remains constant during the measurement of the input characteristics for the single pressure differences $p_{E1} - p_{E2}$. So when one control port pressure is increased the other has to be decreased the same amount, keeping the average of the two at the fixed bias or common mode pressure.

5.2.2   AC-behaviour of diffusers and jet receiver nozzles

For ac-behaviour the diffuser behaves as a nonuniform transmission line which has been discussed in chapter 4.6. The jet receiver nozzle can be interpreted as an ac-pressure source with an internal resistance r_i according to chapter 3.2.3 by the relation

$$(5.22) \quad P_1 = P_Q - r_i \dot{m}$$

where r_i differential internal resistance.

In fluidic circuits it will be important to determine the pressure transfer function P_E / P_Q according to equ. (5.4) and (5.5) and Fig. 5.1. It is obvious that this is not possible for an arrangement in as shown in Fig. 5.1. b. It is therefore convenient to simulate the receiver nozzle by an abrupt nozzle as shown in Fig. 5.13. The source pressure can be directly measured before this nozzle (ref. 9).
A total agreement with the arrangement of Fig. 5.1 a can not be expected because to velocity profiles at nozzle inlets will be different.

5.3   Linear lumped components

5.3.1   Inductor and capacitor (ref. 24,36)

Using the surge impedance and the propagation factor we are able to calculate the input impedance of a uniform transmission line with arbitrary load impedance (Fig.5.14).
Of special interest are the blocked and the short circuited line (Fig.5.15).
The input impedance of the short circuited line results in

$$(5.23) \quad W_{10} = Z_0 \tanh \gamma_i l$$
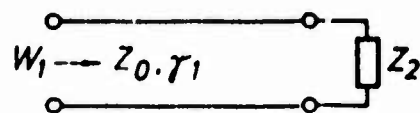
Fig.5.14   Input resistance of a fluidic transmission line
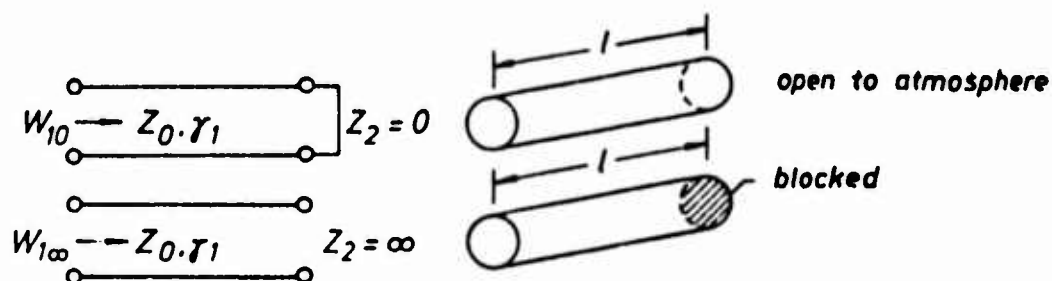
Fig.5.15   Blocked and short-circuited lines
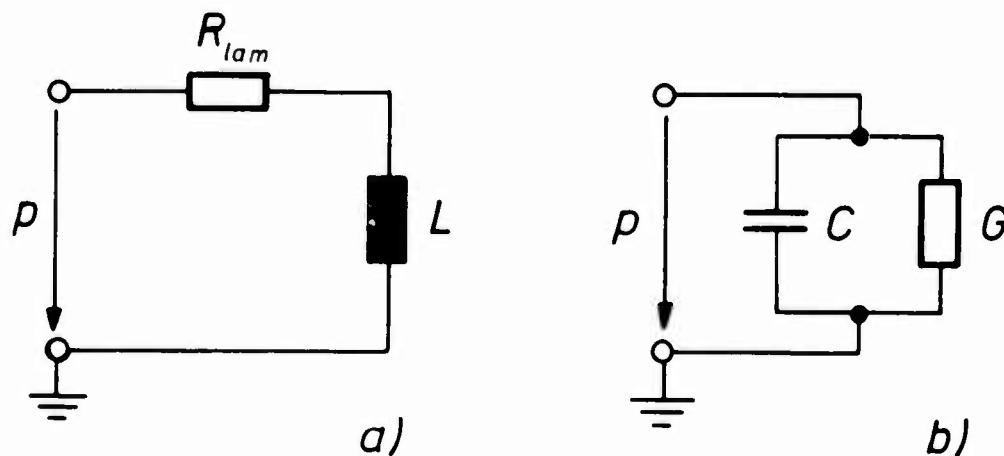
Fig.5.16   Equivalent circuit of short
a) short-circuited line,   b) blocked line

and the input impedance of the blocked line in

$$(5.24) \quad W_{1\infty} = \frac{z_o}{\tanh \eta_1 l}$$

We may expand the hyperbolical tangent per small argument and obtain under the conditions

$$(5.25) \quad \tfrac{1}{3} \eta_1^2 l^2 \ll 1$$

that the short-circuited transmission line may be represented by its series impedance (Fig.5.16a)

$$(5.26) \quad W_{10} = R + j \omega L$$

and the blocked line by its shunt admittance (5.16b)

$$(5.27) \quad W_{1\infty} = \frac{1}{G + j \omega C}$$

The short circuited line therefore behaves as a lossy inductor and the blocked line as a lossy capacitor.
Fig. 5.17 shows the geometrical conditions under which lumped components can be realized. It is assumed that the complex deviation of the lumped components may not exceed 1%. For a frequency of 100 Hz we permit a tube length of 100 mm. For a frequency of 1 kHz this maximum permissible length is reduced to 10 mm.
In electrical engineering the ratio of absorbed wattless power to absorbed wattful power is commonly called energy factor Q. Q is the reciprocal of the loss-factor $\tan \delta$. In the case of the capacitance it is the ratio of susceptance to conductance and in the case of the inductance it is the ratio of reactive to active impedance.

$$(5.28) \quad Q_c = \frac{\omega C}{G}$$

$$(5.29) \quad Q_L = \frac{\omega L}{R}$$

In Fig. 5.18 the energy factor Q of the capacitance and the inductance is plotted as a function of the dimensionless frequency f/f_ν .

Because of their relatively large cross-sections the dimensionless frequencies of technical capacitors are of the order of $f/f_\nu = 1000$. This means they can be regarded as adiabatic. The Q is about 100-200. The dimensionless frequency of technical inductors is about 50-100. From this we find that the Q of an inductor is about 10-20.

The calculation of Q for the inductor has been carried out considering only the frequency dependent laminar resistance. Equation (5.29) therefore is only valid if flow development can be neglected e.g. small or vanishing dc-flow. How to consider the series resistance of the inductance due to flow development and change in cross-section is shown in chapter 5.3.2.
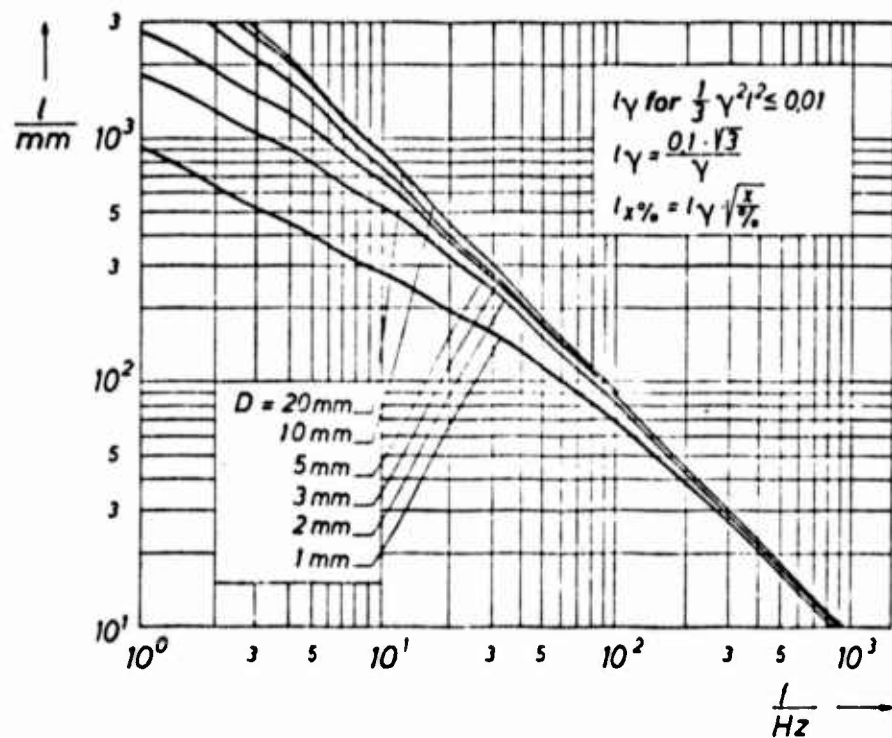
Fig.5.17   Geometrical conditions for lumped components
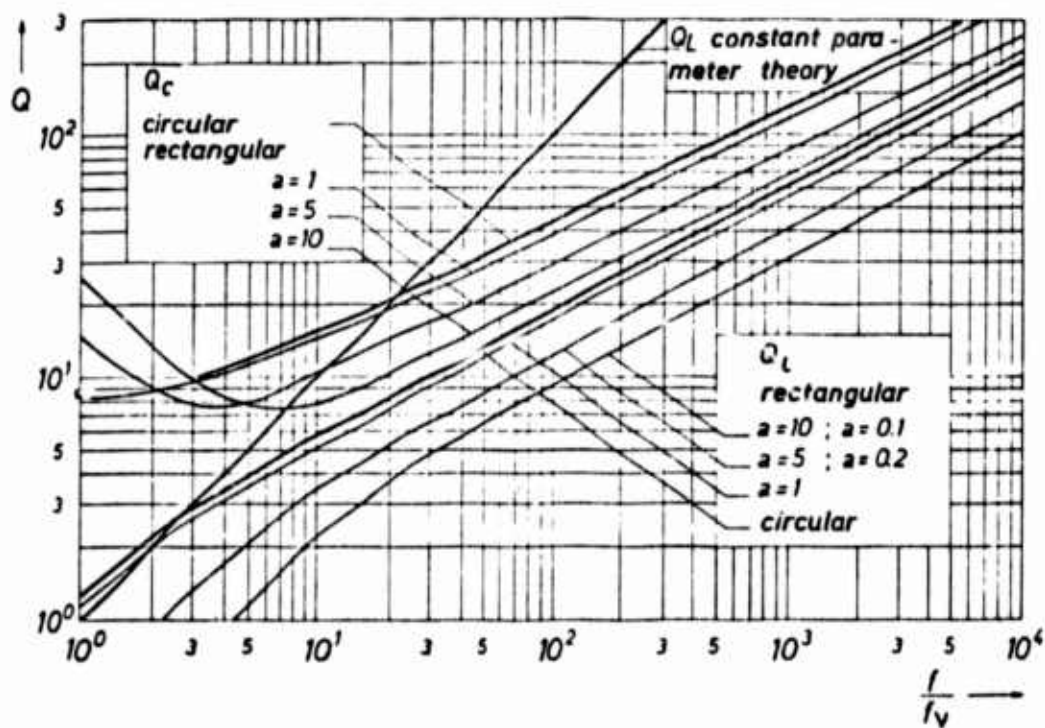
Fig.5.18   Energy factor of capacitors and inductors

For very short inductors the exit correction term of acoustics has to be taken into account.

Caused by the resonating mass of the surrounding medium an apparent elongation of the inductor by $2\Delta l = \lambda/D$ results. Using this the adiabatic inductor becomes

$$(5.30) \quad L_a = \frac{l}{A}\left(1 + \frac{\pi}{4}\frac{D}{l}\right).$$

5.3.2 Resonant Circuits

Fig. 5.19 shows a fluidic resonator using a fluidic inductor and capacitor. The signal passes the resistance R_v and reaches a lossy capacitance. In parallel to the capacitance we find a lossy inductance. The shunt capacitance is represented by a volume and the inductance by a short circuited line. This type of resonator in acoustics is known as Helmholtz-resonator. Fig. 5.20 shows the pressure transfer function. The resonance frequency is

$$(5.31) \quad f_0 = \frac{1}{2\pi\sqrt{LC}}.$$

The energy factor Q can be determined as quotient of resonance frequency to bandwidth

$$(5.32) \quad Q = \frac{\Delta f}{f_0}.$$

The Q of the resonance circuit can be calculated by adding the reciprocals of the single Q factors

$$(5.33) \quad \frac{1}{Q} = \frac{1}{Q_L} + \frac{1}{Q_C}.$$

This means that the loss factors must be added. In any case the Q of the resonator will be smaller than the Q of the single element. From chapter 5.3.1 we know that the Q of the capacitor is about 10 times higher than that of the inductor. Therefore a Q of 10-20 can be expected for the resonator. This is only valid as long as resistance R_v is so high that it does not influence the Q of the resonator.

Usually in a real circuit the internal resistance r_i of the generator feeding the resonator and the load resistance can not be neglected (Fig. 5.21).

Assuming a Q_c of more than 100 the loss resistance, in parallel to the capacitance, will be large compared to the loading resistances. So the resulting energy factor of the capacitance will be determined only by r_i and r_L.

$$(5.34) \quad Q_{cres} = \frac{\omega C}{g_i + g_L}$$

where $g_i = \frac{1}{r_i}$ and $g_L = \frac{1}{r_L}$.

From this the resulting Q of the loaded resonator becomes
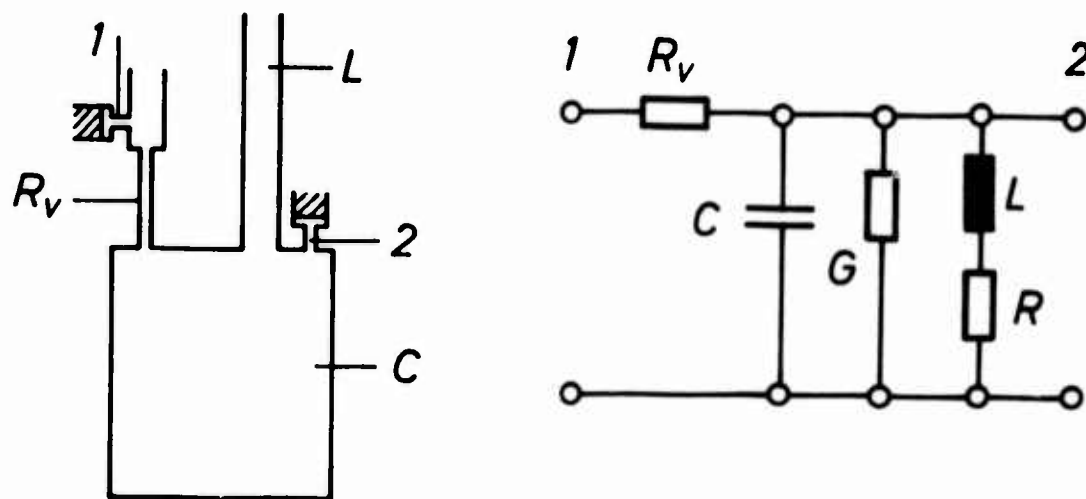
Fig.5.19   Fluidic parallel resonator
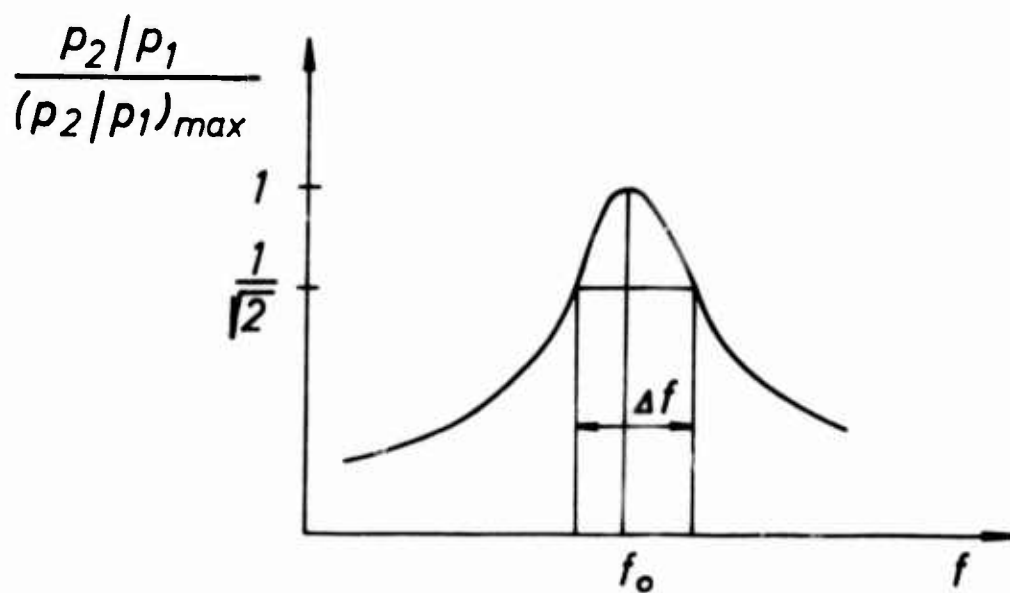
Fig.5.20   Transfer function of a fluidic resonator

270
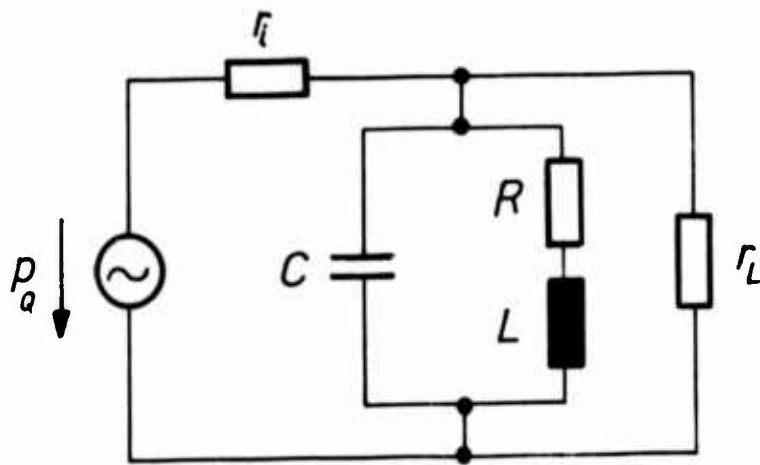
Fig.5.21   Loaded resonator

$$(5.35) \quad \frac{1}{Q} = \frac{1}{Q_L} + \frac{1}{Q_{cres}}.$$

5.3.3 Low pass filters

5.3.3.1 RC low pass filters

The design of fluidic filters should take care of the fact that the input resistance of fluidic amplifiers are relatively low due to flow control. Therefore it should not be tried to copy electronics but to find solutions which consider the peculiarity of fluidics.

For voltage controlled amplifiers in electronics, e.g. valves, a low pass arrangement as shown in Fig. 5.22 is senseful. The transfer characteristic will not be influenced by the high input resistance of the valve for a proper design.

In an equivalent RC-network in fluidics (Fig.5.23) the low input resistance of the amplifier will change the transfer characteristic of the unloaded filter

$$(5.36) \quad \frac{p_2}{p_1} = \frac{1}{1 + j \omega r C}$$

to

$$(5.37) \quad \frac{p_2}{p_1} = \frac{r_c}{r_c + r} \cdot \frac{1}{1 + j \omega \frac{r_c \cdot r}{r_c + r} C}$$

The break frequency then is found as

$$(5.38) \quad \omega_E = \frac{1}{\frac{r_c \cdot r}{r_c + r} C} \cdot \frac{1 + \frac{r}{r_c}}{r \cdot C}.$$

The influence of the resistance of the control input on the break frequency can be minimized by introducing a series resistance as indicated in Fig. 5.24.

$$(5.39) \quad \frac{p_2}{p_1} = \frac{r_c}{r_c + r + r_S} \cdot \frac{1}{1 + j \omega \frac{(r_c + r_S + r)}{r_c + r + r_S} C}.$$

For very low input resistance r_c $(r_c \ll r)$ the series resistance r_s is chosen equal to r. The transfer characteristic then follows as

$$(5.40) \quad \frac{p_2}{p_1} = \frac{1}{2} \cdot \frac{1}{1 + j \omega \frac{r C}{2}}$$

with $r_c \ll r, r_s$ and $r = r_s$.
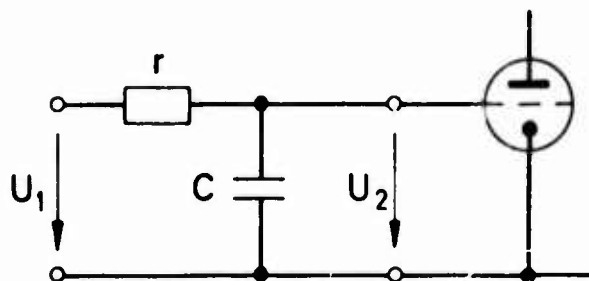
Fig.5.22   RC-low pass filter in electronics
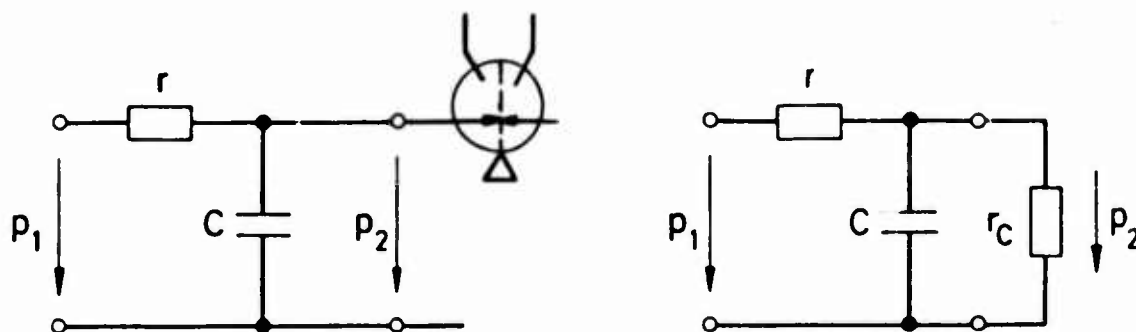
Fig.5.23   RC-low pass filter in fluidics
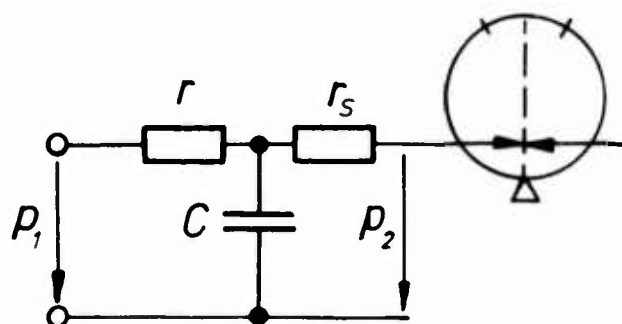
Fig.5.24   RC-low pass filter with series resistance

273

5.3.5.2 RL-low pass filters

An arrangement which is matched to the flow control is the RL-low pass filter in Fig. 5.25 (ref.9).
The massflow rate $\dot{m}$ controls the input for the following amplifier. As long as the length of the line is small compared with the wavelength of the operating frequencies the arrangement of Fig. 5.25 can be described by the network in Fig. 5.26. p_2 take into account the varying nozzle exit pressure as discussed in chapter 5.2.1.2. The dynamic resistance r is composed of the nozzle resistance r_1 , the resistance due to profile development $r_{dev} = kr_1$, and the laminar resistance r_{lam} .
Assuming the linear relationship between p_1 and p_2 in equ. (5.18) $p_2 = -\varepsilon p_1$ and only small overpressures the massflow rate at the amplifier input is found as

$$(5.41) \quad \dot{m} = \frac{p_1 - p_2}{r + j\omega L} = \frac{p_1}{\frac{r + j\omega L}{1 + \varepsilon}} = \frac{p_1}{r/(1+\varepsilon)} \frac{1}{1 + j\omega \frac{L}{r}} .$$

For a line length which is longer than the length of flow development the break frequency becomes

$$(5.42) \quad f_E = \frac{1 + K_{fd}}{t_l} + f_\nu$$

where $r = r_1 + k_{fd}r_1 + R_{lam}$, $L = \frac{l}{A}$

$t_1 = \frac{l}{v}$ transport time in the channel

$f_\nu =$ characteristic frequency

In most cases the line length is smaller than the length of flow development. Using equ. (3.15) the dynamic resistance r for a device with rectangular cross-section is obtained as

$$(5.43) \quad r = \frac{\dot{m}}{\rho A_2^2} + 5.7 \frac{a+1}{\sqrt{a}} \frac{\nu l}{A_2^2} \left(\frac{\dot{m}}{l\mu} \right)^{1/2} .$$

The break frequency follows as

$$(5.44) \quad f_E = \frac{1}{2\pi t_l} \left(1 + 5.7 \frac{a+1}{\sqrt{a}} \left(\frac{\dot{m}}{l\mu} \right)^{-1/2} \right) .$$
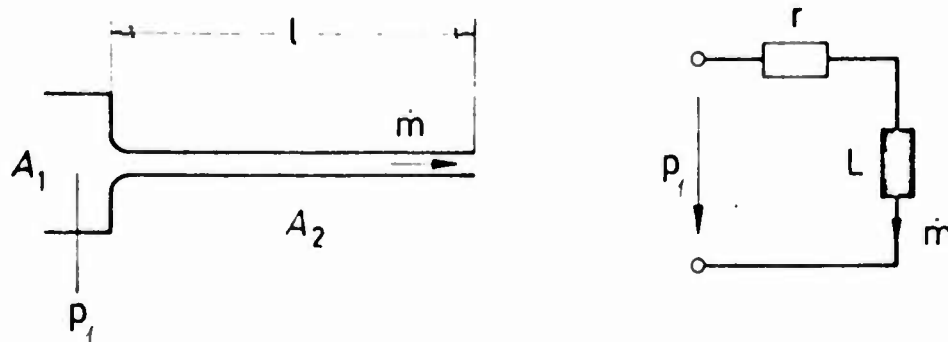
Fig.5.25 RL-low pass filter in fluidics
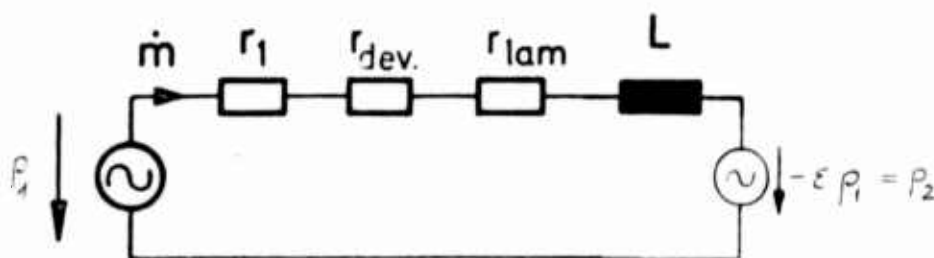
Fig.5.26 Equivalent circuit of a RL-low pass
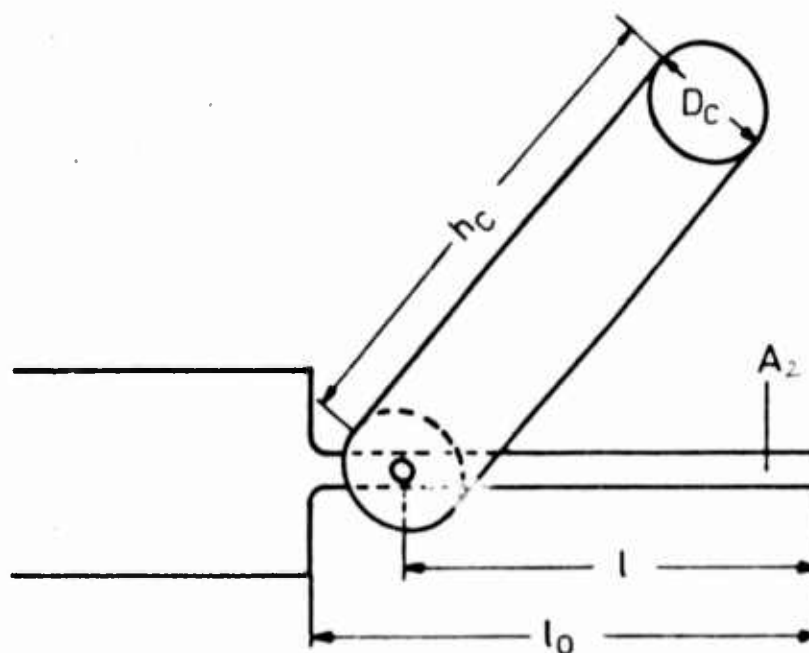
Fig.5.27 RLC-low pass filter

5.5.3.3   RCL-low pass filter (ref.9)

The low pass characteristic of the arrangement described above
can be made steeper by adding a capacitor as shown in Fig. 5.27
thus obtaining a second order system.
The equivalent circuit is given in Fig. 5.28.
To avoid additional series resistances r_c to the capacitor the
coupling hole has to be taken as large as possible. The con-
ductance of the capacitor usually can be neglected.
The massflow in the inductance results as

$$(5.45) \quad \dot{m}_l = \frac{p_1}{\frac{r_0 + r_l}{1 + \varepsilon}} \cdot \frac{1 + j\omega \frac{\varepsilon}{1+\varepsilon} r_0 C}{1 + j\omega \frac{r_0 r_l}{r_0 + r_l} C - \omega^2 \frac{r_0}{r_0 + r_l} LC}$$

if r_c can be neglected.

For neglicable pressure variations at the nozzle exit
we obtain a pure second order systems where

$$(5.46) \quad f_0 = \frac{1}{2\pi} \sqrt{\frac{r_0 + r_l}{r_0}} \frac{1}{\sqrt{LC}} \qquad \text{resonant frequency}$$

$$D = \frac{1}{2} \frac{\sqrt{LC}\left(\frac{1}{r_0 C} + \frac{r_l}{L}\right)}{\sqrt{(r_0 + r_l)/r_0}} \qquad \text{damping ratio.}$$

If ε is not neglicable a PD-term with a break frequency

$$(5.47) \quad f_E = \frac{1}{2\pi}\left(1 + \frac{1}{\varepsilon}\right)\frac{1}{r_0 C}$$

becomes effective, which lowers the steepness of the filter
above that break frequency defined in equ. (5.64).
Measurements at RL and RLC filters have been made in ref. 9.
Some applications in carrier frequency systems can be found
in ref.37, where also methods of coupling the capacitor are
discussed.
RL and RLC-filters are appropriate for integrated circuits
where breakfrequencies of some hundred hertz are needed.
For breakfrequencies below hundred hertz RC-low pass filters
have to be used. Equation (5.60) shows that the lowest break-
frequency for a RL-filter will be $f_a = f_\nu$. For room temperature
we find $f_\nu \approx \frac{60}{A/mm^2} Hz$. This means for a channel of 0.5 mm^2
cross-section that the lowest breakfrequency would be $f \approx 120$ Hz
if the transport time is neglizible.
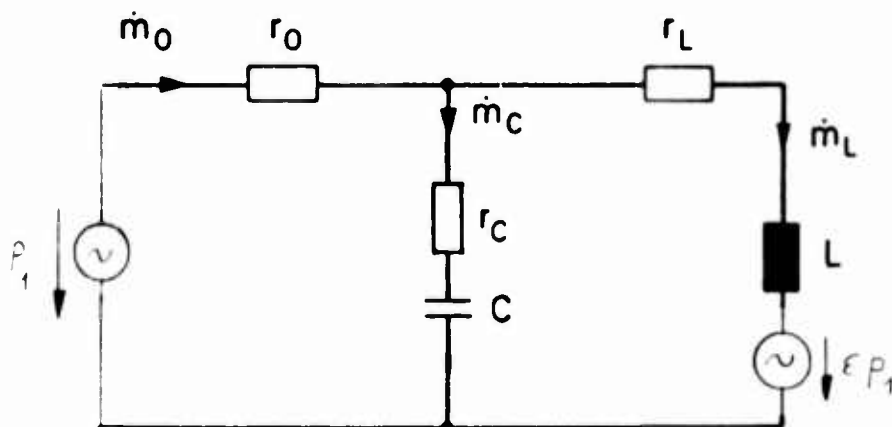
Fig.5.28 Equivalent circuit of an RLC-low pass filter
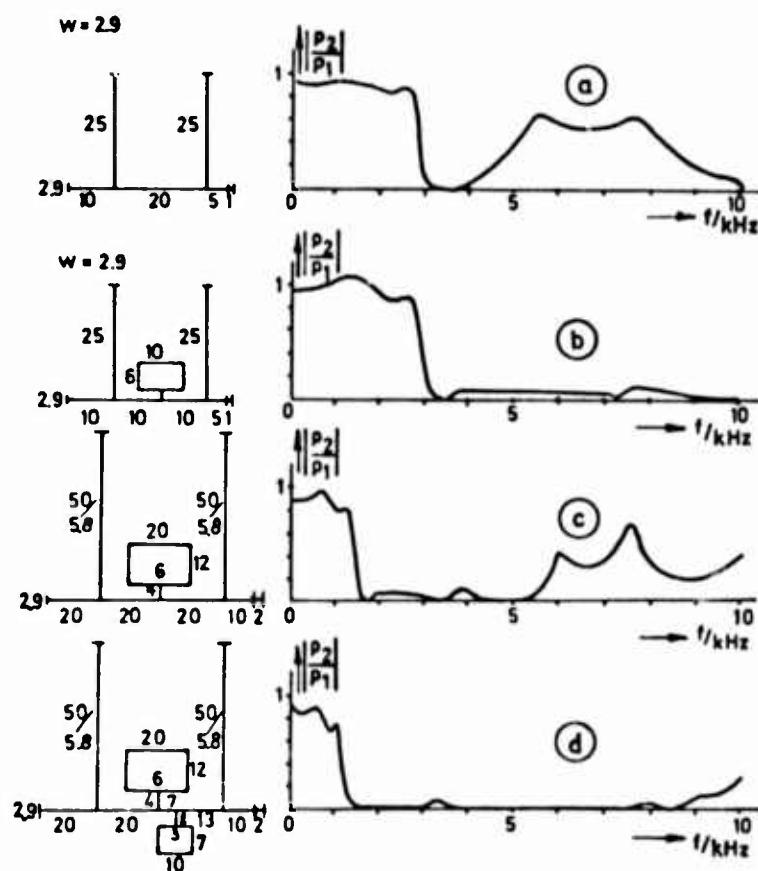
Fig.5.29 OPTIMIZATION OF LOW - PASS FILTER
CONFIGURATION

a,b : $r_n = 7.5 \cdot 10^7$ 1/sm; c : $r = 3.5 \cdot 10^7$ 1/sm
d : $Z_n = 4.25 \cdot 10^7$ 1/sm $+ j\omega 2.0 \cdot 10^3$ 1/m

277
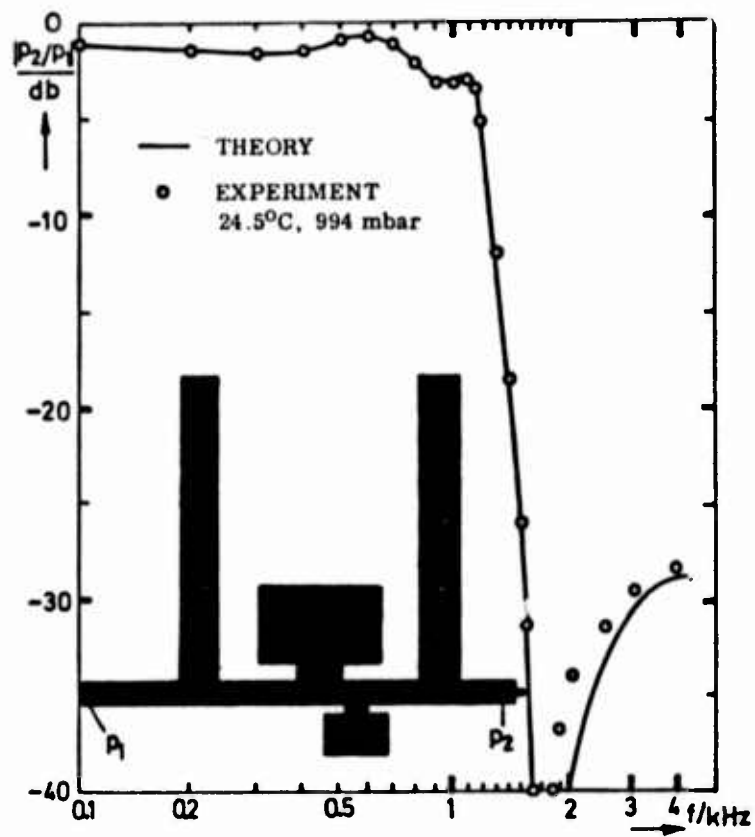
Fig.5.30 Frequency response of a low-pass filter according to Fig.5.29
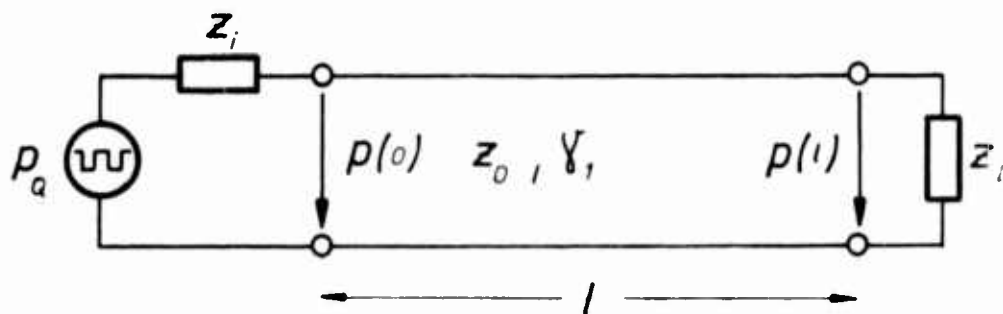
Fig.6.1 Equivalent circuit for a fluidic transmission line

Fig.6.2 Trapezoidic pulse

278
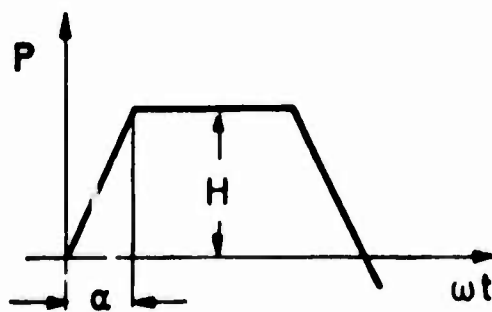
5.4   Filters using multiple branched transmission lines

In ref. 38 Kohl proposes to use multiple branched transmission lines as fluidic low-pass, high-pass, band-pass and band-stop filters.

Fig. 5.29 demonstrates the computer aided optimization of a lowpass filter configuration. In Fig. 5.29a the two blocked loaded lateral transmission lines cause a relatively sharp cut-off combined with a good signal attenuation in the frequency range from 3 to 4 kHz. This range coincides with the range of minimal input impedance of the lateral lines. For frequencies where $1 = \lambda/4$ a blocked line has its minimum input impedance. Using equ. (5.24) for a blocked line the input impedance results as

$$(5.24) \quad W_{1\infty} = \frac{z_0}{\tanh f_1 l}$$

Assuming a lossless transmission line where $f_1 = j\beta = j\frac{\omega}{c}$, the input impedance of a blocked line at $1 = \lambda/4$ vanishes.

The proper location of the lateral lines is investigated experimentally by a computer programme. The reduce the peak at higher frequencies a blocked line with stepped cross-section is introduced. This configuration gives a lower input impedance, when oscillating on a $\lambda/4$ wave length, compared to lines with uniform cross-sections. This blocked line with stepped cross-section can be interpreted as a Helmholtz-resonator. The result in Fig. 5.29b is a very good low-pass filter with a low signal attenuation in the pass-band, a very sharp cut-off behaviour and a very high signal attenuation.

If the low-pass filter geometry is enlarged by a scaling factor of two, we get the characteristic of a low-pass filter with half the cut-off frequency (Fig. 5.29c). The frequency behaviour of this filter can be improved by introducing a third blocked line as shown in Fig. 5.29d.

The low-pass configuration of Fig. 5.29d has been investigated experimentally. Fig. 5.30 shows the results compared with theory in the frequency range from 0 - 4 kHz.

The way of using line branching systems for filtering technique seems to be very promising as to their high attenuation in the stop-band and low attenuation in the pass-band compared with FC, RL and RLC-filters. It seems, however, that they will be restricted to frequencies of some kilohertz because their geometrical dimensions will become too large for frequencies of some hundred Hertz. For a frequency of 100 Hz $\lambda/4$ is about 0,85 m for air. So the main application will be in carrier frequency systems with carrier frequencies of some kilohertz or as noise filters.

6. Pulses in fluidic networks

Like in electronics, pulse distortions on transmission lines in digital fluidic networks are determined by the line characteristics as well as by the load impedance. When rise times are less than the propagation time on the transmission line reflections from the beginning and the end of the line cause distortions.

6.1 Predicting pulse distortions on fluidic transmission lines with linear load and source resistance

The transmission of sinusiodal signals on uniform fluidic transmission lines has been investigated theoretically and experimentally with success. From this the problem for periodic trapezoidal pulses can be handled without difficulty.
Using Fourier analysis the periodic trapezoidic pulses can be separated into the harmonics. Each of those harmonics suffers a certain phase shift and attenuation along the transmission line. At the end of the line the single harmonics are superimposed again.
Fig.6.1 shows the equivalent circuit for a fluidic transmission line which is fed by a source p_Q with an internal impedance Z_i and terminated by the impedance Z_L. The characteristic impedance of the line is Z_0, the propagation factor Γ_1, and the line length l. Propagation factor and characteristic impedance depend on frequency and cross-section (see chapter 4.5). We assume that the source impedance and the load impedance are linear so that superimposing of the single harmonics is permissible.
Pressure p and massflow $\dot{m}$ at the end of the line for a sinusoidal signal are given by equ. (5.4) and (5.5) in chapter 5.1.

$$(5.4) \quad p(l) = p_Q \, \frac{z_0}{z_i + z_0} \, e^{-\Gamma_1 l} \, \frac{1 + \Gamma_2}{1 - \Gamma_1 \Gamma_2 e^{-2\Gamma_1 l}}$$
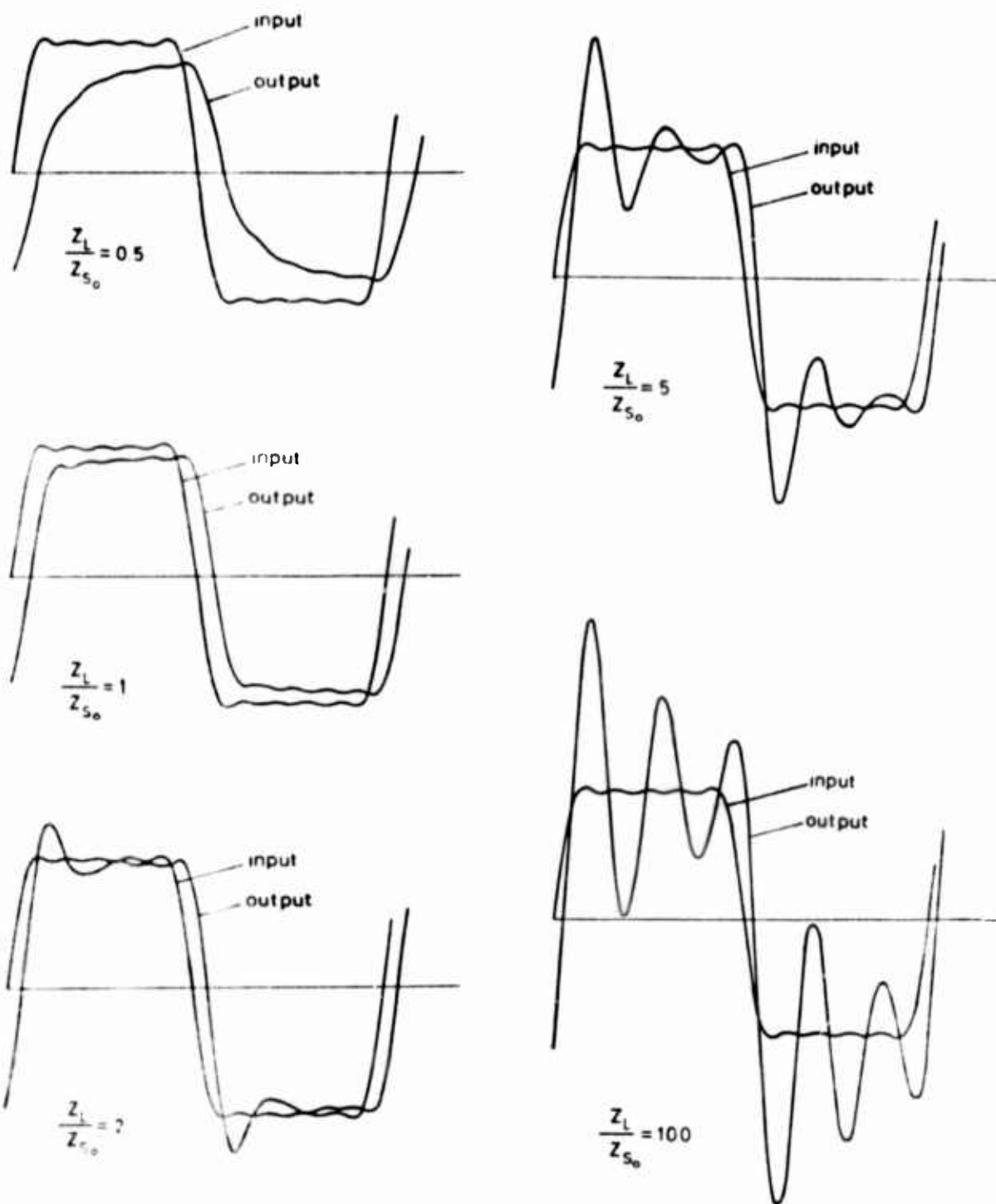
$f = 100 \text{ Hz}$
$\alpha = 0.1 \pi$
$l = 150 \text{ mm}$
$Z_i = 0$

Fig.6.3 Calculated response of a transmission line to periodic pulses for various linear load resistance and zero source resistance

$$(5.5) \quad \ldots \quad \approx \quad \frac{1 - T_2}{1 + T_2} \cdot 2 f_i l$$

The Fourier analysis of periodic trapezoidic pulses (Fig.6.2)
is given by

$$(6.1) \quad p \ldots = \frac{\ldots}{\ldots} \left(\ldots \quad \ldots \cdot \ldots + \frac{1}{9} \sin 3\alpha \sin 3\omega t + \ldots \right)$$

The pressure signal at the end of the line is found by super-
imposing the single sinusoidal signals as

$$(6.2) \quad z(t) = \frac{\ldots}{\ldots} \left(\ldots \cdot \ldots \sin(\omega t - f_1) + D_3 \frac{1}{9} \sin 3\alpha \sin(3\omega t - f_3) + \ldots \right)$$

where the attenuation J_n and the phaseshift f_n are calculated
using equ. (5.4) and (5.5).
Fig. 6.3 shows the computer results for a uniform line with
rectangular cross-section with the following dimensions
length of the line $l = 150$ mm
cross-sectional area $A = 3$ mm
aspect ratio $a = 3$

The pulse repetition rate is 100 Hz with a rise angle of $\alpha = 0.1$.
The source impedance has been chosen $Z_i = 0$ and the load impedance
has been changed between $Z_L / Z_o = 0.5$ and $Z_L / Z_{io} = 100$. The
influence of line mismatch is evident.

For nonlinear source- and load resistances the procedure dis-
cussed above is not applicable, because super-position of signals
is only valid in linear networks.
The transient response of infinite or matched fluidic transmission
lines has been subject to many investigations, mostly using the
Laplace transform (ref.22). In ref. 45 Tsao gives computer results
for dead ended transmission lines showing the pressure transient
at the end of the line and profile development along the line.
The results are obtained by integrating the linearized governing
differential equations by numerical methods.

6.2 Predicting pulse distortions on fluidic transmission lines with nonlinear source and load resistance

Fig. 6.4 shows a transmission line which is loaded by a nozzle
and fed by a free jet that is periodically interrupted by a
chopper-wheel.
If the receiver nozzle at the beginning of the transmission line
is fed by the free jet, it can be interpreted by a constant
pressure source with the internal resistance Z_i. If the jet is
seperated from the nozzle by the chopper-wheel[1] the receiver
nozzle directly is connected to the atmosphere. The beginning
of the line is short-circuited. The switching 'on' and 'off'
of the jet therefore can be interpreted in the equivalent circuit
by a switch alternatively connecting the beginning of the trans-
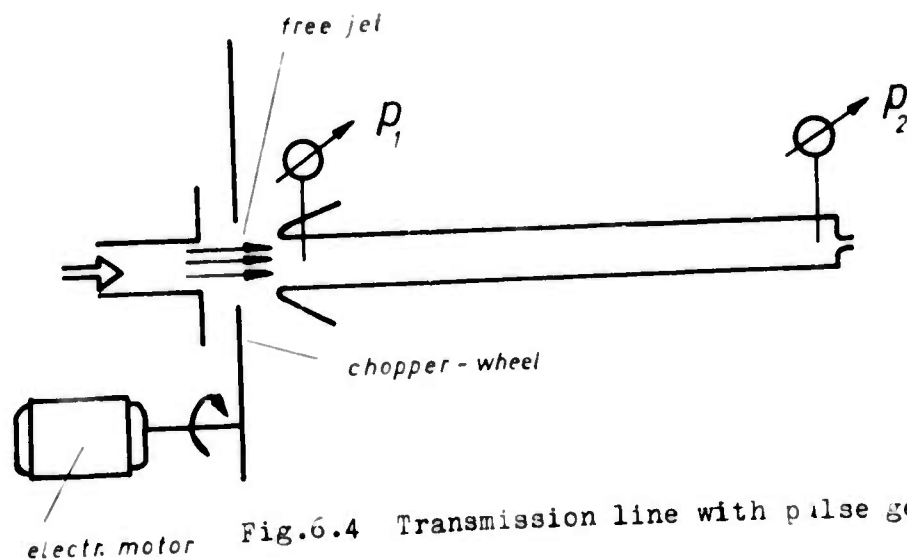
Fig.6.4   Transmission line with pulse generator
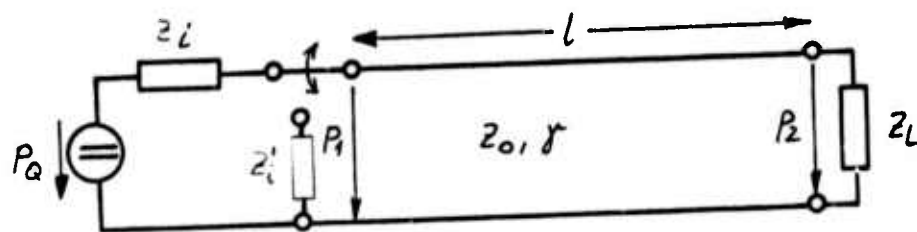
Fig.6.5   Equivalent circuit for a pulsed transmission line
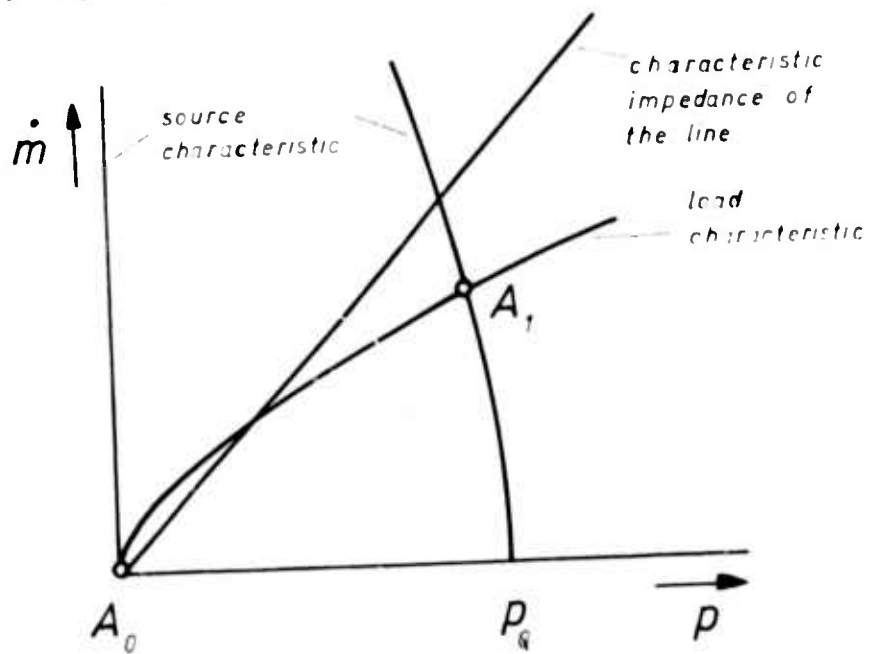
Fig.6.6   Characteristics of a transmission line with
           nonlinear load and source resistance

283

mission line to the atmosphere and to the pressure source with internal impedance Z_i. In general it will be necessary to consider an additional impedance Z_i' for the line switched to atmosphere.

The configuration in Fig.6.4 can be regarded as a simulation of a digital element feeding a transmission line.

6.2.1 Predicting pulse distortions on lossless fluidic transmission lines with nonlinear source and load resistance

Assuming negligible losses a very simple graphical method can be applied to the problem, the fundamentals of which have been given by Bergeron (ref.39).
In Fig.6.6 the source and loaded characteristics of a network described by Fig. 6.5 are plotted.
The free jet being switched off the source characteristic is identical with the ordinate (short circuit). The dc operating points are A_0 and A_1. For a lossless transmission line the surge impedance becomes pure resistive and therefore also a characteristic can be plotted in Fig. 6.6.

Pressure and flow along a transmission line result out of the superposition of a wave travelling in positive z-direction and a wave travelling in negative z-direction (see chapter 4.2.2). Out of equations (4.14) and (4.15) we find

(6.3) $p = p_f \cdot p_r$ f = forward $(+z)$

(6.4) $\dot{m} = \dfrac{p_f}{z_0} - \dfrac{p_r}{z_0}$ r = reverse $(-z)$

The forward travelling flow wave is related to the forward travelling pressure wave by the positive surge impedance and the reverse travelling flow wave is related to the reverse travelling pressure wave by the negative surge impedance.

We now send an observer along the line who travels with wave speed. Travelling in forward direction he will only see the reverse travelling wave where pressure and flow are related by the negative surge impedance. Travelling in reverse direction he will only see the forward travelling wave where pressure and flow are related by the positive surge impedance.

Let us consider the line in Fig. 6.7 where at the time $t = t_i$ at the locus E a change occures that causes two waves in z and -z-direction. The initial conditions at the locus E are to be p_i and $\dot{m}_i$.

If an observer leaves the locus E where we have the initial conditions p_i and $\dot{m}_i$, at the time t_i travelling with wave speed he will state that at any locus of the line pressure p and massflow $\dot{m}$ are related by the same linear equation which only depends on surge impedance, travelling direction and initial conditions (see Fig.6.8).
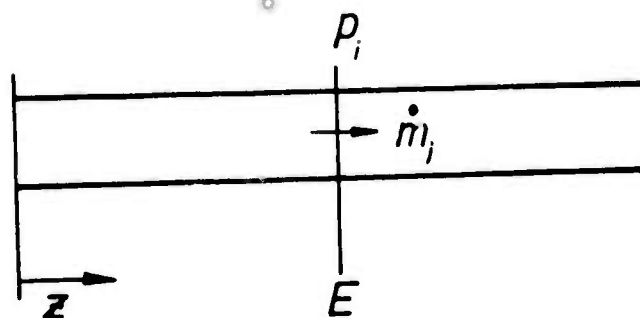
Fig.6.7 Initial conditions on a line at the locus E
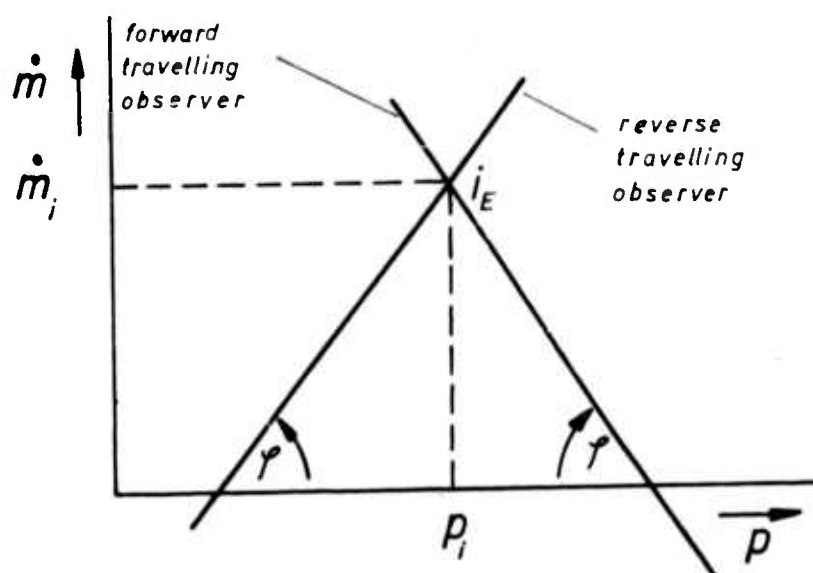
Fig.6.8 Characteristics of a forward and reverse
travelling observer

We will now investigate the case when the line is switched on at the time $t = 0$. The time the wave needs to travel from one end of the line to the other results as $\tau = 1/c_q$. The observer is to start at $t = -\tau$ at the end of the line so that he reaches the beginning of the line at $t = 0$, where the line is switched on.

At the time $t = -\tau$ pressure and flow at the end of the line are zero. This condition is described by the operating point $(1, -\tau)$ in Fig.6.9. During the travel from the end to the beginning of the line pressure and flow are related by the characteristic of the positive surge impedance. At the moment when the observer reaches the beginning of the line at $t = 0$ the jet is switched on. The point of intersection of the characteristics of the surge impedance and the source yields pressure and massflow rate at the time $t = 0$ at the beginning of the line.

The observer now starts at the time $t = 0$ for the end of the line and finds pressure and flow related by the characteristic of the negative surge impedance. The intersection of the characteristics of the load and the surge impedance $(1, \tau)$ yields pressure and massflow rate at the time $t = \tau$.
Continuing in this way the static operating point (OP) is approximated in a sort of cobb-web.
Fig. 6.10 shows the step response at the end of the line.
With the same procedure the switching-off process can be evaluated. At the time $t = 0$ the jet is switched of the receiver nozzle of the line.

Whilst in Fig.6.9 an overmatched line was shown, in Fig. 6.11 the line is undermatched. The observer in Fig. 6.11 leaves the end of the line at the time $t = -\tau$. In contrary to the ringing in Fig. 6.10 now the final value of the pressure at the end of the line is slowly approximated continously decreasing steps.

Out of the considerations made above the procedure to match the line is obvious. As demonstrated in Fig.6.12a and b the characteristic of the surge impedance has to cross the intersections of the load and source characteristics. In the point of intersection the load resistance is equal to the surge resistance.

It should be pointed out that for a given geometry a complete matching is only possible for a distinct source pressure. An increase or decrease of the source pressure will cause mismatching. On the other hand a mismatch can be compensated by a proper change of source pressure.

An other case (ref.40) can be considered in which the transmission line is oversized but intersects the source characteristic at a point such that the reflected wave readjusts flow conditions in the line to the final, steady-state value (see Fig.6.13) for the switching-on process. The oversized lines, because of their larger internal diameter, will have much lower frictional losses and pulse distortions than lines acoustically matched to the load impedance.

Care must, however, be taken that operating point A_0 is reached in the same way for the switching - off process. This will exactly only be possible if the source resistances in the switched-on and switched conditions are the same.

The graphical method described above is applicable to arbitrary
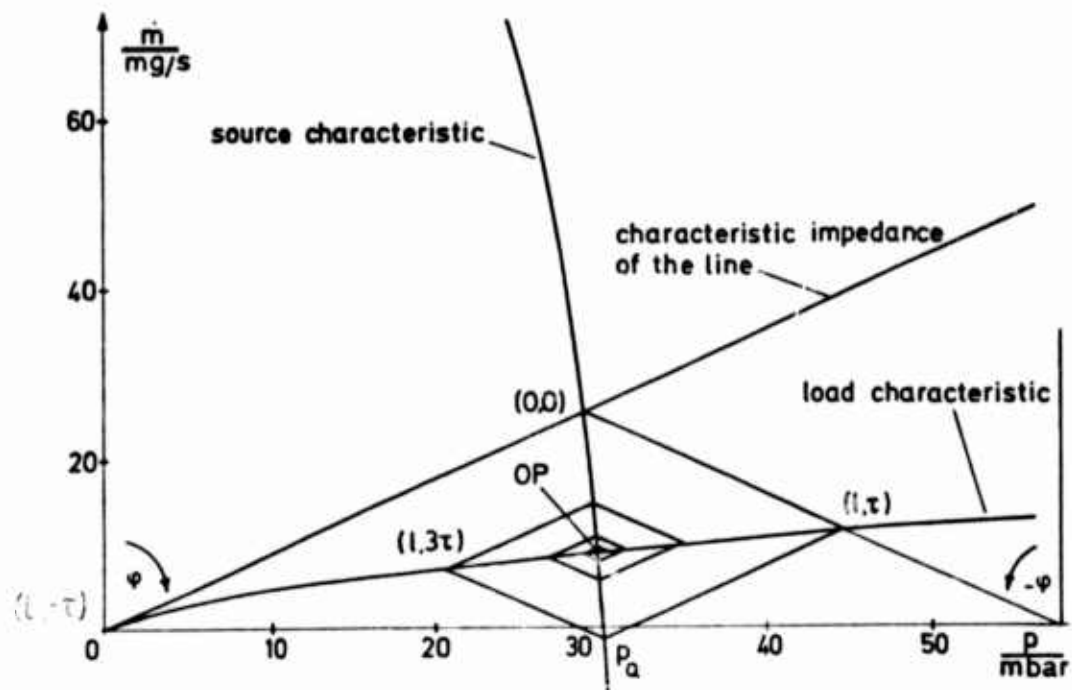
Fig.6.9 Graphical determination of the switching process
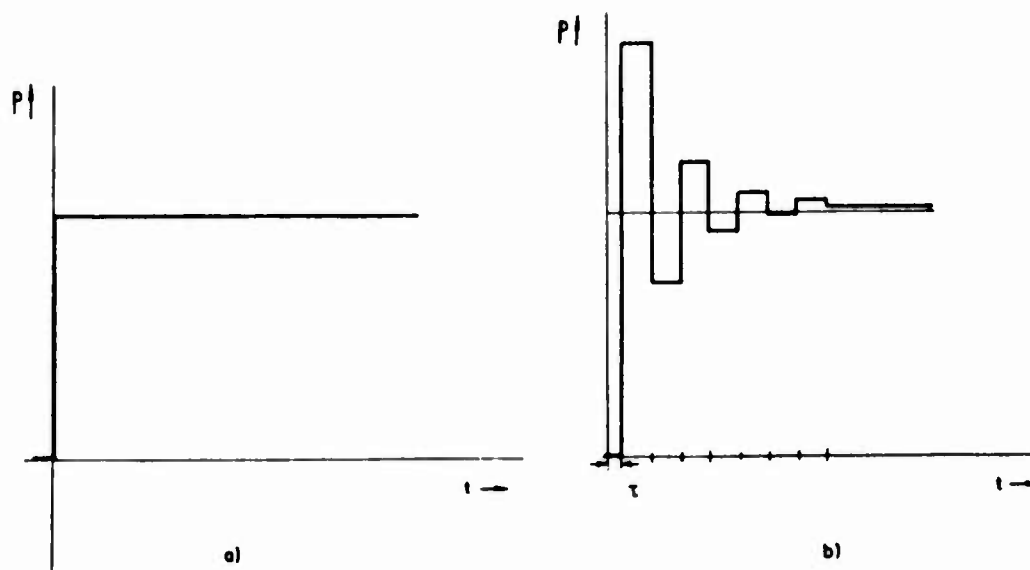
Fig.6.10 Step response according Fig. 6.9
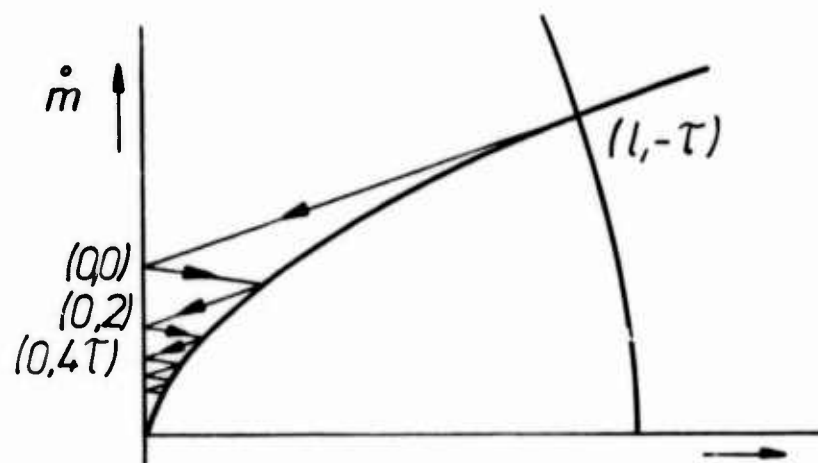
Fig.6.11 Graphical determination of the switching process
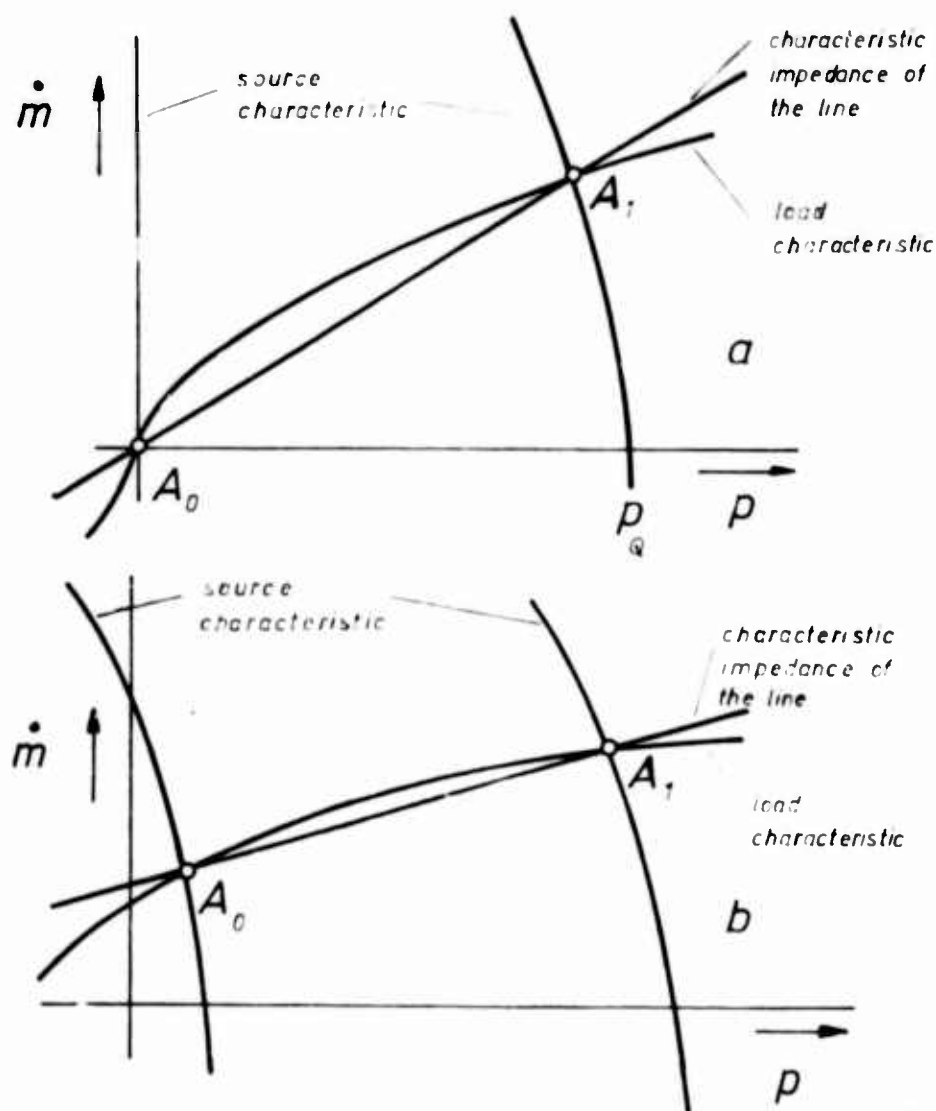
Fig.6.12 Line matching
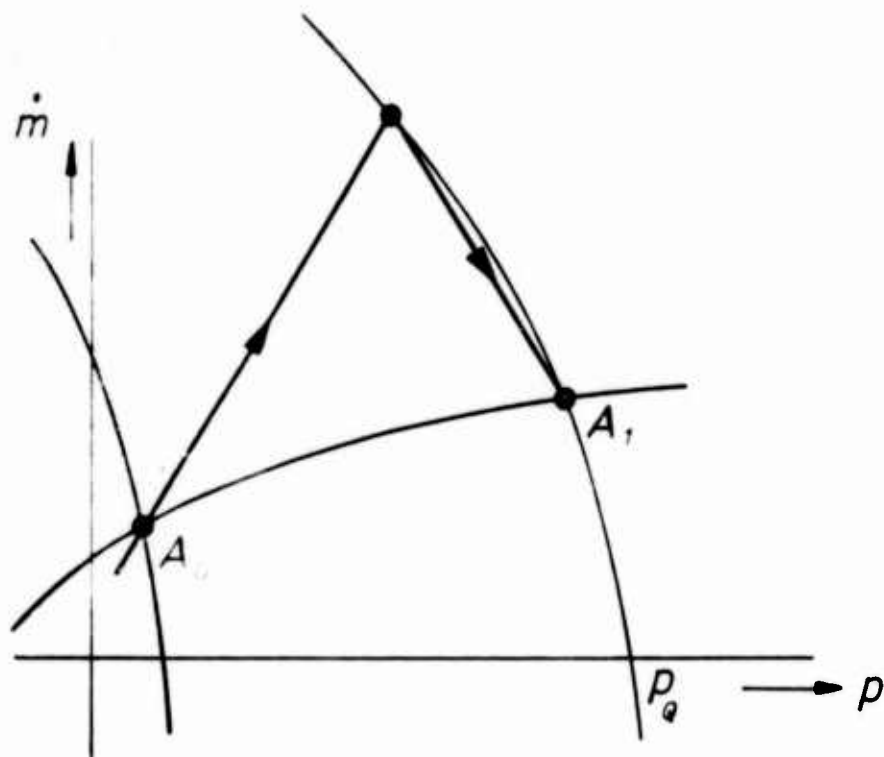
Fig.6.13 Matching by an oversized transmission line

pulse trains and arbitrary nonlinear load and source characteristics, which also can be time dependent. Further applications of this method are branched and stepped lines. In general it will be necessary to establish an accurate time table for the fictive observer.

In Fig.6.14a and 6.15a the oscilloscope traces and the graphical results are shown for a line with the following dimensions (ref.41).

$$l = 150 \text{ mm}$$
$$A = 3.25 \text{ mm}^2$$
$$a = h/b = 2,75$$

The characteristics for both cases considered are plotted in Fig. 6.14b and Fig. 6.15b. In Fig. 6.14 the line is undermatched and in Fig. 6.15 the line is overmatched.

It is remarkable that rise and fall of the output pulses are different, which is predicted rather accurately by the graphical procedure. Due to the neglection of friction the height of the output pulses is overpredicted.

In ref.42 this graphical method has been used to investigate the influence of the switching process of a bistable amplifier on the pulse matching at the amplifier input. By the application of this method if could be shown that a dynamic input characteristic exists in addition to the static characteristic.

In ref.43 Keto determines the area ratio for which no reflections at an orifice terminated line exist (see Fig.6.16). The solution is found by seeking the nozzle size that will sustain the same upstream flow rate as would exist if the line were continuous and is not concerned with the transient reflections

$$(6.5) \quad \frac{A_n}{A_{line}} = \frac{\sqrt{\frac{2}{\kappa-1}}\left(\frac{p_1^*}{p_0}\right)^{\frac{1}{\kappa}}\left(\left(\frac{p_1^*}{p_0}\right)^{\frac{\kappa-1}{2\kappa}}-1\right)}{\sqrt{\frac{T_Q}{T_0}\left(\frac{p_Q}{p_0}\right)^{\frac{1-\kappa}{\kappa}}\left(\left(\frac{p_1^*}{p_0}\right)^{\frac{\kappa-1}{\kappa}}-1\right)\frac{2}{\kappa-1}\left(\left(\frac{p_1^*}{p_0}\right)^{\frac{\kappa-1}{\kappa}}-1\right)^2}}$$

where

p_Q source pressure

p_1 pressure wave amplitude

p_0 ambient pressure

T_Q source temperatur

T_0 ambient temperature .

The assumptions of ref.43 are

a) ideal gas
b) one-dimensional flow
c) inviscid flow
d) subsonic flow
e) homenergic flow
f) inelastic walls

290
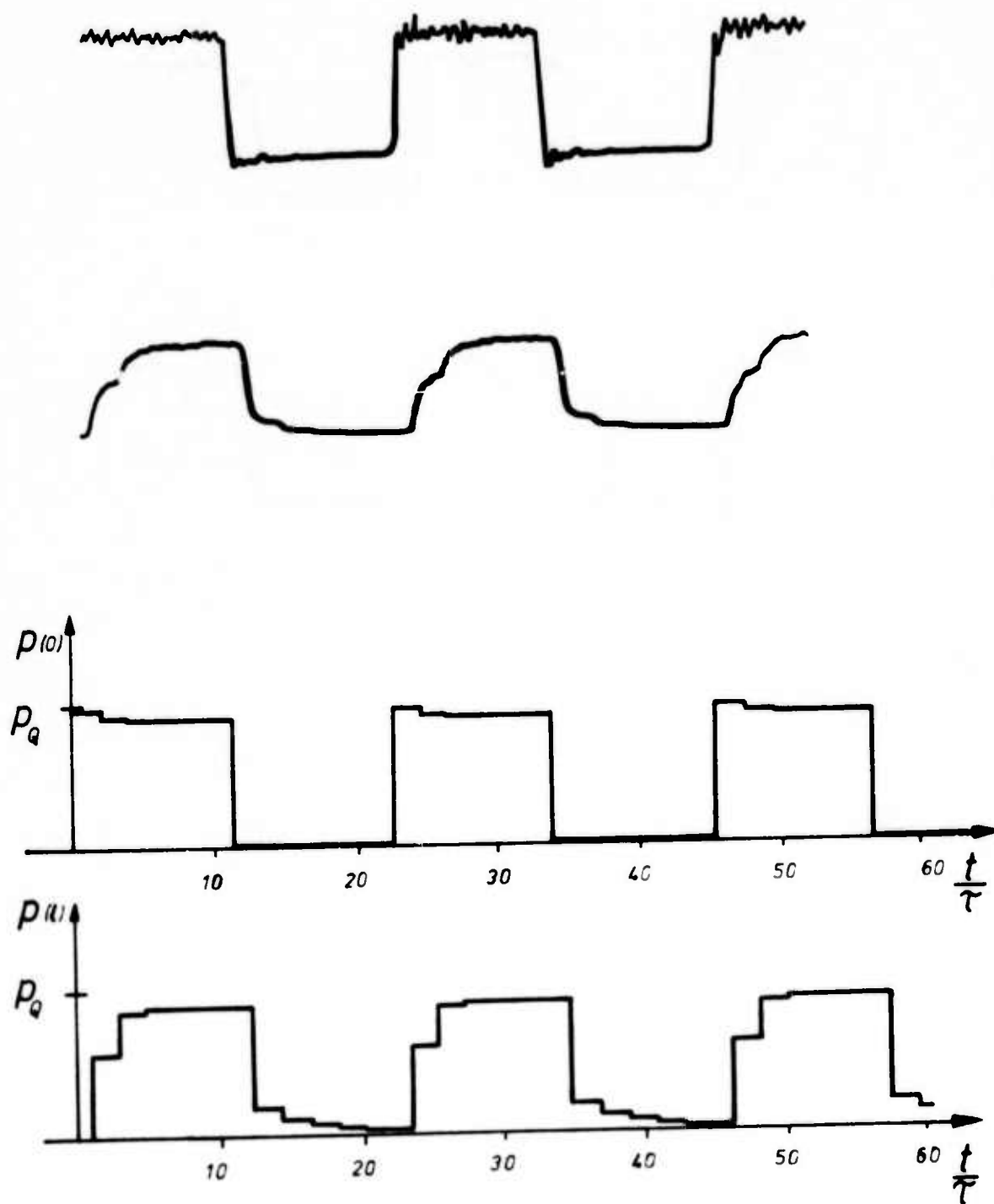
Fig.6.14 a) Oscilloscope traces and graphical results for an undermatched line
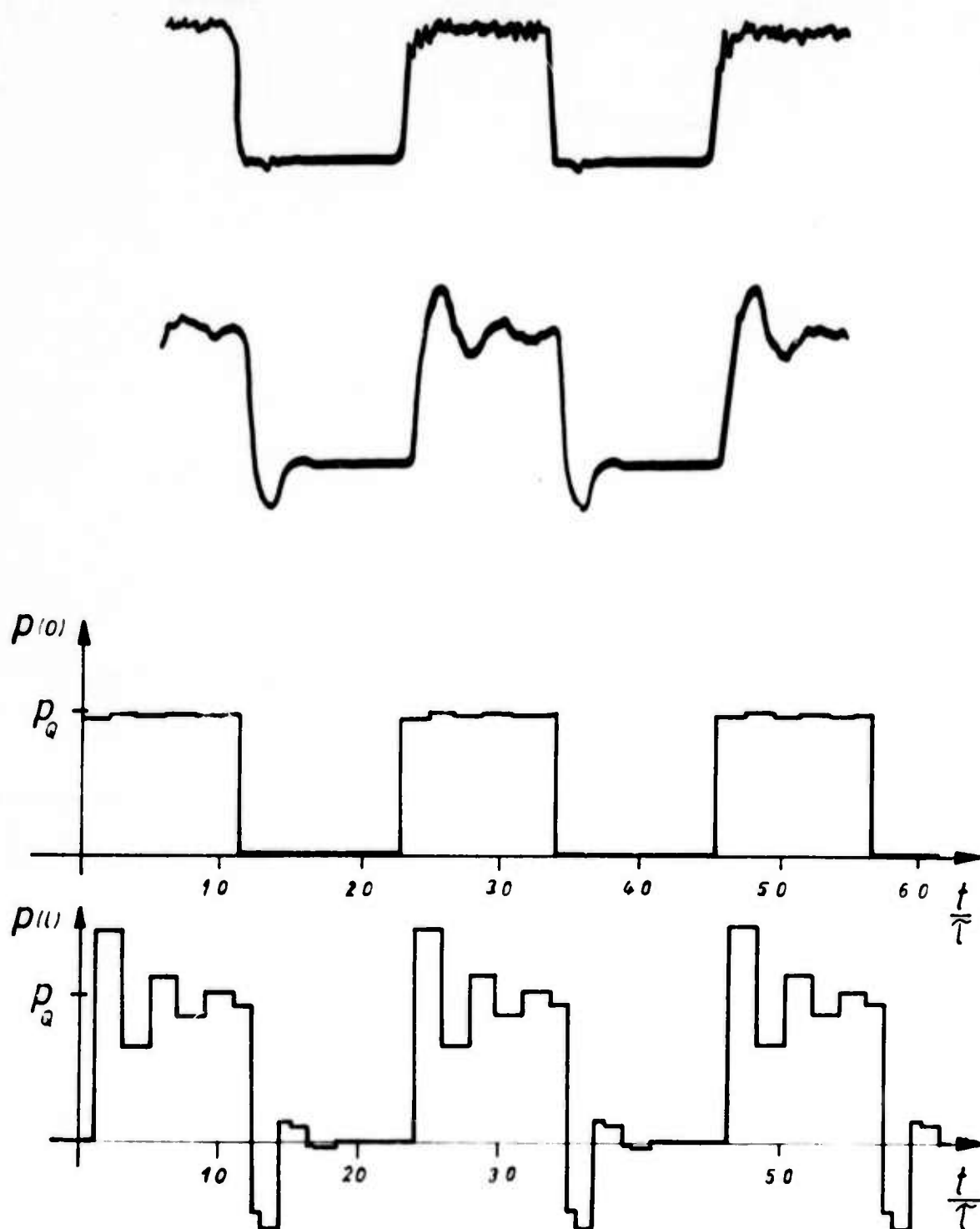
Fig.6.15 a) Oscilloscope traces and graphical results for an
overmatched line
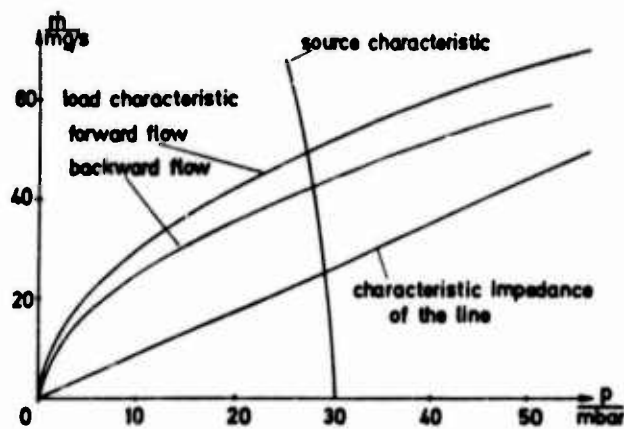
Fig. 6.14 b Line and termination characteristics
of an undermatched transmission line
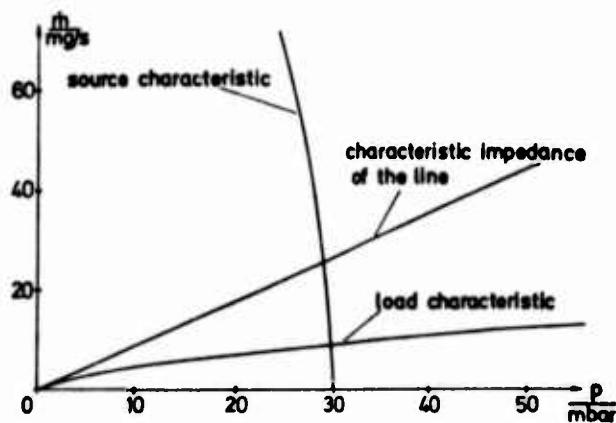
Fig. 6.15 b Line and termination characteristics
of an overmatched transmission line

If T_Q results from isentropic compression from T_o the term

$$\left(\frac{T_Q}{T_o}\right)\left(\frac{p_o}{p_Q}\right)^{\frac{\kappa-1}{\kappa}}$$

becomes equal to unity and equ. (6.5) reduces to

$$(6.6)\ \frac{A_n}{A_{Line}}\ =\ \frac{\sqrt{\frac{2}{\kappa-1}}\ \left(\frac{p_l{}^*}{p_o}\right)^{\frac{1}{\kappa}}\left[\left(\frac{p_l{}^*}{p_o}\right)^{\frac{\kappa-1}{2\kappa}}-1\right]}{\sqrt{\left[\left(\frac{p_l{}^*}{p_o}\right)^{\frac{\kappa-1}{\kappa}}-1\right]+\frac{2}{\kappa-1}\left[\left(\frac{p_l{}^*}{p_o}\right)^{\frac{\kappa-1}{2\kappa}}-1\right]^2}}\ .$$

In the acoustic case, when overpressure and density are considered very small equation (6.6) can be written as

$$(6.7)\ \frac{A_n}{A_{line}}\ =\ \frac{1}{\sqrt{2\kappa}}\ \sqrt{\frac{\bar{p}_l}{p_o}}\ .$$

In this case the dc nozzle resistance R_n is equal to the surge impedance Z_{so}. Equation (6.7) is equivalent to equ. (5.16) for small signal matching, where $r_n = Z_{so}$.

6.2.2 Predicting pulse distortions on lossy fluidic transmission lines with nonlinear load resistance

The graphical method evaluated by Bergeron (ref.39) can also be applied to lossy transmission lines by considering the losses in additional resistances. The simplest way will be to introduce resistance at the beginning and (or) the end of the line (ref.42).

If the reflections at the end of the line have to be determined the dc-resistance of the line is added to that of the pressure source. If the reflections at the beginning of the line are of interest the dc-resistance of the line is added to that of the terminating nozzle (Fig.6.17).

This procedure guarentees exact operating points. The dynamic behaviour, however, can not be predicted exactly because the losses in reality are distributed along line causing a dispersion of the waves. A much better approximation is acnieved by distributing single resistors along the line which in sum are equal to the dc transmission line resistance. The results will be much better than for one single resistance at the beginning or the end of the line. But the amount of graphical work will increase rapidly with the number of resistors, because the reflections at every resistor have to be considered. A further disadvantage is, that the frequency dependence of the losses can not be taken into account.

294
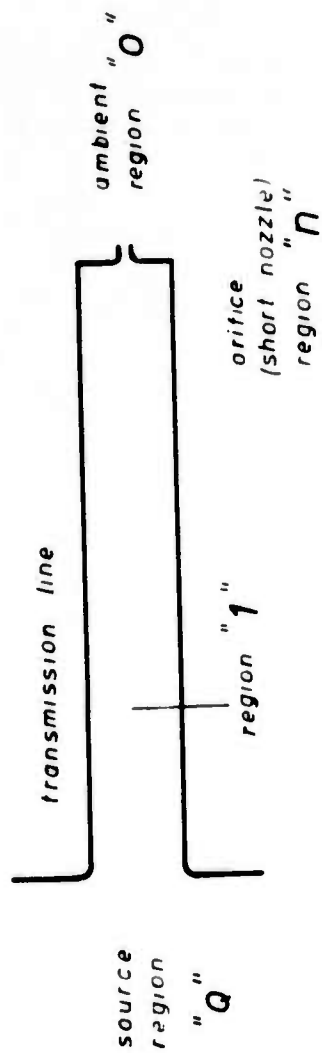
Fig.6.16 Orifice terminated transmission line
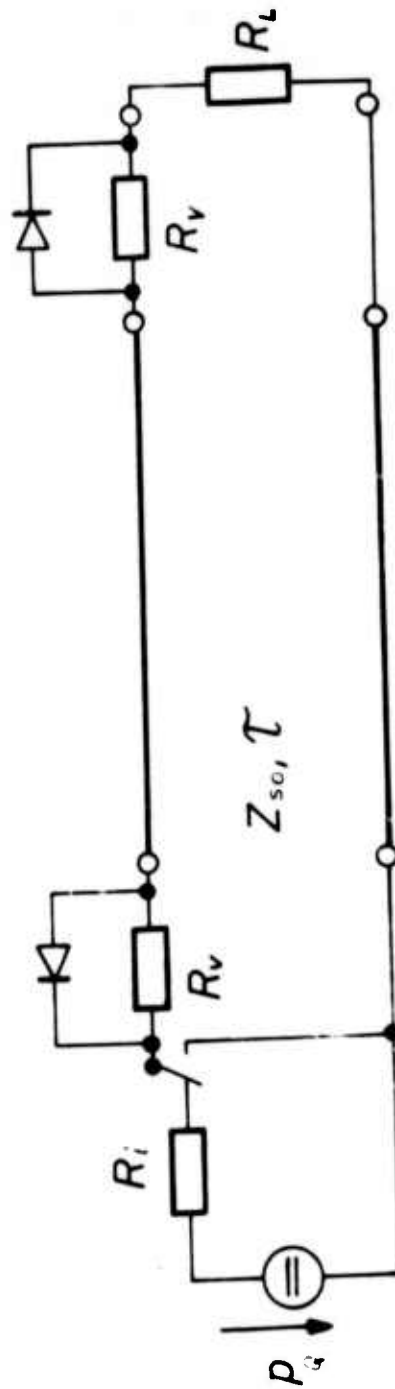
Fig.6.17 Eqivalent circuit of a pulsed transmission line
with losses

when the frequency dependent wall shear is to be considered, computerized methods should be applied to solve the governing equations (ref.30, 44 and 45).

In ref.44 Manning presents a computerized method of characteristics, which can be applied to systems where the gas velocity is not negligibly small relative to local wave velocity. The convective terms in the equations of motion and the actual variation of wave speed with gas pressure and temperatur must not be neglected.

A very remarkable work in the field of numerical solutions of transients in pneumatic networks seems to be that of Tsao (ref.45). The assumptions in ref.45 are the same as in chapter 4.5. In part I the dead end response of circular transmission lines and the pressure and velocity profile development along the line are shown. Part II discusses the problem of nonlinear loads and part III network problems with branchings.

References

1   Kirshner, J.M.   "Fluid Amplifiers"
Mc Graw-Hill Book Co., New York,1966.

2   Schaedel, H.M.   "Transmission lines and nonlinear
components in fluidic ac networks"
Paper E3, pp. E3-29 to E3-56,
Proc. 4th Cranfield Fluidics conf.
Brit. Hydrom. Res.Ass., Cranfield,
March 1970.

3   Taplin, L.B.   "Small signal analysis of vortex
amplifiers" AGARD Lecture series on
"Fluid control-components and systems"
September 1966. AGARDograph 118.

4   Sparrow, E.M.   "Experiments on laminar flow develop-
Hixon, C.W. and   ment in rectangular ducts". Trans.
Shavit, G.   A.S.M.E., 89, Series D, 1. pp.116-
124 (March 1967).

5   Lundgren, T.S.   "Pressure drop due to the entrance
Sparrow, E.M. and   region in ducts of arbitrary cross-
Starr, J.B.   section." Trans. A.S.M.E., 86,
Series D, 3pp. 620-626. (September
1964).

6   Han, L.S.   "Hydrodynamic entrance lengths for
incompressible laminar flow in
rectangular ducts" Trans. A.S.M.E.,
27, Series E, 3.pp. 403-409 (Sep-
tember 1960).

7   Kline, S.J.   "Optimum design of straight-walled
Abbot, D.E. and   diffusers" Trans. A.S.M.E., 81,
Fox, R.W.   Series D, 3 pp. 321-331 (September
1959).

8   McDonald, A.T. and   "An experimental investigation of
Fox, R.W.   incompressible flow in conical
diffusers" A.S.M.E. Paper 65-FE-25.
9 pp. incl. 15 figs. (June 1965).

9   Schaedel, H.M.   "Investigations on fluidic jet
Kessel, G.W.   deflection amplifiers in dc and ac
networks" Paper D2, pp. D2-13 to
D2 36.Proc. 5th Cranfield Fluidics
conference Uppsala, Sweden, June
1972.

10   Gibson, A.H.   "On the resistance to flow of
water through pipes or passages
having divergent boundaries"
Trans. of the Royal Society of
Edinburgh, Vol. 48 (1911) Part 1,
No. 5, pp.97-116.

11   Kessel, G.W.   "Theoretical and experimental in-
                            vestigations on the static and dy-
                            namic behaviour of fluidic jet
                            deflection amplifiers"
                            Ph.D. Thesis, T.H. Aachen 1974.

12   Schaedel, H.   "The dc-equivalent circuit of fluidic
      Kessel, G.   line branchings"
                            Fluidics Quarterly, Vol.IV, No.2,
                            April 1972.

13   Vazsonyi, A.   "Pressure loss in elbows and duct
                            branches"
                            Transactions A.S.M.E., Vol.66, pp.
                            177-183, April 1944

14   Schütt, H.   Mitteilungen des Hydraulischen Inst.
                            der T.H. München (1926) Heft 1, p.42.

15   Vogel, G.   "Untersuchungen über den Verlust in
      Petermann, F.   rechtwinkligen Rohrverzweigungen"
                            "Der Verlust in schiefwinkligen
                            Rohrverzweigungen"
                            Mitteilungen des Hydraulischen Inst.
                            der T.H. München, Heft 1,2,3 (1926,
                            1928,1929).

16   Kohl, A.   "The dc-equivalent circuit of
                            fluidic line junctions"
                            Internal report No.71/4. Inst. f.
                            Nachrichtengeräte und Datenverarbei-
                            tung. T.H. Aachen.

17   Reid, K.N.   "Dynamic models of fluid trans-
                            mission lines"
                            Proc. Symposium on fluidics and
                            internal flows. pp.I-143 to I-163
                            (1968)

18   Crandall, I.B.   Theory of vibrating systems and sound.
                            Appendix A, pp.229-241. D.v.Nostrand
                            Company, Inc. 1927.

19   Richardson,   Proc. phys. Soc. London 40, 206 (1928).

20   Iberall, A.S.   "Attenuation of oscillatory pressures
                            in instrument lines"
                            Journal of Research, National Bureau
                            of Standards, Vol.45, pp.85-108 (1950).

21   Nichols, N.B.   "The linear properties of pneumatic
                            trnasmission lines" Trans. of the
                            Instrument Society of America, Vol.1
                            pp. 5-14 (1962).

22   Brown, F.T.   "The transient response of fluid
                            lines" Journal of basic engineering,
                            Trans. A.S.M.E., Series D, Vol.84,
                            1962, pp.547-553.

23   Schaedel, H.M.   "A theoretical investigation of
                              fluidic transmission lines with
                              rectangular cross-section" Paper K3,
                              pp.K3-33 to K3-52. Proc. 3rd Cranfield
                              Fluidics Conf., Brit. Hydrom. Res. Ass.
                              Cranfield (1968).

24   Schaedel, H.M.   "Theoretical and experimental in-
                              vestigations on fluidic transmission
                              lines and lumped components"
                              Ph.D.Thesis, T.H. Aachen 1968.

25   Shearer, J.L.   "Highlightsof fluidics research in
                              the S.C.L." Proc. Symposium on
                              fluidics and internal flows. pp.I-
                              132 to I-138 (1968).

26   Franke, M.E.   "The frequency response of volume-
      Wilda, R.W.   terminated pneumatic lines with cir-
      Miller, R.N.   cular and rectangular cross-sections"
      Fada, C.V.   Proc. of the 1969 Joint Automatic
                              Control Conference. University of
                              Colorado (August 1969).

27   Karam, J.T.   "The frequency response of blocked
                              pneumatic lines" Wright-Patterson
                              AFB, Ohio: Air Force Institute of
                              Technology, M.S. Thesis, GAM/ME/
                              66B-3, 1966.

28   Gerlach, C.R.   "Wave propagation in viscous fluid
      Parker, J.D.   lines including higher mode effects"
                              Journal of basic engineering, Trans.
                              A.S.M.E., Series D., Vol.89, pp.782-
                              788 (Dec. 1967).

29   Zielke, W.   "Frequency-dependent friction in
                              transient pipe flow" Journal of Basic
                              Engineering, Trans. A.S.M.E. Series D,
                              Vol.90, No.1, pp.109-115 (March 1968).

30   Brown, F.T.   "A quasi method of characteristics
                              with application to fluid lines with
                              frequency dependent wall shear and
                              heat transfer" ASME paper No.68-WA/
                              Aut-7.

31   Brown, F.T.   "Samll-amplitude frequency behaviour
      Margolis, D.L.   of fluid lines with turbulent flow"
      Shak, R.P.   ASME paper No.69-FE-11.

32   Brinkmann, R.   "Numerische Simulation inhomogener
                              Doppelleitungen bei vorgeschriebener
                              Rechengenauigkeit"
                              PH.D. Thesis, T.H. Aachen 1970.

33   Kirszenblat, A.   "Transmission of a fluidic signal
                             at intermediate distances"
                             Fluidics Quarterly, Vol.IV, No.2,
                             pp.1-18 (1972).

34   Tarantine, F.J.   "Fluid pressure transients in a
                             tapered transmission line"
                             Trans. of the A.S.M!E.-Journal of
                             Basic Engineering, 89, pp.181-190
                             (March 1967).

35   Dat, J.   "A frequency study of pneumatic
      Piquemal, J.   convergent and divergent lines"
      Caen, R.   Paper D 1, IVth International Fluidics
                            Conference, Varna, Bulgaria (Oct.
                            1972).

36   Schaedel, H.M.   "The behaviour of transmission lines
                            and nozzles in fluidic networks"
                            AGARD Lecture Series XXXV on Fluidic
                            Control Systems for Aerospace Pro-
                            pulsion, AGARDograph 134 (Sept. 1969).

37   Schaedel, H.M.   "Some investigations on frequency
      Kessel, G.W.   demodulating systems with fluidic
      Franke, M.E.   jet deflection amplifiers"
                            The second international I.S.M.E.
                            Symposium on Fluid Machinery and
                            Fluidics, Tokio, Japan (Sept. 1972)

38   Kohl, A.   "Theoretical and experimental in-
                            vestigations of fluidic signal and
                            noise filters with application to dc
                            and ac fluidic systems"
                            Paper G2, pp.G2-21 to G2-42. Proc.
                            5th Cranfield Fluidics Conf., Brit.
                            Hydrom. Res. Ass., Cranfield (1972).

39   Bergeron, L.   "Water hammer in hydraulics and wave
                            surges in electricity"
                            J. Wiley and Sons, Inc. 1961.

40   Griffin, W.S.   "Simplified interconnection technique
                            for digital fluid jet amplifiers"
                            Appendix in "A breadboard   -
                            controlled pneumatic stepping motor
                            system" NASA Lewis Research Center,
                            Cleveland, Ohio, (October 1967).

41   Schaedel, H.M.   "A simple method of predicting pulse
      Zwethov, G.   distortions on fluidic transmission
                            lines" Appendix in "Transmission
                            lines and nonlinear components in
                            fluidic ac networks"
                            Paper E2, pp.E3-42 to E3-46, 4th
                            Cranfield Fluidic Conference. Brit.
                            Hydrom. Res.Ass., Cranfield (March
                            1970).

42   Osthorst, J.   "Investigations on the pressure pulse
      Schaedel, H.M.   transfer between fluidic wall attach-
                            ment amplifiers"
                            Paper D2, IVth International Fluidics
                            Conference, Bulgaria (October 1972).

43   Keto, J.R.   "Transient response of some flueric
                            components to step waves and appli-
                            cation to matching"
                            HDL-TR 1531 (September 1970).

44   Manning, J.R.   "Computerized method of characteristics
                            calculations for unsteady pneumatic
                            lineflows" Journal of Basic Engineering
                            pp.231-240 (June 1968).

45   Tsao, S.   "Numerical solutions of transients
                            in pneumatic networks"
                            Part I - "Transmission line calcula-
                            tions" Trans.of the A.S.M.E. pp.588-
                            595 (September 1960).
                            Part 2 - "Nonlinear terminations
                            problems" Journal of Applied Mech.,
                            Paper 69-APM-M.
                            Part 3 -"Network problems with
                            branching" Journal of Applied Mech.,
                            Paper 69-APM-N.

TWO TERM ANALOGUE FLUERIC CONTROLLER

*E.C. HIND** and *J.D. BLACK**

ABSTRACT

A proportional plus integral flueric pneumatic controller is described
which uses the principle of flow summation at each of two control
ports and operates over the standard signal range of 3 psi to 15 psi .
Only proprietary proportional fluid amplifiers were used each having
only one pair of control ports. Equations are developed which define
the conditions necessary for an ideal integral component in the control
action, when only a moderately high open loop gain is used, and the
conditions necessary for equal controller gains for set point and
measured value inputs. The performance of the controller was evaluated
by testing it in isolation and when used in place of a conventional
pneumatic controller to control a fourth order level process subjected
to set point changes and process flow disturbances.

LIST OF SYMBOLS

A   Dimensionless open loop gain of operational amplifier.

C   Pneumatic capacitance, $in^5 lb^{-1}$.

G   Dimensionless proportional gain of controller.

ℓ See $\Sigma\ell$.

P_b Bias Pressure, $lb\ in^{-2}$.

$P_{c\ell}$ Left hand control port pressure, $lb\ in^{-2}$.

P_{cr} Right hand control port pressure, $lb\ in^{-2}$.

P_ℓ Left hand input pressure, $lb\ in^{-2}$.

P_o Output pressure, $lb\ in^{-2}$.

P_r Right hand input pressure, $lb\ in^{-2}$.

$R_{b\ell}$ Left hand bias resistance, $lb\ sec\ in^{-5}$.

R_{br} Right hand bias resistance, $lb\ sec\ in^{-5}$.

* The University of New South Wales, Australia.

$R_{c\ell}$ Left hand control port resistance, lb sec in^{-5} .

R_{cr} Right hand control port resistance, lb sec in^{-5} .

R_f Left hand feedback resistance, lb sec in^{-5} .

R_{fI} Right hand feedback resistance, lb sec in^{-5} .

R_I Integral resistance, lb sec in^{-5} .

R_ℓ Left hand input resistance, lb sec in^{-5} .

R_r Right hand input resistance, lb sec in^{-5} .

r See Σr .

S Laplace transform variable, sec^{-1} .

T_I Integral time constant $(R_I C)$, sec .

T_I' Effective integral time constant $T_I \left(\dfrac{1}{1 + \dfrac{R_I}{R_{fI}}} \right)$, sec .

t time, sec .

Z Resistance valve opening, in .

$\Sigma\ell$ Sum of left hand reciprocal resistances,

$$\Sigma\ell = \frac{1}{R_\ell} + \frac{1}{R_{b\ell}} + \frac{1}{R_f} + \frac{1}{R_{c\ell}} , \qquad \text{in}^5 \text{ lb}^{-1} \text{ sec}^{-1} .$$

Σr Sum of right hand reciprocal resistances,

$$\Sigma r = \frac{1}{R_r} + \frac{1}{R_{br}} + \frac{1}{R_{fI}} + \frac{1}{R_{cr}} , \qquad \text{in}^5 \text{ lb}^{-1} \text{ sec}^{-1} .$$

$\Sigma\ell d$ Dominant term only in $\Sigma\ell$,

i.e. $\Sigma\ell d = \dfrac{1}{R_{c\ell}}$,   in^5 lb^{-1} sec^{-1} .

$\Sigma r d$ Dominant term only in Σr ,

i.e. $\Sigma r d = \dfrac{1}{R_{cr}}$,   in^5 lb^{-1} sec^{-1} .

INTRODUCTION

The purpose of this paper is to report the results of a study of the use of the principle of flow summation at each of two control ports in the first stage of the flueric operational amplifier for the generation of proportional plus integral control action. Of particular interest in the study was the problem of obtaining an ideal integral component in the control action.

The controller was to have no moving parts. It was to be constructed using only proprietary proportional amplifiers each having only one pair of control ports and using proprietary needle type resistance valves and a capacitance tank. It was to replace a conventional pneumatic controller operating on the signal range 3 psi to 15 psi (or 20 k Pa to 100 k Pa) which was mostly set at about 100% proportional band with an integral time constant in the vicinity of one minute.

Of the work on fluidic controllers reported in the literature [(1), (2), (3), (4), (5), (6), (7), (8), (9), (10) *] some refer to special applications, some to controllers in which four control ports are used in the first stage amplifier and some refer to controllers in which the modular approach is used for function generation; resulting in as many as four fluidic operational amplifiers in the one controller. As far as the authors are aware, only one paper refers to the use of flow summation at a control port of a fluid amplifier. B.G. Bjornsen (11) has described a controller which uses the principle of flow summation at an input to the first stage of a five stage high gain amplifier. His controller used a summing impact modulator as the first stage followed by three transverse impact modulator stages and then an output stage consisting of a conventional moving part pneumatic relay of gain 10 : 1. He claims a very high gain in the open loop condition of between 30,000 and 50,000, a figure which the authors believe cannot at this time be matched by five stages of proprietary proportional fluid amplifiers.

DESCRIPTION OF TWO TERM CONTROLLER

A schematic arrangement of the proportional plus integral controller using a five stage amplifier is shown in Fig.1. As the performance of the amplifiers was best when the control port pressures were approximately 10% of the power jet pressures, the two bias resistors $R_{b\ell}$ and R_{br} were used to achieve this optimum first stage mean

---

* Numbers in brackets refer to the list of references at the end of the paper.

305

pressure and also to compensate for any differences between left and right control ports, and to enable the output pressure P_o, to be set at the required value when the two inputs P_ℓ and P_r were at specific initial values.

The output signal pressure had to range from 3 psi to 15 psi . Tests on the last stage amplifier showed that this could easily be achieved if the power jet pressure was set to 25 psig although this was above the maximum power jet pressure shown on the characteristic curves supplied by the manufacturer.

The seven resistance valves were of the tapered needle type fitted with isolating diaphragms and spring loaded against micrometer heads which enabled valve openings to be read in thousandths of an inch. The needles were cones of included angle 4° . The matching conical valve seats were of length 0.34" and the small end diameter was 0.04" .

The two input pressures to the controller P_ℓ and P_r represent set value and measured value inputs or vice versa. The input signal ranges were also 3 psi to 15 psi . The resistance valves R_ℓ and R_r provide left hand input and right hand input gain adjustments.

The valves R_f and R_{fI} provide negative feedback and positive feedback gain adjustment, and hence controller stability adjustment. The valve R_I provides integral time constant adjustment and the volume chamber provides the fixed capacitance for the generation of the integral action.

CONTROLLER ANALYSIS

In the following analysis, the flueric operational amplifier is assumed to have a moderately high pressure gain (e.g. 100 to 1,000), and to respond fast enough for time dependent terms to be neglected. The amplifier may consist of any suitable number of stages. A stage may be any type of fluid amplifier such as conventional analogue or proportional amplifier, impact modulator or vortex amplifier, provided its characteristic is essentially proportional. It is further assumed that all resistances and the capacitance are linear.

The block diagram of the proportional plus integral controller is shown in Fig. 2 , with output pressure, P_o , and inputs left hand side pressure, P_ℓ , right hand side pressure, P_r , and bias pressure P_b.

306

The bias pressure input was useful for studying the effect of noise emanating from the bias pressure regulator. For the following analysis the bias pressure is assumed constant so that $P_b = 0$ in the block diagram.

Let $\Sigma \ell = \dfrac{1}{R_\ell} + \dfrac{1}{R_{b\ell}} + \dfrac{1}{R_f} + \dfrac{1}{R_{c\ell}}$,

$\Sigma r = \dfrac{1}{R_r} + \dfrac{1}{R_{br}} + \dfrac{1}{R_{fI}} + \dfrac{1}{R_{cr}}$

and $T_I = R_I C$.

The block diagram of Fig.2 may be reduced to that shown in Fig.3.

Provided the term $\dfrac{R_I}{R_{fI}} \left(\dfrac{1}{R_{fI}\Sigma r} \right)$ is much smaller than unity, it

may be neglected (for this controller its value is about 0.0025, and neglecting it results in an error of only about $\frac{1}{4}\%$ which is acceptable.

When the term $\dfrac{R_I}{R_{fI}} \left(\dfrac{1}{R_{fI}\;\Sigma r} \right)$ is neglected, the block diagram of

Fig.3 may be reduced to that shown in Fig.4. The effective integral time constant is

$$T_I' = \frac{T_I}{1 + \dfrac{R_I}{R_{fI}}} \quad .$$

It may be seen from Fig.4 that for an ideal proportional plus integral controller it is necessary that

$$\left(\frac{R_f\;\Sigma \ell}{R_{fI}\;\Sigma r} \right) \left(\frac{1}{1 + \dfrac{R_I}{R_{fI}}} \right) \left(\frac{1}{1 + \dfrac{R_f\;\Sigma \ell}{A}} \right) = 1 \qquad (1)$$

. If the left hand side of equation (1) is greater than unity then the controller is unstable as shown in Fig.5a.

. If the left hand side of equation (1) is equal to unity then the controller is critically stable as required and the integral component in the controller response is ideal as shown in Fig.5b.

. If the left hand side of equation (1) is less than unity, then the controller is stable as shown in Fig.5c.

Equation (1) may be written in the following form, which is more useful when selecting controller resistance values:

$$\frac{R_f \ \Sigma\ell}{(R_{fI} + R_I)\Sigma r} \ = \ 1 + \left(\frac{R_f \ \Sigma\ell}{A}\right) \tag{2}$$

Alternatively, the following form of equation (1) is useful for the determination of R_f

$$R_f \ \left[\frac{\Sigma\ell}{(R_{fI} + R_I)\Sigma r} \ - \ \frac{\Sigma\ell}{A}\right] \ = \ 1 \ . \tag{3}$$

From Fig.4, it can be seen that the condition for the controller to have a right hand side proportional gain of G is:

$$\frac{R_f \ \Sigma\ell}{R_r \ \Sigma r} \ = \ \left[1 + \frac{R_f \ \Sigma\ell}{A}\right] \ G \tag{4}$$

The condition for the controller to have the same gain on the left hand side and right hand side can be seen from Fig.4 and is:

$$R_r \ \Sigma r \ = \ R_\ell \ \Sigma\ell \tag{5}$$

Another useful relationship may be derived from equations (2) and (4) which allows R_r to be determined, i.e.:

$$R_r \ = \ \frac{R_{fI} + R_I}{G} \tag{6}$$

A condition imposed on A by equation (3) is that

$$A \ > \ (R_{fI} + R_I)\Sigma r \ .$$

ESTIMATION OF INITIAL RESISTANCE VALUES

It is not possible to solve the above equations to determine the required resistance values, as there are too many unknowns for the number of equations available. Hence an Engineering approach must be used if estimates are required for the resistance values and hence for valve settings.

308

For these values to be determined, the following details must be known (in some cases reasonable estimates will suffice): The open loop pressure gain of the operational amplifier; the pressure-flow characteristics of the first stage control ports; the pressure-flow characteristics for the type of valve to be used; the required controller proportional gain and integral time constant; and the value of the integral capacitance likely to be used.

The steps in estimating the initial values of resistance are as follows:

1. From T_I and C choose R_I .

2. Fig.3 may be reduced to Fig.4, provided the term

$$\frac{R_I}{R_{fI}} \left(\frac{1}{R_{fI}} \Sigma r \right) \ll 1 .$$

It will therefore be necessary to keep $\frac{R_I}{R_{fI}}$ small. Provided $G \geqslant 1$, choose R_{fI} as the value corresponding to the smallest convenient valve opening. If $G < 1$, the input resistances R_ℓ and R_r will be the higher values, and the smallest convenient valve opening will fix these values approximately. In this case $(G < 1)$ the approximation $\frac{R_{fI}}{R_\ell} = G$ or $\frac{R_{fI}}{R_r} = G$ will determine the initial value of R_{fI} .

3. As the effective integral time constant is

$$T_I' = T_I \left(\frac{1}{1 + \frac{R_I}{R_{fI}}} \right) ,$$

this equation should now be used to make a new estimate of T_I and hence R_I by using the ratio $\frac{R_I}{R_{fI}}$ determined in step 2. This will result in a second estimate of R_I and so $\frac{R_I}{R_{fI}}$.

4. Obtain R_r from equation (6)

5. Assuming that the control port resistances are much smaller than the other resistances, they will dominate the terms $\Sigma \ell$ and Σr. Hence as a first approximation, substitute $\Sigma \ell d = \frac{1}{R_{c\ell}}$ for $\Sigma \ell$

and $\Sigma rd = \dfrac{1}{R_{cr}}$ for Σr in equation (3) which becomes

$$R_f \left[\frac{\Sigma\ell d}{(R_{fI} + R_I)\,\Sigma rd} - \frac{\Sigma\ell d}{A} \right] = 1 \qquad \qquad (3d)$$

$R_{c\ell}$ and R_{cr} being determined from the slopes of the pressure-flow characteristics of the control ports at their optimum operating points will allow the first estimate of R_f to be made.

6. Substituting $\Sigma\ell d$ for $\Sigma\ell$ and Σrd for Σr in equation (5) will allow an estimate to be made for R_ℓ .

7. Using the pressure-flow characteristics for the valves and assuming that input and output controller signals are at mid range, i.e. at the nominal zero level of 9 psig , $P_\ell = P_r = P_o = 9$ psig , and that the control port pressures $P_{c\ell}$ and P_{cr} are at their optimum values, the sum of the flows through R_ℓ and R_f into the left hand summing point may be found. Also if the pressure in the capacitance is assumed to be 8 psig , the flows into the right hand summing point through R_r and R_{fI} may be determined. Now from the control port characteristics, the flows from the summing points into the amplifier may be determined. Hence the bias flows can be determined by difference and, provided a bias pressure P_b is known or assumed, the valve characteristics will yield the bias resistance values $R_{b\ell}$ and R_{br} .

8. Estimate $\Sigma\ell$ and Σr from

$$\Sigma\ell = \frac{1}{R_\ell} + \frac{1}{R_{b\ell}} + \frac{1}{R_f} + \frac{1}{R_{c\ell}}$$

and

$$\Sigma r = \frac{1}{R_r} + \frac{1}{R_{br}} + \frac{1}{R_{fI}} + \frac{1}{R_{cr}} \ .$$

9. It is advisable to make a second estimate of R_f from equation (3) using the values of $\Sigma\ell$ and Σr determined in step 8 and hence determine the initial setting for R_f .

From the above nine steps, resistance values, mean operating points and valve openings are determined for R_ℓ, $R_{b\ell}$, R_f, R_r, R_{br}, R_{fI} and R_I which may be used in the controller setting up procedure.

310

SETTING UP PROCEDURE

The setting up procedure for the controller is based on the input and output signal range of 3 psig to 15 psig with a nominal zero signal of 9 psig . It involves matching input, bias and feedback resistors to achieve the following:

. The required controller gains for left hand and right hand inputs.

. A good integration component of the control action with an integral time constant in the vicinity of that required.

. Correct zeroing of the controller.

. The operational amplifier functioning in the maximum gain region.

. The control port pressures of the first stage amplifier operating in the region of optimum performance.

The following recommended setting up procedure for the controller assumes that the operational amplifier has been previously set up and is operating satisfactorily.

1. Set bias pressure P_b to an appropriate value. Set pressures P_ℓ and P_r to 9 psig with all resistance valves shut.

2. Open the left or right bias valve so as to cause the amplifier to function in the region of maximum gain with the output pressure somewhere near mid range. When the open loop gain is relatively high, the output will be extremely sensitive to very small changes in bias valve setting.

3. Gradually open both left and right bias valves to increase the control port pressures to the optimum value with the amplifier operating still in the maximum gain region.

4. Gradually open left and right input valves, and compensate with bias valves, to hold the amplifier operation in the maximum gain region and with control pressures at their optimum values. Continue until the input valves are set at their initial values.

5. Gradually open the left hand feedback valve R_f , and compensate with the left hand bias valve to hold the required operating condition until R_f is at its initial value and the output pressure, P_o is at 9 psig.

6. Open the integral valve R_I wide open and gradually open the integral feedback valve R_{fI} , compensating with the right bias valve so that the controller output will HOLD (i.e. not drift), in mid range with the control port pressures at optimum, until R_{fI} is at the required initial value. By setting R_I wide open, the maximum integration rate will result and drift tendencies will be more

311

readily observed.

7. Set the integral valve to the required initial opening and check left and right gains. If necessary, adjust left and right input resistors to correct gain errors and compensate with bias valves to maintain optimum operation.

8. Use step changes in left and right inputs to check integral action time and if necessary adjust the integral valve R_I to obtain the required integral action time and hence the required effective integral time constant T_I'.

9. Re-check left and right hand gains, input error linearity and hold characteristics. Check also to see that the integral component in the control action is ideal. If the integral action is not ideal, adjust the integral feedback resistance R_{fI}. It will be seen by referring to Fig.4 or equation (1), that the stability of the controller, and hence the nature of the integral action component is influenced directly by the ratio $\dfrac{R_f}{R_{fI}}$.

Reference to Fig.5 shows that if the controller is unstable R_{fI} should be increased, whereas if the controller is stable R_{fI} should be reduced, i.e. valve opened further. Note that changes in R_{fI} may require compensation by adjusting R_{br}.

While a change in any one resistance setting will have a number of effects, the following summary of the main functions of each resistance valve will assist in setting up and subsequent adjustment of the controller:

R_ℓ	Left hand side gain;
R_r	Right hand side gain;
R_f	Gains of both sides similarly affected and the nature of the integral action or controller stability;
R_{fI}	Controller stability;
$R_{b\ell}$	Left hand control port pressure and so amplifier operation;
R_{br}	Right hand control port pressure and so amplifier operation;
R_I	Integral time constant.

CONTROLLER PERFORMANCE

Experimental verification of the feasibility of using the principle of flow summation at each of two control ports in the first stage of a flueric operational amplifier was obtained by using proprietary proportional amplifiers having only one pair of control ports each and proprietary resistance valves.

The controller was set up as described earlier in the paper using both a four stage and a five stage operational amplifier.

The controller was first set up and tested in isolation and the foregoing theory and setting up procedure verified. Of particular interest in the study was controller stability. The controller was adjusted so that it operated as an unstable element, as a stable element, and as a critically stable element, producing quite a satisfactory integral component of the control action when adjusted for this critically stable condition.

Fig.6 shows a plot of the controller output when subjected to an input step change of 1 psi in the right hand input pressure P_r , after being adjusted for ideal proportional plus integral action.

The pressure-flow characteristics of the resistance valves were significantly non-linear. This had a noticeable effect on the zeroing of the input signals at the low pressure end of the signal range. For the valves used in this study, the effect could be minimised by selection of bias pressure. Fig.7 shows a plot of values of right hand input pressure plotted against left hand input pressure, which indicated to the controller that zero error existed at the input.

The controller performed satisfactorily over a range of gains (0.5 to 2.0) and over a range of integral action times (20 sec to 120 sec) .

Some indication of the relative values of the terms in the equations developed earlier can be obtained by considering a particular case.

The values in the following table applied when the controller was set up for unit gain. The operational amplifier open loop gain was 750 , when the first stage control port pressures were in the vicinity of 0.8 psig.

As all resistances are non-linear, the values quoted were obtained by taking the tangent to the pressure-flow curve at the nominal zero controller signal level, i.e. $P_\ell = P_r = P_o = 9$ psig ; for a bias pressure P_b of 15 psig ; and for the first stage control port pressures of 0.8 psig . The pressure-flow curve, used to evaluate the adjustable resistors, was for the type of valve used, and no information was available on the likely variation from one valve to another, which could be quite significant at small openings such as 0.015" . To the authors' surprise, the two control port resistances were significantly different.

Resistance	R_ℓ	$R_{b\ell}$	R_f	$R_{c\ell}$	R_r	R_{br}	R_{fI}	R_{cr}	R_I
Valve opening inch	0.016	0.026	0.015	–	0.014	0.025	0.016	–	0.050
Resistance Value lb sec in^{-5}	83	26	90	2.0	105	28	83	2.4	8.3

Table 1:

Valve openings and resistance values for the controller when set up for unit gain.

$$\Sigma\ell = \left(\frac{1}{R_\ell} + \frac{1}{R_{b\ell}} + \frac{1}{R_f} + \frac{1}{R_{c\ell}}\right) = \frac{1}{83} + \frac{1}{26} + \frac{1}{90} + \frac{1}{2.0}$$

$$= 0.012 + 0.038 + 0.011 + 0.500 = 0.561$$

$$\Sigma r = \left(\frac{1}{R_r} + \frac{1}{R_{br}} + \frac{1}{R_{fI}} + \frac{1}{R_{cr}}\right) = \frac{1}{105} + \frac{1}{28} + \frac{1}{83} + \frac{1}{2.4}$$

$$= 0.010 + 0.036 + 0.012 + 0.417 = 0.475 .$$

Check the condition for ideal integration, equation (1)

$$\left(\frac{R_f \ \Sigma\ell}{R_{fI} \ \Sigma r}\right) \left(\frac{1}{1 + \frac{R_I}{R_{fI}}}\right) \left(\frac{1}{1 + \left[\frac{R_f \ \Sigma\ell}{A}\right]}\right) = 1 \tag{1}$$

$$\text{LHS} = \left(\frac{90 \times 0.561}{83 \times 0.475}\right) \left(\frac{1}{1 + \frac{8.3}{83}}\right) \left(\frac{1}{1 + \frac{90 \times 0.561}{750}}\right)$$

$$\text{LHS} = \frac{1.28}{1.1 \times 1.067} = 1.09$$

Indicated error is 9% .

Check proportional gain of left hand side (see Fig.4)

$$G = \frac{R_f}{R_\ell} \left(\frac{1}{1 + \left[\frac{R_f \ \Sigma\ell}{A}\right]}\right) = \frac{90}{83} \left(\frac{1}{1.067}\right) = 1.016$$

Indicated error is about 2% high.

Check proportional gain of right hand side using equation (4).

314

$$G = \frac{R_f \; \Sigma\ell}{R_r \; \Sigma r} \left[\frac{1}{1 + \left(\dfrac{R_f \; \Sigma\ell}{A}\right)}\right] = \left(\frac{90 \times 0.561}{105 \times 0.475}\right)\left(\frac{1}{1.067}\right) = 0.949$$

Indicated error is about 5% low.

Check the condition that the term $\dfrac{R_I}{R_{fI}}\left(\dfrac{1}{R_{fI}\;\Sigma r}\right)$ should be much less than unity.

$$\frac{R_I}{R_{fI}}\left(\frac{1}{R_{fI}\;\Sigma r}\right) = \frac{8.3}{83}\left(\frac{1}{83 \times 0.475}\right) = 0.00254$$

Indicated error caused by discarding this term is about ½% .

Determine the value of the effective integral time constant, T_I' , in terms of the integral time constant, T_I .

$$T_I' = T_I\left(\frac{1}{1 + \dfrac{R_I}{R_{fI}}}\right) = \frac{T_I}{1 + \dfrac{8.3}{83}} = \frac{T_I}{1.1}$$

$$T_I' = 0.91 \; T_I \; .$$

The controller was also tested by using it in place of a conventional pneumatic controller to control a fourth order liquid level process which was subjected to set point changes and process flow disturbances (12).

The controller performed at least as well as the conventional controller. However, changes in the settings of the flueric controller, particularly gain settings, were more difficult to accomplish than was the case for the conventional pneumatic controller. In addition, the flueric controller did use much more air than the conventional controller.

CONCLUSION

A proportional plus integral flueric controller, using the principle of flow summation, and constructed by using proprietary proportional fluid amplifiers has been described. Equations have been developed which define the conditions necessary for an ideal integral component in the control action, when only a moderately high open loop gain is used. The conditions necessary for equal controller gains for set point and measured value inputs have also been determined.

A method for determining the initial resistance settings for the controller has been outlined, and a setting up procedure given. These are especially useful when the two control port resistances of the flueric operational amplifier are significantly different.

Some indication has been given of the controller performance, when tested in isolation and in closed loop control of a process subjected to set point and load disturbances.

LIST OF REFERENCES

(1) Dexter, E.M. and Colston, J.R. *Pure Fluid Controls for Ship's Boiler*, Control Engineering, September, 1964.

(2) Colston, J.R. *A Pure Fluid Turbine Speed Control*, ASME Paper No. 64 WA/AUT-8.

(3) Chou, Q.B. *A Study of Analog Fluid Flow Amplifiers*, M.E. Thesis, University of New South Wales, 1965.

(4) Reason, J. *Boiler Control Proves Analog Fluidics*, Control Engineering, March, 1967.

(5) Barrett, J.A. and Wagner, R.E. *Developement of a Three Mode Control Using High Gain Fluid Amplifiers*, ASME Paper No. 67 WA/FE 35.

(6) Chou, Q.B. *Development of a Simple Fluidic Three Mode Controller*, 1969 Canadian National Conference on Automatic Control, University of Alberta, August, 1969, Preprint Volume.

(7) Payne, D.A. *A Design of a Fluidic Three Term Controller*, Preprint Volume, Automation and Fluid Power Symposium, Sydney, Australia, February, 1971.

(8) Carroll, J.J. and others, *Design and Development of a Fluidic Chamber Pressure Control Subsystem for the NERVA Engine*, Journal of Spacecraft and Rockets, September, 1971.

(9) Payne, D.A. *Design of a Fluidic Three Term Controller*, M.Eng.Sc. Thesis, Monash University, 1972.

(10) Stern, H. *Analog Fluidic Control is Now*, Chemical Technology, February, 1973.

(11) Bjornsen, B.G. *A Fluid Amplifier Pneumatic Controller*, Control Engineering, June, 1965, pp.88-93.

(12) Black, J.D. *Development of a Fluidic Process Controller*, M.Eng.Sc. Thesis, University of New South Wales, 1973.
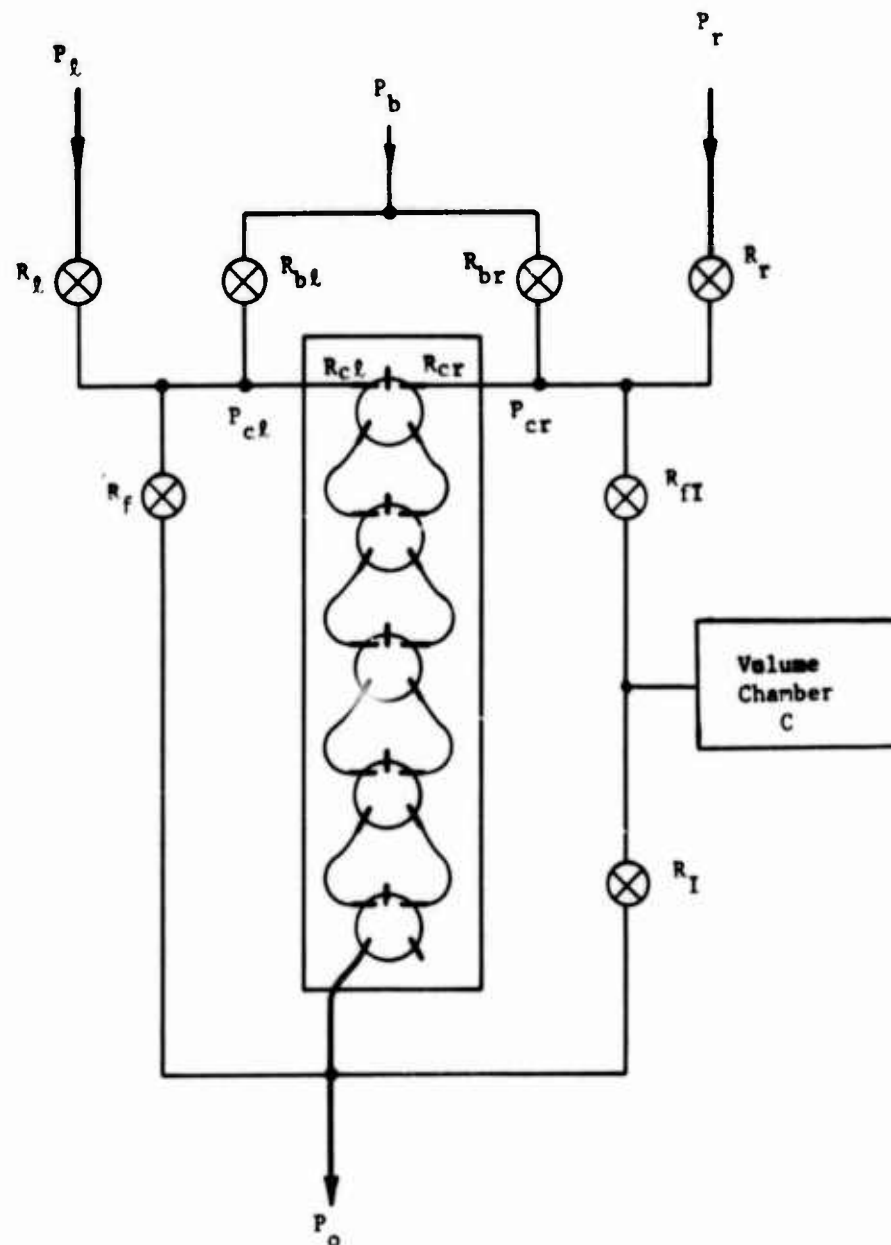
FIGURE 1

Schematic arrangement of proportional plus integral flueric
controller with five stage amplifier.
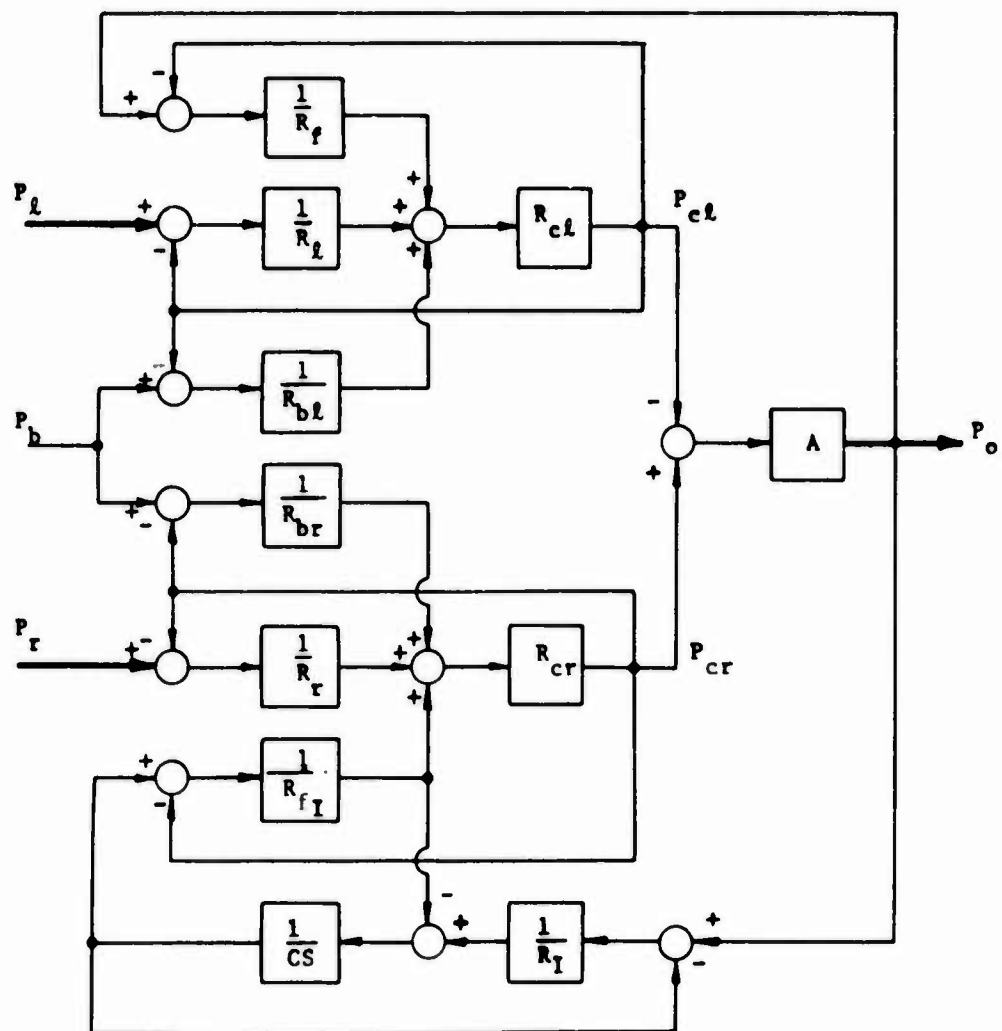
FIGURE 2

Block diagram of proportional plus integral flueric controller.

319
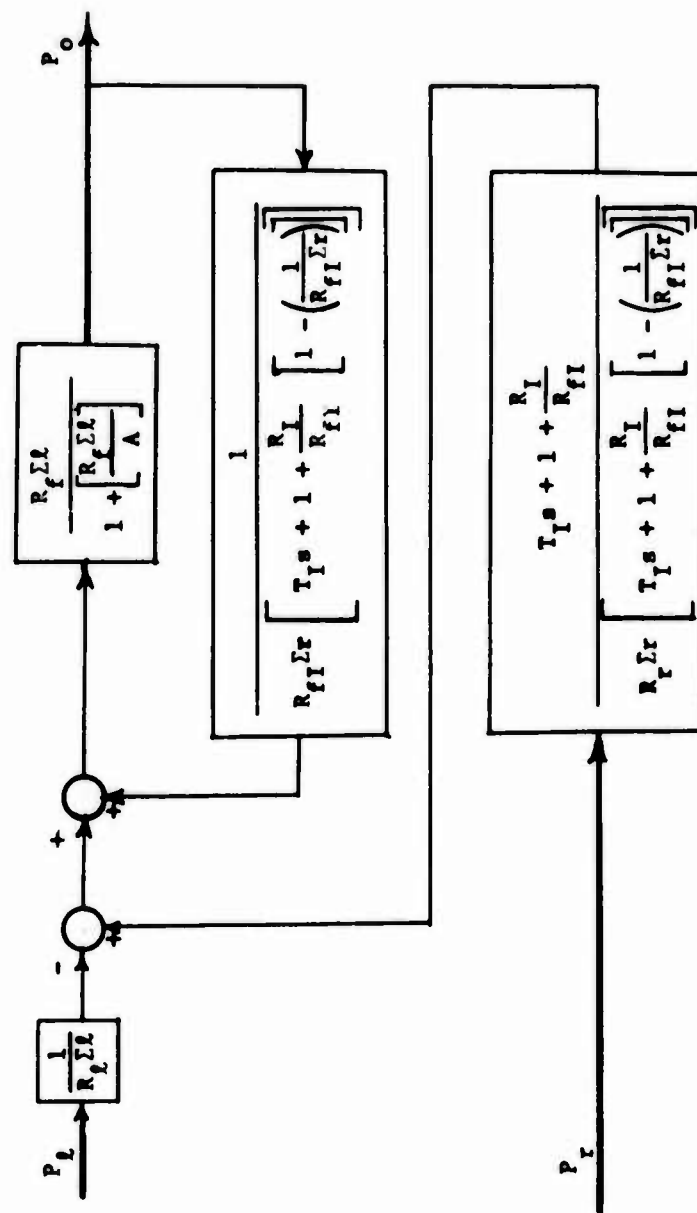
FIGURE 3

Partially reduced block diagram of proportional plus integral flueric controler.

320
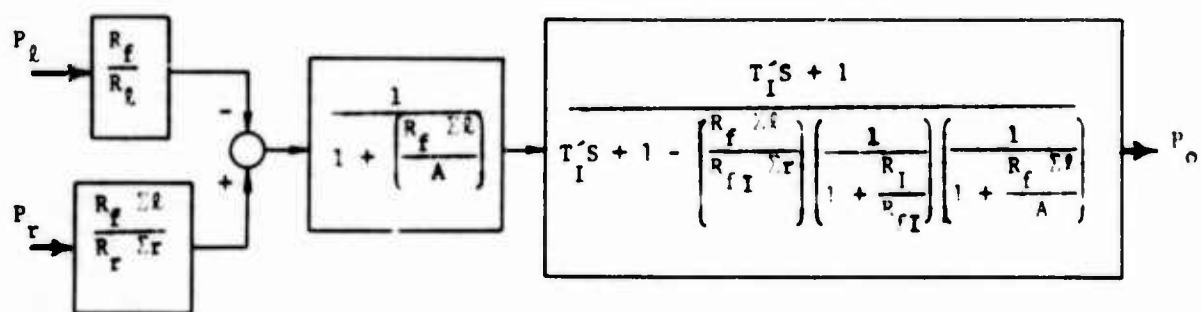
<u>FIGURE 4</u>

Reduced block diagram of proportional plus integral flueric controller.
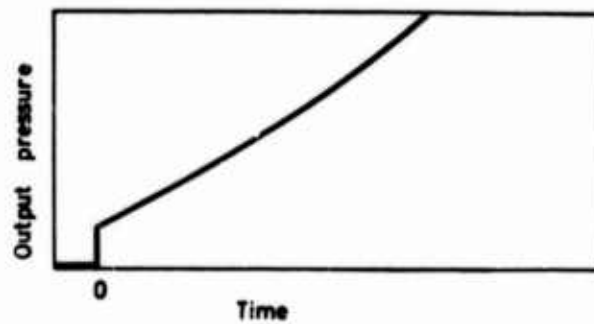
(a) Response of Unstable Controller.
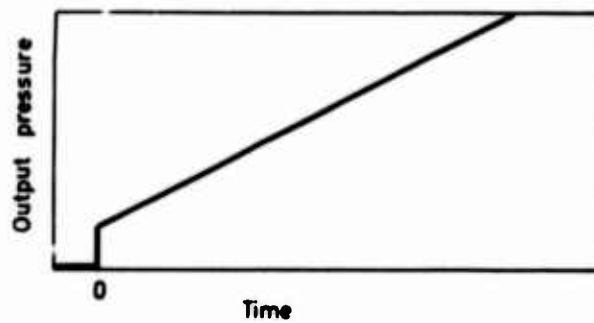
(b) Ideal response of critically stable controller.
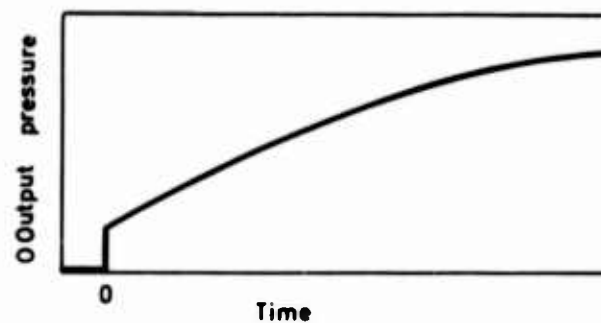
(c) Response of stable controller.

FIGURE 5

Responses of the two term controller to a step change in either
input at $t = 0$. The responses apply for the following values
of the Left Hand Side of equation (1):

Diagram (a) applies when LHS > 1
Diagram (b) applies when LHS = 1
Diagram (c) applies when LHS < 1

322
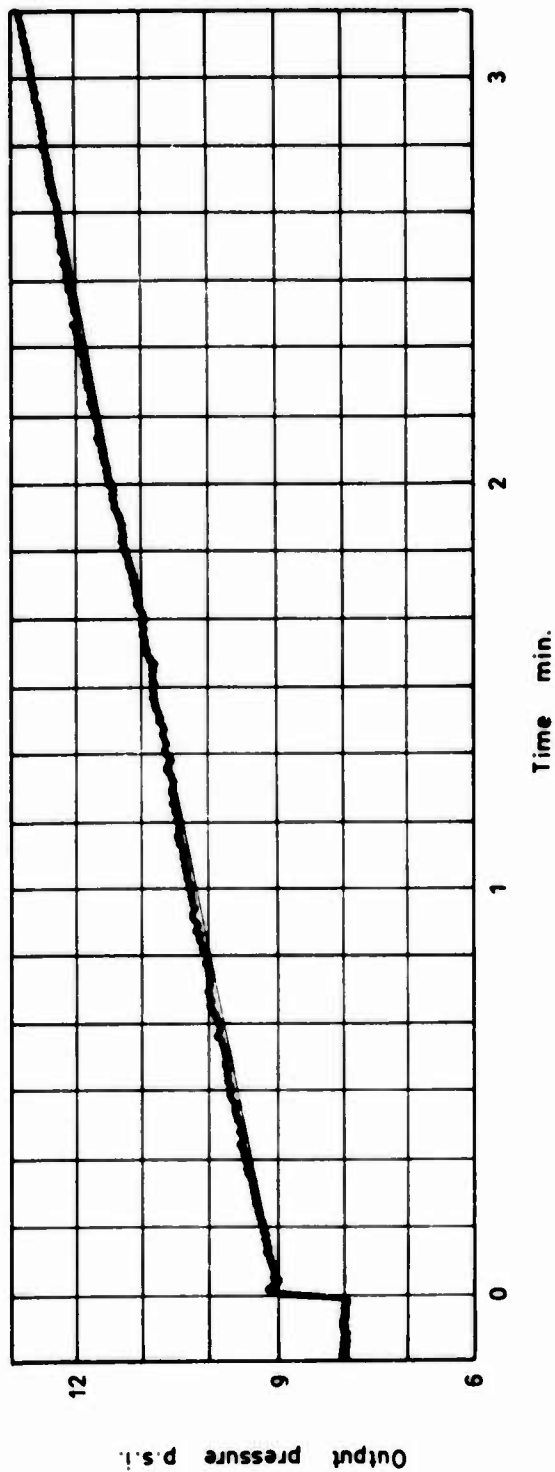
FIGURE 6

Response of isolated controller to a step change of 1 psi in right hand side input pressure after being adjusted for an ideal integral component of the control action.

Output pressure, P_o = 9 psig constant

Right hand input pressure p.s.i.

Left hand input pressure p.s.i.
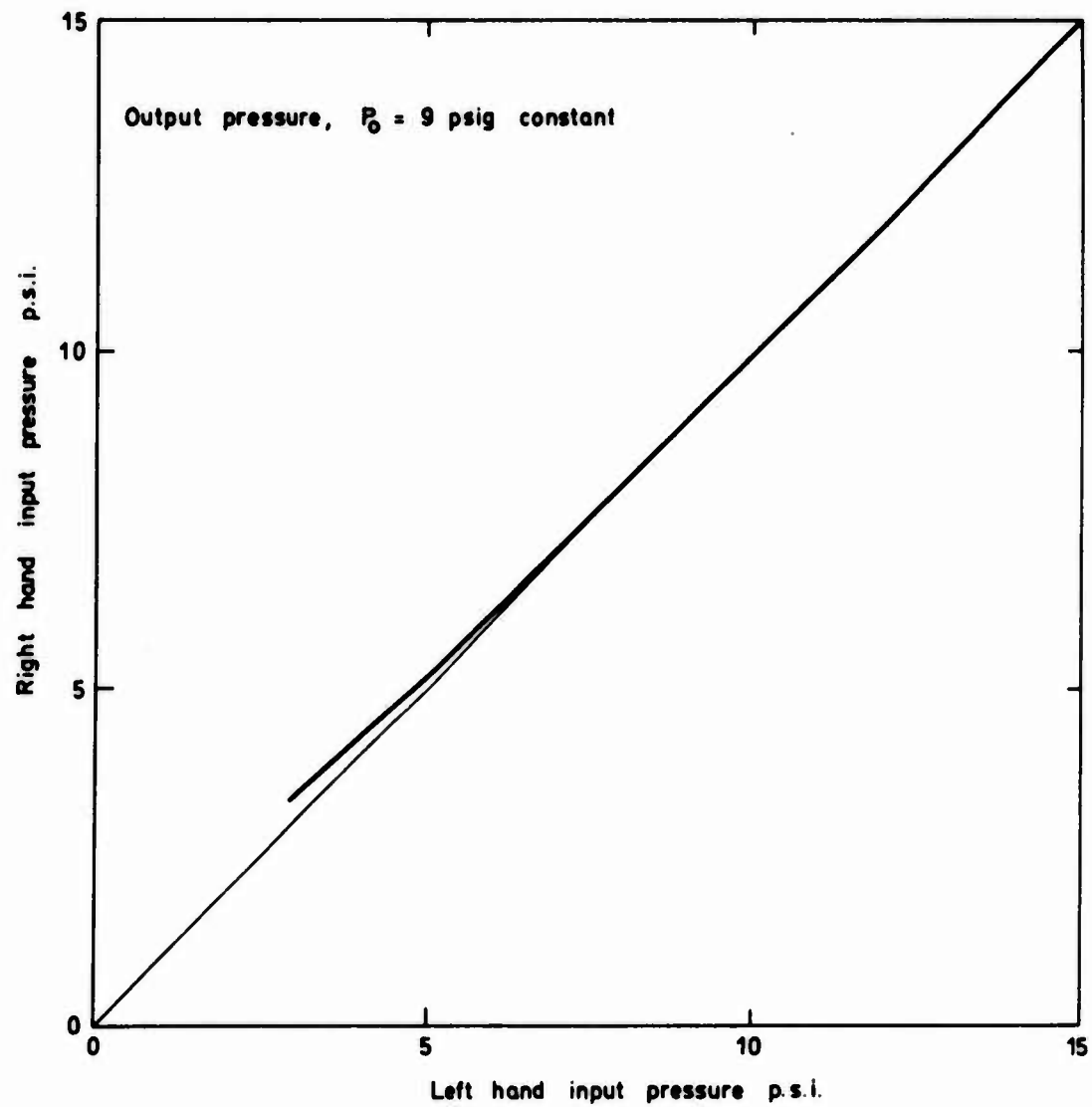
FIGURE 7

Values of right hand side input pressure P_r, which caused the controller to experience zero error, plotted against left hand side input pressure P_ℓ when the output pressure P_o was 9 psig.

324

FLUIDIC CARRIER TECHNIQUES

Willis A. Boothe

and

Carl G. Ringwall

General Electric Company
Schenectady, New York

March 1974

ABSTRACT

Both proportional (DC) and carrier modulation (AC) fluidic techniques have their own particular advantages in fluidic control system applications. In some cases, one is preferable over the other due to types of sensors used, length of signal transmission, and complexity of computation to be done by fluidics. In many cases, a combination of the two techniques is used.

This paper deals primarily with fluidic carrier techniques including pulse modulation. Proportional fluidic operational amplifiers are also briefly described, since they often appear in conjunction with fluidic carrier systems. In addition to the "building block" techniques of fluidic carrier systems, examples are given of their applications ranging from air motor governors to jet engine and missile controls.

NOMENCLATURE

f	=	Frequency of sensor output	(Hz)
Δf	=	Differential frequency between two sensor outputs	(Hz)
G	=	Forward gain of closed loop	
H	=	Feedback gain of closed loop	
K	=	Open loop gain of operational amplifier	
K_1, K_2	=	Gain constants of temperature sensors	$(Hz/{}^{\circ}R^{1/2})$
P	=	Pressure	(psig)
ΔP	=	Differential pressure	(psid)
R	=	Fluid resistance	(sec/in^2)
S	=	Laplace operator	(sec^{-1})
t	=	Absolute temperature	$({}^{\circ}R)$
T	=	Time constant	(sec)
W	=	Weight flow	(pound/sec)

FLUIDIC CARRIER TECHNIQUES

by

Willis A. Boothe*
General Electric Co.
Gas Turbine Products Division
Schenectady, N. Y.

and

Carl G. Ringwall
General Electric Co.
Specialty Fluidics Operation
Schenectady, N. Y.

1.0 INTRODUCTION

Fluidic devices are particularly attractive for use in many applications due to their insensitivity to vibration, radiation, and temperature extremes as well as their potential for high response and reliability. Equally important is the fact that fluidics presents an opportunity to use techniques analogous to electronic circuitry but without the restrictions imposed by the electronic art. Other papers presented at this symposium cover digital devices and proportional or analog circuitry. In this paper, the use of carrier techniques in fluidics is described. Temperature, position and shaft rotational velocity are among the parameters that can be sensed fluidically to produce a frequency proportional to the sensed parameter. Techniques for comparing such sensed signals to various frequency references are described in this paper as well as applications including pure carrier systems and those where a combination of proportional and carrier techniques have been used. Among the former are speed governors and temperature controls. Combined carrier and proportional control applications include a control for J-79 jet engine, a gas turbine overspeed control, and missile thrust vector controls.

2.0 PROPORTIONAL FLUIDIC TECHNIQUES

2.1 Basic Amplifiers

Since most fluidic carrier systems ultimately employ some proportional stages in their circuits, a brief review of proportional amplifiers is in order. (Professor Brown covers them in greater detail in his paper.

* Formerly with Corporate Research and Development, Schenectady, N.Y.

A basic typical proportional amplifier stage is a beam deflector amplifier of the type shown in Fig. 1 with a steady-state characteristic as shown in Fig. 2. The device has relatively low gain and the negative gain region after passing the maximum output point shown in Fig. 2 can be troublesome in circuits where it is possible to over-drive the amplifiers. However, the single stage proportional amplifier is entirely adequate for many applications. Each of these is a special case, the performance of each being dictated by the characteristics of the individual amplifier stage.

The advent of the high gain fluidic operational amplifier[5,14] has changed this picture completely. By use of a high gain, multi-stage fluidic operational amplifier, fluid circuits of considerable sophistication can be constructed without the need for detailed understanding of the internal characteristics of the individual fluidic elements. In addition, significant performance advantages are obtained.

2.2 Operational Amplifiers

The basic building block of fluidic operational amplifiers for air operation is the five stage proportional amplifier or gain block shown in Fig. 3. (This paper will deal with the air operated version, although a hydraulic fluidic operational amplifier has also been developed.)[1] Constructed of precision photo-etched metal laminates, the fluidic gain block has linear forward gains ranging up to 4000 and higher. Using advanced fluidic noise reduction techniques,[13] this gain block represents a significant advance in signal-to-noise ratio.

Normally, the operational amplifier is operated in a push-pull manner. As seen in Fig. 4, the input signal is a differential pressure, $p_{i_1} - p_{i_2}$, and the output is also a differential pressure, $p_{o_1} - p_{o_2}$. Operation in the push-pull manner provides increased linearity and also allows simple sign inversion by crossing over connections.

Open loop steady state characteristics of the gain block are shown in Fig. 5. It can be seen that the gain block has a flat saturation when over-driven by large input signals. Many single stage fluidic amplifiers have an undesirable gain reversal when over-driven in this manner. The five-stage gain block is balanced to assure a flat saturation characteristic with inputs up to 200 times that required to produce saturation. It will be seen later where this permits use of the gain block to perform accurate signal limiting functions in control circuits.

The output vs input curve of Fig. 5 is an actual x-y plotter trace that has been retraced five times to evaluate repeatability and hysteresis. In spite of the excessive over-driving of the gain block, no performance degradation has resulted. Figure 6 shows the same trace with the horizontal sensitivity increased by 20 in order to evaluate the linearity and stability

of the gain block. The output is linear over 80% of its range and demonstrates good stability with no hysteresis.

Along with a high gain amplifier, linear resistors and capacitors are used to generate feedback networks. The linear resistors are capillary passages etched in laminates, while the capacitors are simply volumes.

Using the powerful technique of feedback with a high gain amplifier, a number of desirable performance characteristics are obtained. Steady state characteristics that can be produced include:

- fixed gain under varying conditions of load and supply pressure

- accurate signal summation or subtraction

- signal limiting

- isolation amplifier

- very low output impedance amplifier

- adjustable gain amplifier

By choice of input and feedback circuitry, a variety of dynamic characteristics can also be generated:

- flat frequency response amplifier

- lag-lead

- lead-lag

- integrator (approximate)

- notch network

Techniques for obtaining these characteristics are given in Appendix I.

3. 0 FLUIDIC CARRIER TECHNIQUES

3. 1 Why "AC" Fluidics

A striking parallel exists between fluidics and electronic control development. The DC or proportional control approach has led to the development of operational amplifiers in both the fluidic and electronic case. This has proven to be an excellent solution for many control problems; yet, as in electronics, the fluidic engineer has gone on to exploit the field of carrier modulation, or AC techniques.

The reasons for this are several; the most compelling two being the availability of several types of AC fluidic sensors and the ability to transmit information accurately in modulated carrier form. The transmitted

330

information in the modulated carrier approach no longer depends on level or amplitude, but only the AC frequency characteristic of the signal. This results in a transmission system which is relatively insensitive to DC level changes, extraneous noise pickup, line losses and particularly leaks in the sensing lines.

Since precise fluidic frequency references are available, the AC fluidic techniques offer a means for high precision control not usually associated with straight DC fluidic systems.

To best describe the AC fluidic system approach, this section of the paper will first consider the characteristics of the AC fluidic signal, then describe typical AC fluidic system elements, and finally will explain specific AC fluidic circuits.

3.2 Characteristics of the AC Fluidic Signal

The use of the term "AC" when applied to fluidic signals may be misleading to those who carry the analogy between electrical and fluidic circuits too far. A more precise description of what is meant by the term AC (with respect to fluidic signals) might be "an undulating flow," or "an oscillatory flow superimposed on a steady flow." The important difference between the electrical and fluidic AC signal is that the fluidic signal always has a DC component in addition to the AC signal component.

The term signal, as generally used throughout this section will refer to the pressure changes occurring in the circuit. These pressure variations can either be referenced to the local atmospheric pressure, or to some other point in the circuit in which case the signal is differential pressure. The terms "single sided" and "push-pull" are sometimes used to describe the individual signal and the differential signal pair respectively. Signal amplitude encountered in AC fluidic circuit generally range from about 0.01 to 10 psi. More typical values are between 0.1 and 1.0 psi.

Operating frequencies for AC fluidic circuits are limited only by the response capabilities of the individual circuit elements and the interconnecting signal lines. Typical carrier frequencies used in present fluidic control systems range from about 100 Hz to over 3 K Hz depending on the type of control system. Speculation on the ultimate frequency limit for fluidic devices range from a conservative 10 K Hz up to a rather optimistic 100K Hz.

Transmission lines used in carrying AC carrier signals from sensors and transducers to the fluidic circuits have varied in length from a few inches up to 100 feet. One particular investigation carried out at the General Electric Company successfully demonstrated the capability to transmit a 400 Hz fluidic signal over 70 feet of line. The signal speed for AC

331

fluidic transmission is approximately equal to the acoustic velocity of the operating fluid. For air under normal conditions the acoustic velocity is about 1000 ft/sec. The corresponding time delay is thus about one milli-second per foot of transmission line.

3.3 AC Fluidic "Building Blocks"

To date, most AC fluidic work has used jet deflector type fluidic elements. The discussion of the basic building blocks is confined to these elements, but obviously many of these techniques can be implemented using other types of elements as well.

3.3.1 Amplifiers

The proportional amplifier is also used in ac fluidic systems. The characteristics of individual amplifier elements are well known, and the very high gain five-stage operational amplifier has been described in the Section 2.0 of this paper.

A third type of high gain amplifier is shown in Fig. 7. This device consists of three individual amplifier stages stacked in a vertical fashion. Typical gains achieved with this single module are around 100:1.

3.3.2 "Rectifiers"

In addition to the proportional amplifiers described above, a second class of amplifier is used extensively in AC fluidic circuits. This is the so-called rectifier or absolute value amplifier. It is essentially a conventional proportional amplifier with a single receiver centered in line with the power nozzle. Its input-output characteristic for steady-state conditions is shown in Fig. 8. If the differential input signal is zero, the power jet impinges fully on the single receiver and a maximum output level is achieved. If the jet is deflected on either direction, recovery decreases proportionally.

Figure 9 illustrates the output response of the rectifier to sinusoidal input signals of different amplitudes. After filtering, the average output pressure of the rectifier is seen to be inversely proportional to the input signal amplitude. This performance characteristic is made use of in most of the AC circuits which will be described later.

3.3.3 Decoupler (Derivative Circuit)

The "decoupler" circuit is shown schematically in Fig. 10. This element is used to convert a single-ended pressure signal to a differential push-pull signal. An AC input signal is divided into two separate paths by means of a pair of matched resistors. One leg of the divided signal is connected directly to one side of a proportional amplifier. The other signal leg is connected through a capacitor to the opposite side of the amplifier.

At very low frequencies the filtering effect of the capacitor is negligible resulting in a small differential control signal at the input to the amplifier. As the frequency increases the capacitor tends to attenuate the AC signal passing through it which results in a corresponding increase in the differential AC signal across the amplifier control ports. The transfer function describing this circuit arrangement is of the form:

$$\frac{\Delta P_o}{\Delta P} = \frac{Ks}{(1 + TS)} \tag{1}$$

3.3.4 Resonators

One of the most important passive devices in AC fluidics is the tuned resonator. It is frequently used as a frequency reference in modulated carrier systems employing either amplitude or phase discrimination.

The most common fluid resonator is the Helmholtz resonator which can best be characterized by the equivalent circuit of an inductance and capacitance in series. Better suited to fluidic applications due to impedance matching characteristics is the "parallel Helmholtz resonator." It consists of a parallel combination of a capacitor and inductor connected in a circuit as shown in Fig. 11. When the operating frequency of the input signal, P_i, approaches the tuned frequency of the resonator both the amplitude and phase of the resonant signal change as shown in Fig. 12. These rapid changes in the characteristic of the responding resonator signal can be used to provide closed loop control action to maintain the operating frequency at the resonant point. An application using this technique in a speed control system is discussed later.

In addition to the purely fluidic resonator shown in Fig. 11, an equivalent mechanical spring-mass system can be used to provide the same results. The primary reason for resorting to the spring-mass system in place of the Helmholtz resonator lies in the fact that the natural frequency of the Helmholtz device depends on the value of capacitance in the circuit. The capacitance in turn is a function of the gas temperature and is therefore subject to change if the ambient temperature is not constant.

In those cases where it is necessary to maintain a very accurate frequency reference a spring-mass resonator is used with special spring materials having low temperature coefficients. Figure 13 shows a miniature mechanical resonator designed for use in a governor system where the operating temperature is expected to vary over a wide range.

333

3.4 Typical AC Fluidic Circuits

3.4.1 Frequency-to-Analog Circuits

Three basic circuits have been used for the purpose of converting frequency signals to analog pressure signals. The most commonly used one is shown in Fig. 14. A rectifier is overdriven by the output of a fluidic flip-flop. The rate at which the rectifier is driven from one limit to the other is controlled by a time constant comprised of a capacitance and the output impedance of the flip-flop. The output of the rectifier is thus a constant area pulse, two pulses occur for each input cycle. The filtered output is an analog pressure directly related to the number of pulses per unit time.

Another circuit also utilizes a constant area pulse as shown in Fig. 15. The constant area pulse is generated by a capacitor in one leg of an "AND" element. The "AND" drives a flip-flop whose output is a pulse with the width determined by the time constant and the height determined by the supply pressure of the output flip-flop. This circuit produces one pulse for each input cycle and is characterized by very good linearity over the complete operating range.

A second frequency detecting circuit is shown in Fig. 16. In this particular case, the frequency sensitive element is a small inductive shorting tube connected across the control ports of the rectifier. At low frequencies the shorting tube effectively cancels the differential pressure signal across the rectifier input ports resulting in a maximum filtered output, P_o. As the operating frequency is increased, the inductive reactance of the shorting tube increases resulting in an increase in the differential amplitude across the rectifier input ports. The corresponding filtered output of the rectifier decreases in proportion to the increase in operating frequency.

3.4.2 Beat Detector

The difference between two independent frequency signals can easily be detected with fluidic elements. Figure 17 shows a circuit schematic for a fluidic beat frequency detector. Differential input signals from two separate frequency sources are first summed at the control ports of a proportional amplifier by means of fixed summing resistors. The amplified output signal from the proportional amplifier is connected to a rectifier element which provides the desired beat frequency detection after proper filtering. Figure 18 shows the characteristics of a typical beat detector.

3.4.3 Phase Discriminator

The fluidic phase discriminator detects both the polarity and magnitude of phase shift between a single-ended reference signal, and a differential phase-shifted signal. The circuit consists of two identical rectifier elements

334

connected in a symmetrical bridge arrangement as shown in Fig. 19. The average amplitudes of the differential control pressures acting on the rectifiers vary with the relative phase difference between the reference signal C, and the phase varying signal at A-B, as shown in Fig. 20. This variation in the average control signals results in a differential output signal (after filtering) which indicates both direction and magnitude of the phase difference. An application of this circuit will be described in Section 3.5.

3.4.4 Pulse Duration Modulation Circuits

The fluidic PDM circuit converts an analog input signal to a square wave AC carrier where the relative high pressure and low pressure duration in each cycle are a function of the input. PDM techniques are particularly attractive in applications requiring high power gain or high power output levels. The signal to noise ratio of a PDM Amplifier is established primarily by the low level summing of an analog signal and a triangular waveform. Additional power amplification by cascaded digital amplifier stages has only a second order effect on the overall S/N ratio.

A typical PDM circuit is shown in Fig. 21.

The circuit consists of a square wave oscillator followed by an integrator to convert the square wave to a triangular wave shape. The output of the integrator is summed with an analog signal in a proportional amplifier. A low hysteresis digital amplifier follows the summer. This amplifier is switched when the output of the summer reaches the switching threshold of the amplifier.

Linearity of the PDM circuit is determined by the integrator and summer. A high quality triangular wave must be generated and summed in an amplifier whose input impedance remains linear over the operating range.

The range of the circuit is determined by hysteresis of the digital amplifier following the summer.

An application of the PDM circuit to a thrust vector control is presented in Section 4.3.

4.0 AC FLUIDIC APPLICATIONS

The previous sections describe some of the building block elements and circuits of AC fluidics. It remains to show how these various pieces can be brought together to form a complete control system. The particular applications which will be described are considered typical and representative of the present state-of-the-art in AC fluidics.

335

4.1 AC Fluidic Governors

Governing shaft speed of a turbine or reciprocating engine is a natural application for fluidics. AC speed pickoffs can be used without need for gearing or any direct contact with the rotating shaft, and can produce a "single sided" or "push-pull" signal at the choice of the system designer.

Figure 22 shows the arrangement of AC fluidic components to perform the speed error detection for such a governor. In this case, a push-pull AC fluidic speed signal is used. The sensed speed signal is first amplified and converted to a differential signal A-B. This differential signal pair is connected to a phase discrimination circuit identical to Fig. 19. One side of the differential signal is also connected to a tuned resonator which in turn is connected to the third input port on the phase discriminator.

When the sensed speed signal is equal to the tuned resonator frequency, a 90° phase lag occurs across the resonator as shown. If the speed is varied above or below the natural frequency of the resonator a corresponding increase or decrease in phase shift results across the resonator. The differential signal amplitudes appearing across the control ports of the rectifiers in the phase discriminator circuit are dependent on the vector differences between B-C and A-C as illustrated in Fig. 23. When the operating frequency equals the natural frequency of the resonator a 90° phase difference occurs across both B-C and A-C which results in equal outputs from both rectifiers (zero differential signal). Varying the operating frequency above or below the resonant point results in an unbalance of input amplitudes to the rectifier pair. This in turn results in a corresponding variation in the differential output pressure from the discriminator circuit as shown in Fig. 24.

Normally, from this point on, the signal processing in governing systems uses dc techniques as described in Section 2.0.

4.1.1 Overspeed Sensor for Gas Turbine

The more demanding control applications frequently call for a combination of proportional and carrier modulation techniques. One such control is a fluidic overspeed sensor for a small turbo-shaft engine. Here, the use of a "chopper" type fluidic speed sensor precludes the need for one power take-off shaft and reduction gearing. This provides the opportunity for considerable simplification of the engine design which could represent a major weight saving on smaller engines. [6, 7]

The "overspeed sensor" actually includes the power turbine rotor speed sensor (chopper), speed reference oscillator and associated circuitry, signal summer and gain amplifier, ground checkout means and a built-in filter and regulator. The engine to be controlled is an advanced 1500 SPH

turboshaft engine. The control must handle "worst case" system failures such as sudden loss of load. One example is failure and breakaway of one or more helicopter rotor blades. Another case would result from certain conceivable failures of a main power transmission gearbox. Under such conditions, the overspeed sensor must effect engine shutdown within 2% of set point speed.

In such an application, fluidics has unique capabilities unmatched by other control means. To protect against a power turbine shaft failure, the chopper speed pickoff is located near the power turbine at the hot aft end of the engine. (Although a more favorable environment exists at the forward end, location of the speed pickoff, there would be no protection against power turbine shaft failure.) The signal lines from the chopper pass through the hot exhaust section of the turbine. Sensing of power turbine speed is accomplished without mechanical contact with the rotor shaft and without compromises to the design of the rotor bearings, bearing sump, or air-oil seals.

The functional block diagram of the control is shown in Fig. 25 and the schematic diagram in Fig. 26. Basically, the control uses an AC speed signal from the chopper, runs through a decoupler to convert to push-pull AC signal and, after amplification, is run through a frequency-to-analog-converter circuit resulting in a DC pressure signal, P_c, proportional to the sensed shaft frequency. The AC output of a fixed frequency oscillator using a mechanical resonator reference is run through a similar circuit resulting in a reference pressure, P_r, proportional to the set point frequency. This is done to eliminate effects of drifts in supply air pressure and temperature. Pressures P_r and P_c are compared in a summing amplifier and, when P_c exceeds P_r, a sharp proportional rise in output P_o results. The output P_o is transmitted to the main fuel control of the engine where a diaphragm operated pilot valve varies the reference fuel pressure behind the bypass pressure regulator valve. Upon the onset of overspeed, the regulator reference pressure is decreased, causing more fuel to be bypassed thus sharply reducing fuel flow to the engine. The net result is a proportional or droop overspeed governor action.

Figure 27 shows the overspeed sensor with and without its cover. The basic manifold is hexagonal in shape with the various fluidic circuit modules mounted on the flats. The supply air filter and pressure regulator are contained in the center of the hexagon. This assembly is designed for supply air temperature of -65° to 400°F with ambient temperatures of -65° to 250°F, and uses a compensated resonator reference torsional spring which maintains a frequency band within 0.25% over this range. All of the major elements, components and circuits have been tested for functional performance at varying supply and ambient pressures typical of sea level to over 25000 ft. altitude. The assembly weight is 0.7 pounds compared to an initial design goal of 1.0 pounds. One means of weight reduction is the use of an aluminum manifold which is sufficient for this temperature range.

Substitution of stainless steel for the aluminum manifolding, higher temperature resonator pivot material in place of Ni-Span C, and metal seals for the elastomeric O rings will raise temperature capability to 1200°F.

The fluidic overspeed sensor represents a conceptually simple combination of AC and DC fluidics which has proven capable of meeting a demanding application.

4.1.2 Speed Control for Air Motor

Air motors, when operated from a fixed supply source, experience wide variations in motor speed with load and have excessive air consumption when unloaded. These characteristics can be significantly improved by a speed governing system. Such a system detects the speed of the motor and adjusts the supply to maintain a preselected speed.

One approach to the speed control of an air motor is an all-pneumatic system making use of fluidic techniques for sensing, amplifying, and comparing the speed signal with a preselected reference. A governor utilizing this approach (Fig. 28) has been successfully applied to industrial air motors ranging from 1/25 to over 5 HP.

Figure 29 illustrates the functional arrangement of a governed air motor system. The speed of the motor is detected by connecting a tube (typically 1/4 in. OD) between the exhaust port and the input to the governor. The pressure pulsations caused by the vanes or pistons passing the exhaust port are transmitted through the tubing to the governor as an acoustic frequency. These pressure pulsations are interfaced with the governor by means of a simple diaphragm which acts as a blocking capacitor, passing the desired frequency signal while blocking the steady-state pressure level.

The pneumatic frequency signal is next converted to a proportional pressure level and compared with a preset reference pressure to produce a differential speed error signal. This speed error signal is then amplified by means of a multi-stage fluidic amplifier and interfaced with a volume booster valve to produce the required air supply pressure for the motor.

Exhaust Speed Signal

The pressure pulsations associated with the air motor exhaust are caused by the passage of the vanes or pistons by the exhaust port, allowing the sudden release of the working pressure. Typically, the pressure drop across the exhaust port of an air motor is about 80 percent of the incoming supply pressure. This rather high discharge pressure is due to the limited expansion permitted through the motor. A typical time trace of the pressure pulsations in air motor exhaust is shown in Fig. 30. Considerable

338

attenuation has occurred due to the internal volume between the exhaust port and the point of measurement.

From the general shape and spacing of the exhaust pulsations, it is seen that the wave form is made up of a number of higher harmonics in addition to the fundamental frequency representing motor speed. Unless some care is taken in adapting the sensing line to the exhaust port, these higher harmonics can be accentuated and transmitted to the governor as an erroneous signal.

Selection of a non-resonating type exhaust muffler will usually insure successful signal detection. Muffler designs which provide a diffusing flow through a porous media, such as felt or sintered metal, are generally preferred over a reflecting chamber design.

A second cause of faulty signal transmission is the transmitting line itself. If the line is not sized properly, it is possible to set up various standing wave patterns which will cause signal cancellation at certain frequencies. This problem can be solved in a classical manner by terminating the transmission line with its characteristic impedance (proper size orifice venting at atmosphere). A simpler approach, which avoids the need for "fine tuning", is to use a line that is sufficiently "lossy" to minimize reflected waves and avoid cancellation. A 1/4-in. tube in excess of 2 ft. in length will generally provide satisfactory performance.

Signal De-coupler

The acoustic signal is interfaced to the governor through a flexible diaphragm which acts similar to an audio speaker. Acting on one side of the diaphragm is the total exhaust pressure made up of the steady-state back pressure due to the muffler and the small pressure pulsations due to the cyclic discharge of working volume. The opposite side of the diaphragm produces an oscillating pumping action in response to the exhaust pulsations. Any variation in steady-state exhaust pressure is rejected by the diaphragm. The diaphragm also serves two other important functions. It provides some additional signal rejection of the higher harmonics that may be present, and it prevents any oil or contamination from entering the governor circuit.

Frequency to Analog Conversion

The decoupled speed signal is processed by a frequency to analog circuit similar to the circuit used in the overspeed sensor (Fig. 26).

Comparator Amplifier

Once the motor speed has been detected and converted to a useable pressure signal, it is compared to a reference pressure representing the

339

desired operating speed. The difference between the actual speed signal and the reference is the error signal used to provide the necessary corrective action. This error signal is produced by means of a differential fluidic amplifier which sums the tachometer signal with a preselected reference pressure. The difference is amplified and then used to operating a conventional volume booster relay valve. The relay valve provides an additional pressure amplification as well as the required volume flow to power the air motor. This added pressure gain is needed to match the relatively low fluidic pressure levels (typically 10 psi) with the maximum operating pressures required by the air motor.

Dynamic Considerations

As with any closed loop controller, it is necessary to consider total system dynamics to some extent before going too far with the application. The size of motor, type of load, and characteristic of the duty cycle all play some part in the overall performance of the system.

At one extreme, an application may consist of a large motor driving a low inertia load with little damping. In this case, care must be exercised to insure a stable operating condition is achieved by slowing down the high frequency response. In other applications, the opposite extreme may be encountered where the nature of the load is such that a very sluggish performance will exist unless special effort is made to maximize the higher frequency response.

In most applications, it is impractical to change the various gain values or load characteristics to satisfy particular stability requirements. Instead, it is much simpler to design a system which is slightly unstable but has the ability to be compensated.

The compensation technique used on the fluidic governor is to simply add a small volume in the tachometer circuit. This volume (which can be a pressure gage) slows down the speed signal sufficiently to prevent any undesirable oscillations. From a performance standpoint, the delay volume in the tachometer circuit acts similar to an increase in load inertia. Typical crossover frequencies for properly compensated governor systems range between 5 and 10 rad/sec.

4.2 Fluidic Control for a J-79 Engine

Another earlier application[12] of combined AC and DC fluidics represents a more complex system requirement. This application consisted of a fluidic demonstrator control of the J79-GE-15 jet engine. The broad scope of this program was to develop fluidic hardware to perform the function of engine-speed governing and transient-fuel control. Transient-fuel control

includes control of fuel flow during engine starting and during engine speed changes, and is required to prevent compressor stall and turbine over-temperature.

4.2.1 Control Mode

The first item of work under the program was to establish a method of controlling the engine that was compatible with the engine requirements and the capabilities of fluidics. This was accomplished using both analog and digital-computer simulations in parallel with preliminary component and sub-system development. As a result of these studies, the following control mode evolved:

Steady State

- The corrected rotor speed of the engine is scheduled as a function of the pilot's throttle position (α_{fa}) and is maintained by varying engine fuel flow (W_f).

- A maximum speed-limit circuit is incorporated to prevent the engine physical speed from exceeding the maximum allowable speed limit of 7420 rpm.

Transient

In the starting range, the engine fuel flow is scheduled as a function of compressor discharge static pressure (CDP). At a speed just below idle (4200 rpm), control of fuel flow is switched to the acceleration fuel limit.

During engine accelerations, the rate of change of fuel flow (dW_f/dt) is limited as a function of compressor discharge static pressure. This schedule was established to provide as fast an acceleration as possible and still prevent compressor stall and turbine overtemperature.

The deceleration fuel schedule, required to prevent a combustor blow out during a throttle chop, was made the mirror image of the acceleration schedule.

4.2.2 Control Mechanization

Figure 31 shows the control system block diagram. The regular hydro-mechanical main fuel control was modified to include an interface unit to accept a pneumatic differential pressure input from the fluidic control. The interface unit, consisting of a bellows-operated servo valve, provides a hydraulic supply output to the metering valve power piston which slews the fuel-metering valve at a velocity proportional to the pneumatic differential pressure input signal. Pressure drop across the fuel metering valve ports

341

is maintained by a pressure-drop regulator and fuel bypass valve. Thus, the position of the fuel valve is directly related to engine fuel flow. A fluidic transducer on the fuel valve provides a position feedback signal from the fuel valve to the fluidic control.

A manually operated mode selector valve permits selection of engine fuel control by the normal hydromechanical control or by the pneumatic input signal from the fluidic control.

For engine checkout purposes, the selector valve can be positioned to allow operation in the normal hydromechanical control mode. During either mode of fuel control, the compressor variable stators are controlled by the hydromechanical control.

The fluidic control provides the following four functions:

1. Control of steady-state corrected speed as a function of fuel

2. Protection of the engine by imposing limits on

   - overspeed

   - stall margin

   - turbine inlet temperature

3. Provision for servo stability by compensating the engine time constant.

4. Engine start.

Figure 32 shows a simplified circuit schematic for normal operation. A brief description of the four control functions follows.

Speed Controls. Engine speed is sensed by a specially-designed tachometer which converts speed to pneumatic sine wave; two speed-governor receive this pneumatic signal. One governor compares corrected speed with that requested by the pilot (via throttle motion). The other governor is a fixed frequency topping governor. Both governors use circuitry as in Fig. 22. In the case of the corrected speed governor, the resonator is a variable volume Helmholtz resonator. The volume is a function of throttle motion, and it is continually flushed with compressor inlet air by means of an ejector. Hence, a given throttle position calls for a given corrected speed by setting resonator volume. The fixed frequency topping governor uses a mechanical resonator similar in principle to that of Fig. 13 set to hold a maximum engine speed of 7420 rpm. The two governor output signals are differential pressures representing speed error of each governor. These two signals are processed by the selector-limiter circuit so as to pass the signal of the governor demanding the lowest set point speed. As will be explained shortly, this selected error is subsequently limited proportional to CDP to provide the acceleration and deceleration schedules. The

limited output ΔP is applied to the servo loop input as a fuel-metering-valve rate demand. To understand operation of the selector, refer to the simplified circuit diagram, Fig. 33. Assume engine speed is at 98 percent speed and the topping governor is set to override at 100 percent speed. Further assume that the pilot demands an overspeed condition of 105 percent speed. The polarities of the speed signals are indicated by the presence of dashed lines at the input to proportional amplifiers 3 and 4. Actually, pressures are applied on all four input lines but, since only differential values are of interest, we will assume for simplicity that the solid lines are at zero/gage pressure. Since the pilot-controlled corrected speed governor is set above the topping governor, its speed error is proportionally greater as noted by the heavier dashed lines. A comparison between these signals is made at amplifier number 1 and a proportional jet deflection is obtained. Amplifier 2 is a digital device which is triggered by amplifier 1. This amplifier has only on-off capability and is actually the power supply to amplifier 3 or 4. For the example chosen, only the top-speed error amplifier has its power supply activated, since element number 2 is switched to element number 4. Therefore, the top-speed governor pressure signal is passed through to the selector output. Even though a corrected speed error is present at all times, this signal is disabled because amplifier number 3 has no power supply. The control is automatically switched back to the corrected governor when the throttle is retarded since, for this case, the lowest set point would then be corrected speed.

Limits Control. Transient fuel limit control is performed by limiting the selected speed error signal proportional to CDP thereby generating acceleration/deceleration schedules which protect the engine from compressor stall and turbine over-temperature. The final output of this loop is a differential pressure signal which requests a safe metering-valve rate on which to control the engine.

The limiting of the selector speed error signal is accomplished by taking advantage of the inherent characteristics of fluidic operational amplifiers. The saturation levels at the amplifier output are directly related to the power supply. If the amplifier supply pressure is proportional to CDP, the amplifier output will saturate and the speed-error limit will be controlled directly by CDP. Proper design of the saturation levels effectively controls the acceleration and deceleration schedules. Operational amplifiers are used here because of their flat saturation characteristics and because negative feedback around the amplifier maintains nearly constant forward gain independent of supply pressure--an important consideration when operating between the limit conditions.

Operation of the limiter can be best illustrated by referring to an X-Y recording of the amplifier characteristics at variable supply pressures (variable CDP). Figure 34 is an X-Y recording of output differential pressure versus input differential pressure.

343

For low values of CDP, low saturations are achieved. When speed demand is nulled with engine speed, circuit operation is within the proportional band of the limiter. Negative saturations are the deceleration limit and positive saturations are the acceleration limit. As CDP increases so do the saturation levels.

Servo Loop. The function of the servo loop is to convert the output of the limit circuit to fuel flow and actually control engine speed. Beginning with the outermost loop, the action of the rate transducer is to make possible an integration between speed error and fuel flow which makes the overall control isochronous, i.e., capable of holding speed at zero error. This transducer is lagged at a time constant to compensate the engine dynamics. The integrator inserted in the loop makes the loop a type 1 servo capable of controlling metering-valve rate at zero error. The action of the integrator converts metering-valve rate error to its integral which is metering-valve position. This position command signal, in the form of a differential pressure, is converted to actual metering-valve position in the innermost position loop. (This innermost position loop has already been discussed in Section 2.3.2.) A tapered metering port then produces fuel flow proportional to position. Ultimately, fuel flow drives the engine, and the entire loop is closed through engine speed.

Implementation of the servo loop was by operational amplifier techniques. Of particular interest is the integrator which, using techniques similar to those of section 2.3.7 achieved integration rates on this control using 3 cubic inch volumes which would have required a 1 gallon can using the more usual approach to integration (high forward gain lagged with RC networks).

Start Controls. Fluidic circuits are used to convert the control loop to a start configuration as shown in Fig. 35. A single pressure pulse, applied by the pilot, disconnects both the selector output and rate feedback to the servo loop. Simultaneously, fluidic pressure feedback is established around the integrator, making the combination a simple pressure repeating loop. CDP, applied to the input, then effectively becomes fuel to the engine. As speed builds up so does CDP, and a start schedule of fuel flow versus CDP is established. Design of the start schedule must be such that sufficient fuel flow is added to accelerate the engine but not overtemperature the turbine or stall the compressor. At a speed of 4200 rpm, the circuitry automatically switches from the start configuration to the operate configuration and engine speed moves in a smooth transient to the speed set on the pilot's speed governor. Normal procedure is to set the pilot's throttle to idle speed on start.

The speed switch circuit functions are as follows:

1. Generate a speed signal which is directly proportional to the speed of the engine.

344

2. Recognize the one speed where controlling is required and generate a digital output signal at the speed; this digital output is the power supply to an operational amplifier in the start circuit.

The latter circuit requirements dictate the following components.

1. A speed sensor which is mounted to the engine generates a speed signal. Actually the unused output of one speed-governor circuit driver is employed, thus requiring no additional hardware to generate this signal.

2. A Helmholtz resonator which is used for speed recognition.

3. A Helmholtz coupler amplifier (OR/NOR Fluid Amplifier) which is used for coupling the resonator to an amplifier.

4. Amplification (digital-amplifier element) and final conversion (Flip-flop element).

The complete speed switch circuit is shown in Fig. 36. The curve of Fig. 37 represents amplitude characteristics of the Helmholtz resonator.

Operation of the speed switch can be best summarized by considering the circuit operation as the engine is accelerated through the switch point. Assume initially that a reset pulse is applied to the converter's control port "H" (refer to Fig. 36) and that the speed signal applied to the Helmholtz resonator is well below the resonant frequency of the resonator. This corresponds to the circuit condition at LIGHTOFF.

A summary of the state of the circuit elements is as follows:

(A) Coupler's supply flow-directed toward digital amplifier's control port "E"

(B) Digital amplifier's supply flow-dumping to atmosphere through output port "F"

(C) Converter's supply flow-directed toward load R_K through port "K"

Assume that engine speed increases due to the action of the start schedule and the pressure signal to the Helmholtz resonator is increased in frequency until the Helmholtz output signal is sufficient in amplitude to switch the coupler element. Most repeatable switching characteristics are achieved if the switch point is set at the resonator half-power point which is the largest rate of change of amplitude with frequency.

Once the switch is obtained, the positive feedback connected between the output of the circuit to the coupler input effectively "latches" the control onto the rate schedule. The output will remain in this condition until a reset pulse is applied to port "H".

345

4.2.3 Control Construction

A modular design approach was employed in the control hardware assembly. Circuits performing like functions or circuits that could be identified as a development module were individually mounted on aluminum panels and interconnected with stainless steel tubing. The modular approach also allowed a maximum of development flexibility and ease of measurement at key points in the system.

The control is engine mounted and consumes 1 lb/min of air at 25 psig. If bled from the compressor at a pressure ratio of 3:1, this air consumption would require approximately 1.3 hp turbine power. It is estimated that, if aircraft packaging techniques were used, the fluidic as well as all hydraulic components (including the variable stator system) could be packaged in a volume of 360 cu in.

Figure 38 is a photo of the control.

4.2.4 Engine Test Results

The complete control system was entirely engine mounted and steel tubing was used for all fluidic system interconnections.

In over 11 hours of engine operation, the fluidic control system successfully controlled the engine during starting and during steady-state and transient operation between idle and 100 percent speed. The transient operation included numerous throttle bursts and chops between 5400 rpm (idle) and 7420 rpm (100 percent). The acceleration time from idle to 100 percent speed was approximately 4 sec. Also, throttle "Bodes,"* in which the throttle was chopped from 100 percent speed to idle and as speed was passing through approximately 6000 rpm was readvanced to 100 percent speed, were made. A typical time trace of engine speed during a throttle Bode is shown in Fig. 39. In this severest of transient tests, no stalls were encountered.

One problem area identified during the engine test was an approximate ±0.4 percent speed fluctuation about a steady-state speed point. A post-engine test investigation on an engine-simulator bench test stand has indicated that excessive phase shift across the metering valve and engine caused the observed speed fluctuation. Figure 40 is an oscilloscope photograph taken on the simulator stand and shows the instanteous speed-holding accuracy of the control. The top trace shows transient speed wobble (approximately ±0.12 percent) at the nominal anticipated loop phase shift.

_____

*A throttle chop followed by an advance of the throttle when the engine is passing through a specified speed range.

Additional phase shift, over and above that for which the fluidic control dynamics were designed, was probably present during the engine test run. The lower trace illustrates the effect of 30° less phase margin on the speed-holding capability of the control. In this case, the oscillation increased to ±0.48 percent of set point, a condition representative of actual engine test experience. The oscillations were not a servo instability but rather amplified noise resulting from underdamping of the entire loop through the engine. This effect has been substantiated analytically and is eliminated by increased phase lead across the servo loop.

The ability of the control to hold the <u>average</u> set-point speed was excellent. Figure 41 presents four digital tapes taken during the post-engine test-bench investigation. Readings were sampled six times per minute. On a statistical basis, the worst speed-holding accuracy obtained was 0.033 percent of set point (one standard deviation); the lower part of Fig. 41 summarizes the reduced data. Due to the long sampling times, transient speed perturbations are not reflected in Fig. 41.

Subsequent to the engine test, the control was returned to the bench test setup and subjected to air-inlet temperatures up to 750F while varying the power supply pressure ±20 percent. Satisfactory control operation was obtained under these extended conditions.

4.3 Temperature Controller

The ability to accurately sense and control high gas temperatures is a serious problem, particularly in propulsion engines. Conventional methods using thermoelectric devices are limited by the relatively low operating temperature capability of the materials. Oxidation and corrosion can also be serious problems when using these devices in typical hot gas atmospheres. Fluidic techniques now offer the ability to sense gaseous temperatures up to the limits imposed by the material properties of the sensors.

The operation of the fluidic temperature sensor makes use of the temperature sensitivity of an acoustical whistle. A portion of the hot gas to be controlled is used to produce a high frequency whistle in a specially designed cavity. The actual frequency produced by the whistle is proportional to the acoustic velocity of the gas which in turn is approximately proportional to the square root of the absolute gas temperature. For a particular sensor design the operating temperature can be calibrated in terms of the resulting whistle frequency.

The frequency level generated in most fluidic temperature sensors is in the range of several thousand cycles per second. This very high frequency level can be scaled down by an order of magnitude or more by comparing the sensor frequency to a reference frequency. The frequency difference between the sensor and reference is obtained in a beat frequency detector and used for control purposes.

347

A particular circuit arrangement for a fluidic temperature control[8] which has been successfully demonstrated by the General Electric Company is shown in Fig. 42. This design uses two whistle type sensors tuned such that their frequency difference is relatively small. Each individual sensor frequency is proportional to the square root of the absolute gas temperature. If the difference of these relatively high frequencies is obtained, then it too will be proportional to the square root of the absolute temperature.

$$f_1 = K_1 \sqrt{t}$$

$$f_2 = K_2 \sqrt{t}$$

$$\Delta f = f_1 - f_2 = (K_1 - K_2)\sqrt{t}$$

The detection of the frequency difference signal is accomplished by means of a fluidic beat frequency detector as previously described and shown in Fig. 17.

Conversion of the relatively low frequency temperature signal from the beat detector to a DC or analog pressure can be accomplished with a frequency-to-analog circuit. Another method for providing this final DC control signal is to use the same basic speed control circuit illustrated in Fig. 22. The input frequency in this case would represent temperature rather than speed and the tuned resonant frequency would correspond to a desired operating temperature. The output differential pressure represents deviation of temperature from the desired value.

4.4 A Fluidic PDM for Thrust Vector Control

A PDM unit shown in Fig. 43 was developed for a specific missile application in which a pneumatic analog signal from a two axis attitude gyro reference required conversion to a PDM output capable of driving the two sets of guidance control actuators on a missile.

Design Requirements

The requirements for this PDM circuit were as follows:

● Input command signal levels of less than ±0.3 psi pressure and 0.05 scfm flow.

● Output control pressures to the actuators of 10 psi differential across the load at a minimum flow rate per channel of 2.8 scfm.

● The linearity of output pressure ΔP_o for the full range of input control pressure ΔP_c to be within ±10% of the point setting or 2% of the maximum ΔP_o, whichever is greater.

- Operating range of PDM modulation up to ±90%.

- Gain of the unit to be adjustable over the range 87%/0.1 psi to 29%/0.1 psi.

- Operate within the above specifications over a temperature range of -20 to 165F.

- The PDM circuit design must also meet all missile shock and vibration design specifications.

Circuit Design

The circuit design shown in block diagram form in Fig. 44 employs commercially available fluidic element and resistor components. A single oscillator drives two identical PDM circuits each controlling one attitude axis.

The triangular wave oscillator is made of an integrator (12) and flip-flops (10 and 11) interconnected as a negative feedback oscillator. Thus, when flip-flops (10 and 11) switch they provide a step input to the integrator. The integrated step input provides a ramp output. When the amplitude of the ramp output from the integrator equals the threshold of the flip-flop (10), the latter switches and provides the opposite polarity step input to the integrator. The integrator then provides a ramp output in the opposite direction. Thus, the output of the integrator produces a triangular wave. The integrator is of the positive feedback type using one stage of amplification.

The triangular wave and the analog input signal are summed in amplifier (2). An amplifier stage (1) is used between the command input signal from the rate gyros and the proportional summer to provide necessary signal level matching at the summing point. The resistors on the output of amplifier #1 are of a variable type which can be independently adjusted. Gain, or percent modulation/psi, is adjusted by changing each resistor an equal amount. Bias is adjusted by changing only one resistor to maintain gain exactly constant.

The output of the proportional summer drives a staged digital amplifier made up of elements (3) through (6) utilizing flip-flops to provide the function of bistability with memory. Supply pressures are cascaded from 5 to 60 psi to provide the necessary power amplification to drive the final output amplifiers.

The final output amplifier, elements (8) and (9) have 0.02 x 0.064 inch power nozzles. Two amplifiers per channel are used each providing 1.4 scfm at 10 psi. The outputs of these two amplifiers can then be paralleled to provide the design flow requirement of 2.8 scfm. Element (7) is similar to elements (8) and (9) and provides the necessary power gain. Elements (7) through (9) operate with 60 psig supply. This circuit diagram (Fig. 3) illustrates the magnitude and number of the various types of fluidic elements required to mechanize the PDM.

KEY COMPONENTS

The successful implementation of the PDM circuit resulted from three key components; namely (1) the trangular wave oscillator, (2) the summer, and (3) a highly efficient output amplifier stage. As a result of an innovative oscillator circuit configuration a reliable and clean sawtooth triangular pressure wave shape was developed. A typical trace of the oscillator output is shown in Fig. 45.

In the design of the summing amplifier attention was directed toward minimizing the switching hysteresis by impedance and level matching techniques to achieve the performance accuracies required of the PDM.

4.4 PDM Circuit Fabrication

The unit was constructed entirely of stainless steel laminates except for the end plates and resistor knobs, which were machined elements. Final assembly of the unit was performed by diffusion bonding. The PDM circuit when completely assembled and bonded, contains 44 differently configured laminates of various stacked numbers, 0.010 + 0.004 inches in thickness, totaling 175 laminations per PDM circuit stack. The configuration as shown provides an integrated circuit possessing an extremely high packaging density. The material used in the fabrication was Type 304 stainless steel.

PDM Performance Results

Figure 46 is a direct tracing of an oscillograph recording of the typical PDM output at 0% modulation and at both $\pm 85\%$ modulation. The percent modulation determined from this recorded data is measured at the switching initiating points for each cycle. It should be noted that the recording equipment could not completely follow the pressure changes during the switching cycle; hence, the variance in spike height is not meaningful.

The output linearity and gain change capability obtainable with this PDM unit are shown in Fig. 47. The symmetry of both channel outputs for the fluidic circuit is also graphically shown. The data in this figure was obtained at both the 29% modulation minimum gain and 87% modulation maximum gain settings.

This development effort has included the fabrication of 20 PDM units under contracts to the U.S. Army Missile Command Guidance and Control Directorate, Redstone Arsenal, Alabama.

5.0 CONCLUSIONS

Both proportional and carrier techniques offer their own unique advantage to the control designer. At the risk of oversimplification it can be said

that AC techniques offer advantages where signals must be transmitted over a distance or face attenuation or interference by other means; where very accurate references are needed, and where AC types of sensors are preferable due to accuracy, response, or installation requirements. For flexibility of circuitry and ability to perform a variety of computations including frequency shaping, DC techniques usually have an advantage. Certain AC circuits are available to perform a limited number of such functions, [11] but each is fairly specialized. In general, where a-c techniques are used, they appear in conjunction with d-c amplifiers to close the loop.

It is apparent that fluidics offers a demonstrated tolerance to difficult environments that is not achievable by other means. This and the expanding functional capabilities of fluidics gives the control designer important new tools for solving the control problems of the 70's.

6.0 REFERENCES

1. W. A. Boothe and L. R. Kelley, "Hydraulic Fluidics," ASME Paper No. 68-WA/FE-26 (Nov. 1968).

2. W. A. Boothe, C. G. Ringwall, and J. N. Shinn, "New Fluid Amplifier Techniques for Speed Controls," SAE Paper No. 650355 (May 1965).

3. W. A. Boothe and C. W. Woodson, "AC Fluidic Systems," General Electric TIS Report 66-C-434 (Nov. 1966).

4. J. R. Colston and E. M. Dexter, "Applications of Pure Fluid Techniques to a Speed Control," 1964 HDL Fluid Amplification Symp. Proceedings.

5. M. C. Doherty, "Applying Fluidic Operational Amplifiers," ISA Paper No. 68-943 (Oct. 1968).

6. R. G. Furgurson, "Accessories for Small Gas Turbine Engines," SAE Paper No. 680450 (1968).

7. H. B. Kast and D. E. Jehling, "Fluidic Overspeed Sensor for a Power Turbine," ASME Paper.

8. L. R. Kelley, "A Fluidic Temperature Control Using Frequency Modulation and Phase Discrimination," JACC Conf., Seattle, Wash., Aug. 1966.

9. R. Khol, "AC Fluidics," Mach. Design, Feb. 6, 1969.

10. R. T. Mattle and J. N. Shinn, "Fluidic Compensation for a Pneumatic Position Servo," Oct. 1967, Report prepared for NASA, Marshall Space Flight Center, Huntsville, Ala., Contract NAS 8-5408, by the General Electric Research and Development Center.

11. C. G. Ringwall, "Fluidic Processing of Alternating Pressure Signals," ASME Paper No. 67-WA/FE-43.

12. R. K. Rose and W. L. Phipps, "Fluidic Control of a J-79 Turbojet Engine," ASME Paper No. 67-WA/FE-33.

13. J. N. Shinn and L. R. Kelley, "Noise in Fluidic Proportional Amplifiers," Paper G-1, Third Cranfield Fluidic Conf., May 9, 1968.

14. T. F. Urbanosky, "Fluidic Operational Amplifier Survey," SAE Paper No. 670707 (Oct. 1967).

15. C. W. Woodson, "AC Fluidics," 1968 Wescon Conf. Paper.

16. C. W. Woodson, "Speed Control for an Air Motor using Fluidics Techniques," ASME Paper No. 73-DE-35.

APPENDIX I

Operational Amplifier Analysis and Dynamic Compensation

I. Basic Operational Amplifier Analysis

A simple first order analysis shows some of the direct analogies between the electronic and fluidic operational amplifier. Figure I-1 shows a basic single-sided operational amplifier circuit of the simplest type. It consists of an input resistor R_i, a feedback resistor R_f, the high gain amplifier of gain $-K$, and its inherent input resistance R_c. Current or flow is designated as W and pressure as P. Applying Kirchoff's law to the flow into the summing function:

$$W_1 + W_2 = W_3. \tag{1}$$

Rewriting in terms of resistance and pressure gives

$$\frac{P_i - P_g}{R_i} + \frac{P_o - P_g}{R_f} = \frac{P_g}{R_c} \tag{2}$$

Noting that $P_o = K P_g$, $\tag{3}$

P_g can be eliminated from Eq. (2) to give

$$\frac{-P_o}{P_i} = \frac{R_f}{R_i} \left[\frac{K\left(1 + \dfrac{\dfrac{1}{R_f}}{R_i} + \dfrac{R_f}{R_c}\right)}{1 + K\left(1 + \dfrac{\dfrac{1}{R_f}}{R_i} + \dfrac{R_f}{R_c}\right)} \right] \tag{4}$$

It can be shown in a similar manner that when a push-pull amplifier of the form of Fig. 1 of the main text is used, the relationship of the push-pull output signal ΔP_o to the push-pull input signal ΔP_i is

$$\frac{-\Delta P_o}{\Delta P_i} = \frac{R_f}{R_i} \left[\frac{K\left(1 + \dfrac{1}{\dfrac{R_f}{R_i} + \dfrac{R_f}{R_c}}\right)}{1 + K\left(1 + \dfrac{1}{\dfrac{R_f}{R_i} + \dfrac{R_f}{R_c}}\right)} \right] \tag{4a}$$

This implies, of course, that the usual practice be that the input resistors R_i be the same on both inputs and the feedback resistors be the same on both outputs.

Now, rewrite Eq. (4) in the more familiar control system terms by the substitution of

$$G = K \tag{5}$$

for the forward gain of the loop, and

$$H = \frac{1}{1 + \dfrac{R_f}{R_i} + \dfrac{R_f}{R_c}} \tag{6}$$

for the feedback gain. The result is

$$\frac{-\Delta P_o}{\Delta P_i} = \frac{R_f}{R_i} \left(\frac{GH}{1 + GH}\right) \tag{7}$$

Now note that, when the loop gain, GH, is large Eq. (7) shows that the transfer function is determined primarily by the passive input and feedback resistors. As long as the loop gain GH is large, variations in the value of G (amplifier gain) due to variations in loading or supply pressure are virtually eliminated from the transfer function.

The above analysis is simplified in many ways. In particular, the circuit itself is the simplest possible. By adding capacitors to various parts of the circuit, frequency shaping functions can be accomplished. By using parallel input resistors, signal summing or subtraction are possible. These variations will be discussed in later sections.

The other major simplification of the above analysis is the assumption that the gain block is a pure gain. In reality, the gain block dynamics are approximately those of a pure time delay without attenuation in the frequency range of interest (less than 1000 Hz). This fact must be considered when

354

evaluating the stability of any fluidic operational amplifier. To have stability, the open loop transfer function, GH, of the operational amplifier must be attenuated below unity gain before 180° of phase shift are accumulated. Where G is a pure time delay with no attenuation, and H is made up entirely of resistive terms as in Eq. (6), it is obvious that 180° of phase lag will build up without any attenuation. In practice, the gain block can be represented by the equation

$$G = Ke^{-T_1 S}. \tag{8}$$

where T_1, the transport lag, has an approximate value of 5.5×10^{-4} sec and S is the Laplace operator.

To assure stability, some attenuation must be added. This is done by use of small capacitors (volumes) on the output of the amplifier, resulting in the open loop transfer function

$$GH = \frac{KH}{1 + T_2 S} e^{-T_1 S} \tag{9}$$

where H is already defined by Eq. (6) and T_2 is the RC time constant of the stabilizing volumes. Normally, T_2 is relatively large so that it can be considered to contribute 90° of phase lag to GH at loop crossover frequency. The lag contribution of the gain block is about 0.2 deg/Hz. Thus, if 40° of phase margin is desired, the gain block lag can be only 50° which occurs at 250 Hz. T_2 and H must, therefore, be adjusted to assure unity gain at 250 Hz or less.

The closed loop transfer function is not limited in frequency response directly by the break frequency of the stabilizing volumes. The lag in this expression appears as

$$\frac{\Delta P_o}{\Delta P_i} = \frac{R_f}{R_i} \left(\frac{GH}{1 + GH} \right) \left(\frac{1}{1 + \frac{T_2}{1 + GH} S} \right) \left(e^{-T_1 S} \right) \tag{10}$$

Thus, the closed-loop lag time constant is the stabilizing lag, T_2, reduced by the quantity $(1 + GH)$. This is the frequency where the open loop transfer function has unity gain.

In normal system design, the small phase lag contributed by the operational amplifier is neglected and the simple transfer function of Eq. (7) is employed.

2.3 Operational Amplifier Circuit Characteristics

2.3.1 Flat Response Amplifier

This is the simplest and most common application of fluidic operational amplifiers. The principal requirements are that the transfer function be an accurate and constant amplification independent of the input frequency, supply pressure variations, load conditions, and input null level (bias level).

The basic circuit is shown in Fig. I-2.

Figure I-3 shows plotter tracers of pressure-gain characteristics of a Model FS-12 amplifier with supply pressure and load variations. Note the insensitivity of gain to changes in load, indicating virtually no closed loop output resistance. Feedback also assures no change of gain with supply pressure.

Typical frequency response is shown in Fig. I-4. The gain is frequency independent, or flat out to approximately 200 Hz.

2.3.2 Summation Amplifier

By adding input resistors, additional inputs can be used to provide signal summation, as shown in phantom lines of Fig. I-2. This type operational amplifier is used in many fluidic control circuits where sensing, computation, and logic are accomplished at very low power levels and then amplified to a higher power level actuatior. Large power ampification can cause inaccuracies so that often a closed loop is required. The FS-12 can provide a block of the amplification and the summation junction for this type of loop.

A typical application is the fuel valve position loop shown in Fig. I-5. (This loop is part of the J-79 fuel control described in a later section of this paper.) The fuel valve position loop, shown in Fig. I-5 provides fuel flow proportional to a low pressure fluidic input signal. The fixed gain amplifier is used to provide an amplification of 45 and to sum the feedback position signal of the rotary fuel metering valve with the input signal. The position feedback transducer consists of an eccentric cam on the fuel valve shaft and a flapper nozzle sensor.

The transfer function for the summing amplifier can be developed in a manner similar to the single input amplifier of Eq. (7) as

$$\Delta P_o = \Delta P_a \, \frac{R_f}{R_a}\left(\frac{GH}{1 + GH}\right) + \Delta P_b \, \frac{R_f}{R_b}\left(\frac{GH}{1 + GH}\right)$$

or   (11)

$$\Delta P_o \simeq \Delta P_a \; \frac{R_f}{R_a} + \Delta P_a \; \frac{R_f}{R_b} \qquad\qquad (11 \text{ Cont'd.})$$

Typical pressure-gain plots for this type of amplifier are shown in Fig. I-6. Each input channel is shown to have a gain of 45. Summing accuracy is demonstrated by the plot of a single input signal summed with itself and subtracted from itself. The gains for these two cases are 90 and zero which agree with the predicted gain from Eq. (11).

2.3.3 Isolation Amplifier

The characteristic high input impedance of the fluidic operation amplifier has frequently been used as an isolation amplifier. The FS-12 has been used to uncouple or isolate a pneumatic sensor from a fluidic circuit either to minimize the loading effects on the sensor, or because of a high dc level on the sensor output. An operational amplifier has been designed for this purpose which has an input impedance 100 times greater than that of a typical 0.020" x 0.020" power nozzle fluidic amplifier.

2.3.4 Adjustable Gain Amplifier

A recent additional feature of the operational amplifiers has been the use of a variable feedback resistor. Pressure-gain performance plots of this type device are shown in Fig. I-7. All the features of the fixed gain amplifier are maintained and the gain is adjustable with an external knob over a 10 to 1 range. Figure I-8 is a photo of this amplifier which also has the capability of summing three input signals. In almost all controls work is desirable to have some external gain adjustable to have some external gain adjustment to compensate for design inaccuracies. The adjustable gain operational amplifier provides this function for fluidic control systems.

2.3.5 Simple Lag

Occasionally only a moderate lag is required in fluidic systems. If a passive RC lag is employed it introduces attenuation or requires large volumes. When this is undesirable the operational amplifier circuit of Fig. I-2 can be modified by the addition of a capacitor in the input resistor to provide this function. This device provides up to a one second lag with a gain of five using small volumes on a compact hardware module. This type device has been applied to compensate for lags in engines or actuators, or in series with the lag-lead circuit to cancel out the lead term. Accurate summing can also be performed by this device. Two such amplifiers are being used in a fluidic circuit under development for a Naval aircraft carrier approach power compensator control. Angle of attack of the aircraft is sensed and the requirement is to treat it with the following transfer function.

$$\frac{\Delta P_o}{\Delta P_i} = \frac{1.23}{S} + \frac{9}{1 + 0.75S} \cdot \qquad (12)$$

The fluidic circuit has been mechanized as shown by the block diagram of Fig. I-9. The two leg circuits and one lag-lead provide this precise dynamic transfer function in three simple blocks.

2.3.6 Lead-lag

Many high performance analog control circuits require derivative action to compensate either the dynamics of the load or of other control components. This function is readily accomplished with fluidic operational amplifier techniques by adding a capacitor into the feedback path of Fig. I-2. This produces a lead-lag circuit or proportional plus derivative action. A typical application is a fluidic position control loop for a rocket engine actuator[10]. Figure I-10 is a block diagram of the control. The lead-lag circuit in series with two single stage flow amplifiers and a servovalve accept the position error signal from a flapper-nozzle valve and drive a 1000 psi hot gas actuator. The dynamic response characteristics of the lead-lag are shown in Fig. I-11. This device produces 65° of phase lead to compensate the compliance of the actuator. The addition of the two stage of flow amplification reduce this phase lead by less than 5°.

2.3.7 Integration

Integration is the most difficult frequency dependent function to mechanize in fluidics because of the absence of the series capacitor. Whether the connections to a fixed volume capacitor are in series or parallel the resulting transfer function is that of a shunt capacitor to ground. This precludes the use of the analogous electronic circuit to obtain integration, an operational amplifier with a series capacitor as the feedback.

Proportional plus integral action, which approximates integral, has been mechanized in fluidics by using positive feedback. A capacitor to lag a positive feedback path and an equal but un-lagged negative feedback path result in a lag-lead circuit having the following transfer function

$$\frac{\Delta P_o}{\Delta P_i} = K T_2 \frac{(1 + T_1 S)}{(1 + T_2 S)} \qquad (13a)$$

where K is the integrating rate or the gain at 1 radian/sec, T_2 is the lag or integrating time constant and T_1 the lead time constant. The lag time constant can be up to 60 seconds so that the approximation

$$1 + T_2 S \approx T_2 S \text{ for } T_2 S \gg 1$$

The transfer function becomes

$$\frac{\Delta P_o}{\Delta P_i} \simeq \frac{K}{S} + T_1 \tag{13b}$$

This is proportional plus integral control action. It is used in closed loop control systems subjected to sustained disturbances or load variations to eliminate steady-state error or droop. The lead term of equation (13a) could be eliminated with the addition of a simple lag in series, but this is rarely required because pure integral control tends to produce instability.

A typical application for a fluidic lag-lead circuit is in an isochronous governor for a shipboard steam turbine. The block diagram of this control is shown in Fig. I-12. A fluidic speed error signal is treated to produce a proportional plus integral action pressure signal. This signal is amplified and drives the main steam valve. The actual control has governed a simulated turbine-generator in accordance with the latest stringent military specification for shipboard governors, MIL-G-21410. Frequency response data for the lag-lead circuit are shown in Fig. I-13.
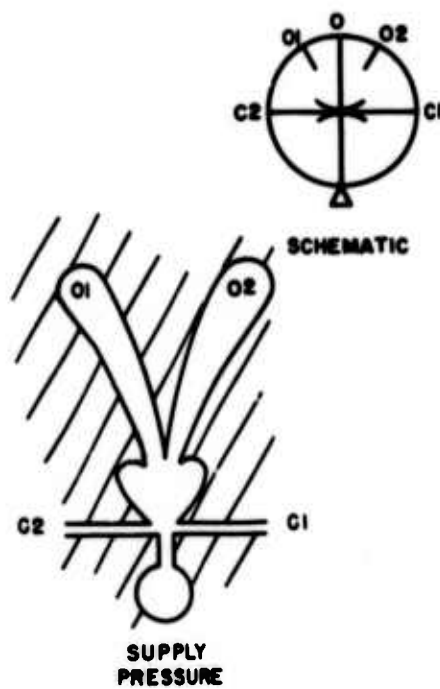
BEAM DEFLECTOR AMPLIFIER

Figure 1
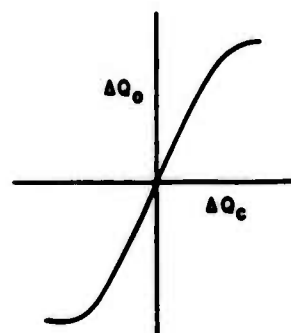
$$\Delta Q_o = Q_{o2} - Q_{o1}$$
$$\Delta Q_c = Q_{c2} - Q_{c1}$$

CHARACTERISTIC

STEADY-STATE CHARACTERISTIC

Figure 2

360
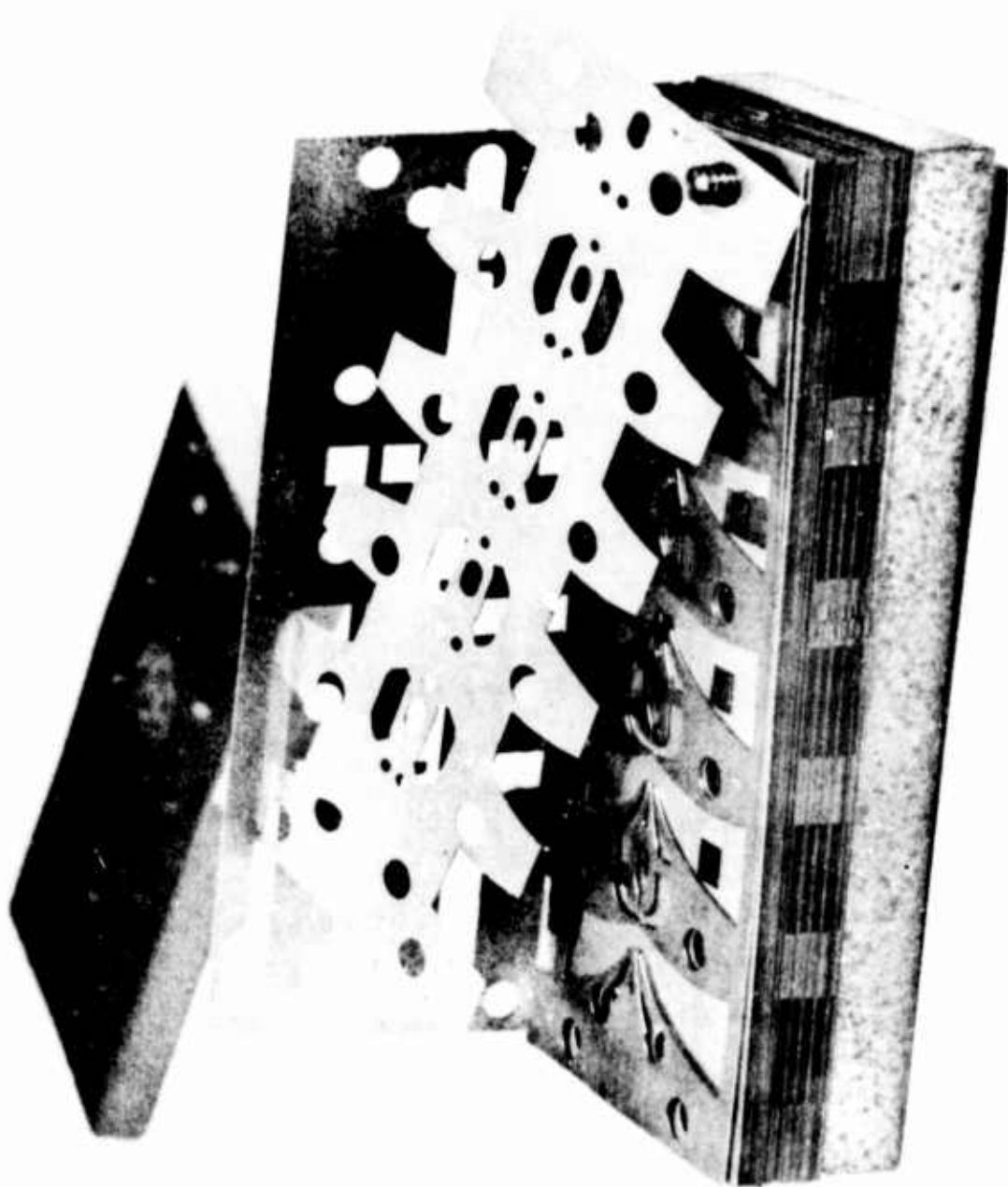
FIGURE 3. FIVE-STAGE PROPORTIONAL AMPLIFIER
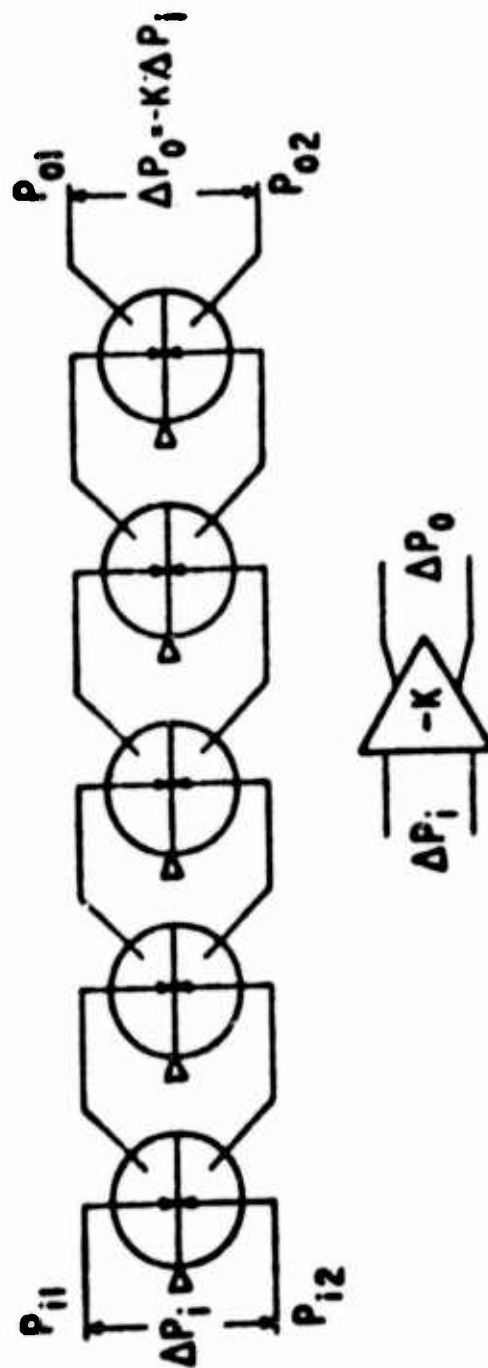
FIGURE 4 Gain block schematic diagrams.
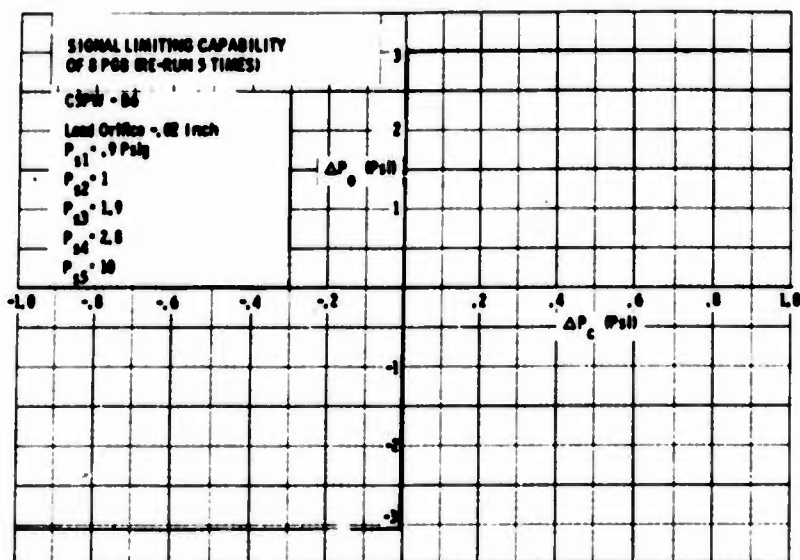
FIGURE 5. SIGNAL LIMITING CAPABILITY OF GAIN BLOCK
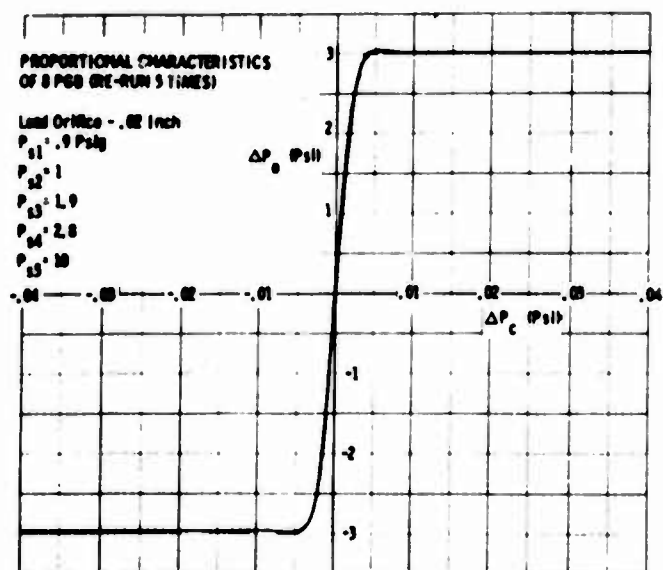
FIGURE 6. PROPORTIONAL CHARACTERISTICS OF GAIN BLOCK
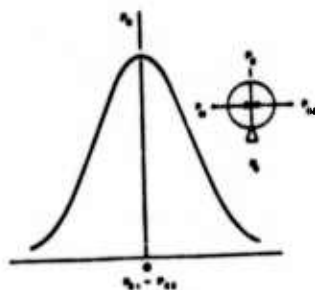
363
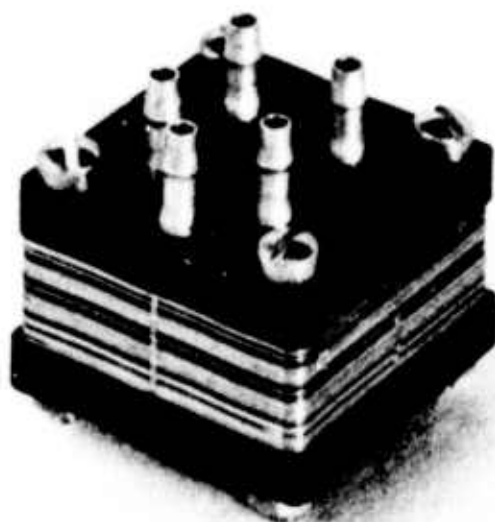
FIGURE 7. THREE-STAGE GAIN MODULE
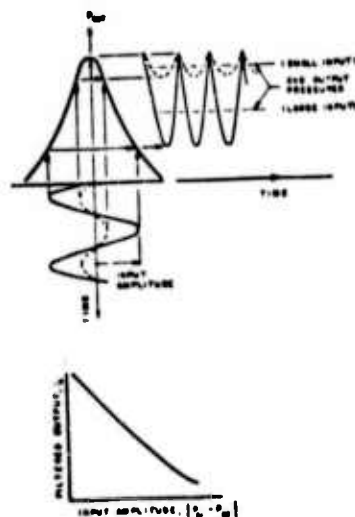
364

Fig. 8 Rectifier steady-state performance.

Fig. 9 Rectifier ac characteristics.
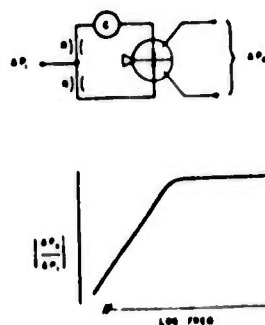
Fig. 10 Decoupler circuit.

365
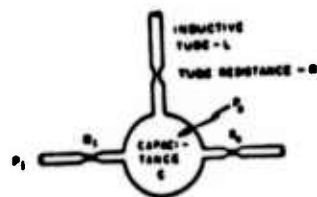
(a) Fluidic schematic
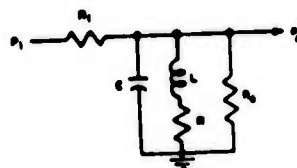
(b) Electrical analogy

FIGURE 11. PARALLEL HELMHOLTZ RESONATOR
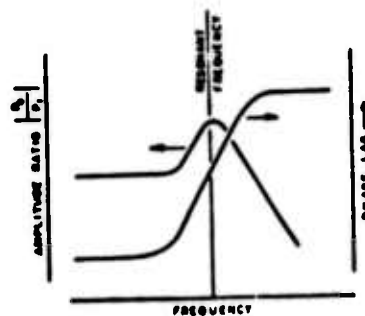
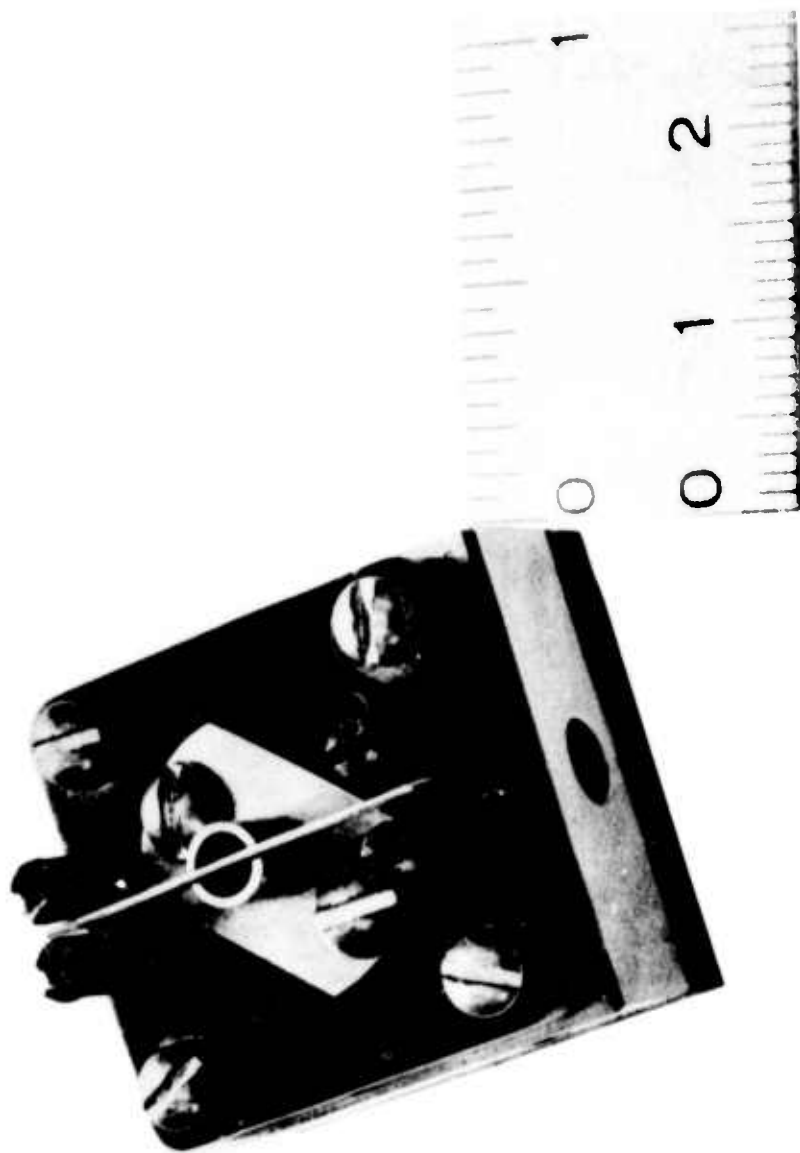**FIGURE 12. RESPONSE CHARACTERISTICS OF THE HELMHOLTZ RESONATOR**
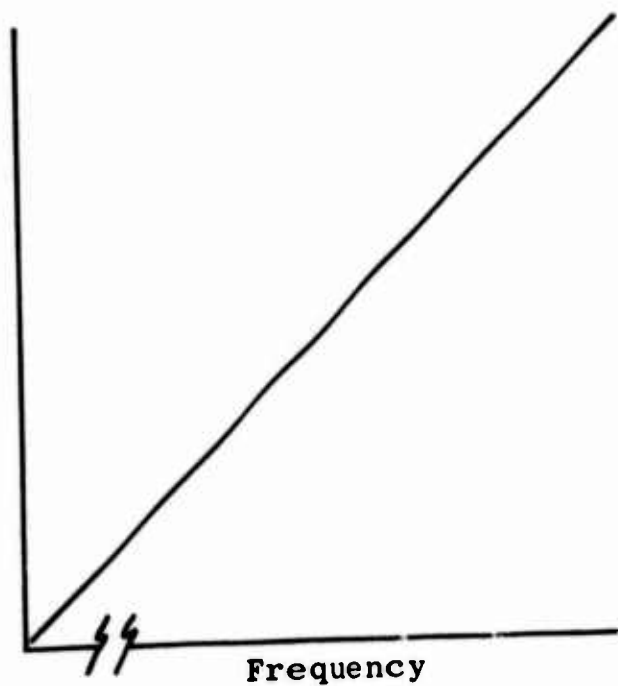
366

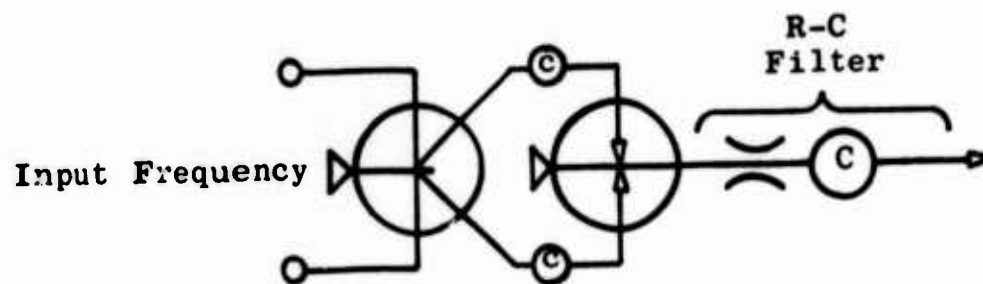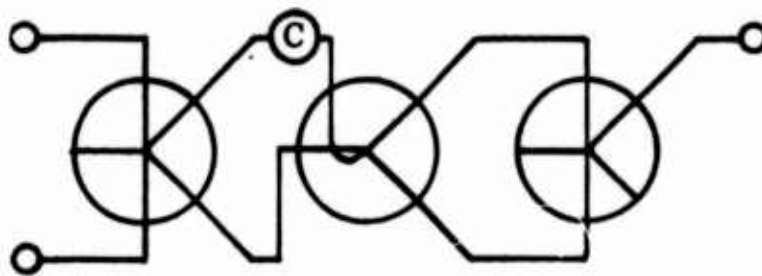FIGURE 13. MECHANICAL FREQUENCY REFERENCE

Figure 14

FREQUENCY CONVERTER CIRCUIT
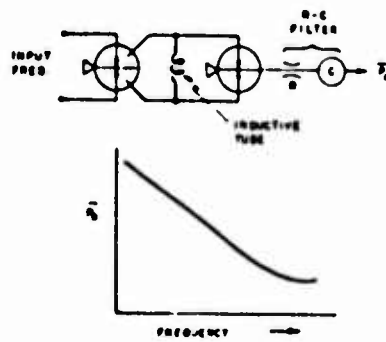
Figure 15

FREQUENCY DETECTING CIRCUIT

Figure 16

FREQUENCY CONVERTER CIRCUIT

Figure 17

BEAT DETECTOR CIRCUIT

f_1 INPUT
400 HZ

f_2 INPUT
350 HZ

$\Sigma f_1 + f_2$

RECTIFIED
FILTERED
OUTPUT
$f_0 = 50$ HZ
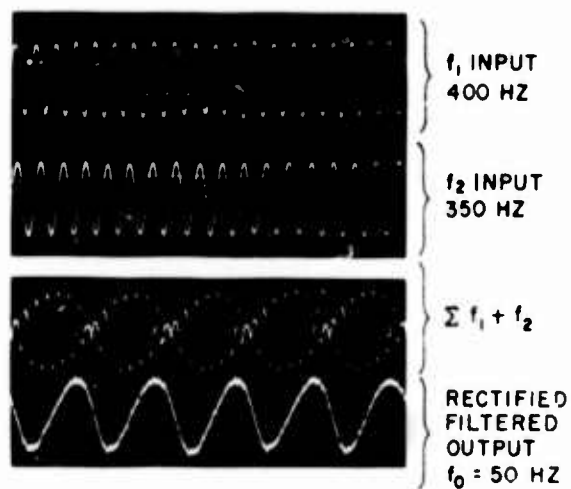
Figure 18

BEAT DETECTOF SIGNAL CHARACTERISTICS
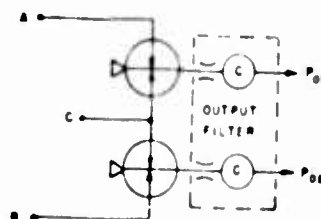
Figure 19

PHASE DISCRIMINATOR CIRCUIT

(a) $P_{o1} = P_{o2}$

(b) $P_{o1} > P_{o2}$

(c) $P_{o1} < P_{o2}$
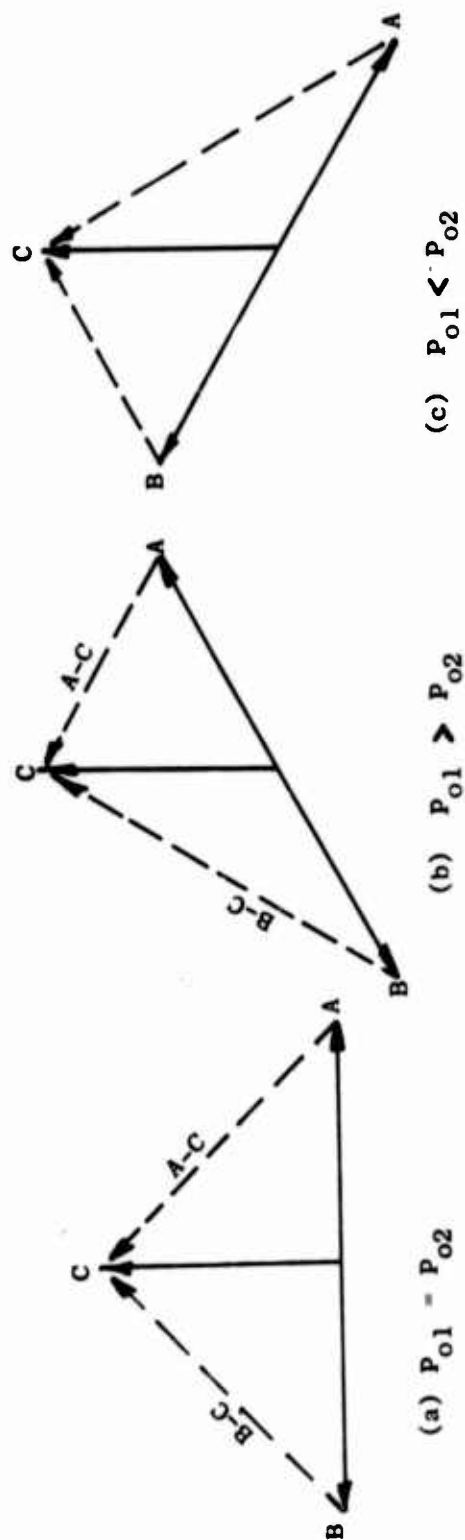
Figure 20 PHASE DIAGRAMS FOR PHASE DISCRIMINATOR SIGNALS

371

Figure 21

372
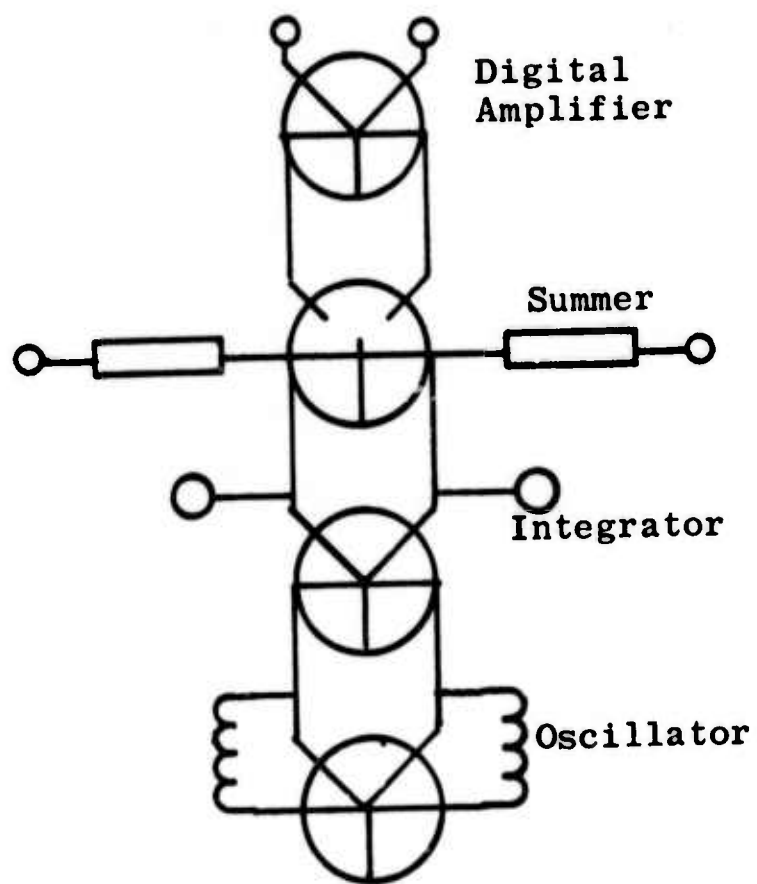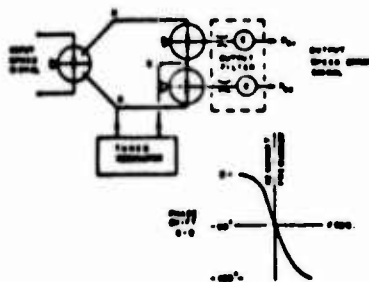
Fig. 22 Schematic for turbine governor circuit.
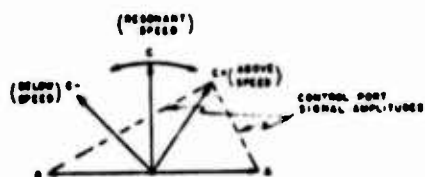
Fig. 23 Phase discriminator vector diagram.
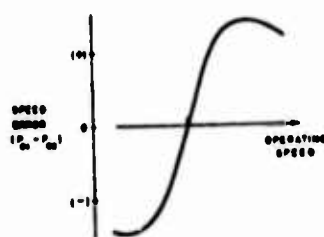
Fig. 24 Speed error signal from phase discriminator.

373
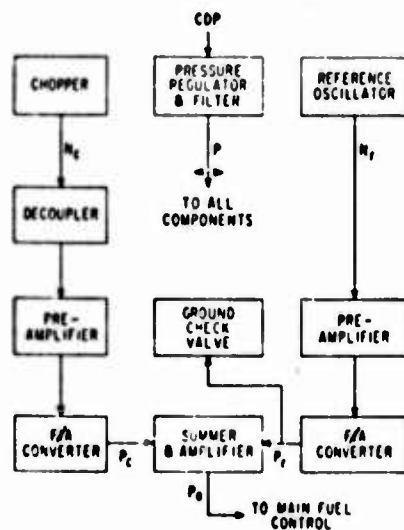
Fig. 25   Block diagram of overspeed sensor.
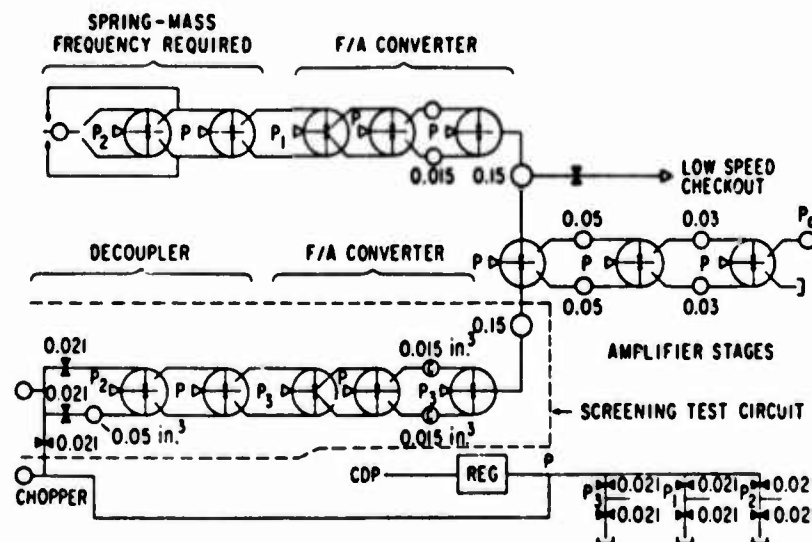
Fig. 26   Circuit diagram of overspeed sensor.

374
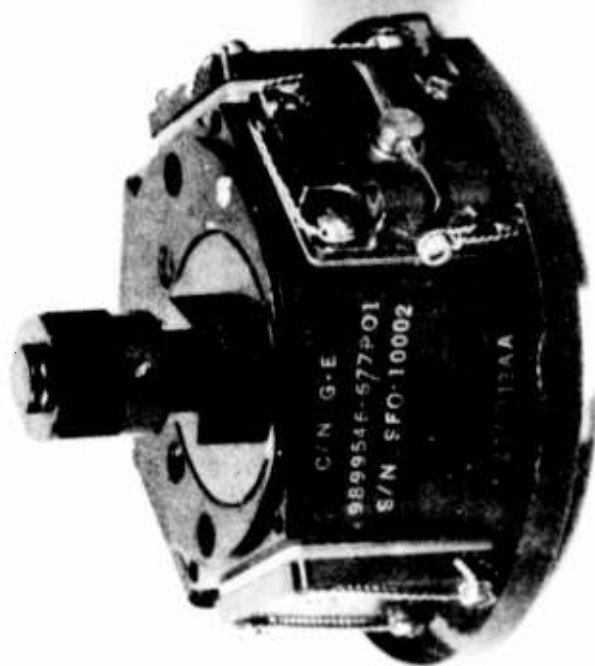
FIGURE 27. FLUIDIC OVERSPEED GOVERNOR WITH AND WITHOUT COVER

INDUSTRIAL AIR MOTOR GOVERNOR

Figure 28
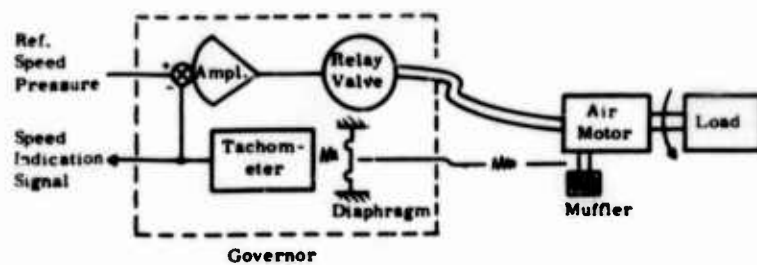
FIGURE 29. GOVERNED AIR MOTOR SYSTEM
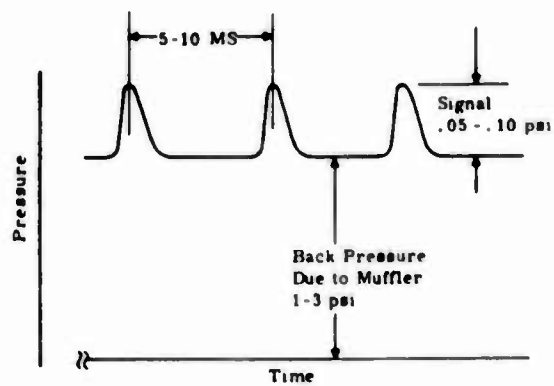
FIGURE 30. TYPICAL EXHAUST SYSTEM

377
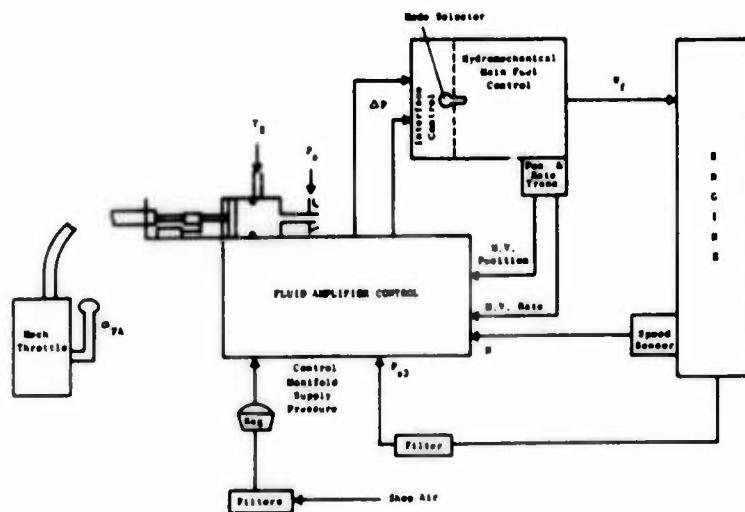
FIGURE 31. CONTROL SYSTEM BLOCK DIAGRAM
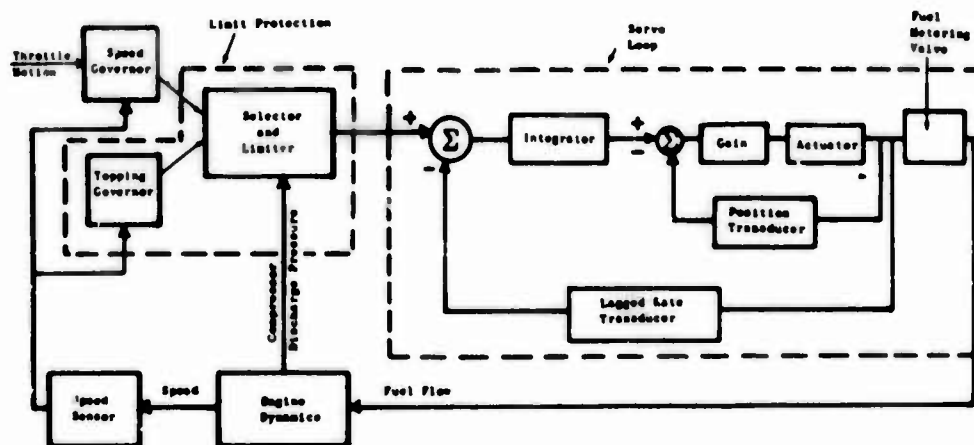
FIGURE 32. SIMPLIFIED CONTROL CIRCUIT

378

FIGURE 33. SELECTOR LIMITER CIRCUIT

FIGURE 34. ACCEL/DECEL LIMITER OPERATION

379
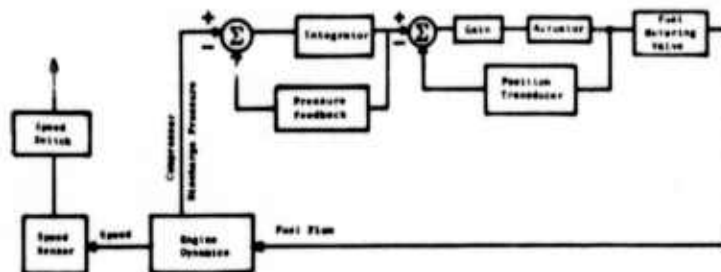
FIGURE 35. CONTROL START CONFIGURATION
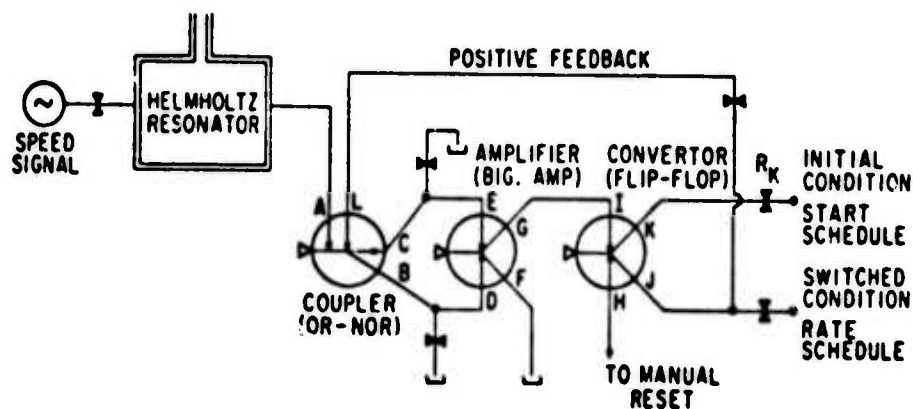
FIGURE 36. SPEED SWITCH SCHEMATIC

380
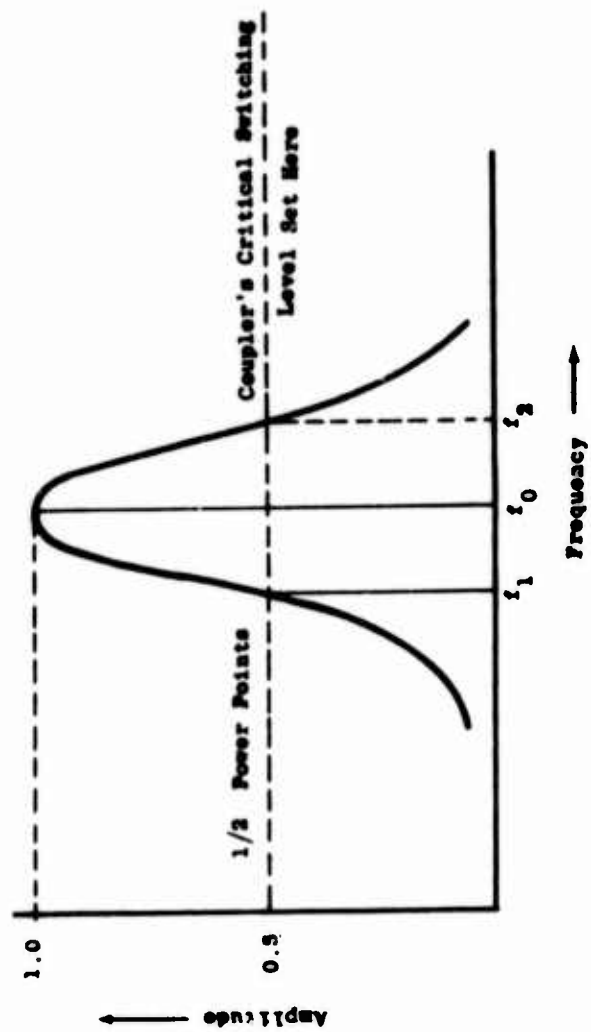
FIGURE 37. HELMHOLTZ AMPLIFIER CHARACTERISTICS
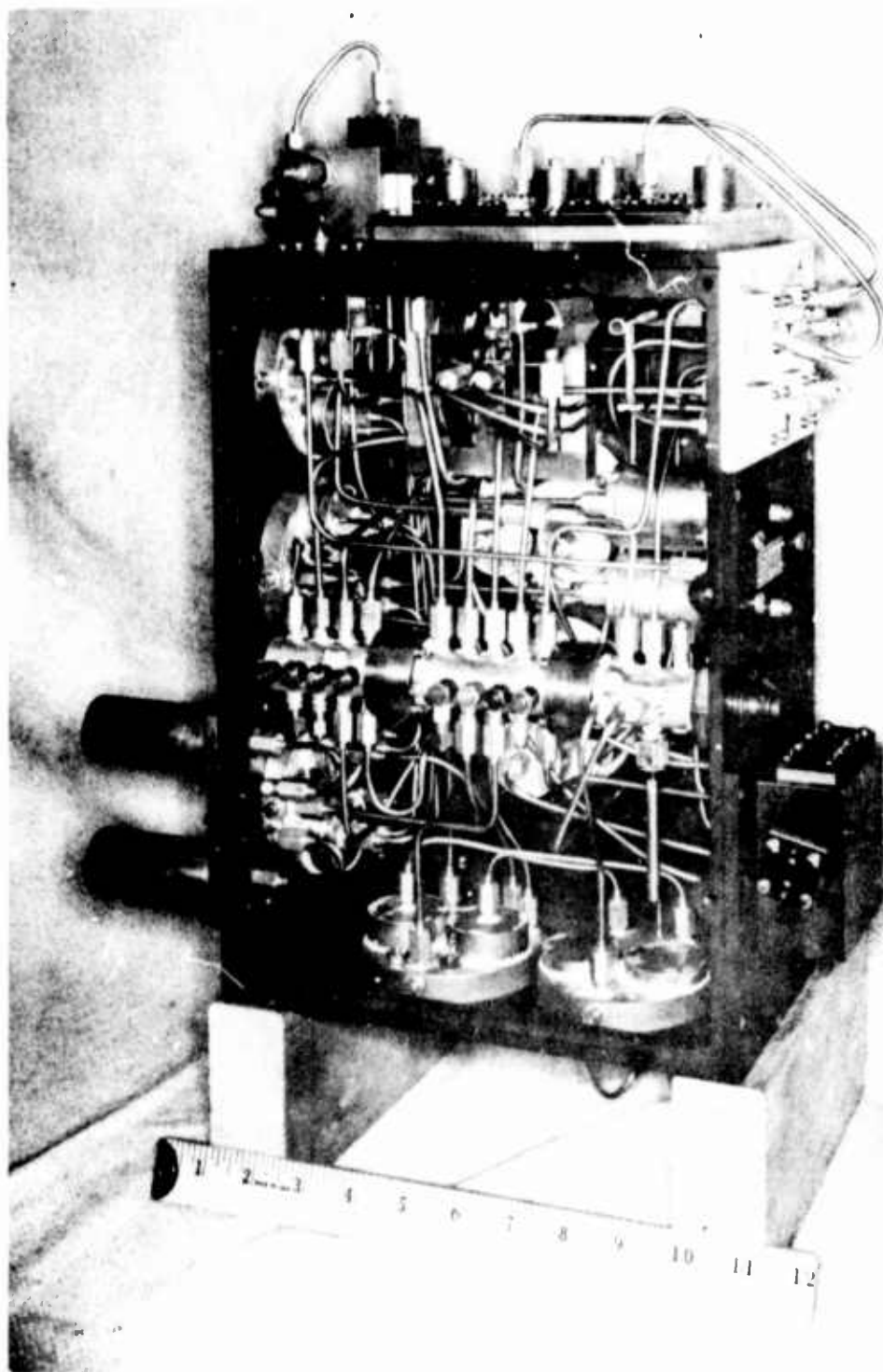
FIGURE 38. BACK VIEW OF ASSEMBLED CONTROL
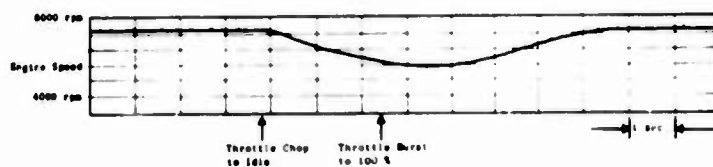
FIGURE 39. SPEED RESPONSE TO THROTTLE "BODE"
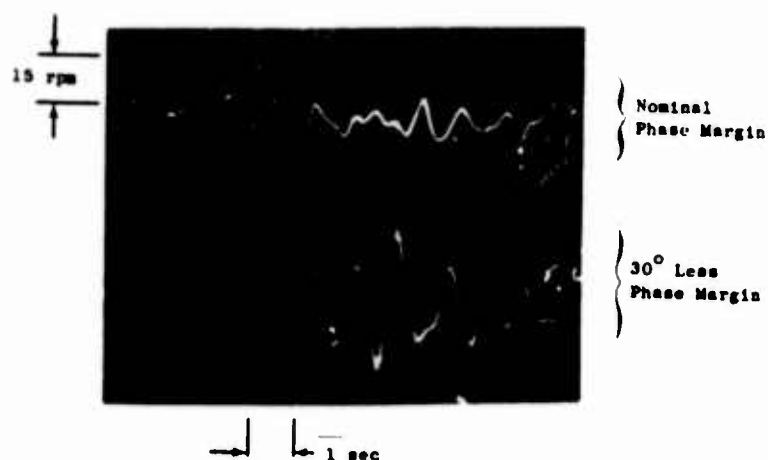
FIGURE 40. SPEED FLUCTUATION ABOUT SETPOINT

383

Speed	272.2 Lps (67.5)	Corrected Speed Governor 342.2 (84)	195.5 (97)	Topping Governor 405.5 (201P)
Test Time	6.5 min	6.7	7.5	6.5
Standard Deviation	0.074 Lps (0.027.5)	0.101 (0.030)	0.132 (0.033)	0.076 (0.019)
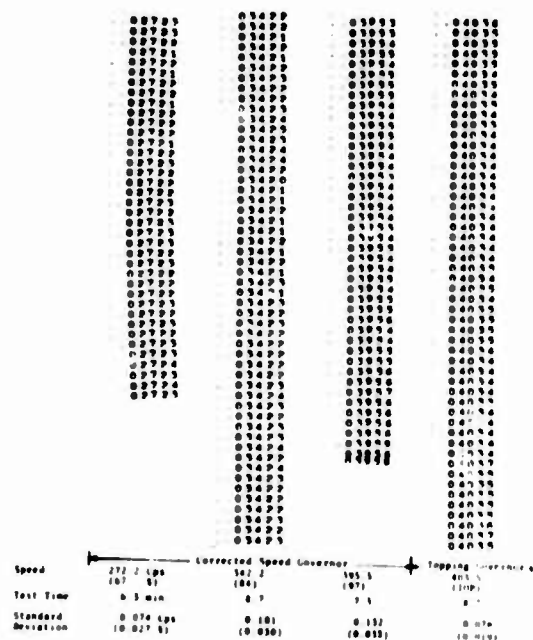
FIGURE 41. DIGITAL TAPES SHOWING SPEED HOLDING ACCURACY
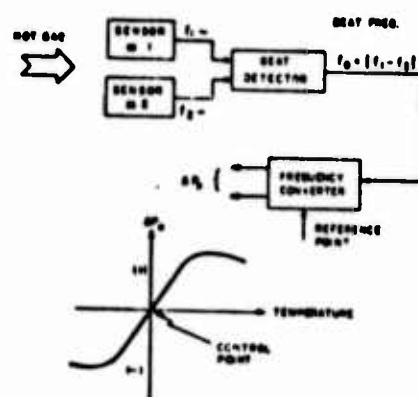
FIGURE 42. TEMPERATURE SENSOR CIRCUIT

384

FIGURE 43. ASSEMBLED PDM UNIT
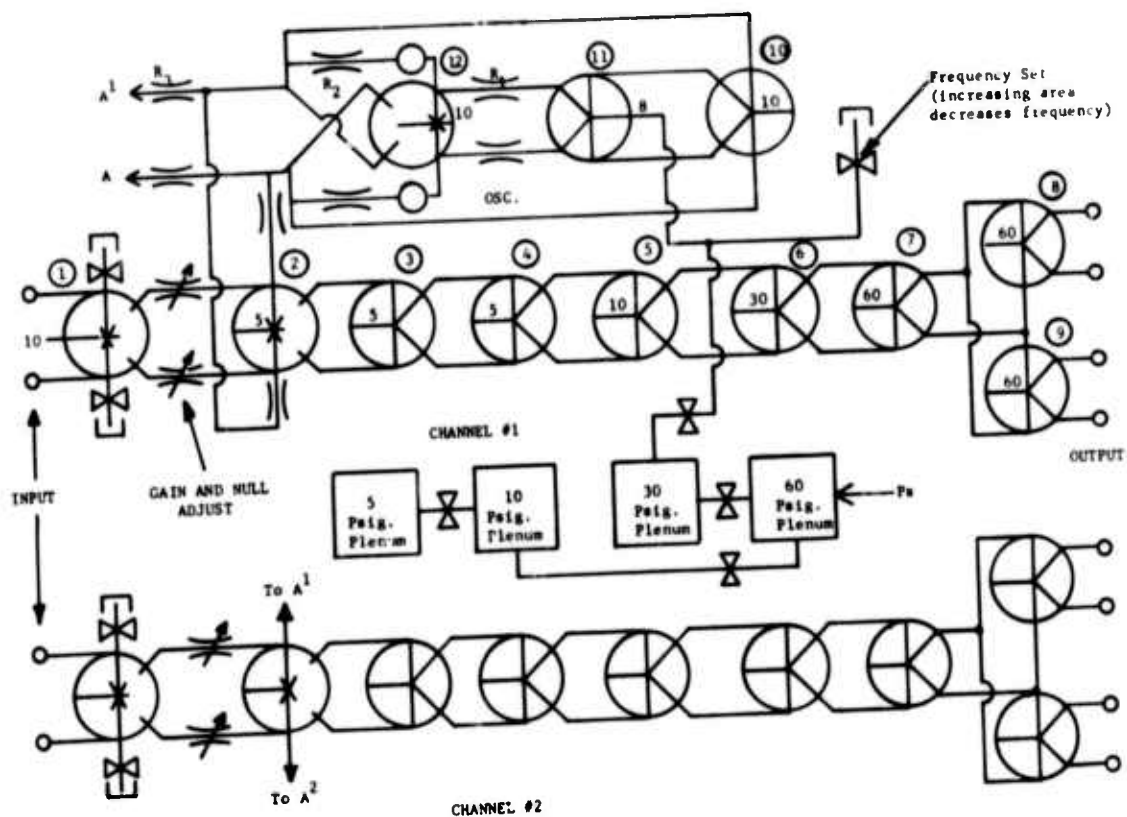
Fig. 44   PDM Circuit Diagram.
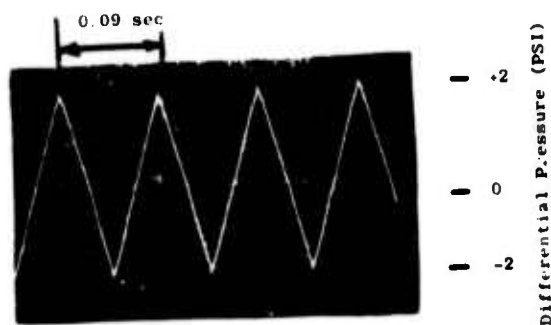
Fig. 45 Typical Trace of Oscillator Output.

386

OSCILLOGRAPH RECORDING
PDM OUTPUT

Modulation
.85%

Modulation
10

Modulation
-85%

0.09 sec
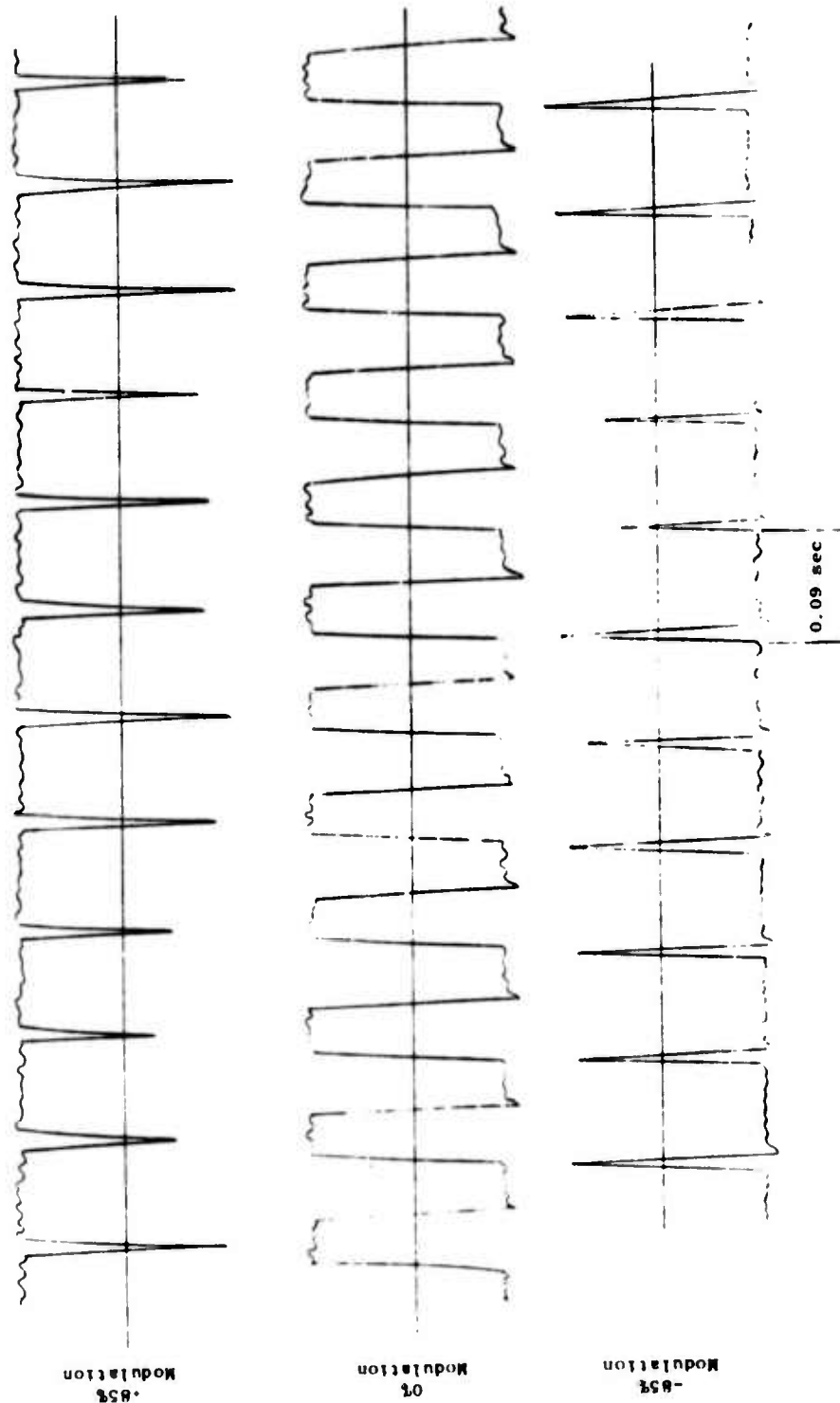
FIGURE 46. OSCILLOGRAPH RECORDING PDM OUTPUT

387
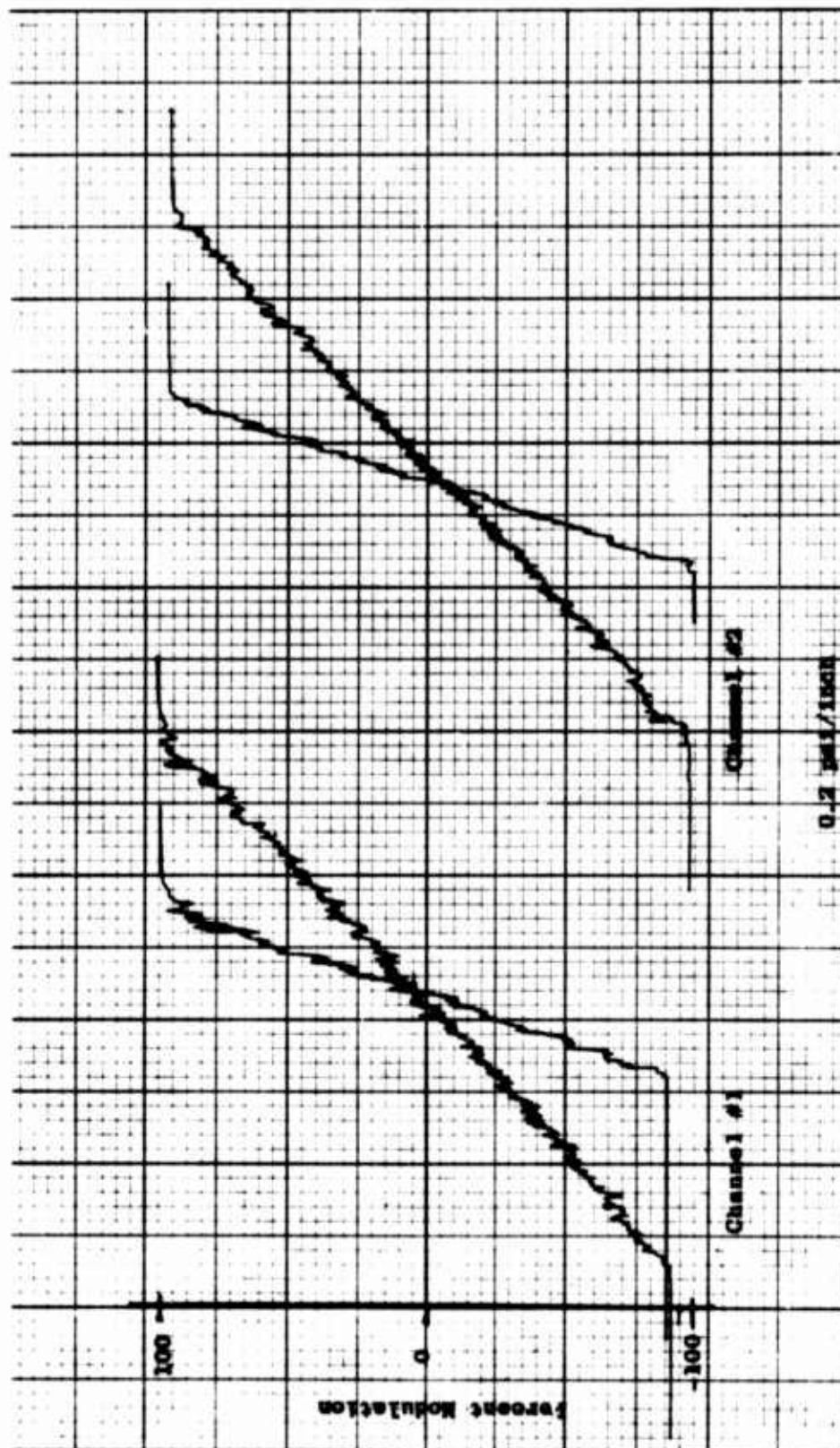
FIGURE 47. MINIMUM-MAXIMUM GAIN VARIATIONS (S/N 003)
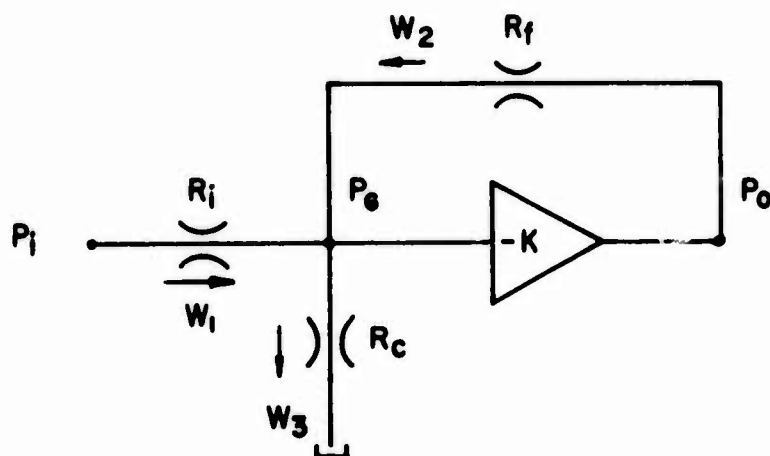
FIGURE I-1. BASIC OPERATIONAL AMPLIFIER CIRCUIT
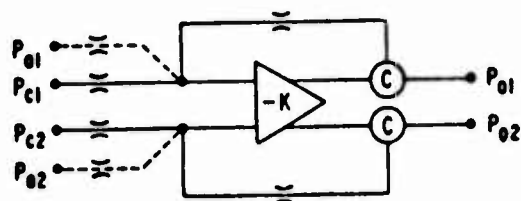
FIGURE I-2. FLAT RESPONSE AMPLIFIER AND SUMMING AMPLIFIER CIRCUIT
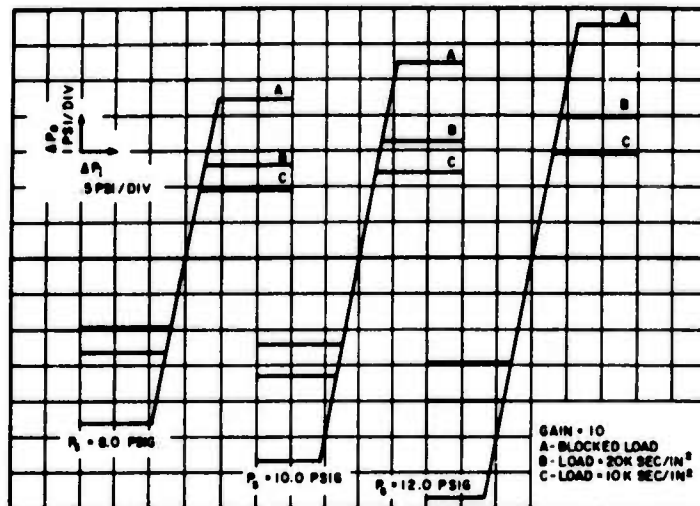
FIGURE I-3. PRESSURE-GAIN CHARACTERISTICS, FS-12 AMPLIFIER
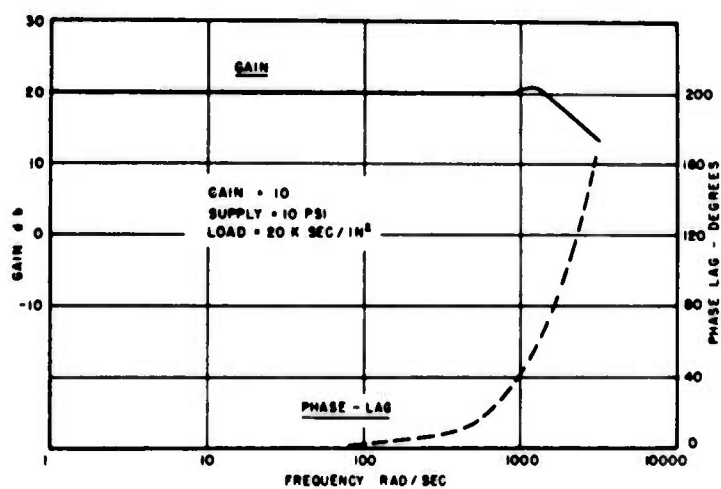
FIGURE I-4. FREQUENCY RESPONSE OF A SUMMING AMPLIFIER

390
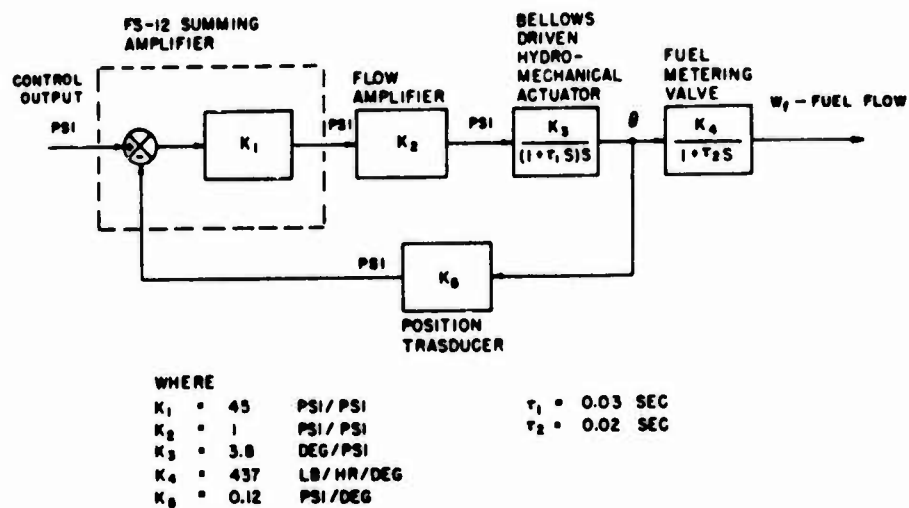
FIGURE I-5. FS-12 SUMMING AMPLIFIER IN J79 TURBOJET ENGINE CONTROL
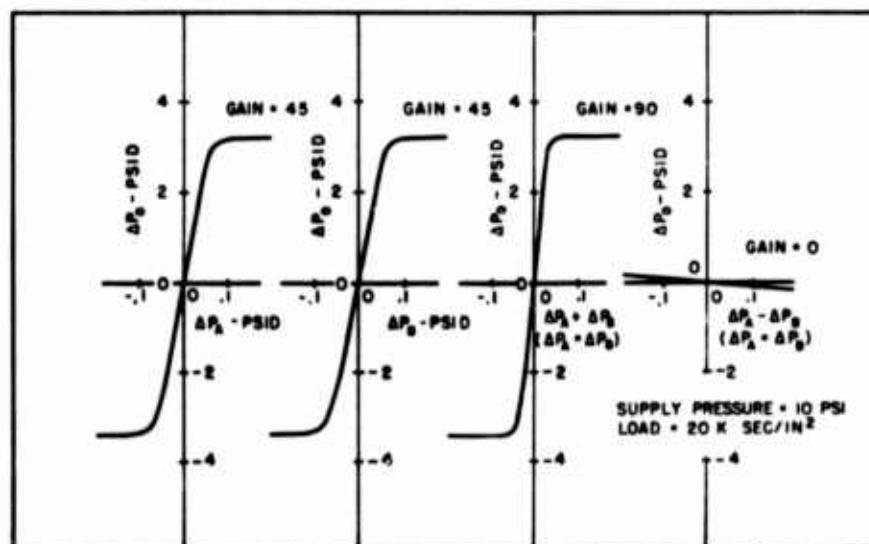
FIGURE I-6. PRESSURE GAIN CHARACTERISTICS, FS-12 SUMMING AMPLIFIER

391
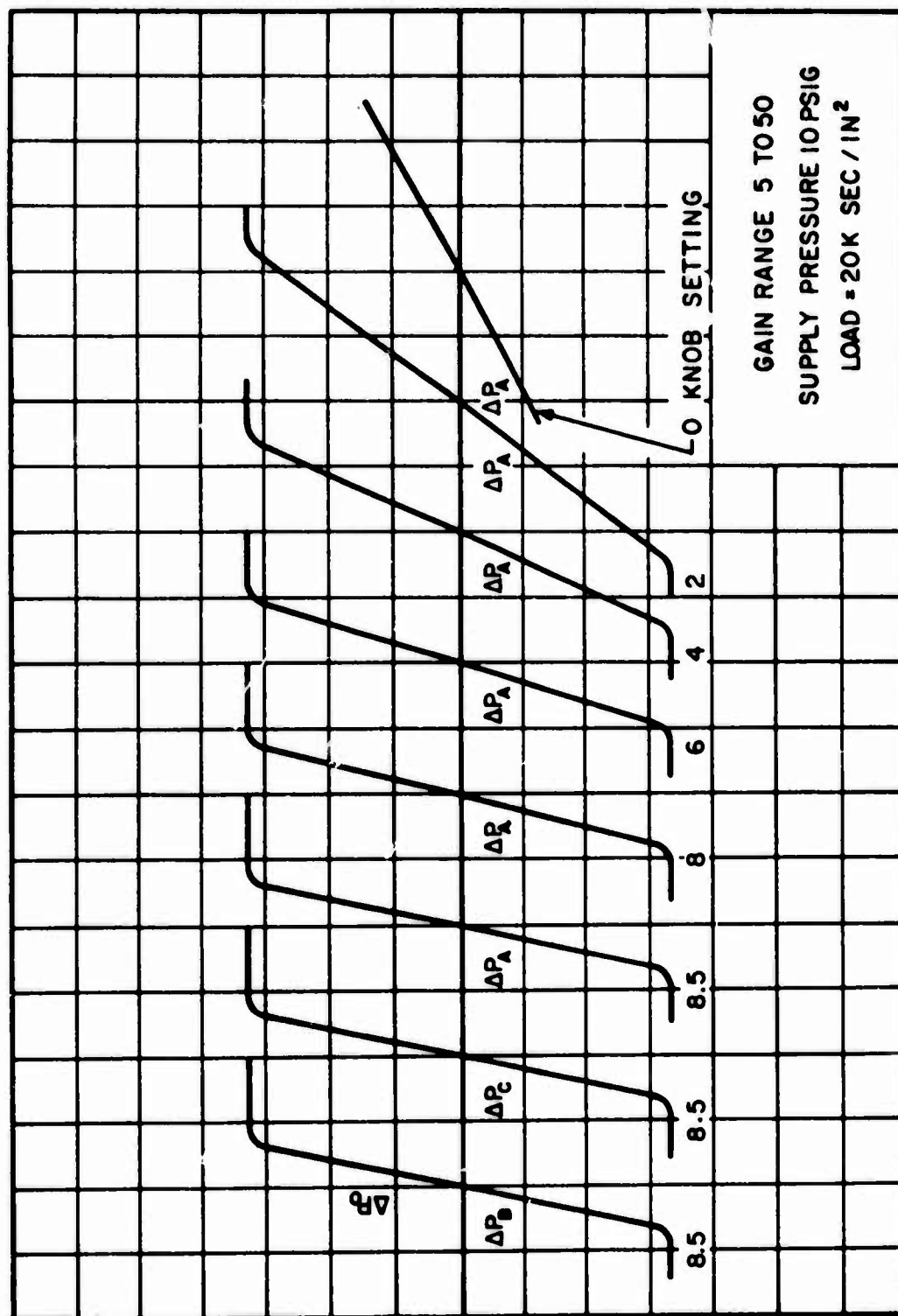
FIGURE I-7. PRESSURE–GAIN CHARACTERISTICS, VARIABLE GAIN AMPLIFIER
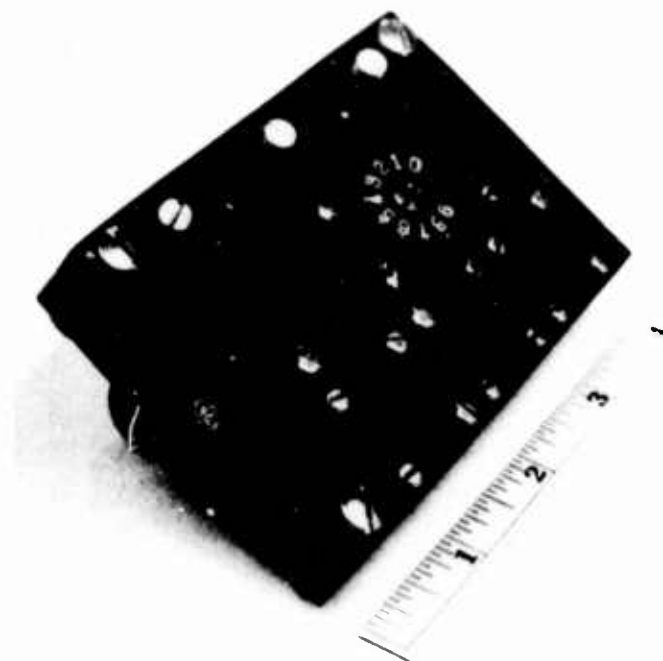
FIGURE I-8. VARIABLE GAIN OPERATIONAL AMPLIFIER
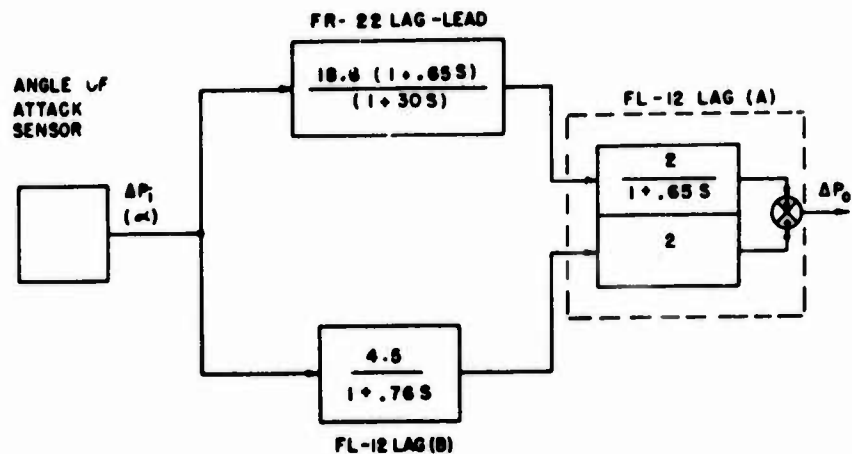
FIGURE I-9. FL-12 LAG CIRCUITS IN NAVAL AIRCRAFT CARRIER LANDING CONTROL

K_L = 13,700 LBS / IN W_V = 100 RAD / SEC
M = 2.12 LB-SEC^2/IN τ_1 = 1/10 SEC
K_V = 100 LBS / PSI τ_2 = 1/300 SEC
K_0 = 5.4 PSI / IN
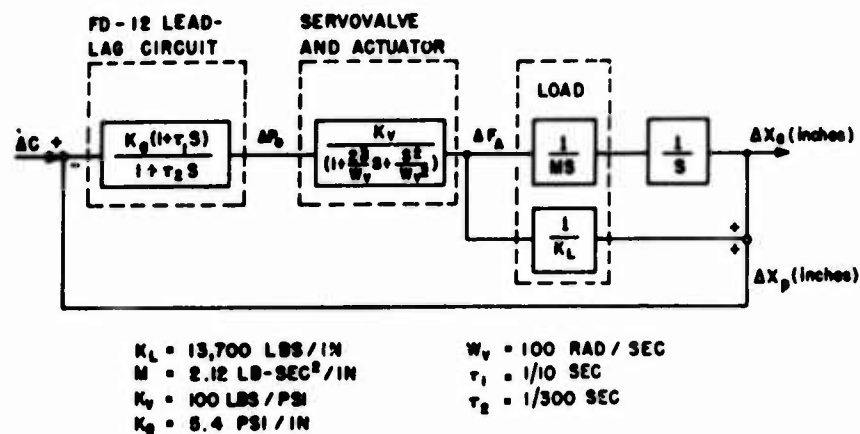
FIGURE I-10. FD-12 LEAD-LAG CIRCUIT IN ROCKET ENGINE ACTUATOR LOOP

394
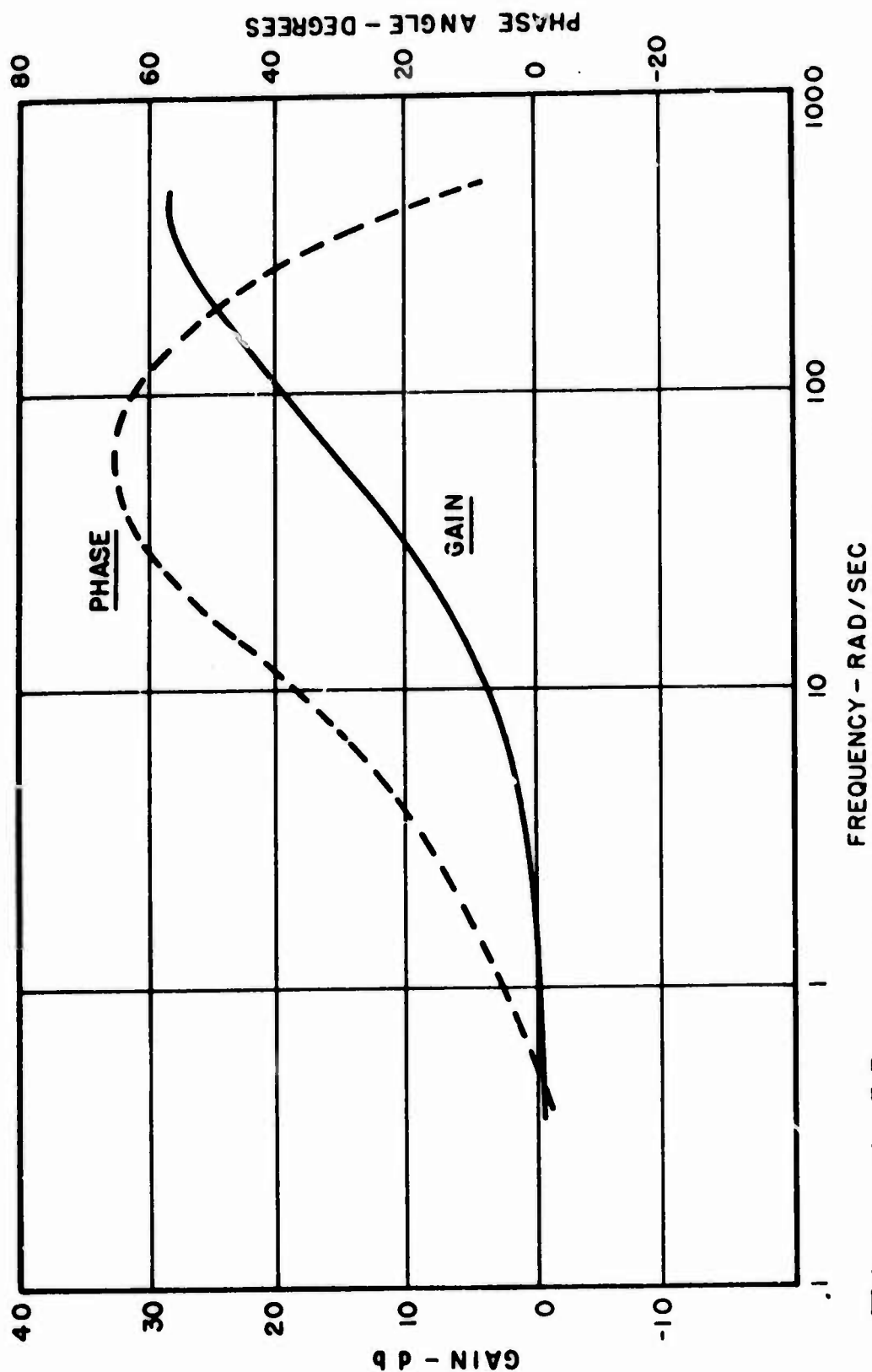
Fig. I-11 FREQUENCY RESPONSE OF A LEAD-LAG NETWORK

395

ANALOG FLUIDIC CIRCUITRY: REVIEW, CRITIQUE AND A
NEW OPERATIONAL AMPLIFIER

Forbes T. Brown
Professor of Mechanical Engineering
Lehigh University
Bethlehem, Pa. 18015

Abstract:

Two different approaches to analog fluidic circuitry are
found in the literature. The first utilizes high gain ampli-
fiers with feedback (operational amplifiers) to achieve easy
design, excellent linearity, low noise and low sensitivity to
disturbances at a cost of limited bandwidth, high power con-
sumption and high expense. The second utilizes fewer ampli-
fiers with feed-forward and a minimum of feedback to achieve
the opposite consequences.

A new operational amplifier is proposed which, through
resonance tubes placed in the forward loop upstream of the
gain block, has a greatly extended bandwidth at a cost of
increased sensitivity to load changes at high frequencies.

1.   INTRODUCTION

Most active fluidic elements in use today are bistable.
Frequently, however, conditions arise favoring the use of
proportional or so-called analog devices:

1.   The input energy level is too low to drive a digital
      device with sufficient resolution.

2.   Digital switching is too slow.

3.   A continuous output is desired.

4.   The simplicity of the analog alternative is com-
      pelling.

5.   Modulation schemes are desired.

Items 1 and 2 involve implicit advantages of analog devices,
including electronic analog computers. The major drawbacks
of analog fluidics involve the reliability and sensitivity
in the face of changes in pressure levels, load impedances,
load disturbances, temperature, and the inherent noise. Con-
sequently, analog fluidic circuits are often harder to design.

Kirshner and Manion [1] have given a fine review of pro-
portional amplifiers. Boothe and Ringwall [2] are contrib-
uting a review on modulation circuits (or AC fluidics) to the
present symposium. The present paper is directed at the

Preceding page blank

elements of the circuitry of proportional amplifiers, empha-
sizing the linear operations of summation, integration, fil-
tering or wave shaping, etc. Although the paper is largely
a review, a new type of operational amplifier also is intro-
duced.

2. COMPONENTS AND CIRCUIT THEORY

The heart of most analog systems is the proportional
amplifier. Most applications use jet-deflection amplifiers,
which are assumed herein. Vortex amplifiers can be very
useful also, however, especially in high-power applications
where efficiency is an important concern. Jet-impact ampli-
fiers also have been used.

Good linearity of the proportional amplifier is desir-
able, although it may not be necessary if feedback is to be
employed. Often more important is the flatness of the satu-
ration for very large input differential pressures. The
usual jet-deflection amplifier suffers a return to low output
pressure for very high input pressure. One remarkable excep-
tion is a design due to Griffin [3]. If several amplifiers
are to be cascaded, another approach is to stagger the onsets
of saturation so the last stage saturates first and the first
stage last. This procedure has helped lead to the dramati-
cally flat saturation of the 5-stage General Electric gain
block reported by Urbanosky [4], at some expense of increased
noise.

Other characteristics of the amplifier which are impor-
tant in circuit design include the input impedance, which is
usually nearly linear, the output impedance, which often has
significant nonlinearities, the pressure, flow and power
gains, and the signal-to-noise ratio. Several papers cited
below report that the frequency response of the gain of jet
amplifiers is virtually flat until the phase angle exceeds
180°; the behavior is close to that of a pure delay. Florea
and Stanescu [5] and Belsterling [6] give simple analytic
models for the internal dynamics, and Brown and Humphrey [7]
give a more complicated model as well as data on all the
important linearized dynamic characteristics of a particular
amplifier. Similar data for commercially available ampli-
fiers would be very helpful to circuit designers, but is very
hard to collect. One simple technique for partial informa-
tion up to very high frequencies, based on acoustic waves,
is described by Toda et al [8]. A more awkward but complete
method, which becomes inaccurate at high frequencies, uti-
lizes calibrated resistances comprised of a bundle of short
capillary tubes [9]. Toda and Katz [10] use single capillary
tubes and apply a correction for known dynamic effects. The
data of Brown and Humphrey included hot wire anemometry.

Gottron and Weinger, in the book edited by Kirshner [11], Sarpkaya [12] and Massen [13] discuss the inherent problem of noise and turbulence in the jets and receivers of jet amplifiers. Sarpkaya gives hot-wire data within the jet on a large-scale model, while Massen describes a rather sophisticated facility for small models using pressure transducers and correlation techniques. Considerable data is given by Kelley and Kantola [14] on the trade-offs between noise and gain, output impedance, and sensitivity to Reynold's numbers. Brown [15] has found that an excitation introduced at one frequency can reduce the noise at other frequencies, and related advantages in signal-to-noise ratio result from the use of modulated signals as presumably discussed by Boothe [2].

Passive elements also play a key role in analog circuit design. Resistors based on orifice flow are nonlinear, and thus of limited usefulness, although the multiple irregular cascaded orifices in porous sintered metal filters is an exception. Resistors based on viscosity and using channels with rectangular or circular cross-sections are analyzed by Lee and Kwok [16, 17]. The length of a resistor should be at least an order of magnitude less than the acoustic wavelengths of interest, occasionally dictating a bundle of small parallel channels. A resistance which is nearly temperature-independent, described by Bedard [18], uses a channel which changes in cross-section.

Inductors are not often used with air, although Bowles et al [19] provides a significant exception. The kinematic viscosity is too high to give a high Q with small elements, and the compressibility is too great to permit large elements without significant capacitive effects. The compressibility problem vanishes when a liquid is used, and the kinematic viscosity problem is greatly reduced with water. Boddy [20] points out that the paucity of good inductors is compensated for by using active elements; even in electrical circuits "active RC" networks are increasingly preferred, for economic reasons, over passive LRC circuits.

Capacitors with one side grounded usually use simple rigid volumes when air is the medium. Unfortunately, the capacitance varies with time or inverse frequency from the adiabatic value toward the isothermal value, for a 40% change, and the transition is extremely gradual. Some analyses are given by Dagan and Kwok [21] and Katz and Hastie [22]. If one is determined to achieve as nearly adiabatic performance as possible, the capacitor should be spherical with the supply tube possibly penetrating to near the center. Any scavenging effect or heat transfer surface pushes the behavior toward the isothermal extreme, however, and since either extreme is better than a compromise the designer should consider increasing the heat transfer surface, for example by inserting steel wool into the cavity.

399

Capacitors which do not use a gas or which do not have one side grounded are normally avoided, since they must involve mechanical strain such as in a bellows.

A large literature exists on the dynamics of fluid lines in circular tubes; the basic aspects involving laminar flow are cited in a review paper by Goodson and Leonard [23]. Healy and Carlson [24] and Schaedel [25] give theoretical results for rectangular channels which are used in modular fluidic devices. A fluid line has resistance, capacitance and inertance. Optimum design of fluidic circuits may well involve explicitly a continuous distribution of these elementary properties, somewhat in the fashion of microelectronics, but this is beyond the state of the art.

Elementary techniques for circuit synthesis developed by analogy to electronics are given by Belsterling [6, 26], examples are given by Chou et al [27], and some more general techniques are given by Brown [15]. Kirshner and Katz [11] present a more complete physical basis for circuit analysis, which unfortunately requires simplification to make most circuit problems tractable.

3. BASIC CIRCUITS

The basic linear operations which comprise the building blocks of analog circuitry are

1. amplification, multiplication by a constant, or buffering

2. summation (positive and negative)

3. integration

4. filtering, including differentiation, lag-lead, etc.

Modulation circuits also make fundamental use of rectifier circuits including a nonlinear active element [2].

Each of the basic operations can be carried out either of two different ways: with and without feedback. As discussed below, feedback greatly enhances linearity and low output impedance, but at the expense of speed of response and complexity. Thus both approaches have appropriate domains of application.

3.1 Operational Amplifier Circuits

Summation and amplification was first carried out without feedback, as typified by Roffman and Katz [28], because the gain of the single stage of amplification used was low. The basis for the more classical operational amplifier was

set with the advent of multi-stage gain blocks which typically have a pressure gain over 1000. The resulting operational amplifier-summer, shown in Figure 1, is discussed by Wagner and Barrett [29], Parker and Addy [30], Foster and Parker [31], Urbanosky [4], Doherty [32], and Brown et al [9]. Presuming the input and output admittances of the gain block are Y_i and $1/Z_o$, respectively, the load admittance is Y_o, and the pressure gain of the amplifier for zero load flow is g, the static behavior is easily deduced to be

$$\frac{P_O}{P_i} = - \frac{R_2}{R_1} \frac{1}{1 + a/g} \tag{1}$$

$$a = (1 + \frac{R_2}{R_1} + \frac{R_2}{R_1} + R_2 Y_i)(1 + Z_o Y_o) + \frac{Z_o}{R_1} + \frac{Z_o}{R_1} + Y_i Z_o \tag{2}$$

If $g > 1000$, and Y_i, Y_o and Z_o are not excessively large, this behavior is nearly ideal:

$$\frac{P_O}{P_i} \simeq - \frac{R_2}{R_1} \tag{3}$$

Unfortunately the circuit as shown in Figure 1 (and in most other papers) is unstable and oscillates wildly. The reason is obvious from the typical data of Parker and Addy [30], given in Figure 2: the loop gain vastly exceeds unity when the phase lag reaches 180°. One novel approach, proposed by Lloyd [33], is to let the circuit oscillate, saturating each cycle to give a square wave, and to utilize the pulse-width modulation which results from the input pressures. He further suggests reducing the complication by using three switching amplifiers (nearly bistable) rather than five lower-gain proportional amplifiers. The basic advantage is a fast response time, which is essentially one oscillation period if the necessary output filtering is discounted. Linearity appears to be a major difficulty, although use of better components than employed by Lloyd should improve substantially upon his results.

The traditional solution to the instability has been to place capacitance volumes at the output, as shown in Figure 3. This introduces an additional 90° phase lag, unfortunately, so the break frequency of the circuit must be reduced to the value at which the lag of the gain block itself is about 50°, as noted by Urbanosky [4]. Parker and Addy [30] and Foster and Parker [31] properly note that this can require break frequencies in the loop gain below 1 Hz, but then seem to confuse this break with the closed-loop behavior which actually retains its break, for the case cited, at 250 Hz, presuming linear behavior. The actual behavior is not always linear,

however, and the conclusion of these authors turns out to be not quite as false as its premises, as seen below.

Wagner and Barrett [29] had a low closed-loop break frequency (about 5 Hz), due to the volume of interconnecting tubes, and thus did not study the dynamics beyond a false claim that their closed loop response should break at as high as 500 Hz simply by employing integrated circuitry. Doherty [32] and the General Electric Co. [34] (same amplifier) give data supporting the linear theory, but the results can be misleading as seen below.

The gain block can be modeled closely as a gain with a pure delay, or ge^{-Ts}, with $g > 1000$. The closed-loop pressure gain then becomes, neglecting the reactances of the passive elements other than the capacitors,

$$\frac{P_o}{P_i} = -\frac{R_2}{R_1} \frac{e^{-Ts} - \dfrac{Z_o}{R_2 g}}{e^{-Ts} + \dfrac{(\tau s + 1)a}{g}} \tag{4}$$

in which a is given by equation (2) and

$$a\tau = (1 + \frac{R_2}{R_1} + \frac{R_2}{R_1'} + Y_i R_2) Z_o C \tag{5}$$

As an example consider the typical values

$$g = 2500; \quad Z_o = 1.4 \text{ lb sec/in}^5; \quad Y_o = 0$$

$$R_1 = 5.66 \text{ lb sec/in}^5; \quad R_2 = 56.6 \text{ lb sec/in}^5$$

$$Y_i = 0.4 \text{ in}^5/\text{lb sec}$$

Further, for stability it is necessary that $a\tau > \frac{2}{\pi} gT$; we choose

$$a\tau = \frac{4}{\pi} gT \tag{6}$$

This gives

$$\frac{P_o}{P_i} = -10 \frac{e^{-Ts} - 1 \times 10^{-5}}{e^{-Ts} + .0179(71.2Ts + 1)} \tag{7}$$

The second term in the numerator represents the signal path through the feedback channels from input to output, and is obviously negligible. The break frequency occurs when $T\omega \simeq \pi/4$, or essentially the same as discussed above. At

402

zero frequency the result reduces to

$$\frac{p_o}{p_i} = - 10 \frac{1}{1.0179}$$ (8)

showing the powerful effect of the feedback gain which is $g/a = 56$.

The sensitivity to changes in the load admittance Y_o is desirably small:

$$\frac{\partial (p_o/p_i)}{\partial Y_o} = \frac{R_2}{R_1} \frac{(1 + \frac{R_2}{R_1} + \frac{R_2}{R_1}r + R_2 Y_i) \frac{z_o}{g} e^{-Ts}}{[e^{-Ts} + \frac{a(\tau s + 1)}{g}]^2}$$ (9)

For the example,

$$\frac{\partial (p_o/p_i)}{\partial Y_o} = 10 \frac{0.0174 \, z_o e^{-Ts}}{[e^{-Ts} + 0.0179(71.2Ts + 1)]^2}$$ (10)

or, at zero frequency,

$$\frac{\partial (p_o/p_i)}{\partial Y_o} = 0.169 \, z_o$$ (11)

A potentially serious limitation of this circuit has been pointed out by the author [9]. The output flow of the gain block consistent with the above is virtually

$$\frac{Q_g}{p_i} = - \frac{1}{R_1} \frac{(R_2 Cs + 1 + Y_o R_2) e^{-Ts}}{e^{-Ts} + (\tau s + 1)a/g}$$ (12)

For the example,

$$\frac{Q_g}{p_i} = - \frac{1}{R_1} \frac{(2950 \, Ts + 1) e^{-Ts}}{e^{-Ts} + 0.0179(71.2Ts + 1)}$$ (13)

The denominator does not change dramatically with increasing frequency, but over the useful frequency band the numerator term 2950 Ts forces the ratio to increase by roughly a factor of 1600. Therefore, at the break frequency the maximum input amplitude which does not saturate the gain block is 1/1600 the corresponding amplitude at zero frequency. The saturation accompanying anything larger than this trivial amplitude then vastly reduces the output amplitude, seriously reducing

the break frequency. Thus, the need to charge a large pair of volumes from a saturable source introduces serious rate limiting.

Care is suggested in reading advertising literature. Consider the General Electric data, given in Figure 4. This data shows a break at about 200 Hz, not much below the linear theory. Since the closed-loop gain is unity and the gain of the gain block is over 2000, a loop gain of several hundred would have been possible. Why, then, was the loop gain chosen as small as 20? It is not clear a'so how the loop gain was made so small, although the large load admittance clearly helped. Nevertheless, a calculation suggests that the amplitude of the input and output signals was large enough to produce incipient saturation of the gain block; larger signals would have lowered the break frequency by as much as a decade or more.

An entirely different approach which eliminates this problem is suggested in Section 4.

Since series capacitors are not practical, fluidic feedback integrators are constructed a way different from electronic integrators. The circuit of Figure 5 has been described by Katz and Roffman [35], Doherty [32], Wagner and Barrett [29], Pavlin and Facon [36] and others. Presuming an infinite gain in the forward loop, and making the critical choice

$$\frac{R_3}{R_1} = 1 + \frac{R_2}{R_1} + \frac{R_2}{R_4} \tag{14}$$

balances the lagged positive feedback and unlagged negative feedback to give the desired integration function

$$e_o = - \frac{R_3}{CR_1R_2} \frac{1}{s} e_i \tag{15}$$

A typical response to a step input, given by Urbanosky [4], is given in Figure 6. Other authors report proper magnitude behavior over a band of four or more decades of frequency; this must be recognized as inconclusive unless proper phase data is also reported.

Differentiation is an impractical function to generate, but a useful related function is the lead-lag of Figure 7, discussed by Doherty [32], Wagner and Barrett [29] and Rose [37]. The two break frequencies can easily be set a decade apart. A variety of other filter or shaping functions also can be created with considerable accuracy and insensitivity to load, presuming feedback is placed around a high-gain

fluidic amplifier.

Applications using operational amplifier circuits are reported by Stern [38], Holoubeck [39], Gelin and Jardinier [40], Florea et al [41], and Schrader [42]. Hydraulic operational amplifiers are presented by Kelley and Boothe [43], with applications and further development by Boothe [44], and Kelley and Boothe [45]. Dvoretsky and Molchanov [46] present a hydraulic operational amplifier using fluid impact modulators.

3.2 Other Circuits

One may wish to operate above the usual break frequency of an operational amplifier, or wish to use cheaper or fewer components, and be willing to sacrifice some linearity and load insensitivity. Boddy [20] has proposed a series of filter circuits which, with the exception of two circuits designed to achieve complex poles, employ no feedback whatsoever. They are comprised of passive RC circuits with a single stage amplifier as an output buffer, or a cascade of such circuits. The example of a lead-lag circuit is given in Figure 8. The special case of $R_1 = R_2$ is a high-pass filter, earlier described by Kelley [47] as "decoupler element". This approach does not give summers or integrators.

Parker and Addy [30] propose circuits which attempt to improve the performance without the liabilities of operational amplifiers. Their summer, shown in Figure 9, is based on the implicit assumptions of linear resistive output and load impedances. Their "differentiator circuit", shown in Figure 10, is actually a disguised version of Boddy's [20] lead-lag (Figure 8) when, as is actually assumed, $V_1 = 0$. The essential difference is the introduction of two buffer amplifiers at the input. Their integrator circuit, shown in Figure 11, employs a volume and positive feedback like the operational amplifier approach. Since the signal is buffered by amplifiers at each stage, the behavior is adequate for many applications. Note the "gain control resistors"; good balance, in this case of the gains of the upper and lower amplifiers, is needed in any active integrator circuit.

Positive feedback around a fluidic amplifier also has been frequently utilized to make oscillators. Discussions are offered by Brown [9], Ashikian [48], and Frey and Wilson [49]. Foster and Carley [50] suggest the use of a pressure-dependent oscillator as the heart of an analog-digital converter. This and other applications of oscillators involves the use of modulated carrier systems, discussed by Boothe [51] and Boothe and Ringwall [2]. The tuned or band-pass amplifier of Bowles et al [19] which is intended for such systems, shown in Figure 12, is particularly interesting in

its use of fluid inductors which together with volumes make moderate-Q Helmholz resonators.

Fluidic analog position sensing is surveyed by Chitty and Lenaerts [52].

A variety of applications using analog amplifiers are given by Clark [53], Kast and Uehling [54], Mayne [55, 56], Schaedel et al [57], Reid and Woods [58] and Burton [59], the last using hyraulic fluidics which seems to be a current thrust.

4. DESIGN OF A NEAR-OPTIMAL OPERATIONAL AMPLIFIER

Vastly better dynamics should be realized with the operational amplifier shown in Figure 13, which is an improvement over a design of the author's [9] having a pair of unnecessary resistors. Using the same assumptions for the gain block as before, again neglecting reactance in the passive elements, and setting $R_3 = Z_c$ (the characteristic impedance of the cross-section of the resonance tubes), the overall pressure gain is

$$\frac{P_o}{P_i} = - \frac{R_2}{R_1} \frac{1}{\Delta} (e^{-Ts} - \frac{Z_o}{gR_2}) \tag{16}$$

$$\Delta = (1 - \frac{R_b}{2Z_c g}) e^{-Ts} + (Y_i + \frac{1}{2Z_c}) \frac{R_b}{g} + \frac{r}{g} \tag{17}$$

$$R_b = Z_o + R_2(1 + Z_o Y_o) \tag{18}$$

$$r = (1 + \frac{R_2}{R_1'} + \frac{R_2}{R_1}) (1 + Z_o Y_o) + \frac{Z_o}{R_1} + \frac{Z_o}{R_1'} \tag{19}$$

Note that the round-trip wave delay time in the resonance tubes is set equal to the delay time of the gain block. Further, we now set

$$R_b = 2gZ_c \tag{20}$$

which gives

$$\frac{P_o}{P_i} = - \frac{R_2}{R_1} \frac{e^{-Ts} - \frac{Z_o}{gR_2}}{1 + 2Y_i Z_c + \frac{2Z_c}{R_1'} + \frac{2Z_c}{R_1} + \frac{1}{g}(1 + Z_o Y_o)} \tag{21}$$

406

For the same example values as before, plus

$$Z_c = 0.0116 \text{ lb sec/in}^5$$

this gives

$$\frac{P_o}{P_i} = -10 \ \frac{e^{-Ts} - 1 \times 10^{-5}}{1.018} \tag{22}$$

This result is virtually ideal; the second term in the numerator is absolutely negligible, the denominator is a constant differing by less than 2% from the nominal value, and the response is merely an amplified and delayed reproduction of the input over an infinite bandwidth. Optimal control theory shows that the delay e^{-Ts} is absolutely unavoidable, and thus the circuit can be described even in the theoretical sense as virtually optimal.

There are limitations not evident in equation (22), of course. If the reactances of the various elements were included, some limitation in the bandwidth would appear. More fundamentally, we should examine the load sensitivity:

$$\frac{\partial (P_o/P_i)}{\partial Y_o} = \frac{R_2 Z_o}{R_1 g} \ e^{-Ts} \ [\ 1 + \frac{R_2}{2Z_c}(1 - e^{-Ts})$$

$$+ Y_i R_2 + \frac{R_2}{R_1 r} + \frac{R_2}{R_1}] \tag{23}$$

At zero frequency ($s = 0$) this gives, for the example,

$$\frac{\partial (P_o/P_i)}{\partial Y_o} = 0.21 \ Z_o \tag{24}$$

which is similar to the traditional design.

On the other hand, at higher frequencies this becomes

$$\frac{\partial (P_o/P_i)}{\partial Y_o} = 10[0.976(1 - e^{-Ts}) + 0.021]Z_o e^{-Ts} \tag{25}$$

It can be seen that the sensitivity to load errors or load changes increases tremendously with frequency, reaching a maximum when $T\omega = \pi$. The traditional design does not share this problem, and thus has one advantage which can be important in applications involving large and uncertain load admittances.

The flow emanating from the gain block is

$$\frac{Q_g}{P_i} \simeq -\frac{1}{R_1} \frac{e^{-Ts}}{1.018} \tag{26}$$

This is virtually the same as the traditional circuit (equation (13)) for $\omega = 0$, but for higher frequencies illustrates the total absence of rate limiting due to saturation.

The behavior including this key feature perhaps can best be understood for a step input. Most of the flow and energy of the step initially goes into the creation of a pair of waves which propagate down the resonance tubes. A tiny fraction of the flow and energy of the step enters the gain block, just enough for the vastly amplified initial step output of the gain block to equal the final steady-state output (producing no surge which might saturate the gain block!). This initial step output is then transmitted through the feedback paths, arriving at the resonance tubes just as the initial wave fronts in the tubes have returned to their starting positions. The two incident waves now cancel identically, and all further transients cease: static equilibrium has been reached.

In practice the very small value of R_3 is difficult to achieve except with the use of porous disks (e.g., sintered filter disks, etc.) It is possible to retain part of the virtue of the concept, however, including the banishment of transient saturation, and to improve on the load sensitivity, by using any properly balanced scheme with the dynamic filtering of the loop gain placed in the forward path upstream of the gain block. To the author's knowledge, however, no one has done this before, instead placing the filters downstream of the gain block or in the feedback paths. Compromises between the two designs might offer advantages, also.

5. CONCLUSIONS

Sarpkaya [60] suggests that the point of diminishing returns has been reached for fundamental fluid mechanical studies of fluidic amplifiers. Rather, effort should be directed toward making practical circuits. The review herein reveals that analog circuitry has been developed to the point where application can be a routine procedure.

If a bandwidth of 200 Hz is adequate, the use of available operational amplifiers gives simple and reliable behavior within certain power and noise limitations. Less elaborate but less reliable alternative circuits can be used to handle design problems where the cost of operational amplifiers is excessive or the frequency response is inadequate.

A particular design for a new operational amplifier circuit has been advanced which promires greatly extended dynamic performance at the cost of an increased sensitivity, at high frequencies, to load changes, and the need for more critical balancing.

Related Symposium Papers

The author has been informed that in addition to references [2] and [10] the present symposium includes related papers by H. Schaedel, G. Roffman and J. Iseman on circuits and circuit analysis, by R.A. Comparin on fluidic interconnections, and by M.E. Franke with E.F. Moore and S. Katz with A. Hausner and N. Eisenberg on fluid lines.

Acknowledgement

References

1. J. Kirshner and F. Manion, "Jet Deflection Proportional Amplifiers", ASME paper 70-Flcs-17, 1970, and Fluidics Quarterly, v2 n4 1970 p15-39.

2. W.A. Boothe and C.G. Ringwall, "Fluidic Carrier Techniques", 1974 HDL symposium.

3. W.S. Griffin, "Fluid-Jet Amplifier with Flat Saturation Characteristics", J. Basic Eng., ASME Trans., v91 n4 1969 p734-9.

4. T.F. Urbanosky, "Flueric Operational Amplifier Summary", SAE paper 670707, 1967.

5. S. Florea and A.M. Stanescu, "A Circuit Viewpoint for Studying Beam Deflection Amplifiers", paper DA, 2nd IFAC Symposium on Fluidics, 1971.

6. C.A. Belsterling, "Fluidic Systems Design", Wiley-Interscience, N.Y. 1971.

7. F.T. Brown and R.A. Humphrey, "Dynamics of a Proportional Fluidic Amplifier, Part I" and "..., Part II", J. Basic Eng., ASME Trans., v92 Series D n2 June 1970 p302-321.

8. K. Toda, G. Roffman, and A.I. Talkin, "Matched Acoustic Generator", J. Dyn. Syst. Meas. and Control, ASME Trans., v94 Series G n1 Mar 1972 p11-14.

9. F.T. Brown, J.S. Boparai and T.M. Sheikh, "Design of a Near-Optimal Fluidic Operational Amplifier", Tech. Rep't n16 Themis Project, Dept. of Mech. Eng. and Mechanics, Lehigh University, for Office of Naval Research, Jun 1973.

10. K. Toda and S. Katz, paper in 1974 HDL symposium.

11. J. Kirshner, ed., Fluid Amplifiers, McGraw-Hill, N.Y., 1966.

12. T. Sarpkaya, "On Mean Motion, Jet Turbulence and Noise in Proportional Fluid Amplifiers", 2nd IFAC Symposium on Fluidics, Prague, 1971, and Fluidics Quarterly, v4 n1 1972 p30-36.

13. R. Massen, "On the Measurement of Signal Noise in Proportional Fluidic Amplifiers", 2nd IFAC Symposium on Fluidics, Prague, 1971, and Fluidics Quarterly, v4 n1 1972 p37-49.

14. L.R. Kelley and R. Kantola, "Fluidic/Flueric Low Frequency Noise Investigation", Final Report, Research and Development Center, General Electric Co., Schenectady, N.Y., under Contract N00019-69-C-0571 for Naval Air Systems Command, Aug 1970.

15. F.T. Brown, "Stability and Response of Fluid Amplifiers and Fluidic Systems", Engineering Projects Lab. MIT, Cambridge, Mass., prepared for NASA under contract NAS 3-5203, Oct 1967.

16. P.M. Lee and C.K. Kwok, "Design Method for Laminar Resistors", Fluidics Quarterly, v4 n3 1972 p1-12.

17. P.M. Lee and C.K. Kwok, "Design Rule for Rectangular Laminar Resistors", preprints Joint Automatic Control Conference, 1971, p414-9.

18. A.J. Bedard, Jr., "The Design of a Temperature-Independent D-C Flow Resistor", ASME paper 72-WA/Flcs-12, 1972, also Fluidics Quarterly, v5 n2 p31-50.

19. K.E. Bowles, E.M. Dexter, R.F. Turek, L.R. Moose, and J.J. Zalondek, Jr., "Fluidic AC Amplifiers", paper G2, Third Cranfield Fluidics Conference (Turin) 1968.

20. D.E. Boddy, "Synthesis of Transfer Functions Using RC Fluidic Circuits", paper F3, Fourth Cranfield Fluidics Conference (Coventry) 1970, also Fluidics Quarterly, v3 n1 1971 p1-15.

21. J. Dagan, C.K. Kwok, "Study of Pneumatic Capacitors",
    ASME paper 71-WA/Flcs-3, 1971.

22. S. Katz and E. Hastie, "The Transition from Isothermal
    to Adiabatic Capacitance in Cylindrical Enclosures",
    Harry Diamond Laboratories report HDL-TM-71-35, Dec 1971.

23. R.E. Goodson and R.G. Leonard, "A Survey of Modeling
    Techniques for Fluid Line Transients", J. Basic Eng.,
    ASME Trans., v94 n2 June 1972 p474-82.

24. A.J. Healy and Carlson, "Frequency Response of Rectan-
    gular Pneumatic Transmission Lines", ASME paper
    69 WA/Flcs-5, 1969.

25. H. Schaedel, "A Theoretical Investigation of Fluidic
    Transmission Lines with Rectangular Cross-Section",
    paper K3, Third Cranfield Fluidics Conference (Turin)
    1968.

26. C.A. Belsterling, "Fluidic Component Descriptions and
    Systems Synthesis", Fluidics Quarterly, v1 n3 1968 p9-32.

27. Q.B. Chou, E.C. Hind, J.Y. Harrison and R.A.A. Bryant,
    "Analyses of Proportional Fluid Amplifiers in Cascade
    and with Feedback", preprints Joint Automatic Control
    Conference, 1969, p. ix-xviii.

28. G.L. Roffman and S. Katz, "Experimental Flueric Analog
    Computation", no 15 of HDL series on Fluerics (Fluid
    Amplification), TR-1292, Washington, D.C., 1965.

29. R.E. Wagner and J.A. Barrett, "Study of Basic Analog
    Amplifier Networks Using High Gain Fluid Amplifiers",
    paper K6, Third Cranfield Fluidics Conference (Turin)
    1968.

30. G.A. Parker and M.K. Addy, "The Use of Low Gain Fluidic
    Beam Deflection Amplifiers in Shaping Networks", pre-
    prints Joint Automatic Control Conference (JACC) 1969.

31. K. Foster and G.A. Parker, Fluidics — Components and
    Circuits, Wiley-Interscience, N.Y.-London, 1970.

32. M.C. Doherty, "Applying Fluidic Operational Amplifiers",
    Adv. in Instrumentation, v23 part II, ISA, 1968, also
    "A Second Generation of Analog Fluidics", Fluidics
    Quarterly, v2 n1 1970 p7-12.

33. G.F.H. Lloyd, "A Fluidic Proportional Amplifier Using
    Pulse-Width Modulation Technique", paper H4, Fourth
    Cranfield Fluidics Conference (Coventry) 1970.

34. "Fluidics – Operational Amplifier Model FS-12", advertising flyer and specification sheet, Specialty Fluidics Operations Section 37-365 General Electric Co. Schenectady, N.Y., undated (about 1970).

35. S. Katz and G. Roffman, "Flueric Feedback Integration and Computation", preprints 1966 Joint Automatic Control Conference, p150-157.

36. C. Pavlin and P. Facon, "A Fluidic Chain for Missile Altitude Control", paper L2, Fourth Cranfield Fluidics Conference (Coventry) 1970.

37. R.K. Rose, "Fluidic Power Control Systems", ibid, paper L3.

38. H. Stern, "Analog Fluidic Controls Is Now", Chem. Tech., v3 n2 Feb 1973 p111-14.

39. F. Holoubeck, "A Study of a Fluidic Open Loop Damping Flight Stability Augmentation System", paper C3, Fifth Cranfield Fluidics Conference (Uppsala) 1972.

40. A. Gelin and J. Jardinier, "Fluidic Application to Missile Control System", paper L1, Fourth Cranfield Fluidics Conference (Coventry) 1970.

41. S. Florea, I. Dumitrache, and A.M. Stanescu, "Fluidic Controller for Slow Processes in Chemistry", paper J2, ibid, 1970.

42. G.R. Schrader, "A Fluidic Operational Amplifier Computing Relay", Fluid Logic Conference Milwaukee, 1969, and Fluidics Quarterly, v2 n3 1970 p63-66.

43. L.R. Kelley and W.A. Boothe, "Hydraulic Fluidics", ASME paper 68-WA/FE-26, 1968.

44. W.A. Boothe, "Applying Fluidics to Hydraulic Controls", paper C4, Fifth Cranfield Fluidics Conference (Uppsala) 1972.

45. L.R. Kelley and W.A. Boothe, "Hydraulic Fluidics", J. Dynamic Systems, Measurement and Control, ASME Trans., v95 Series G n2 June 1973 p161-6.

46. V. Dvoretsky and K. Molchanov, "A Hydraulic Operational Amplifier with Fluid Impact Modulators", paper E8, 2nd IFAC Symposium on Fluidics, 1971.

47. L.R. Kelley, "A Fluidic Temperature Control Using Frequency Modulation and Phase Discrimination", preprints of Joint Automatic Control Conference, 1966, p123-31.

48. B. Ashikian, P. Darmedru, and R. Caen, "Proportional Fluid Amplifiers As Feedback Oscillators", J. Applied Mech., ASME Trans., v37 Series E n3 Sept 1970 p801-811.

49. J.R. Frey, J.N. Wilson and R.W. Besant, "A Study of the Parameters Affecting the Performance of Fluidic Feedback Oscillators", paper H2, Fourth Cranfield Fluidics Conference (Coventry) 1970.

50. K. Foster and J.B. Carley, "Analysis of Branched Pneumatic Transmission Lines Employed in High Frequency External Feedback Oscillators", paper H3, ibid.

51. W.A. Boothe, "New Fluid Amplifier Techniques for Speed Controls", preprints Joint Automatic Control Conference 1965.

52. A. Chitty and P. Lenaerts, "Analogue Fluidic Position Sensors", Fl. Power Int., v37 n433 Apr 1972 p49-51, and "Fluidic Displacement Sensing", ibid, v37 n431 Feb 1972 p25-28,49.

53. R.R. Clark, "Survey of Recent Developments in Semi-Fluidic, Proportional Control Systems", Fluidics Quarterly, v2 n1 1970 p13-20.

54. H.B. Kast and D.E. Uehling, "Fluidic Overspeed Sensor for a Power Turbine", ASME paper 69-GT-17, 1969.

55. R.W. Mayne, "Study of a Flueric Extremum Controller", paper D6, 2nd IFAC Symposium on Fluidics, 1971.

56. R.W. Mayne, "Fluidic Implementation of a Perturbation Extremum Controller", Fluidics Quarterly, v4 n3 1972 p58-69.

57. H.M. Schaedel, G. Kessel and M.E. Franke, "Some Investigations on Frequency Demodulating Systems with Fluidic Jet Deflection Amplifiers", Second International JSME Symposium on Fluid Machinery and Fluidics, Tokyo, 1972.

58. K.N. Reid and R.L. Woods, "Fluidic Control of a Hydrostatic Transmission in a Vehicle Propulsion System", J. Dyn. Systems, Meas. and Control, ASME Trans., v95 Series G n2 June 1973 p114-124.

59. R.V. Burton, "Hydrofluidic Servos for Industry", SAE preprint n 730787 1973 9p.

60. T. Sarpkaya, "On the Art of Advancing the Science of Fluidics", J. of System Dynamics, Measurement and Control, ASME Trans., v95 Series G n2 June 1973 p110-13.
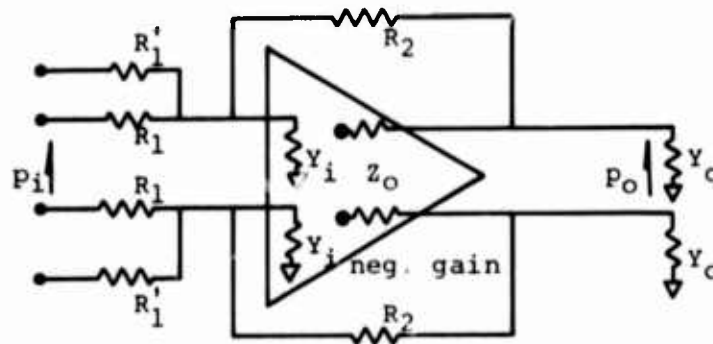
Fig. 1   Summing Operational Amplifier, Nominal Design
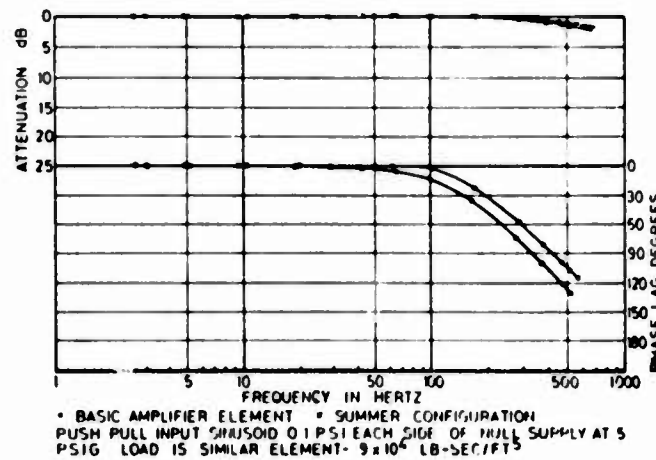
Fig. 2   Dynamics of Gain Block (Basic Amplifier Element)
(from Parker and Addy [30])
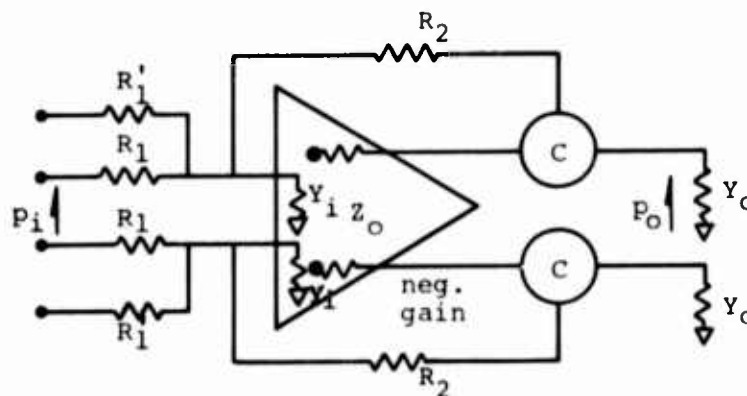
Fig. 3   Summing Operational Amplifier, Traditional Design

414

GAIN VS. INPUT SIGNAL FREQUENCY

Fig. 4 Advertised Data
for G.E. Opera-
tional Amplifier
(from [34])
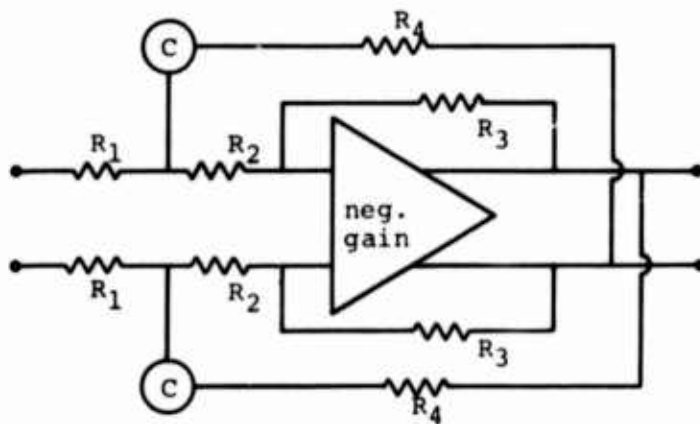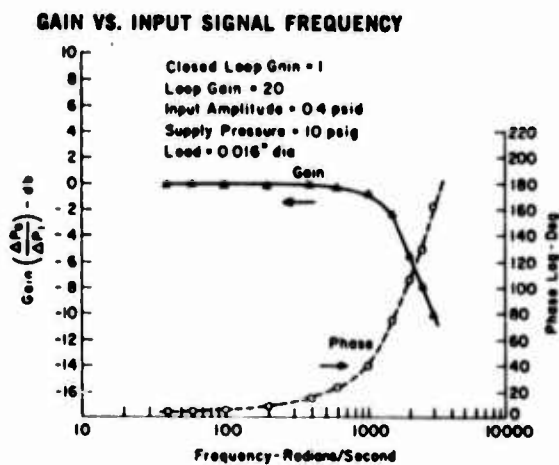
Fig. 5 Integrator Based on Operational Amplifier
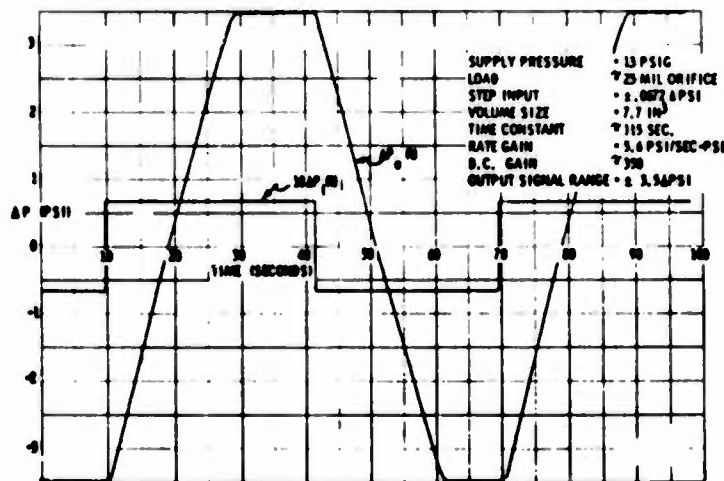
Fig. 6 Response of Integrator Including
Saturation (from Urbanosky [4])

415
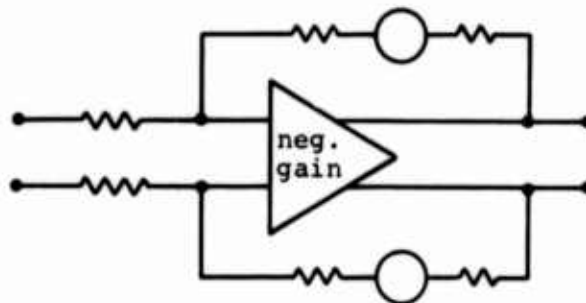
Fig. 7   Lead-Lag Based on Operational Amplifier
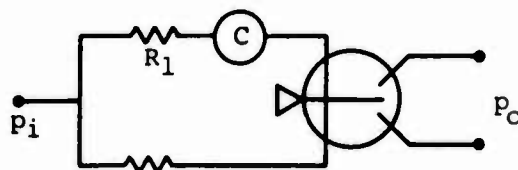
Fig. 8   Simple Lead-Lag
(from Boddy [20])
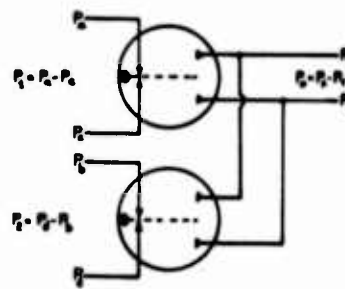
Fig. 9   Simple Summer (from
Parker and Addy [30])
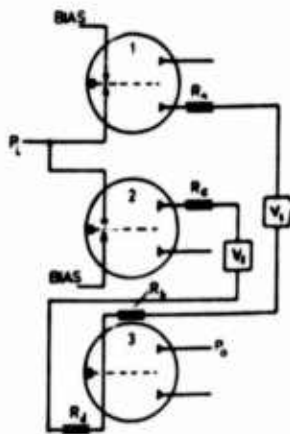
Fig. 10   Intermediate Com-
plexity Lead-Lag
(from Parker and
Addy [30])
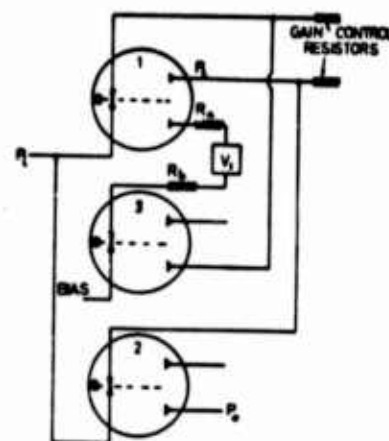
Fig. 11   Integrator (from
Parker and Addy [30])

(a) Tuned Flow Amplifier

(b) Tuned Pressure Amplifier

(c) Tuned Power Amplifier
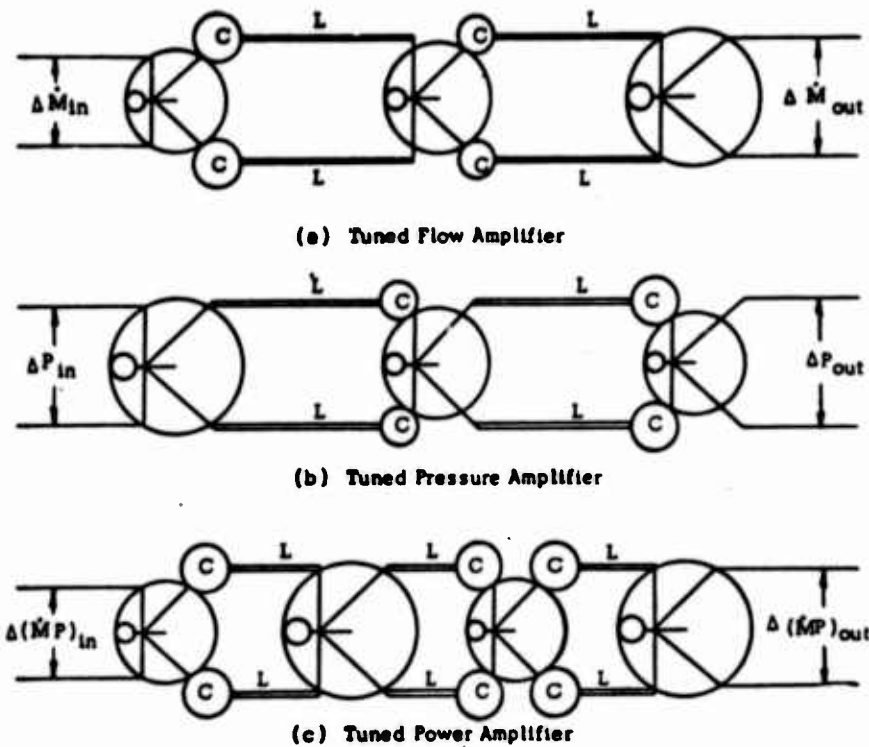
Fig. 12   Use of Fluid Inductances for Interstage Tuning
(from Bowles et al [19])
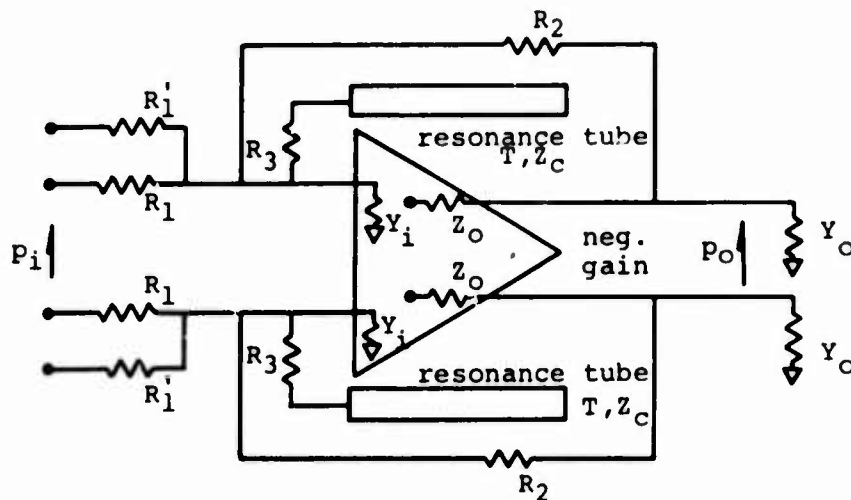
Fig. 13   Summing Operational Amplifier, Proposed Design

417

FLUIDIC NOTCH FILTERS

by

Gary L. Roffman
Harry Diamond Laboratories

Prepard for
Presentation at HDL
Fluidics State-of-the-Art Symposium
30 Sept - 04 Oct 74

ABSTRACT

Ten notch-filter circuits with biquadratic transfer functions are described. Notch filters are used in control systems to prevent instabilities due to mechanical resonances. The electronic circuit literature was searched to find circuits with biquadratic transfer functions that could be implemented with fluidic amplifiers. The amplifiers are assumed to have equal input and output impedances, and all high-gain amplifiers used are assumed to have a pressure gain of 2000. Using these characteristics, the frequency response of the circuits is calculated using a digita', circuit-analysis program. The best circuit, based on accuracy in producing a required transfer function for the M60A1 tank control system, gain insensicivity, and least number of compliances (bellows) requires three high-gain amplifiers. Advantages and disadvantages of all the circuits are discussed.

420

FLUIDIC NOTCH FILTERS

1. INTRODUCTION

This paper is concerned with the theoretical design of a fluidic notch filter. Notch filters are used in control systems to eliminate instability problems caused by resonances (usually mechanical) of the plant. The purpose of the notch filter is to reduce the system gain to less than unity at the resonant frequency. This prevents control loop oscillations that would occur if the (mechanical) resonance makes the system open loop gain greater than unity. An ideal notch has the frequency response shown in figure 1. One of the required characteristics for such a filter is that the gain (attenuation) be relatively constant in the vicinity of the notch center frequency. The reason for this is that the mechanical resonant frequency may shift slightly for one reason or another. If the notch were very sharp, it would no longer coincide with the resonant frequency if the resonant frequency shifted slightly. A second requirement is that the phase shift be small at the lower frequencies at which the system open loop gain is unity (the zero-dB crossover frequency). Finally, it is also necessary that the frequency response of the filter be relatively insensitive to changes in value of the components. This latter requirement is imposed by the fact that fluidic component values change with temperature and it may not be possible to hold the temperature constant in all cases.
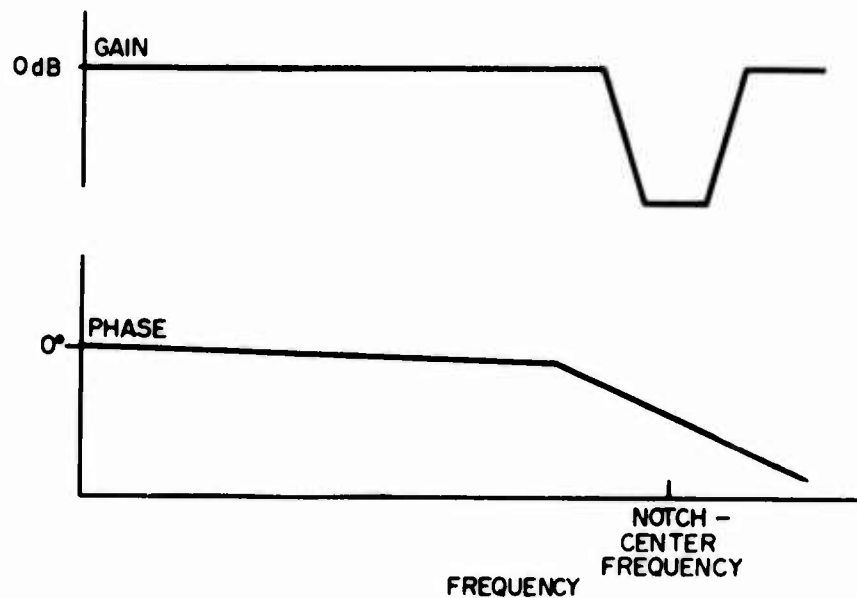
Figure 1. Ideal notch filter frequency response.

The method of approach was to adapt electronic notch-filter concepts for the parameters obtainable with fluidic devices. The electronic circuit literature was therefore searched. It was found that the ratio of two quadratic transfer functions (biquadratic transfer function or Biquad) can have a frequency response that approximates that of an ideal notch filter. On the basis of rough estimates ten biquadratic notch-filter circuits that seemed most likely to be capable of adaption to fluidics were selected and are described in this paper.

For each of the circuits analysed the proper values of the components were found by equating the coefficients found from the circuit equations with those of a Biquad for a specific c' rol system. This involved the solution of a set of simultaneous equations. A perturbation of the resistor values was then carried through on a computer and the effect on the transfer function determined.

2. TANK GUN STABILIZATION COMPENSATOR BIQUAD

The particular notch-filter frequency characteristics chosen was one that fullfilled the requirements for use with the M60A1 tank gun stabilization control system.

The transfer function $G(s)$ of the compensator circuit used in the gun elevation axis of the M60A1 tank is [1]

$$G(s) = \frac{(.046s + 1)(7.0 \times 10^{-5}s^2 + 1.5 \times 10^{-3}\, s + 1)}{(2.1\, s + 1)(2.1 \times 10^{-4}s^2 + 7.0 \times 10^{-3}\, s + 1)} \tag{1}$$

where s is the Laplace transform variable. The first fractional factor on the right side of the equation gives the single pole and zero of a lag-lead network. The ratio of the two quadratic terms is a biquadratic transfer function (Biquad). The notch-filter circuits developed in this paper are Biquads; and the Biquad in equation 1 is used as a realistic example to demonstrate the capabilities and difficulties associated with the notch-filter circuits.

The Biquad in equation 1 can also be written as

$$\frac{A(s^2 + 21s + 1.4 \times 10^4)}{(s^2 + 33s + 4.8 \times 10^3)} = \frac{A(s^2 + 2\zeta_n\omega_n s + \omega_n^2)}{(s^2 + 2\zeta_d\omega_d s + \omega_d^2)} \tag{2}$$

where
   A = constant,
   ζ_n = damping ratio of numerator,
   ω_n = natural radian frequency of numerator, $2\pi f_n$
   ζ_d = damping ratio of denominator, and
   ω_d = natural radian frequency of demoninator, $2\pi f_d$

The numerator quadratic has a resonant frequency f_n of 19 Hz and a damping ratio ζ_n of 0.09; the denominator quadratic has a resonant frequency f_d of 11 Hz and a damping ratio ζ_d of 0.24.

3. CIRCUIT CHOICE CONSIDERATIONS

The roots of the quadratic in the numerator of equation 2 are complex if $\zeta_n^2 \omega_n^2 < \omega_n^2$, i.e., if $\zeta_n < 1$. It is apparent that both the zeros (numerator) and the poles (denominator) of equation 2 are complex.

3.1 Passive and Active Circuits

A passive circuit composed of resistances, inductances, and capacitances (RLC circuit) can produce a Biquad with complex poles and zeros. Inductances are, however, often impractical to use. This is particularly true in fluidic circuits where inductance (inertance) is always accompanied by resistance and large diameter tubing would be required to minimize the resistance with respect to the inertance. The sizes required are often impractical.

A passive RC circuit cannot be used to produce a Biquad with complex poles [2], but a passive circuit can be built such that its Biquad has complex zeros and real poles. Adding a lead-lag circuit to one of the latter type circuits can produce a passive circuit whose transfer function approximates the required Biquad at the critical frequency bands for a notch filter.

An active RC circuit is required to build a Biquad with complex poles [2]. We therefore have examined one RLC passive circuit and one RC passive circuit but we have concentrated primarily on active circuits involving amplifiers whose Biquads have complex poles and zeros.

3.2 Fluidic Considerations

We have already pointed out the problems associated with inertance and will therefore concentrate primarily on circuits involving resistance and capacitance; however, the problem of inertance associated with passages is still with us. The major problem due to unwanted inertance is that the circuit capacitance present may, when combined with this inertance, result in resonant peaks (parasitics). It is therefore necessary that the tubing be small enough so that the associated inertance is small. If the inertance is sufficiently small the parasitic resonance will occur at frequencies higher than the frequency band of interest in the system.

Fluidic resistance is usually obtained by the use of capillary tubing which result in an almost linear resistance or by the use of orifices which result in a resistance that varies with flow. Linear resistors are easier to analyse and will not change value if the flow changes. They are, however, dependent on the viscosity of the fluid.

423

The large viscosity change of liquids as compared with gases due to temperature changes makes hydraulically supplied amplifiers and capillary tube resistors more sensitive than air to temperature variations. Using orifices for resistors reduces the temperature dependence. But orifice flow is nonlinear, and a linearizing bias flow is necessary. For linear flow resistance, the orifices operate with small signals around a bias flow. The bias flow must be kept constant or the resistance value will change, and the need for small signal levels reduces the dynamic range. Since it is impossible to supply bias flow through resistors that are blocked by capacitors (fig. 2a), circuits with capacitors shunted or bypassed by resistors are better for use with hydraulic oil; also they can be designed to be self-purging of air (fig. 2b).

a. Capacitor-blocked resistors

b. Capacitors shunted and bypassed by resistor

Figure 2. Fluidic RC circuits

Fluidic capacitance is obtained by the use of diaphrams, or bellows when the fluid is a liquid or when a point-to-point capacitance is required with a gas. Point-to-ground capacitance may be obtained in a gas by using its compressibility properties, but the effect is very small in a liquid. Since point-to-point capacitances are required for the circuits found for the notch-filter, we concern ourselves only with bellows type capacitances.

The use of fluid amplifiers for the active circuits involves some problems that are not significant in electronic amplifiers. A critical one is the fact that the input impedance of a fluid amplifier is relatively low. Notch-filter designs given in the electronics literature assume

that the amplifier input impedance is essentially infinite so that the electronic circuits must be modified to account for the finite input impedance of fluid amplifiers.

Furthermore the output impedance of an electronic amplifier is usually small enough to neglect and the amplifier is essentially level independent. Much more care must be exercised in the case of fluid amplifiers where the ratio of output to input resistance is usually of the order of unity.

If the notch filter is not to degrade the dynamic range of the control system significantly, noise must be kept to a minimum in the amplifiers that are part of the active networks. Consequently laminar fluid amplifiers must be used. The gain of a laminar proportional amplifier is dependent on the Reynolds number at lower Reynolds numbers. The Reynolds number on the other hand is a function of temperature. Thus at the higher temperatures (and associated higher Reynolds numbers), the gain of the amplifier is essentially independent of temperature; but if the temperature is sufficiently low (with associated small Reynolds numbers), the gain of the amplifier may decrease appreciably.

If the gain is to be kept constant over a temperature range that includes sufficiently low temperatures, an operational amplifier may prove more useful than an ordinary amplifier. An operational amplifier consists of a high gain amplifier (or chain of amplifiers) together with a feedback circuit such that the overall gain is essentially dependent on the passive components and is almost independent of the amplifier gain provided that the amplifier gain is high. Thus the temperature dependence is transferred from the amplifiers to the passive components.

Small fluidic amplifiers with low-flow requirements are desired to keep flow consumption low. If the amplifier is small, the amplifier resistances will be relatively large. Therefore, even the relatively large time constant-corresponding to the 19 Hz numerator resonant frequency (equation 2) could require only a small value of capacitance. If the parasitic capacitances due to compressibility effects are comparable in value to the required capacitance, the circuit frequency response will be highly dependent on the parasitic capacitance. Since this is undesirable, unduly small amplifiers and the small capacitance values associated with them cannot be used particularly if the medium is air.

For this paper amplifier resistance values of $5.0 \times 10^{10} \frac{N\text{-sec}}{m^5}$ ($120 \frac{PSI}{CIS}$) have been chosen. This resistance value is produced by an amplifier with a power jet nozzle .05 cm (.020 in) square operating with hydraulic fluid. This size amplifier provides a low flow drain while still allowing reasonable capacitance sizes. The smallest capacitance value used is $1.0 \times 10^{-13} \frac{m^5}{N}$ ($4.2 \times 10^{-5} \frac{in^3}{PSI}$). A bellows capacitor with this value should have parasitic capacitances to ground, due to the fluid volume on either side of the bellows, several orders of magnitude below the point-to-point value.

Section 7.1 shows that for the same Reynolds number flow the resistance of an orifice depends on fluid viscosity. Amplifier resistances are essentially orifices; thus, at the same Reynolds number an amplifier using air would have a much lower resistance than that of the same amplifier using hydraulic fluid. Regardless of the fluid medium laminar fluid amplifiers have similar gain characteristics for the same Reynolds number flow [3]. Unfortunately, the bulk modulus of elasticity of air is much less than that of hydraulic fluid. As a result the improvement in output resistance using air is offset by the problems due to the increase in circuit parasitic capacitances.

Although hydraulic amplifier resistance values are used in this paper, circuit impedance values can be scaled easily for air operation or for different sized amplifiers. To scale for air operation, resistance values should be multiplied by the ratio of amplifier resistance using air, to the resistance using hydraulic fluid; and circuit capacitances should be multiplied by the inverse of this ratio.

4. CIRCUIT CHOICES

Since the best way of overcoming the problems due to temperature is still to be determined, many (ten) circuits of different configurations were chosen for analysis. Eight are active, two are passive. Some of the active circuits require only a relatively low-gain amplifier so that a single stage is usually adequate. Other active circuits use operational amplifiers which, as indicated earlier, require a gain block and a feedback network.

Circuit selection for any particular case will depend on the notch characteristics required, the supply fluid, and the fluidic components available. Some circuits use fewer passive components than others, which is particularly important with respect to the relatively large bellows used as fluidic capacitors.

Although circuits using both high- and low-gain amplifiers are described, high-gain amplifiers in operational-amplifier circuits will probably be required because of the gain in sensitivity and the isolation provided by the low output impedance.

5. LOW-GAIN AMPLIFIER CIRCUITS

A wider range of transfer functions can be produced if an amplifier is used with a passive RC circuit. However, the frequency response of the circuit is sensitive to the amplifier gain, and the input and output impedances of the fluidic amplifiers must be included in the circuit. A circuit that uses only one amplifier could not be designed to meet the specifications associated with the tank gun stabilization compensator. However, a single-amplifier circuit was found that could produce a notch filter with a deeper and narrower notch and greater phase shift than that desired. On the other hand a two-amplifier circuit could be made with the necessary characteristics.

426

5.1 Low-Gain Two-Amplifier Circuit

Figure 3 shows a circuit with unspecified RC one ports. The circuit transfer function [4] is shown equated to the Biquad in equation 2:

$$\frac{P_O}{P_I} = \frac{\alpha \, [Y_3 - \mu Y_4]}{Y_1 + Y_3 + Y_4 - (\alpha - 1)Y_2} = \frac{s^2 + 21s + 1.4 \times 10^4}{s^2 + 33s + 4.8 \times 10^3} . \qquad (3)$$

The RC one ports needed to produce the Biquad are found by a circuit synthesis technique [4]. The numerator and denominator of the Biquad are divided by the term (s+A), yielding

$$\frac{\dfrac{s^2 + 21s + 1.4 \times 10^4}{s + A}}{\dfrac{s^2 + 33s + 4.8 \times 10^3}{s + A}} = \frac{(s+B) + \dfrac{(21 - A - B)s + 1.4 \times 10^4 - AB}{s + A}}{(s+D) + \dfrac{(33 - A - D)s + 4.8 \times 10^3 - AD}{s + A}}$$
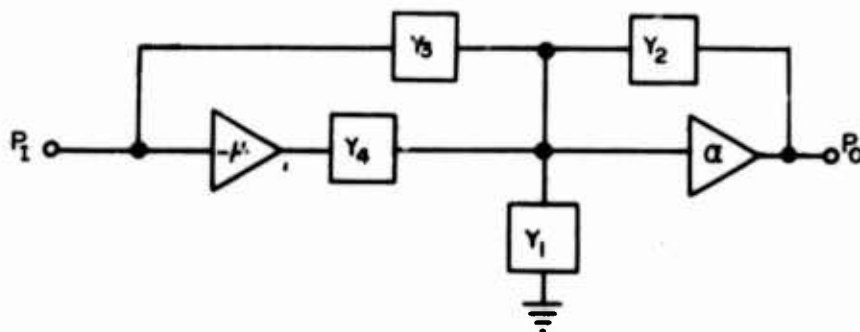
Figure 3. Two amplifier Biquad circuit

A is chosen so that the remainder quotients in the numerator and denominator are negative; then the corresponding positive and negative terms in equations 3 and 4 can be equated. From the resulting equations, the values of the one ports can be solved. The one ports are simple expressions for which circuits can be recognized easily. The value of A determines the magnitude of the one-port time constants and the one-port circuit configuration. Proper choice of A will provide reasonable circuit component values and allow the amplifier parasitic resistances to be included in the circuit (see also sect. 6.3).

Choosing A = 120 in equation 4 allows the amplifier resistances to be included in the circuit. Figure 4 shows a circuit with the one ports in figure 3 evaluated to produce the required Biquad. The component values were
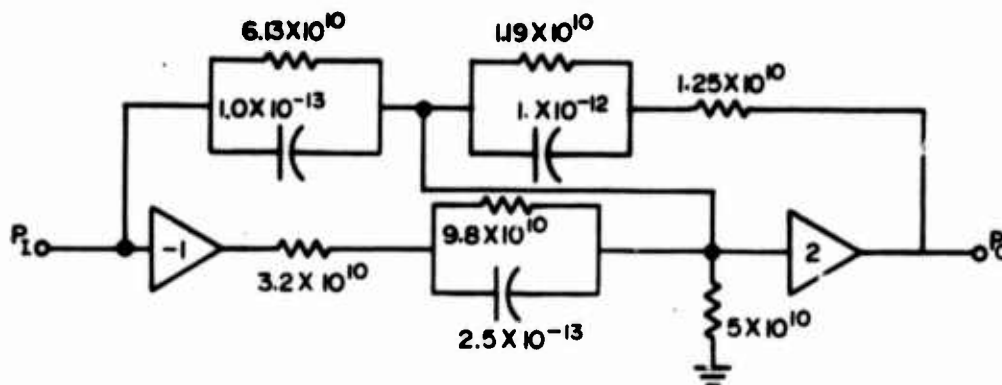
Figure 4. Coefficients for two amplifier Biquad circuit

scaled so that the smallest capacitor is $1.0 \times 10^{-13} \frac{m^5}{N}$ (see sect. 3). The units of resistance are $\frac{N-sec}{m^5}$. For simplicity, this circuit and all other circuits in the paper are shown single sided rather than differential. Since the fluidic amplifiers are differential amplifiers, a symmetric differential circuit will be needed for fluidic circuits. All capacitors in this circuit are shunted by resistors; thus, the circuit can be used with hydraulic supplies. The circuit cannot produce the required Biquad unless the driving source impedance is low. With the exception of the input impedance of the first amplifier, the input and output impedances of the amplifiers are included in the circuit. This impedance has no effect on the circuit frequency response if a low-impedance driving source is used. Although the amplifier parasitic impedances are included in the circuit, a value of A could not be found to make all amplifier resistances $5.0 \times 10^{10} \frac{N-sec}{m^5}$. Since some of the resistance values are less than $5.0 \times 10^{10} \frac{N-sec}{m^5}$, additional resistances cannot be added. The circuit resistance values cannot be scaled up without reducing the capacitance values, and one capacitor is already at the assumed minimum value of $1.0 \times 10^{-13} \frac{m^5}{N}$ (sect. 3). Also to avoid output loading problems the parallel, two-amplifier circuit in figure 5 is required.

Table I shows the frequency response of the Biquad in equation 2 at a low frequency (1 Hz), the zero-dB crossover-frequency band (5-8 Hz; exact frequency depends on system gain), and at the notch frequency (17-21 Hz). The phase at the notch frequencies is not given since it is not important for system stability. The gain and phase are only given at certain critical frequencies where the filter frequency response most affects the control system response. The tabular data display provides an easy method of comparing the responses at these critical frequencies. Table II (sect. a) is the frequency response of the low-gain, two-amplifier circuit shown in figure 4. The frequency response of this circuit and the other circuits in the paper were calculated using Net 2, a digital circuit simulation language [5]. The circuit of figure 4 and the Biquad of equation 2 have frequency responses that are nearly identical.

TABLE I. - Biquad Frequency Response

FREQ (Hz)	1	5	6	7	8	17	18	19	20	21
Gain (dB)	.04	1	1.6	2.3	3	-15.8	-19.5	-21.6	-21	-19.5
Phase(deg)	-2	-12.5	-17	-23	-31.5	—	—	—	—	—

TABLE II. Low-Gain Two-Amplifier Circuit with Parametric Variations

(a) Low-gain two-amplifier circuit

FREQ (Hz)	1	5	6	7	8	17	18	19	20	21
Gain (dB)	.04	1	1.5	2.1	2.8	-15.8	-19.5	-21.5	-20.8	-19
Phase (deg)	-2	-12.6	-17	-23	-31	—	—	—	—	—

(b) Resistance x 1.05

Gain (dB)	.03	1.1	1.7	2.3	3	-19	-21.4	-20.8	-19	-17.5
Phase (deg)	-2.1	-13.7	-18.5	-25	-35	—	—	—	—	—

(c) Resistance x 0.95

Gain (dB)	.04	.9	1.3	19	2.5	-12.6	-16	-19.6	-21.5	-20.9
Phase (deg)	-1.9	-11.7	-15.5	-20.5	-27	—	—	—	—	—

(d) Gain x 1.05

Gain (dB)	-7.6	-7.8	-8	-8	-8.5	-17.3	-18.8	-19.8	-19.8	-19.1
Phase (deg)	-2.7	-14	-17	-20	-24	—	—	—	—	—

(e) Gain x 0.95

Gain (dB)	+7.8	3	1.4	-.3	-3.7	-25	-33	-33	-26.6	-23
Phase (deg)	-8.5	-26	-27	-27	-27	—	—	—	—	—

429
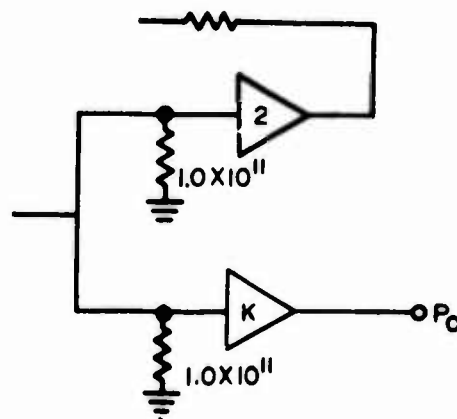
Figure 5. Output load reducing circuit

Varying all the resistors in the circuit in figure 4 by ±5 percent results in the frequency responses in table 11 (sect. b, c). Changing the resistor values shifts the notch center frequency, but the effect on the zero-dB crossover-frequency band is negligible. Changing the resistor values demonstrates the sensitivity of the circuit to resistance changes as would occur with temperature. When the resistance is produced predominantly by viscous forces, the ±5 percent resistance change corresponds to a ∓ 3°C change for hydraulic oil [6] and a +8°C and -15°C change for air [7] for an initial 20°C temperature. The relationship between viscosity and temperature is quite nonlinear [6], but hydraulic oil is more sensitive especially for large temperature changes. Changing the amplifier gains by ±5 percent (table 2d, e) changes the frequency response significantly, especially at the lower frequencies. The amplifier gains will, therefore, have to be kept constant to maintain the desired frequency response.

5.2 Single Amplifier Circuits

Figure 6 shows a Biquad circuit configuration suggested by Balabanian [8], and figure 7 shows a cirlct configuration proposed by Kuh [9]. These circuits can produce a biquadratic transfer functions and both have configurations that can be used in fluidic circuits. Unfortunately, neither circuit can produce the Biquad in equation 1 unless some of the passive components have negative values.

430
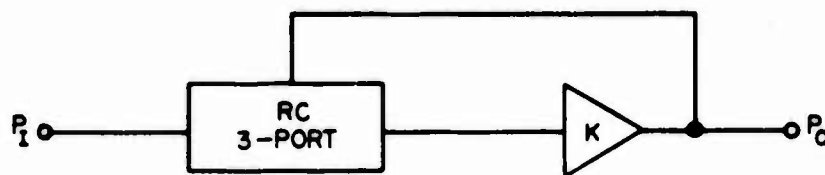
Figure 6. Circuit proposed by Balabanian
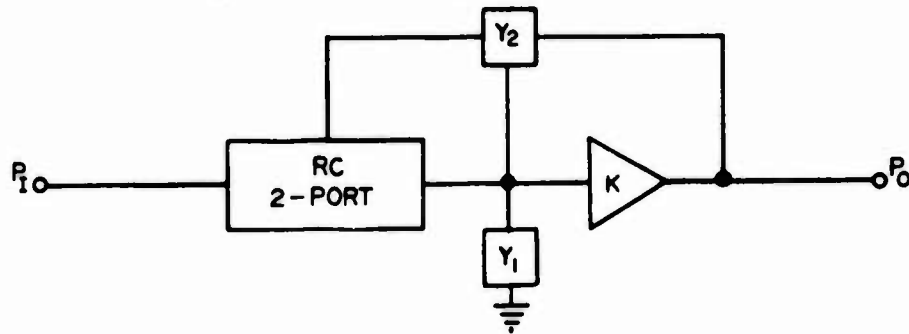
Figure 7. Circuit proposed by Kuh
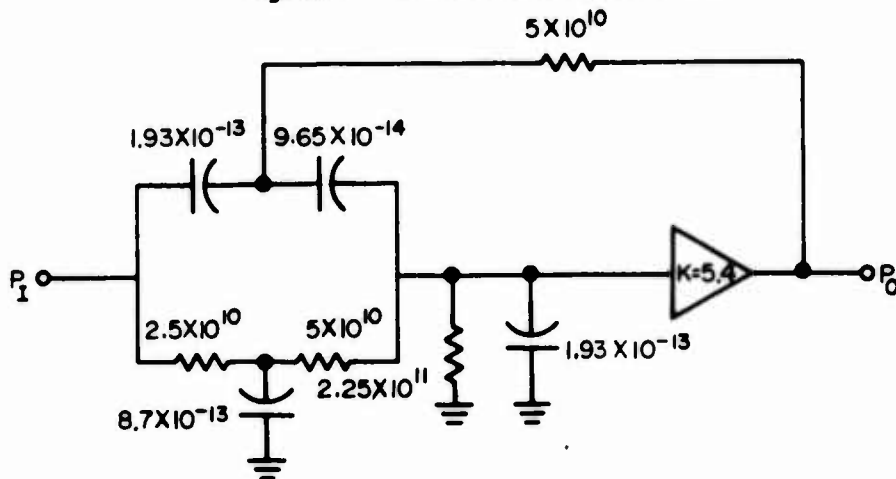
Figure 8. Elliptic filter circuit

5.3 Elliptic Filters

Figure 8 shows a circuit proposed by Kerwin and Huelsman [10] for an elliptic filter. An elliptic filter is a Biquad circuit with zero damping in the numerator. Although this transfer function is different from the Biquad in equation 2, a useable notch filter is produced. It is also a good circuit for fluidic use, since amplifier input and output impedances can be included in the circuit. However, since the feedback resistor is blocked by capacitors, this circuit is better for pneumatic operation.

The transfer function for the elliptic filter shown in figure 8 is

$$\frac{s^2 + 1.4 \times 10^4}{s^2 + 33s + 4.8 \ 10^3} \tag{5}$$

431

The component values are easily found from a set of equations given by Kerwin and Huelsman [10].

Table III shows the frequency response of the elliptic filter. The phase shift at the zero-dB crossover frequencies is greater than that of the required Biquad (table I), but the notch depth is much greater. Varying the resistor values by ±5 percent moves the notch-center frequency; but because of the greater notch depth, the rejection at the notch center frequency, 19 Hz, is still greater than that of the Biquad in equation 1 (table IIIb, c). Changing the gain by ±5 percent has little effect on the notch frequency response, but the phase lag at the zero-dB cross-over frequencies is affected. (table IIId, e).

5.4 Boddy-Feedforward Circuit

Boddy [11] describes a number of fluidic RC circuits that include a Biquad (figure 9). The circuit corresponding to the block diagram in figure 9 has the same transfer function form as Boddy's circuit but provides more insight into the circuit design and simplifies the transfer-function calculation. The transfer function for the circuit of figure 9 is

$$\frac{P_O}{P_I} = \frac{B \left[s^2 + (\alpha + \beta)s + \frac{\alpha\beta B + C}{B} \right]}{s^2 + (\alpha + \beta)s + \alpha\beta + AC} \tag{6}$$

Matching these coefficients to the resonant frequencies and damping coefficients in equation 2 yields

$$\omega_n = \sqrt{\alpha\beta + C/B} \qquad \zeta_n = \frac{\alpha + \beta}{2\sqrt{\alpha\beta + C/B}} \tag{7a}$$

$$\omega_d = \sqrt{\alpha\beta + AC} \qquad \zeta_d = \frac{\alpha + \beta}{2\sqrt{\alpha\beta + AC}} \tag{7b}$$
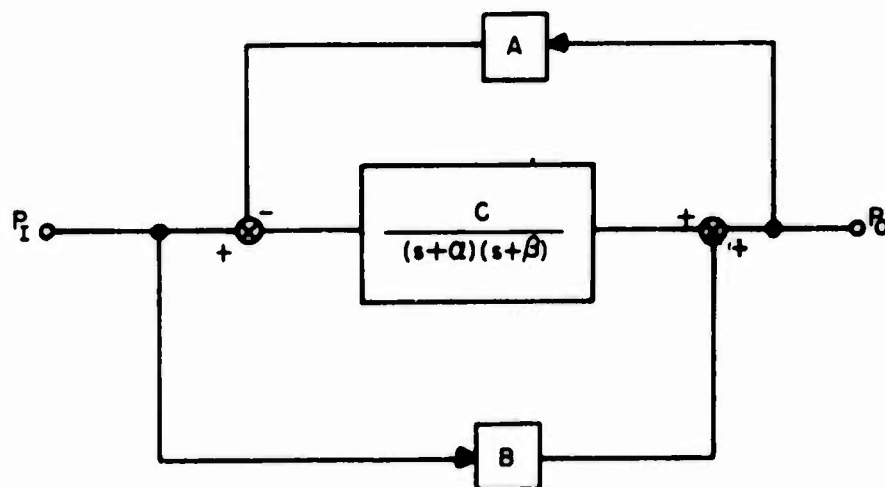
Figure 9. Feedforward circuit given by Boddy

432

TABLE III. Elliptic Filter with Parametric Variations

(a) Elliptic Filter

FREQ (Hz)	1	5	6	7	8	17	18	19	20	21
Gain (dB)	0	1.	1.6	2.2	3.	-17.8	-25	-56	-27.5	-22
Phase(deg)	-2.5	-15	-20	-27	-36	—	—	—	—	—

(b) Resistance x 1.05

Gain (dB)	0	1.2	1.8	2.5	3.3	-23	-44	-28	-22	-19
Phase(deg)	-2.6	-16	-22	-30	-41	—	—	—	—	—

(c) Resistance x 0.95

Gain (dB)	0	.6	.9	1.4	2	-13.4	-18.4	-25.4	-56	-28
Phase(deg)	-2.4	-14	-19	-24	-32	—	—	—	—	—

(d) Gain x 1.05

Gain (dB)	.5	1.6	2.2	3	4	-17	-24	-55	-27	-21.6
Phase(deg)	-2	-12	-16	-22	-30	—	—	—	—	—

(e) Gain x 0.95

Gain (dB)	-.5	.5	.9	1.4	1.9	-18.7	-25.7	-56	-28	-23
Phase(deg)	-3	-18	-24	-31	-42	—	—	—	—	—

From equations 7a and 7b,

$$\omega_n \zeta_n = \omega_d \zeta_d = \frac{\alpha + \beta}{2} \qquad (8)$$

For the Biquad in equation 2, the product of the resonant frequency and the damping ratio of the numerator and denominator quadratic terms, respectively, are not equal. Therefore, Boddy's circuit cannot be used to produce this transfer function. Another difficulty with Boddy's circuit is that equation 8 limits the values of α and β; thus, the gain C must be very large ($C = 10^4$) to produce the required resonant frequencies. Accuractely maintaining such high gains is not feasible.

5.5 Low-Gain Amplifiers Summary

The two-amplifier circuit (sect. 5.1) is the only circuit found with low gain that can accurately produce the required Biquad. The elliptic circuit is relatively insensitive to gain changes and, if a way to add damping to the numerator quadratic could be found, it would also be relatively insensitive to resistance changes. Both of these circuits require low impedance driving sources and constant amplifier gains. It may be necessary to use the operational amplifier circuits described in the next section to provide these requirements.

6. OPERATIONAL-AMPLIFIER CIRCUITS

If the amplifier block has sufficiently high gain, the gain of the operational amplifier, scaling circuit in figure 10 is determined by the ratio of the feedback resistor R_F to the input resistor R_I. Also the high-gain amplifier input impedance R_I and output impedance R_o can be neglected when the scaler is used in a larger circuit. If the scaler circuit is used as the amplifier in section 5, the scaler gain will remain constant as long as R_F/R_I is constant and the gain is sufficiently high. Also because of the low output impedance of the scaling circuit, it can be used to drive the circuits in section 5.
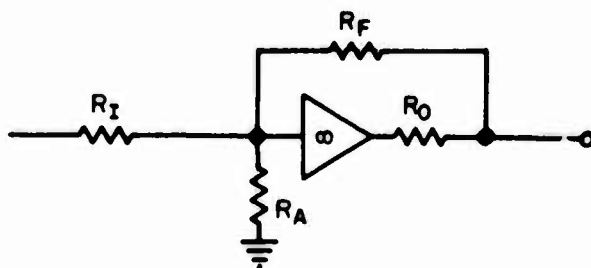

Figure 10. Operational amplifier circuit for low gain scaler

By using RC circuits in the input and feedback of high-gain amplifiers (operational amplifiers), the frequency response of the circuits is

434

dependent only on the passive components as long as the gain is sufficiently high. Because of the relatively low input impedance, relatively high output impedance and only moderately high gain of fluidic gain blocks, the loading effects of the amplifier parasitic impedance cannot be neglected. Phase delay in the gain block can also cause stability problems [12,13]. In this section of the paper six circuits using high-gain amplifiers are described, and the frequency response of the circuits including amplifier parasitic resistances is calculated.

6.1   Input and Feedback Transfer-Impedance Ratio Circuits

Figure 11 shows a high-gain amplifier with a two-port input and feedback circuit. The overall circuit transfer function is

$$\lim_{k \to \infty} \frac{P_o}{P_I} = \frac{Z_{21F}}{Z_{21I}} \tag{9}$$

where

Z_{21} is the transfer impedance of the two port,

F   is the feedback subscript, and
I   is the input subscript.

The transfer impedance of RC two-port circuits are catalogued and can be found in many references [14, 15, 16]. Producing the required Biquad becomes a task of finding RC transfer impedances with complex poles. The placement of the transfer-impedance zeros, the spread of the component values, and the circuit configuration lead to several circuit possibilities.
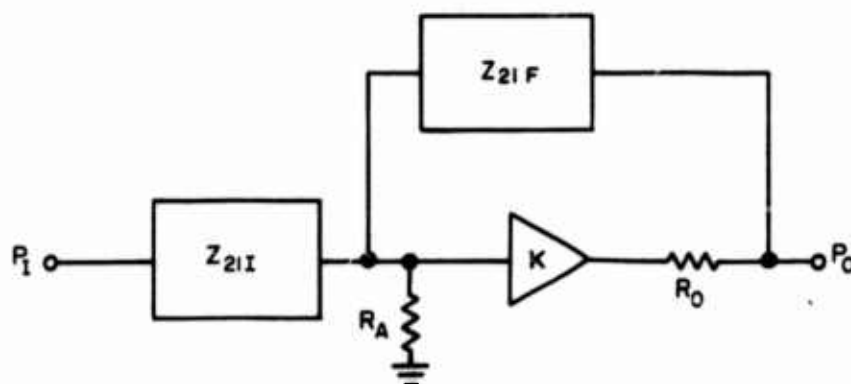

Figure 11.   Input and feedback ratio operational amplifier circuit

435

6.1.1 Simple Bridge-Tee Biquad

Figure 12 shows a bridged-tee circuit with the transfer impedance [17]

$$Z_{21} = \frac{A (T_1 s + 1)}{T_1 T_2 s^2 + T_1 s + 1} \tag{10a}$$

and $A = R_2$, $T_1 = 2R_1 C$, and $T_2 = R_2 C/2$; (10b)

using this transfer impedance in equation 9

$$\frac{P_O}{P_I} = \frac{A_F (T_{1F} s + 1)(T_{1I} T_{2I} s^2 + T_{1I} s + 1)}{A_I (T_{1I} s + 1)(T_{1F} T_{2F} s^2 + T_{1F} s + 1)} \tag{11}$$

The coefficients of equation 11, obtained by comparing like coefficients of equations 1 and 11, are

$$
\begin{array}{ll}
T_{1I} = 1.5 \times 10^{-3} & T_{2I} = 4.7 \times 10^{-2} \\[2mm]
T_{1F} = 7.0 \times 10^{-3} & T_{2F} = 3.0 \times 10^{-2}
\end{array}
\tag{12}
$$

The component values are calculated by using these values in equation 10b. The pole frequency in equation 11 is $1/T_{1I} = 670$ rad/sec or 107 Hz, and the zero frequency is $1/T_{1F} = 140$ rad/sec or 23 Hz. The pole can be ignored, but the zero will affect the desired transfer function (equation 1).

Figure 13 shows the simple bridged-tee circuit with components evaluated to produce the required Biquad. The high-gain amplifier is assumed to have a gain of -2000 with both input and output impedances equal to $5.0 \times 10^{10} \frac{N\text{-sec}}{m^5}$. The dynamics of the gain blocks are assumed to be second order, with a resonant frequency of 200 Hz and a damping ratio of 0.5. The impedance values were picked for a hydraulic amplifier, but the circuit values can easily be scaled for different impedance values by a different choice of A. The amplifier dynamics were chosen to represent the lowest resonant frequency measured in fluid amplifier frequency response tests [18].

Table IVa shows the frequency response of the simple bridged-tee circuit. Because of the additional zero at 23 Hz, the notch is not as deep as the required Biquad notch (table I), but the phase shift at the zero-db crossover frequencies is less (tables I and IVa). Reducing T_{1I} in equation 11 would reduce not only the notch depth but also the notch width, making the circuit more sensitive to notch center frequency shifts. Some tradeoffs of the desired Biquad (equation 1) characteristics might be considered because of the low phase shift and simplicity of this circuit. Table IV (sect. b, c) shows the frequency response with resistance changes of ±5 percent. The notch center frequency does not change significantly, and the low-frequency phase shift is still small.

436
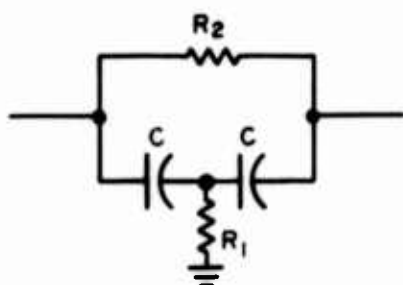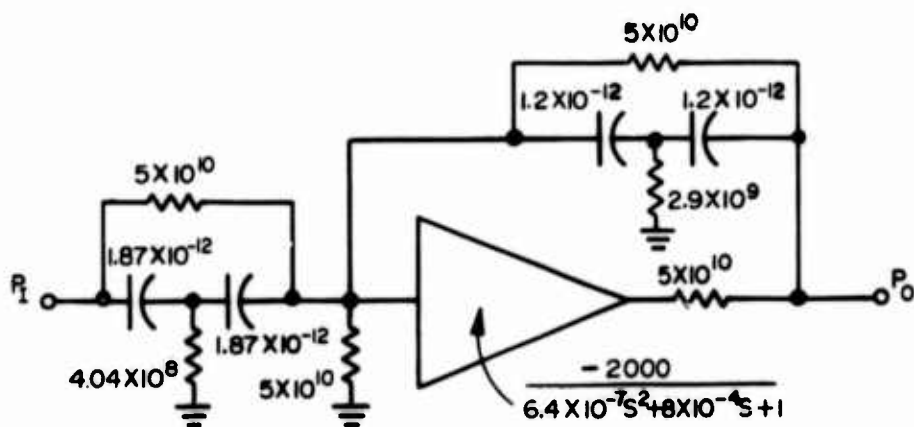
Figure 12.   Simple bridged-tee circuit

Figure 13.   Simple bridged-tee biquad circuit

437

TABLE IV. Simple Bridged-Tee Circuit with Parametric Variations

(a) Simple Bridged-Tee Biquad

FREQ (Hz)	1	5	6	7	8	17	18	19	20	21
Gain (dB)	0	1.2	1.9	2.6	3.5	-14.4	-17.8	19.6	-18.9	-17
Phase (deg)	-1	-3.5	-6	-11	-18	—	—	—	—	—

(b) Resistance x 1.05

Gain (dB)	0	1.4	2	2.9	3.7	-17.3	-19.6	-18.9	-17	-15.4
Phase (deg)	0	-4	-7	-13	-22	—	—	—	—	—

(c) Resistance x 0.95

Gain (dB)	0	1	1.6	2.3	3	-11	-15	-18	-19.6	-18.9
Phase (deg)	0	-3	-5	-9	-15	—	—	—	—	—

TABLE V. Compound Bridged-Tee Biquad

FREQ (Hz)	1	5	6	7	8	17	18	19	20	21
Gain (dB)	.28	5.8	-.75	-5.6	-9	-35	-38	-40	-39	-37
Phase (deg)	-4	-128	-151	-159	-163					

TABLE VI. Dual of Bridged-Tee for Lag-Lead and Biquad

(a) Lag-Lead and Biquad

FREQ (Hz)	1	5	6	7	8	17	18	19	20	21
Gain (dB)	-2.2	-10.6	-10.5	-10.2	-9.6	-29	-33	-35	-34	-33
Phase (deg)	-72	-47	-46	-49	-54	—	—	—	—	—

(b) Dual of Compound Bridged-Tee Biquad

Gain (dB)	-3	-14	-15	-17	-18	-37	-40	-41	-40	-38
Phase (deg)	-80	-82	-87	-92	-96	—	—	—	—	—

438

The grounded resistor in figure 13 is blocked by capacitors; thus, this circuit is better for pneumatic operation. The dual of the bridged-tee is shown in figure 14. This circuit can be used with hydraulic fluid; but now the pole and zero depend on T_{2I} and T_{2F}, respectively (equations 11 and 12), which are at lower frequencies. This pole and zero radically change the frequency response from the desired values.

6.1.2 Compound Bridged-Tee Biquad

Adding a capacitor in parallel to the circuit in figure 12 produces the circuit in figure 15, which has the transfer impedance [17]

$$Z_{21} = A \frac{T_3s + 1}{T_1T_2s^2 + T_1s + 1} \tag{13}$$

with $T_3 < T_1$.

The zero can be arbitrarily chosen as long as $T_3 < T_1$. Choosing $T_3 = 0.50 \times 10^{-3}$ for both input and feedback impedances, the pole and zero produced in the operational amplifier circuit (equation 11) cancel. The circuit element coefficients are found by using equation 12, setting $T_3 = 0.50 \times 10^{-3}$, and by using the following equations [17]

$$R_1 = \frac{AT_3^2}{4[T_1T_2 - T_3(T_1 - T_3)]} \qquad\qquad R_2 = A$$

$$C_1 = \frac{2[T_1T_2 - T_3(T_1 - T_3)]}{AT_3} \qquad\qquad C_2 = \frac{T_1 - T_3}{A} \; . \tag{14}$$

Figure 16 shows the circuit used to produce the required Biquad. The operational amplifier has the same gain and phase characteristics as the amplifier in figure 13. The frequency response of the circuit is shown in table V and is quite different from that of the required Biquad (table I). This difference was attributed to the small resistance values that load down the amplifiers output. To overcome this problem, greater gains or lower output impedances are required.

6.1.3 Compound Bridged-Tee for Biquad and Lag-Lead

Figure 17 shows the dual of the compound bridged-tee circuit. Since the resistors are not blocked by capacitors, this circuit can be used with hydraulic supplies. The transfer impedance of the circuit is [19]

$$Z_{21} = \frac{A(T_3s + 1)}{T_1T_2s_2 + T_1s + 1} \; , \tag{15}$$

where $T_3 > T_2$.

The zero and pole produced by T_{3F} and T_{3I}, respectively, can have arbitrary values as long as $T_3 > T_2$; it is, therefore, possible to make these time constants similar to the lag-lead in the tank compensator
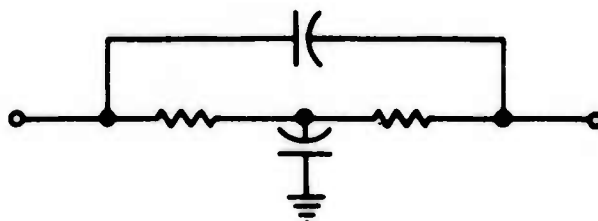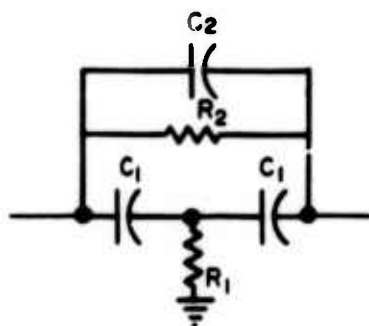
Figure 14.   Dual of simple bridged-tee

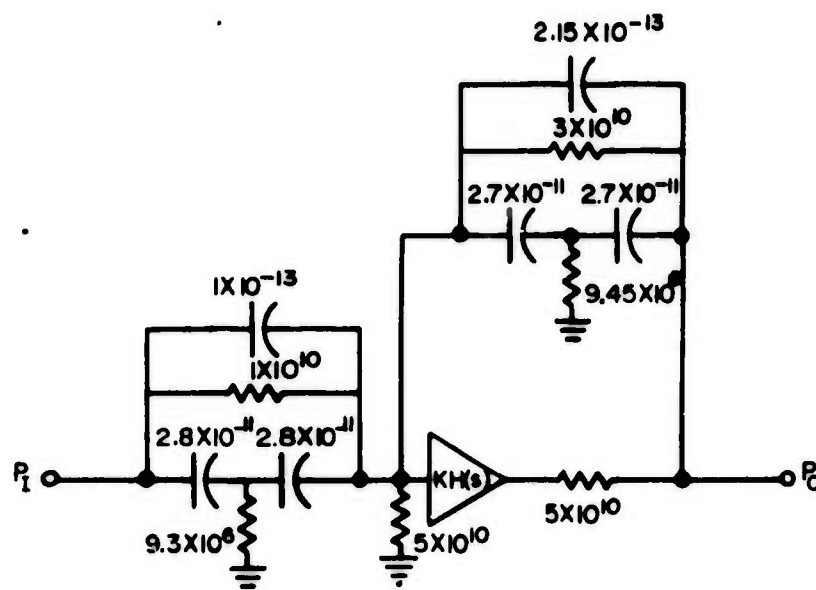Figure 15.   Compound bridged-tee circuit

Figure 16.   Compound bridged-tee biquad circuit

440

control system (equation 1). Using the time constants in equations 1 and 12 in the following equations gives the component values of figure 18

$$R_1 = \frac{AT_3^2}{2\,[T_3^2 - T_1(T_3 - T_2)]} \qquad R_2 = \frac{AT_3^2}{T_1(T_3 - T_2)} \qquad (16)$$

$$C_1 = \frac{4[T_3^2 - T_1(T_3 - T_2)]}{AT_3} \qquad C_2 = \frac{T_1 T_2}{AT_3}$$

$$A = \frac{2R_1 R_2}{2R_1 + R_2} \quad .$$

Table VI(a) shows the frequency response of equation 1 and table VI(b) shows the response of the circuit in figure 18. Again the amplifier is loaded by the circuit as can be seen by the large phase shift at the zero-dB crossover frequencies. A lower output impedance amplifier is needed for satisfactory performance.

6.2 Bohn's Biquad Circuit

Figure 19 shows a multiple feedback circuit configuration proposed by Bohn [20,21]. The boxes represent one-port admittance circuits. The transfer function for this circuit is

$$\frac{P_o}{P_I} = \frac{Y_3 Y_1 + Y_6 (Y_1 + Y_2 + Y_3 + Y_4)}{Y_3 Y_4 + Y_5 (Y_1 + Y_2 + Y_3 + Y_4)} \qquad (17)$$

when the amplifier gain is large. Various one-ports could be chosen [21], but a satisfactory choice for a fluidic circuit is shown in figure 20. Following are the circuit values that were found. First, the one ports in figure 19 are

$$Y_1 = G_1 \qquad Y_2 = C_2 s \qquad Y_3 = G_3$$

$$Y_4 = C_4 s + G \qquad Y_5 = Y_6 = C_o s \qquad (18)$$

where $G_i = 1/R_i$.

Using these values, equation 17 becomes

$$\frac{P_o}{P_I} = \frac{s^2 + \dfrac{(G_1 + G_3 + G_4)}{C_2 + C_4}\,s \qquad \dfrac{G_1 G_3}{C_0(C_2 + C_4)}}{s^2 + \dfrac{[G_3 C_4 + C_0(G_1 + G_3 + G_4)]s}{C_0(C_2 + C_4)} + \dfrac{G_3 G_4}{C_0(C_2 + C_4)}} \quad . \qquad (19)$$

Equating like coefficients of equations 19 and 2 provides four simultaneous equations and six unknowns. By setting two of the unknowns to the values

$$C_0 = 1.0 \times 10^{-13} \qquad \text{and } G_3 = \frac{1}{R_3} = 1.0 \times 10^{-10}; \qquad (20)$$

and using a digital computer routine for sets of nonlinear, simultaneous equations to solve for the remaining unknowns, the component values in figure 20 were evaluated.
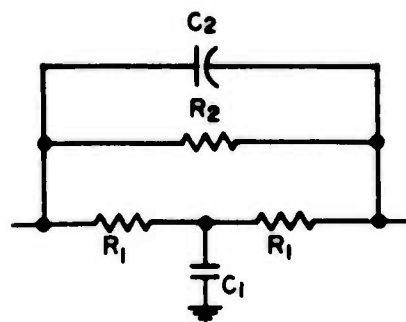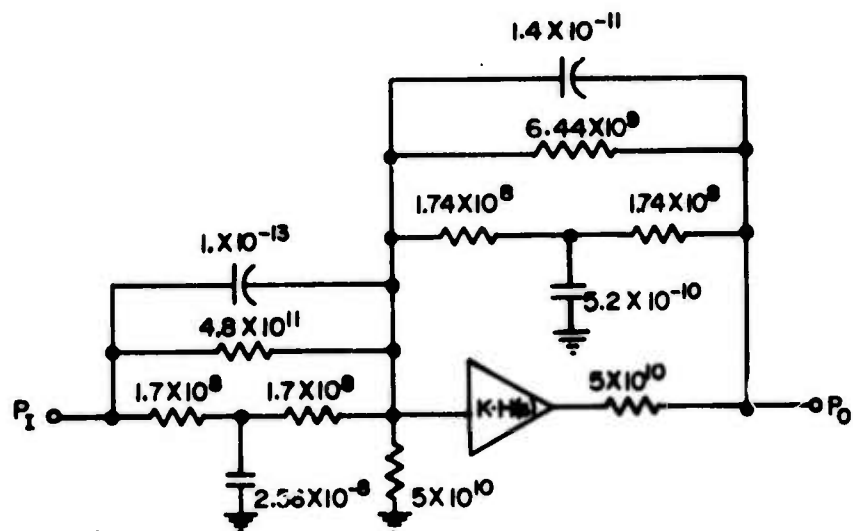
Figure 17. Dual of compound bridged-tee

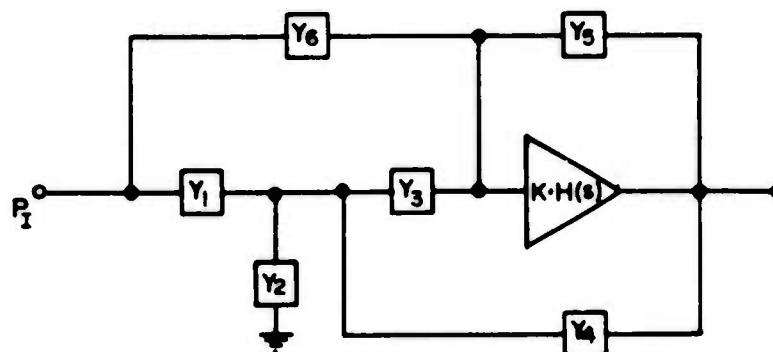Figure 18. Dual compound bridged-tee biquad circuit

Figure 19. Circuit configuration for Bohn's circuit

442

The amplifier in figure 20 has the same gain and phase characteristics as previously used. Table VII (a) shows the frequency response of the circuit in figure 20. The response is slightly different from that of the required Biquad because of amplifier loading, but the response is much closer to that of the required Biquad than the two previous circuits. Tables VII (b,c) show the effects of changing the resistors by ±5 percent. The frequency response is relatively insensitive to the resistance changes.

Because the amplifier in this circuit is only slightly loaded by the circuit, the effects of lowering the output impedance were investigated. Since for fluidic amplifiers a decrease in output impedance causes a decrease in gain, the gain was scaled down by the same ratio as the input impedance. Table VII(d, f) shows that there is no improvement in the matching of the circuit frequency response to the required Biquad as the output impedance R_o and gain are reduced. However, the change in the circuit frequency response is quite small. Thus, if amplifiers with lower gain and lower output impedance were available, this technique might be useful. The gain and output impedance tradeoff will work for other circuits when the output impedance is the major resistance term limiting the accuracy of the frequency response [22]. One advantage of a lower pressure-gain amplifier is a lower output-pressure bias level. Because of the feedback to the amplifier input, a lower output-pressure bias level would produce a lower bias-pressure level at the amplifier input. The gain of most fluidic amplifiers depends on the input-pressure bias level [23].

6.3 Two-Operational-Amplifier Circuit

The circuit configuration shown in figure 21 has the transfer function [24]

$$\lim_{k \to \infty} \frac{P_o}{P_I} = \frac{Y_1 Y_5 - Y_2 Y_3}{Y_3 Y_6 - Y_4 Y_5} = \frac{Y_1 - Y_2}{Y_6 - Y_4} . \tag{21}$$

if $Y_3 = Y_5$.

Setting equation 21 equal to equation 2 gives

$$\frac{Y_1 - Y_2}{Y_6 - Y_4} = \frac{s^2 + 21s + 1.4 \times 10^4}{s^2 + 33s + 4.8 \times 10^3} \tag{22}$$

Dividing the numerator and denominator of equation 22 by $s + \alpha$ gives

$$\frac{\dfrac{s^2 + 21s + 1.4 \times 10^4}{s + \alpha}}{\dfrac{s^2 + 33s + 4.8 \times 10^3}{s + \alpha}} = \frac{s + \beta + \dfrac{(21 - \alpha - \beta)s + 1.4 \times 10^4 - \alpha\beta}{s + \alpha}}{s + \gamma + \dfrac{(33 - \alpha - \gamma)s + 4.8 \times 10^3 - \alpha\gamma}{s + \alpha}} . \tag{23}$$
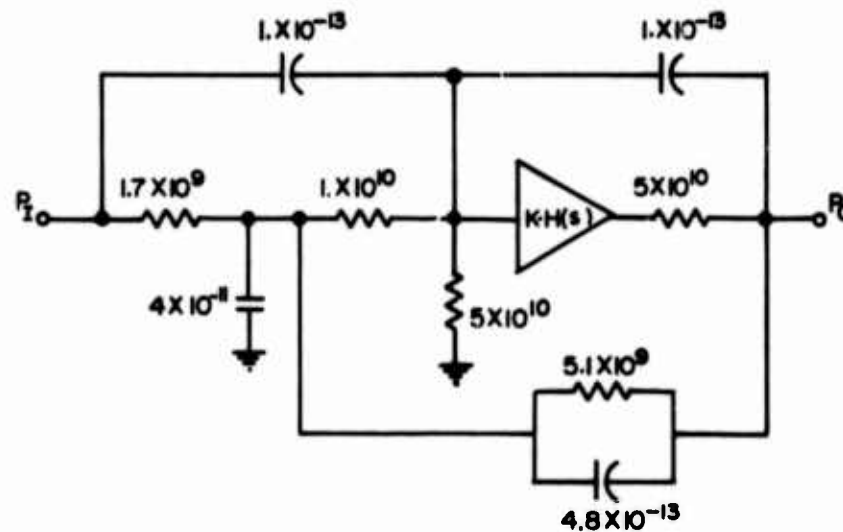
443

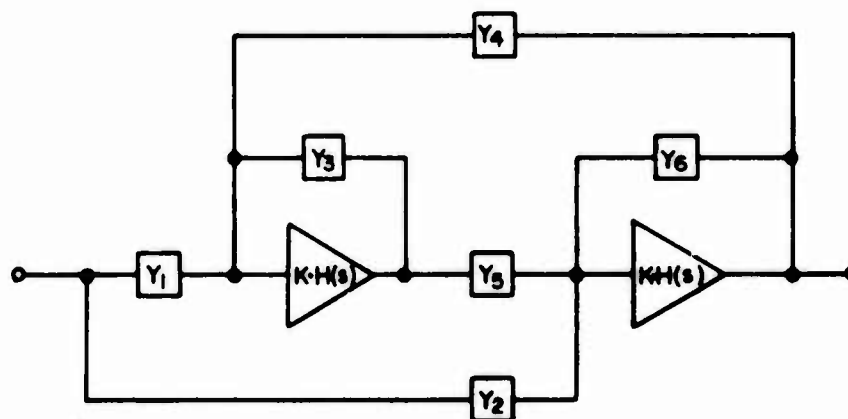Figure 20. Bohn's circuit for producing complex biquad

Figure 21. Two-operational-amplifier configuration

TABLE VII. Bohn's Circuit with Parametric Variations

(a) Bohn's Biquad Circuit

FREQ (Hz)	1	5	6	7	8	17	18	19	20	21
Gain (dB)	.03	1	1.4	2	2.5	-16.5	-20	-22	-21	-19.7
Phase(deg)	-2.5	-15	-20	-27	-36.5	——	——	——	——	——

(b) Resistance x 1.05

Gain (dB)	.03	1.0	1.6	2.15	2.65	-19.6	-22	-21	-19.6	-18
Phase(deg)	-2.5	-16	-22	-30	-41	——	——	——	——	——

(c) Resistance x 0.95

Gain (dB)	.02	.9	1.3	1.8	2.3	-13	-17	-20	-22	-21
Phase(deg)	-2.5	-14	-19	-25	-33	——	——	——	——	——

(d) R_0 and Gain ÷ 2

Gain (dB)	0	.93	1.4	1.9	2.4	-16.6	-20	-22	-21	-19.6
Phase(deg)	-2.5	-15.4	-21	-27.5	-37	——	——	——	——	——

(e) R_0 and Gain ÷ 4

Gain (dB)	0	.8	1.2	1.7	2.2	-16.7	-20	-22	-21.4	-19.7
Phase(deg)	-2.6	-16	-22.5	-28.5	-38	——	——	——	——	——

(f) R_0 and Gain ÷ 10

Gain (dB)	0	.65	1	1.4	1.8	-17	-20.5	-22.4	-21.6	-19.9
Phase(deg)	-2.8	-17	-23	-30	-40	——	——	——	——	——

445

Equating corresponding parts of equations 21 and 23 gives

$$Y_1 = s + \beta \qquad Y_2 = \frac{(21 - \alpha - \beta)s + 1.4 \times 10^4 - \alpha\beta}{s + \alpha} \qquad (24)$$

$$Y_6 = s + \gamma \qquad Y_4 = \frac{(33 - \alpha - \gamma)s + 4.8 \times 10^3 - \alpha\gamma}{s + \alpha}$$

By choosing different values of α, β, and γ, the admittances of different simple RC circuits are realized. The terms α, β, and γ should be chosen to maximize time constants so larger capacitor values can be used and to ensure that Y_2 and Y_4 are negative. Also, if no resistors blocked by capacitors are desired, then it is required that $\alpha\beta > 1.4 \times 10^4$ and $\alpha\gamma > 4.8 \times 10^3$.

Figure 22 shows a circuit with components evaluated for $\alpha = 160$, $\beta = 160$, and $\gamma = 82$. Table VIII(a) shows the circuit frequency response to be very close to that of the required Biquad. Changing the resistor values by ±5 percent (table VIIIb, c) shows that the circuit is relatively insensitive to resistance changes.

6.4 Three-Operational-Amplifier Circuit

A Biquad circuit using three, operational amplifiers is shown in figure 23 [25,26]. This circuit has the transfer function

$$\frac{P_o}{P_I} = \frac{ms^2 + cs + d}{s^2 + as + b} = \frac{\frac{R_8}{R_6} s^2 + \left[\frac{1}{R_1 C_1} \frac{R_8}{R_6} - \frac{R_1 R_8}{R_4 R_7}\right] s + \frac{R_8}{R_3 R_5 R_7 C_1 C_2}}{s^2 + \frac{1}{R_1 C_1} s + \frac{1}{R_2 R_3 C_1 C_2} \cdot \frac{R_8}{R_7}} . \qquad (25)$$

The values for m, c, d, a, and b can be evaluated by comparing equation 25 with equation 2. The circuit element values are given by [25]

$$R_1 = \frac{1}{aC_1}, \qquad\qquad R_2 = \frac{K_1}{\sqrt{b}\, C_2} ,$$

$$R_3 = \frac{1}{K_1 K_2 \sqrt{b}\, C_1} , \qquad R_4 = \frac{1}{K_2(ma-c)C_1} , \qquad (26)$$

$$R_5 = \frac{K_1 \sqrt{b}}{dC_2} , \qquad\qquad R_6 = \frac{R_8}{m} ,$$

$$R_7 = K_2 R_8 .$$

Because there are five equations and ten unknowns, C_1, C_2 and R_8 are chosen to determine impedance levels, and K_1 and K_2 are arbitrary constants. Making $R_3 C_1 = R_2 C_2$ minimizes circuit sensitivity, and making $K_1^2 K_2 = 1$ distributes the amplifier gains. Figure 24 shows the circuit with components evaluated to produce the required Biquad.
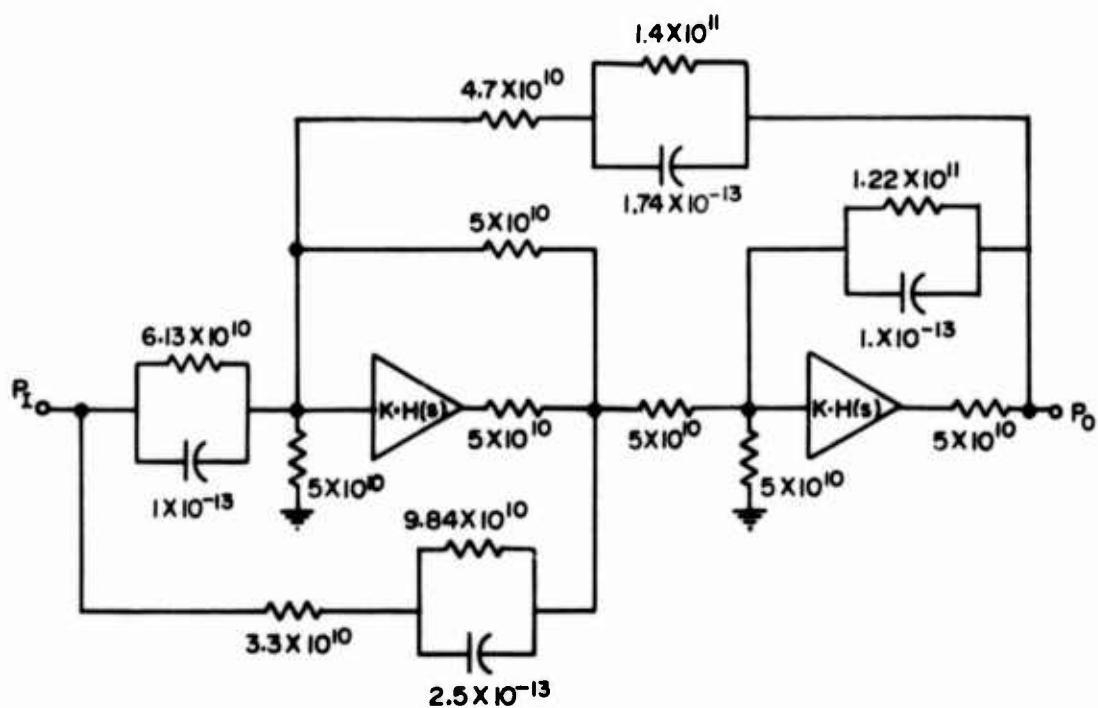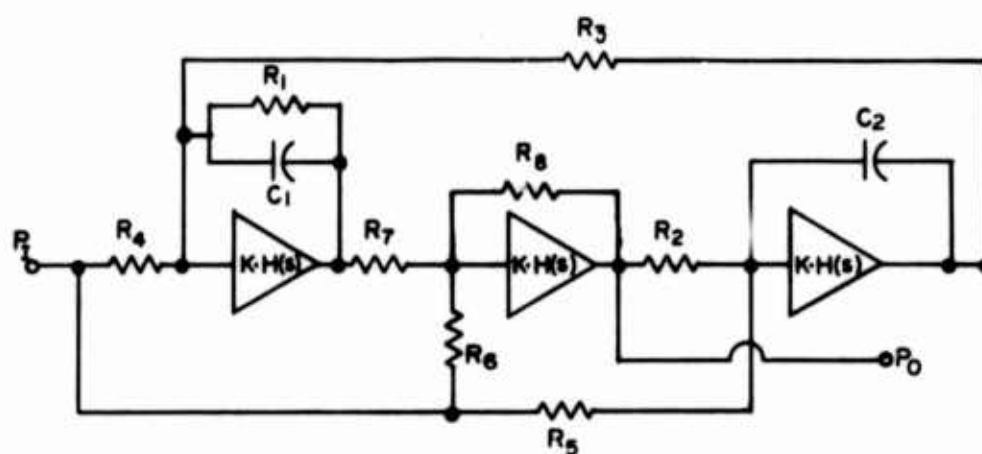
446

Figure 22. Two-operational-amplifier biquad circuit

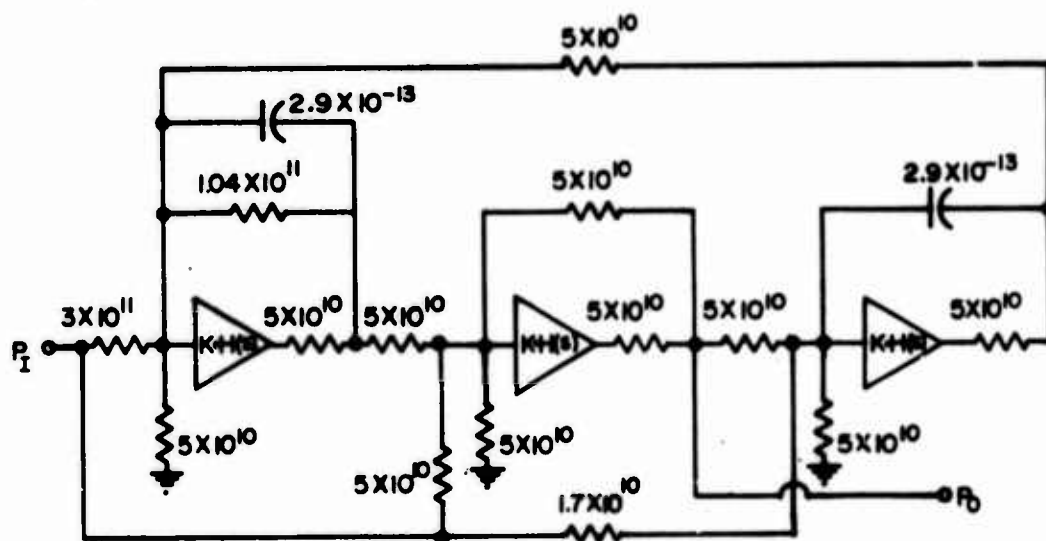Figure 23. Three-operational-amplifier circuit configuration

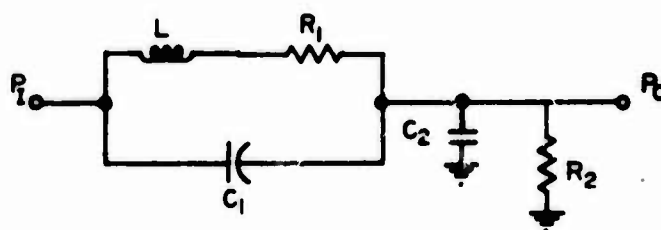447

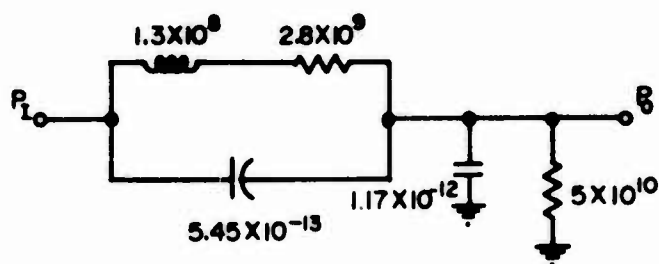Figure 24. Three-operational-amplifier biquad circuit

Figure 25. RLC configuration

Figure 26. RLC biquad circuit

448

TABLE VIII. Two-Operational-Amplifier Circuit with Parametric Variations

(a) Two-Operational-Amplifier Biquad Circuit

FREQ (Hz)	1	5		7	8	17	18	19	20	21
Gain (dB)	0	1	1.5	2.1	2.8	-16.5	-20.4	-22.6	-21.7	-19.8
Phase(deg)	- 2	-13.7	-18.4	-24.8	-33.7	—	—	—	—	—

(b) Resistance x 1.05

Gain (dB)	0	1.1	1.7	2.4	3	-19.9	-22.6	-22	-19.8	-18
Phase(deg)	-2.3	-14.7	-20	-27.5	-38	—	—	—	—	—

(c) Resistance x 0.95

Gain (dB)	0	.9	1.4	1.9	2.5	-13	-17	-20.6	-22.6	-21.8
Phase(deg)	-2	-12.7	-16.8	-22.3	-29.8	—	—	—	—	—

TABLE IX. Three-Operational-Amplifier Circuit with Parametric Variations

(a) Three-Operational-Amplifier Biquad Circuit

FREQ (Hz)	1	5	6	7	8	17	18	19	20	21
Gain (dB)	0	1.0	16	2.2	2.9	-16	-19.6	-21.6	-21	-19.4
Phase(deg)	-2	-13	-17.4	-23.5	-32.3	—	—	—	—	—

(b) Resistance x 1.05

Gain (dB)	0	1.1	1.8	2.5	3.2	-19	-21.5	-21	-19.4	-17.9
Phase(deg)	-2.2	-14	-19	-26	-37	—	—	—	—	—

(c) Resistance x 0.95

Gain (dB)	0	.9	1.4	2	2.7	-13	-16.4	-19.7	-21.6	-21
Phase(deg)	2	-12	-16	-21	-28.4	—	—	—	—	—

Table IX(a) shows the circuit frequency response. This circuit has a frequency response that is very close to the frequency response of the required Biquad. The additional amplifiers make possible the use of passive component values that do not load down the amplifiers. Table IX(b, c) shows that the effects of a ±5 percent resistance change are relatively small.

6.5 Summary of Operational-Amplifier Circuits

The three-operational-amplifier circuit (sect. 6.4) produces the required Biquad accurately. The circuit also requires relatively few passive components. Only four capacitors are needed for a differential circuit. However, three high-gain fluidic amplifiers are needed for the circuit. The two-operational-amplifier circuit (sect. 6.3) produces the next best frequency response. Eight capacitors are needed for the differential circuit. Since a low-impedance driving source is needed for this circuit, three high-gain amplifiers may actually be required. Because the driving source of the three-operational-amplifier circuit in figure 24 drives only resistors connected to the amplifier input, which is effectively grounded, a driving-source resistance changes the circuit gain but not the frequency response. The two- and three-operational-amplifier circuits may therefore require three amplifiers.

The Bohn circuit (sect. 6.2) is relatively simple but is less accurate in producing the required Biquad. The phase shift at the zero-dB crossover frequency is greater than that of the required Biquad and will reduce the phase margin of the system. The other single-amplifier circuits, which depend on the ratio of the input and feedback networks, load down the amplifier so that the frequency response is very inaccurate. The only exception is the simple bridged-tee circuit (sect. 6.1.1) which does not load the amplifier but does produce an extra zero in the transfer function. This zero reduces the notch depth but decreases the low-frequency phase shift.

7. PASSIVE BIQUAD CIRCUITS

The main advantage of passive circuits over active circuits is that ideally there are no amplifiers to affect the circuit frequency response. However, in practice the fluidic passive circuits do require amplifiers to increase the signal level and to provide isolation between circuits.

An RLC circuit that can produce the required Biquad was found, but the high resistance of the fluidic inertances (tubes) did not allow for practical-sized components. A passive RC notch-filter circuit with a complex-numerator but real denominator quadratic transfer function was also found. Compensating this notch with a lead-lag circuit decreased the excessive phase shift at the zero crossover frequencies. However, the transfer function of the circuit still only approximated that of the required Biquad.

450

7.1 RLC Circuit

Figure 25 shows an RLC circuit with the transfer function

$$\frac{P_o}{P_I} = \frac{R_2}{R_1 + R_2} \cdot \frac{LCs^2 + R_1C_1s + 1}{(\frac{R_2}{R_1 + R_2}) L(C_1 + C_2)s^2 + \left[\frac{R_1R_2(C_1 + C_2)}{R_1 + R_2} + \frac{L}{R_1 + R_2}\right]s + 1} \tag{27}$$

$$= \frac{K(7.0 \times 10^{-5}s^2 + 1.5 \times 10^{-3}s + 1)}{2.1 \times 10^{-4}s^2 + 7.0 \times 10^{-3}s + 1},$$

where K is an arbitrary scaling constant. Equation like coefficients gives four equations and five unknowns. By letting $R_2 = 5.0 \times 10^{10}\frac{N\text{-sec}}{m^5}$, the element values in figure 26 are found.

From the numerator of equation 27

$$\frac{LC_1}{R_1C_1} = \frac{L}{R_1} = \frac{7.0 \times 10^{-5}}{1.5 \times 10^{-3}} = 4.7 \times 10^{-2} \tag{28}$$

The ratio of inertance to resistance of a tube is

$$\frac{L}{R_1} = \frac{(\frac{4\rho\ell}{3\pi r_o^2})}{(\frac{8\mu\ell}{\pi r_o^4})} = 4.7 \times 10^{-2} \tag{29}$$

where

ℓ = length of tube, m,

r_o = radius of tube, m,

ρ = density of fluid, kg/m^3, and

μ = viscosity of fluid, $\frac{N\text{-sec}}{m^2}$.

Solving equation 29 for the tube radius yields

$$r_o = \sqrt{0.28 \frac{\mu}{\rho}}, \tag{30}$$

where μ/ρ, the kinematic viscosity of a typical hydraulic fluid, is $2.1 \times 10^{-5} \frac{m^2}{sec}$,

so that $r_o = 2.4 \times 10^{-3}m$ (0.1 in.), $\tag{31}$

The length of tube with this radius needed to produce the inertance value in figure 26 is

$$\ell = 1.3 \times 10^8 \cdot \frac{(3\pi r_o^2)}{(4\rho)} \approx 2m, \tag{32}$$

using $\rho = 8.8 \times 10^2$, which is much too long for most applications.

To perform the same calculations for the RLC circuit using air, it is necessary to first scale the component values for the lower impedances in air. Assuming the amplifier impedances are orifices

451

$$P = \frac{\rho v^2}{2} = \left(\frac{\rho v h}{\mu}\right) \frac{v S \mu}{2hS} = N_R \frac{Q\mu}{2hS} \qquad (33)$$

where
  h = amplifier nozzle height, m,
  v = fluid velocity, m/sec,
  S = area, m^2,
  Q = vS, volume flow, m^3/sec, and
  N_R = Reynolds number, dimensionless.

From equation 33,
$$R = \frac{P}{Q} = \frac{N_R \mu}{2hS} \qquad (34)$$

Thus, for a constant Reynolds number, the resistance of an orifice is pro-
portional to the fluid viscosity. The viscosity of air is approximately
1000 times less than that of hydraulic oil. The inertance and resistances
in figure 26 should be reduced by a factor of 1000. Using 1.5×10^5 for
the kinematic viscosity of air in equation 30, the tube radius that
provides the proper damping to produce the required Biquad is

$$r_o = 2.1 \times 10^{-3} m \ (\approx 0.08 in). \qquad (35)$$

This is approximately the same radius tube found for hydraulic fluid
since the kinematic viscosities of the two fluids are nearly the same.
From equation 32, the length of tubing required to produce an inertance
1000 times smaller with air is

$$\ell = 1.3 \times 10^5 \ \frac{(3\pi r^2)}{(4\rho_{air})} \approx 1.1m \qquad (36)$$

where $\rho = 1.2$, which is still very long.

From equation 30, it was found that relatively large diameter tubes
are required to produce the low damped inertances for the required Biquad.
This large diameter tubing in turn requires long tube lengths to provide
the inertance values for the required time constants. If large amplifiers
with lower amplifier resistances are used, the inertance values (and thus
the tube lengths) can be reduced. Equation 34 shows that the resistance
is inversely proportional to the tube area. Increasing the radius 4.5
times reduces the resistance by a factor of approximately 20, and the
tube length by the same factor. However, the amplifiers will now require
20 times more flow. Another problem of the RLC circuit is that the circuit
is very temperature sensitive because of the capillary flow resistance.
It is also necessary to drive the circuit with a low-impedance source.

7.2 Passive RC Compensated Notch Filters

Figure 27 shows a parallel-tee circuit which has a transfer function
with a complex quadratic numerator but a real quadratic denominator.
The circuit includes a source resistor R_o and an input resistor R_I. The
easiest way to find component values for a given notch width, notch
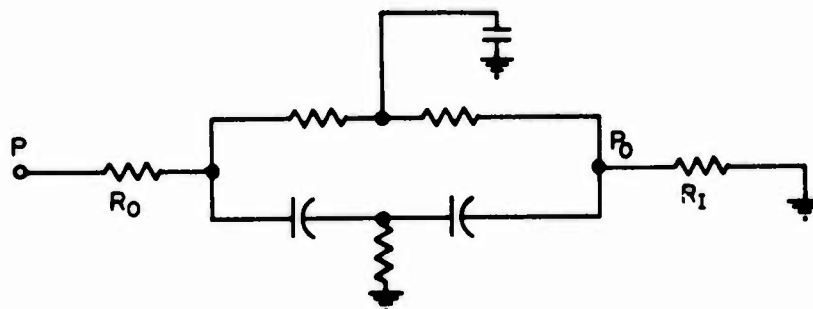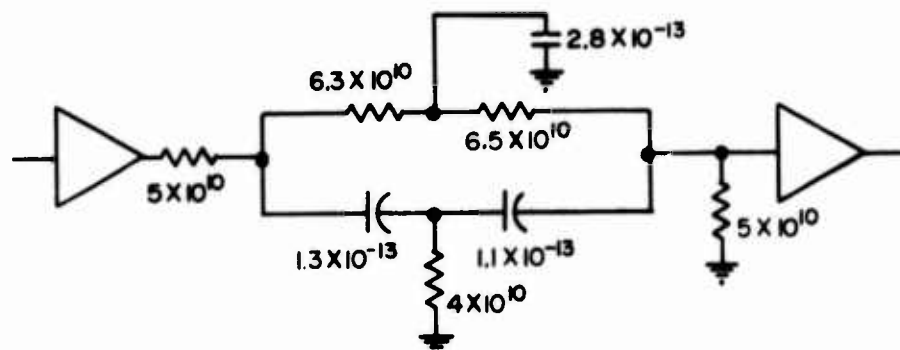
Figure 27. Parallel tee circuit configuration
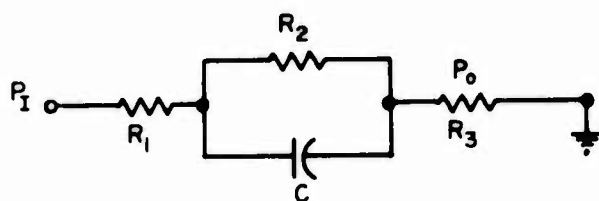

Figure 28. Parallel tee biquad circuit
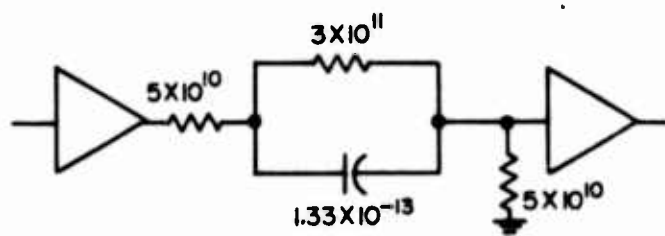

Figure 29. Lead-lag circuit configuration

Figure 30. Lead-lag circuit

453

center frequency, and values of R_o and R_I is to use the graphical technique described by Bocast [27]. The circuit with the component values shown in figure 28 has the frequency response shown in table X. This circuit has much more phase shift at the zero-dB crossover frequencies than the required Biquad (table !), as well as a deeper notch.

A lead-lag circuit can be used to decrease the phase shift at the zero-dB crossover frequency. Placing the zero at 4 Hz and the pole at 16 Hz decreases the phase shift at the lower frequencies. Figure 29 shows a passive, lead-lag circuit which has the transfer function

$$\frac{P_o}{P_I} = \frac{R_3}{R_1 + R_2 + R_3} \frac{R_2Cs + 1}{\frac{R_1R_2 + R_2R_3}{R_1 + R_2 + R_3} Cs + 1} = K \frac{.04s + 1}{.01s + 1},\qquad(38)$$

where K is an arbitrary scaling constant. Setting $R_1 = R_3 = 5.0 \times 10^{10} \frac{N\text{-sec}}{m^5}$ (amplifier input and output resistors) leaves two unknown circuit elements that can be found by equating the like coefficients in equation 37. All the circuit values are shown in figure 30.

It was found that a slightly different lag-lead in equation 1 when used with the parallel tee notch and lead-lag circuit produced a better approximation of the original transfer function (equation 1). The circuit for the passive lag-lead shown in figure 31 has the transfer function

$$\frac{P_o}{P_I} = \frac{R_2Cs + 1}{2\frac{(R_1 + 2R_2)}{2} Cs + 1} = \frac{.06s + 1}{2[3s + 1]}\qquad(39)$$

which differs slightly from the lag-lead in equation 1. Setting $R_1 = 5.0 \times 10^{10} \frac{N\text{-sec}}{m^5}$ (amplifier resistances), R_2 and C are found by equating like coefficients in equation 38. All of the circuit values are shown in figure 32.

Putting the circuits in figures 28, 30 and 32 together gives a passive circuit with isolating amplifiers that approximates the transfer function in equation 1. Table XI shows the frequency response of the combined circuit. Comparing this frequency response with the response of equation 1 in table VI(a) shows that the passive circuit has less phase shift at the zero-dB crossover frequencies and a deeper but sharper notch. If the resistance values are changed ±5 percent, the low-frequency response stays relatively constant, but the gain at the notch frequency changes greatly (table XIb, c). Table XI(c) shows that the notch center frequency drops 5 dB below the desired value (table VIa). If either temperature remains constant or the system can tolerate notch depth variations caused by temperature changes without becoming unstable, this circuit provides a means of building a notch filter with passive elements and low-gain fluidic amplifiers.
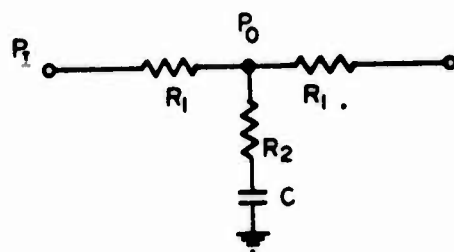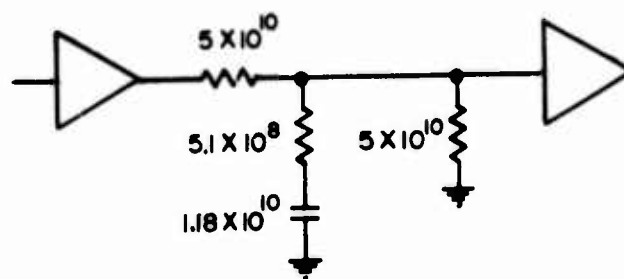
Figure 31.   Lag-lead circuit configuration

Figure 32.   Lag-lead circuit

455

TABLE X. Twin Tee Circuit

FREQ (Hz)	1	5	6	7	8	17	18	19	20	21
Gain (dB)	0	-2.3	-3.2	-4.3	-5.3	-24	-32	-35	-26	-22
Phase(deg)	-.9	-41	-47	-52	-57	—	—	—	—	—

TABLE XI. Passive RC Circuit with Parametric Variations

(a) Passive RC Compensated Notch

FREQ (Hz)	1	5	6	7	8	17	18	19	20	21
Gain (dB)	-4.8	-11.7	-12	-12.4	-13	-29	-36	-39	-30	-25.5
Phase(deg)	-65	-34	-34	-36	-38	—	—	—	—	—

(b) Resistance x 1.05

Gain (dB)	-5.1	-11.8	-12	-12.6	-13	-35	-40.6	-30	-26	-22
Phase(deg)	-64	-34	-35	-37	-39	—	—	—	—	—

(c) Resistance x 0.95

Gain (dB)	-4.4	-11.7	-12	-12.3	-12.7	-25	-29	-37	-39	-30
Phase(deg)	-65	-34	-34	-35	-37	—	—	—	—	—

7.3 Summary of Passive Circuits

The RLC circuit, although theoretically capable of producing the required Biquad, is limited by the large size of the inertances or by the large supply flows required by larger fluidic amplifiers needed to produce lower amplifier impedances. The RC circuit only approximates the required Biquad response. Although the zero-dB crossover-frequency phase response is good, the notch is very sharp and therefore very sensitive to component value changes. Because of these problems, it is probably better to use the active circuits. But where supply flow is plentiful and temperature is relatively constant, it could be less expensive to use the passive circuits.

8. SUMMARY OF BIQUAD CIRCUITS

Ten notch-filter circuits have been investigated to determine whether they can fulfill the requirements for the M60A1 tank control system. Table XII provides a summary of some of the more important characteristics of the circuits investigated. We note that the circuits that require a low-impedance driving source will need an additional low-output-impedance amplifier or other low-impedance source. The number of passive and active components in the circuits is given in the table since this is important for determining packaging size and flow requirements. The relative sensitivity of the circuits frequency response to resistor value changes listed in the table is indicative of the effect of temperature variations. The degree to which a circuit produces the required transfer function is indicated qualitatively in the column labled "Biquad Performance". The behavior of the high-gain circuits depends on the values assumed for amplifier gain and parasitic resistances. If the amplifier gain and resistances are different from those assumed in this paper, the circuit frequency response will also be affected.

9. CONCLUSIONS

Of the various circuits described in the paper, the three-operational-amplifier circuit appears to be the most practical fluidic notch-filter circuit for the M60A1 control system. First the circuit accurately produces the required Biquad, and although three high-gain amplifiers are required, the other high-gain amplifier circuit that can accurately produce the Biquad also requires three amplifiers. Most importantly, this circuit requires fewer capacitors than the other circuits, and all of the capacitor values are equal. Because the capacitor values are equal, the resistor values, which are more easily controlled, can be scaled to provide the required transfer function if bellows with an exact capacitance value cannot be obtained.

Although the three-operational-amplifier circuit appears to be the best circuit for meeting the requirements of this investigation, other circuits might be a better choice for producing different notch-filter transfer functions.

457

Table XII. Summary of Circuit Performance

Circuit	Driving Source Impedance	No. of Cap.*	No. of Res.*	No. of Induc.	No. of Amp.	Amp. Gain	Circuit Sensitivity to Resistor Variations	Biquad Performance	Section of Paper
Low-gain two-amp.	Low	6	12	0	2	Low	High	Good	5.1
Elliptic	Low	6	7	0	1	Low	Medium	Fair	5.3
Simple bridged-tee	Low	8	7	0	1	High	Low	Fair-Good	6.1.1
Compound bridged-tee	Low	12	7	0	1	High	-	Poor	6.1.2
Dual of compound bridged-tee	Low	7	12	0	1	High	-	Poor	6.1.3
Bohn circuit	Low	7	6	0	1	High	Low	Fair	6.2
Two-op-amp.	Low	8	16	0	2	High	Low	Good	6.3
Three-op-amp.	Low or High	4	16	0	3	High	Low	Good	6.4*
(Passive) RLC	Low	3	3	2	2	Low	-	-	7.1
RC	Low or High	7	21	0	4	Low	High	Fair	7.2

* Differential circuits

458

LITERATURE CITED

1. Kaminski, A. P., "A Mathematical Representation of the M60A1 Azimuth and Elevation Control and Add-On Stability System," Chrysler Defense Engineering System Analysis, Report No. CDE-SA-TR-71-09, 1971, pp. 86.

2. Haykin, S. S., "Sythesis of RC Active Filter Networks," (McGraw-Hill, NY 1969), pp. 1.

3. Manion, Francis M., and Mon, George, "Fluerics: 33. Design and Staging of Laminar Proportional Amplifiers," HDL-TR-1608, Sept 1972.

4. Mitra, Sanjit K., "Analysis and Synthesis of Linear Active Networks," (John Wiley and Sons, Inc. NY, 1969), pp. 326.

5. Malmberg, Allan B., "Users Manual-NET 2 Network Analysis," HDL-050-1, Sept. 1973.

6. Blackburn, John F. et.al., "Fluid Power Control," (The MIT Press, Boston MA, 1960), pp. 18-28.

7. Streeter, Victor L., "Handbook of Fluid Dynamics," (McGraw-Hill, NY, 1961), pp. 9-6.

8. Balabanian, N., "Active Realization of Complex Zeros," IEEE Transaction on Circuit Theory, Vol. CT-10, Mar 1963, pp 299-300.

9. Mitra, Sanjit K., Loc. cit., p 311.

10. Kerwin, W. J. and Huelsman, L. P., "The Design of High Performance Active RC Band-Pass Filters," IEEE International Conv. Rec., Vol. 14, pt. 10, 1966, pp 74-80; Mitra, Sanjit K. (editor), "Active Inductorless Filters," IEEE Press, 1971, pp 63-69.

11. Boddy, D. E., "Synthesis of Transfer Functions Using RC Fluidic Circuits," Fourth Cranfield Fluidics Conference, March 1970, Conventry, Paper F3.

12. Tobey, Gene E. et al. "Operational Amplifiers Design and Applications," (McGraw-Hill, NY, 1971), ch. 5.

13. Brown F. T. et al. "Design of a Near-Optimum Fluidic Operational Amplifier," Lehigh Unversity, Themis Project: Fluid Amplifiers, Office of Naval Research, Code 461, Contract No. N00014-69-A-0417, Technical Report No. 16, 1973.

14. Jackson, Albert S., "Analog Computation," (McGraw-Hill, NY, 1960), pp. 621-626.

15. Truxal, John G., "Control Engineers Handbook," (McGraw-Hill, NY, 1958). pp 6-38 to 6-42.

16. Korn, Granino A. and Korn, Theresa M., "Electronic Analog and Hybrid Computers," (McGraw-Hill, NY, 1964), pp. 554-559.

459

17. Jackson, Albert S., loc. cit., p 624.

18. Manlon, Francis M., loc. cit., pp 33-38.

19. Jackson, Alberts., loc. cit., p 625.

20. Mitra, Sanjit K., loc. cit., pp 485-486.

21. Holt, A. G. J. and Sewell, J. I., "Active RC Filters Employing a Single Operational Amplifier to Obtain Biquadratic Responses," Proc. IEE (London), 112, Dec 1965, pp 2227-2234.

22. Jackson, Albert S., loc. cit., p 44.

23. Manlon, Francis M., loc. cit., p 32.

24. Huelsman, Lawrence P., "Theory and Design of Active RC Circuits," (McGraw-Hill, NY, 1968), p. 201.

25. Fleischer, P. E. and Tow, J., "Design Formulas for Biquad Active Filters Using Three Operational Amplifiers," Proceedings of the IEEE, Vol. 61, No. 5, May 1973, pp. 662-663.

26. Mitra, Sanjit J., loc. cit., pp 97-103;   Kerwin, W. J. et. al., "State Variable Synthesis for Insensitive Integrated Circuit Functions," IEEE Journal of Solid-State Circuits, Vol. S6-2, Sept 1967, pp. 114-116.

27. Bocast, Donald R., "Graphical Solution for Twin-T Networks," Electronics, 17 Jun 60, pp 67-70.

LOW-POWER HYDRAULIC CONTROL COMPONENTS

by

RICHARD DEADWYLER

Prepared for
Presentation at the Harry Diamond Laboratories
Fluidic State-of-the-Art Symposium

30 Sept - 04 Oct 74

ABSTRACT

This report presents the initial results of an effort to determine whether low-power, passive hydraulic, fluidic control components operated in the linear laminar regime can be used in high-performance control systems, i.e., control systems with a dynamic range $\geq$ 1,000 and negligible parasitic dynamics below 100 Hz. Hydraulic resistive and capacitance summing junctions and compensation circuits were tested and found to have low frequency dynamic ranges of 1,7?0 and 20,000, respectively. They also have good frequency response. The parasitic dynamics were found to cause 6 to 8 degrees phase shift at 100 Hz for both the summing junction and compensation circuit.

These results were obtained with a low-noise-level pump (0.007 kP_a or 0.001 psi), nearly constant oil temperature ($\pm 2^{\circ}C$), and very little entrained air bubbles in the oil. They indicate that low-power, passive hydraulic fluidics can be used in high-performance control systems under these conditions.

INTRODUCTION

Low-power, hydraulic control which involves sensing, amplification, compensation, etc. is currently limited by (1) the lack of basic design procedures and (2) the nonlinearities, and inaccuracies of those procedures which are available. Therefore, low-power control is presently accomplished by electrical, mechanical or electromechanical means [1]. Hydraulic fluidics, which can be used to amplify, sense, etc., offers a mean for overcoming the limitations mentioned above. The use of low-power, hydraulic control in a system with hydraulic power transmission has the following advantages over electrical, mechanical, or electromechanical control:

a. The hydraulic to electrical or mechanical, etc., interface devices are eliminated.

b. The transmission power supply can be used to power the control circuit.

c. The overall system is more rugged, (few moving parts).

d. The overall system can possibly be produced and operated at lower cost (few moving parts, no auxiliary power supply for electrical, or mechanical components [2]); and

e. The overall system is simpler [2].

This paper presents the initial results of an effort to determine whether low-power, passive, hydraulic, fluidic control components operated in the linear, laminar regime can be used in high performance control systems. A high performance control system is defined as one with a dynamic range or operating range $\geq$ 1,000 and negligible parasitic or unwanted dynamics below 100 Hz open loop. The study was made using the analogies between elementary fluid theory and simple lumped-parameter, electrical circuit theory. The results presented here are performance and design criteria with respect to dynamic range, (DR), and frequency response. Hydraulic resistive summing junctions and resistive-capacitive, compensation circuits are considered.

HYDRAULIC RESISTIVE SUMMING JUNCTION

A summing junction is a necessary element in most feedback control systems. Therefore, the hydraulic summing junction shown in figure 1 was investigated. It consists of three capillary tubes and a fixed volume. The tubing impedes fluid flow due to wall shear with impedance magnitude, Z, given by equation (1)

$$Z(s) = R + sL \qquad (1)$$

where

R = fluid resistance = $\dfrac{128\mu\ell}{\pi D^4}$ $\qquad$ L = fluid inertance = $\dfrac{4\rho\ell}{\pi D^2}$

ℓ = tube length $\qquad\qquad\qquad$ μ = absolute viscosity of the fluid

D = tube diameter $\qquad\qquad\quad$ ρ = density of the fluid

s = Laplace operator

When ℓ and D are the same for each impedance, the pressure drops across the impedances in SI units are then given as

$$\Delta P_1(s) = P_1(s) - P_3(s) = \left[\frac{128\mu\ell}{\pi D^4} + s\,\frac{4\rho\ell}{\pi D^2}\right] Q_1(s) = Z_1(s) \quad Q_1(s)$$

$$\Delta P_2(s) = P_2(s) - P_3(s) = \left[\frac{128\mu\ell}{\pi^{-4}} + s\,\frac{4\rho\ell}{\pi D^2}\right] Q_2(s) = Z_2(s) \quad Q_2(s) \qquad (2)$$

$$\Delta P_3(s) = P_3(s) - P_4(s) = \left[\frac{128\mu\ell}{\pi D^4} + s\,\frac{4\rho\ell}{\pi D^2}\right] Q_3(s) = Z_3(s) \quad Q_3(s)$$

where the pressure in the volume is assumed to be uniform. The fluid is incompressible and the junction volume is fixed so that the volume flow, Q, is

$$Q_3(s) = Q_1(s) + Q_2(s) \qquad (3)$$

From equation (2) the sum of the input pressures to the volume $P_1(s)$ + $P_2(s)$ is given as

$$P_1(s) + P_2(s) = 2P_3(s) + \left[\frac{128\mu\ell}{\pi D^4} + s\,\frac{4\rho\ell}{\rho D^2}\right] [Q_1(s) + Q_2(s)] \qquad (4)$$

Substituting (3) into (4) gives

$$P_1(s) + P_2(s) = 2P_3(s) + P_3(s) - P_4(s) = 3P_3(s) - P_4(s) \qquad (5)$$

If $P_4(s)$ is the systems ambient or return pressure then,

$$P_3(s) = \frac{P_1(s) + P_2(s)}{3} \qquad (6)$$

Therefore, when used as a summing junction, neither the magnitude nor the reactive component of the impedance affect the junction dynamics. Moreover, since the output of the junction is not a function of impedance magnitude, it is not a function of temperature.

Capillary tubing with 1.585 mm and 0.762 mm ID was used because it was readily available. The lower impedance, 1.585 mm ID, tubing was used to build the summing junction since the junction pressure P_3(see fig. 1), must drive subsequent circuit components whose input impedance must be high with respect to $Z(s)$ or R to minimize loading effects.

The experimentally determined DR and frequency response of the junction are discussed in the following sections.

SUMMING JUNCTION DYNAMIC RANGE

The tubing impedance Z is primarily resistive over the frequency range of interest; therefore, the DR of the junction is essentially determined by the resistance.

Hydraulic resistance, R, due to wall shear is given

$$R = \frac{128\mu\ell}{\pi D^4} \qquad (7)$$

The dynamic range of hydraulic resistance due to wall shear is given as the ratio of the maximum pressure difference across the resistor to the minimum pressure difference for which expression (7) is valid.

$$DR = \frac{\Delta p_{max}[\text{expression (7) valid}]}{\Delta p_{min}[\text{expression (7) valid}]} \qquad (8)$$

The maximum pressure difference across the given tube, for which the loss is linear and given by expression (7), is determined by the maximum flow or Reynolds Number, N_R. From studies by Shapiro, et al [3] the maximum N_R for which equation (7) holds is given by

$$N_{Rmax} = 5\frac{\ell}{D} \qquad (9)$$

For N_R higher than $5\frac{\ell}{D}$ the flow is not fully developed and equation (7) is not valid. For $N_R \le 5\frac{\ell}{D}$ the ΔP across the tube is

$$\Delta P = \frac{128\mu\ell}{\pi D^4} Q \qquad (10)$$

The Reynolds number can be written as

$$N_R = \frac{VD\rho}{\mu} = \frac{4Q\rho}{\pi D\mu} \qquad (11)$$

where
   V = velocity.

Thus flow as a function of N_R is

$$Q = N_R \frac{\pi D\mu}{4\rho} \qquad (12)$$

Substituting (12) into (10) gives

$$\Delta P = \frac{128\mu\ell}{\pi D^4} \cdot N_R \cdot \frac{\pi D\mu}{4\rho} = \frac{32\mu^2\ell}{\rho D^3} N_R \qquad (13)$$

and substituting (9) in (13) gives

$$\Delta P_{max} = \frac{128\mu\ell}{\pi D^4} \cdot 5 \left(\frac{\ell}{D}\right) \cdot \frac{\pi D\mu}{4\rho} \qquad (14)$$

The minimum pressure difference ΔP_{min} for a resistor connected to another fluid element using hydraulic fluid so that there is no air interface, is determined by the system noise level. However, if the hydraulic fluid flowing through the resistor exits into air (which is the case in the summing junction discussed above), then the minimum pressure difference for oil flow in a horizontal tube is the pressure needed to overcome the surface tension force at the tube exit. The surface tension force, σ, for MIL-H-5606B oil is

$$\sigma = 31.9 \frac{dynes}{cm} = 31.9 \times 10^{-3} \frac{N}{m} \qquad (15)$$

The total force is

$$F = \sigma \pi D \qquad (16)$$

Therefore, the pressure acting on the surface, due to surface tension is

$$P = \frac{F}{A_{tube}} = \frac{4F}{\pi D^2} = \frac{4\sigma}{D} \qquad (17)$$

Thus, the upstream pressure P, must be $> \frac{4\sigma}{D}$. The exit pressure is atmospheric, therefore

$$\Delta P_{min} = \frac{4\sigma}{D} \qquad (18)$$

Using this expression gives the maximum obtainable or upper limit on the DR as

$$DR_{max} = \frac{\frac{128\mu\ell}{\pi D^4} \cdot 5(\frac{\ell}{D}) \cdot \frac{\pi D \mu}{\rho}}{\frac{4\sigma}{D}} = \frac{160\mu^2 \ell^2}{\rho \sigma D^3} \qquad (19)$$

Using expression (19) the DR for a capillary resistor of length $\ell = 7.62$ cm (3 inches) and ID = 1.585mm (0.062 inches) is 680.

The low frequency dynamic range was determined using the test setup shown in figure 2. The regulated pressure from the source was applied to the first volume so that for this test $P_1 = P_2$ and $P_3 = 2/3 \; P_1$, (see fig. 1). The low-pressure measurements were made with variable reluctance pressure transducers which convert the applied pressure signals to electrical signals. The electrical signals are amplified (then attenuated for use in one of five output voltage ranges) by the signal conditioners and measured with a vacuum tube voltmeter. The high-pressure measurements were made with bourdon-type pressure gauges. The experimental accuracy of the measurement was ±3% for each reading. Data on the dynamic range, taken throughout the input-output pressure range is shown in figure 3 where the intermediate range is omitted so that the complete range may be shown in one figure. The experimental data is within ±3% of the ideal value at a point far above the upper limit for linear operation (fig. 3). This limit was imposed based on our study of experiments by Shapiro et al [3]. The data in figure 3 indicates that our choice of $N_{Rmax} = 5 \; \ell/D$ for linear operation is conservative and that a value of $N_{Rmax} \cong 12 \; \ell/D$ may be more appropriate. The lower limit ΔP_{min} agrees with equation (18). From figure 3 the DR of the junction is

$$DR = \frac{141 \; kP_a}{0.0805 \; kP_a} \doteq 1,751 \qquad (20)$$

Since this is a linear system, the DR is given by the ratio of the maximum to minimum input or output pressures. The ratio $P_{3(max)}/P_{3(min)}$ is used here. The data also indicates that larger ID tubing might be used to provide better impedance matching with the subsequent component and still

obtain a DR of 1,000. If there is no liquid-to-air interface, then the lower limit on the element DR is determined by the system noise level as previously stated. This condition leads to a much higher DR as will be seen in the discussion of the RC compensation circuit.

Testing was limited to low frequencies because a large amplitude AC signal could not be generated. However, subsequent tests of the RC circuit makes it appear that the dynamic range is good to 100 Hz.

SUMMING JUNCTION FREQUENCY RESPONSE

The frequency response of the junction was determined using a test setup similar to that shown in figure 2, where $P_1 = P_2$. From equation 6 the junction transfer function (fig. 1) is

$$G_1(s) = \frac{P_3(s)}{P_1(s)} = \frac{2}{3} \tag{21}$$

Quartz-type pressure transducers, which have negligible fluid capacitance, were used. The junction frequency response is shown in figure 4 where the low-frequency data is in good agreement with the ideal design response. These data were obtained after eliminating essentially all the air bubbles from the junction volume. Parasitics are unwanted dynamics which are due to unaccounted for inductance and capacitance in the circuit. The symbol, I, is used to indicate the amount of uncertainty or spread in the data. The uncertainty occurs at high frequencies because the signal generator output decreases with increasing frequency and its output in the 60-100 Hz region was just above the noise level for the electronic phase meter. The parasitics that occur at high frequencies between 70 to 100 Hz are in the form of phase lag. The high-frequency phase lag is due primarily to transmission delay. At 100 Hz it is approximately six degrees.

RC COMPENSATION CIRCUITS

Hydraulic resistive and capacitive impedance elements have been used to build lag-lead compensation circuits. The hydraulic circuit is shown in figure 5a and its equivalent in 5b. The circuit transfer function is

$$G_2(s) = \frac{P_0(s)}{P_1(s)} = \frac{R_0 Cs + 1}{(R_0 + R_1)Cs + 1} \tag{22}$$

It can be rewritten as

$$G_2(s) = \frac{T_1 s + 1}{T_2 s + 1} \tag{23}$$

where $T_1 = R_0 C$
$T_2 = (R_0 + R_1)C$
$C = \frac{\Delta \text{Volume}}{\Delta \text{Pressure}} = (\frac{(\text{Area})^2}{\text{Spring Rate}}$ for bellows).

467

The numerator (or lead) break frequency, f_{lead}, and denominator (or lag) break frequency, f_{lag}, are given as

$$f_{lead} = \frac{1}{2\pi T_1}; \quad f_{lag} = \frac{1}{2\pi T_2} \tag{24}$$

For given resistors, R_I and R_o, and available capacitors the break frequencies were computed using expression (24). The circuit DR and frequency response will be discussed in the following sections.

RC CIRCUIT DYNAMIC RANGE

The DR of resistive elements (ℓ = 7.62 cm, ID = 1.585 mm) exiting to atmosphere was determined in the previous section. Smaller, 0.762 mm ID tubing was used in this circuit to provide high input impedance and minimize inductive effects. From figure 5 it is seen that the resistors in this circuit do not exit into air and consequently the DR is higher since ΔP_{min} is determined by the system noise level. The maximum pressure difference, ΔP_{max} expression (14), for a resistor of length 5.08 cm (2 inches) and ID of 0.762 mm (0.03 inches) is approximately 450 kP_a (65 psi).

The dynamic range of the capacitor is given as

$$DR = \frac{\Delta P_{max}}{\Delta P_{min}} \tag{25}$$

In equation 25, ΔP_{max} is the maximum pressure difference which may be applied across the capacitor for which there is no permanent set in the moving member, a bellows in this case. The minimum pressure difference, ΔP_{min}, is the system noise level. The data on the RC circuit will give the DR of the combined RC circuit and indicate the extent to which the DR of the individual elements coincide. The circuit has the following calculated impedance:

$$R_I = 3.3 \times 10^{11} \frac{Ns}{m^5}; \quad ID = 0.762 \text{ mm} \quad \ell_1 = 15.24 \text{ cm (6 in)}$$

$$R_o = 1.1 \times 10^{11} \frac{Ns}{m^5}; \quad ID = 0.762 \text{ mm} \quad \ell_o = 5.08 \text{ cm (2 in)}$$

$$C = \frac{A_B^2}{K_b} = 2.32 \times 10^{-13} \frac{m^5}{N}$$

Spring Rate, K_b = 219 × 10^2 N/m (125 lb/in)

Area, A_B = 7.13 × 10^{-5} m^2 (0.1104 in)

The experimentally determined value of C is 7.48 × 10^{-13} m^5/N. The difference between the calculated and experimental value is very large in this case. There was about a 10% difference in other capacitors that were

468

tested. The spring rate for this particular bellows was different from the manufacturer's specification. It was probably overstressed during testing. Since there is no resistance to ground in this circuit, the minimum input-pressure signal is determined by the system noise level. The system noise level ΔP_{min} in the test setup used to determine the circuit DR was found to be < 7 Pa (0.001 psi). For peak-to-peak input signal pressures of 145 kP_a (21 psi) in the 1-100 Hz range, DR $\geq$ 21,000, qualitative studies of the circuit input and output signal spectrums show little or no circuit-produced distortion, see figure 6. Figure 6 shows large amplitude inputs at 1 and 20 Hz, (the signal at approximately 40 Hz is the second harmonic of the electronic signal generator signal at approximately 20 Hz) where the top trace is the circuit input and the bottom trace the circuit output. The circuit frequency response for this large-input-amplitude testing will be discussed in the next section. The system noise level for these tests is the noise level of the measurement system. The dynamic range data indicates that hydraulic resistive and capacitive impedance elements have very high dynamic ranges. In actual hydraulic control system applications, the system noise level will be different, probably much higher. This would suggest a lower circuit DR. However, many proposed applications of hydraulic fluidic control use differential circuits, so that noise such as vibrations, shock, etc. that is common to both ports, will be rejected if the amplifiers have good common-mode rejection. A study of laminar amplifier, common-mode rejection is now being conducted at HDL.

RC CIRCUIT FREQUENCY RESPONSE

The frequency response of this circuit was obtained experimentally, using the test setup shown in figure 7. The signal generator provides an electrical sine-wave signal which is fed into the electrohydraulic servovalve. The servovalve provides a proportional hydraulic sine-wave signal in response to the electrical input signal which is used to drive the RC compensation circuit. The circuit input and output pressures (P_I and P_o from fig. 5) are monitored by quartz-type piezoelectric transducers These transducers convert the hydraulic pressure signals into electrical charges. The charges in turn, are ampliferd by the charge amplifiers and displayed as Lissajous patterns on the oscilloscope. This Lissajous data were verified by additional tests using a Drantz phase meter and a Bafco system analyzer, respectively, in place of the oscilloscope. From expression (24) the lag-lead break frequencies are

$$f_{lag} = \frac{1}{2(32.9 \times 10^{-2})} \approx 0.48 \text{ Hz}; \quad f_{lead} \approx \frac{1}{2(8.24 \times 10^{-2})} = 1.9 \text{ Hz} \qquad (26)$$

The theoretical circuit response with the above break frequencies is plotted on the same graph (dashed lines) as the experimentally determined response, figure 8. The experimental response is seen to be in good agreement with the theoretical response using the individual component values. The response is the same for small as well as large (145 kP_a) input signal amplitudes.

The high frequency parasitic phase lag is due to transport delay. The parastic phase shift is approximately 8 degrees at 100 Hz. The design of these circuits is simple and the actual circuits perform very close to the theroetical value. However, in this case the value of capacitance had to be determined experimentally.

CONTROL SYSTEM APPLICATION

The control components discussed in the previous sections could be used in a feedback-control system such as shown in figure 9. Components designated G_1 and G_2 are cascaded (fig. 10) and have a transfer function $T(s)$ where

$$T(s) = G_1(s) \, G_2(s) \tag{27}$$

CASCADE COMPONENTS DYNAMIC RANGE

The static or low frequency DR of the cascaded elements depends on the range of the individual components and the extent to which the ranges coincide. The DR of the cascade components is shown in figure 11 where the maximum and minimum output levels of $G_1(s)$ are plotted with the maximum and minimum input levels of $G_2(s)$. The combined DR is determined by the inner most curves B and C, that is 1,750. The measured low frequency DR of the summing junction, which was limited by the test facility, is projected to 100 Hz. The loading effect, dynamic range, and frequency response of these cascade elements will be discussed in the following sections.

LOADING EFFECT

The cascade transfer function, expression (27), is valid if the input impedance of $G_2(s)$ is high, so that there is little loading effect on $G_1(s)$. The combined equivalent circuit of the elements is shown in figure 10. Its transfer function is

$$T(s) = \frac{2}{3} \, \frac{R_o Cs + 1}{(R_1 + R_o + \frac{R_s}{3}) \, Cs + 1} \tag{28}$$

where $R_1 = R_2 = R_3 = R_s$, from figure 1. The ideal dynamic portion of the transfer function is given by expression (22). The error in the lag term between expression (22) and (29) is about 1% $[(R_1 + R_o) = 4.4 \times 10^{11} \, \frac{Ns}{m^5}$ and $R_s = 9 \times 10^9 \, \frac{Ns}{m^5}]$.

From figure 9 it is seen that the output of $G_2(s)$ is the input signal to the system plant. Normally the compensation circuit output signal $P_o(s)$, must be amplified. The result depends on the input impedance of the fluid amplifier used to amplify the signal. Amplifiers currently being studied have input impedances, R_i, approximately equal to R_o where $R_o = 1.1 \times 10^{11} \, \frac{Ns}{m^5}$, figure 10. Considering the amplifier

input impedance, R_i, the cascade transfer function expression (28) becomes

$$T(s) = \left(\frac{2}{3}\right) \frac{R_i}{R_l + R_i + R_s/3} \left(\frac{R_o C_s + 1}{\left\{ \frac{R_l R_l + R_l R_o + R_l R_o + (R_s/3)(R_o + R_l)}{R_l + R_i + R_s/3} \right\} Cs + 1} \right)$$

If R_i were increased by a factor of 10, that is $R_i = 10^{12} \frac{Ns}{m^5}$ then the error in the lag term would be nearly 4.3% and signal amplitude would be only 75% of the value given by the expression (22). An even higher input impedance is desirable. Such an increase appears possible through amplifier modification at the expense of amplifier gain.

CASCADE FREQUENCY RESPONSE

The cascade response can be found by adding the response of the two components (figs. 4 and 8). This combined response has a parasitic phase shift of approximately 15 degrees at 100 Hz. This response assumes $R_i \gg R_o$. For the case where $R_i = 10 R_o$ the lag break frequency would be 4.3% higher than the value given by expression (22). Other than this change the response should be the same as given by the addition of the response shown in figures 4 and 8.

CONCLUSIONS

A static or low frequency DR of 1,750 was experimentally determined for the resistive summing junction where the experimental transfer function was within 3% of the ideal value. The junction frequency response is in good agreement with the ideal response. The parasitic or unwanted dynamics occur at high frequencies where there is measurable phase lag between 70-100 Hz, primarily due to transport delay. At 100 Hz the lag is approximately six degrees. This lag is acceptable for high performance operation. If this circuit did not have a liquid-to-air interface, a much higher DR would be possible.

A dynamic range of 20,000 was determined experimentally for the RC compensation circuit. The circuit frequency response is in good agreement with the ideal response. The parasitic or unwanted dynamics occur in the 70-100 Hz region. They are primarily due to transport delay. At 100 Hz, there is a parasitic phase shift of approximately 8 degrees. Thus, it appears that low-power, hydraulic fluidics can be used in high performance control systems under the conditions previously stated. These results are for essential constant temperature oil. The oil temperature in most hydraulic systems may vary over a considerable range. Oil temperature changes constitute the major difficulty in using laminar hydraulic compensation circuits. This difficulty can be overcome in two ways; first, the oil can be kept at constant temperature by appropriate heating and cooling. Second, since the low-pass character of this filter shifts upward with increasing temperature, i.e., it passes higher frequency components, it may be possible to design the

471

filter so that at the maximum oil temperature it provides sufficient gain and phase margin to ensure system stability. This will ensure system stability throughout the temperature range; however, the systems response at lower oil temperatures will be degraded.

REFERENCES

1. Merritt, H. E., "Hydraulic Control Systems," John Wiley and Sons, 1967, p 3.

2. Kelley, L. R. and Boothe, W. A., "Hydraulic Fluidics," ASME, 68-WA/FE-26, 1968, p 1, 7.

3. Shapiro, H. H., Siegel, R., and Kline, S. J., "Friction Factor in Laminar Entry Region of a Smooth Tube," Proceedings of the 2nd U.S. National Congress of Applied Mechanics, 1954, pp 934-936.

ACKNOWLEDGEMENT

a. PHYSICAL CONFIGURATION

b. EQUIVALENT CIRCUIT

FIGURE 1

475

FIGURE 2

476

FIGURE 3

FIGURE 4

$R_I, R_O =$ CAPILLARY RESISTORS
C = BELLOWS CAPACITOR

a. PHYSICAL CONFIGURATION

b. EQUIVALENT CIRCUIT

FIGURE 5

479

Amplitude Level, 20DB/Div

Frequency, 5Hz/Div

a. Circuit Input and Output Signal Spectrums for a 1 Hz Input Signal (Input Trace on Top)

Amplitude Level, 20DB/Div
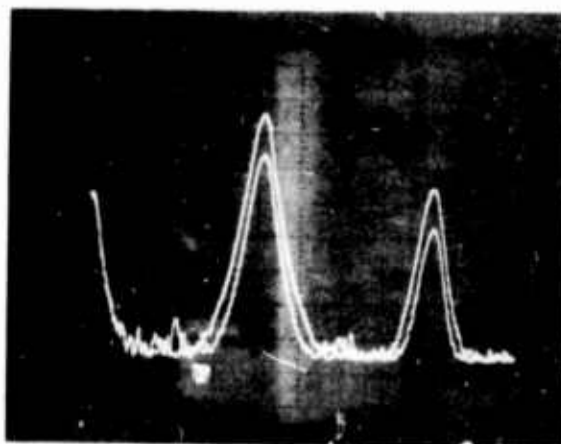
Frequency, 5Hz/Div

b. Circuit Input and Output Signal Spectrums for a 20 Hz Input Signal (Input Trace on Top)

FIGURE 6
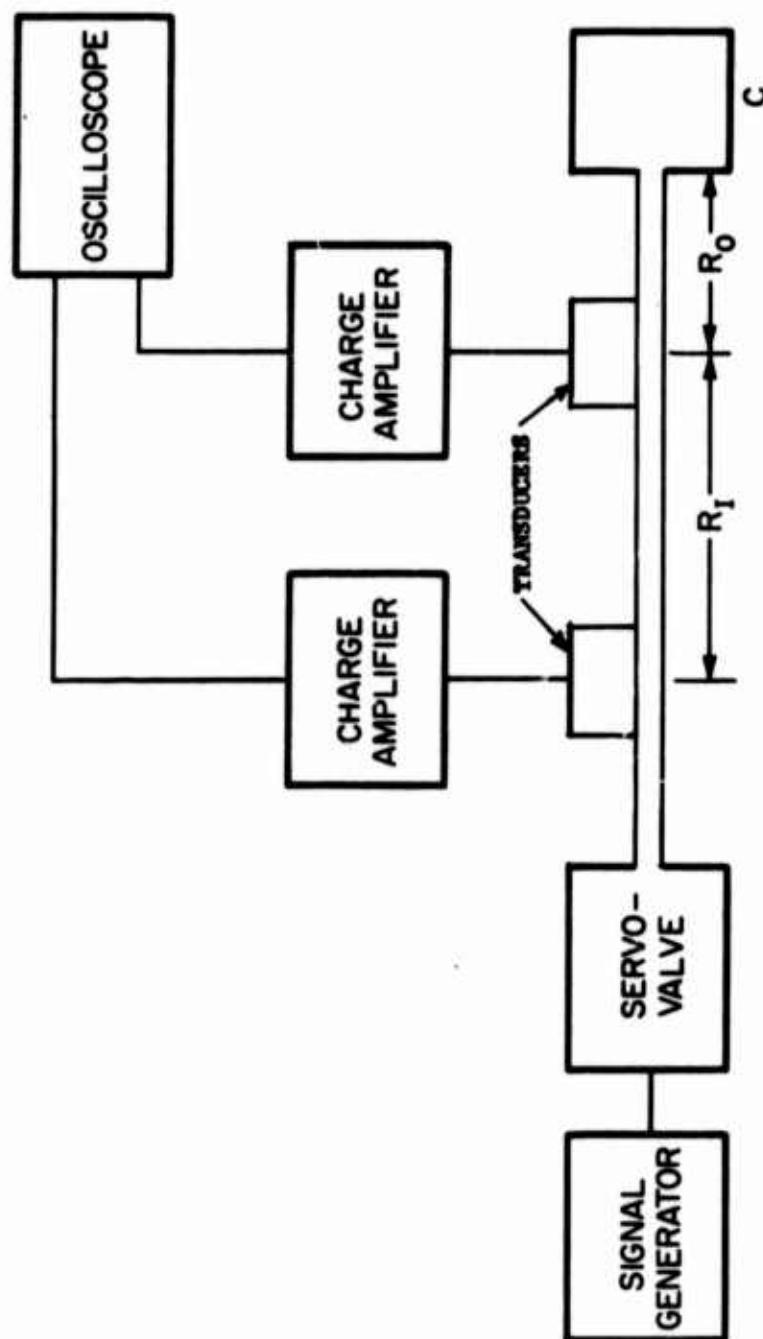
480
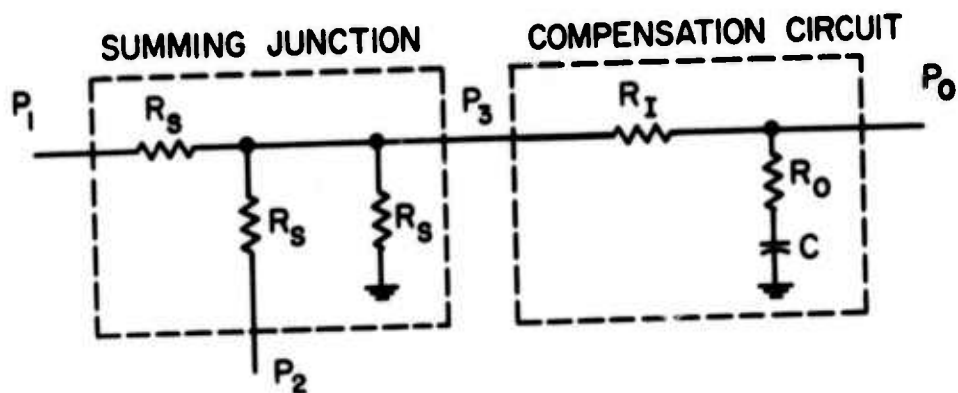
FIGURE 7

FIGURE 8

FIGURE 9

483
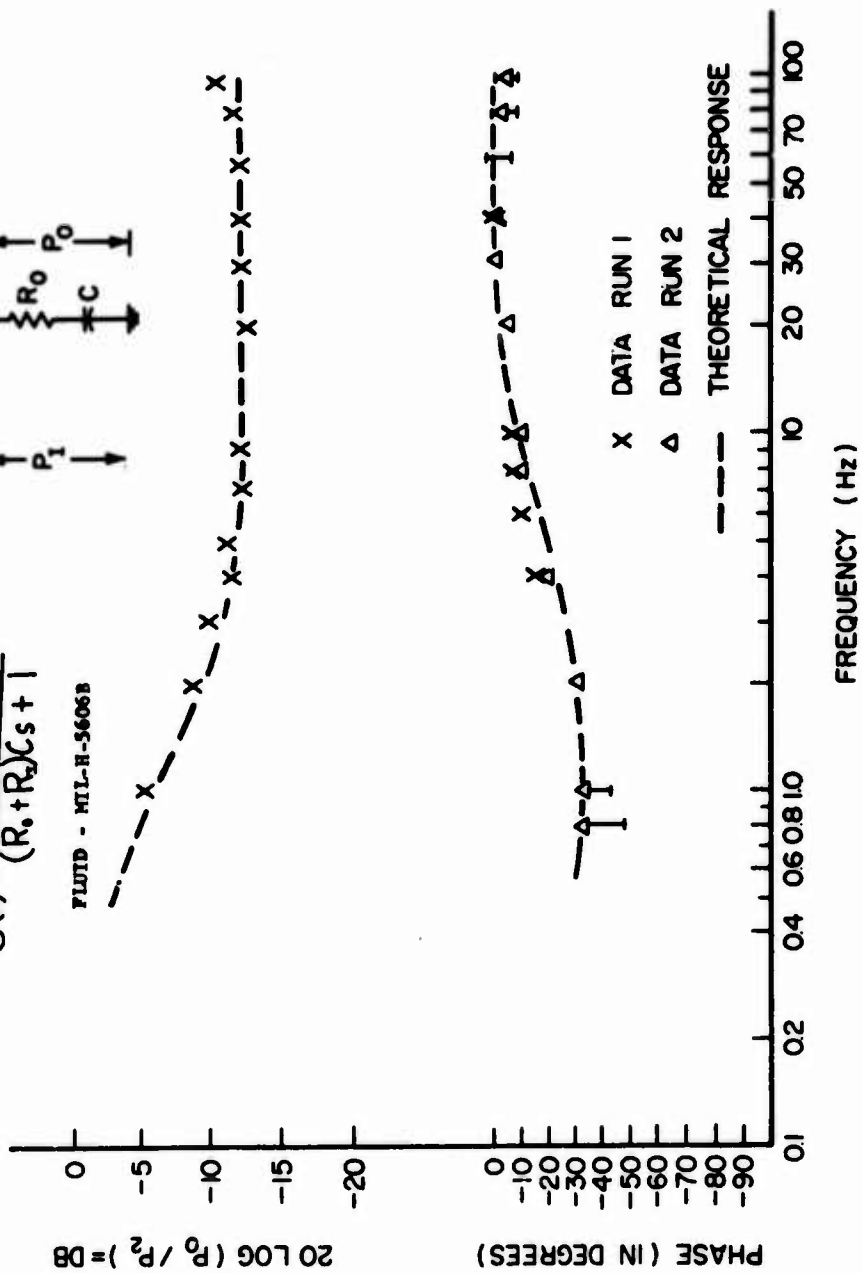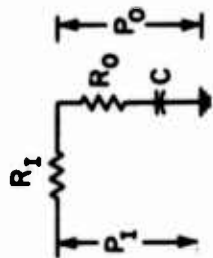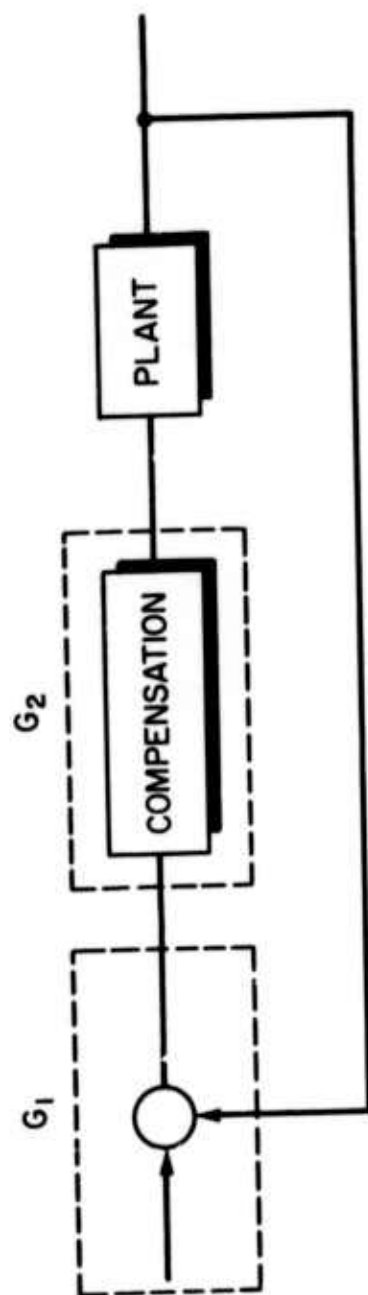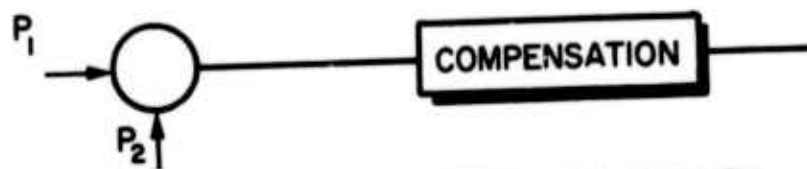
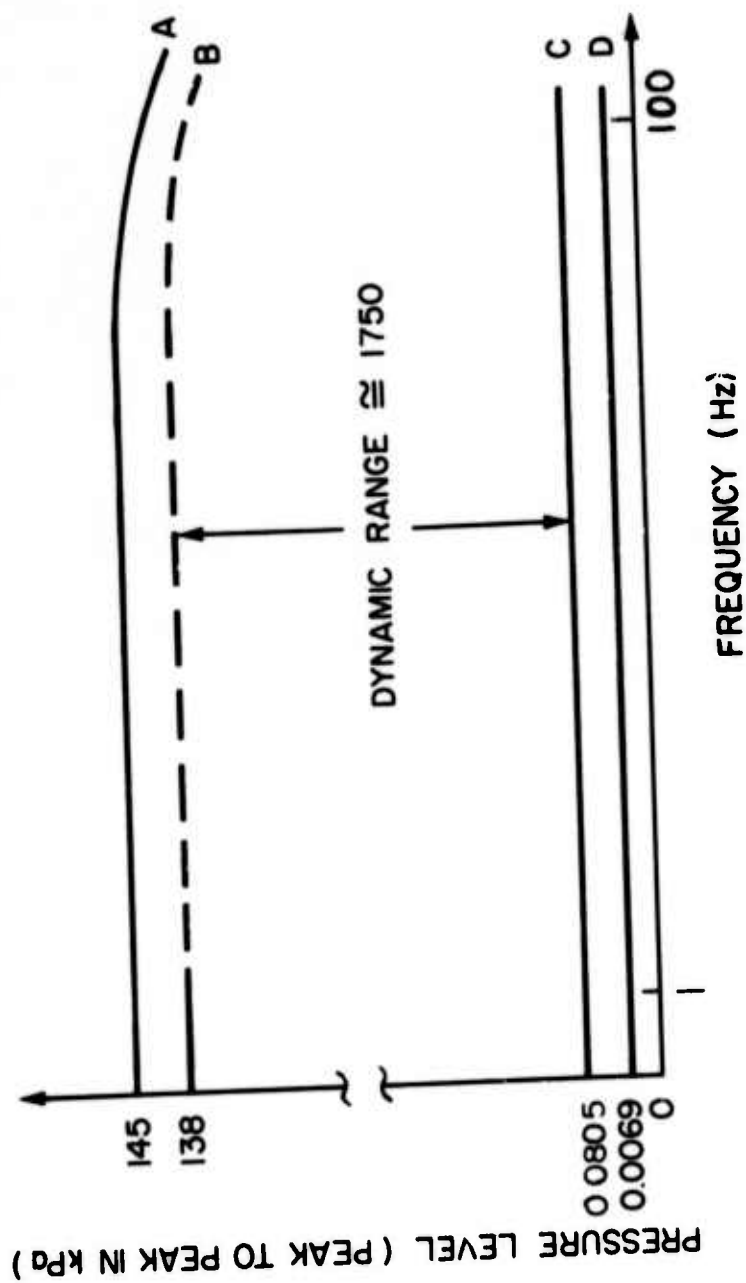a. TWO CONTROL SYSTEM COMPONENTS

b. RC IMPLEMENTATION

FIGURE 10

FIGURE 11